THE PHYSICAL REVIEW

VOLUME 89 *Second Series* NUMBER 2

JANUARY 15, 1953

Published for the

AMERICAN PHYSICAL SOCIETY

by the

AMERICAN INSTITUTE OF PHYSICS

LANCASTER, PA., AND NEW YORK, N. Y.

REVIEW

A journal

Published by the American Institute
for the

AMERICAN PHYSICAL

Officers

President

J. H. VAN VLECK
Harvard University
Cambridge, Massachusetts

Vice-President

ROSCOE FRASER
Institute for Nuclear
University of Chicago
Chicago 37, Illinois

Secretary

K. K. DARROW
Bell Telephone Laboratories
Office
Columbia University
New York 27, New York

Treasurer

G. B. PEGRAM
Columbia University
New York 27, New York

Local Secretary
for the Pacific Coast

J. KAPLAN
University of California
Angeles
Los Angeles, California

Managing Editor

S. A. GOUDSMIT
Brookhaven National
Upton, Long Island
New York

BOARD OF EDITORS

Associate Editors

W. Lawrence

THE
PHYSICAL REVIEW

A journal of experimental and theoretical physics established by E. L. Nichols in 1893

SECOND SERIES, VOL. 89, NO. 2 JANUARY 15, 1953

Distribution in Energy of the Neutrons from the Interaction of 14-Mev Neutrons with Some Elements*

ELIZABETH R. GRAVES AND LOUIS ROSEN
University of California, Los Alamos Scientific Laboratory, Los Alamos, New Mexico
(Received October 6, 1952)

The neutron spectra from the interaction of 14-Mev neutrons with a number of elements have been determined by nuclear plate techniques. The plates were exposed to neutrons from the bombardment of a Zr-T target by 200-kev deuterons when the target was as nearly as possible isolated from all scattering material and when the target was surrounded by a spherical shell of the element to be investigated. The variation of $F(E_n)$, the number of emitted neutrons per unit energy interval with energy (E_n), appears to be Maxwellian in the region 0.5 to 4.0 Mev and may be represented by

$$F(E_n)dE_n = CE_n e^{-E_n/T}dE_n.$$

I. INTRODUCTION

THERE now exist considerable experimental data on the inelastic scattering of fast neutrons by various elements. However, very few of the experiments permit a detailed evaluation of the absolute cross section for inelastic scattering as a function of the energy of the emitted neutrons.

Barschall *et al.*[1] investigated the inelastically scattered neutrons from a number of different elements and for several incident neutron energies below 3.0 Mev. By counting proton recoils in a proportional counter, they measured the cross section for inelastic scattering to below predetermined energies which were varied from 0.4 to 2.25 Mev. These data were interpreted by Feld[2] in terms of the statistical theory of Weisskopf and coworkers[3] and also in terms of individual levels. Feld found that, although the inelastic scattering of tungsten at these low excitation energies agrees quite well with the statistical theory, the data on iron and lead cannot readily be so interpreted, but do lend themselves to interpretation in terms of an individual level theory, applicable when only a few levels of the target nucleus are involved.

Gittings *et al.*[4] performed an experiment in which the cross sections for inelastic collision of 14.5-Mev neutrons with lead were measured by Al(n,p) and Cu$(n,2n)$ detectors. Similar measurements were made by Phillips *et al.*,[5] with the addition of $P(n,p)$ detectors, for a number of elements. Both investigations indicated that secondary neutrons, i.e., inelastically scattered or $n,2n$ neutrons appeared mostly to have energies of less than $\sim$3 Mev.

Stelson and Goodman,[6] using photographic emulsion techniques, measured the distribution in energy of the inelastic neutrons from the interaction of 15-Mev neutrons with lead, iron, and aluminum. Their results confirm those cited above, as do also the results of Whitmore and Dennis[7] who used similar photographic emulsion techniques to investigate the neutron spectra from 14-Mev neutrons interacting with lead and bismuth.

The method used to obtain the results presented in this paper differs from the method utilized by Phillips *et al.*[5] in that the material to be investigated surrounds the source instead of the detector, and the neutron spectra are measured with nuclear emulsion techniques in order to obtain better energy resolution and more

* Work performed under the auspices of the AEC.
[1] Barschall, Battat, Bright, Graves, Jorgensen, and Manley, Phys. Rev. **72**, 881 (1947); Barschall, Manley, and Weisskopf, Phys. Rev. **72**, 875 (1947).
[2] B. T. Feld, Phys. Rev. **75**, 1115 (1949).
[3] V. F. Weisskopf, Phys. Rev. **52**, 295 (1937); V. F. Weisskopf and D. H. Ewing, Phys. Rev. **57**, 472 (1940); V. F. Weisskopf, *Lecture Series in Nuclear Physics* (U. S. Government Printing Office, Washington, D. C., 1947); V. F. Weisskopf and J. M. Blatt, MIT Technical Report No. 42 (May 1950) (unpublished).
[4] Gittings, Barschall, and Everhart, Phys. Rev. **75**, 610 (1949).
[5] Phillips, Davis, and Graves, Phys. Rev. **88**, 600 (1952).
[6] P. H. Stelson and C. Goodman, Phys. Rev. **82**, 69 (1950).
[7] B. G. Whitmore and G. E. Dennis, Phys. Rev. **84**, 296 (1951).

precise values for the cross section for inelastic neutron production as a function of the energy of the inelastic neutron. An inelastic neutron is defined as a neutron produced by interaction of the primary neutron with the target nucleus by any means other than elastic scattering. The threshold detector data permit the determination of only a rough energy distribution for the inelastic neutrons, since only a few suitable detectors are presently available whose thresholds and energy sensitivity have been sufficiently investigated.

II. EXPERIMENTAL METHOD

Figure 1 represents the experimental arrangement. The shell thickness of all the scatterers was chosen to be approximately one-quarter of a mean free path for inelastic collision of 14-Mev neutrons. Neutrons of energy 13.4 to 14.8 Mev were generated by the bombardment of a thick tritium-zirconium target[8] by a magnetically analyzed molecular beam of 200-kev deuterons. The number of neutrons generated was measured by counting in a proportional counter the He^4

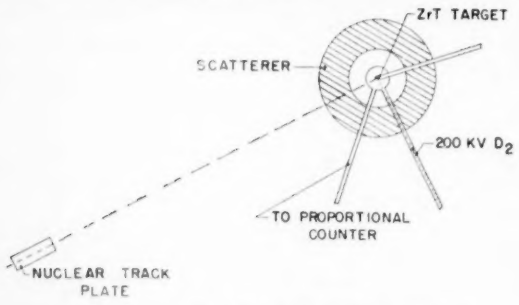

FIG. 1. Schematic view of experimental arrangement.

particles from the $H^3(d,n)He^4$ reaction. Ilford 200-μ C-2 nuclear track plates, the emulsion of each covered by a foil of 0.010-inch platinum, were wrapped in black paper and placed 65 cm from the neutron source. A line through the center of the plates, parallel to the long dimension, intersected the center of the neutron source at an angle of approximately 90° to the direction of the deuteron beam. The maximum angle between a scattered neutron path and the plate axis was $\approx 9°$.

Plates were exposed to neutrons from the bare target assembly to check on the accuracy of absolute neutron counting by the photographic emulsion method and to obtain a background spectrum in the region below the primary peak. Exposures to the source surrounded by thin shells of the various materials were carried out in the same manner as the "background" exposures.

The plates were processed by the "two solution method"[9] and their analysis carried out under 90X apochromatic objectives and 6X compensating eyepieces using Leitz Ortholux microscopes. The microscope stage is fitted with a micrometer screw to which is attached a graduated drum on which one division represents a transverse motion along the screw of 2.5 microns. This adaptation, which was engineered and built by Erb and Gray of Los Angeles, makes possible the measurement of a displacement along the screw axis with an accuracy of approximately ± 3 microns in 1000 microns. For tracks shorter than 50 microns a calibrated eyepiece graticule is used.

For each plate, three to twelve swaths, one cm long by approximately 100 microns wide, were analyzed. The traverses were made in a direction parallel to that of the incident neutrons. All proton tracks originating in the emulsion volume covered by the swaths, which were completely contained within the emulsion within a rectangular pyramid of half-angle 15° in the unprocessed emulsion, were measured. The emulsion volume analyzed was taken at the edge of the plate nearest the source in order to avoid the possibility of attenuation of the neutrons by emulsion, glass backing, and platinum covering. From the ranges of the tracks, corresponding proton recoil energies are deduced, using the range-energy curves of Rotblatt,[10] corrected for water content of the plates on the basis of the range in the emulsion of proton recoils from 14.2-Mev neutrons. The proton recoil energies are transformed to incident neutron energies by the relation $E_p = E_n \cos^2\theta$, where E_p is the proton energy, E_n is the neutron energy, and θ is the average angle between the incident neutron and the recoil proton in the unprocessed emulsion. θ was determined from the scatterer-detector geometry and angle of acceptance for the recoil protons and was approximately 10° in all cases.

In order to calculate the absolute neutron flux at the detector as a function of energy, it is useful to define the following symbols:

$N(E_p)\Delta E_p \equiv$ number of proton recoils having energy between E_p and $E_p+\Delta E_p$, which are projected from unit emulsion volume and into a given solid angle, $d\Omega$.

$n_0 \equiv$ number of hydrogen atoms per unit emulsion volume.

$\sigma_{n,p}(E_n) \equiv$ neutron-proton scattering cross section as a function of energy. The neutron-proton cross sections were taken from the compilation of Adair.[11]

$P(l) \equiv$ probability that a track of given length, l, does not leave the emulsion.

Then the flux of neutrons in any given energy interval between E_n and $E_n+\Delta E_n$ is

$$F(E_n)\Delta E_n = \frac{4\pi N(E_p)\Delta E_p}{4P(l)n_0\sigma_{n,p}(E_n)\cos\theta d\Omega}. \quad (1)$$

[8] Graves, Rodrigues, Goldblatt, and Meyer, Rev. Sci. Instr. **20** 579 (1949).
[9] M. Blau and J. de Felice, Phys. Rev. **74**, 1198 (1948).
[10] J. Rotblatt, Nature **167**, 550 (1951).
[11] R. K. Adair, Revs. Modern Phys. **22**, 249 (1950).

In compiling the data, ΔE_p was always chosen such that ΔE_n would be 0.5 Mev.

The difficulties involved in making absolute neutron flux measurements with nuclear emulsions have been adequately described and referenced in a paper by Barschall *et al.*[12] The value for n_0 was taken as given by the manufacturer with a small correction for the additional water content due to the relative humidity prevailing during exposure. (Dr. Webb of Eastman Kodak very kindly performed accurate experiments on the variation of water content with relative humidity.)

In the course of attempts to increase the accuracy of the absolute neutron flux measurements, the following procedures were found helpful in the determination of n_0 and $d\Omega$:

(1) The thickness of the emulsion is measured prior to development by removing the emulsion from one or more corners of the plate and measuring the emulsion thickness with a dial indicator. This gives the initial emulsion thickness, which, together with the correction for relative humidity, is used to calculate n_0.

(2) After development, the emulsion thickness is measured with the fine focus screw of the same microscope which is to be used to analyze the plate. This measurement, along with the measurement referred to in (1), makes possible the use of the fine focus screw to measure track dips and hence to define $d\Omega$, in one dimension, in terms of the undeveloped emulsion thickness. This procedure makes an accurate determination of emulsion shrinkage and an absolute calibration of the microscope fine focusing adjustment unnecessary. It is only necessary that the fine focus screw motion is a linear function of the resultant stage motion within the region in which it is used.

(3) The calculation of $P(l)$ assumes that the tracks proceed in a straight line without suffering scattering. Consequently if the product of the length of tracks and the sin of the angle of acceptance is less than the emulsion thickness, the effective value of $d\Omega$ is less than calculated because of the loss of singly or multiply scattered tracks which undeflected would have remained in the emulsion volume. In the present experiment there were few neutrons between 4 and 12 Mev. Since scattering introduces negligible error in the evaluation of $P(l)$ for neutrons below 4 Mev, ($P(l)$ differs little from unity for 200-μ emulsions at this energy) the procedure was adopted, somewhat at expense of resolution, of permitting a rather large half-angle for track acceptance (15°). This implies that all protons projected by neutrons of energy >12 Mev at an angle of 15° with the neutron direction will leave the top or bottom of the emulsion if they do not scatter. However, those which scatter in such a way as to end in the emulsion will be counted and will to a large extent compensate for the proton recoils which are destined to end within the emulsion but do not do so as a result of single or multiple scattering.

The absolute flux measurements of high energy neutrons arriving at the detector agree to an accuracy of ±12 percent, when statistical accuracies are 5 percent or better, with the values calculated from the source strength determined by alpha-counting, the cross section measurements of Phillips *et al.* and the material thicknesses. However, at low energies (≈1 Mev) the absolute accuracy is probably not better than ±20 percent.

From the flux and energy distribution of the inelastic neutrons corresponding to a given flux of primary neutrons, and the number of atoms per cm² of scatterer, it is possible to determine the cross section for the production of neutrons as a function of the energy of the emitted neutrons. Let $\sigma(E_0, E_n)$, the differential cross section for the emission of neutrons of energy E_n when the incident neutron energy is E_0, be defined by

$$\int_{0.5\ \mathrm{Mev}}^{12\ \mathrm{Mev}} \sigma(E_0, E_n)dE_n = \frac{NT_r\sigma_i}{(1-T_r)N_0}, \qquad (2)$$

where N is the flux of inelastic neutrons of energy between 0.5 and 12 Mev, N_0 is the flux of neutrons (transmitted) of energy 12 to 15 Mev, T_r is the fraction of the neutrons which have not suffered inelastic collisions and σ_i is the cross section for inelastic collision.[5] T_r and σ_i are related by

$$T_r = e^{-\sigma_i t}, \qquad (3)$$

where t is the number of atoms per cm² in the spherical shell. It should be noted that

$$\int_{0.5\ \mathrm{Mev}}^{12\ \mathrm{Mev}} \sigma(E_0, E_n)dE_n$$

may be larger than σ_i because of $n,2n$ processes.

III. RESULTS

Table I presents all the data obtained on the elements investigated. The rows give consecutively (I) the elements investigated; (II) the wall thickness of each spherical shell used; (III) transmission of 14-Mev neutrons through each shell as calculated from the inelastic cross sections;[5] (IV) values for transmission as given by the ratio of neutrons above 12 Mev determined from the nuclear plates with and without the scatterer in place; (V) the number of tracks measured for each element; (VI) the total cross section for the emission of neutrons of energy 0.5 to 12 Mev. The lower half of the table gives, for each element investigated, the energy distribution of the neutrons. The neutrons above approximately 12 Mev are transmitted neutrons, i.e., they have not suffered inelastic collision.

The values of σ_i used to evaluate $\int\sigma(E_0, E_n)dE_n$ were taken from reference 5 since those values of σ_i are

[12] Barschall, Rosen, Taschek, and Williams, Revs. Modern Phys. **24**, 1 (1952).

TABLE I. Summary of data for the interaction of 14-Mev neutrons with various elements. Row I gives the elements investigated; Row II lists the wall thickness of each spherical shell used; Row III lists the transmission of 14-Mev neutrons through each shell as calculated from the inelastic cross sections (see reference 5); Row IV lists values for transmission as given by the ratio of neutrons above 12 Mev determined from the nuclear plates with and without the scatterer in place; Row V gives the number of tracks measured for each element; Row VI gives the total cross section for the emission of neutrons of energy 0.5 Mev to 12.0 Mev for incident neutrons of E_0 = approximately 14 Mev; Row VII gives the results of the calculation of T for each element using Eq. (4); Row VIII gives the values of a obtained from Eq. (6). The lower half of the table gives, for each element investigated, the energy distribution of the neutrons, corrected for background, resulting from the interaction of 14-Mev neutrons with the element. The neutrons above approximately 12 Mev are transmitted neutrons, i.e., they have not suffered collision.

I	Element	C	Al[a]	Fe	Cu	Zn	Ag	Cd	Sn	Au	Pb	Bi
II	$t(10^{24}$ atoms/cm$^2)$	0.597	0.223	0.174	0.175	0.169	0.151	0.139	0.130	0.130	0.105	0.0985
III	T_r (reference 5)	0.60 0.61	0.79 0.71	0.78 0.76	0.77 0.64	0.77 0.70	0.75 0.78	0.77 0.77	0.78 0.57	0.72 0.64	0.76 0.63	0.78 0.74
IV	T_r (present data)	±0.09	±0.10	±0.11	±0.10	±0.10	±0.12	±0.12	±0.10	±0.10	±0.10	±0.10
V	Number of tracks measured	1500	1884	1020	1031	1344	1039	1012	1035	1166	1108	1496
VI	$\int_{0.5\text{ Mev}}^{12.0\text{ Mev}} \sigma(E_0, E_n)dE_n$(barns)	0.52 ±0.2	0.65 ±0.17	1.3 ±0.3	1.0 ±0.25	1.3 ±0.3	1.6 ±0.4	2.2 ±0.6	1.8 ±0.5	2.1 ±0.5	3.3 ±0.8	3.9 ±1.0
VII	$T=\frac{-d[\ln\{F(E_n)/E_n\}]}{dE_n}$(Mev)	1.04 ±0.11	1.01 ±0.10	0.76 ±0.08	0.77 ±0.08	0.73 ±0.07	0.63 ±0.06	0.66 ±0.07	0.56 ±0.06	0.66 ±0.07	0.76 ±0.08	0.95 ±0.10
VIII	a(Mev)$^{-1}$	52.0 ±10.0	56.0 ±11.0	98.0 ±20.0	95.0 ±19.0	105.0 ±21.0	143.0 ±29.0	129.0 ±25.0	182.0 ±36.0	129.0 ±25.0	97.0 ±19.0	63.0 ±13.0

Energy (Mev)	Neutron flux $\times 10^{-6}$ (neutrons/cm^2)										
0.5– 1.0	7.7	5.0	11.6	14.2	15.4	27.0	23.5	24.1	25.6	19.5	20.9
1.0– 1.5	8.0	5.1	9.5	8.3	8.4	15.3	17.2	14.3	18.4	25.5	17.3
1.5– 2.0	6.5	4.4	5.9	4.8	6.3	7.8	7.3	8.3	10.3	13.4	13.7
2.0– 2.5	4.1	3.5	5.5	3.7	5.2	6.0	7.9	2.4	6.4	11.0	10.5
2.5– 3.0	4.8	2.0	2.8	3.7	3.2	3.5	4.4	1.7	4.7	7.7	9.2
3.0– 3.5	1.3	1.9	1.6	1.3	1.3	2.5	1.9	1.9	0.4	3.2	6.1
3.5– 4.0	2.6	0.5	1.4	0.0	1.6	0.5	1.0	2.1	0.8	2.9	2.4
4.0– 4.5	2.7	1.4	2.3	2.2	0.9	0.0	2.8	0.6	1.6	1.1	2.5
4.5– 5.0	3.6	1.4	1.5	0.5	1.4	0.0	0.0	0.6	0.7	0.9	2.3
5.0– 5.5	1.9	2.0	0.1	0.8	0.0	0.0	0.6	0.0	0.6	0.0	0.3
5.5– 6.0	0.4	1.1	0.6	0.5	0.9	1.3	0.8	0.0	0.2	0.3	0.5
6.0– 6.5	2.2	0.7	0.0	0.2	1.6	1.1	0.7	0.2	0.9	0.0	0.4
6.5– 7.0	2.1	0.9	0.4	0.5	1.7	0.3	1.3	0.3	0.0	1.1	1.2
7.0– 7.5	5.0	0.9	0.0	0.0	0.3	0.0	0.1	0.2	0.7	0.2	1.6
7.5– 8.0	1.2	0.3	0.0	0.0	2.0	0.0	0.4	0.3	0.0	0.8	0.9
8.0– 8.5	3.0	0.3	1.0	0.5	0.6	0.5	0.0	0.0	1.3	0.3	0.4
8.5– 9.0	4.0	0.8	0.0	0.0	0.0	0.0	1.3	0.0	0.8	0.0	0.0
9.0– 9.5	3.3	0.2	0.4	0.0	0.1	0.0	0.3	0.6	0.0	0.6	2.4
9.5–10.0	6.3	2.6	0.9	1.0	1.0	0.0	1.3	0.8	0.0	0.5	0.4
10.0–10.5	1.8	1.2	0.6	0.7	2.2	0.9	2.6	0.0	1.4	2.1	1.0
10.5–11.0	3.0	1.7	0.0	0.4	1.3	1.5	0.0	0.0	1.5	0.8	1.2
11.0–11.5	2.6	0.0	0.0	0.0	0.6	0.0	1.3	0.7	0.0	2.0	0.0
11.5–12.0	5.4	0.0	0.0	0.0	0.0	0.7	0.0	0.0	0.0	0.4	0.0
12.0–12.5	4.7	5.9	1.6	0.9	1.0	0.0	1.5	0.0	0.0	1.0	3.5
12.5–13.0	13.8	10.4	5.9	8.8	1.4	0.8	1.7	6.1	5.8	0.0	3.0
13.0–13.5	35.7	22.8	21.8	14.0	20.1	20.1	12.8	12.2	15.6	12.6	17.6
13.5–14.0	60.9	57.9	59.1	47.7	56.1	59.1	63.8	54.5	85.0	55.5	72.0
14.0–14.5	85.2	91.8	77.9	99.1	102.3	128.8	118.9	83.6	98.4	97.4	104.1
14.5–15.0	7.3	10.4	7.2	18.8	22.4	36.1	29.2	7.3	11.0	21.9	11.4

[a] Contains 2.5 atomic percent copper.

considerably more accurate than the values obtainable from this experiment. σ_i for Ag and Sn were interpolated from the empirical relationship between σ_i and the atomic weight.

The data given in Table I have been corrected for background. These corrections were made on the basis of the runs without scatterer and on the assumption that the ratio of the background neutrons to the neutrons of energy 12 to 15 Mev is not significantly altered by the presence of the scatterer.

IV. DISCUSSION

The statistical theory of Weisskopf and co-workers[3] is applicable to interactions of neutrons with nuclei under the conditions that the incident neutron interacts with all the nucleons of the target nucleus and the incident neutron energy is large compared to the level spacing of the residual nucleus in the region of maximum excitation produced by the interaction. It is predicted that the energy distribution of the inelastically scattered neutrons is Maxwellian and is given by

$$[d\sigma(E_0, E_n)/dE_n]dE_n = \text{const} \times E_n \sigma_c e^{-E_n/T} dE_n, \quad (4)$$

where $d\sigma(E_0, E_n)/dE_n$ is the differential cross section per unit energy interval for the scattering of incident neutrons of energy E_0 into the energy interval between E_n and E_n+dE_n, σ_c is the cross section for the formation of a compound nucleus, and T is a parameter which is analogous to a temperature, at an excitation energy of E_0 of the residual nucleus and will be called the temperature. This implies, assuming that T does not vary with E in the energy region in which Eq. (4) obtains, that

$$\ln\left[\frac{1}{E_n}\cdot\frac{d\sigma(E_0, E_n)}{dE_n}\right] vs\ E_n$$

should give a straight line of negative slope $1/T$, that

the mean energy of the inelastic neutrons is $2T$, and that the maximum intensity occurs at T.

According to the theory, if the maximum energy of the residual nucleus after $n, 2n$ reaction is high enough, it may be expected that the energy of the second neutron emitted will have a Maxwellian distribution characterized by a constant $T(E_0-\Delta)$, where Δ is the binding energy of the second neutron, which temperature is associated, not with the target nucleus but with the residual nucleus after the $n, 2n$ reaction. Hence the function $F(E_n)/E_n$ will be the sum of two exponentials, the relative proportion of each governed by the ratio of the number of inelastic scattering reactions to $n, 2n$ reactions. The resolution obtained in the present experiment is probably not good enough to separate two exponentials if they were present. For equal probability of inelastic scattering and $n, 2n$ reaction from a medium

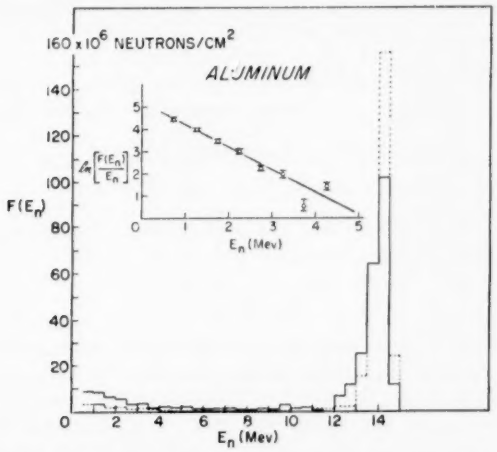

FIG. 2. Neutron spectrum from Al. Solid line represents the energy distribution of the neutrons from the source surrounded by Al sphere; broken line represents the distribution from source alone. The inset is a semilogarithmic plot of the inelastic neutron distribution divided by the neutron energy *vs* neutron energy. Background has been subtracted.

weight element, an apparent T approximately 20 percent lower than T for first neutron emission would be deduced. In any case the value of T deduced from the data will be a lower limit of T for the target nucleus associated with inelastic scattering.

The values of T deduced from the data are given in row VII of Table I. Figs. 2, 3, and 4 are typical of the spectra obtained. The insets show

$$\ln[F(E_n)/E_n] \text{ vs } E_n,$$

indicating to what extent the neutron distributions are Maxwellian. None of the elements investigated appeared to show evidence of a second exponential component. There are a measurable number of neutrons above 5 Mev and these do not follow the exponential which fits the lower energy neutrons. The number of neutrons

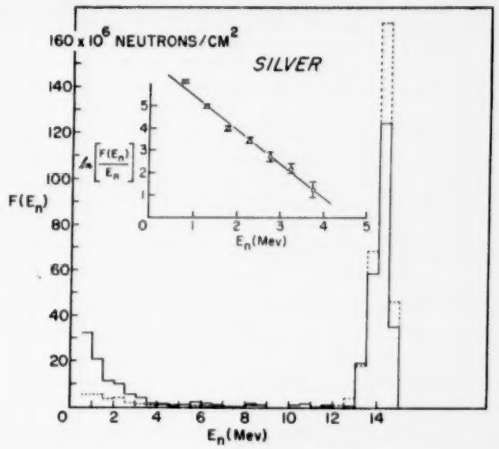

FIG. 3. Neutron spectrum from Ag. Solid line represents the energy distribution of the neutrons from the source surrounded by Ag sphere; broken line represents the distribution from source alone. The inset is a semilogarithmic plot of the inelastic neutron distribution divided by the neutron energy *vs* neutron energy. Background has been subtracted.

above 4 Mev appears to increase with decreasing mass number. It must be emphasized that for carbon, and perhaps even for aluminum, Eq. (4) would not be expected to hold from the very nature of the assumptions upon which it is based.

Stelson and Goodman, applying the statistical analysis, obtained values for T of 1.1, 0.6, and 0.7 Mev for Al, Fe, and Pb, respectively. Whitmore and Dennis obtained temperatures of 0.8 and 0.9 Mev for Pb and Bi, respectively. As can be seen from Table I, our results on these three elements are in quite good agreement with theirs. Stelson and Goodman used scatterers which

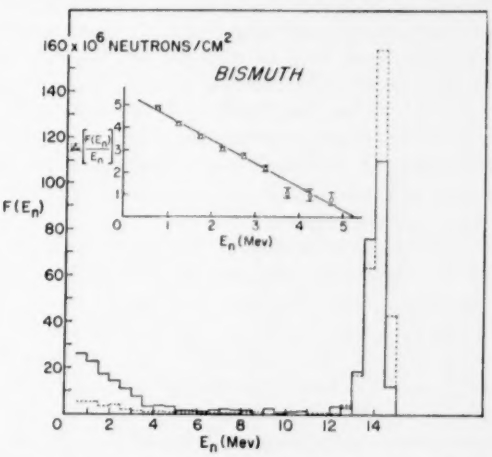

FIG. 4. Neutron spectrum from Bi. Solid line represents the energy distribution of the neutrons from the source surrounded by Bi sphere; broken line represents the distribution from source alone. The inset is a semilogarithmic plot of the inelastic neutron distribution divided by the neutron energy *vs* neutron energy. Background has been subtracted.

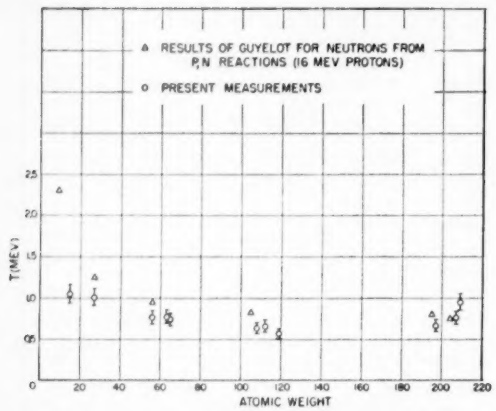

FIG. 5. Variation of T with mass number. Guyelot should read Gugelot.

had a thickness of one mean free path (1λ) for inelastic collision, Whitman and Dennis used scatterers of ½λ thickness, and in the present experiment the scatterers were of thickness ¼λ.

On the assumption of an inelastic cross section which is independent of the primary neutron energy it may be shown that for a thickness of ½λ approximately 25 to 45 percent of the inelastically scattered neutrons have had more than one inelastic collision. For a thickness of ¼λ this fraction drops to approximately 15 to 20 percent. However, the inelastic cross section for Pb and Bi for 1–3 Mev neutrons is less than one-third of its value for 14-Mev neutrons. A study of the data leads to the conclusion that the neutron spectrum for Pb will not be appreciably affected by the difference in sample thickness in the various experiments. For Fe, measured by Stelson and Goodman and in the present work, the difference between 1λ and ¼λ scatterers by the same analysis may be expected to be not large. Also the dearth of low energy neutrons reduces the accuracy of the measurements, so that smaller differences would go undetected. Aluminum has zero inelastic cross section for lower energies so that the spread in scatterer thickness should not cause large differences in results for this element.

In developing the statistical theory of nuclear reactions the assumption is made that the mode of disintegration of the compound nucleus depends only upon the excitation energy and angular momentum and is independent of the method of formation. This implies that the neutron spectra from (p,n) reactions should not differ appreciably from the energy distributions of neutrons from (n,n) processes, provided the compound nuclei and their excitation energies are the same. Gugelot[13] has determined the variation of nuclear temperature, T, with mass number for a large number of elements by measuring the neutron spectra resulting from (p,n) reactions for 16-Mev protons. Figure 5 is a plot of both his results and those presented here. No attempt has been made to correct for the fact that excitation energies produced by 16-Mev protons are not precisely the same as by 14-Mev neutrons. Gugelot's T values have been adjusted by him for contributions from postulated second neutrons while the present data have not been so treated. It is to be seen, however, that with the exceptions of the low masses, the values of T from the two sets of experiments are in quite good agreement.

According to the statistical theory, the neutron energy distribution $F(E_n)/E_n$ is, to a first approximation, proportional to the level density function $W(E_0-E_n)$ which describes the density of levels in the residual nucleus as a function of excitation energy (E_0-E_n), i.e.,

$$W(E_0-E_n)=F(E_n)/E_n$$
$$=\text{const}\times\exp\{[a(E_0-E_n)]^{\frac{1}{2}}\}. \quad (5)$$

For all of the elements investigated, a plot of

$$\ln[F(E_n)/E_n] \quad vs \quad (E_0-E_n)^{\frac{1}{2}}$$

gives a straight line and hence the value of a in the level density function. An equivalent result is obtained by setting

$$T=(4E_0/a)^{\frac{1}{2}}, \quad (6)$$

where T is defined by Eq. (4). The values of a are given in row VII of Table I. These, with Eq. (5) suffice to determine the relative level densities of the elements investigated for a given excitation energy. The values of a, do not increase smoothly with increasing mass number as would be predicted on the basis of statistical theories.

The concept of the statistical theory that the energy introduced into the nucleus is shared by all the particles is equivalent to a requirement that T be a decreasing function of the atomic weight A. However, T appears to be essentially independent of A. Correction for the effect of $n,2n$ reactions can only raise the values of T for high values of A which is an even greater departure from prediction. It is concluded that the simple sharing of energy by all the particles of the nucleus is not supported by the results of the present experiment.

The authors are indebted to R. W. Davis for work with the 14-Mev neutron source and to Pat Agee, May Bergstresser, and Pearl Norwood for analysis of the plates and for much of the computing work involved in the reduction of the data.

[13] P. C. Gugelot, Phys. Rev. **81**, 51 (1950).

Elastic Scattering of 6.5-Mev Protons from Copper*

L. M. GOLDMAN†
Physics Department, University of Rochester, Rochester, New York
(Received September 29, 1952)

The 6.5-Mev protons from the 27-inch Rochester cyclotron have been used to determine the angular distribution of protons elastically scattered from copper. Significant differences from pure Coulomb scattering were observed. The results have been compared with the predictions of the Feshback-Weisskopf schematic theory and appear to disagree with these.

INTRODUCTION

MANY investigators[1–6] who have examined the angular distribution of energetic protons scattered from atomic nuclei have reported significant differences from pure Coulomb scattering. Since these differences must be attributed to a non-Coulomb interaction between the proton and the atomic nucleus, they are of interest in the study of nuclear forces.

Recently Shapiro[7] has applied the Feshbach-Weisskopf schematic theory[8] to the problem of elastic scattering of charged particles, and in particular he calculated an angular distribution for 7.3-Mev protons on copper. The measurement reported here of the angular distribution of the elastic scattering of 6.5-Mev protons from copper was undertaken as a check on the nuclear model used by Shapiro.

EXPERIMENTAL METHOD

The measurements were made with a 12-inch diameter circular scattering chamber containing a scintillation counter detector. A schematic diagram of the experimental arrangement is shown in Fig. 1. The 6.5-Mev protons from the Rochester cyclotron entered the scattering chamber through a set of three collimating apertures, traversed the target, and when undeflected stopped in the Faraday cup. The scattered particles were detected by the scintillation counter. The counter was supported inside the chamber in a mounting attached to a rotatable stainless steel arm. By rotating this arm from outside the chamber, the position of the counter could be adjusted to any angle from 0 to 160 degrees with respect to the incident beam. Since the axis of rotation of the counter coincided with the intersection of the beam with the target, the solid angle subtended by the detector at the target was the same for all angles of observation. Details of the construction of the chamber can be seen in Fig. 2.

A 1P21 photomultiplier and a NaI(Th) phosphor constituted the detector. The NaI crystal was mounted on a Lucite light pipe and covered with a 0.0002-inch aluminum foil. The clouding effect of water vapor on the surface of the crystals was no great problem as the crystals were in vacuum during the experiments.

Figure 3 is a block diagram of the electronic equipment used. All the instruments were of standard design with the exception of the 30-channel pulse-height analyzer which has been described elsewhere.[9] To insure that all the pulses entering the analyzer were of the same shape. The rise time and clipping time of the Model 500 amplifier were adjusted to 2 μsec and 8 μsec, respectively.

The copper foils bombarded in this research were obtained from the International Chromium Corporation of New Haven, Connecticut. Two different foils were used: one of thickness $(0.95\pm0.02)\times10^{-4}$ inch and the other $(2.07\pm0.03)\times10^{-4}$ inch.

The energy of the incident protons was ascertained from the range of the particles in aluminum. This range was found by observing the attenuation of the beam when successive thicknesses of aluminum foil were placed in front of the Faraday cup. The particles were found to have a mean range of 79.3 ± 1.0 mg/cm^2 of aluminum. This range corresponds to an energy of 6.50 ± 0.10 Mev.

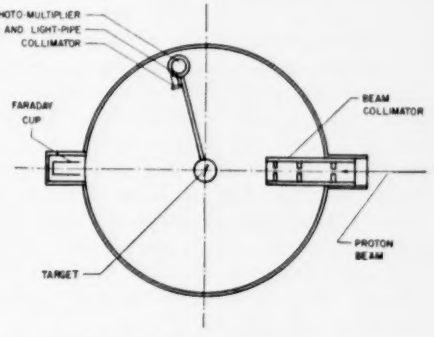

FIG. 1. Experimental arrangement.

* This research supported in part by the AEC.
† Now at Project Matterhorn, Forrestal Research Center, Princeton, New Jersey.
[1] E. G. Dymond, Proc. Roy. Soc. (London) **A157**, 30 (1936).
[2] Kanne, Taschek, and Ragen, Phys. Rev. **58**, 693 (1940).
[3] T. R. Wilkins, Phys. Rev. **60**, 365 (1941).
[4] Heitler, May, and Powell, Proc. Roy. Soc. (London) **A190**, 180 (1947).
[5] Baker, Dodd, and Simmons, Phys. Rev. **85**, 1051 (1952).
[6] J. W. Burkig and B. T. Wright, University of California at Los Angeles Technical Report No. 6 (1951) (unpublished).
[7] M. M. Shapiro, doctoral dissertation, Massachusetts Institute of Technology, 1950 (unpublished).
[8] H. Feshbach and V. Weisskopf, Phys. Rev. **76**, 1550 (1949).
[9] Fulbright, McCarthy, and McCutchen, Phys. Rev. **87**, 184 (1952).

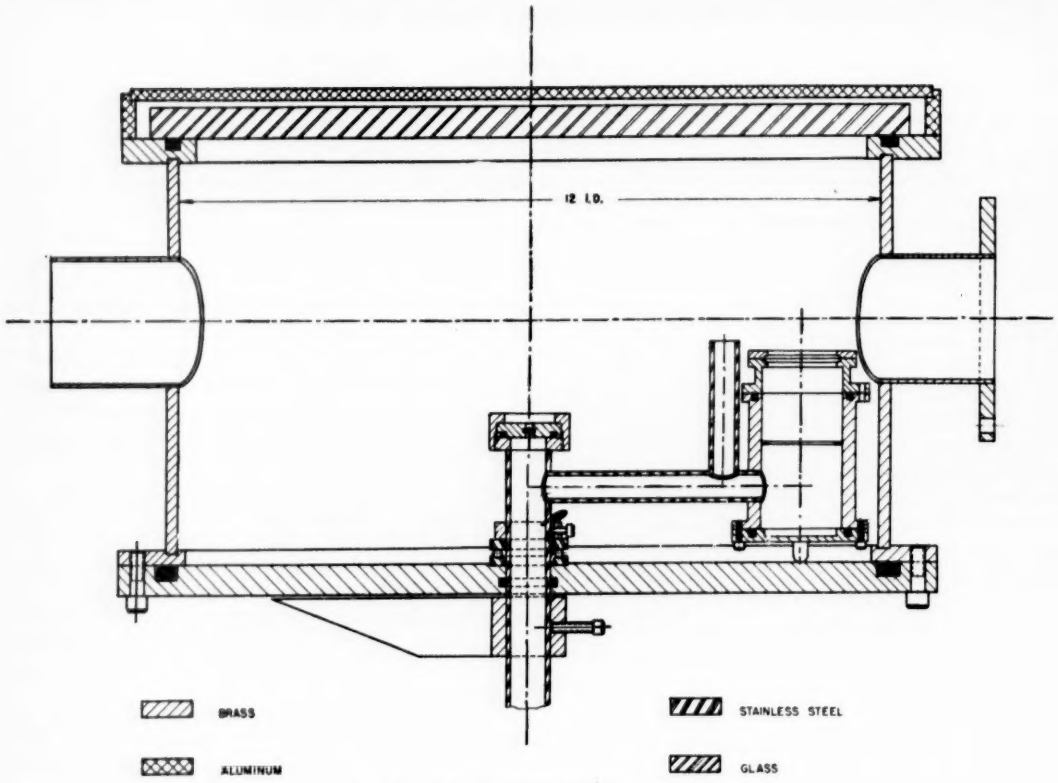

FIG. 2. Side view of the scattering chamber.

In determining the angular distribution of protons elastically scattered from copper, observations were made at 5-degree intervals from 20 to 135 degrees and at 10-degree intervals from 135 to 155 degrees. For each observation the detector angle and the target angle were set, the number of protons collected in the Faraday cup was measured, and the pulse-height spectrum of the detected particles was recorded by the 30-channel analyzer. Each of the pulse distributions showed a distinct peak which was attributed to the elastically scattered protons (see Fig. 4). This assignment was made for three reasons: one, the peak occurred at the same pulse height for the scattering from gold as it did for scattering from copper; two, there was only one peak; and three, the angular distribution that was determined for gold using this peak followed the expected Rutherford distribution to within 5 percent.

Thus the number of protons scattered into the angular region between θ and $\theta+d\theta$ was found by summing all the counts under the θ peak. $d\theta$ was determined by the finite size of the detector and was equal to 0.093° for this case.

EXPERIMENTAL RESULTS

Data from two separate runs were used to determine the angular distribution of the elastic scattering of 6.5-Mev protons from copper. The averaged results of these runs are shown in Fig. 5. The points plotted in Fig. 5 are the ratios of the observed relative differential cross sections to those predicted on the assumption of pure Coulomb scattering. The distribution was normalized by taking the ratio to be equal to 1 at 20 degrees. The error bars on the points are statistical standard deviations. With this normalization, appreciable differences from Rutherford scattering were found over the range between 30 and 150 degrees. The most prominent features of the distribution are the maxima at 45 and 125 degrees and the minimum at 75 degrees.

Different foils were used in the two runs to investigate the possibility of a systematic error due to target geometry. In addition, in one run the target was ad-

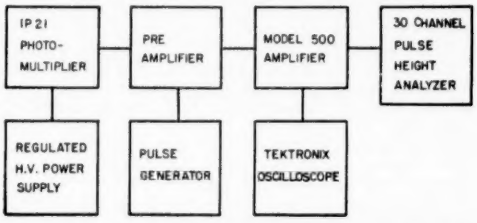

FIG. 3. Block diagram of the electronic apparatus.

justed so that the angle it made with the beam was just half the angle made by the counter, whereas in the second run the target was maintained at 45 degrees for all observations. The consistency of the two runs showed that no error caused by target geometry was detectable.

The accuracy of the whole experimental arrangement was determined by examining the angular distribution of protons elastically scattered by gold. As the Coulomb barrier for gold is more than 5 Mev above the energy of the incident protons, one would expect no nuclear scattering to contribute and therefore a pure Rutherford distribution should be observed. As can be seen in Fig. 6, the observed distribution for gold agrees with a pure Coulomb distribution to within 5 percent. An over-all accuracy of 5 percent is therefore claimed for the relative distribution presented here.

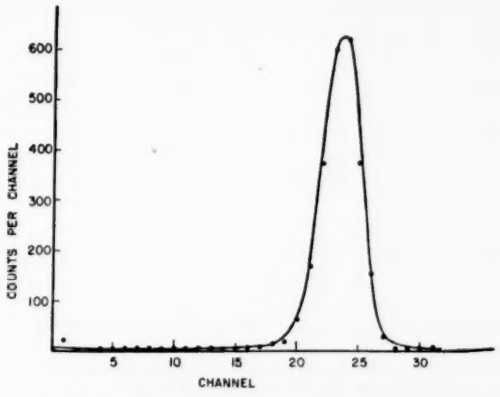

FIG. 4. Pulse-height spectrum observed at 30 degrees with a copper target.

DISCUSSION

The ratio of the differential cross section, including nuclear effects, to the Coulomb differential cross section can be written as

$$\frac{d\sigma}{d\sigma_c}=\frac{1}{\eta^2}\left|\sum_L\left\{(2L+1)\sin^2\frac{\theta}{2}e^{2i(\sigma_L-\sigma_0)}\times[e^{2i\Delta_L}-1]P_L(\cos\theta)+\eta\exp\left[-\left(\eta\sin^2\frac{\theta}{2}-\frac{\pi}{2}\right)\right]\right\}\right|^2, \quad (1)$$

where the only unknown quantities are the nuclear phase shifts Δ_L. The notation is the standard one used by Mott and Massey.[10]

An attempt was made to determine the unknown Δ_L's by fitting the observed distribution with real phase shifts alone. Only the first three phase shifts were considered, as the Coulomb barrier is too high for $L=3$ waves to make any appreciable contributions. The method used was a graphical one suggested to the author by Dr. J. B. French. For this method Eq. (1) was expressed in terms of seven vectors, three of which contain the unknown phase shifts. One therefore looks for a set of Δ_L's such that the sum of the seven vectors is proportional to the observed $\{d\sigma/d\sigma_c\}^{\frac{1}{2}}$ for all angles. It was definitely found that the experimental results could not be described in terms of the real phase shifts alone.

[10] N. F. Mott and H. S. W. Massey, *Theory of Atomic Collisions* (Clarendon Press, Oxford, 1949), second edition.

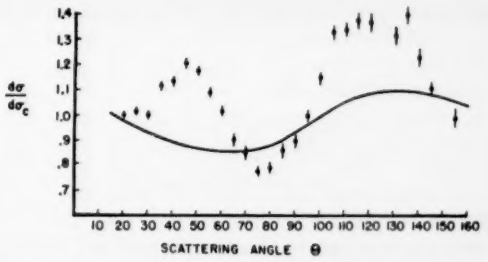

FIG. 5. The angular distribution of the elastic scattering of 6.5-Mev protons from copper. The points represent the relative differential cross section plotted as a ratio to Coulomb scattering. The solid curve is the prediction of the Feshbach-Weisskopf theory for $r_0=1.46$, and $V=20$ Mev.

It was therefore necessary to consider complex phase shifts, implying the presence of nuclear absorption. Nuclear absorption in this case would include all reactions other than elastic scattering.

The schematic theory of Feshbach and Weisskopf which was used by Shapiro to describe this problem assumes nuclear absorption and thus predicts complex phase shifts. This theory describes the interaction of the incident proton and the nucleus in terms of the nuclear radius R and the average effective potential V_0 which the nucleon sees inside the nucleus. The theory assumes that a nucleon entering the nuclear surface will not emerge in the same state in which it entered, i.e., that the target nucleus acts as a "sink" for the incident particles. This assumption determines

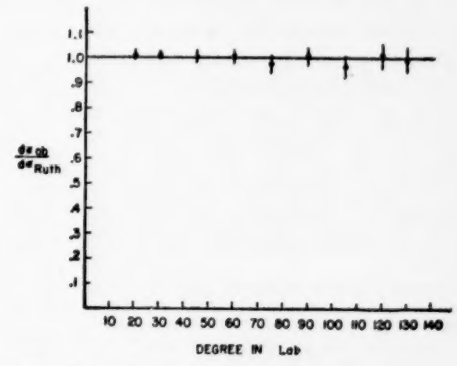

FIG. 6. Angular distribution of elastic scattering of 6.5-Mev protons from gold.

the logarithmic derivative at the nuclear surface and thus the phase shifts. Assuming the radius $R=r_0A^{\frac{1}{3}}$, $r_0=1.48\times10^{-13}$ cm, and $V_0=20$ Mev the phase shifts given by this theory are

$$\Delta0=(-0.367+0.178i),$$
$$\Delta1=(-0.209+0.128i),$$
$$\Delta2=(-0.069+0.062i).$$

By introducting the above values into Eq. (1), a theoretical angular distribution for the elastic scattering of 6.5-Mev protons from copper was determined. This distribution is shown by the solid curve in Fig. 5. The distribution does not differ appreciably from those calculated by Shapiro[7] for 7.35 Mev using the same parameters. Decreasing r_0 to 1.35 or increasing V_0 to 28 Mev does not greatly alter the shape of the distribution.

Comparing the theoretical distribution with the experimental, one finds very little agreement. The maximum at 45 degrees and the rapid decrease in the cross section at large angles which appear in the experimental distribution are not present in the theoretical one. The appearance of a minimum in both curves constitutes the only real agreement.

One may therefore conclude that: (1) definite nuclear effects are present in the elastic scattering of 6.5-Mev protons by copper; (2) the observed distribution cannot be fitted using only real phase shifts, implying that appreciable nuclear absorption takes place; and (3) the Feshbach-Weisskopf theory does not appear to describe adequately the interaction of a 6.5-Mev proton with a copper nucleus.

The author would like to express his indebtedness to Professors H. W. Fulbright and J. B. Platt for their continued interest and valuable advice. He wishes to thank Dr. J. B. French for many enlightening discussions. The complete cooperation and assistance of Dr. D. A. Bromley contributed largely to the conduct of this research.

PHYSICAL REVIEW VOLUME 89, NUMBER 2 JANUARY 15, 1953

Transition Probability for Photoelectric Emission from Semiconductors*

H. B. HUNTINGTON† AND L. APKER
General Electric Research Laboratory, Schenectady, New York

(Received October 6, 1952)

An adaptation of Makinson's theory of photoelectric emission from metals is used to treat simple one- and three-dimensional semiconductor models. The probability of excitation from a state of initial energy ϵ lying near ϵ_0, the top of an occupied band, is found proportional to $\epsilon_0-\epsilon$. Thus, the transition probability vanishes at the top of the band. For a density of states having the normal form, $n\sim(\epsilon_0-\epsilon)^{\frac{1}{2}}$, the energy distribution of the emitted electrons contains a factor $(\epsilon_0-\epsilon)^{\frac{1}{2}}$ and is thus concave upward near the band edge.

For certain simple surfaces, the photoelectric threshold may be high because transitions requiring low energy are forbidden. It is pointed out that this feature is an idealization probably not found for real surfaces having the usual inevitable irregularities. In a qualitative discussion, more realistic cases are mentioned. It is suggested that the results retain the form derived above, although the high threshold energy disappears.

An energy distribution proportional to $(\epsilon_0-\epsilon)^{\frac{1}{2}}$ near the band edge is in good agreement with previous experimental results on Te and other monatomic semiconductors. With the graphical methods of analysis previously applied to data on these materials, the point of view taken above permits more definite location of the edges of occupied bands. Improved estimates of upper limits to the density of occupied surface levels are then possible.

I. INTRODUCTION

RECENT experiments indicate that the external photoelectric effect can give useful information on the electronic energy structure of solids.[1] There is interest in certain monatomic semiconductors and semimetals, for which photoelectric data are available in the form of a product $n(\epsilon)\cdot s(\nu,\epsilon)$. Here the quantity of interest is n, the density of electronic energy states expressed as a function of the energy ϵ; s is a photoelectric excitation probability which may be a function of both ϵ and the frequency ν.[2] In the absence of theoretical information, it has not been possible to isolate n without making questionable assumptions about the form of s. This paper attempts to improve this situation by showing that in certain idealized cases s is proportional to $\epsilon_0-\epsilon$ in the vicinity of ϵ_0, the top of the occupied energy band. These restricted conclusions are then qualitatively extended to more complicated and realistic situations.

There have been many attempts to develop a satisfactory theory of the external photoelectric effect at surfaces of simple metals.[3] A recent and elegant treatment of the problem has been given by Makinson.[4] His

* Presented in part at the Chicago meeting of the American Physical Society, November, 1950 [see Phys. Rev. **81**, 321 (1951)].

† On summer leave (1949) from Rensselaer Polytechnic Institute, Troy, New York.

[1] Apker, Taft, and Dickey, Phys. Rev. **76**, 270 (1949), and foregoing papers.

[2] Apker, Taft, and Dickey, Phys. Rev. **74**, 1462 (1948).

[3] For a review and recent theory, see K. Mitchell, Proc. Roy. Soc. (London) **146**, 442 (1934).

[4] R. E. B. Makinson, Phys. Rev. **75**, 1908 (1949).

approach may be summarized briefly as follows: Free-electron wave functions of the metal are perturbed by light falling on the surface. This interaction gives rise to an excited state described by a wave function consisting of plane waves propagating away from the surface in both directions. Thus, the volume photoelectric effect[3] is excluded. An auxiliary wave function is introduced for mathematical convenience, and simple manipulation yields the amplitude of the excited wave moving away from the metal into the vacuum. The resulting contribution to the photocurrent arising from the electrons that were initially in an infinitesimal region of momentum space $d\mathbf{k}$ is

$$dJ \propto E(\mathbf{k}, \nu)D(r)d\mathbf{k}. \tag{1}$$

Here E is an excitation probability involving the initial and auxiliary wave functions, the x component of the vector potential (the x direction is the surface normal), and the wavelength of the excited wave in the metal. D is the transmission coefficient of the surface barrier for the photoelectrons in question, which have a wavelength $2\pi/r$ in the vacuum. One of the most valuable features of Makinson's work is the separability of E and D in a general way. For real surfaces, it is practically always conceded that $D=1$ when escape is energetically possible.[5]

After some modification, this theory for metals may be applied to simple models of semiconductors. The free-electron wave functions must be replaced by functions appropriate to the periodic potential in the emitter. This will be done here for initial states. The effect of the periodic field on the excited electrons is considered briefly in the subsequent paper.

The optical properties of nonmetals are more complex than those of simple metals, since the light wave is affected in a different way in the important region near the surface. For the free-electron model used by Makinson,[6] it was possible to assume that the action of the incident light involved no appreciable absorption by the electron system. More complicated effects may occur in nonmetals and some real metals since absorption is important in the spectral regions involved.[7] Detailed consideration of optical phenomena must depend, then, on the particular substance investigated. The present paper attacks an aspect of the emission problem which, we believe, is not influenced in character by these details. The following crude point of view is, therefore, adopted: The dielectric constant is assumed to change abruptly at the surface to a positive value, and the three components of the electric vector are assumed to behave as in Makinson's work.[8] The absolute magnitude of the result will not be significant. However, the dependence of the excitation probability on initial energy should not be greatly affected.

[5] C. Herring and M. H. Nichols, Revs. Modern Phys. **21**, 245 (1949).

[6] R. E. B. Makinson, Proc. Roy. Soc. (London) **162**, 367 (1937).

[7] See, for example, W. H. Brattain and H. B. Briggs, Phys. Rev. **75**, 1705 (1949), for data on Ge.

[8] R. F. Miller, J. Opt. Soc. Am. **10**, 621 (1925) has shown that the real part of the dielectric constant is of the order of $+3$ at the pertiment frequency in Te, a material of interest here.

II. AN EXAMPLE IN ONE DIMENSION

For purposes of illustration, we first consider the behavior of electrons at the surface of an idealized one-dimensional crystal.[9] In the region $x<0$, we assume a periodic potential with an average value that is negative. Taking the surface at $x=0$, we set the constant potential in the region $x>0$ equal to zero. In the periodic field, we choose two superposed Bloch running wave functions in the form

$$\varphi_k(x)=u_k(x)\exp(-ikx)+Au_k^*(x)\exp(+ikx), \quad x<0, \tag{2}$$

to describe electrons of negative total energy. At $x=0$, this must be matched to the function

$$\varphi_k(x)=B\exp(-px), \quad x>0. \tag{3}$$

We find

$$A=c(-p+ik-d)/(p+ik+d^*), \tag{4}$$

$$B=u_k(0)(+2ik-d+d^*)/(p+d^*+ik), \tag{5}$$

where

$$c=u_k(0)/u_k^*(0), \quad d=u_k'(0)/u_k(0).$$

When the potential inside the crystal is constant, u_k is constant, $c=1$, and $d=0$. In this case, we have the familiar Sommerfeld model of a metal. Equations (4) and (5) then express two well-known results: (1) the standing plane waves describing the free electrons inside the metal have very closely a node at $x=0$ when k is small; (2) the coefficient B which measured the amplitude of the wave function in the vicinity of the surface is proportional to k.

Mitchell[3] and Makinson[4] have shown that this same proportionality to k appears in the matrix element M for photoelectric emission from the state k in a Sommerfeld metal. Thus, in Eq. (1) Makinson's excitation function E becomes proportional to $M^2 \propto k^2$, which is proportional in turn to the kinetic energy of the metallic electrons in question; hence E vanishes linearly with kinetic energy at the bottom of the Fermi band. (The k vector of the light wave is neglected as small in this treatment.)

Except in one instance, a similar argument may be applied to the more complex case of electrons in a potential that is periodic rather than constant. We consider electrons near the top of an occupied band in a semiconductor. We take k to be the wave number vector of the "hole" (or of the envelope of the Bloch wave function). It can be shown by perturbation methods[10] that in this case

$$u_k(x)=u_0(x)+ikv(x), \tag{6}$$

[9] We are indebted to Professor H. Bethe for generalizing this argument.

[10] F. Seitz, *The Modern Theory of Solids* (McGraw-Hill Book Company, Inc., New York, 1940), p. 352; J. Bardeen, J. Chem. Phys. **6**, 367 (1938).

where $u_0(x)$ is the wave function for the state at the top of the band. The question arises as to how far into the band the perturbation treatment is valid. For one case, at least,[11] it appears to have a sufficiently wide range of validity to be of interest here.

We may apply (6) in (5) and find that B is proportional to k except for one rare case. This occurs when the surface is so located that

$$-2p=d^*+d=2u_0'(0)/u_0(0),$$

where terms of order k^2 are neglected in the last expression. Then $A=c$ and $B=2u_k(0)$, which is not proportional to k. At the surface, a resonance occurs between the modulational (short wavelength) part of the interior wave function and the damped exterior wave. A node in the envelope of the Bloch function is no longer required in the neighborhood of the surface. Because of the highly special surface condition required to produce this phenomenon, we shall look upon it as an artificiality and shall not consider it further here.

Except for the rare case above, then, the amplitude of the wave function at the surface of our periodic one-dimensional crystal behaves in the same way as that at the surface of a Sommerfeld free-electron metal. In place of the wave vector of the free electron in the metal, we substitute the wave vector k of the "hole" corresponding to the state in question near the top of the occupied zone in the periodic structure. We find that the amplitude of the damped part of the wave function outside the crystal surface (as measured by the constant B) is proportional to k.[12]

We may now apply Makinson's technique in an approximate way and calculate the transition probability for photoelectric emission from this one-dimensional system. For simplicity, we neglect the effect of the periodic field on the wave functions of the excited states and treat these electrons as practically free inside the crystal. Thus, we may use excited wave functions θ_k and auxiliary functions χ_r identical with Makinson's [see Eqs. (4) and (5), reference 4]. The part of the integral in Makinson's Eq. (6) which lies outside the metal involves the damped wave function. It is, therefore, proportion to B and so to k. Inside the metal, the wave function can be written

$$\varphi_k=[(1+A)\cos kx-i(1-A)\sin kx]u_0(x)+[(1+A)\sin kx+i(1-A)\cos kx]kv(x). \quad (7)$$

When integrated with a traveling wave, which is slightly damped as it goes into the metal, $\sin kx\cdot u_0(x)$ gives a contribution proportional to k. From Eq. (4) it can be seen that $(1+A)$ varies as k. It follows, therefore, that the part of the matrix integral arising from the region inside the metal is also proportional to k. Hence, the excitation function E in Makinson's Eq. (8) is proportional to k^2.

On the basis of this application of Makinson's methods, we conclude that the transition probability for photoelectric emission from a state near the top of an occupied zone in our one-dimensional crystal is proportional to the energy of the hole formed by the transition. In the symbols used here (and in reference 2), the probability is proportional to $\epsilon_0-\epsilon$, where ϵ_0 is the energy at the top of the band and ϵ is the energy of the state in question.[13]

III. THREE-DIMENSIONAL CASES

Consideration of real semiconductors involves problems that are necessarily three-dimensional. (In the foregoing section, any mention of the density of states would have been pointless because momenta parallel to the surface were either excluded or treated like those of free electrons.) Though the variety of possible situations is large and the detailed analysis is complex, it is possible to show that the character of the result in Sec. II is preserved in passing from the one- to the three-dimensional crystal.

The surface of the semiconductor is taken to be the plane $x=0$. Inside the crystal the wave function has the form

$$\phi_k(\mathbf{r})=\exp[-i(k_x x+\mathbf{k}_\rho\cdot\boldsymbol{\varrho})]u_k(+,\mathbf{r})+A\exp[i(k_x x-\mathbf{k}_\rho\cdot\boldsymbol{\varrho})]u_k(-,\mathbf{r})+S(\mathbf{r}), \quad (8)$$

where $\boldsymbol{\varrho}$ is the component of $\mathbf{r}$ parallel to the surface plane, i.e., $\rho=(y^2+z^2)^{\frac{1}{2}}$. The quantities $\mathbf{k}_\rho$ and k_x are the components of the wave number vector of the hole respectively parallel and perpendicular to the surface. The three-dimensional analog of Eq. (6) is

$$u_k(\pm,\mathbf{r})=u_0(\mathbf{r})+i\mathbf{k}(\pm)\cdot\mathbf{v}(\mathbf{r}), \quad (9)$$

where $\mathbf{k}(\pm)=\mathbf{k}_\rho\pm k_x$, and is valid for a limited range at the top of the band.

In Eq. (8), the last term, $S(\mathbf{r})$ is a surface-type function possessing the periodicity of the surface but falling off rapidly toward the interior of the semiconductor. The introduction of this function is important to fit boundary conditions. It can be expanded as a series of functions all corresponding to the same energy as the wave function in the volume:

$$S(\mathbf{r})=\sum_m S_m(x)\exp[-i(\mathbf{k}_\rho+\mathbf{K}_\rho+\mathbf{K}_m)\cdot\boldsymbol{\varrho}]. \quad (10)$$

Here $\mathbf{K}_\rho$ refers to the ρ-components of the free-electron $\mathbf{k}$ for the state at the top of the band. The $\mathbf{K}_m$ are the translation vectors of the two-dimensional space reciprocal to the semiconductor surface. The $S_m(x)$ decrease rapidly as a function of x going into the solid.

[11] P. M. Morse, Phys. Rev. **35**, 1310 (1930). This point is most clearly displayed in Morse's Fig. 5, which shows the Fourier coefficients for the functions that we symbolize here by u. At the top of the lowest zone, a relation like (6) holds over the range in which the quantities b_0, b_{-1}, involving Morse's first two Fourier coefficients, are linear in k.

[12] A proportionality of this type for "almost-free" electrons in a one-dimensional periodic structure was first proposed, to our knowledge, in unpublished work by H. Brooks.

[13] This result differs from that assumed by V. Weisskopf and L. Apker, Phys. Rev. **60**, 170 (1941) and from that tacitly assumed by E. U. Condon, Phys. Rev. **54**, 1089 (1938).

Outside the metal, the wave function has the form

$$\phi(\mathbf{r})=\sum_n s_n \exp[-p_n x - i(\mathbf{K}_p+\mathbf{K}_n)\cdot\boldsymbol{\rho}], \quad (11)$$

where the $\mathbf{K}_m$ are the same set of vectors as the $\mathbf{K}_m$. The s_n and the p_n are constants.

One method for determining a finite number of the constants S_m and s_n would be to satisfy boundary conditions for a continuous wave function and a continuous normal derivative at a finite number of points on the surface. In general, a straightforward procedure would be to work with a number of inhomogeneous, linear equations equal to the number of unknown quantities. One could obtain a solution for A, the s_n, and the S_m. However, it is more illuminating for our purpose to consider $(1+A)$ as an unknown and to solve our equations in terms of $(1-A)$. From the form of Eqs. (7) and (9), it is apparent that wherever $(1-A)$ appears it will be multiplied by k_x. It therefore follows in our solution that $(1+A)$, the s_n and the S_m will all be proportional to k_x, if our set of linear equations is linearly independent. The possibility of linear dependence has been noted already in our one-dimensional example. There this contingency appeared as a resonance effect, when a particular relationship between the wave functions inside and outside the surface was satisfied. Except when this occurs, the important amplitudes in the wave function are proportional to k_x in three dimensions as well as in one.

In passing, we note the following fundamental difference between this situation and that for a simple metal. An electron occupying an energy state inside a Sommerfeld metal has a definite momentum parallel to the surface. It appears externally as a photoelectron with this same momentum, since there is no binding in the surface plane. Simple wave functions describe the electron adequately on both sides of the surface and and match at the interface. On the other hand, an electron in a three-dimensional crystal does not have a definite momentum parallel to the surface. Rather, it possesses a distribution of momenta (all leading to the same reduced momentum) determined by the crystal potential. The individual terms in the initial wave function outside the surface [see Eq. (11)], however, are associated with respectively distinct momenta, and each has a different damping constant perpendicular to the surface. A series of these simple functions must be used to match the internal wave function. Likewise, for the excited functions, for each traveling wave representing a freed photoelectron a series of functions inside the metal are needed for boundary fitting. All these functions will have the same reduced momentum parallel to the surface.

One of us has extended Makinson's treatment to the case of the periodic potential[14] in three dimensions by using the expressions for the unexcited wave function ϕ_k [see Eqs. (8)–(11), inclusive], the excited wave function θ_k, and the auxiliary wave function χ_r appropriate to the periodic field.

On the basis of this work, we have come to the following conclusions:

(1) The matrix element M is proportional to k_z, and the transition probability is proportional to k_z^2 as in the one-dimensional case.

(2) For certain simple surfaces, important transitions may be forbidden. As an example, we may consider the (100) surface of a simple cubic crystal. The lowest Brillouin zone for such a structure is a cube in free-electron k space with sides at k_x, k_y, $k_z=K/2$, where $2\pi/K=a$, the lattice constant. The states of highest energy in this zone lie at the corners of the cube. Thus, $k_y\cong k_z\cong K/2$. Now the periodicity of the simple (100) surface is such that the crystal may absorb only momenta $s\hbar K$ in the y and z directions, where s has integral values. Thus, transitions from initial states near the band edge to final states having zero or very small momentum parallel to the surface are not permitted, since a momentum transfer of the type $\hbar K/2$ would be required. In the extension of Makinson's Eq. (5a) to three dimensions, the integrations over y and z automatically impose these restrictions.

Hence, the photoelectrons must emerge from the surface with y and z momentum components at least as large as $\hbar K/2$ and with a corresponding amount of kinetic energy. This means that the photoelectric threshold energy will be greatly increased, because this kinetic energy might otherwise be available in the x direction to overcome the surface barrier. This situation is, thus, quite different from that involving a simple metal, in which all of the initial energy may be used to overcome the surface barrier and for which photoelectrons consequently emerge with zero kinetic energy when ejected by quanta having the threshold energy.

These restrictions on the momentum parallel to the surface depend on the presence of a highly regular and especially simple surface structure. They probably would not appear in practice, therefore, since real surfaces do not possess such perfect configurations. Thus, a slight deviation from a (100) surface orientation immediately introduces periodicity on a much larger scale. This permits the absorption by the crystal of smaller quantities of momentum. A final state with y and z momenta very close to zero may, thereby, be permitted. Obviously, the probability of this kind of process may vary widely for different types of surfaces.

If the momentum restrictions described above for a simple surface should actually exist, they would be simple to detect experimentally, since only photoelectrons with kinetic energies of several electron volts would be emitted. Thus, a concentric-sphere phototube would show saturated currents even with large retarding fields. This would be difficult to overlook. It is not surprising, however, that it has not been observed. Apart from the ideal surfaces and special zone struc-

[14] See the following article for details of this treatment, H. B. Huntington, Phys. Rev. **89**, 357 (1952).

tures required, other influences such as electron interactions could mask the effect. We note further that forbidden transitions do not arise when the state of highest energy lies at the center of the zone (in a reduced-zone scheme).

To obtain the excitation probability $s(\nu, \epsilon)$ mentioned in the introduction,[2] we must integrate the transition probability in k space over the shell of constant energy ϵ. In the case of our simple cubic crystal, for instance, this shell is composed of small spherical octants centered at the corners of the cubical zone.[15] After excitation, the electrons in the crystal occupy relatively small portions of a much larger spherical shell centered at the origin in free-electron k space. (At this point, we neglect the zone structure in the case of these higher energies.) A fraction of these excited electrons can emerge as photoelectrons. If we consider values of $h\nu$ appreciably larger than the threshold energy $h\nu_0$ required for emission from the state ϵ_0 at the top of the band, the value of this emergent fraction will be a slowly varying function of ϵ near ϵ_0. (It will drop to zero when $\epsilon_0-\epsilon=h(\nu-\nu_0)$.)

Thus, the energy distribution of the photoelectrons from initial states near the band edge is dominated by only two rapidly varying factors. One is the density of states, which goes to zero like $(\epsilon_0-\epsilon)^{\frac{1}{2}}$. The other is the excitation probability $s(\nu, \epsilon)$ which is proportional to $\epsilon_0-\epsilon$. We conclude that the energy distribution goes to zero like $(\epsilon_0-\epsilon)^{\frac{1}{2}}$.

In the graphical method of analysis used in reference 2, this result leads to a value $\frac{3}{2}$ for the parameter m.[16]

IV. DISCUSSION OF THE RESULT

In this paper we have used a highly simplified approach to a very complex problem. We have neglected the detailed behavior of optical phenomena and the effect of zone structure on excited states, in the belief that the character of the result would in general not be affected. From this viewpoint, we shall proceed at once to direct comparison with experiment.

The result obtained here is in good agreement with available data on Te, since it arrives theoretically at the $\frac{3}{2}$ power dependence on energy shown by the function $N/E\sim n(\epsilon)s(\nu, \epsilon)$ for this element.[2] (The same dependence is shown by the high energy portion of the energy distribution N.)

There is a further possibility that the very small tail found on the energy distributions for Te is due to thermal lattice vibrations[17] (see Figs. 4 and 5, reference 2). If such be the case, we have interpretations of all the effects observed for Te. This requires that the upper limit estimated for the density of surface levels on Te in reference 2 be revised downward by an order of magnitude. There is no need to postulate superposed energy distributions from patches with different Fermi levels. This was done, in the previous work, for the case in which the transition probability was tentatively assumed to be independent of energy. The patch phenomenon or surface levels might still be of some importance for Ge and B. For these materials, the experimental results were less clear-cut than for Te. The energy distributions were roughly parabolic in form at higher energies. From the present point of view, however, these other effects need only explain the difference between the exponents 2 and $\frac{3}{2}$ instead of that between 2 and $\frac{1}{2}$ as formerly. Thus, the high estimated surface-state densities associated in reference 2 with exponents m smaller than $\frac{3}{2}$ are not required.

Finally, we note that the data on the function N/E for As, Sb, and Bi[1] can be interpreted more satisfactorily as overlapping $\frac{3}{2}$ power characteristics than as $\frac{1}{2}$ power characteristics. The behavior shown by each of these elements arises because the occupied band overlaps the conduction band. If the band edges have the normal form, one expects the density $n(\epsilon)$ of occupied states to show a sharp minimum slightly below the top of the occupied region and near the lower edge of the conduction band. The photoelectric data on the product $n(\epsilon)\cdot s(\nu, \epsilon)\sim N/E$ did not show such a behavior, although a plateau was observed in the case of Sb. If the transition probability s has the form suggested in this paper, the product sn for a semimetal is composed of two $\frac{3}{2}$ power characteristics. These overlap and produce a composite characteristic without a sharp minimum. This interpretation is in better agreement with the observations than is the assumption of a transition probability independent of energy.

We are indebted to Dr. R. E. B. Makinson for the privilege of reading his recent paper before publication and for supplying a copy of the thesis on which it was based. We wish to thank Professor H. Bethe for valuable discussions, particularly of the material given in Sec. III. We are grateful to Dr. Harvey Brooks for his unflagging interest and critical comments, and to Dr. Malcolm Hebb for many illuminating conversations.

[15] As pointed out by W. Shockley, Phys. Rev. **78**, 177 (1950), equal-energy surfaces need not be spherical in general.

[16] An assumption made in using this method was that an excited electron had a probability of escape which varied linearly with the kinetic energy E of the external photoelectron. This is a reasonable first approximation when the excited electrons are uniformly distributed over a spherical shell in free-electron k space. If the shell is only partially occupied, as in the present case, the escape probability may exhibit structure. Then higher powers of E may become more important. This, however, does not affect the conclusions of this paper.

[17] W. Shockley and J. Bardeen, Phys. Rev. **77**, 407 (1950).

Extension of Makinson's Theory of Photoelectric Emission to a Periodic Potential

H. B. HUNTINGTON
Physics Department, Rensselaer Polytechnic Institute, Troy, New York
(Received October 6, 1952)

The results of Makinson's treatment of the transition probability for photoelectric emission for a free-electron model has been extended to Bloch wave functions in a periodic field. The particular application of these results to the case of electrons at the top of a filled band has been developed, thereby filling in some of the details of the preceding paper.

MAKINSON[1] has shown that for a free-electron metal the probability for photoelectric emission for the kth electron is given by the product of D the transmission coefficient of the surface barrier for the excited electron, and $E(\mathbf{k}, \nu)$ which plays the role of an excitation function and determines the probability that the kth electron absorbs a photon of frequency ν. This function is proportional to the square of the component of the incident light normal to the surface and to the square of a particular integral which is linear in the wave function of the unexcited electron. This integral $N(\mathbf{k}, \nu)$ is given according to Makinson's notation by

$$N(\mathbf{k}, \nu)=\int_{-\infty}^{\infty}(\chi_r\phi_k'-\chi_r'\phi_k)/\{\epsilon_1+i\epsilon_2\}dx, \quad (1)$$

where ϕ_k is the wave function for the unexcited electron, χ_r is an auxiliary wave function with an energy corresponding to that of the electron after a photon of frequency ν has been absorbed, and ϵ_1 and ϵ_2 are the real and imaginary parts of the dielectric constant. The direction of x is taken to be perpendicular to the surface ($x=0$) of the metal.

Though Makinson's original treatment was limited to a free-electron model, this limitation is not an essential one. The purpose of the present paper is to apply the development to the corresponding wave functions appropriate to the problem of photoelectric absorption at the surface of an insulator or semiconductor. In such physical situations, the periodicity of the potential inside the solids cannot be ignored and the wave function cannot be represented simply by plane waves. The more generalized functions necessary here can be expressed in terms of a double Fourier series in the primitive translational vectors of the surface whose coefficients are functions of x. All functions used in calculating the excitation function for a particular electron have the same properties with respect to the surface translations.

For the wave function of the unexcited electron, one uses expressions equivalent to those in Eqs. (8), (10), and (11) of the preceding article.[2] Inside the crystal one has

$$\phi_k(\mathbf{r})=\exp(i\mathbf{k}_\rho\cdot\boldsymbol{\rho})\sum_m\exp(-i\mathbf{K}_m\cdot\boldsymbol{\rho}) \times[\sum_n(A_{nm}\exp\{-i(L_n+k_x)x\} +A_{nm}^*\exp\{i(L_n+k_x)x\})+S_m(x)]. \quad (2)$$

Nere x measures distance perpendicular to the surface and $\boldsymbol{\rho}$ is a vector lying in the plane of the surface. The symmetry of the wave function with respect to the surface translations is determined by $\mathbf{k}_\rho$. The translation vectors of the lattice reciprocal to the surface net are represented by the K_m, and the L_n are $2\pi n$ divided by d, the shortest unit translation perpendicular to the surface. The functions $S_m(x)$ falls rapidly to zero for $x\rightarrow-\infty$ going from the surface into the solid. These functions are required to fit the surface boundary conditions, whereas the A_{nm} are determined by solving the Schrödinger equation for the interior of the solid. Outside the solid for $x>0$ one has, assuming a uniform potential,

$$\phi_k(\mathbf{r})=\exp(-i\mathbf{k}_\rho\cdot\boldsymbol{\rho})\sum_m s_m\exp(-p_mx-i\mathbf{K}_m\cdot\boldsymbol{\rho}), \quad (3)$$

where the p_m and s_m are constants.

Similar expressions for the wave functions of the excited electron can be constructed. Inside the solid, one has

$$\theta_k(\mathbf{r})=\exp(-i\mathbf{k}_\rho\cdot\boldsymbol{\rho}) \times\sum_m\exp(-i\mathbf{K}_m\cdot\boldsymbol{\rho})[C_m(x)+T_m(x)], \quad (4)$$

where the T_m decrease rapidly going into the crystal and the C_m each represent one or more plane waves of the type $\exp(iqx)$ modulated by a function periodic in d. For a free-electron metal, the value for q was determined uniquely to be $[k_x^2+(8\pi^2m/h^2)\nu]^{\frac{1}{2}}$; but for the more general case under consideration, multiple values of q (even for the same m) may exist which satisfy the conditions for conservation of energy and momentum parallel to the surface. Whether or not such complications occur depends on the complexity of the Brillouin zone structure. Multiple values of q will be most probable for multiple-leaved surfaces in the same energy range. Outside the crystal one has

$$\theta_k(\mathbf{r})=\exp(-i\mathbf{k}_\rho\cdot\boldsymbol{\rho})[\sum_m B_m\exp i(r_mx-\mathbf{K}_m\cdot\boldsymbol{\rho}) +\sum_m' t_m\exp(-r_m'x-i\mathbf{K}_m\cdot\boldsymbol{\rho})]. \quad (5)$$

The unprimed summation includes only those values of surface momentum which leave enough normal energy

[1] R. E. B. Makinson, Phys. Rev. **75**, 1908 (1949).
[2] H. B. Huntington and L. Apker, Phys. Rev. **89**, 352 (1952).

for the electron to escape. The primed summation includes the remaining (larger) values of $\mathbf{K}_\rho$.

The construction of the auxiliary function depends upon the purpose for which it is to be used. To calculate the probability that the electron will escape with particular momentum parallel to the surface $(\mathbf{k}_\rho+\mathbf{K}_1)\hbar$, one takes for inside the solid

$$\chi_r(\mathbf{r})=\exp\{i(\mathbf{k}_\rho+\mathbf{K}_1)\cdot\boldsymbol{\rho}\}\times[\textstyle\sum_i \exp(-iq_ix)u_i(\mathbf{r})+V(\mathbf{r})], \quad (6)$$

and for outside the solid

$$\chi_r(\mathbf{r})=\exp\{i(\mathbf{k}_\rho+\mathbf{K}_1)\cdot\boldsymbol{\rho}\}[G_1e^{ir_1x}+H_1e^{-ir_1x}+v(\mathbf{r})]. \quad (7)$$

The summation over i takes care of possible multiple values of q. $V(\mathbf{r})$ has the periodicity of the surface and falls off rapidly toward the interior. The u_i have the periodicity of the lattice and are individually normalized so that the integral of the amplitude squared over the solid gives unity. The function v has the periodicity of the surface and dies off rapidly at large distances from the crystal. The quantity r measures the normal momentum of the escaping electron and can be found from the relation

$$(\hbar^2/2m)[(k_\rho+K_1)_2+r_1^2-k_\rho^2-k_z^2]=h\nu-\epsilon_0, \quad (8)$$

where ϵ_0 is the energy difference from the bottom of the filled band to the vacuum level and the energy level of the kth electron is approximated by the free-electron formula.

According to Makinson's Eq. (4), the relation between ϕ and θ can be expressed as

$$\nabla^2\theta_k+\{r^2+(k_\rho+K_1)^2-(8\pi^2m/h^2)U_k(\mathbf{r})\}\theta_k = -(4\pi ie/ch)\{a_x\phi_k'+i\phi_k(a_yk_2+a_zk_3)+\tfrac{1}{2}\phi_ka_x'\}. \quad (9)$$

$U_k(\mathbf{r})$ is the periodic potential of the lattice as referred to the vacuum level. The a_x, a_y, and a_z are the components of a vector field equal to the amplitude of the time-varying vector potential of the incident light. One multiplies Eq. (9) through by χ_r and integrates over x, y, and z using an extinction factor $e^{\Delta x}$ inside the solid, where Δ is positive. Two applications of Green's theorem to the left side of Eq. (9) so modified reduces it to the sum of a volume integral, which vanishes by virtue of the fact that χ_r is a solution of the Schrödinger equation for the excited electron, and a surface integral over the boundary of our space. The part of the surface integral over the x–y and x–z planes vanishes if one employs the usual periodicity requirements as boundary conditions for $\exp(-i\mathbf{k}_\rho\cdot\boldsymbol{\rho})$. At the surface $x=-\infty$, the integral vanishes because of the extinction factor. At $x=+\infty$, one is left with only $2ir_1B_1H_1$ per unit area from the surface integral. For the volume integral on the right, the terms involving a_y and a_z give a negligible contribution, and a_x is inversely proportional to $\epsilon_1(x)+i\epsilon_2(x)$, where we have assumed that the dielectric constant is independent of y and z. The integrations over y and z can now be carried out making use of the orthogonality of factors containing different $\mathbf{K}_\rho$. The remaining integration over x becomes (after integration by parts) proportional to a modified form of Eq. (1):

$$\int_{-\infty}^{\infty}\textstyle\sum_m(\chi_{rm}\phi_{km}'-\phi_{km}\chi_{rm}')/[\epsilon_1(x)+i\epsilon_2(x)]dx. \quad (10)$$

Outside the solid, there is only one term in the summation over m, ϕ_{k1} is $s_1\exp(-p_1x)$, and χ_{r1} is the square bracket term in Eq. (7). Inside the solid, the θ_{km} are the square bracket terms in Eq. (2) and the χ_{rm} are the mth Fourier components of the expressions in square brackets in Eq. (6).

For the case where there is only one q_i, Makinson's results obtain practically unmodified [$(M(\mathbf{k},\nu)$ is represented by Eq. (10) rather than (1)]. With multiple values for q, the transmission coefficient of the barrier is no longer simply defined. One can extend the Makinson formalism to these cases by introducing a $\bar{D}$, defined as the average transmission coefficient for equal flux into each of the f states with different q, and an average value for q namely $\bar{q}$. As a result the quantity D/q which appears in Makinson's (7a) is replaced by $f\bar{D}/\bar{q}$. Since it is customary to treat electrons excited to the conduction band as essentially free, the case of multiple q's is probably physically unimportant.

From the standpoint of physical interest also, attention should be centered on transitions for minimum $(\mathbf{k}_\rho+\mathbf{K}_m)$, since there is no experimental evidence of electrons coming off with large components of momentum parallel to the surface.

Our main concern in extending the Makinson treatment to Bloch-type wave functions is to apply it to the electrons at the top of a filled band. The preceding paper[2] was given to the consideration of this problem and it is convenient to use its expressions for ϕ_k as given in Eqs. (8), (10), and (11) of reference 2. The most significant change is that there $\mathbf{k}$ refers to the wave number vector of the hole rather than of the electron as in Eqs. (2) and (3) of this paper. For states near a zone boundary, the additional relation given by Eq. (9) of reference 2 also holds approximately. It has been shown that for small k_z the s_m, the S_m and $(1-A)$ are proportional to k_z (unless an accidental resonance exists). Consequently every part of ϕ_k is either directly proportional to k_z or contains a factor $(1-A)\sin(k_zx)$. Those with the $\sin(k_zx)$ factor give contributions proportional to k_z after the integration over $x<0$ in (10) has been carried out. It follows that $M(\mathbf{k},v)$ will be proportional to k_z, and the transition probability for photoelectric emission from the top of the band is proportional to k_z^2. Consequently, the transition probability averaged over an equi-energy contour in k space is proportional to the hole energy, and the contribution to the photocurrent from states in an infinitesimal shell at such a contour will be proportional to the $\frac{3}{2}$ power of the hole energy. This result holds for elliptical as well as spherical energy contours.

It is a pleasure to acknowledge the author's indebtedness to Dr. L. Apker for many valuable suggestions and stimulating conversations on the subject of this paper.

PHYSICAL REVIEW VOLUME 89, NUMBER 2 JANUARY 15, 1953

Electron Capture by Protons Passing through Hydrogen

J. DAVID JACKSON AND HARRY SCHIFF
McGill University, Montreal, Quebec, Canada
(Received September 29, 1952)

A theoretical calculation is made of the capture of an electron by a particle of charge $Z'e$ passing a hydrogen-like atom of charge Ze. Numerical results are presented for protons passing through hydrogen gas. In contrast to earlier treatments of this problem, the complete interaction Hamiltonian is retained as the perturbation causing the electron transfer. Previous workers assumed that the interaction between the incident particle and the electron was the only perturbation causing the transition and ignored the interaction between the incident particle and the nucleus of the atom. Such a neglect is unjustified. The results of this paper show that when the complete interaction is used the agreement between theory and experiment is good for all energies greater than 25 kev ($hv/e^2 \geq 1$) in the case of protons in hydrogen, even though the Born approximation is employed. This is a marked improvement over previous calculations which were approximately four to five times larger than experiment.

1. INTRODUCTION

THE capture of electrons by ions traversing matter has been extensively studied in the laboratory.[1] Theoretical work on the capture problem has been done by Oppenheimer,[2] Brinkman and Kramers,[3] and Massey and Smith,[4] while a survey of capture and loss phenomena with estimates for various cross sections has been given by Bohr.[5] Recently, precise experiments on the capture of electrons by protons in hydrogen gas have been performed by Keene,[6] Ribe,[7] and Whittier.[8] As a result, the capture cross section is known with good accuracy in the energy range from 2 to 150 kev.

BK,[3] with whose work we shall be most concerned in this paper, evaluated the Born approximation cross section for the capture of an electron by a particle of charge $Z'e$ passing a hydrogen-like atom of charge Ze. When applied to protons in hydrogen, their formula gives values for the cross section which are approximately four times the experimental results at 100 kev and still higher at lower energies (see Fig. 4). The discrepancy between BK's result and experiment has been largely attributed to the failure of the Born approximation in the energy range of the experiments. While it is true that e^2/hv equals unity at 25 kev and has only dropped to 0.41 at 150 kev, it will be shown in this paper that there is a much more important source for the discrepancy than the failure of the Born approximation. The perturbation Hamiltonian consists of two terms, the Coulomb interaction between the electron and the incident particle of charge $Z'e$, and the Coulomb interaction between the nucleus of charge Ze and the incident particle. Following Oppenheimer, BK considered only the (electron)-(incident particle) interaction, neglecting the (nucleus)-(incident particle) term. Such a neglect is well known, and completely justified, in inelastic collision problems. However, as is pointed out by Bohr,[9] the capture collision is a three-body problem, whereas ionization and excitation collisions are essentially two-body problems. Consequently, the neglect of the (nucleus)-(incident particle) interaction is unjustified.* Indeed, when it is taken into account, agreement between theory and experiment for protons in hydrogen is good for all energies above 25 kev ($hv/e^2 \geq 1$), even though the Born approximation is still used (see Fig. 4). For energies less than 25 kev it is evident that the Born approximation will not be valid, and other methods of calculation must be employed.[10]

In Sec. 2 we briefly discuss rearrangement collisions as they pertain to the problems of this paper. In Sec. 3 the cross section for the capture of an electron from a hydrogen-like atom of charge Ze to form a hydrogen-like atom of charge $Z'e$ is set up, and detailed results are presented for the ground state captures for protons in hydrogen. Section 4 deals with the contribution to the

[1] For references to the various experiments, see H. S. W. Massey and E. H. S. Burhop, *Electronic and Ionic Impact Phenomena* (Oxford University Press, New York, 1952).
[2] J. R. Oppenheimer, Phys. Rev. **31**, 349 (1928).
[3] H. C. Brinkman and H. A. Kramers, Proc. Acad. Sci. Amsterdam **33**, 973 (1930), referred to as BK in the text.
[4] H. S. W. Massey and R. A. Smith, Proc. Roy. Soc. (London) **A142**, 142 (1933).
[5] N. Bohr, Kgl. Danske Videnskab. Selskab. Mat.-fys. Medd. **18**, No. 8 (1948).
[6] J. P. Keene, Phil. Mag. **40**, 369 (1949).
[7] F. Ribe, Phys. Rev. **83**, 1217 (1951).
[8] A. C. Whittier, Ph.D. thesis, McGill University, 1952 (to be published).
[9] Reference 5, pp. 105, 111.
* *Note added in proof.*—The situation is not really so clear-cut. It has been pointed out to us by Professor G. C. Wick that in an *exact* calculation of the capture process the (nucleus)-(incident particle) interaction will give a negligible contribution (of order m/M). This can be seen most easily by considering the nuclei to be infinitely heavy and setting the problem up as an impact parameter calculation. It is then evident that the (nucleus)-(incident particle) interaction can be removed from the Hamiltonian by an appropriate canonical transformation. Consequently it cannot effect the exact transition probability.
The good agreement with experiment obtained in the present paper implies that use of the whole perturbation Hamiltonian in an approximate calculation of the capture process greatly improves the convergence of the approximation scheme, even though it can be shown that some parts of the perturbation will give rise to negligible effects in an exact calculation. This is perhaps plausible physically in the light of Bohr's remarks.
[10] N. F. Mott and H. S. W. Massey, *Theory of Atomic Collisions* (Oxford University Press, New York, 1949), second edition, p. 140 *ff*.

cross section by captures into higher orbits, while Sec. 5 contains the comparison of theory with experiment for protons in hydrogen and a discussion of the reliability of the Born approximation in such problems.

2. REARRANGEMENT COLLISIONS

The capture of an electron by an ion passing another atom is an example of a rearrangement collision.[10,11] When such a problem is treated by perturbation theory, there is an ambiguity as to just what is to be treated as the perturbation. Consider a collision process in which systems A and B collide to form two different systems C and D. Assuming that the center of mass of the whole system is at rest, the complete Hamiltonian can be written in two ways:

$$H=T_i+H_A+H_B+V_i, \tag{1}$$

or

$$H=T_f+H_C+H_D+V_f, \tag{2}$$

where H_A, H_B, H_C, H_D are the internal Hamiltonians of the systems A, B, C, D; T_i and T_f are the kinetic energies of relative motion of systems A and B, and systems C and D, respectively; while V_i and V_f are the perturbation Hamiltonians. V_i and V_f are not equal in a rearrangement collision, and so there is an ambiguity as to which term to use in a perturbation calculation for the transition probability. These remarks are well known. The reason for mentioning them here is that in the particular problem that we are considering—that of the transfer of an electron from one hydrogen-like atom to form another hydrogen-like atom—there is *no ambiguity in the result* for the transition probability. In a first-order (Born-approximation) calculation for the transition probability V_i and V_f can be shown to lead to the same results, even though there is an apparent asymmetry because the charges are different and the capture may occur into various excited states. This result is proved in Appendix I.

The coordinate system for the capture problem is shown in Fig. 1. We consider the electron (3) of charge $-e$ and mass m initially bound around a nucleus (1) of charge Ze and mass AM, where M is the mass of a proton. As a result of the interaction of the passing particle (2) of charge $Z'e$ and mass $A'M$, the electron is captured into a bound state around particle (2). The Hamiltonian can be written initially in the form of Eq. (1) with

$$T_i=-\frac{\hbar^2}{2\mu_i}\nabla_R^2, \quad \mu_i=\frac{A'M(AM+m)}{(A+A')M+m}, \tag{3}$$

$$H_A=-\frac{\hbar^2}{2m_i}\nabla_r^2-\frac{Ze^2}{r}, \quad m_i=\frac{AMm}{AM+m}, \tag{4}$$

$$V_i=\frac{Z'Ze^2}{|\mathbf{R}+[m/(AM+m)]\mathbf{r}|}-\frac{Z'e^2}{|\mathbf{R}-[AM/(AM+m)]\mathbf{r}|}, \tag{5}$$

where H_B is irrelevant since particle (2) is assumed structureless. All terms of the Hamiltonian have been expressed in terms of the initial coordinates, $\mathbf{r}$ and $\mathbf{R}$. The first term in V_i is the (nucleus)-(incident particle) interaction, while the second is the (electron)-(incident particle) interaction $(-Z'e^2/r')$.

The Hamiltonian can be rearranged for the final configuration into the form of Eq. (2) with

$$T_f=-\frac{\hbar^2}{2\mu_f}\nabla_{R'}^2, \quad \mu_f=\frac{AM(A'M+m)}{(A+A')M+m}, \tag{6}$$

$$H_C=-\frac{\hbar^2}{2m_f}\nabla_{r'}^2-\frac{Z'e^2}{r'}, \quad m_f=\frac{A'Mm}{A'M+m}, \tag{7}$$

$$V_f=\frac{Z'Ze^2}{|\mathbf{R}'-[m/(A'M+m)]\mathbf{r}'|}-\frac{Ze^2}{|\mathbf{R}'+[A'M/(A'M+m)]\mathbf{r}'|}. \tag{8}$$

In Eq. (8) the first term is identical with the first term of Eq. (5), while the second term is just $(-Ze^2/r)$.

We note that BK considered only the second term of Eq. (5) [or Eq. (8)] as the perturbation producing the capture process. We shall keep both terms of the interaction, but will still employ the Born approximation. In treating the problem of protons in hydrogen, we have ignored the identity of the protons. This introduces a negligible error in the results because the cross section for capture is so peaked in the forward direction (the mean angle is of order m/M) that the protons are, in practice, distinguishable.[12]

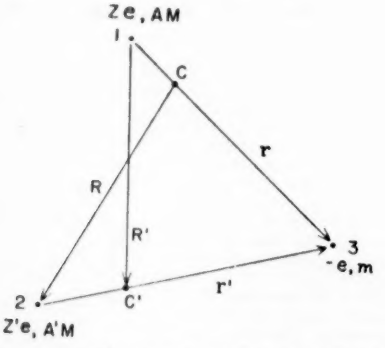

FIG. 1. Coordinate system. The points marked C and C' are the centers of mass of the initial and final atoms.

[11] L. I. Schiff, *Quantum Mechanics* (McGraw-Hill Book Company, Inc., New York, 1949), p. 230 *ff*.

[12] Reference 10, p. 290.

3. CALCULATION OF THE CROSS SECTION

The Born-approximation cross section for the capture of the electron into a final state f is given by[10]

$$\frac{d\sigma_f}{d\Omega}=\left(\frac{\mu_f}{2\pi\hbar^2}\right)^2\left(\frac{v'}{v}\right)|I_f|^2, \tag{9}$$

with

$$I_f=\int \exp(-i\mathbf{k}'\cdot\mathbf{R}')\psi_f^*(\mathbf{r}')V\exp(i\mathbf{k}\cdot\mathbf{R})\psi_0(\mathbf{r})d\mathbf{r}d\mathbf{R}, \tag{10}$$

where ψ_0 is the ground state wave function for the electron in atom Z; ψ_f is the wave function for the electron in the state f of the atom Z'; V is either V_i or V_f; $\hbar\mathbf{k}=\mu_i\mathbf{v}$, $\hbar\mathbf{k}'=\mu_f\mathbf{v}'$, where $\mathbf{v}$ is the velocity of the incident particle relative to the atom Z at rest, and $\mathbf{v}'$ is the corresponding outgoing velocity of atom Z' relative to the stripped nucleus Z. The conservation of energy requirement is

$$\tfrac{1}{2}\mu_i v^2-\epsilon=\tfrac{1}{2}\mu_f v'^2-\epsilon', \tag{11}$$

where ϵ, ϵ' are the binding energies of the electron in atoms Z, Z'.

It is convenient, following BK, to use $\mathbf{r}$ and $\mathbf{r}'$ as independent coordinates in the evaluation of the integral in Eq. (10). By reference to Fig. 1, it can be seen that I_f can be written

$$I_f=\int \exp(-i\mathbf{C}\cdot\mathbf{r}')\psi_f^*(\mathbf{r}')V(\mathbf{r},\mathbf{r}')\times\exp(i\mathbf{B}\cdot\mathbf{r})\psi_0(\mathbf{r})d\mathbf{r}d\mathbf{r}', \tag{12}$$

where

$$\mathbf{C}=\mathbf{k}-\frac{A'M}{A'M+m}\mathbf{k}', \quad \mathbf{B}=\frac{AM}{AM+m}\mathbf{k}-\mathbf{k}'. \tag{13}$$

The interaction [Eq. (5) or (8)] becomes

$$V_i=Z'Ze^2/|\mathbf{r}-\mathbf{r}'|-Z'e^2/r', \tag{5'}$$

$$V_f=Z'Ze^2/|\mathbf{r}-\mathbf{r}'|-Ze^2/r. \tag{8'}$$

The integration in Eq. (12) involving the second term in Eq. (5') or (8') is straightforward (see Appendix I), and leads to the well-known BK result for capture into the ground state and similar expressions for capture into excited states.[13] The first term of the interaction is somewhat more difficult to handle. The integral in question is

$$I_f'=Z'Ze^2\int \exp(-i\mathbf{C}\cdot\mathbf{r}')\psi_f^*(\mathbf{r}')\frac{1}{|\mathbf{r}-\mathbf{r}'|}\times\exp(i\mathbf{B}\cdot\mathbf{r})\psi_0(\mathbf{r})d\mathbf{r}d\mathbf{r}.$$

[13] M. N. Saha and D. Basu, Indian J. Phys. **19**, 121 (1945).

We introduce the Fourier transform of $1/|\mathbf{r}-\mathbf{r}'|$ to get

$$I_f'=\frac{Z'Ze^2}{2\pi^2}\int\frac{d\mathbf{k}}{k^2}\int \exp[-i(\mathbf{C}-\mathbf{k})\cdot\mathbf{r}']\times\psi_f^*(\mathbf{r}')d\mathbf{r}'\int\exp[i(\mathbf{B}-\mathbf{k})\cdot\mathbf{r}]\psi_0(\mathbf{r})d\mathbf{r}.$$

We define the Fourier transforms of the wave functions ψ_0 and ψ_f:

$$\phi_0(\mathbf{K})=\int\exp(i\mathbf{K}\cdot\mathbf{r})\psi_0(\mathbf{r})d\mathbf{r}, \qquad \phi_f(\mathbf{K}')=\int\exp(i\mathbf{K}'\cdot\mathbf{r}')\psi_f(\mathbf{r}')d\mathbf{r}'. \tag{14}$$

Then the integral I_f' can be written as a single integral in $\mathbf{k}$ space:

$$I_f'=\frac{Z'Ze^2}{2\pi^2}\int\phi_0(\mathbf{B}-\mathbf{k})\phi_f^*(\mathbf{C}-\mathbf{k})\frac{d\mathbf{k}}{k^2}. \tag{15}$$

For the ground state of a hydrogen-like atom of charge Ze the Fourier transform is

$$\phi_0(\mathbf{K})=8(\pi)^{1/2}(Z/a_0)^{5/2}[(Z/a_0)^2+K^2]^{-2}, \tag{16}$$

while the excited states have similar, but more involved, transforms.

The evaluation of I_f' in Eq. (15) is outlined in Appendix II, with the ground state capture for $Z'=Z=1$ being used as an illustration. The calculation for arbitrary Z' and Z, even for the relatively simple case of capture into the ground state, is too involved algebraically to warrant discussion here.

As was mentioned earlier, the angular distribution is peaked very sharply in the forward direction. The mean angle of the distribution in the center-of-mass system is of the order of $\theta_0=(A+A')m/2AA'M$. It should be mentioned that the only place that the masses of the heavy particles enter is in the angular distribution. $|I_f|^2$ can be written as a function of Z', Z, $h\nu/e^2$, and $y=(\theta/\theta_0)^2$. When the differential cross section Eq. (9) is integrated over angles, the solid angle $d\Omega$ is approximately $\pi d(\theta)^2$ for the angles of interest and the factor μ_f^2 is equal to $(m/2\theta_0)^2$, so that $\mu_f^2 d\Omega$ is proportional to dy. Thus the total cross section is independent of the values of A and A'. However, the cross section does depend in detail on the values of Z' and Z.

For protons in hydrogen ($Z'=Z=1$) the partial cross section for captures into the ground state is

$$\sigma_1=\sigma_{BK}\left[\frac{1}{192}\left(127+\frac{14}{E}+\frac{2}{E^2}\right)-\frac{1}{96}\frac{\tan^{-1}E^{\frac{1}{2}}}{E^{\frac{1}{2}}}\left(83+\frac{15}{E}+\frac{2}{E^2}\right)+\frac{1}{96E}(\tan^{-1}E^{\frac{1}{2}})^2\left(31+\frac{8}{E}+\frac{1}{E^2}\right)\right], \tag{17}$$

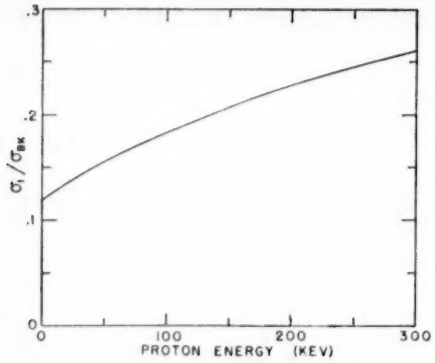

FIG. 2. Ratio of the ground-state capture cross section σ_1 to the Brinkman-Kramers cross section σ_{BK} for protons in hydrogen ($Z'=Z=1$) as a function of the incident proton energy.

where

$$\sigma_{BK}=\frac{112.5\times10^{-17}\ \text{cm}^2}{E(1+E)^6} \tag{18}$$

is the BK cross section for capture into the ground state, and $E=(hv/2e^2)^2$ is the proton energy in units of 100 kev. The ratio (σ_1/σ_{BK}) is shown as a function of incident proton energy in Fig. 2. The limiting values of the ratio are 0.117 at zero energy and 0.661 at very high energies (the high energy limit is approached very slowly, e.g., at 1 Mev the ratio is only 0.369). Figure 2 shows that the inclusion of the incident particle-nucleus interaction has a decisive influence on the cross section, even at high energies. This term produces destructive interference with the other term of the interaction to reduce the cross section from the BK value by a factor of from 5 to 3 over the energy range from 0 to 1 Mev. Both σ_{BK} and σ_1 are plotted in Fig. 4 over the energy range where there is experimental data.

4. CONTRIBUTION FROM CAPTURES INTO EXCITED STATES

The captures into higher orbits of the atom Z' will contribute to the cross section and increase its value over the ground-state result. Oppenheimer[2] showed that at high velocities ($hv/e^2\gg1$) only the higher s states contribute, and that the ratio $(\sigma_n/\sigma_1)=n^{-3}$, where n is the principal quantum number. Thus, at high velocities, the complete capture cross section σ_c is

$$(\sigma_c)_{BK}\simeq\sigma_{BK}\sum_1^\infty n^{-3}=1.202\sigma_{BK}.$$

For protons in hydrogen we have evaluated the partial cross sections for capture into the $2s$ and $2p$ states, using the complete interaction, Eq. (5′) or (8′). The methods of Sec. 3 and Appendix II were used, along with numerical integration of some of the more involved expressions which result. In Fig. 3 we have plotted the ratios of these partial cross sections to the ground-state cross section σ_1, Eq. (17), for the energy range from 0 to 200 kev. Also plotted are the corresponding ratios in the approximation of BK. The remarkable thing is the similarity in the shape and magnitude of the ratio curves from the present calculations and the BK calculations, even though the absolute magnitudes differ by a factor of five.

We wish to exploit the similarity of the ratio curves in Fig. 3 in order to estimate the partial cross sections for the capture into states with $n\geqslant3$. It is found that for the higher partial cross sections in the BK approximation the ratios to the ground-state cross section have roughly the same energy dependence as the $n=2$ ratios but are down in magnitude by the factor n^{-3}. From the evidence for $n=2$ shown in Fig. 3, it is reasonable to assume that a similar behavior occurs for the (small) higher partial cross sections calculated with the complete interaction, Eq. (5′) or (8′). Thus we can write approximately that $\sigma_n\simeq(8/n^3)\sigma_2$ for $n\geqslant3$. As a result, the complete-capture cross section σ_c can be written to a good approximation as

$$\sigma_c=\sum_1^\infty\sigma_n\simeq\sigma_1\left[1+\frac{8\sigma_2}{\sigma_1}\left(\sum_1^\infty n^{-3}-1\right)\right],$$

or

$$\sigma_c=\sigma_1(1+1.616\sigma_2/\sigma_1). \tag{19}$$

The ratio (σ_c/σ_1) of the complete-capture cross section to the ground-state cross section given by Eq. (19) is plotted as the solid curve in Fig. 3. We see that for protons in hydrogen the captures into excited states account for about one-third of the total cross section in the energy region 25 to 100 kev, and about 17 percent at very high velocities as found by Oppenheimer.

Although we have not calculated in detail the partial cross sections for captures into excited states for values of Z' and Z other than unity, it is evident that the

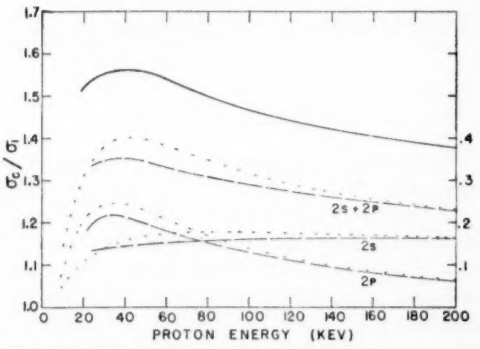

FIG. 3. (a) Ratios of the capture cross sections for the $2s$ and $2p$ states to the ground-state capture cross section for protons in hydrogen as functions of the incident proton energy (right-hand ordinate scale). Present results ———. Brinkman-Kramers results – – – –. (b) Ratio of the total capture cross section σ_c to the ground-state cross section σ_1 for protons in hydrogen as a function of incident proton energy (left-hand ordinate scale)—solid curve at the top.

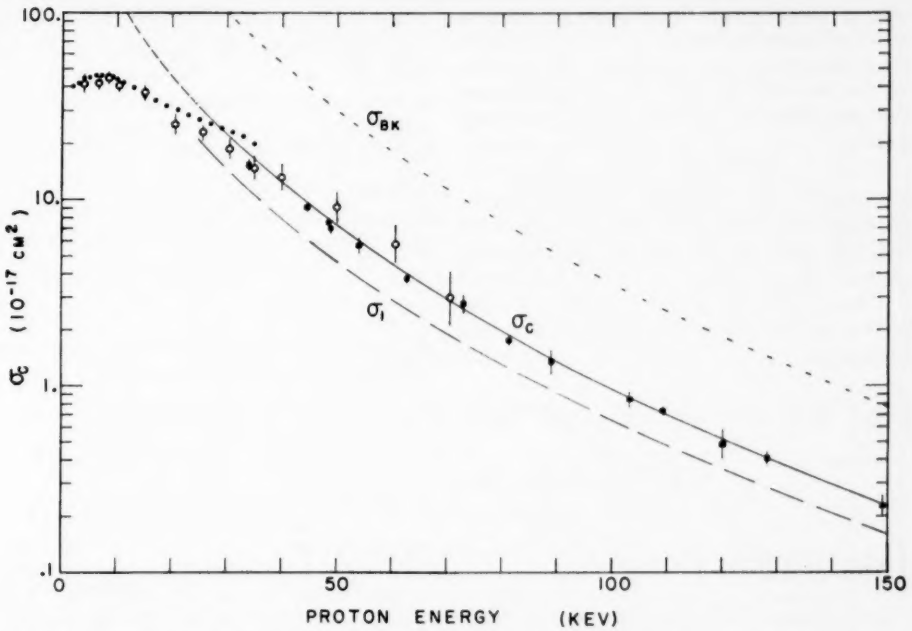

FIG. 4. Electron-capture cross section σ_c per atom for protons in hydrogen gas as a function of incident proton energy. The solid curve labeled σ_c is the theoretical result [Eq. (19)] for the total capture cross section; the dashed curve labeled σ_1 is the partial cross section for capture into the ground state [Eq. (17)], while the dotted curve labeled σ_{BK} is the corresponding cross section due to Brinkman and Kramers [Eq. (18)]. The experimental data are those of Keene (●), Ribe (■), and Whittier (○).

relative magnitude of these cross sections will not necessarily be similar to that found for $Z'=Z=1$. For example, for alpha-particles in hydrogen ($Z'=2$, $Z=1$), a case in which we have evaluated the ground-state cross section, it is expected that σ_2 may be comparable with, or even larger than, σ_1, at least at low velocities ($hv/e^2\sim 1$), since there is no difference in the binding energies ϵ and ϵ' [Eq. (11)] and a resonance phenomenon occurs.

5. COMPARISON WITH EXPERIMENT; REMARKS ON THE USE OF THE BORN APPROXIMATION

For protons in hydrogen gas the total cross section σ_c [Eq. (19)] is shown plotted in Fig. 4 along with the most recent experimental data of Keene,[6] Ribe,[7] and Whittier.[8] For energies below 25 kev, where hv/e^2 is less than unity, the curve is shown dotted to indicate that the Born approximation certainly cannot be used at such low velocities. At energies above 50 kev the agreement between theory and experiment is excellent, and even down to 25 kev is adequate.

It is perhaps somewhat surprising that the Born approximation leads to such good agreement even for relatively low velocities. This may be merely another example of the well-known empirical rule that the Born approximation is, at least in atomic physics, often much better than it has any right to be. There is another qualitative rationalization for its reliability in this particular problem. The capture of an electron by a proton in hydrogen is the transfer of an electron from one neutral atom to form another neutral atom. The force exerted by a neutral atom on an incident charged particle is of relatively short range. This means that the incident (or outgoing) wave describing the relative motion will be distorted only at close distances, so that the approximation involved in using plane waves will not be too great. This is substantiated by an impact parameter calculation made by BK which showed that most of the captures occur for distances of the order of, or greater than, $a_0(e^2/hv)$; when $(e^2/hv)\ll 1$, the Born approximation is valid, while for $(e^2/hv)\sim 1$ the captures occur at distances of the order of a_0 where the neutral atom's potential is weak. This argument would apply with equal validity to any singly ionized atom capturing an electron in any substance. It would indicate that the Born approximation would be less successful in the case of more highly ionized atoms, at least in the velocity region $hv/e^2\gtrsim 1$.

It should be noted that we have ignored molecular effects in these calculations. It is not clear to what extent the fact that the incident proton actually captures the electron from a hydrogen molecule instead of an isolated hydrogen atom will modify the present results. This aspect of the problem, as well as other examples of electron capture, are being studied at present.

The authors wish to thank Dr. Whittier for allowing them to quote his measurements of σ_c before publication. One of the authors (H.S.) was the recipient of a fellowship from the National Research Council of Canada during the year 1951–52, and wishes to acknowledge this support.

APPENDIX I

We wish to show that in the Born approximation the initial and final perturbations, V_i and V_f, lead to the same results for the capture cross section. Since the first terms in V_i [Eq. (5′)] and V_f [Eq. (8′)] are equal, all that is necessary is to prove that the following integrals (the two alternative forms of the BK matrix element) are equal:

$$I_{BK}=\int \exp(-i\mathbf{C}\cdot\mathbf{r}')\psi_f^*(-Z'e^2/r')d\mathbf{r}' \times\int \exp(i\mathbf{B}\cdot\mathbf{r})\psi_0 d\mathbf{r}, \quad \text{(I.1)}$$

$$I_{BK}'=\int \exp(-i\mathbf{C}\cdot\mathbf{r}')\psi_f^* d\mathbf{r}'\int \exp(i\mathbf{B}\cdot\mathbf{r}) \times\psi_0(-Ze^2/r)d\mathbf{r}. \quad \text{(I.2)}$$

Using the internal Hamiltonian H_C [Eq. (7)] with eigenvalue ϵ' [see Eq. (11)], we can write I_{BK} in the form

$$I_{BK}=\int \exp(-i\mathbf{C}\cdot\mathbf{r}')\left(\frac{\hbar^2}{2m_f}\nabla_{r'}{}^2-\epsilon'\right)\psi_f^* d\mathbf{r} \times\int \exp(i\mathbf{B}\cdot\mathbf{r})\psi_0 d\mathbf{r}.$$

Integration by parts twice leads to the result

$$I_{BK}=-\left(\frac{\hbar^2C^2}{2m_f}+\epsilon'\right)\int \exp(-i\mathbf{C}\cdot\mathbf{r}')\psi_f^* d\mathbf{r}' \times\int \exp(i\mathbf{B}\cdot\mathbf{r})\psi_0 d\mathbf{r}.$$

Or, introducing the Fourier transforms Eq. (14),

$$I_{BK}=-\left(\frac{\hbar^2C^2}{2m_f}+\epsilon'\right)\phi_0(\mathbf{B})\phi_f^*(\mathbf{C}). \quad \text{(I.3)}$$

A similar treatment of I_{BK}' leads to the form

$$I_{BK}'=-\left(\frac{\hbar^2B^2}{2m_i}+\epsilon\right)\phi_0(\mathbf{B})\phi_f^*(\mathbf{C}). \quad \text{(I.4)}$$

By means of the conservation of energy Eq. (11), it is easy to show that

$$(\hbar^2C^2/2m_f)+\epsilon'=(\hbar^2B^2/2m_i)+\epsilon,$$

so that $I_{BK}=I_{BK}'$, as required.

APPENDIX II

We will outline the evaluation of I_f' [Eq. (15)], using the capture into the ground state for $Z'=Z=1$ as an example. The method can be readily extended to arbitrary Z' and Z and captures into excited states. For the special case we have, using Eq. (16),

$$I_0'=\frac{32e^2}{\pi a_0{}^5}\int (a_0{}^{-2}+C^2+k^2-2\mathbf{k}\cdot\mathbf{C})^{-2} \times(a_0{}^{-2}+B^2+k^2-2\mathbf{k}\cdot\mathbf{B})^{-2}\frac{d\mathbf{k}}{k^2}. \quad \text{(II.1)}$$

By introducing an auxiliary integral of the type used by Feynman[14] in another connection,

$$(ab)^{-2}=\int_0^1 \frac{6x(1-x)dx}{[ax+b(1-x)]^4},$$

we can transform (II.1) into the form

$$I_0'=\frac{32e^2}{\pi a_0{}^5}\int_0^1 6x(1-x)dx\int \frac{d\mathbf{k}}{k^2(k^2+\Delta-2\mathbf{k}\cdot\mathbf{q})^4}, \quad \text{(II.2)}$$

where

$$\Delta=a_0{}^{-2}+xC^2+(1-x)B^2, \quad \text{and} \quad \mathbf{q}=x\mathbf{C}+(1-x)\mathbf{B}.$$

Differentiation of the integral,

$$\int \frac{d\mathbf{k}}{k^2(k^2+\Delta-2\mathbf{k}\cdot\mathbf{q})^2}=\pi^2(\Delta)^{-1}(\Delta-q^2)^{-\frac{1}{2}},$$

twice with respect to Δ, gives 6 times the integral over $\mathbf{k}$ space in (II.2). Consequently, I_0' becomes

$$I_0'=\frac{32\pi e^2}{a_0{}^5}\int_0^1 x(1-x)\left[\frac{2}{\Delta^3(\Delta-q^2)^{1/2}} +\frac{1}{\Delta^2(\Delta-q^2)^{3/2}}+\frac{\frac{3}{4}}{\Delta(\Delta-q^2)^{5/2}}\right]dx. \quad \text{(II.3)}$$

Now $C^2=B^2$ in this case, so that Δ does not depend on x (this is true for the ground state capture for arbitrary Z' and Z) but does depend upon angle. $(\Delta-q^2)$ can be written as $(\alpha x^2+\beta x+\gamma)$ where α, β, γ depend upon Z', Z, and v, but not on angles. Thus (II.3) can be written as

$$I_0'=(32\pi e^2/a_0{}^5)(2\lambda_0\Delta^{-3}+\lambda_1\Delta^{-2}+\tfrac{3}{4}\lambda_2\Delta^{-1}), \quad \text{(II.4)}$$

where

$$\lambda_n=\int_0^1 x(1-x)(\Delta-q^2)^{-n-\frac{1}{2}}dx =\int_0^1 x(1-x)(\alpha x^2+\beta x+\gamma)^{-n-\frac{1}{2}}dx,$$

[14] R. P. Feynman, Phys. Rev. **76**, 769 (1949), Eqs. (14a) and (15a) in the Appendix.

and

$$\Delta = a_0^{-2} + B^2 \simeq a_0^{-2}[1+(hv/2e^2)^2(1+y)] + O(m/M),$$

where

$$y = [2A'AM\theta/(A'm+Am)]^2 = (\theta/\theta_0)^2.$$

We note that $I_{BK} \sim \Delta^{-3}$ [see Eq. (I.3) and Eq. (16)], so that the differential cross section, Eq. (9), is proportional to Δ^{-2} and higher reciprocal powers of Δ. Consequently, the angular distribution is largely confined to angles less θ_0, as discussed in Sec. 3.

When the integral I_0' is combined with I_{BK} in Eq. (9) and integrated over angles, the resulting total cross section can be expressed in the form of Eq. (17). For arbitrary Z' and Z and/or captures into excited states the general procedure is the same. However the algebraic complexity grows enormously, and it is advantageous in some instances to evaluate certain expressions (such as the integrals λ_n) numerically rather than analytically.

PHYSICAL REVIEW VOLUME 89, NUMBER 2 JANUARY 15, 1953

The $C^{12}(p,p)C^{12}$ Differential Cross Section*

H. L. Jackson, A. I. Galonsky, F. J. Eppling, R. W. Hill, E. Goldberg,† and J. R. Cameron†
University of Wisconsin, Madison, Wisconsin

(Received July 28, 1952)

The $C^{12}(p,p)C^{12}$ differential cross section has been observed at four scattering angles by using differentially pumped gas targets of propane and ethylene. The scattering angles employed were 106.4, 127.8, 148.9, and 169.2 degrees in the center-of-mass system, and the energy range covered extended from 0.4 to 4.3 Mev. These measurements show the angular behavior of the previously discovered scattering anomalies at 0.46 and 1.7 Mev and give values of the absolute cross section accurate to within five percent. A careful search in three- and six-kev steps failed to reveal any indication of any hitherto unknown scattering resonances within the energy range surveyed.

I. INTRODUCTION

In a previous article[1] we reported the results of a partial wave analysis of the differential cross section for elastically scattered protons from ordinary carbon obtained by Goldhaber and Williamson.[2] Although that analysis yielded definite values for the momenta and parities of the excited states of N^{13}, it also led to values of the resonant energies and widths which differed somewhat from those obtained from the proton capture data.[3] In addition, the experimental and calculated scattering cross sections could not be brought into agreement below one Mev. In the hope of removing these discrepancies, we have measured the $C^{12}(p,p)C^{12}$ differential cross section with increased accuracy at four scattering angles and have analyzed the new data by the same method. This paper describes the experiment and presents the data obtained. The following paper will deal with the analysis.

II. APPARATUS

Unless the absolute value of the scattering cross section is known to within a few percent, the phase shift analysis is extremely difficult and the results uncertain. In view of this fact, one of the major considerations in planning the experiment was the type of target to be used and the technique for measuring its thickness. Solid targets of the required purity and uniformity of thickness are difficult to prepare and are liable to additional carbon deposition during bombardment. The final decision was to employ a gas target, since its thickness depends only upon the dimensions of the counter slit system, the scattering angle, and the pressure and temperature of the scattering gas. All these quantities are readily measurable to a degree of accuracy somewhat higher than required for the projected experiment.

The gas actually used for most of the experiment was propane, although ethylene was used for some of the data at low bombarding energies, because it gives rise to less small angle scattering than propane at the same pressure. Being compounds of hydrogen and carbon only, these gases behave like pure carbon targets at scattering angles greater than 90 degrees. They have the further advantage of giving satisfactorily high yields of scattered protons at feasible chamber pressures and incident beam intensities.

Figure 1 is a cross-sectional view of the apparatus as seen from above. Its four principal components are the differential pumping column A, the scattering chamber B, the collector cup assembly C, and the two proportional counters together with their collimating slit systems D and D'. In operation the incident beam from

* Work supported by the AEC and the Wisconsin Alumni Research Foundation.
† AEC Predoctoral Fellow.
[1] H. L. Jackson and A. I. Galonsky, Phys. Rev. **84**, 401 (1951).
[2] G. Goldhaber and R. M. Williamson, Phys. Rev. **82**, 495 (1951).
[3] W. A. Fowler and C. C. Lauritsen, Phys. Rev. **76**, 314 (1949); D. M. Van Patter, Phys. Rev. **76**, 1264 (1949); and J. D. Seagrave, Phys. Rev. **84**, 1219 (1951).

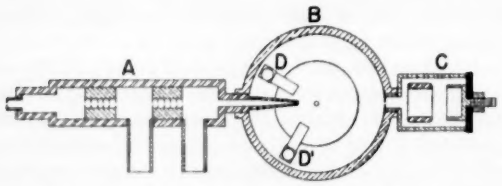

FIG. 1. Cross-sectional view of the scattering chamber as seen from above. The differential pumping column *A* isolates the scattering chamber from the electrostatic analyzer and collimates the incident beam. It consists of three stages, each separated from the adjoining ones by small circular apertures. The scattering chamber *B* is a bronze casting with an inside diameter of nine inches and a depth of two and one-half inches. The collector cup housing *C* incloses the collector cup and a ring magnet to suppress secondary electrons. The magnet is mounted on Lucite supports and is also used as an electrostatic suppressor electrode. A 0.00002-in. nickel foil prevents the gas in the chamber from entering the collector cup housing. The two proportional counters *D* and *D'*, together with their collimating slit systems, are mounted on a turntable which can be rotated from the outside.

the proton accelerator, after passing through the electrostatic analyzer, enters the differential pumping column where it is collimated. It crosses the scattering chamber and is finally stopped by the collector cup. In the meantime those protons which have been scattered from the incident beam and whose trajectories pass through the counter slit systems enter the counters and are recorded. The collector cup is connected to a current integrator which shuts off the counter recording circuits as soon as a predetermined charge (10 microcoulombs) has been collected.

The differential pumping column prevents the target gas in the chamber from entering the electrostatic analyzer. It is superior to a thin foil for several reasons. First, the scattering chamber undergoes continuous flushing so that contaminant gases and vapors do not accumulate. Second, the problem of energy degradation and straggling of the incident beam, which would occur both in a foil and in the carbon deposits, which would gradually build up on it, does not arise. Third, the small angle scattering which a foil would introduce into the beam, especially at low energies, is absent. The deleterious effects of the gas within the column are negligible, since the column pressures are far less than that in the chamber itself. As is clear from the figure, the differential pumping column consists of three pressure dropping stages. A fast forepump (5 liters/second capacity) exhausts each of the first two sections, and an oil diffusion pump (250 liters/sec capacity) the last.

The aperture at each end of the column is a 1.5-mm hole drilled in a 0.003-inch stainless steel disk. In addition to restricting the gas flow, these apertures collimate the incident beam. As they are about 43 cm apart, the maximum half-angle spread in the incident beam, when it enters the chamber, is approximately 12 min. Each of the two intermediate capillaries consists of twenty-two stainless steel apertures, each of which is 2.0 mm in diameter and 0.003 inches thick. All apertures, including the ones at the ends, were electropolished until they were free from irregularities under microscopic examination. When the pressure in the scattering chamber is 10 mm Hg, the flow rate through the column is from 10 to 15 liters STP per hour, and the pressures in the successive stages are roughly 0.5, 10^{-2}, and 10^{-5} mm Hg, respectively.

The scattering chamber used in the present experiment is similar in design to the one described by Herb, Kerst, Parkinson, and Plain.[4] It is a bronze casting with an inside diameter of 9 in. and a depth of $2\frac{1}{2}$ in. A turntable, rotatable from the outside and situated just above the chamber floor, supports the proportional counters and their slit systems. The degree marks on the rim of the turntable together with a vernier index secured to the floor of the chamber, enable the operator to read the scattering angle to 0.1 degree.

The design of the collector cup assembly is conventional. An alnico ring magnet, $2\frac{1}{2}$ in. inside diameter with a uniform transverse field of about 300 gauss, rests on Lucite supports and is connected to an external electrode so that it can be used to provide electrostatic as well as magnetic suppression of secondary electrons. A 0.00002-inch nickel foil prevents the target gas from entering the collector cup housing which is kept evacuated to about 5×10^{-6} mm Hg.

Each of the two proportional counters used consisted of an inconel tube $1\frac{3}{4}$ in. long and $\frac{5}{8}$ in. inside diameter, with a 0.005-in. Kovar wire suspended along the center axis. Since propane and ethylene are good counting gases, it was thought advantageous to avoid the complication of a separate counter filling system by letting the counters operate with the same gas and at the same pressure as the chamber itself. Because the proton entrance slots were necessarily rather large, they had to be covered with a thin metal foil (0.00002-in. nickel) to prevent the electric field from extending outside the counter volume. A small separate opening was provided for the gas inflow. In practice, the open style counters proved to be difficult to adjust and the range of pressures suitable both for satisfactory counting and for accurate current integration was inconveniently narrow, especially at low energy. Below 0.6 Mev the open style counters had to be abandoned because the usable pressure range disappeared altogether. In order to cover the lower scattering anomaly, we sealed the counters and provided them with a separate filling system.

The sensitive volume of the scattering chamber and the solid angle subtended by the counter are determined by two rectangular slits, 2.0×9.0 mm placed $1\frac{3}{4}$-in. apart. The slit edges are made from stellite ground to 0.0001-inch tolerance. Two slightly larger sets of auxiliary slits stand between the two defining slits to prevent protons scattered from the slit support blocks from entering the counter. Figure 2 shows the details of the counter slit system assemblies.

[4] Herb, Kerst, Parkinson, and Plain, Phys. Rev. **55**, 998 (1939).

The recording circuits connected to each counter include a pre-amplifier, amplifier, and two discriminator-scalers operating in parallel. In operation the two discriminators were set at substantially different minimum pulse height acceptance voltages so as to monitor the number of pulses outside the main proton group.

A glass arm manometer filled with Octoil-S measured the chamber pressure. One arm was connected directly to the chamber and the other to the collector cup diffusion pump. The cathetometer built by Findley, McGruer, and Worthington[5] was used to observe the displacement of the oil menisci.

The propane vapor from the bottle was admitted into the chamber through a long-taper needle valve. In order to stabilize the vapor pressure of the liquified propane in the bottle, we immersed it in a bath of crushed ice and water. The sections of tubing between the bottle and the chamber were quite long in order to bring the vapor up to room temperature before it entered the chamber.

The pressure stability was quite good. The principal variation was that caused by the "pumping" action of the proton beam. This effect is an increase of pressure that occurs when the intensity of the incident beam is increased. The change of pressure associated with a change of beam current from zero to the maximum attainable value was roughly 0.1 to 0.2 mm Hg, the exact amount varying somewhat with the chamber pressure and the energy of the beam. The seriousness of the effect was minimized by keeping the beam as steady as possible and by continuously monitoring the pressure. To accomplish this, a team of three worked together in taking data; one member controlled the proton accelerator and the electrostatic analyzer, one recorded counter data, and the third observed the chamber pressure and recorded as many values per run as time permitted.

III. EXPERIMENTAL RESULTS

In the present experiment we measured the $C^{12}(p,p)C^{12}$ differential cross section from 0.4 to 4.3 Mev at four different scattering angles. Figure 3 shows the results obtained. In order to simplify the subsequent analysis as much as possible, we calculated the scattering angle and the absolute value of the cross section in the center-of-mass system but left the energy of the incident beam in the laboratory system. At two angles, 169.2 and 106.4 degrees, observations were made every three kev up to two Mev, and every six kev thereafter in an effort to locate any narrow resonances hitherto undiscovered. The results show no evidence whatever of any additional levels in the energy range surveyed. Except over the region of the 1.7-Mev anomaly, only about one-fifth of the total number of points recorded at these angles appear in the figure.

[5] Findley, McGruer, Worthington, Phys. Rev. (to be published).

The counters were sealed and pressurized to obtain data between 0.4 and 0.6 Mev. As the counter design included no provision for eventual sealing, the task of attaching foils to the proton entrance slots, securely enough to withstand the required internal pressure, was most difficult. After many trials, we successfully sealed one counter with a 0.00002-in. nickel foil, but never succeeded with the other. We finally covered the second counter slot with a 0.00005-in. nickel foil instead. In operation over the energy region of the lower scattering anomaly, the latter foil introduced so much straggling into the energy of the protons entering the counter that the voltage spread of the proton pulses was unacceptably broad. Consequently, the data from this counter had to be rejected and, for lack of time, we did not cover the two lower scattering angles with the usable counter.

The cross section at 169.2 degrees is quite similar to that obtained earlier at 164 degrees from a solid target,[2] except that its absolute value in the vicinity of the 0.46-Mev anomaly is about 20 percent larger. Thus, the serious discrepancy in the low energy region between the original data and the analysis based on it[1] is resolved. The crucial point of interest in the 169.2-degree data is the unmistakable presence of two maxima and minima near 1.7 Mev. Their existence is good evidence that the scattering anomaly at this energy is not the result of a single narrow energy level.

IV. DISCUSSION OF ERRORS

Most of the points in the present data are based on more than ten thousand counts and all on more than

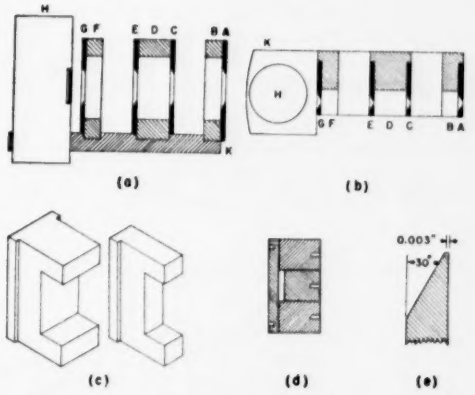

FIG. 2. Drawings *a* and *b* are cross-sectional views of the counter and slit system assembly as seen from the side and from above, respectively. *A* and *G* are the slits which define the solid angle subtended by the counter; *C* and *E* are auxiliary slits whose function is to prevent multiply scattered protons from reaching the counter; *B*, *D*, and *F* are the slit support blocks; *K* is the slit assembly base plate; and *H* is the proportional counter. Drawing *c* shows the shape of the slit support blocks. Drawing *d* shows the shapes of the stellite plates forming the slit and their arrangement on the face of the support block. Drawing *e* is a cross-sectional view of the slit forming edge of the stellite plates.

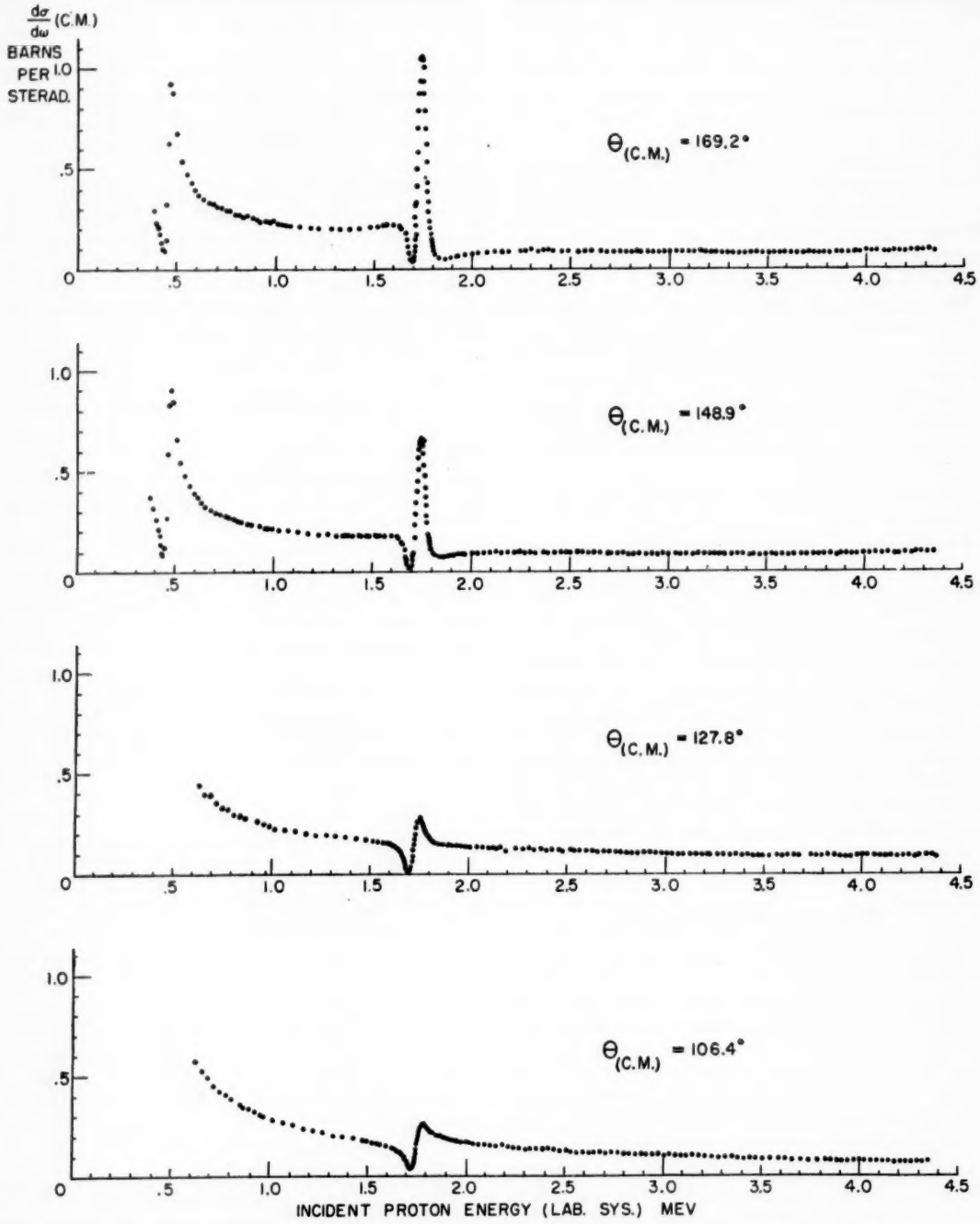

FIG. 3. The $C^{12}(p,p)C^{12}$ differential cross section. The values of the cross section and of the scattering angles are given in the center-of-mass system, while the bombarding energy is given in the laboratory system. At 106.4 and 169.2 degrees, observations were made every three kev up to two Mev and every six kev thereafter in an effort to locate any unknown scattering anomalies. However, except over the resonance at 1.7 Mev, only about one-fifth of these points are plotted. The 0.46-Mev scattering anomaly does not appear at the two smaller scattering angles because the data at these angles below 0.6 Mev were defective.

twenty-five hundred. Therefore, the statistical uncertainty is usually less than one percent and never more than two percent.

Three important sources of error that can affect the accuracy of current integration are the failure of an appreciable fraction of the incident beam to reach the collector cup, failure to suppress secondary electrons, and deficiencies in the current integration circuit. As we used the current integrator built by Findley *et al.*,[5] for the recently completed proton-proton scattering experiment, the errors from the last-mentioned cause should be negligible since the circuit was designed to be accurate to one part in ten thousand.

The effect of unsuppressed secondary electrons was investigated by plotting yield *versus* suppressor voltage curves at constant incident proton energy and target gas pressure. These curves indicated complete suppression within statistics at sixty volts, but as an additional precaution we used a bias of 300 volts while taking data.

The failure of a fraction of the beam to reach the collector cup because of small angle scattering was fairly troublesome, especially at low energies with the open style counters. To check the seriousness of this effect, we plotted numerous yield/pressure *versus* pressure curves below 1.5 Mev. We accepted yield data in any given energy region only when the appropriate curve of Y/P *versus* P was horizontal up to pressures 1.5 to 2.0 times the pressure used to obtain data for cross-section calculation. In the 0.6- to 1.0-Mev region, small angle scattering in propane was excessive at the minimum usable pressure with the open style counters. In this region, therefore, ethylene was used instead. During sealed counter operation, the effect was reduced to a tolerable level by using a chamber pressure of about 3 mm Hg. The error in the current integration therefore lies within the statistics of the Y/P curves, or about one percent.

No direct means of testing the efficiency of the open style counters was available. However, there are many regions of overlap in the data where yields were obtained for a wide range of gas pressure and counter voltage. Since these regions show no discrepancies greater than statistics, it is plausible to assume that the counters are reliable to within statistics or one percent.

The propane used has an advertised purity of 99.9 percent. No analysis was made to check the supplier's[6] claim. On the assumption that the impurities present are mostly light hydrocarbons, the resulting error would be negligible. The purity of the ethylene used is unknown, but in the regions where ethylene and propane data overlap, no discernable discrepancy exists.

As stated earlier, the target thickness depends upon the gas pressure and temperature, the dimensions of the counter slit systems, and the scattering angle. The combined error of the pressure, temperature, and slit dimension measurements should not exceed 0.1 percent, but an error of 0.1 degree in the scattering angle introduces an error of one percent into the value of the absolute cross section at 169.2 degrees. The error introduced at the smaller scattering angles is, of course, somewhat less.

Ordinary carbon is about 99 percent C^{12} and one percent C^{13}. Since the differential cross section for elastically scattered protons from C^{13} has not been measured, the error introduced by the isotopic contamination at any given energy and scattering angle cannot be estimated.

The errors cited are those which affect the magnitude of the cross section at a given energy and scattering angle. The sum of these errors is about 5 percent plus whatever error the presence of C^{13} introduces. Of the errors mentioned, that in the scattering angle affects only the absolute cross section, while the others may or may not affect the relative cross section as well, depending upon whether they are or are not functions of time and/or energy. The sum of the errors that may affect the relative cross section is therefore about four percent plus the C^{13} effect.

Under the conditions of the experiment, the error in the absolute value of the energy of the incident beam is not greater than 0.2 percent. An additional source of error arises in correcting for the stopping power of the gas between the last analyzer slit and the sensitive volume of the scattering chamber. The magnitude of the limit of this error is hard to estimate, but it is believed that it could hardly exceed 2 kev in the worst case.

[6] Matheson Company, East Rutherford, New Jersey.

The Excited States of the N^{13} Nucleus*

HERBERT L. JACKSON† AND AARON I. GALONSKY
University of Wisconsin, Madison, Wisconsin

(Received July 28, 1952)

The properties of the excited states of N^{13} were reinvestigated by applying dispersion theory to the $C^{12}(p,p)C^{12}$ differential cross section reported in the preceding paper. The quantity and accuracy of the data were sufficient to permit extraction of the experimental S wave phase shift up to 1.4 Mev. The remainder of the data was fitted by successive readjustment of the level parameters.

The present analysis corroborates the previous momentum and parity assignments but gives somewhat different values for the resonant energies and widths. The level assignments together with the revised widths and resonant energies are as follows: The 0.46-Mev scattering anomaly is due to a virtual $(j=1/2, +)$ level in the compound nucleus N^{13} with $E_r=2.369$ Mev and $\Gamma=31$ kev. The 1.7-Mev scattering anomaly is the result of two virtual levels, a $(j=3/2, -)$ level with $E_r=3.511$ Mev and $\Gamma=55$ kev and a $(j=5/2, +)$ level with $E_r=3.558$ Mev and $\Gamma=61$ kev. E_r and Γ are calculated in the center-of-mass system and E_r is measured from the ground state of N^{13}. These new values for E_r and Γ agree quite well with those obtained from the $C^{12}(p,\gamma)N^{13}$ reaction provided it is assumed that the $(j=5/2, +)$ level does not participate appreciably in the capture process. The values of the reduced widths of the levels indicate that the two even-parity levels arise mainly from single particle excitation, but that the odd-parity level involves appreciable excitation of the core.

THE purpose of this paper is to present the information about the excited states of N^{13} obtained from the analysis of the $C^{12}(p,p)C^{12}$ differential cross section reported in the preceding article. For the most part, this analysis is similar to that of the original data of Goldhaber and Williamson,[1,2] but because the more recent measurements include data at four scattering angles and are of relatively high accuracy, the widths and resonant energies of the excited levels as determined in this investigation are more reliable than those previously proposed. Unlike the earlier values, they agree with those obtained from the $C^{12}(p,\gamma)N^{13}$ reaction.

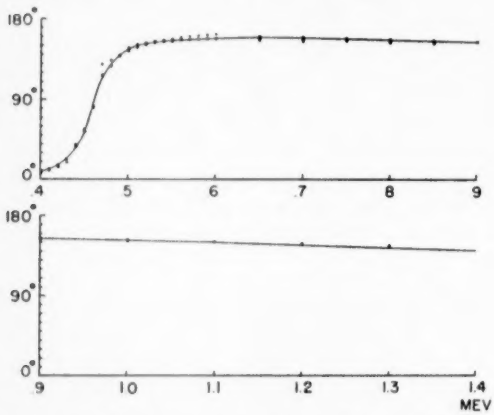

FIG. 1. The $C^{12}(p,p)C^{12}$ S wave phase shift as a function of energy. The points are the values of δ_0 extracted from the experimental cross section. The solid line is the phase shift calculated from the parameters in Table I.

I. METHOD

As the dispersion theory formalism used in this analysis and the usual methods of applying it are already described in the literature,[2-5] they will not be repeated in detail here. Instead this section will merely summarize the procedures which are of especial importance in the present work.

Whenever practicable, a dispersion theory analysis should begin with the extraction of the phase shifts of each partial wave from the experimental cross section. Once these are known as explicit functions of the bombarding energy, the task of identifying the parameters characteristic of the energy levels present is relatively simple and their numerical values reasonably dependable.

In dealing with the present data, we were able to obtain the S wave phase shift as a function of energy up to 1.4 Mev. Beyond this point, however, the contribution of higher momentum components could no longer be ignored at any of the scattering angles studied. As both the P and D waves appeared to enter in approximately equal strengths, further attempts at

TABLE I. Parameters of the first three excited states in N^{13}.

Level:	$a=1.45(12^{\frac{1}{3}}+1^{\frac{1}{3}})\times10^{-13}$ cm $(j=1/2, +)$	$(j=3/2, -)$	$(j=5/2, +)$
E_p(Mev)[a]	0.461	1.698	1.748
Γ(kev)[a]	34	60	66
E_r(Mev)	2.369	3.511	3.558
Γ(kev)	31	55	61
E_λ(Mev)	0.951	3.516	3.612
$\gamma\lambda^2$(Mev-cm)	7.58×10^{-13}	0.440×10^{-13}	2.92×10^{-13}
$\gamma\lambda^2\div\hbar^2/\mu a$	0.81	0.047	0.31

[a] Laboratory system. All other numbers apply to the center-of-mass system.

* Work supported by the AEC and the Wisconsin Alumni Research Foundation.

† Now at the University of Basel, Basel, Switzerland.

[1] G. Goldhaber and R. M. Williamson, Phys. Rev. **82**, 495 (1951).

[2] H. L. Jackson and A. I. Galonsky, Phys. Rev. **84**, 401 (1951).

[3] C. L. Critchfield and D. C. Dodder, Phys. Rev. **76**, 602 (1949).

[4] R. A. Laubenstein and M. J. W. Laubenstein, Phys. Rev. **84**, 18 (1951).

[5] L. J. Koester, Phys. Rev. **85**, 643 (1952).

explicit extraction were abandoned as unrewarding, and the analysis was continued by successive readjustment of the level parameters just as in the analysis[2] of the Goldhaber-Williamson data.

Whenever the elastic scattering cross section involves only Rutherford and S wave effects, the partial wave expansion of the differential cross section[2] can be written in the two-dimensional vector form $\mathbf{X}=\mathbf{R}+\mathbf{S}$, where

$$|\mathbf{X}|=k(d\sigma/d\omega)^{\frac{1}{2}},$$

$$\mathbf{R}=-\tfrac{1}{2}\eta\csc^2\theta/2\exp(i\eta\ln\csc^2\theta/2),$$

and

$$\mathbf{S}=\sin\delta_0 e^{i\delta_0}.$$

The only unknown quantities in the equation are δ_0 and the phase of $\mathbf{X}$, the latter being of no interest. The solution for the unknowns is straightforward, both graphically and analytically. In general, the solution at any one scattering angle gives two values for the phase shift. The one which is physically meaningful can usually be identified by comparing the solutions obtained at different scattering angles.

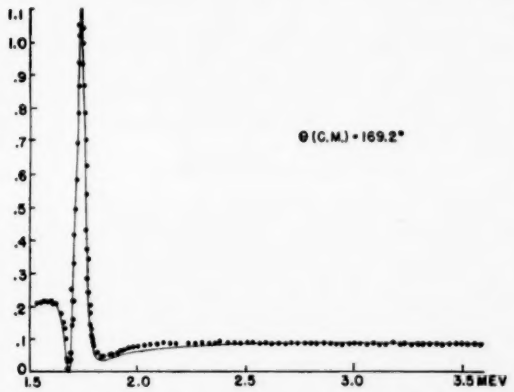

FIG. 2. Comparison of the calculated and experimental cross sections at 169.2 degrees center-of-mass. The points are the experimental cross sections reported in the preceding paper. The solid line is the cross section calculated from the parameters in Table I together with the modifications of δ_0 and δ_2^- discussed in the text. Vertical scale is in barns per steradian c.m.

II. RESULTS

According to the analysis of the Goldhaber-Williamson data,[2] the 0.46-Mev scattering anomaly in the $C^{12}(p,p)C^{12}$ reaction is due to a $(j=1/2,+)$ level in N^{13} and the 1.7-Mev scattering anomaly is due to two levels about fifty kev apart. These two levels were classified as $(j=3/2,-)$ and $(j=5/2,+)$, the latter lying higher in energy. The present analysis corroborates the momentum and parity assignments of these levels but gives somewhat different values for their widths and resonant energies. The remainder of this section will present only those results which are different from or supplementary to the previous work.

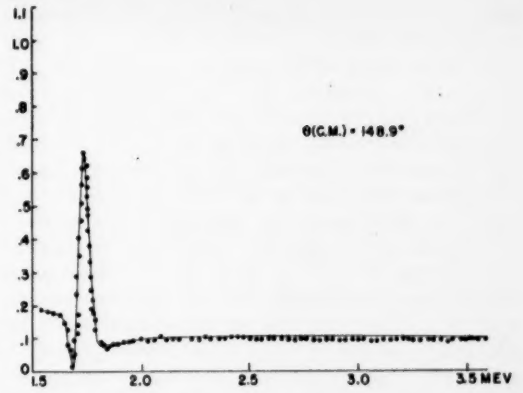

FIG. 3. Comparison of the calculated and experimental cross sections at 148.9-degrees c.m. The points are the experimental cross sections reported in the preceding paper. The solid line is the cross section calculated from the parameters in Table I together with the modifications of δ_0 and δ_2^- discussed in the text. Vertical scale is in barns per steradian c.m.

The points in Fig. 1 are the values of the S wave phase shift determined from the experimental cross section. Below 1.2 Mev the effects of the higher momentum phase shifts appear to be less than the statistical uncertainty of the experimental cross sections. Between 1.2 and 1.4 Mev, the values for δ_0 obtained from the data at different scattering angles no longer agree, thus indicating the presence of higher momentum components. The points plotted in the figure above 1.2 Mev are those obtained from the data at 127.8 degrees. The cross section at this angle is believed to be relatively free from the effects of higher momentum components because the P and D vectors at this angle happen to be rather small in magnitude and are so oriented as to have little effect. The solid line in the

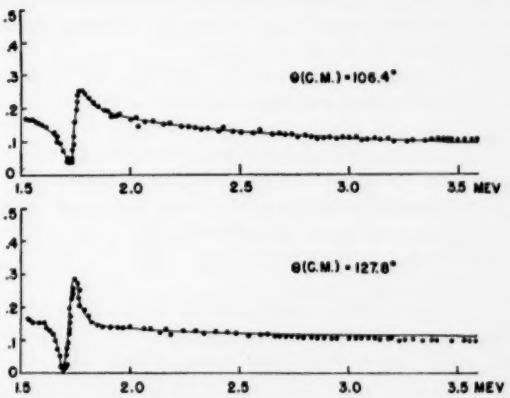

FIG. 4. Comparison of the calculated and experimental cross sections at 127.8-degrees and 106.4-degrees c.m. The points are the experimental cross sections reported in the preceding paper. The solid lines are the cross sections calculated from the parameters in Table I together with the modifications of δ_0 and δ_2^- discussed in the text. Vertical scale is in barns per steradian c.m.

figure is the S wave phase shift calculated from the parameters in Table I.

The final values of the parameters characteristic of the $(j=3/2, -)$ and the $(j=5/2, +)$ levels are listed in Table I and the cross section calculated from these values is shown by the solid lines in Figs. 2, 3, and 4. The calculated cross sections also include modifications in the values of δ_0 and δ_2^- to be discussed below. The points in these figures are the experimentally determined cross sections reported in the preceding paper.

As the figures show, the fit is quite good except at the largest scattering angle. In this curve discrepancies exist both below the first minimum and above the principal maximum of the 1.7-Mev anomaly. Investigation has shown that it is possible to reduce the disagreement at this scattering angle without seriously disturbing the fit elsewhere, but to do so would require a number of simultaneous readjustments of the S, P, and D waves. We believe that further work of this sort with the present data is not wortnwhile, mainly because the required readjustment in any one phase shift would apparently not amount to more than one or two degrees at any given energy. This being the case, little change would be introduced into the resonant energy (where the resonant part of the phase shift is equal to ninety degrees) or into the width of the level at half-maximum. Furthermore, the observed cross section almost certainly differs from the true cross section because of isotopic contamination. The $C^{13}(p,\gamma)N^{14}$ reaction has several resonances between 1.0 and 2.2 Mev,[6] some of them quite broad, which undoubtedly give rise to corresponding anomalies in the elastic scattering. If the maximum of any such anomaly is equal to or greater than one barn, and if it occurs at an energy where the $C^{12}(p,p)C^{12}$ cross section is low, then the resulting increase in the observed yield could easily amount to twenty percent or more. Thus, it is by no means certain that further refinement of the fit would result in any actual improvement in the accuracy of the values of the level parameters.

The discrepancy between the calculated and experimental cross sections happens to occur at 169.2 degrees rather than at some other angle because we worked mostly at the lower scattering angles while fitting the data over the region of the 1.7-Mev anomaly. As a result, the effects of errors both in the phase shifts and in the value of the experimental cross section would tend to accumulate at the unfitted scattering angle, 169.2 degrees.

This procedure of fitting at the lower angles was adopted because of certain properties of the incoherent scattering. As is clear from the expansion of $d\sigma/d\omega$,[2] the incoherent term (that is, the term beginning with the factor $\sin^2\theta/k^2$) involves only P and higher waves, is increasingly important for scattering angles nearer ninety degrees, and makes its principal contribution when $|\delta_l^+ - \delta_l^-| \sim \pi/2$. Thus, over the maximum of the 1.7-Mev anomaly, which is due to resonances in the $P_{\frac{1}{2}}$ and $D_{\frac{3}{2}}$ waves, the value of the cross section at angles near ninety degrees is relatively more sensitive to small changes in δ_1^+ and δ_2^+. This increased sensitivity results because these phase shifts, together with δ_1^- and δ_2^-, affect both the coherent and incoherent parts of the scattering while the Rutherford and S wave effects are confined to the coherent part.

The S wave phase shift as calculated from the parameters given in Table I does not permit an acceptable fit of the experimental data above 1.4 Mev. Trial and error readjustments of δ_0 showed that a positive increment varying linearly with energy from 0° at 1.2 Mev to 8° at 3.6 Mev added to the calculated S wave phase shift was satisfactory. The fit is further improved by setting δ_2^- equal to zero over all energies up to 3.6 Mev. The value of this latter phase shift, calculated from the expression $\delta_2^- = -\arctan F_2/G_2|_a$ is about zero below 1.7 Mev and decreases to −5° at 3.6 Mev. The calculated cross sections shown in the figures include the just mentioned deviations of δ_0 and δ_2^- from the values given by the dispersion theory formula.

III. DISCUSSION

An interpretation of the results of analyses of this kind requires consideration of the assumptions entering the dispersion theory formalism.[7] The basic hypothesis upon which the theory rests is that the Hamiltonian for the scattering system is known for all space excepting a finite region within which the particles interact strongly. The treatment begins by surrounding this part of space with a closed surface which in practice is usually a sphere of radius a. In the present development of the theory, a must be large enough to permit description of the system outside the sphere by a single-particle Hamiltonian of known form but is otherwise arbitrary. As thus introduced, the radius a has no direct connection with the physical processes under study.

In order that the remainder of this discussion may be explicit, we shall assume that the formalism has been specialized for the elastic scattering of protons from spinless nuclei and that the single-particle wave functions in the outer region are expanded in spherical harmonics in the usual way.[3]

Since the Hamiltonian is known in the outer region, the wave functions are determined explicitly in this region except for an arbtrary phase shift $\delta_l^\pm$ in each radial component. The value of each of these phase shifts is fixed by the requirement that the external wave function join the internal wave function smoothly on the surface of the sphere which separates the inner and outer regions. However, no solution for the internal wave functions is practicably obtainable because of

[6] J. D. Seagrave, Phys. Rev. **85**, 197 (1952). Levels are reported at 1.16, 1.25, 1.76, and 2.10 Mev with widths of 6, 500, 2.1, and 45 kev, respectively.

[7] E. P. Wigner and L. Eisenbud, Phys. Rev. **72**, 29 (1947).

the complexity of the system. Consequently, the phase shifts must be determined experimentally and used to infer information about the internal wave functions. The value of dispersion theory lies in the fact that it provides relationships between the phase shifts of the external wave functions and certain constants E_λ and γ_λ characteristic of the internal wave functions χ_λ. In general, the number of χ_λ and, hence, the number of pairs of $(E_\lambda, \gamma_\lambda)$ associated with each phase shift is infinite. Hence, in its general form, the dispersion theory cannot be applied to any specific scattering process because knowledge of any phase shift $\delta_l^{\pm}$ over a finite energy range is insufficient to determine the infinite set of $(E_\lambda, \gamma_\lambda)$ pairs associated with it. Application of the theory to specific nuclear processes is possible only if there exists an energy range within which the number of $(E_\lambda, \gamma_\lambda)$ pairs appreciably affecting the value of $\delta_l^{\pm}$ is finite—and for practical purposes—small. Obviously the validity of this condition depends upon, among other things, the choice of a used to bound the interior region, because not only the values of E_λ and γ_λ but also the extent in energy of the influence of each such pair depends upon the magnitude of a. Usually, the larger the value of a, the greater the number of $(E_\lambda, \gamma_\lambda)$ pairs which must be introduced to explain the behavior of $\delta_l^{\pm}$.

The special form of dispersion theory used in this analysis is usually called the one-level approximation. This means that the expression for $\delta_l^{\pm}(E_\lambda, \gamma_\lambda)$ is derived on the assumption that not more than one energy level, and hence not more than one $(E_\lambda, \gamma_\lambda)$ pair affects the value of $\delta_l^{\pm}$ in the energy range under consideration. Whether this assumption is ever even approximately appropriate to the description of a scattering process is still debated, but if so, the most favorable circumstance is that the separation of successive levels of given parity and angular momentum in the compound nucleus be much larger than their widths both within and near the energy region under study. Whenever this condition holds, it is not unreasonable to suppose that only one level contributes to the phase shift at a given value of the bombarding energy.

This assumption, together with the requirements of continuity on the surface of the sphere separating the inner and outer regions, leads to the expression

$$\delta_l^{\pm}=\left[-\arctan\frac{F_l}{G_l}+\arctan\frac{k\gamma_\lambda^2/A_l^2}{E_\lambda+\Delta_\lambda-E}\right]_{r=a}$$

where F_l and G_l are the regular and irregular radial Coulomb wave functions, respectively, E_λ and γ_λ^2 are, respectively, the characteristic energy and reduced width of the level $k=p/\hbar$ in center-of-mass units,

$$\Delta_\lambda=\left[-\frac{k\gamma_\lambda^2}{\rho}\left(\frac{\rho}{A_l}\frac{dA_l}{d\rho}+l\right)\right]_{\rho=ka}$$

where $\rho=kr$, $A_l^2=F_l^2+G_l^2$, E is the bombarding energy of the incident particle.

From the above expression for $\delta_l^{\pm}$ it is at once clear that the non-Coulomb scattering has been mathematically divided into two parts. The first, represented by the term $[-\arctan(F_l/G_l)]_a$, happens to be mathematically equal to the phase shift which would be produced by a hard-sphere potential of range a. The second term may be called the resonant part of the phase shift since its principal contribution occurs in the vicinity of the energy $E_r=E_\lambda+\Delta_\lambda$.

Therefore, any cross section that can be fitted by the present formalism may be thought of as owing to three causes, namely: (a) a Coulomb potential Ze^2/r, (b) a hard sphere potential of range a, and (c) a resonant interaction characterized by the parameters E_λ and γ_λ. However crude this model may be, it at least has the advantage of providing a simple mental picture of the process and of permitting the cross section to be completely described over the observed energy range by $4x+1$ numerical constants, x being the number of energy levels present. These constants are E_λ, γ_λ, parity, and j for each level, and the parameter a.

The one-level approximation imposes restrictions upon the acceptable numerical values of a which do not appear in the general formulation of the theory. This situation arises from the fact that we have excluded the possibility of introducing an unlimited number of $(E_\lambda, \gamma_\lambda)$ pairs to account for the behavior of the phase shift. Since only one such pair is allowed, a reasonable fit can be achieved only for a limited range of a values. To illustrate the point, let us consider the phase shift shown in Fig. 1. This phase shift is a slowly and monotonically decreasing function of energy except for the rather rapid increase of about 180 degrees near 0.46 Mev. We will now show that the off-resonance behavior of the phase shift determines the appropriate value of a.

Since the term $-\arctan F/G$ decreases monotonically with increasing energy, the positive increase in the phase shift must be attributed to the resonant term, $\arctan(k\gamma_\lambda^2/A_l^2)/(E_\lambda+\Delta_\lambda-E)$. The value of this term depends upon E_λ, γ_λ, and also upon a which appears implicitly in the quantities Δ_λ and A_l^2. However, over the energy range of a narrow resonance, the values of Δ_λ and A_l^2 are practically independent of energy regardless of the value of a. Such being the case, it is obvious from the mathematical form of the resonant term, that E_λ is fixed by the value of the bombarding energy for which $\delta_l^{\pm}+\arctan(F_l/G_l)=90°$ and γ_λ is determined by the rapidity with which $\delta_l^{\pm}$ increases near this energy. Thus, the acceptable values of E_λ and γ_λ depend almost entirely upon the behavior of $\delta_l^{\pm}$ near resonance. Consequently these two parameters are not available for fitting the off-resonance behavior of the phase shift. Since the only other parameter at our disposal is a itself, it follows that, in the single level approximation, a becomes a measure of the strength of the off-resonant interaction between the target nucleus and the incident proton.

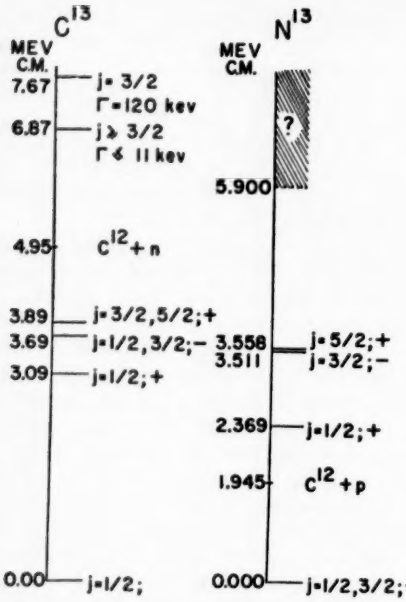

FIG. 5. Comparison of the energy levels in N^{13} and C^{13}. The characteristics of the first three levels in C^{13} were obtained by Rotblat from the $C^{12}(d,p)C^{13}$ stripping reaction. Those of the two highest levels were obtained by Bockelman *et al.* from the $C^{13}(n,n)C^{13}$ total cross section. The characteristics of the excited states in N^{13} are the results of the present analysis.

IV. CONCLUSION

The necessity for the alterations introduced into δ_0 and δ_2^- may be "accounted for" in a variety of ways, but since the alterations are positive and increase with energy, it is plausible to assume that they reflect the influence of higher resonances.‡ In the case of the S wave, any high energy resonance could be very broad because the barrier factor is relatively small. Consequently the low energy tail of any such resonance could be appreciable over an extensive range of energy.

On the basis of Mayer's hypotheses[8] a $(j=3/2,+)$ level is expected to lie a few Mev above the $(j=5/2,+)$ level. Although the position and width of this level are as yet unknown, reasonable estimates show that it is possible for its low energy effect to extend into the observed region and so give the required positive increment to δ_2^-.

The widths and resonant energies of the proposed levels as obtained from the present analysis agree satisfactorily with those found from the study of the $C^{12}(p,\gamma)N^{13}$ reaction. For the lower capture level, Fowler and Lauritsen[9] obtain the values $E_p=0.456\pm0.002$ Mev and $\Gamma=35$ kev. Our values are $E_p=0.461$ Mev and $\Gamma=34$ kev. Since the error in locating the resonant energy may easily be as much as 3 kev, the agreement is satisfactory.

For the upper capture level, Van Patter[10] obtains the values $E_p=1.697\pm0.012$ Mev and $\Gamma=74\pm9$ kev, while Seagrave[11] gets the values $E_p=1.698\pm0.005$ Mev and $\Gamma=70\pm10$ kev. These values of the resonant energy are in excellent agreement with our value of 1.698 Mev for the $(j=3/2,-)$ level. Our value for the width of this level is 60 kev. This value is somewhat smaller than those obtained from the $C^{12}(p,\gamma)N^{13}$ reaction, but because of the uncertainties both in our analysis and in the just-cited experimental results, the discrepancy is probably not significant. In any event, the inference is that the $(j=5/2,+)$ level makes relatively little, if any, contribution to the gamma-yield.

Figure 5 shows the known energy levels in N^{13} and C^{13} up to 8 Mev. In N^{13} the region above 5.9 Mev is unexplored. The parities and possible momentum values of the first three excited states in C^{13} are those obtained by Rotblat[12] from the $C^{12}(d,p)C^{13}$ stripping reaction. The values of the parameters of the two highest levels are those of Bockelman *et al.*[13]

As the figure shows, the parities and momenta of the corresponding levels agree in so far as they are known, thus lending support to the hypothesis of equal *nn* and *pp* forces.

The ratio $\mu a\gamma_\lambda^2/\hbar^2$ for a given level is usually regarded as a measure of the degree to which that level arises from the excitation of a single nucleon. Qualitatively, the numerical value of this ratio should be about one for single-particle levels, and much less for levels due to multiparticle excitation. As shown in Table I, the values of this ratio are 0.81, 0.047, and 0.31 for the $(j=1/2,+)$, $(j=3/2,-)$ and the $(j=5/2,+)$ levels in N^{13}, respectively. On the basis of these numbers, it is probable that the even parity levels arise from the excitation of the outer nucleon and the odd parity level involves excitation of the core.

The arguments concerning the uniqueness of the level assignment based on the analysis of the Goldhaber-Williamson data,[2] of course, remain valid. The fact that this level assignment also explains the behavior of the cross section as a function of the scattering angle is also strong evidence of its correctness.

‡ *Note added in proof.*—See discussion of T. Teichman and E. P. Wigner, Phys. Rev. **87**, 123 (1952).

[8] M. G. Mayer, Phys. Rev. **78**, 16 (1950).

[9] W. A. Fowler and C. C. Lauritsen, Phys. Rev. **76**, 314 (1949).

[10] D. M. Van Patter, Phys. Rev. **76**, 1264 (1949).

[11] J. D. Seagrave, Phys. Rev. **84**, 1219 (1951).

[12] J. Rotblat, Nature **167**, 1027 (1951), and Phys. Rev. **83**, 1271 (1951).

[13] Bockelman, Miller, Adair, and Barschall, Phys. Rev. **84**, 69 (1951).

Neutron Capture γ-Rays from Titanium, Chromium, Iron, Nickel, and Zinc

B. B. KINSEY AND G. A. BARTHOLOMEW
Physics Division, Atomic Energy of Canada, Limited, Chalk River, Ontario, Canada
(Received September 10, 1952)

The neutron capture γ-rays emitted by the even-charge elements, from titanium to zinc, have been investigated with the aid of a pair spectrometer.

Titanium emits a very simple spectrum. Two strong γ-rays, 6.756 ± 0.006 and 6.412 ± 0.006 Mev, are produced by capture in Ti^{48}. Neither the direct transition to the ground state of Ti^{49}, nor the transitions to the ground states of Ti^{48} and Ti^{50} were detected. From chromium the γ-rays corresponding to transitions to the ground state (9.716 ± 0.007 Mev) and to the first excited state (8.881 ± 0.007 Mev) of Cr^{54} are prominent and have intensities of 13 and 35 photons per 100 captures in Cr^{53}. The direct transition to the ground state of Cr^{51} was not detected. The iron spectrum is dominated by a strong γ-ray with the energy 7.639 ± 0.004 Mev resulting from neutron capture in Fe^{56}. This γ-ray is produced in the transition in Fe^{57} either to the ground state or to the excited state at 14 kev. Two weaker γ-rays with nearly equal energies close to 6 Mev are also produced in this isotope. The ground state γ-ray and the γ-rays leading to the first two excited states of Fe^{56} have been identified. Of these, the ground-state γ-ray (9.298 ± 0.007 Mev) is strong, about 50 photons per 100 captures in Fe^{54}. A part of the counting rate ascribed to this γ-ray, however, may be due to the γ-ray producing the first excited state of Fe^{58} in a direct transition. The ground state γ-ray in Fe^{58} (10.16 ± 0.04 Mev) accounts for about 5 percent of all captures by Fe^{57}. The nickel spectrum contains an intense γ-ray with an energy of 8.997 ± 0.005 Mev, which is produced in 50 percent of the captures in Ni^{58}. Another prominent γ-ray at 8.532 ± 0.008 Mev may represent the transition to the ground state in Ni^{61}; if so, it accounts for some 80 percent of captures in Ni^{60}. From considerations of intensity, five of the remaining nickel γ-rays can be ascribed to transitions to excited states in Ni^{59}. In the spectrum of zinc, few discrete γ-rays can be discerned above a background of unresolved radiations. Of these, a very strong γ-ray, with an energy to 7.876 ± 0.007 Mev, probably producing directly the ground state of Zn^{65}, is emitted in 40 percent of neutron captures by Zn^{64}.

INTRODUCTION

IN earlier communications,[1] we have reported investigations of the neutron capture γ-rays produced by various elements between beryllium and calcium. These measurements were made with the aid of a pair spectrometer. In this paper we describe the results obtained for the even-charge elements: titanium, chromium, iron, nickel, and zinc. The preliminary survey of the γ-ray spectra from these elements was made in 1949, and a few of these results have already been published.[2] Since that time the apparatus has been modified, and the spectra have been carefully remeasured. The coincidence counting rates have been increased, and this improvement has been used to obtain better resolution. The stability and control of the magnetic field has also been improved, and it has been possible to count coincidences automatically at a series of predetermined values of the magnetic field. The strength of the field, averaged over the orbits of the electron pairs, is known absolutely to 0.05 percent, while relative values are known to 0.002 percent.

Absolute measurements of the intensities of capture radiations were made by comparison with the 9.0-Mev capture γ-ray produced by nickel. In this method, as previously described,[1] use was made of a calculated curve for the variation of the peak coincidence counting efficiency with the energy. Previously published intensity measurements, however, were certainly too high in the 5-Mev region. In the present paper, the intensity measurements were made on the basis of a semi-empirical counting efficiency curve and are undoubtedly much more reliable. Full details of the derivation of this curve and of the method of energy measurement are given elsewhere.[3] Ignoring errors introduced by uncertainties in the values of the thermal neutron absorption cross sections, the intensity measurements from 3 to 5 Mev should not now be in error by more than 15 percent, and from 6 to 8 Mev, by not more than 10 percent. From 8 to 11 Mev, the counting efficiency is much more difficult to estimate, and at the latter energy, the error may be 30 percent.

In the present experimental arrangement, the sample to be studied is enclosed in an aluminum container fitted with Bakelite ends, and is located, as before, in a hole in the concrete radiation shield of the Chalk River pile. A bismuth block, about six inches in length, is placed between the sample and the reactor and prevents unwanted γ-radiation from entering the spectrometer. The center of the pair spectrometer is about fifteen feet from the sample, and two collimators ensure that any point on the radiator of the spectrometer is exposed only to radiations from the central part of the sample. Unwanted radiations produced by the aluminum container, or by the walls of the hole in the pile shield, are thereby eliminated. Those parts of the collimating system which are, of necessity, located in a strong neutron flux are made of bismuth which emits little capture radiation of its own; the remainder is made of lead.

In the absence of a sample, a low background of unresolved radiations is obtained on which is superposed a coincidence peak near 4 Mev, due to bismuth, and two low peaks at 7.3 and at 7.6 Mev, produced, respectively, by the capture radiations of lead and aluminum. Except in the case of materials of excep-

[1] Kinsey, Bartholomew, and Walker, Phys. Rev. **83**, 519 (1951); **85**, 1012 (1952); Can. J. Phys. **29**, 1 (1951).
[2] Kinsey, Bartholomew, and Walker, Phys. Rev. **78**, 481 (1950).
[3] B. B. Kinsey and G. A. Bartholomew, Can. J. Phys. (to be published).

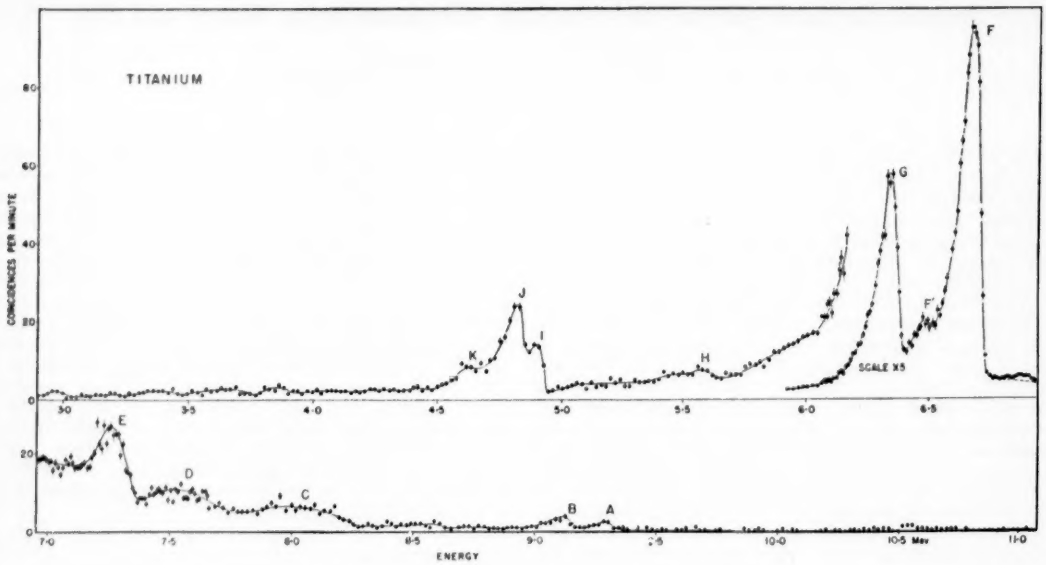

FIG. 1. Coincidence spectrum produced by titanium.

tionally low cross section, these background radiations are of little practical importance; after taking into account the absorption in the sample and in the materials between it and the spectrometer, suitable corrections can be applied to the coincidence spectrum.

The intensity of the fast neutrons in the γ-ray beam from the sample is reduced with a plate of polythene $\frac{3}{4}$ inch in thickness, and the slow neutrons are filtered out by a disk of similar size containing boron carbide. The absorption of the γ-rays, by these filters and the air, is about 10 percent at 4 Mev.

The present measurements were made with gold slits in front of the stilbene crystals used as detectors. The slits were 1 mm wide and 1.5 mm thick and about 23 cm apart. In these circumstances, for a homogeneous γ-ray, the width of a coincidence peak at half-maximum, hereafter called the line width, is about 100 kev at all energies. This slit width represents a satisfactory compromise between the higher counting rates with less resolution obtained with a wider slit, and the much lower counting rate with only slightly improved peak width obtained when the slits are made much narrower.

TABLE I. Energies and intensities of titanium γ-rays.

γ-ray	Energy in Mev	Intensity in photons per 100 captures in natural Ti	Probable origin
A	9.39 ±0.03	0.1	Ti^{48} ?
B	9.19 0.03	0.2	
C	8.27 0.02	0.4	
D	7.80 0.04	0.8	
E	7.38 0.01	1.5	Ti^{49}
F	6.756 0.006	53	Ti^{49}
F'	6.53 0.02	4	Ti^{49}
G	6.412 0.006	32	Ti^{49}
H	5.65 0.03	0.4	
I	4.96 0.01	3.5	Ti^{49}
J	4.88 0.01	5.0	Ti^{49}
K	4.67 0.03	1.4	

A tail, produced by the scattering of the pair components within the vacuum chamber, is observed beyond the upper end of each intense coincidence peak. At the point where the tail joins the upper edge of the peak, it is about 5 percent of the peak height; beyond that point, it rises to a maximum of about 6.5 percent and then falls slowly producing a spurious peak. This ghost peak is the result of scattering of the pair components from an aluminum frame in which the slits are recessed. It did not appear in the measurements made with the previous apparatus in which the slits were differently mounted. In the figures illustrating this paper, the spurious peaks are distinguished from the genuine peaks by a broken line, drawn beneath the experimental points (for example, see Fig. 9 near 9.2 Mev).

The method of correcting the coincidence pair spectrum to find the γ-ray spectrum has been described in other communications.[1,3] In Figs. 2, 5, 7, 10, and 12, the ordinates $\nu(E)$ of the corrected γ-ray spectra are given in absolute units, i.e., the number of photons emitted per unit energy range per capture. The height of a coincidence peak of unit intensity, i.e., one photon per capture, is equal to 6.7 Mev^{-1}.

TITANIUM

The coincidence pair spectrum from a sample of about 500 g of titanium dioxide is shown in Fig. 1. Except for the two very strong γ-rays *F* and *G*, few other γ-rays appear in the spectrum and the background of unresolved radiation at the lower energies is

low. The energies and intensities of the more intense resolved radiations are listed in Table I. The absolute intensities were determined by comparing the coincidence counting rate of the peak F with that of the 9.00-Mev nickel γ-ray, both γ-rays being emitted from an intimate mixture of titanium and nickel oxides in the ratio of roughly 5:1 by weight. The capture cross section of titanium for thermal neutrons was assumed to be 5.8 barns. The corrected γ-ray spectrum is shown in Fig. 2. This was obtained from the coincidence spectrum by correcting for γ-ray absorption in the titanium sample and in the neutron filters, and by correcting for the counting efficiency of the spectrometer as a function of the energy.

The abundances and the contributions to the total capture cross section of the separate titanium isotopes and the neutron binding energies of the product nuclei are listed in Table II. The neutron binding energies were calculated from recent mass values obtained by Collins, Nier, and Johnson,[4] and from measurements on the (d,p) reaction by Harvey[5] and by Pieper.[6] Of the five stable isotopes of titanium, it will be seen that only the first four, Ti^{46}, Ti^{47}, Ti^{48}, and Ti^{49}, contribute appreciably to the thermal neutron capture cross section of natural titanium. Of these isotopes, by far the greater part[7] of the capture cross section is due the more abundant isotope Ti^{48}.

An inspection of Table I and Fig. 1 will show that there is no distinct γ-ray corresponding to any of the neutron binding energies listed in Table II. We estimate that the direct transitions to the ground states of Ti^{48} and Ti^{50} produce γ-rays for which the intensities are less than 0.02 photon per 100 captures in natural titanium. Since Ti^{47} and Ti^{49} each contribute roughly 2 percent of the capture cross section of natural titanium, these ground state γ-rays are weaker than 1 photon per 100 captures in the separate isotopes.

TABLE II. Abundances, neutron capture cross sections, and neutron binding energies of titanium isotopes.

Isotope	Abundance percent	Contribution to cross section in percent	Neutron binding energy of product nucleus in Mev: From Harvey[c]	From Collins, Nier, and Johnson[d]	From Pieper[e]
Ti^{46}	8.0	0.8[a]	8.74±0.1	8.64±0.11	
Ti^{47}	7.8	2.1[a]	11.05±0.4	11.63±0.11	
Ti^{48}	73.4	95 [a]	8.15±0.05	7.99±0.08	8.04±0.05
Ti^{49}	5.5	1.6[a]		10.99±0.06	
Ti^{50}	5.3	0.2[b]			

[a] See reference 7.
[b] See reference 25.
[c] See reference 5.
[d] See reference 4.
[e] See reference 6.

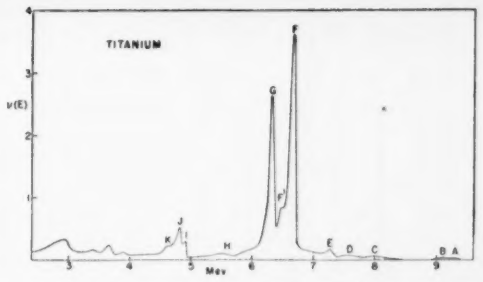

FIG. 2. Corrected γ-ray spectrum of titanium.

From Table II, it is clear that the neutron binding energy of Ti^{49} is close to 8.05 Mev. This energy lies near the middle of the broad peak C in Fig. 1, which clearly represents the contribution of several unresolved γ-rays. If the ground-state γ-ray in Ti^{49} is present, and there is no clear evidence in Fig. 1 for its existence, it must contribute a peak coincidence counting rate of less than 2 counts per minute, which corresponds to an intensity of less than 0.2 photons per 100 captures in Ti^{48}.

The main feature of the titanium spectrum is the presence of the two very strong γ-rays F and G, both of which must originate in Ti^{49}. Between them lies a small peak F', which, on account of its intensity, must also come from Ti^{49}. The γ-rays I and J, and probably also E and K, are produced by this isotope.

From a study of the (d,p) reaction, Pieper[6] has shown that excited states exist in Ti^{49} at 1.40, 1.74, 2.45, and 3.14 Mev. If the energies of the γ-rays F and G are added to the energies of the first two of these excited states, we obtain 8.16 and 8.15 Mev, respectively, in fair agreement with the neutron binding energies listed in Table II. It seems probable, therefore, that the γ-rays F and G derive from transitions to the first and second excited states of Ti^{49} found by Pieper (see Fig. 3). Transitions to the third excited state are not found. The group of γ-rays I, J, and K may originate in transitions to a group of levels near the fourth excited state at 3.14 Mev. The γ-rays E and F' have not been identified though their high intensities suggest that they are emitted by Ti^{49}. It is possible that they represent transitions to low-lying levels not detected in Pieper's experiments.

Two excited states in Ti^{48}, at 0.98 and at 2.31 Mev, are known from the decay[8] of Sc^{48} and V^{48}; these states have also been produced[9] in the reaction $Sc^{45}(\alpha,p)Ti^{48}$. Assuming that the neutron binding energy of Ti^{48} is 11.63±0.11 Mev (from Table II), γ-rays producing these states directly will have the energies 10.65±0.11 and 9.32±0.11 Mev. There is an indication in Fig. 1 of a γ-ray at an energy of about 10.6 Mev, although the statistics are not good enough to establish its existence

[4] Collins, Nier, and Johnson, Phys. Rev. **86**, 408 (1952).
[5] J. A. Harvey, Phys. Rev. **81**, 353 (1951).
[6] G. F. Pieper, Phys. Rev. **87**, 215 (1952).
[7] H. Pomerance, Phys. Rev. **88**, 412 (1952). We are indebted to Dr. Pomerance for the privilege of seeing his results before publication.
[8] W. C. Peacock and M. Deutsch, Phys. Rev. **69**, 306 (1946); also C. T. Hibdon and M. L. Pool, Phys. Rev. **67**, 313 (1945); C. E. Mandeville, Phys. Rev. **64**, 147 (1943).
[9] E. Pollard, Phys. Rev. **54**, 411 (1938).

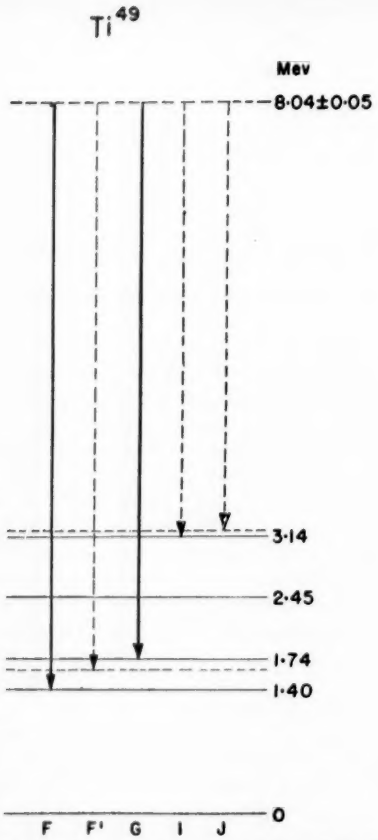

FIG. 3. Decay scheme for the capture γ-rays from Ti^{49}. The level energies are those obtained by Pieper.[6] Other possible levels, inferred from the capture γ-ray spectrum, are indicated by broken horizontal lines.

with certainty. Probably one of the γ-rays *A* or *B*, represents a transition to the second of these two states. There is little doubt that these weak γ-rays are produced by titanium, for a spectrographic analysis of the sample material revealed no impurities in sufficient concentration to account for the weak radiations with energies about 7.5 Mev.

The γ-rays which contribute to the broad peak at *C* have not been identified. Some of the γ-rays in Fig. 1 must be produced by capture in Ti^{49}, but no details of the positions of the excited states in Ti^{50} have been published, and such radiations therefore cannot be distinguished.

CHROMIUM

The sample consisted of about a kilogram of chemically pure chromic oxide. The coincidence spectrum of the neutron capture γ-rays is shown in Fig. 4, and the energies and intensities are listed in Table III. In previous measurements, no chromium γ-rays were detected between the energy of peak *A* and 12.4 Mev. Since the peak *B* in the chromium spectrum overlaps that produced by the 9.00-Mev nickel γ-ray, the absolute intensities of the chromium γ-rays were measured by comparing the peak coincidence counting rate of the γ-ray *B* with that of the 9.30-Mev γ-ray *B* of the iron spectrum, using an equal mixture of Cr_2O_3 and Fe_2O_3. The chromium capture cross section was assumed to be 2.90 barns. The corrected chromium spectrum is shown in Fig. 5.

Natural chromium possesses four stable isotopes, Cr^{50}, Cr^{52}, Cr^{53}, and Cr^{54}, of which only the first three contribute appreciably to the thermal neutron capture cross section in the natural element. The abundances and the contributions of the various isotopes to the cross section,[10] together with the neutron binding energies of the product nuclei are given in Table IV.

The neutron binding energy of Cr^{51}, obtained from the *Q* of the reaction[11] $V^{51}(p,n)Cr^{51}$, is 9.07 ± 0.09 Mev. This value can be checked by subtracting the neutron binding energy of Cr^{52} from the sum of the binding energies (21.4 Mev) of two neutrons in Cr^{52} obtained from the mass measurements.[4] For the former, Sher, Halpern, and Mann,[12] find 11.80 ± 0.25 Mev. A more accurate value can be deduced from the *Q* of the reaction, $V^{51}(p,n)Cr^{51}$; the neutron binding energy[5] of V^{52}, 7.3 Mev; and the energy[13] of the decay of V^{52}, 4.2 Mev. The value obtained is 12.2 ± 0.1 Mev. When this is subtracted from the binding energy of two neutrons in Cr^{52}, the neutron binding energy of Cr^{51} is found to be 9.2 ± 0.2 Mev.

The neutron binding energies of Cr^{53} and Cr^{54}, given in Table IV, were calculated from the mass measurements. Since the activity of Cr^{55} has not been identified with certainty, its binding energy cannot be calculated;

TABLE III. Energies and intensities of chromium γ-rays.

γ-ray	Energy in Mev	Intensity in photons per 100 captures in natural Cr	Probable origin
A	9.716 ± 0.007	7	Cr^{54}
B	8.881 0.007	19	Cr^{54}
C	8.499 0.007	7	
D	7.929 0.008	8	
D'	7.67 0.02	0.2	
E	7.54 0.02	0.2	
F	7.364 0.007	3	
F'	7.21 0.02	0.2	
G	7.097 0.006	2.6	
H	6.872 0.008	0.6	
I	6.644 0.006	3.0	
J	6.358 0.007	0.3	
K	6.26 0.02	0.9	
L	6.12 0.01	0.7	
M	6.00 0.01	1	
N	5.61 0.01	2	
O	5.26 0.02	1	
P	4.83 0.01	0.6	
Q	3.72 0.02	0.5	

[10] H. Pomerance, Phys. Rev. **76**, 195 (1949).
[11] R. V. Smith and H. T. Richards, Phys. Rev. **74**, 1257 (1948).
[12] Sher, Halpern, and Mann, Phys. Rev. **84**, 387 (1951).
[13] R. Bouchez and G. A. Renard, J. phys. et radium **8**, 289 (1947).

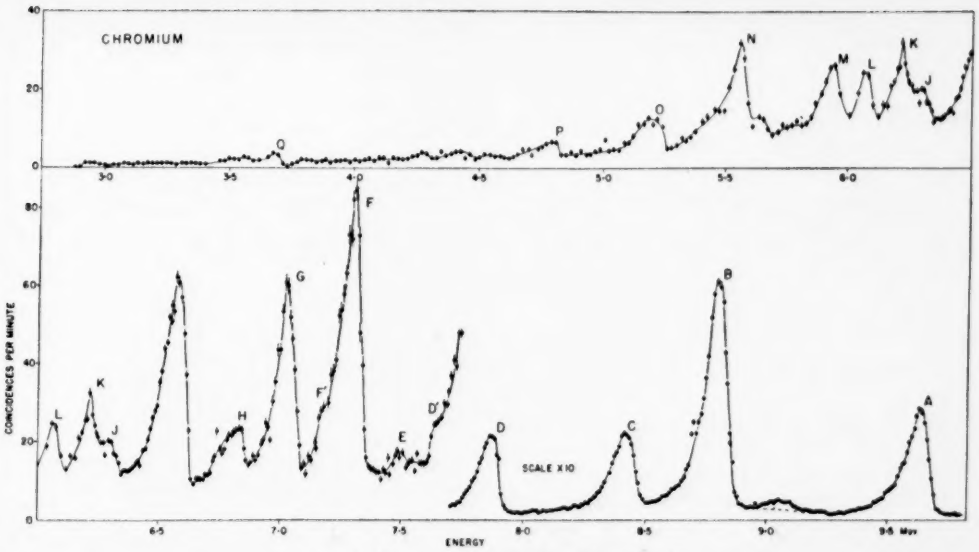

FIG. 4. Coincidence spectrum produced by chromium.

however, this binding energy is not relevant to the present work, for the contribution of that isotope to the cross section of natural chromium is negligible.

The energy of the γ-ray *A* is very close to that of the neutron binding energy of Cr^{54}. The difference between the energies of the γ-rays *A* and *B* is 0.835±0.005 Mev. The error in this difference is smaller than the error in either γ-ray measurement, because it depends only on the statistical errors, the systematic errors in the measurement of the magnetic field disappearing in the difference. This difference is in excellent agreement with the energy of the γ-ray produced in the decay of Mn^{54}, which is 0.835±0.015 Mev, according to Deutsch and Elliott.[14] We conclude that the γ-ray *A* is emitted in the direct transition to the ground state of Cr^{54} and that the γ-ray *B* is emitted in the transition to the first excited state. Both *A* and *B* are very strong γ-rays, and together account for half of the captures in Cr^{53}. No other excited states of Cr^{54} are known, and it is not possible, therefore, to identify any other γ-rays in Fig. 4 with capture in Cr^{53}.

It can be seen from Fig. 4 that a 9.1-Mev γ-ray, corresponding to the ground-state transition in Cr^{51}, would be superposed on the spurious peak caused by the γ-ray *B*. There is no evidence for such a γ-ray at this energy, and if it exists, its intensity is less than one photon per 100 captures in Cr^{50}. The positions of four excited states in Cr^{51} have been determined by Stelson, Preston, and Goodman[15] in their study of the neutron energies of the reaction $V^{51}(p,n)Cr^{51}$. If the neutron binding energy of Cr^{51} is assumed to be 9.07±0.09 Mev, it follows that the γ-rays producing these states in direct transitions should have energies of 8.29±0.11, 7.90±0.11, 7.65±0.13, and 7.54±0.13 Mev. From Table III it will be seen that these energies are in rather good agreement with the energies of the γ-rays *C*, *D*, *D'*, and *E*. If this identification is correct, then the intensities of the γ-rays *C* and *D* are both about 30 photons per 100 captures in Cr^{50}. Now the neutron binding energy of Cr^{53} is 7.76±0.11 Mev; with an equal validity, therefore, it is possible to identify one or the other of the γ-rays *D* or *D'* with the ground-state transition in that isotope. It is clear that much more accurate measurements on the neutron binding energies and on the level energies of the chromium isotopes are

TABLE IV. Abundances, neutron capture cross sections, and neutron binding energies of the chromium isotopes.

Isotope	Abundance percent	Contribution to cross section in percent[a]	Neutron binding energy of product nucleus in Mev
Cr^{50}	4.4	24.5	9.07±0.09
Cr^{52}	83.7	20.5	7.76±0.11[b]
Cr^{53}	9.5	55	9.70±0.20[b]
Cr^{54}	2.4		

[a] See reference 10.
[b] See reference 4.

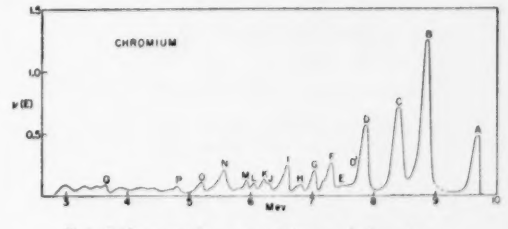

FIG. 5. Corrected γ-ray spectrum of chromium.

[14] M. Deutsch and L. G. Elliott, Phys. Rev. **65**, 211 (1944).

[15] Stelson, Preston, and Goodman, Phys. Rev. **80**, 287 (1950).

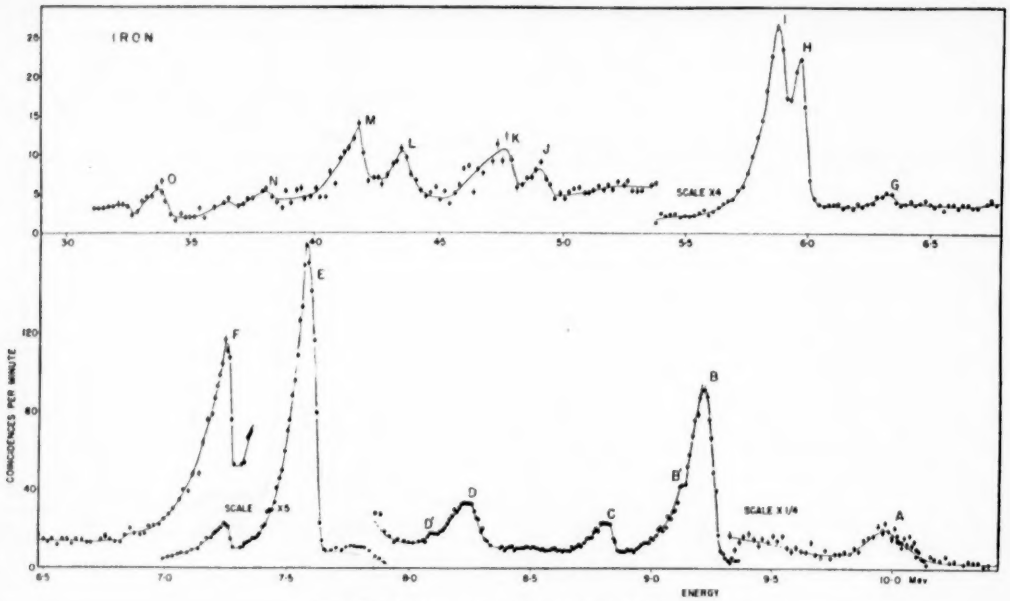

FIG. 6. Coincidence spectrum produced by iron.

required before these radiations can be identified with certainty.*

IRON

The coincidence spectrum of the neutron capture γ-rays from a very pure sample of metallic iron[16] are shown in Fig. 6, and the energies and intensities of individual γ-rays are listed in Table V. The absolute intensities were measured by a comparison of the counting rates of the 7.64-Mev γ-ray (peak *E*) and the 8.53-Mev γ-ray of nickel in a mixture of iron and nickel oxides. This procedure was chosen because the 9.00-Mev nickel γ-ray which is usually used for comparison has an energy too close to that of the 9.30-Mev iron γ-ray (peak *B*). The 8.53-Mev nickel γ-ray, however, lies between two peaks in the iron spectrum, and only small corrections need to be applied to allow for the contribution of the spectrum of the one element to the counting rate produced by the other. The capture cross section of iron was assumed to be 2.43 barns. The corrected γ-ray spectrum is shown in Fig. 7.

TABLE V. Energies and intensities of iron γ-rays.

γ-ray	Energy in Mev	Intensity in photons per 100 captures in natural iron	Probable origin
A	10.16 ±0.04	0.1	Fe^{58}
B	9.298 0.007	2.7	Fe^{58}, Fe^{56}
C	8.872 0.010	0.5	Fe^{55}
D	8.345 0.011	0.8	Fe^{55}
E	7.639 0.004	36	Fe^{57}
F	7.285 0.009	3.5	Fe^{57}
G	6.369 0.009	0.4	
H	6.015 0.007	5.6	Fe^{57}
I	5.914 0.010	5.2	Fe^{57}
J	4.968 0.011	0.5	
K	4.81 0.02	1	
L	4.44 0.03	1	
M	4.21 0.03	2	
N	3.86 0.05	0.5	
O	3.43 0.03	2.0	

Iron has four stable isotopes, Fe^{54}, Fe^{56}, Fe^{57}, and Fe^{58}. The abundances, the contributions[7] to the total thermal neutron capture cross section, and the neutron binding energies are listed in Table VI. The greater part of the neutron capture cross section of natural iron is due to Fe^{56}, and therefore the stronger γ-rays in the iron spectrum can be ascribed to capture by that isotope.

The dominant features of the coincidence spectrum are the very strong peak *E*, and the weaker, but higher energy, peak *B*. The energy of the γ-ray *E* (7.639±0.004 Mev) is in very good agreement with the neutron binding energy deduced from the *Q* value of the stronger of the two high energy groups of protons found by Harvey[5] in the (d,p) reaction. The *Q* values of these two groups are 5.42 and 7.11 Mev. The intensity of the stronger shows that it is derived from Fe^{56}, and therefore the neutron binding energy of Fe^{57} is 7.65±0.10 Mev, in agreement with the energy of the γ-ray *E*.

* *Note added in proof:* McFarland, Bretscher, and Shull [Bull. Am. Phys. Soc., **27** (No. 5) 7 (1952)] have reported measurements on the $Cr^{50}(d,p)Cr^{51}$ reaction, from which it follows that the energies of the γ-rays leading to the ground state and to the first excited state of Cr^{51} are 7.93 and 7.39 Mev, respectively, in good agreement with the energies of the γ-rays *D* and *F*.

[16] We are indebted to the Division of Physical Metallurgy, Department of Mines and Technical Surveys, Ottawa, for the provision of this sample.

Harvey has shown that the weaker group of protons corresponds to the production of Fe^{55} in its ground state and that the neutron binding energy obtained (9.34 ±0.05 Mev) is consistent with the neutron binding energy of that nucleus deduced from disintegration data. It is also consistent with the value 9.24±0.10 Mev deduced from mass measurements[4] and the Q of the $Mn^{55}(p,n)Fe^{55}$ reaction.[17] These results are in good agreement with the energy of the γ-ray B, which, we conclude, represents the direct transition to the ground state of Fe^{55}.

The γ-rays with energies above that of E must be due to capture in Fe^{54} or Fe^{57}, because the highest energy produced by capture in Fe^{56} is that of the γ-ray E, and the energy produced by capture in the heavier even isotope Fe^{58} must be lower. The weak γ-rays, C and D, correspond to transitions to the first and second excited states of Fe^{55} (see Fig. 8). This can be seen from Table VII. The first column contains the positions of the excited states of Fe^{55} found by Stelson and Preston[17] from a measurement of the energies of the neutrons

TABLE VI. Abundances, neutron capture cross sections, and neutron binding energies of the iron isotopes.

Isotope	Abundance percent	Contribution to cross section in percent	Neutron binding energy of product nucleus in Mev	
Fe^{54}	5.9	5.1[a]	9.34±0.05[b]	9.24±0.10[a,d]
Fe^{56}	91.6	92 [e]	7.65 0.10[b]	7.62 0.13[e]
Fe^{57}	2.2	2.0[a]		9.8 0.4[e]
Fe^{58}	0.3	0.5[e]		

[a] See reference 7.
[b] See reference 5.
[c] See reference 4.
[d] See reference 17.
[e] See reference 25.

in the $Mn^{55}(p,n)Fe^{55}$ reaction; the second column contains the position of the excited states found by Deutsch and Hedgran[18] from the study of the decay of Co^{55}; and the third column, the differences in the energies of neutron capture γ-rays. The errors in these energy differences are the root mean square values of the sums of the statistical errors of measurement; as in the case of the two most energetic chromium γ-rays, the systematic errors are approximately the same for each γ-ray and disappear in their differences. For the first two excited states, there is quite close agreement between the energies obtained by the different measurements. The third excited state of Fe^{55} near 1.4 Mev, which, according to the neutron measurements, may consist of two or more closely spaced levels, could be excited directly by a γ-ray with an energy of about 7.94 Mev. This energy lies near the upper end of the scattering tail of the peak E, and consequently, the detection of a weak γ-ray in this position is difficult. If this γ-ray is present, the counting rate produced by it must be less than 5 counts per minute, which at this

[17] P. H. Stelson and W. M. Preston, Phys. Rev. **82**, 655 (1951).
[18] M. Deutsch and A. Hedgran, Phys. Rev. **75**, 1443 (1949).

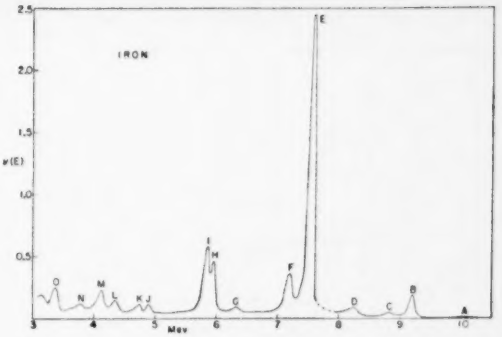

FIG. 7. Corrected γ-ray spectrum of iron.

energy, is equivalent to an intensity of less than 4 photons per 100 captures in Fe^{54}. The energy of the γ-ray F is equal to that expected from a transition to the fourth excited state of Fe^{55} at 2.08 Mev. The intensity of this γ-ray, however, would seem to be rather high; a more probable alternative explanation of F is given below.

We return to a consideration of peak B. The sum of the intensities of B, C, and D together corresponds to about 80 percent of the neutron capture rate in Fe^{54}. If the peak B is produced only by the direct transition to the ground state in Fe^{55}, it occurs very frequently, *viz.*, in about 50 percent of all captures in Fe^{54}. This intensity, however, is an upper limit, for it will be shown below that the peak B may contain a contribution from Fe^{58}.

The γ-ray responsible for the bump B' has an energy about 100 kev less than that of B and cannot be interpreted as the transition to the ground state in Fe^{55} in view of the good agreement in the energy differences obtained with the γ-ray B in Table VII. It will also be shown below that B' cannot be produced in Fe^{58}. We conclude that B' indicates the presence of a low-lying excited state in Fe^{55}, possibly connected with the emission of the 95-kev radiation observed by Deutsch and Hedgran[18] in the decay of Co^{55}.

Excited states are known[18,19] to exist in Fe^{57} at 0.014 Mev and at 0.131 Mev. Although the energy of the γ-ray E is in agreement with that deduced from the strong proton group found by Harvey in the (d,p) reaction, it is not clear from the present measurements

TABLE VII. Excited states of Fe^{55}.

From Stelson and Preston[a] in Mev	From Deutsch and Hedgran[b] in Mev	γ-ray differences in Mev
0.42		B–C 0.425±0.009
0.94	0.935	B–D 0.953 0.011
1.36	1.41	γ-ray not detected
2.08		B–F 2.013±0.010

[a] See reference 17.
[b] See reference 18.

[19] L. G. Elliott and M. Deutsch, Phys. Rev. **64**, 321 (1943).

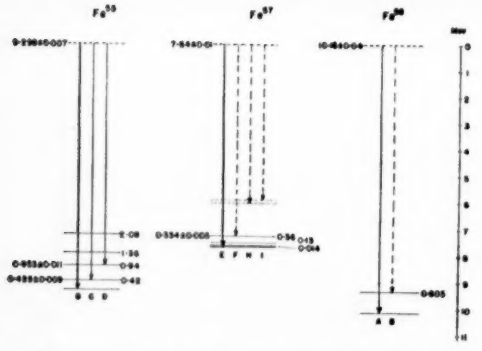

FIG. 8. Decay scheme for the capture γ-rays from Fe^{55}, Fe^{57}, and Fe^{58}. The level energies on the left are obtained from the γ-ray measurements, those on the right from the results of other authors (see text). Two levels, whose presence is inferred from the γ-ray spectrum, are shown in the level scheme of Fe^{57}.

whether E represents the direct transition to the ground state or the transition to the first excited state of Fe^{57}, for the line width used in the present measurements does not allow of the resolution of two γ-rays separated by only 14 kev. The proton group found by Harvey, however, is of exceptional width, and he has interpreted his results as showing the presence of an excited state at 0.36 Mev. This energy is equal to the difference between the energies of the γ-rays E and F, 0.354 ± 0.005 Mev, and the latter γ-ray, therefore, is very probably the direct transition to that excited state. A direct transition to the excited state at 0.131 Mev must be very infrequent by comparison with the intensity of the γ-ray E, for the width of peak E is normal and there is no evidence for the presence of any γ-ray between E and F.

The γ-rays producing the peaks at H and I in Fig. 6 are of such a strength that it is clear that they must both arise from the capture of neutrons in Fe^{56}. The transitions represented by these γ-rays and those of lower energy cannot be identified with certainty for no details of the positions of the higher excited states of Fe^{57} have yet been published. However, it is very probable that these γ-rays produce directly excited states at 1.73 and 1.62 Mev, respectively. Between the peaks H and F there is a continuous background part of which may be due to γ-rays emitted by highly excited states.

From the mass measurements, the neutron binding energy of Fe^{58} is found to be 9.8 ± 0.4 Mev. The energy of the γ-ray A, 10.16 ± 0.04 Mev, is in agreement with this value, and we identify this γ-ray, therefore, with the direct transition to the ground state in that nucleus. Its intensity, 0.10 photon per 100 captures, is equivalent to 5 photons per 100 captures in Fe^{57}.

An excited state is known[14] to exist in Fe^{58} at 0.805 ± 0.012 Mev; we should expect, therefore, to find a γ-ray corresponding to the direct transition to this state with an energy of 9.35 ± 0.04 Mev. From natural iron, such a γ-ray would be hard to distinguish from the γ-ray B, the ground state transition in Fe^{55}. The γ-ray B' cannot be confused with this transition for its energy is certainly too low.

Neutron capture in Fe^{58} accounts for only 0.5 percent of the total absorption cross section. The neutron binding energy of Fe^{59} may be calculated from the neutron binding energy[12] of Co^{59} and the decay energies[14] of Co^{58} and of[20] Fe^{59}. Assuming that the latter quantities are 2.30 and 1.56 Mev, respectively, the neutron binding energy of Fe^{59} is found to be 6.4 ± 0.2 Mev. Another value for the same quantity can be found from the masses of Fe^{58} and Ni^{58}, the neutron binding energy of Ni^{59} and the decay energy[21] of Ni^{59} and of Fe^{59}: it is 7.2 ± 0.4 Mev. These values are too inaccurate to permit the identification of any of the iron γ-rays with the ground state transition in Fe^{59}.

NICKEL

In the previous investigation of nickel, no γ-rays were detected between 9.0 and 14.0 Mev. Consequently, when studying the nickel spectrum again with the improved apparatus, we have only examined the spectrum from 3 to 9 Mev. The coincidence spectrum obtained from a kilogram of chemically pure Ni_2O_3 is shown in Fig. 9, the corrected spectrum in Fig. 10. Table VIII contains the energies and intensities of the γ-rays observed. The absolute intensities were obtained by comparison of the relative intensities with that of the 9.00-Mev γ-ray, for which the absolute intensity had been previously determined[3] by direct comparison with the 2.75-Mev γ-ray of Na^{24}. The intensities are based on capture cross sections of 0.54 and 4.80 barns for sodium and nickel, respectively. Below 5 Mev no distinct peaks can be detected on the continuous unresolved background. As in the iron spectrum, this background is low, the γ-rays in Table VIII accounting for some 75 percent of the total energy emitted.

TABLE VIII. Energies and intensities of nickel γ-rays.

γ-ray	Energy in Mev	Intensity in photons per 100 captures in natural nickel	Probable origin
A	8.997 ± 0.005	35	Ni^{59}
B	8.532 0.008	14	Ni^{61}
C	8.119 0.010	2.8	
D	7.817 0.008	6.5	Ni^{59}
E	7.528 0.011	4	Ni^{59}
F	7.22 0.02	0.5	
G	7.05 0.02	0.5	
H	6.839 0.010	9	Ni^{59}
I	6.58 0.02	2.0	
J	6.34 0.02	0.6	
K	6.10 0.02	1.0	
L	5.99 0.02	0.3	
M	5.82 0.02	3	Ni^{59} ?
N	5.70 0.02	0.4	
O	5.31 0.02	1	

[20] Deutsch, Downing, Elliott, Irvine, and Roberts, Phys. Rev. **62**, 3 (1942).
[21] J. J. G. McCue and W. M. Preston, Phys. Rev. **84**, 384 (1951).

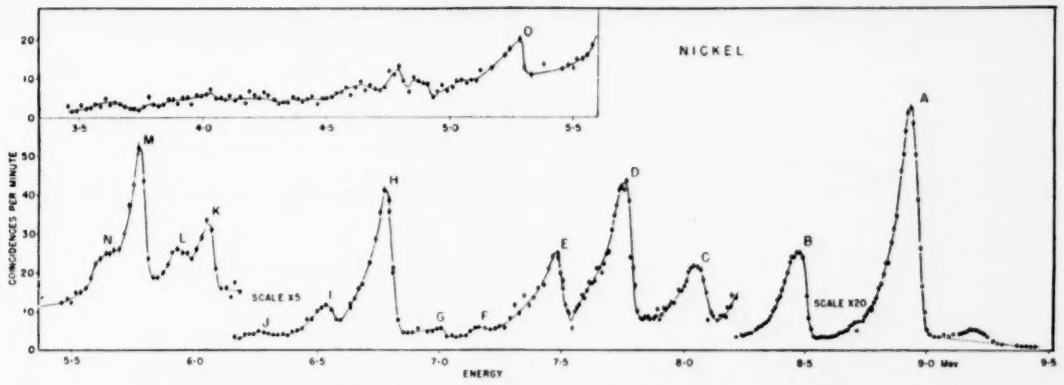

FIG. 9. Coincidence spectrum produced by nickel.

Nickel contains five isotopes of which only Ni^{58}, Ni^{60}, and Ni^{62} contribute appreciably to the cross section of the natural element. The abundances, the contributions to the thermal neutron capture cross section, and neutron binding energies are given in Table IX. The contributions to the cross section were calculated from the results obtained by Pomerance.[10]

The neutron binding energy of Ni^{59} may be deduced from Harvey's measurements[5] of the energy balance in the (d,p) reaction. The result obtained, 9.01 ± 0.10 Mev, is in good agreement with the energy of the γ-ray A. In the absence of any evidence of γ-radiation with energies above that of A, we conclude that this γ-ray represents the direct transition to the ground state in Ni^{59}. It is emitted in 50 percent of all captures in Ni^{58}. There is no evidence for a γ-ray leading to the first excited state[22] of Ni^{59} at 0.33 ± 0.05 Mev; if it is present, its intensity must be less than 0.5 photons per 100 captures in Ni^{59}.

The energy of the γ-ray B (8.532 ± 0.008 Mev) is close to the neutron binding energy of Ni^{61} deduced from the masses of Ni^{60} and Ni^{61} (see Table IX). This value, however, disagrees with the tentative binding energy (7.5 Mev) of Ni^{61} found by Sherd, Halpern, and Stephens.[12] In a previous communication, we have identified the γ-ray B with the ground-state transition in Ni^{61}. This identification would appear to be correct, for the energy of the γ-ray B is in agreement with the neutron binding energy of Ni^{61} deduced from the Q of the reaction $Ni^{60}(d,p)Ni^{61}$ recently measured by Hoesterey.[23] The γ-ray B, therefore, like A, is exceptionally strong, and is produced in about 80 percent of all neutron captures by Ni^{60}.

The γ-rays D, E, H, and I cannot be emitted by Ni^{62} or Ni^{65} since their intensities separately exceed the contributions of either Ni^{61} or Ni^{64} to the cross section of the natural element; they cannot be emitted by Ni^{63} since their energies exceed the neutron binding energy of that nucleus. Moreover, if the γ-ray B is indeed emitted by Ni^{61}, the combined intensity of the remaining Ni^{61} γ-rays is only about 2 photons per 100 captures. This difference, which may be in error by a factor of two, is equal to the intensity of the γ-ray I, but is less than that of D, E, or H. We conclude, therefore, that the γ-rays D, E, and H, and perhaps also the γ-ray I, are all emitted by Ni^{59}.† Together with the

TABLE IX. Abundances, neutron capture cross sections, and binding energies of nickel isotopes.

Isotope	Abundance percent	Contribution to cross section, in percent	Neutron binding energy of product nucleus in Mev
Ni^{58}	67.9	69 [a]	9.01 ± 0.10 [c]
Ni^{60}	26.2	16 [a]	8.31 0.34 [d]
Ni^{61}	1.2	0.5 [a]	10.46 0.23 [d]
Ni^{62}	3.7	13 [a]	6.0 0.1 [e]
Ni^{64}	1.0	0.4 [b]	5.5 0.1 [f]

[a] See reference 10.
[b] See reference 25.
[c] See reference 5.
[d] Deduced from the results of Collins, Nier, and Johnson, see reference 4.
[e] Deduced from mass measurements and the decay of Ni^{62} (0.05 Mev).
[f] Deduced from the mass measurements and the decay of Ni^{65} (2.1 Mev).

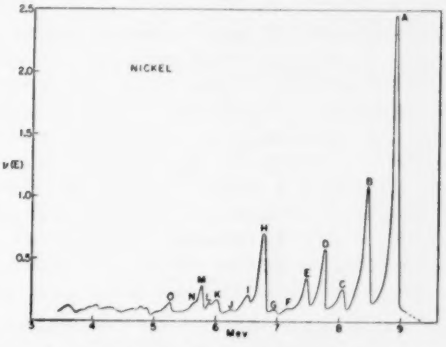

FIG. 10. Corrected γ-ray spectrum of nickel.

[22] P. H. Stelson and W. M. Preston, Phys. Rev. **86**, 807 (1952).

[23] D. C. Hoesterey, private communication.

† *Note added in proof.*—All of these assignments may be incorrect, for, according to McFarland, Bretscher, and Shull (see note added in proof, page 380), the first excited state of Ni^{59} is 0.42 Mev and the second at 3.08 Mev. These results suggest that

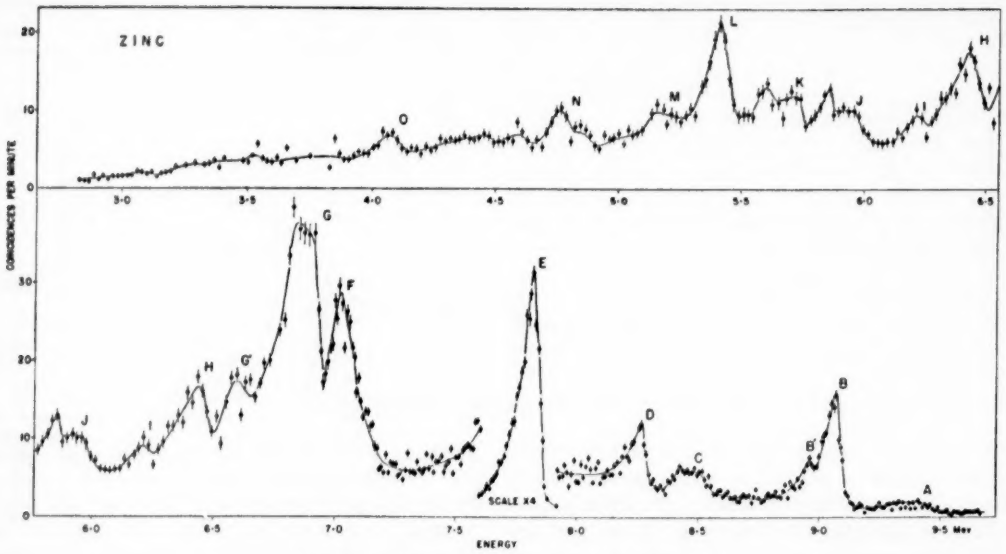

FIG. 11. Coincidence spectrum produced by zinc.

γ-ray A, these radiations then account for about 80 percent of the captures in Ni^{58}.

Three excited states are believed to exist[24] in Ni^{61} at the energies 0.655 ± 0.003, 0.939 ± 0.004, and 1.015 ± 0.004 Mev. Direct transitions to these states would produce γ-rays with the energies 7.877 ± 0.008, 7.593 ± 0.009, and 7.517 ± 0.009 Mev. Since the combined intensities of these γ-rays must be, at most, about two photons per 100 captures, they cannot be detected with certainty in the presence of the stronger radiations D and E.†

Because of the small contributions of both Ni^{61} and Ni^{64} to the thermal cross section, no radiations produced by capture in these isotopes can be identified.

ZINC

The γ-rays emitted from a sample of about 2 kg of very pure zinc metal[16] are shown in Fig. 11 and are listed in Table X. In the preliminary investigation, the γ-ray spectrum was explored to a maximum energy of 10 Mev, and, therefore, in the recent and more detailed investigation no attempt was made to search above the energy of the γ-ray A. Table X contains only the more prominent of the numerous γ-rays which make up the zinc spectrum. Of those coincidence peaks which cannot be resolved by the present instrument, e.g., C, F, G, etc., the energies listed in Table X are those of the components of highest energy. The absolute intensities were measured by comparing the counting rate of the peak E with the counting rates of the two nickel peaks A and B. A composite source was used, consisting of three similar zinc plates, about $\frac{1}{2}$ inch in thickness, each sandwiched between two sheets of nickel of 0.1 g per cm^2. The capture cross section of zinc was assumed to be 1.06 barns. The corrected γ-ray spectrum is shown in Fig. 12.

Zinc possesses five stable isotopes, of which only four contribute to the total thermal neutron cross section, that due to Zn^{70} being negligible. The abundances, the contributions to the thermal neutron capture cross section, and the neutron binding energies are listed in Table XI. The contributions to the cross section of Zn^{64} and Zn^{68} are known from activation experiments.[25] The separate contributions of Zn^{66} and Zn^{67} have not been measured. The neutron binding energy of Zn^{65} was calculated from the masses of Zn^{64}

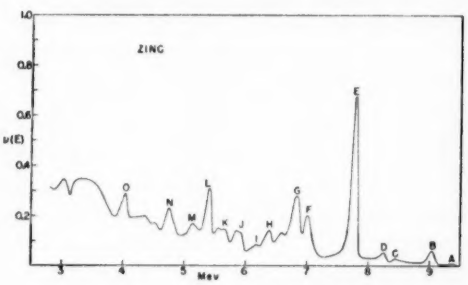

FIG. 12. Corrected γ-ray spectrum of zinc.

part, at least, of peak B (which, however, is of normal width) is caused by Ni^{59}. If this is the correct interpretation of B, it does not follow that the γ-rays D, E, H, and I, are produced by Ni^{59}. The peaks D and E could be produced by Ni^{61}, for it will be noted that the difference between the energies of these γ-rays is very close to the difference between the energies of the first and second excited states of Ni^{61} quoted above.

[24] Owen, Cook, and Owen, Phys. Rev. **78**, 686 (1950); Boehm, Blaser, Marmier, and Preiswerk, Phys. Rev. **77**, 295 (1950).

[25] Seren, Friedlander, and Turkel, Phys. Rev. **72**, 888 (1947).

and Cu^{65}, and the energy of the decay[26] of Zn^{65} (1.34 Mev). The result obtained (8.14±0.06 Mev) is in fair agreement with the value obtained by Harvey from the (d,p) reaction (7.92±0.05 Mev). The neutron binding energies of Zn^{67} and Zn^{68}, listed in Table X, were obtained from mass measurements. The neutron binding energy of Zn^{69} was obtained from the masses[4] of Zn^{68} and Zn^{70} and the (γ,n) threshold[27] of Zn^{70}, 9.20±0.20 Mev.

TABLE X. Energies and intensities of zinc γ-rays.

γ-ray	Energy in Mev	Intensity in photons per 100 captures in natural Zn	Probable origin
A	9.51 ±0.03	0.07	Zn^{68}
B	9.12 0.01	1	Zn^{68}
B′	8.98 0.01	0.2	Zn^{68}
C	8.58 0.03	0.2	Zn^{68}
D	8.31 0.02	0.6	Zn^{68}
E	7.876 0.007	10	Zn^{65}
F	7.19 0.03	2.0	
G	6.94 0.02	2.7	
G′	6.65 0.03	0.5	
H	6.49 0.02	1	
I	6.26 0.03	0.3	
J	6.03 0.02	0.8	
K	5.77 0.02	1	
L	5.48 0.02	2.5	
M	5.23 0.03	0.7	
N	4.84 0.04	1.6	
O	4.14 0.03	1.2	

The agreement between the energy of the γ-ray *E* and the neutron binding energy of Zn^{65} obtained by Harvey, suggests that this γ-ray is the product of the transition either to the ground state or to some low-lying state in that nucleus. If this identification is correct, the γ-ray is of exceptional strength, for it must be produced in 40 percent of all neutron captures in Zn^{64}. However, the possibility that this γ-ray is caused by capture by Zn^{67} is not excluded; capture by this isotope must be frequent, for the product nucleus Zn^{68} is certainly responsible for the emission of the γ-rays *A*, *B*, *B′*, *C*, and *D*.

[26] Mann, Rankin, and Daykin, Phys. Rev. **76**, 1719 (1949).
[27] Hanson, Duffield, Knight, Diven, and Palevsky, Phys. Rev. **76**, 578 (1949).

TABLE XI. Abundances, neutron capture cross sections, and neutron binding energies of zinc isotopes.

Isotope	Abundance percent	Contribution to cross section in percent	Neutron binding energy of product nucleus in Mev	
Zn^{64}	49	25[a]	7.92±0.05[b]	8.14±0.06[c]
Zn^{66}	27.8	52		7.49 0.08[c]
Zn^{67}	4.1			9.57 0.08[c]
Zn^{68}	18.6	23[a]		6.6 0.2[a,d]
Zn^{70}	0.6	0.05[e]		

[a] See reference 25.
[b] See reference 5.
[c] See reference 4.
[d] See reference 27.
[e] National Bureau of Standards Circular No. 499 (1950).

The existence of the γ-ray *A* with 9.51±0.03 Mev is indicated but not well established in Fig. 11. Its energy is equal to the calculated neutron binding energy of Zn^{68} and, therefore, may be produced in the transition to the ground state in that nucleus. The γ-rays *B*, *B′*, *C*, and *D* probably represent transitions to low-lying excited states in Zn^{68}.

Although the positions of some of the excited states of Zn^{67} are known from the decay of Ga^{67}, it is not possible to identify any of the γ-rays of Table X with transitions in this nucleus for most of the capture γ-rays are only partially resolved and their energies cannot be measured with sufficient precision. Similarly, none of the γ-rays in Zn^{69} due to capture by Zn^{68} can be identified.

Neutron Capture γ-Rays from Scandium, Vanadium, Manganese, Cobalt, and Copper

G. A. Bartholomew and B. B. Kinsey
Physics Division, Atomic Energy of Canada, Limited, Chalk River, Ontario, Canada
(Received September 10, 1952)

The neutron capture γ-ray spectrum from scandium consists of an exceptionally large number of γ-rays, and those of highest energy are only partially resolved when the line width in the coincidence spectrum is 130 kev. The γ-ray corresponding to the direct transition to the ground state in Sc^{46} (8.85±0.08 Mev), if correctly identified, has an intensity of 0.3 photon per 100 captures. Vanadium produces several strong γ-rays with intensities of about 10 photons per 100 captures. Of these, the γ-ray with the highest energy, 7.305±0.007 Mev, can be identified with the transition to the ground state of V^{52}. A group of partially resolved γ-rays with energies between 7.6 and 8.0 Mev are tentatively ascribed to capture in the rare isotope V^{50}. If this interpretation is correct, the isotopic capture cross section of V^{50} probably lies between 40 and 400 barns. The transition to the ground state in V^{51} was not detected. In manganese the transition to the ground state (7.261±0.006 Mev) is stronger than any other γ-ray in the spectrum (12 photons per 100 captures). With a line width of 100 kev it is only partially resolved from another strong γ-ray with an energy of 7.15±0.02 Mev. The remainder of the manganese spectrum is complex. From cobalt, about six γ-rays are produced each with intensities of the order of 5 photons per 100 captures. The γ-ray with the highest energy (7.486±0.006 Mev) may be identified with either the transition to the ground state or to the isomeric state at 59 kev. The copper spectrum is dominated by the strong γ-ray producing the ground state in Cu^{64}. Its energy is 7.914±0.006 Mev and its intensity is 24 photons per 100 captures in Cu^{63}. Another strong γ-ray at 7.634±0.006 Mev may be the transition to the ground state of Cu^{66}.

INTRODUCTION

PRELIMINARY pair spectrometer measurements of the neutron capture γ-rays produced by V, Mn, Co, and Cu were made in 1949, and some results have been published.[1] In the present paper we describe more detailed and more accurate measurements. The experimental conditions were similar to those for the measurement of the γ-ray spectra of the even-charge elements described in the preceding paper.[2] As before, we define the line width of the coincidence peak due to a homogeneous γ-ray as the width at half-maximum. The line width was 100 kev for all materials except scandium, for which it was 130 kev.

As in the preceding paper, the absolute intensities of the γ-rays (in photons per capture) were determined by the nickel comparison method. For this purpose we used thermal neutron capture cross sections and assumed that the effect caused by resonance capture was negligible. While this is certainly true for the even-charge elements, it may introduce an error in the case of manganese and cobalt, for it is well known that low-lying resonances can contribute to the activation cross sections of these elements.

To determine the resonance contribution to the capture γ-rays, we measured the intensity of the 7.261-Mev manganese γ-ray emitted by two equal (1 kg) samples of manganese dioxide, one of which was completely enclosed in a thick ($\frac{1}{16}$ in.) cadmium container. The contribution of cadmium radiation to the manganese peak was found from a measurement of the counting rate due to the 8.48-Mev cadmium γ-ray and the previously determined coincidence spectrum of that element. We found that the resonance capture effect was about one percent of that due to thermal

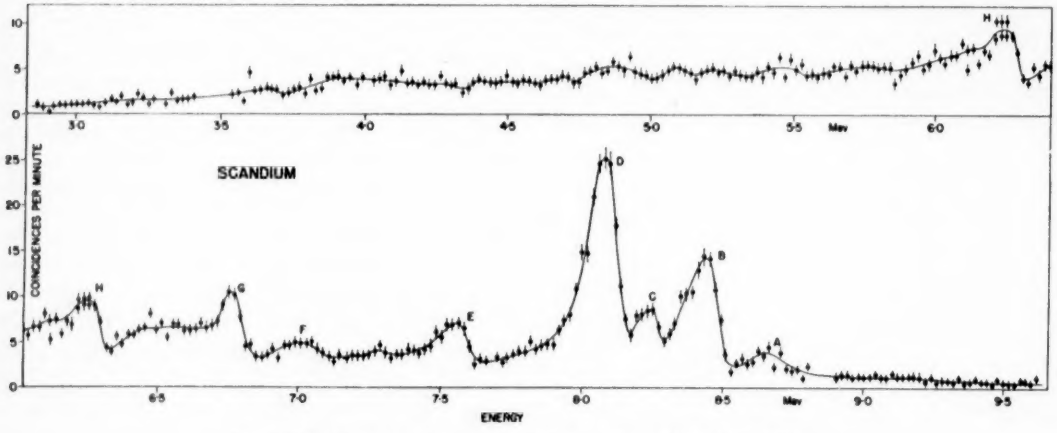

FIG. 1. Coincidence spectrum produced by scandium. Line width: 130 kev.

[1] Kinsey, Bartholomew, and Walker, Phys. Rev. 78, 481 (1950).
[2] B. B. Kinsey and G. A. Bartholomew, preceding paper [Phys. Rev. 88, 375 (1952)].

neutrons. Accordingly, we neglected this effect in the intensity measurements of both manganese and cobalt γ-rays.

SCANDIUM

Scandium has only the single stable isotope Sc^{45} and the capture γ-ray spectrum, therefore, is produced by Sc^{46}.

The scandium sample consisted of four grams of scandium oxide. Impurities capable of producing strong capture γ-rays, such as Al, Fe, and Mn, were present in quantities less than 0.02 percent by weight and hence could not contribute appreciably to the spectrum. Measurements were made from 2.9 Mev to 10 Mev. The results are shown in Fig. 1. There are no peaks in the coincidence spectrum below 6 Mev, and from 6 to 9 Mev a few peaks were observed, partially resolved or superposed on a continuous background.

The lack of structure shows that the level system of Sc^{46} must be exceptionally complicated. The absolute intensity of the γ-ray *D* was obtained by comparison[2] with that of the 9.00-Mev nickel γ-ray using a sample consisting of one gram of powdered Sc_2O_3 mixed with a plastic cement and sandwiched between two nickel sheets of the same area each of thickness of about 0.1 g per cm^2. The cross section of scandium was assumed to be 22 barns. This is the cross section for the production[3] of the 85-day activity of Sc^{46}, and also includes the cross section for the production of the 20-second isomeric state.[4] After correcting the coincidence spectrum (Fig. 1) for the sensitivity of the spectrometer and for the absorption of the radiations in the sample and in the neutron filters, the γ-ray spectrum shown in Fig. 2 was obtained. The ordinate scale in this figure represents the number of photons emitted per capture per unit energy range, and for the line width (130 kev) used in this experiment, a homogeneous γ-ray with an intensity of one photon per capture would produce a peak with a height of 5.6 Mev^{-1}. The energies and absolute intensities of the scandium γ-rays are given in Table I.

The complexity of the spectrum shown in Fig. 2 is remarkable in so light a nucleus. One might be tempted

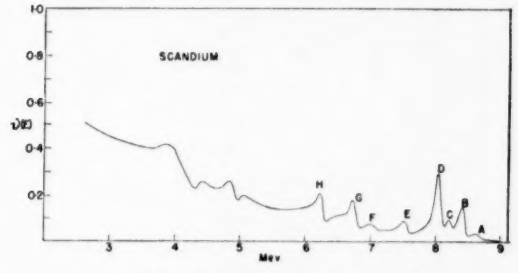

FIG. 2. Corrected γ-ray spectrum of scandium.

[3] Seren, Friedlander, and Turkel, Phys. Rev. **72**, 888 (1947).
[4] M. Goldhaber and C. O. Muehlhause, Phys. Rev. **74**, 1877 (1948).

TABLE I. Energies and intensities of scandium γ-rays.

γ-ray	Energy in Mev	Intensity in photons per 100 captures
A	8.85 ±0.08	0.3
B	8.539 0.010	2.5
C	8.31 0.02	1
D	8.175 0.011	5
E	7.65 0.03	1
F	7.15 0.04	0.7
G	6.84 0.02	2.5
H	6.35 0.01	2

to conclude that impurities of heavy elements not detected in the spectrographic analysis, have contributed to the results obtained. The only heavy elements which have sufficiently large cross sections to contribute are the rare earths, and of these,[5] gadolinium, which can be recognized by a prominent peak in the coincidence spectrum at 6.7 Mev, is the most important. A peak appears at *G* in Fig. 1, but if this were entirely due to gadolinium the coincidence spectrum at lower energies would be much more intense than that found, and therefore we estimate that gadolinium cannot contribute more than 10 percent to the neutron capture rate. Since that element will contribute the greater part of the neutron captures caused by any likely combination of rare earth impurities, we conclude that the complexity of the scandium spectrum is genuine.

None of the γ-rays listed in Table I can be identified with certainty. From the *Q* value (6.78 Mev) of the high energy proton group observed by Davidson in the $Sc^{45}(d,p)Sc^{46}$ reaction,[6] we find 9.0±0.1 Mev for the neutron binding energy of Sc^{46}. This result is in agreement with the value (8.90 Mev) calculated from the masses of Sc^{45} and Ti^{46} given by Collins, Nier, and Johnson[7,8] and the decay energy (2.37 Mev[9]) of Sc^{46}. Two excited states have been reported in Sc^{46}; one is an isomeric level at 0.17 Mev,[4] and the other, at 2.30 Mev, was found in a study of the $Sc^{45}(d,p)Sc^{46}$ reaction.[6] The energy of the γ-ray *A* in Table I is very close to the neutron binding energy of Sc^{46} and may represent the direct transition to the ground state. The difference between the energies of the γ-rays *A* and *B* (0.31±0.08 Mev) seems to be too great for the latter γ-ray to be identified with a transition to the isomeric state.

VANADIUM

Vanadium consists of two isotopes, V^{50} and V^{51}. The abundance of V^{50} is only 0.24 percent and its capture cross section is unknown.

The vanadium sample consisted of 300 grams of V_2O_5 powder enclosed in a Dural container with Bakelite ends. A sodium impurity was present in a concentration of 2 percent by weight, but it did not contribute a

[5] B. B. Kinsey and G. A. Bartholomew (to be published).
[6] W. L. Davidson, Phys. Rev. **56**, 1061 (1939).
[7] Collins, Nier, and Johnson, Phys. Rev. **83**, 228 (1951).
[8] Collins, Nier, and Johnson, Phys. Rev. **86**, 408 (1952).
[9] C. L. Peacock and R. G. Wilkinson, Phys. Rev. **74**, 297 (1948).

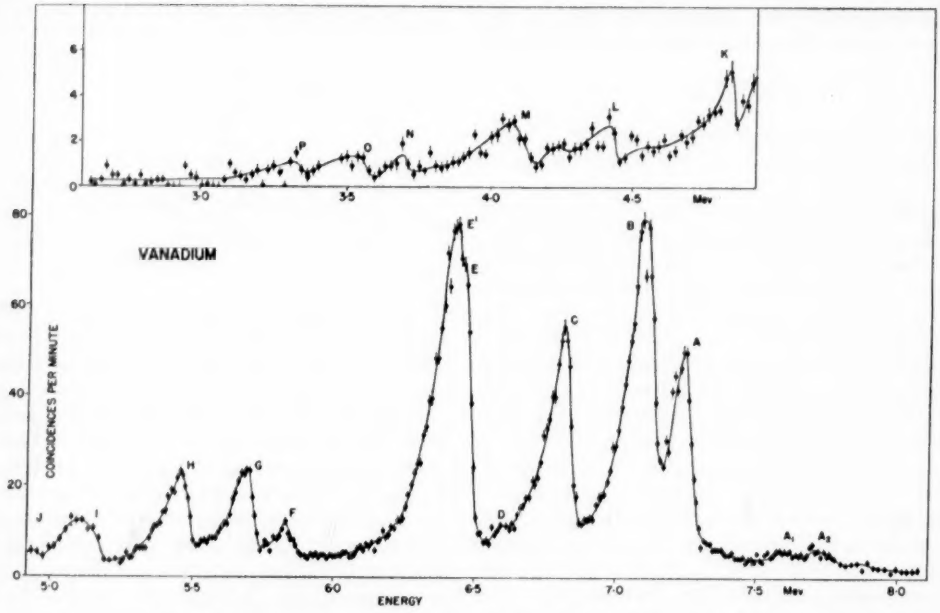

FIG. 3. Coincidence spectrum produced by vanadium. Line width: 100 kev.

detectable amount to the vanadium spectrum since its cross section is only one tenth of that of vanadium. Other impurities, such as Al, Si, Fe, and Pb, were each present in concentrations of about 0.02 percent, which are too low to produce capture radiation detectable in the presence of vanadium γ-rays.

The vanadium capture γ-rays were measured between 2.6 and 8.1 Mev. The coincidence spectrum is shown in Fig. 3. In earlier measurements, the spectrum was explored to an energy of 9.5 Mev with less resolution, and no γ-rays were found with energies above 7.3 Mev. Table II contains the energies and intensities of the vanadium capture γ-rays. The intensities were obtained by comparing the counting rates at the peak E' with that of the 9.00-Mev nickel γ-ray using a mixture of weighed amounts of Ni_2O_3 and V_2O_5, the cross section of vanadium being assumed to be 4.7 barns. The corrected γ-ray spectrum is shown in Fig. 4. In this figure, and in the corrected spectra for Mn, Co, and Cu, the peak height for a homogeneous γ-ray of unit intensity is 6.7 Mev^{-1}.

From the Q-value of the high energy proton group in the $V^{51}(d,p)V^{52}$ reaction, Harvey[10] obtained 7.25 $\pm$0.05 Mev for the neutron binding energy of V^{52}. This result is in agreement with the value (7.4$\pm$0.15 Mev) calculated from the masses of V^{51} and Cr^{52} given by Collins, Nier, and Johnson[5] and the decay energy (4.2$\pm$0.1 Mev[11]) of V^{52}. Both results are in agreement with the energy of the γ-ray A, 7.305$\pm$0.007 Mev, which we therefore identify with the direct transition to the ground state of V^{52}. Less satisfactory agreement is obtained if the work of Abramov[12] and of Davidson[6] is considered, both of whom used the (d,p) reaction. The former leads to a neutron binding energy of 7.66$\pm$0.15 Mev and the latter to a value of 10.0 Mev.

The energy levels of V^{52} were first investigated by Davidson,[6] who found levels at 2.47 and at 4.70 Mev. Because of the discrepancy between the Q values obtained by Davidson and by Harvey, the position of these energy levels is doubtful. A longer list of levels has been published by Abramov.[12] We have attempted

TABLE II. Energies and intensities of vanadium γ-rays.

γ-ray	Energy in Mev	Intensity in photons per 100 captures
A	7.305$\pm$0.007	11
B	7.154 0.008	18.5
C	6.868 0.008	14
D	6.62 0.02	0.7
E	6.508 0.006	25
F	5.879 0.015	3
G	5.744 0.008	9
H	5.511 0.008	10
I	5.21 0.01	6
J	4.98 0.02	2
K	4.85 0.02	2
L	4.45 0.02	3
M	4.15 0.03	4
N	3.73 0.03	3
O	3.59 0.02	3
P	3.36 0.02	2

[10] J. A. Harvey, Phys. Rev. **81**, 353 (1951).
[11] R. Bouchez and G. A. Renard, J. phys. et radium **8**, 289 (1947).
[12] A. Y. Abramov, Doklady Akad. Nauk. U.S.S.R. **73** (No. 5), 92 (1950).

to fit the capture γ-rays into the tentative decay scheme shown in Fig. 5, the position of Abramov's levels being shown on the right. Our level scheme was constructed on the assumption that the γ-ray A is the ground-state γ-ray and that strong high energy γ-rays are always emitted by the capturing state and do not occur as the result of the de-excitation of other high energy states. This assumption is justified by the experimental fact that the most frequent transitions are those producing low-lying excited states; however, it is perhaps unsafe to apply this rule to establish excited states much above 2 Mev.

We assume, therefore, that the γ-rays B and C produce states at 0.15±0.01 and 0.44±0.01 Mev, respectively. No levels at these energies were found by Abramov [although this is possibly not surprising in view of the relatively low yields of the long range proton groups produced in the (d,p) reaction], nor is there a γ-ray leading to an isomeric state at 0.25 Mev reported by Renard.[13]

The partly resolved peak E, E' has a width of about 150 kev at half-maximum. When analyzed, this complex peak may be shown to consist of two peaks differing in energy by 50 kev, each with intensities of about 14 photons per 100 captures. As will be seen in Fig. 5, emission of these γ-rays is assumed to create a pair of levels near 0.8 Mev. A level near this position has been found by Abramov.

The identity of the remaining γ-rays is more obscure. The levels corresponding to the strong γ-rays G, H, I, and K do not agree well with those found by Abramov. Other possible energy levels, produced by weaker radiations, are indicated by horizontal broken lines in Fig. 5. The sum of the energies of the γ-rays N and O add up to 7.32±0.03 Mev, in good agreement with that of the γ-ray A. This agreement suggests that the γ-rays N and O are in cascade, and the two possible configurations are shown in Fig. 5.

Two peaks appear in Fig. 3 corresponding to γ-ray energies above that of the γ-ray A which we have identified with the neutron binding energy of V^{52}. Their positions on the energy scale are such that they cannot be identified as ghost peaks produced by the scattering

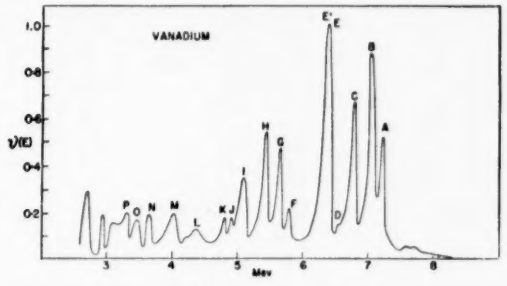

FIG. 4. Corrected γ-ray spectrum of vanadium.

[13] G. A. Renard, Ann. phys. 5, 385 (1950).

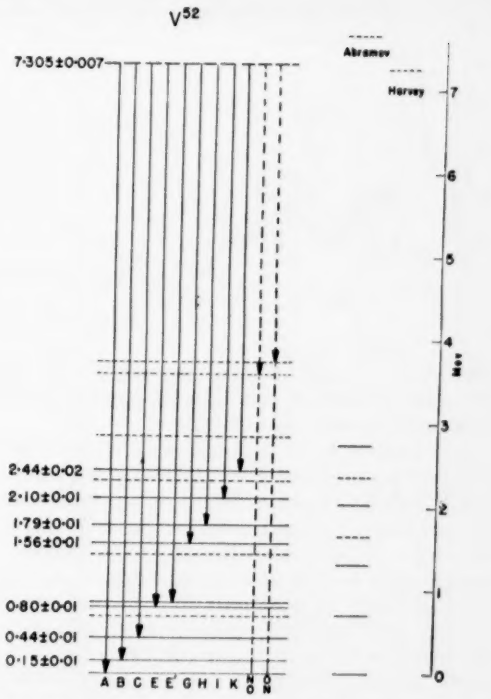

FIG. 5. Tentative decay scheme for the capture γ-rays from vanadium. The full horizontal lines represent levels whose existence is inferred from the strong γ-rays in the spectrum, the broken lines represent possible levels whose existence is suggested by weak γ-rays. The levels from the (d,p) reaction are shown on the right (see text).

effects which were described in the preceding paper. The peak counting rates are too great to be explained in terms of the background radiations of lead and of aluminum, which are known to be present and which produce coincidence peaks in a similar position. We therefore examined this region of the coincidence spectrum in greater detail, using a sample of vanadium oxide obtained from another source. A spectrographic analysis of the new sample material showed no trace of sodium, and only insignificant traces of other elements. In order to get more vanadium into the sample container, the oxide was melted and cast into disks of suitable size. With this sample measurements were made up to an energy of 11.2 Mev. The significant results obtained are shown in Fig. 6. The peaks A_1 and A_2 in Fig. 3, appear again in Fig. 6 in the same proportion to the peak A, which in this new sample has been increased by a factor of three. The proportional increase in the counting rate in A_1 and A_2 suggests that the γ-rays responsible for these peaks are due to vanadium. The expected ghost peaks produced by scattering from peaks A and B are now visible as a sudden change of slope on the upper edge of peak A. In addition, a peak A_3 appears on the high energy side of A_2. The energies and intensities of these γ-rays are listed in Table III.

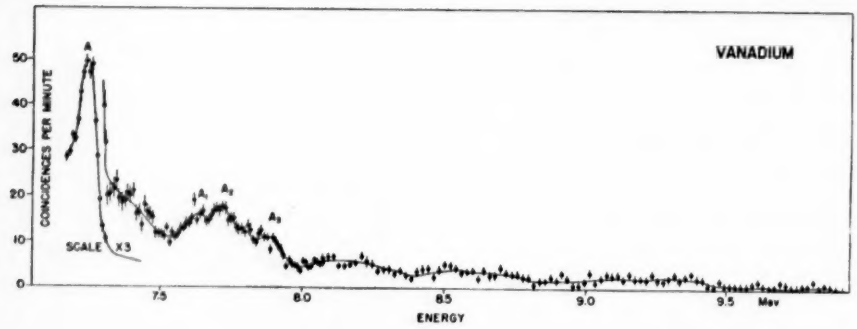

FIG. 6. Coincidence spectrum produced by higher energy vanadium γ-rays. Line width: 100 kev.

Beyond A_3, we find an undulating coincidence curve, with a few breaks in it, indicating the presence of γ-rays with energies extending to 9.5 Mev.

The most probable explanation of these γ-rays is that they are produced in V^{51}, following capture in the rare isotope V^{50}. If this is the correct explanation, the thermal neutron capture cross section of V^{50} must be very high. Since its abundance[14] is 0.24 percent, the capture cross section for the production of the γ-rays listed in Table III is at least 40 barns, and the total capture cross section is probably much higher. It is not likely to be higher than 400 barns because one would then expect to find a difference of more than 20 percent (which has not been detected) between the cross sections determined by activation and by pile oscillator methods.

Two determinations[15] of the (γ,n) threshold of V^{51} have been made giving neutron binding energies in V^{51} of 10.8 ± 0.5 Mev and 11.15 ± 0.2 Mev. From recent measurements of Johnson[16] the value 10.95 ± 0.11 Mev is obtained. No evidence was found for a γ-ray of energy corresponding to the transition to the ground state of V^{51} nor to any excited states up to 1.5 Mev. The intensity of the ground-state γ-ray must be less than 0.06 photon per 100 captures in natural vanadium.

MANGANESE

Manganese has only one stable isotope, Mn^{55}. The neutron capture γ-rays are therefore produced in the product nucleus Mn^{56}.

TABLE III. Energies and intensities of γ-rays probably due to V^{51}.

γ-ray	Energy in Mev	Intensity in photons per 100 captures in natural vanadium
A_1	7.67 ± 0.02	0.25
A_2	7.83 0.02	1.3
A_3	7.98 0.02	0.5

In the earlier measurements on the neutron capture γ-rays of manganese, a sample of metallic manganese was used and the spectrum was examined up to 9.1 Mev. No γ-rays were found above 7.25 Mev. In the more recent investigation, we examined the spectrum between 3.5 and 8.0 Mev emitted by a sample consisting of 1400 g of manganese dioxide. Spectrographic analysis showed that the amounts of other elements present were not sufficient to produce a detectable effect on the manganese spectrum. The coincidence spectrum is shown in Fig. 7.

The absolute intensities were determined from a comparison of the counting rate of the peak A with that of the 9.00 nickel γ-ray, using a sample containing a mixture of weighed amounts of manganese and nickel oxides. In this determination, the capture cross section of manganese was assumed to be 12.6 barns. The energies and intensities are listed in Table IV. The corrected γ-ray spectrum is shown in Fig. 8.

By other methods with less resolution, the manganese capture γ-rays have been studied by Pringle and Isford[17] and by Hamermesh.[18] The former authors report the presence of two prominent groups of radia-

TABLE IV. Energies and intensities of manganese γ-rays.

γ-ray	Energy in Mev	Intensity in photons per 100 captures
A	7.261 ± 0.006	12
B	7.15 0.02	4
C	7.048 0.008	6.5
D	6.779 0.008	2.5
E	6.43 0.01	0.5
F	6.11 0.01	1
G	5.91 0.02	0.5
H	5.77 0.01	1
I	5.63 0.02	0.3
J	5.528 0.010	4
K	5.21 0.01	3
L	5.04 0.02	6
M	4.81 0.01	2
N	4.72 0.02	2
O	4.55 0.01	2
P	4.24 0.01	2
P'	4.10 0.03	1
Q	3.82 0.02	1

[14] D. C. Hess and M. G. Inghram, Phys. Rev. **76**, 1717 (1949); W. Leland, Phys. Rev. **76**, 1722 (1949).
[15] Sher, Halpern, and Stephens, Phys. Rev. **81**, 159 (1951); Sher, Halpern, and Mann, Phys. Rev. **84**, 387 (1951).
[16] W. H. Johnson, Phys. Rev. **87**, 166 (1952).
[17] R. W. Pringle and G. Isford, Phys. Rev. **83**, 467 (1951).
[18] B. Hamermesh, Phys. Rev. **81**, 487 (1951).

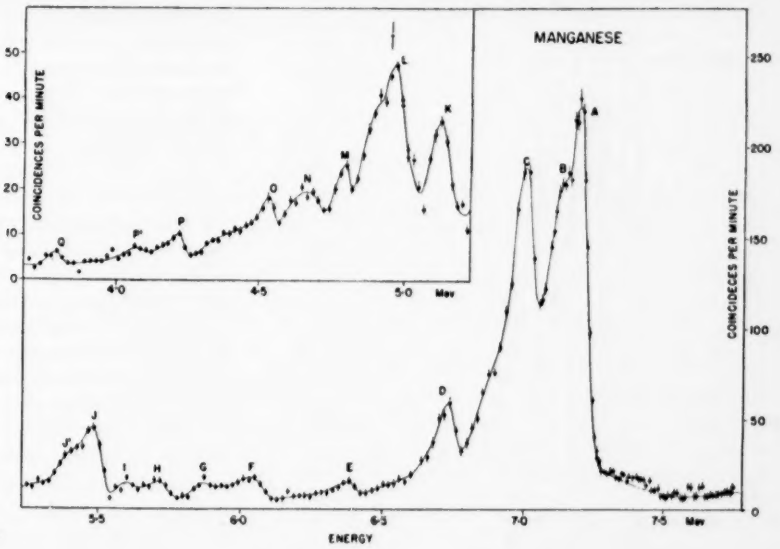

FIG. 7. Coincidence spectrum produced by manganese. Line width: 100 kev.

tions of comparable intensity, with energies of 5.32 ±0.05 and 7.16±0.05 Mev. Similar results were obtained by Hamermesh and Hummel.[19] These observations are in general agreement with the corrected spectrum of Fig. 8, which shows two groups of γ-rays near these energies.

The strong γ-ray *A* has an energy of 7.261±0.006 Mev. There would seem to be no doubt that this γ-ray represents the direct transition to the ground state in Mn^{56}, for its energy is in good agreement with the neutron binding energy determined from the highest *Q* value of the (d,p) reaction. A neutron binding energy of 6.99 Mev is obtained from the measurements of Martin,[20] 7.24 Mev from the more recent measurements of Whitehead and Heydenburg,[21] and 7.32±0.15 Mev from the measurements of Abramov.[12]

The energies of the known excited states in Mn^{56}, obtained from the $Mn^{55}(d,p)Mn^{56}$ reaction, are listed in Table V. With the aid of these results we have constructed the tentative decay scheme shown in Fig. 9, in which the levels from the (d,p) reaction are shown on the right and those inferred from the γ-ray measurements are shown on the left. The γ-rays *B*, *C*, and *D*, are not likely to be produced by transitions from highly excited states to the ground state, since it would be difficult to understand how the transitions producing these excited states could compete with the direct transition to the ground state. Accordingly, these γ-rays are assigned to transitions to three low-lying excited states hitherto undetected, at 0.11±0.02, 0.213±0.009, and at 0.482±0.009 Mev. The existence of the first of these, at least, is not inconsistent with the observations of Whitehead and Heydenburg, and of Martin, whose results showed an unusually broad proton group of highest energy.

The difference between the energies of the γ-rays *A* and *F* is 1.15±0.01 Mev, which corresponds to the energy of the lowest excited state observed by Martin and also that of Abramov. The strong γ-ray *J* is

TABLE V. Energy levels of Mn^{56} from the (d,p) reaction, in Mev.

Martin[a]	Whitehead and Heydenburg[b]	Abramov[c]
1.07	1.54	1.22?
1.77	1.88	1.77
...	2.16	2.07
2.48	...	2.45?
...	...	2.82
3.61	...	...
4.38	4.53	
	4.88	
	5.20	

[a] See reference 20.
[b] See reference 21.
[c] See reference 12.

[19] B. Hamermesh and V. Hummel, Phys. Rev. **83**, 663 (1951).
[20] A. B. Martin, Phys. Rev. **72**, 378 (1947).
[21] W. D. Whitehead and N. P. Heydenburg, Phys. Rev. **79**, 99 (1950).

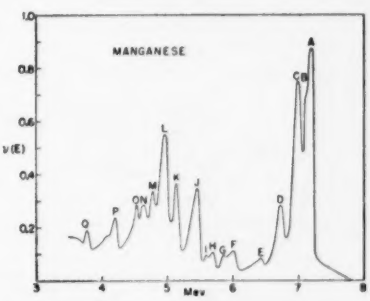

FIG. 8. Corrected γ-ray spectrum of manganese.

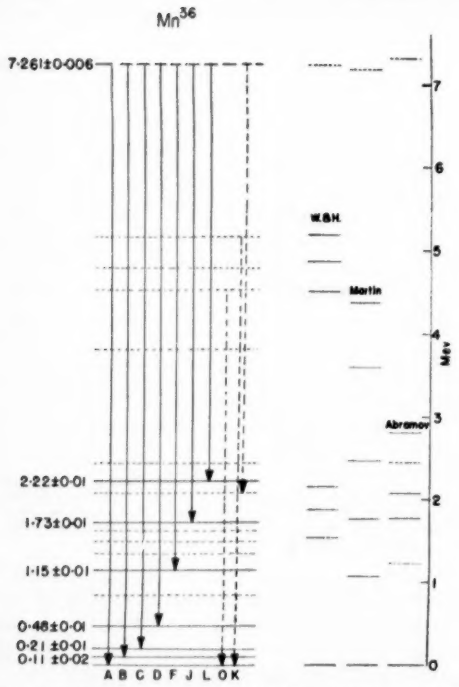

FIG. 9. Tentative decay scheme for the capture γ-rays from manganese. The full horizontal lines represent levels whose existence is inferred from the strong γ-rays in the spectrum, the broken lines represent possible levels whose existence is suggested by weak γ-rays. The levels from the (d,p) reaction are shown on the right (see text).

probably associated with a transition to a level at 1.73 ± 0.01 Mev, for proton groups corresponding to a level near this energy were obtained in all three (d,p) measurements. The γ-rays K and L are more difficult to assign. Two possible alternatives for K are shown in Fig. 9.

COBALT

Cobalt has one stable isotope, Co^{59}. All of the neutron capture γ-rays, therefore, must be ascribed to Co^{60}.

The cobalt sample consisted of 750 grams of very pure cobalt metal[22] mounted in a Dural cylinder with open ends. The spectrum was measured from 2.4 to 8.3 Mev, and the results are shown in Fig. 10. The absolute intensities of the cobalt γ-rays were determined from a comparison of the counting rate at the peak B with that of the 9.00-Mev nickel γ-ray, using a known mixture of nickel and cobalt oxides. The capture cross section of cobalt was assumed to be 34.8 barns. The energies and intensities of the cobalt γ-rays are listed in Table VI, and the corrected γ-ray spectrum is shown in Fig. 11.

The neutron binding energy of Co^{60} can be obtained from the Q value of the $Co^{59}(d,p)Co^{60}$ reaction. From the results of Bateson and Pollard[23] we find a neutron binding energy of 7.42 Mev, from those of Harvey,[10] 7.66 ± 0.2 Mev, and from those of Hoesterey,[24] 7.53 Mev. The binding energy can also be obtained from a consideration of the masses[8] of Ni^{58}, Ni^{60}, the energy[25] (2.81 Mev) of the decay of Co^{60}, the neutron binding

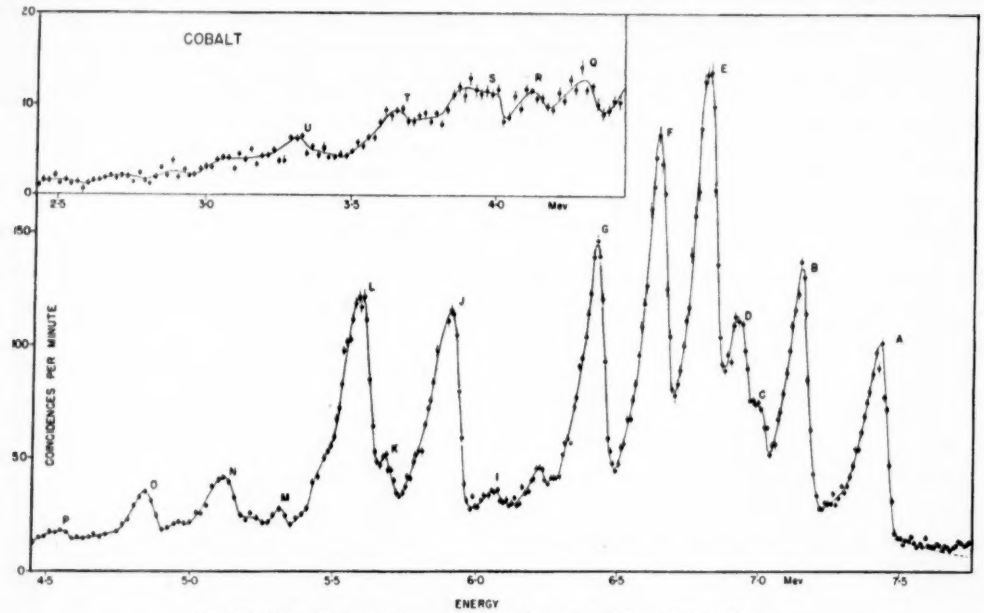

FIG. 10. Coincidence spectrum produced by cobalt. Line width: 100 kev.

[22] We are indebted to the Department of Mines and Technical Surveys, Ottawa, for the provision of this sample.
[23] W. D. Bateson and E. Pollard, Phys. Rev. **79**, 241 (1950).
[24] D. C. Hoesterey, Phys. Rev. **87**, 216 (1952).
[25] Deutsch, Elliott, and Roberts, Phys. Rev. **68**, 193 (1945); Lind, Brown, and DuMond, Phys. Rev. **76**, 591 (1949).

energy[2] of Ni^{59}, and the known mass difference[26] of Ni^{59} and Co^{59}. The result is 7.2±0.3 Mev, which is lower than, but not inconsistent with, the values obtained from the (d,p) reaction.

The energy of the γ-ray A (7.486±0.006 Mev) is close to the above values for the neutron binding energy of Co^{60}. However, the latter is not known with sufficient precision to identify this γ-ray with the direct transition to the ground state, since the energy of the first excited state, the well-known 58.9±0.5 kev[27] isomeric state of Co^{60}, is less than the error in the above values of the neutron binding energy. The γ-ray A must represent a transition either to the isomeric state or to the ground state, and the present measurements also are insufficient to distinguish between the two alternatives, for the width of the peak A in Fig. 10 is normal (100 kev) and there is no evidence for the presence of another γ-ray with an energy 60 kev above or below it. It follows that, if the γ-ray A represents the transition to the ground state, the γ-ray producing the isomeric state is weak, with an intensity less than one-tenth of that of A. On the other hand, if the γ-ray A represents a transition to the isomeric state, the ground-state transition must have an intensity less than 3 percent of A.

TABLE VI. Energies and intensities of cobalt γ-rays.

γ-ray	Energy in Mev	Intensity in photons per 100 captures
A	7.486±0.006	3.0
B	7.201 0.006	4.0
C	7.041 0.010	1.3
D	6.974 0.010	2.5
E	6.867 0.006	7
F	6.690 0.006	6
G	6.474 0.006	5
H	6.250 0.009	0.7
I	6.110 0.015	0.5
J	5.966 0.006	5.6
K	5.726 0.010	1.7
L	5.646 0.006	6.3
M	5.351 0.010	0.7
N	5.179 0.010	2
O	4.903 0.008	2.5
P	4.59 0.02	0.6
Q	4.37 0.02	1
R	4.18 0.02	0.8
S	4.03 0.02	1
T	3.69 0.02	0.7
U	3.36 0.02	1

Six higher excited states in Co^{60} have been reported by Bateson and Pollard at 0.39, 0.81, 1.28, 1.73, 2.17, and 2.80 Mev. Hoesterey[24] reported a level at 0.44 Mev, which perhaps corresponds to the first excited state found by these authors. In Fig. 12 we have constructed a very tentative level diagram for Co^{60} on the assumption that the relatively strong γ-rays B, C, D, E, F, G, J, and L are all emitted in transitions from the capturing state to low-lying excited states, the γ-ray A being the transition to the ground state. All these γ-rays appear to be homogeneous except those producing the peaks J and L which are unusually broad. The positions of the excited states, obtained by subtracting the energies of the γ-rays from that of A are given on the left of Fig. 12, the results of the measurements of Bateson and Pollard on the right. It will be seen that there is agreement between the energies of these levels only for those produced by the γ-rays C, F, and L. If,

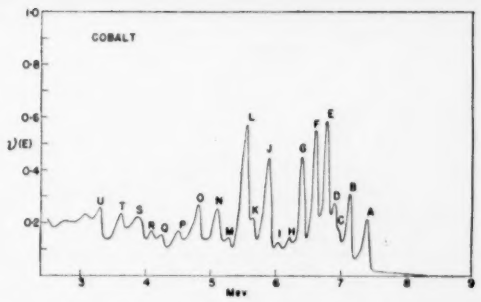

FIG. 11. Corrected γ-ray spectrum of cobalt.

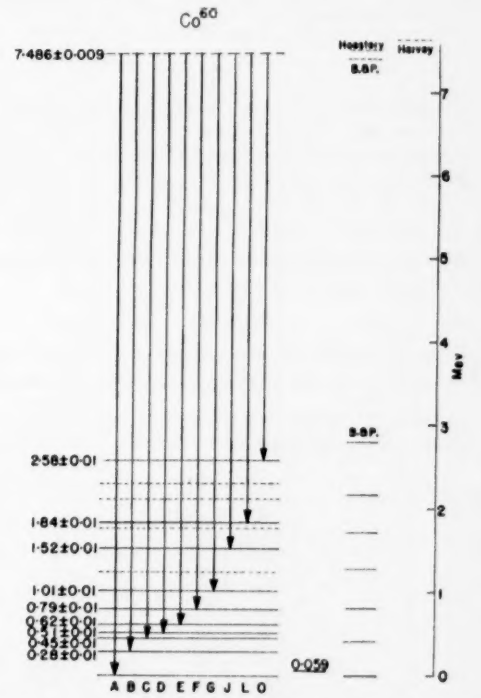

FIG. 12. Tentative decay scheme for the capture γ-rays from cobalt. It is assumed that γ-ray A is produced in the direct transition to the ground state and not to the isomeric state at 59 kev. The full horizontal lines represent levels whose existence is inferred from the strong γ-rays in the spectrum, the broken lines represent possible levels whose existence is suggested by weak γ-rays. The levels from the (d,p) reaction are shown on the right (see text).

[26] J. J. G. McCue and W. M. Preston, Phys. Rev. **84**, 384 (1951).
[27] R. L. Caldwell, Phys. Rev. **78**, 407 (1950).

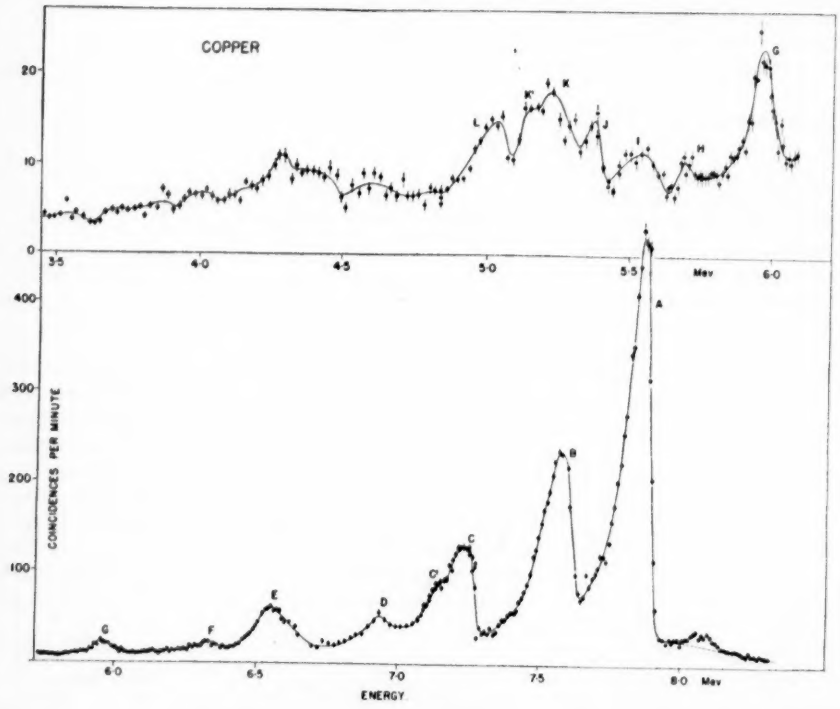

FIG. 13. Coincidence spectrum produced by copper. Line width: 100 kev.

on the other hand, the γ-ray A represents the transition to the isomeric state, the level system given on the left would be shifted upwards by only 59 kev, and the general agreement of the two level schemes would not be improved. It will be clear from this discussion that no progress can be expected in the identification of the capture γ-rays until much more accurate measurements on the (d,p) reaction are available.

COPPER

Copper consists of two isotopes, Cu^{63} and Cu^{65}. According to recent measurements by Pomerance,[28] about 82 percent of the thermal neutron capture cross section of the natural element is due to Cu^{63}.

TABLE VII. Energies and intensities of copper γ-rays.

γ-ray	Energy in Mev	Intensity in photons per 100 captures
A	7.914±0.006	20
B	7.634 0.006	9
C	7.296 0.009	5.5
C'	7.16 0.02	1
D	7.01 0.02	2
E	6.69 0.03	3
F	6.41 0.02	1
G	6.05 0.02	1
H	5.75 0.03	0.2
I	5.64 0.03	0.5
J	5.43 0.02	1
K	5.31 0.03	1
K'	5.18 0.02	0.6
L	5.07 0.02	0.7

The copper sample consisted of a cylindrical bar of very pure copper, 2300 grams, mounted in a Dural cylinder with open ends. The coincidence spectrum, which was measured from 3.4 to 8.2 Mev, is shown in Fig. 13. The energies and intensities of the copper radiations are listed in Table VII. The intensities were determined by comparing the counting rate of the peak A of the copper spectrum with that of the 9.00-Mev nickel γ-ray, using a known mixture of nickel and copper oxides. The capture cross section of copper was assumed to be 3.59 barns. The corrected γ-ray spectrum is shown in Fig. 14.

The neutron binding energy of Cu^{64} has been determined by Harvey[10] from a study of the $Cu^{63}(d,p)Cu^{64}$ reaction. He found the value 7.78±0.2 Mev. Using copper enriched in Cu^{63}, Hoesterey[24] has determined the energy balance in the same reaction; his result corresponds to a neutron binding energy of 7.89 Mev, in good agreement with Harvey's result. Another value in agreement with these measurements can be obtained from a consideration of the reaction cycle involving the positron decay energy of Zn^{63} (2.36 Mev[29]), the β-decay energy of Cu^{64} (0.573 Mev[30]), and the photoneutron threshold of Zn^{64}. For the latter quantity,

[28] H. Pomerance, Phys. Rev. **88**, 412 (1952). We are indebted to Dr. Pomerance for the privilege of seeing his results before publication.

[29] Huber, Medicus, Preiswerk, and Steffen, Helv. Phys. Acta **20**, 495 (1947).

[30] C. S. Cook and L. M. Langer, Phys. Rev. **73**, 601 (1948).

Hanson *et al.*,[31] obtained 11.80±0.2 Mev, and Sher and co-workers[15] obtained 11.65±0.2 Mev. Adopting the mean of the latter results, the neutron binding energy of Cu^{64} is found to be 7.8±0.2 Mev, in agreement with the measurements on the (d,p) reaction. If the masses of Cu^{63} and Zn^{64} obtained by Collins, Nier, and Johnson[8] are used instead, the lower value 7.52±0.06 Mev is obtained. The origin of this disagreement is not clear. However, the strong γ-ray *A* has an energy of 7.914±0.004 Mev in good agreement with the above estimates for the neutron binding energy of Cu^{64} with the exception of that obtained from the mass measurements. There seems to be little doubt, therefore, that the γ-ray *A* represents the direct transition to the ground state in Cu^{64}. According to Hoesterey,[24] excited states exist in Cu^{64} at 0.51 Mev and at 1.29 Mev. These energies agree with the difference between the energy of the γ-ray *A* and the energies of the γ-rays *C* and *E*, respectively, and we conclude that these γ-rays represent transitions to excited states at these positions.

In natural copper, Hoesterey[32] has found a high energy proton group which was absent in the protons emitted from a sample enriched in Cu^{63}. If the binding energy of the deuteron is added to the *Q* value of this group, the energy obtained is very close to the energy of the γ-ray *B* (7.634±0.006 Mev). This γ-ray, therefore, would appear to be the direct transition to the ground state in Cu^{66}. The energy, however, is inconsistent with the neutron binding energy of Cu^{66} deduced from the disintegration energies of Cu^{66} and Zn^{65} and the (γ,n) threshold of Zn^{66}. These quantities are respectively 2.63 Mev,[33] 1.34 Mev,[34] and 11.15±0.2 Mev[15]; and hence the neutron binding energy of Cu^{66} is 7.2±0.2 Mev. Another low value may be obtained from the masses[8] of Cu^{65} and Zn^{66} and the disintegration energy of Cu^{66}; this value is 6.8±0.1 Mev. Until these discrepancies are resolved, the γ-ray *B* cannot be identified with certainty.

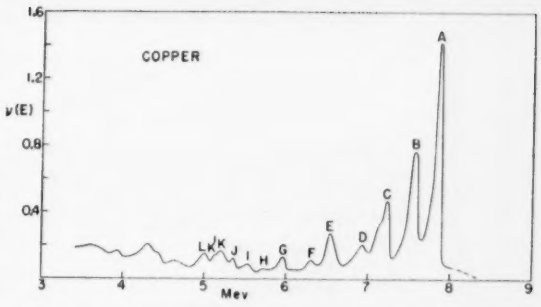

FIG. 14. Corrected γ-ray spectrum from copper.

An interesting feature of the γ-ray spectrum of copper is the great strength of the ground-state γ-ray *A*. It is produced in 24 percent of the captures by Cu^{63}. Also if the γ-ray *B* is caused by capture in Cu^{65}, its intensity is even greater, about 50 photons per 100 captures in that isotope.

[31] Hanson, Duffield, Knight, Diven, and Palevsky, Phys. Rev. **76**, 578 (1949).
[32] D. C. Hoesterey, private communication.
[33] G. Friedlander and D. E. Alburger, Phys. Rev. **84**, 231 (1951).
[34] W. M. Good and W. C. Peacock, Phys. Rev. **69**, 680 (1946).

Angular Distributions of Protons from the Reaction $F^{19}(d,p)F^{20}$†

D. A. Bromley, J. A. Bruner, and H. W. Fulbright
University of Rochester, Rochester, New York

(Received September 29, 1952)

A Teflon (CF_2) target was bombarded with 3.6-Mev deuterons from the Rochester 26-inch cyclotron, and the angular distributions of the resulting proton groups were determined using an ionization chamber detector. The following table gives the angular momentum transfer (determined by comparison with the Butler curves) and the cross sections corresponding to the indicated levels in F^{20}:

Ground state:	$l_n=0$ and 2,	$\sigma=0.92\pm0.18$ mb/sterad (at 45°);
0.65-Mev level:	$l_n=2$,	$\sigma=7.15\pm1.4$ mb/sterad (at 45°);
2.05-Mev level:	$l_n=2$,	$\sigma<8$ mb/sterad (at 45°);
3.49- and 3.53(?)-Mev level:	$l_n=0$,	$\sigma=116\pm23$ mb/sterad (at 7°).

These F^{20} states were found to have even parity, and the ground-state spin was determined to be 1.

INTRODUCTION

A STUDY of the beta-decay of F^{20} has shown that only about 3.5 percent of the transitions are directly to the ground state,[1] indicating that this transition is forbidden. Until now, the spin of the F^{20} ground state had not been measured, and the shell models do not make a definite spin prediction.

A previous study of the $F^{19}(d,n)Ne^{20}$ ground state reaction[2] showed that the F^{19} ground state has even parity and spin $\frac{1}{2}$, in agreement with the known spin value[3] and with the shell model predictions. Consequently, a measurement of the angular distributions of the protons from the reaction $F^{19}(d,p)F^{20}$ makes possible the determination of the parities and possible spins of the F^{20} states which correspond to clearly resolved proton groups.

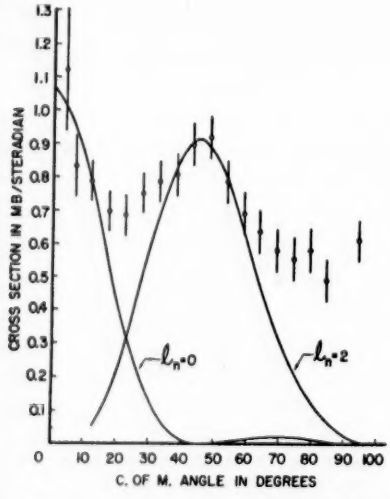

FIG. 1. Angular distribution of protons from the $F^{19}(d,p)F^{20}$ ground-state reaction.

EXPERIMENTAL METHOD

The Teflon (CF_2) target had an areal density of 1.43 mg/cm² and was prepared by slicing a thin film from a Teflon block with a microtome.

The experimental method has been described previously.[4] In brief, the target was mounted at the center of the scattering chamber and bombarded by a collimated beam of 3.6-Mev deuterons, and the protons were detected by a thin-window (0.003-inch Al) ionization chamber mounted on a rotatable arm inside the scattering chamber. At each angle the amplified output of the ionization chamber was analyzed by a 30-channel pulse-height discriminator. The energy scale was calibrated using polonium alpha-particles. Since the $C^{12}(d,p)C^{13}$ reaction has been studied here and elsewhere,[5] we were able to subtract out the corresponding proton group in the pulse height spectra.

The angular distributions obtained by analysis of the pulse-height spectra were transformed from the laboratory system to the center-of-mass system for comparison with the Butler theoretical curves.[6] These curves were calculated for $r_0=5.32\times10^{-13}$ cm and the appropriate Q.[7]

The cross sections were determined from the target areal density, the total deuteron charge measured by the beam integrator, and the geometry of the detector and scattering chamber. The absolute cross sections have an estimated accuracy of ±20 percent.

RESULTS

Watson[7] has reported the observation of eighteen excited levels in F^{20} with excitation energies less than 4.5 Mev. Our system resolution, although better than 0.22 Mev, was inadequate to separate most of these levels.

† This work was supported in part by the AEC.

[1] R. M. Littauer, Phil. Mag. **41**, 1214 (1950).
[2] D. A. Bromley, Phys. Rev. **88**, 565 (1952).
[3] H. G. Gale and G. S. Monk, Astrophys. J. **69**, 77 (1929); J. S. Campbell, Z. Physik **84**, 393 (1933).
[4] Fulbright, Bruner, Bromley, and Goldman, Phys. Rev. **88**, 700 (1952).
[5] D. A. Bromley and L. M. Goldman, Phys. Rev. **86**, 790 (1952), and J. Rotblat, Proceedings of the Chicago Conference, Sept. 17–22, 1951 (unpublished).
[6] S. T. Butler, Proc. Roy. Soc. (London) **A208**, 559 (1951).
[7] H. A. Watson, MIT Progress Report, May 31, 1952, p. 157 (unpublished).

The proton group corresponding to the F^{20} ground state was clearly resolved at all angles. The angular distribution of this group is shown in Fig. 1 with the appropriate theoretical curves.[6]

The group corresponding to the 0.65-Mev level was clearly resolved because of the relatively large energy separation between this group and that corresponding to the ground state, and because of the very low observed cross section ($\ll$1 mb/steradian) for the transition to the 0.83-Mev level. The angular distribution of this group with the corresponding theoretical curve is shown in Fig. 2.

On the basis of Watson's observed relative cross

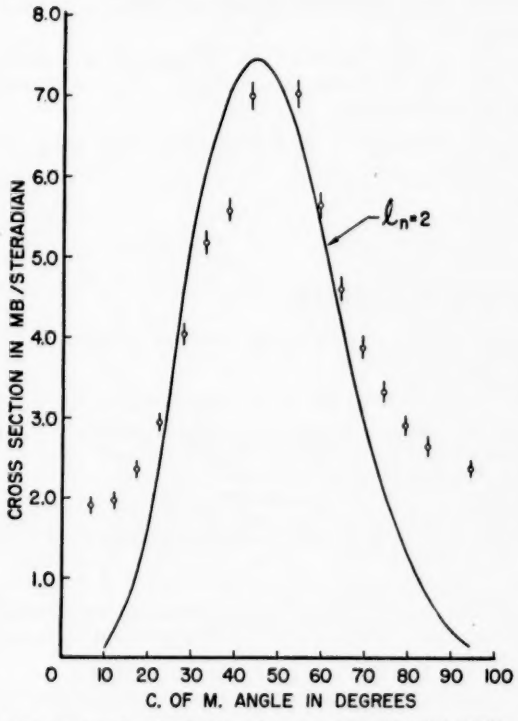

FIG. 2. Angular distribution of protons from the $F^{19}(d,p)F^{20*}$ (0.65-Mev level) reaction.

sections it is probable that the high intensity proton group, which is characterized by the $l_n=0$ angular distribution shown in Fig. 3, corresponds to transitions to the 3.49-Mev level. We cannot, however, exclude the possibility that the transition to the 3.53-Mev level is also characterized by $l_n=0$, in which case the observed distribution is the sum of the two $l_n=0$ distributions.

Our resolution was inadequate to separate the proton groups corresponding to transitions to the 1.95-, 2.05-, and 2.20-Mev levels. The angular distribution shown in Fig. 4 is, therefore, the sum of these three individual distributions. In view of the observed relative intensities[7] of 0.25, 2.0, and 0.85, respectively, it seems prob-

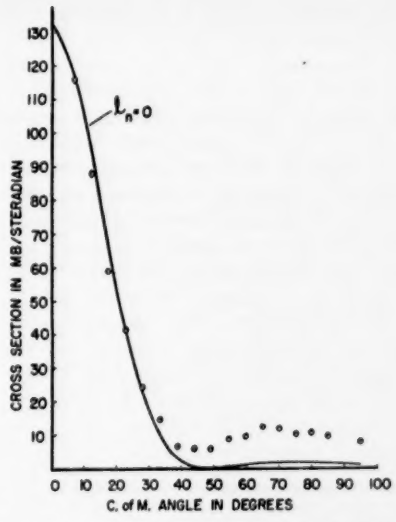

FIG. 3. Angular distribution of protons from the $F^{19}(d,p)F^{20*}$ (3.49-Mev level) reaction.

able that at least the transition to the 2.05-Mev level is characterized by $l_n=2$.

DISCUSSION

The angular distribution of the F^{20} ground-state group indicates a mixture of $l_n=0$ and $l_n=2$ transitions. Consequently, since the F^{19} ground state has spin $\frac{1}{2}$, conservation of angular momentum requires that the F^{20} ground state have spin 1. Furthermore, the F^{19} ground state parity is even, and the F^{20} ground-state parity must therefore be even, also.

With this knowledge and from the F^{20} beta-decay

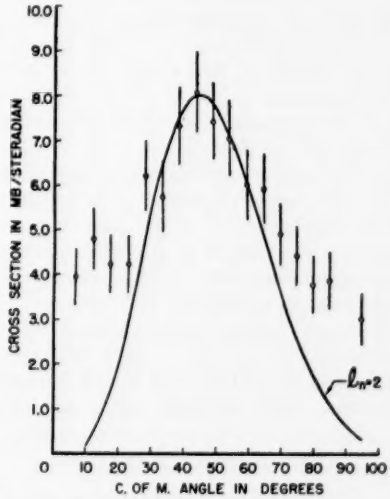

FIG. 4. Angular distribution of protons from the $F^{19}(d,p)F^{20*}$ (2.05-Mev level) reaction.

data, we deduce that the most probable shell model configuration of the F^{20} ground state is $O^{16}+s_{\frac{1}{2}}{}^{1}(p)+D_{\frac{1}{2}}(n)$ (see reference 8) with a small admixture of $O^{16}+s_{\frac{1}{2}}{}^{1}(p)+d_{\frac{1}{2}}{}^{2}(n)+s_{\frac{1}{2}}{}^{1}(n)$ corresponding to $l_n=0$) neutron capture. This admixture cannot constitute the major part of the F^{20} ground state, since it is experimentally observed that the proton intensities corresponding to the $l_n=0$ and 2 transitions are comparable. On the basis of the Butler theory this indicates that the probability of the $l_n=2$ transition is greater by a factor of about 10. Furthermore, this latter configuration would result in a "doubly l-forbidden" F^{20} beta-decay to the Ne^{20} ground state. The configuration cannot be $O^{16}+d_{\frac{1}{2}}{}^{1}(p)+d_{\frac{1}{2}}{}^{2}(n)+s_{\frac{1}{2}}{}^{1}(n)$, because this does not yield spin 1. Finally, the configuration $O^{16}+d_{\frac{1}{2}}{}^{1}(p)+D_{\frac{1}{2}}(3n)$ would lead to an allowed ($\Delta I=1$, no, $\Delta l=0$) beta-transition to the Ne^{20} ground state (contrary to experimental evidence[1]), since the Ne^{20} ground-state configuration is almost certainly $O^{16}+d_{\frac{1}{2}}{}^{2}(p)+d_{\frac{1}{2}}{}^{2}(n)$. We conclude, therefore, that a single-particle model is inadequate to account for the present observations on the F^{20} ground state.[9]

The $F^{20}\rightarrow Ne^{20}$ (ground state) beta-decay is thus characterized by $\Delta=1$, no, and by a change of 2 units of orbital angular momentum of the proton not participating in the beta-decay. The assigned configuration would thus explain the relatively large ft value of the allowed transition ($\log ft=6.9$).

Since the most intense group of beta particles in the F^{20} decay is in coincidence with a 1.63-Mev gamma-ray,[1] a study of the $F^{19}(d,n)Ne^{20}$ reaction, to determine the parity and possible spins of this final state, would be of interest.

We are indebted to Dr. M. Watson for cutting the Teflon film, and to Mr. W. Skillman for the calculation of the Butler curves.

[8] There is an analogous situation involving the 11 protons in the Na^{23} ground state. See M. G. Mayer *et al.*, Revs. Modern Phys. **23**, 315 (1951).

[9] See, for example, L. W. Nordheim, Revs. Modern Phys. **23**, 322 (1951).

PHYSICAL REVIEW VOLUME 89, NUMBER 2 JANUARY 15, 1953

Thermal Treatment of Silicon Rectifiers

LEO ESAKI
Kobe Kogyo Corporation, Hyogo-ku, Kobe, Japan
(Received July 28, 1952)

The effect of thermal treatment on silicon point contact rectifiers over the temperature range between 900°C and 1400°C, both in high vacuum and in an oxygen atmosphere below about 0.1 mm Hg, has been investigated by means of heating a silicon specimen directly. During the treatment above 1250°C in vacuum, the rectification is changed remarkably and is finally lost. It is recovered by successive heat treatment in oxygen. Both the creation of thermal donors or acceptors and the absorbed oxygen may be regarded as causes of these phenomena. The contact area calculated from the ohmic resistance at the non-rectifying contact is the order of 10^{-6} cm².

IN the course of studying the thermal treatment of point contact rectifiers,[1] it has been found that the rectification of both p- and n-type silicon disappears, when the specimen is heated above 1250°C in high vacuum, and it reappears through heating at 1000°C in oxygen from 10^{-1} to 10^{-3} mm Hg.

In the experiment, several silicon specimens were prepared from ingots of p-type or n-type of specific resistivity from 0.05 to 0.135 ohm-cm containing aluminium or phosphorus as impurity. The specimen and tungsten whisker were sealed in a tube, which was evacuated to a pressure below 10^{-6} mm Hg. If necessary, oxygen was admitted after sufficient evacuation. The specimen was heated to high temperature by passing current directly through it, and dc rectification characteristics were measured after quenching the specimen to room temperature. Such successive thermal treatments in high vacuum and in oxygen, as listed in Table I, made the rectification change remarkably, as illustrated in Figs. 1 and 2. In almost all cases the

[1] A comprehensive survey of crystal rectifiers has been given by H. C. Torrey and C. A. Whitmer, *Crystal Rectifiers* (McGraw-Hill Book Company, Inc., New York, 1948).

TABLE I. Conditions for thermal treatment.

Number in Fig. 1	Conditions for treating	Number in Fig. 2	Conditions for treating
I		I	
	930°C, 20 min		1400°C, 1 sec.
	950°C, 20 min	II	
II			1400°C, 1 sec
	1100°C, 120 min	III	
III			1400°C, 5 sec
	1250°C, 30 min	IV	
IV			1100°C, 60 min
	1000°C, 20 min		1300°C, 10 min
	in oxygen at 0.03 mm Hg	V	
			1300°C, 30 min
V		VI	
			1000°C, 10 min in oxygen at 0.12 mm Hg
		VII	
			1000°C, 10 min in oxygen at 0.006 mm Hg

specimen was heated with the whisker being kept in contact with silicon. However, similar results were obtained even when the whisker, having been apart from the silicon surface during heating, was pressed against the silicon in vacuum without exposing it to air. There seems to be no possibility of interaction between tungsten and silicon in heating.

It should be noticed that the rectification is completely lost through the thermal treatment in high vacuum, while it recovers through heating in oxygen,

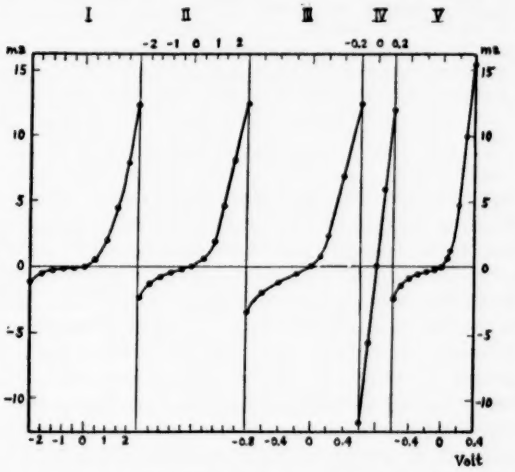

FIG. 1. The changes of rectification characteristics.

whatever impurity may be contained in the specimen. A nonrectifying point contact can be also produced rather easily by heating only the vicinity of the contact, that is, by passing a heavy current of about 500 ma for a short time through the contact. The residual ohmic resistance R of the nonrectifying specimen is given as follows, in terms of the diameter d of the point contact and the specific resistivity ρ of the bulk silicon,

$$R=\rho/2d.$$

For instance, with the known values $\rho=0.072$ and 0.064 ohm-cm, and $R=17.0$ and 12.5 ohm in Figs. 1

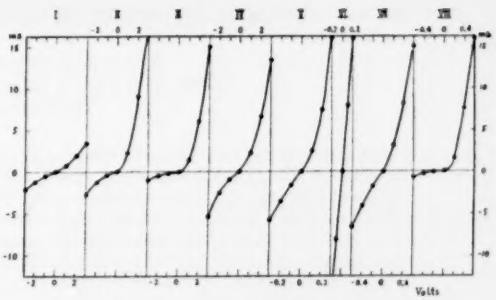

FIG. 2. The changes of rectification characteristics.

and 2, the diameters are evaluated to be 0.0021 cm and 0.0026 cm, respectively, giving a contact area of the order of 10^{-6} cm^2 in good agreement with the value estimated hitherto.

The resistivity at room temperature, which increased or decreased a little through thermal treatment, shows that no donor or acceptor impurities, substituted from silicon atoms in lattice, diffuse and evaporate.[2] There is no indication for the formation of lattice defects which may act as acceptors or donors. Purer specimens will be necessary to detect the effect of lattice defects.[3]

There seem to be two possibilities for losing the rectification; creation of acceptors or donors by the formation of lattice defects by quenching, and freeing of adsorbed oxygen and other kinds of gas from the surface. But the probable relation between these effects and the rectification is quite unknown, because it is not sure whether the initial surface stage such as I in Fig. 1 or III in Fig. 2, is equivalent to the final one such as V in Fig. 1 of VIII in Fig. 2.

The author is very grateful to Dr. T. Arizumi (Technical Department, Kobe Kogyo Corporation) for his advice and encouragement.

[2] B. Serin's theory of heat treatment [Phys. Rev. **69**, 357 (1946)], which assumes the formation of a layer low in impurity concentration as the result of a rapid evaporation of impurity atoms from the surface and a slower influx by the diffusion from the interior, seems to stand on a weak experimental basis.

[3] In the thermal treatment of pure germanium the formation of lattice defects has been verified by the author (to be published).

Spin and Angular Momentum in General Relativity*

PETER G. BERGMANN AND ROBB THOMSON
Department of Physics, Syracuse University, Syracuse, New York

(Received October 6, 1952)

In the general theory of relativity, the group of coordinate transformations gives rise to four point-to-point conservation laws, which are usually identified with energy and linear momentum. In the presence of a semi-classical Dirac field, it is convenient to introduce at each point of space-time an arbitrary set of four orthonormal vectors (quadrupeds, "beine") and to consider the group of "bein" transformations, which then play the role of local, nonholonomic lorentz transformations. A search for the corresponding conservation laws leads to terms that have the form of a spin angular momentum and which, in order to be conserved, must be supplemented by terms representing the orbital angular momentum. The technique of the so-called superpotentials has enabled us to introduce, in addition to the canonical stress-energy, a "contravariant" stress-energy which contains the usual symmetric Dirac and Maxwell terms and also asymmetric, purely gravitational terms. It is this set of expressions which enters into the orbital angular momentum. The techniques presented here are applicable to more general covariant theories, provided the gravitational field is represented by a metric tensor.

1. INTRODUCTION

THE general definition of the angular momentum of a field has been discussed within the framework of Lorentz invariance of the theory by several authors.[1–3] In these and other previous papers the conservation theorem for angular momentum is a direct result of the fact that the Lagrangian is a scalar density with respect to Lorentz transformations.

We have been interested for several years in the possibilities of constructing a completely covariant quantum theory containing the gravitational field.[4–7] One of the aspects of this investigation is, of course, the role of the angular momentum in such a theory. The spin is a fundamental property of a particle in the usual Lorentz-invariant theory; it would be surprising indeed if this property were suddenly lost simply because the theory is made covariant with respect to more general coordinate transformations.

Yet it seems that in the theory of general relativity the concept of angular momentum is not as natural as it has been in special relativity. In general relativity the only identity one obtains from the general covariance of the Lagrangian is the conservation of the energy and momentum. In Lorentz-invariant theories, there are at least two separate types of transformations (each dependent on a set of *parameters*) which lead to two conservation laws. The invariance with respect to linear displacement yields the conservation of linear momentum and energy, while the invariance with respect to the homogeneous Lorentz transformation group yields the conservation of angular momentum. Now in the theory of general relativity, the most important invariance property is the invariance with respect to general (curvilinear) coordinate transformations. This is a group of transformations which depends on a set of four arbitrary *functions*, one for each coordinate. The conservation law obtained as a result of this invariance, as stated earlier, is none other than the conservation of linear momentum and energy. It is true that the theory is also invariant with respect to linear displacements, a subgroup of the group of all coordinate transformations. This invariance leads again to the conservation of linear momentum and energy. One might think that by considering other subgroups, say the Lorentz group, other conservation laws might be found. Such is not the case. Noether[8] has shown that in general, conservation laws obtained in such a way are simply restatements or even special cases of the general conservation law resulting from the invariance with respect to curvilinear transformations. Thus it seems that the angular momentum law will not be obtained by appealing to an invariance argument in the usual theory.

Our program is not to attempt to derive the angular momentum from an invariance argument, but rather to construct a quantity from the energy-momentum "tensor" itself which has the properties of the usual angular momentum. There are several types of quantities which have been used in the past as energy-momentum tensors. Rosenfeld[1] considers only the symmetric matter tensor which describes matter in the gravitational field equations. Others[2,3] start with the canonical "tensor" of a particular field and add terms which are obtained from the Lorentz covariant angular momentum law, to make the result symmetric. These

* Some of this work was performed under the sponsorship of the ONR. One of us (R. T.) gratefully acknowledges a Syracuse University Predoctoral Fellowship, whose tenure coincided with the completion of the major phase of this research. (This work is being submitted in somewhat more extended form by R. T. to the Graduate School of Syracuse University, in partial fulfillment of the requirements for the doctor's degree.)

[1] L. Rosenfeld, Acad. roy. Belg. Classe sci. Mém. **6**, 30 (1940).
[2] F. J. Belinfante, Physica **7**, 887 (1939).
[3] W. Pauli, Revs. Modern Phys. **13**, 203 (1941).
[4] P. G. Bergmann, Phys. Rev. **75**, 680 (1949).
[5] P. G. Bergmann and J. H. M. Brunings, Revs. Modern Phys. **21**, 480 (1949).
[6] Bergmann, Penfield, Schiller, and Zatkis, Phys. Rev. **80**, 81 (1950).
[7] J. L. Anderson and P. G. Bergmann, Phys. Rev. **83**, 1018 (1951).
[8] E. Noether, Nachr. kgl. Ges. Wiss. Göttingen Math.-phys. Klasse 235 (1918).

two methods lead to the same result when applied to a Lorentz-invariant Lagrangian. However, this procedure will have to be modified if the gravitational terms are included in the Lagrangian. First, the symmetric matter tensor, as is well known, is not actually conserved; its *covariant* divergence is zero, and purely gravitational terms must be added to obtain expressions whose *ordinary* divergence vanishes. The essential feature of the procedure of this paper is to find the proper energy momentum "tensor" and then to construct from it a "superpotential" for the angular momentum of the total field. The superpotential will have certain symmetry properties which guarantee the conservation of the angular momentum which is derived from it. We shall show the results of applying this method to the gravitation-electron field.

We have stated that there is no invariance property of the usual theory which leads naturally to the conservation of angular momentum. However, we can introduce into the theory of gravitation one further invariance property which on first inspection seems to point the way toward an angular momentum conservation law. This is "bein" invariance. It is possible to describe the gravitational field in terms of a system of "quadrupeds" or "beine."[3] One introduces at each point of Riemannian space four orthonormal vectors whose components are differentiable functions of the coordinates. Then the metric tensor components may be expressed in terms of the 16 components of these vectors, and the "beine" themselves act as field variables for the gravitational field. The theory is still obviously invariant with respect to coordinate transformations, since the "beine" transform as vectors, but, in addition, it is possible to transform from one system of vectors to another set by rotating the quadruped located at each point of space-time by an amount that may vary with position. Rotation, of course, usually generates angular momentum, and one might reasonably hope that such is the case here. Detailed examination shows that while this procedure does not lead to a complete conservation law, the identity obtained yields the contribution of the spin of the electron field to the total angular momentum.

2. CONSERVATION LAWS

For the derivation of the conservation law of angular momentum, it is assumed traditionally that there is available a symmetric energy-stress tensor that satisfies a conservation law of its own. Hence, we find in the literature a distinction made between the canonical stress tensor which is obtained directly by the requirement that the theory be invariant with respect to rigid displacement along each of the four coordinate axes, and a symmetric stress tensor $\Theta^{\mu\nu}$. The symmetric stress tensor is then made the point of departure for a derivation of the expression for the angular momentum. The symmetric tensor $\Theta^{\mu\nu}$ has the further virtue of being gauge invariant, while the canonical tensor is not. The canonical tensor is written

$$t_\mu{}^\nu=\frac{\partial L}{\partial\zeta_{,\nu}}\zeta_{,\mu}-\delta_\mu{}^\nu L, \tag{2.1}$$

where ζ is short for the totality of all field variables, and L is the Lagrangian density.

In a theory that is generally covariant, the expression (2.1) can be introduced in a natural manner, but it is impossible to introduce, by a general procedure, a symmetric tensor $\Theta^{\mu\nu}$ whose divergence vanishes. What we shall do in this paper is to derive a quasi-symmetric expression consisting of two parts: one that depends exclusively on gravitational terms and which is neither covariant nor symmetric; the other, "the matter tensor," which is covariant, gauge invariant, spin invariant, and symmetric. This result is independent of the special nature of the theory in so far as it does not concern the gravitational field. But we cannot obtain our results without assuming explicitly the existence of a symmetric gravitational tensor $g_{\mu\nu}$ which, in the absence of other fields, satisfies Einstein's field equations $G^{\mu\nu}=0$. We shall, therefore, assume that the Lagrangian of our theory has the form

$$L=\mathfrak{G}'+\mathfrak{M},\quad \mathfrak{G}'=-(c^4/16\pi\kappa)(-g)^{\frac{1}{2}}R, \tag{2.2}$$

where R is the curvature scalar, c the velocity of light and κ the gravitational constant.

In what follows, we shall establish a relationship between the canonical and the quasi-symmetric expressions by means of the so-called strong conservation laws.[4] These laws are actually identities and hold whether the field equations are satisfied or not, simply because of the covariance of the theory with respect to general coordinate transformations. They will, therefore, hold both for the Lagrangian of the whole theory (2.2) and also for the gravitational term $\mathfrak{G}'$ alone. We shall make use of the latter fact. The field equations,

$$\delta L/\delta\rho=0, \tag{2.3}$$

contain two types of terms, originating in the two terms of the Lagrangian (2.2),

$$\delta L/\delta\rho=\delta\mathfrak{G}'/\delta g_{\mu\nu}+\delta\mathfrak{M}/\delta\rho, \tag{2.4}$$

which we shall designate for short as the gravitational and the matter terms, respectively. If we write down the strong conservation laws for the gravitational terms only, we obtain

$$T_{G\mu}{}^\nu{}_{,\nu}=0,\quad T_{G\mu}{}^\nu=t_{G\mu}{}^\nu-F_{G\mu}{}^\nu\delta\mathfrak{G}/\delta\zeta, \tag{2.5}$$

where t_G is the canonical stress "tensor" obtained from the gravitational term of the Lagrangian alone. In obtaining this expression, we must observe one precaution, though. The expression $\mathfrak{G}'$ contains second

[3] L. Eisenhart, *An Introduction to Differential Geometry* (Princeton University Press, Princeton, 1947).

derivatives of the field variables, while the canonical stress "tensor" is defined ordinarily only for Lagrangians depending on zeroth and first derivatives of the field variables. To meet this difficulty we introduce, as is customary, the gravitational Lagrangian $\mathfrak{G}$ which differs from $\mathfrak{G}'$ only by a divergence but is free of second derivatives,

$$\mathfrak{G}=\mathfrak{G}'-Q^{\rho}{}_{,\rho}. \tag{2.6}$$

The variational derivative of the last term on the right vanishes, and we have, therefore,

$$\delta\mathfrak{G}/\delta\rho=\delta\mathfrak{G}'/\delta\rho. \tag{2.7}$$

The canonical stress tensor t_G in Eq. (2.5) is then understood as having been formed from the Lagrangian $\mathfrak{G}$. The $F_{G\mu}{}^{\nu}$ in Eq. (2.5) is defined by means of the transformation properties of the field variables. In an infinitesimal transformation of the field variables, we set

$$\delta\zeta=F_{\nu}{}^{\mu}\xi^{\nu}{}_{,\mu}, \tag{2.8}$$

where the ξ^{ν} are the infinitesimal variations of the coordinates. The subscript G in (2.5) obviously refers to the gravitational field variables.

We may write

$$\begin{aligned} T_{G\mu}{}^{\nu}&=t_{G\mu}{}^{\nu}-F_{G\mu}{}^{\nu}\delta G/\delta\zeta \\ &=t_{G\mu}{}^{\nu}+2g_{\lambda\mu}\delta G/\delta g_{\lambda\nu} \\ &=t_{G\mu}{}^{\nu}-(-g)^{\frac{1}{2}}G_{\mu}{}^{\nu}. \end{aligned} \tag{2.9}$$

$G_{\mu}{}^{\nu}$ stands for the Einstein tensor, with one index raised,

$$G_{\mu}{}^{\nu}=R_{\mu}{}^{\nu}-\tfrac{1}{2}\delta_{\mu}{}^{\nu}R. \tag{2.10}$$

Because of the set of field equations ($\delta L/\delta g_{\mu\nu}=0$), Eq. (2.9) may also be written in the form

$$T_{G\mu}{}^{\nu}=t_{G\mu}{}^{\nu}+\mathcal{T}_{\mu}{}^{\nu}, \tag{2.11}$$

where $\mathcal{T}_{\mu}{}^{\nu}$ is the matter tensor density defined (as usual) as

$$\mathcal{T}^{\mu\nu}=-2\delta\mathfrak{M}/\delta g_{\mu\nu}. \tag{2.12}$$

It is now clear from Eq. (2.11) that $T_{G\nu}{}^{\mu}$ may be interpreted as the total energy-momentum of all fields present, and is the combination of the energy-momentum tensor density of the matter fields with the canonical energy-momentum of the gravitational field.

Because of Eq. (2.5), it is possible to introduce a set of "superpotentials" related to the $T_{G\mu}{}^{\nu}$ in the following way:

$$T_{G\nu}{}^{\mu}=-U_G{}^{[\lambda\mu]}{}_{\nu,\lambda}. \tag{2.13}$$

The brackets indicate antisymmetry in the superscripts. The actual expression for the gravitational superpotentials was obtained by Freud.[10] In the case of a field whose Lagrangian is a scalar density, such as the matter fields, it has the form[11]:

$$U_M{}^{[\lambda\mu]}{}_{\nu}=-(\partial\mathfrak{M}/\partial\rho_{,\lambda})F_{M\nu}{}^{\mu}. \tag{2.14}$$

We shall have no occasion to use the explicit expression for the gravitational superpotentials. It should perhaps be emphasized that there are superpotentials for each of the terms introduced into the Lagrangian. Here we have introduced only the gravitational superpotentials. Later, when a definite expression for the matter tensor is needed, superpotentials associated with the other terms in the Lagrangian will be introduced.

In order to obtain a conservation law for a "contravariant" energy-momentum tensor, we note that it is the antisymmetry property of the superpotentials which leads to a conservation law. We can, therefore, raise and lower the index not involved in the antisymmetry with the help of the metric tensor to obtain the new expression

$$U_G{}^{[\lambda\mu]\nu}=U_G{}^{[\lambda\mu]}{}_{\rho}g^{\rho\nu}. \tag{2.15}$$

The energy-momentum derived from this set of modified superpotentials will also be conserved and will be taken to be the "contravariant" form of the energy-momentum. The conservation law now reads

$$\begin{aligned} &\{\mathcal{T}^{\mu\nu}+t_{G\sigma}{}^{\mu}g^{\sigma\nu}+U_G{}^{[\lambda\mu]}{}_{\sigma}g^{\sigma\nu}{}_{,\lambda}\}_{,\mu} \\ &\qquad=\{\mathcal{T}^{\mu\nu}+\tau_G{}^{\mu\nu}\}_{,\mu}=U_G{}^{[\lambda\mu]\nu}{}_{,\lambda\mu}=0. \end{aligned} \tag{2.16}$$

Here, we have grouped two terms together as $\tau_G{}^{\mu\nu}$; this expression represents the gravitational terms in the "contravariant" energy-momentum. Note, however, that $\tau_G{}^{\mu\nu}$ is not symmetric in its superscripts (though $\mathcal{T}^{\mu\nu}$ is) and that

$$\{\mathcal{T}^{\mu\nu}+\tau_G{}^{\mu\nu}\}_{,\mu}=0, \quad \{\mathcal{T}^{\mu\nu}+\tau_G{}^{\mu\nu}\}_{,\nu}\neq 0. \tag{2.17}$$

In special relativity, the energy-momentum may be symmetrized so that both lines of Eq. (2.17) turn into equalities. Here the energy-momentum will be left unsymmetric as will be discussed below.

Using the $U_G{}^{[\lambda\mu]\sigma}$, we can now construct a superpotential of a quantity which will reduce to the angular momentum of special relativity in the limit of a flat metric. We define

$$W^{[\lambda\mu][\nu\sigma]}=U_G{}^{[\lambda\mu]\nu}x^{\sigma}-U_G{}^{[\lambda\mu]\sigma}x^{\nu} \tag{2.18}$$

and define the angular momentum as

$$\Omega^{\mu[\nu\sigma]}=W^{[\lambda\mu][\nu\sigma]}{}_{,\lambda}. \tag{2.19}$$

Then, as before, because of the antisymmetry of $W^{[\lambda\mu][\nu\sigma]}$ in $[\lambda\mu]$, we have

$$\Omega^{\mu[\nu\sigma]}{}_{,\mu}=0. \tag{2.20}$$

[10] Ph. Freud, Ann. Math. **40**, 417 (1939).

[11] R. Schiller, Ph.D. dissertation, Syracuse University (1952) (to be published).

In terms of the energy-momentum

$$\Omega^{\mu[\nu\sigma]}=(\mathcal{T}^{\mu\nu}x^{\sigma}-\mathcal{T}^{\mu\sigma}x^{\nu})+(\tau_G^{\mu\nu}x^{\sigma}-\tau_G^{\mu\sigma}x^{\nu})+(U_G^{[\sigma\mu]\nu}-U_G^{[\nu\mu]\sigma}). \quad (2.21)$$

The extra terms involving U_G are necessary because of the unavoidable asymmetry of the gravitational energy-momentum $\tau_G^{\mu\nu}$. The only reason for requiring that any stress tensor in classical mechanics be symmetric is to insure that there will be no net torque on the material in the absence of external forces. Here we make up for the fact that the energy-momentum is not symmetric by redefining the torque in (2.21). For the limiting case of zero gravitational field, U_G goes to zero, and the angular momentum assumes the same form as in Lorentz covariant theories.

3. ANGULAR MOMENTUM OF THE ELECTRON FIELD

In this section we will consider the matter tensor density $\mathcal{T}^{\mu\nu}$ by itself and derive an expression for the angular momentum of a Dirac field. Originally $\mathcal{T}^{\mu\nu}$ is defined as $-2(\delta\mathfrak{M}/\delta g_{\mu\nu})$. But as $\mathcal{T}^{\mu\nu}$ represents the contribution of the nongravitational fields, it is preferable to express $\mathcal{T}^{\mu\nu}$ in terms of the "matter" field variables (including the electromagnetic field). This expression for $\mathcal{T}^{\mu\nu}$ can be obtained in a similar way to Rosenfeld.[1] First, however, we shall summarize briefly the results of introducing, in a covariant way, a spinor field into a curvilinear metric.

The Lagrangian for the original Dirac electron may be generalized quite easily so that it is a scalar density with respect to general coordinate transformations. It then becomes

$$\mathfrak{M}=\tfrac{1}{2}\hbar c(-g)^{\frac{1}{2}}(i\psi^{\dagger}\gamma^{\mu}\psi_{;\mu}-i\psi^{\dagger}{}_{;\mu}\gamma^{\mu}\psi+2\epsilon\psi^{\dagger}\psi). \quad (3.1)$$

The γ^{μ} are matrices satisfying the generalized anticommutation law

$$\gamma^{\mu}\gamma^{\nu}+\gamma^{\nu}\gamma^{\mu}=2g^{\mu\nu}, \quad (3.2)$$

and $\psi_{;\mu}$ is defined to be

$$\psi_{;\mu}=\psi_{,\mu}+\Gamma_{\mu}\psi\,, \qquad \psi^{\dagger}{}_{;\mu}=\psi^{\dagger}{}_{,\mu}-\psi^{\dagger}\Gamma_{\mu}, \quad \Gamma_{\mu}+\Gamma_{\mu}{}^{\dagger}=0, \quad (3.3)$$

where the comma is ordinary partial differentiation and the spinors, Γ_{μ}, are the coefficients of connection of the spinor field. They satisfy the equation

$$\gamma^{\mu}{}_{;\nu}\equiv\gamma^{\mu}{}_{,\nu}+\begin{Bmatrix}\mu\\ \lambda\nu\end{Bmatrix}\gamma^{\nu}+\Gamma_{\nu}\gamma^{\mu}-\gamma^{\mu}\Gamma_{\nu}=0, \quad (3.4)$$

and the $\begin{Bmatrix}\mu\\ \lambda\nu\end{Bmatrix}$ are the usual Christoffel symbols.

These equations may also be written in terms of the bein (or quadruped) gravitational variables. The Lagrangian will then be

$$\mathfrak{M}=\tfrac{1}{2}\hbar c(-g)^{\frac{1}{2}}(i\psi^{\dagger}\gamma^{a}\psi_{;a}-i\psi^{\dagger}{}_{;a}\gamma^{a}\psi+2\epsilon\psi^{\dagger}\psi), \quad (3.5)$$

where

$$\gamma^{a}=h^{a}{}_{\mu}\gamma^{\mu}, \quad \psi_{;a}\equiv\psi_{,\mu}h_{a}{}^{\mu}+\Gamma_{a}\psi. \quad (3.6)$$

In all that follows bein indices will be written with Latin letters, and coordinate indices will appear with Greek letters. The bein vectors $h^{\mu}{}_{a}$, are defined so that

$$g_{\mu\nu}=h^{m}{}_{\mu}h^{n}{}_{\nu}\eta_{mn}. \quad (3.7)$$

(Greek indices are raised or lowered by $g_{\mu\nu}$ or $g^{\mu\nu}$ and Latin indices by η_{mn} or η^{mn}.) η_{mn} is the Minkowski flat-metric tensor. The practical importance of the bein is that it is possible to find a particular representation of the ψ field such that for all bein and coordinate systems, the γ^{a} are constants, and are given by the original Dirac-Pauli matrices

$$\gamma^{a}\gamma^{k}+\gamma^{k}\gamma^{a}=2\eta^{ka}. \quad (3.8)$$

In the bein notation it is easier to find a closed expression for the spin connection coefficients in terms of the bein gravitational field variables. (We need this expression because the Γ_{l} appears in the Lagrangian, and we need to know how it depends on the field variables.)

The analog to Eq. (3.4) now becomes

$$\begin{Bmatrix}s\\ kl\end{Bmatrix}\gamma^{k}+\Gamma_{l}\gamma^{a}-\gamma^{a}\Gamma_{l}=0, \quad (3.9)$$

which is a linear expression for the Γ_{l} and does not contain the partial derivatives of γ^{a} (which vanish). Since the γ^{a} generate a hypercomplex number system (sedenions), any spinor of rank 2 may be represented by a linear combination of the γ^{a} and their various products. It turns out that the only nonvanishing terms are of the zeroth and second degrees. The bein Christoffel symbol in Eq. (3.9) is determined as follows:

$$h^{m}{}_{\mu;\,n}\equiv h^{m}{}_{\mu,\,n}-\begin{Bmatrix}\lambda\\ \mu\sigma\end{Bmatrix}h^{\sigma}{}_{n}h^{m}{}_{\lambda}+\begin{Bmatrix}m\\ kn\end{Bmatrix}h^{k}{}_{\mu}=0, \qquad \begin{Bmatrix}m\\ ln\end{Bmatrix}=-h^{m}{}_{\mu,\,n}h^{\mu}{}_{l}+\begin{Bmatrix}\lambda\\ \mu\sigma\end{Bmatrix}h^{\sigma}{}_{n}h^{m}{}_{\lambda}h^{\mu}{}_{l}, \quad (3.10)$$

where the $\begin{Bmatrix}\lambda\\ \mu\sigma\end{Bmatrix}$ are the usual coordinate Christoffel symbols. The solution of Eq. (3.9) becomes then

$$\Gamma_{l}=\tfrac{1}{4}\begin{Bmatrix}m\\ nl\end{Bmatrix}\gamma^{n}\gamma_{m}+i\phi_{l}, \quad (3.11)$$

where ϕ_{l} are four real numbers and equal to $-i/4$ trace-$\{\Gamma_{l}\}$. They are not determined by Eq. (3.9) and are usually interpreted as representing the electromagnetic potentials. The ϕ_{l} transform as vectors with respect to coordinate transformations and are invariant under bein transformations. In this paper we shall set all trace

terms equal to zero as we are not concerned with the electromagnetic field.

We shall now resume our undertaking to express the matter energy-stress tensor density in terms of the bein variables. After a short calculation, we have

$$\frac{\delta\mathfrak{G}}{\delta h^m{}_\mu}=\frac{\delta\mathfrak{G}}{\delta g_{\sigma\lambda}}\frac{\partial g_{\sigma\lambda}}{\partial h^m{}_\mu}=\frac{\delta G}{\delta g_{\mu\lambda}}h^l{}_\lambda\eta_{ml}+\frac{\delta\mathfrak{G}}{\delta g_{\lambda\mu}}h^k{}_\lambda\eta_{km}, \quad (3.12)$$

where the second equation follows from Eq. (3.7).

$$\frac{\delta\mathfrak{G}}{\delta h^m{}_\mu}h^m{}_\nu=\frac{\delta\mathfrak{G}}{\delta g_{\mu\lambda}}g_{\lambda\nu}+\frac{\delta\mathfrak{G}}{\delta g_{\sigma\mu}}g_{\sigma\nu}=\mathcal{T}_\nu{}^\mu. \quad (3.13)$$

Since $(\delta/\delta h^m{}_\mu)\{\mathfrak{G}+\mathfrak{M}\}=0$, then

$$\mathcal{T}_\nu{}^\mu=-\frac{\delta\mathfrak{M}}{\delta h^m{}_\mu}h_\nu{}^m=\frac{\delta\mathfrak{M}}{\delta h}F_{(h)\nu}{}^\mu. \quad (3.14)$$

Having set the electron field in the general framework which we use, we now return to the direct discussion of its contribution to the angular momentum of the theory. In the discussion leading up to Eq. (2.5), we mentioned that each part of the Lagrangian had a set of identities related to the invariance of the Lagrangian density function with respect to coordinate transformations. Equations (2.5) and (2.11) summarize the identities obtained for the gravitational part of the total Lagrangian. Since the electron Dirac Lagrangian function given in Eq. (3.5) is also a scalar density for such transformations, the process which led to (2.5) and (2.11) will lead to a new set of identities pertaining to the electron field. Writing, thus, Eq. (2.5) and (2.11) for the matter fields, we have

$$U_M{}^{[\lambda\mu]}{}_{\nu,\lambda}=-t_{M\nu}{}^\mu+F_{M\nu}{}^\mu\delta\mathfrak{M}/\delta\zeta, \quad (3.15)$$

which then becomes

$$\mathcal{T}_\nu{}^\mu=-\frac{\delta\mathfrak{M}}{\delta\psi}F_{(\psi)\nu}{}^\mu+\frac{\partial\mathfrak{M}}{\partial h^k{}_{\sigma,\mu}}h^k{}_{\sigma,\nu}+\frac{\partial\mathfrak{M}}{\partial\psi_{,\mu}}\psi_{,\nu}+\psi^\dagger{}_{,\nu}\frac{\partial\mathfrak{M}}{\partial\psi^\dagger{}_{,\mu}}-\mathfrak{M}\delta_\nu{}^\mu+U_M{}^{[\lambda\mu]}{}_{\nu,\lambda}. \quad (3.16)$$

The subscripts in parentheses on the F's show that each field variable has its own set of F's, the type of F being indicated by the letter. $U_M{}^{[\lambda\mu]}{}_\nu$ is the same expression obtained before in Eqs. (2.13) and (2.14), but with the Dirac Lagrangian understood. It must also be remembered that there are two distinct sets of terms in $U_M{}^{[\lambda\mu]}{}_\nu$—those containing derivatives with respect to the gravitational variables, and those with derivatives with respect to the matter fields. By a similar argument to that which leads to (3.13), it may be shown that the $t_{G\nu}{}^\mu$ used in Eq. (2.5) is not changed when it is expressed in terms of the bein variables. Hence we still have the equation

$$\{\mathcal{T}_\nu{}^\mu+t_{G\nu}{}^\mu\}_{,\mu}=0, \quad (3.17)$$

where the $\mathcal{T}_\nu{}^\mu$ is now the generalized bein expression for the energy-momentum tensor, (3.16).

It is probably pertinent to remark here that the tensor $\mathcal{T}^{\mu\nu}$ defined by Eqs. (3.14) and (3.16) is symmetric by virtue of the fact that the matter field equations are satisfied. This is a direct result of the invariance of the Lagrangian with respect to the choice of any particular bein system. Different bein systems are related to one another by orthogonal bein transformations.

From here on, we shall change our viewpoint slightly. When heretofore we have used Greek indices for coordinate components, it was not implied that there existed an underlying orthogonal be in system. In all subsequent formulas, even when coordinate indices are used on spinors, it will be understood that some orthogonal quadruped system has been chosen to which all spinors are implicitly referred. In other words, from now on, we shall take

$$\gamma^\mu=h^\mu{}_m\gamma^m, \quad (3.18)$$

and assume, as a matter of course, that the γ^m are the constant Dirac matrices chosen in (3.8). The γ^m are no longer field variables. Of course, the usual notation for ordinary vectors and tensors is still the same as before:

$$A^\mu=h^\mu{}_m A^m. \quad (3.19)$$

It is desirable to eliminate those terms in Eq. (3.16) which contain the partial derivatives of the electron Lagrangian with respect to the gravitational variables. They are hard to evaluate as they stand, and it is possible to eliminate them by the use of certain identities. In order to take advantage of this method, however, it is necessary to put the expression for $\mathcal{T}^{\mu\nu}$ into a form in which its tensor character is explicit. Rosenfeld[1] has done this. His expression is

$$\mathcal{T}_\nu{}^\mu=\frac{\partial\mathfrak{M}}{\partial\psi_{;\mu}}\psi_{;\nu}+\psi^\dagger{}_{;\nu}\frac{\partial\mathfrak{M}}{\partial\psi^\dagger{}_{;\mu}}-\mathfrak{M}\delta_\nu{}^\mu+U_M{}^{[\lambda\mu]}{}_{\nu;\lambda}. \quad (3.20)$$

The terms in question now are

$$\frac{\partial\mathfrak{M}}{\partial h_{,\lambda}}F_{(h)\nu}{}^\mu=\frac{\partial\mathfrak{M}}{\partial h^\alpha{}_{,\lambda}}\delta_\nu{}^\alpha h^\mu{}_\alpha. \quad (3.21)$$

We will need to work with a particular antisymmetric expression of the U's:

$$Z^{\lambda[\mu\nu]}=U_M{}^{[\lambda\mu]\nu}-U_M{}^{[\lambda\nu]\mu}=\frac{\partial\mathfrak{M}}{\partial h^\alpha{}_{,\lambda}}\{h^\mu{}_\alpha g^{\alpha\nu}-h^\nu{}_\alpha g^{\alpha\mu}\}+\frac{\partial\mathfrak{M}}{\partial\psi_{,\lambda}}\{F_{(\psi)\sigma}{}^\mu g^{\sigma\nu}-F_{(\psi)\sigma}{}^\nu g^{\sigma\mu}\}. \quad (3.22)$$

The program is to eliminate $\partial\mathfrak{M}/\partial h_{,\lambda}$ from this expression also, and we do this by means of an identity due to the bein invariance of the electron Lagrangian. We speak now of the transformation

$$\delta h^{a}{}_{a}=\epsilon^{b}{}_{a}h^{a}{}_{b}, \tag{3.23}$$

where the $\epsilon^{b}{}_{a}$ are the Lorentz transformation coefficients which satisfy the relations

$$\epsilon^{b}{}_{a}\epsilon^{a}{}_{c}=\delta_{c}{}^{b}, \quad \epsilon^{ba}+\epsilon^{ab}=0, \quad \epsilon^{ba}=\epsilon^{b}{}_{c}\eta^{ca}. \tag{3.24}$$

The possibility is left open here for the "amount of rotation" of the bein vectors to be a function of position in the space. Under this transformation the variation of the matter part of the action becomes

$$\delta I=\int\left\{\left[\frac{\delta\mathfrak{M}}{\delta h^{a}{}_{a}}\delta h^{a}{}_{a}+\frac{\delta\mathfrak{M}}{\delta\psi}\delta\psi+\delta\psi^{\dagger}\frac{\delta\mathfrak{M}}{\delta\psi^{\dagger}}\right]\right.$$
$$\left.+\left[\frac{\partial\mathfrak{M}}{\partial h^{a}{}_{a,\beta}}\delta h^{a}{}_{a}+\frac{\partial\mathfrak{M}}{\partial\psi_{,\beta}}\delta\psi+\delta\psi^{\dagger}\frac{\partial\mathfrak{M}}{\partial\psi^{\dagger}{}_{,\beta}}\right]_{,\beta}\right\}d^{4}x=0. \tag{3.25}$$

This equation gives rise to two independent identities: that due to the volume integral, and that due to the divergence or surface part. This is because the descriptors of the transformation may be taken zero on the surface, thus making the volume integrand zero; but since the combination is also zero, then the surface contribution must also be zero. In order to obtain the identities themselves, we need the expression for $\delta\psi$ and $\delta\psi^{\dagger}$. Assume

$$\delta\psi=\sigma\psi, \quad \delta\psi^{\dagger}=-\psi^{\dagger}\sigma, \tag{3.26}$$

where σ is some spinor of second rank. Then we must have

$$\delta\gamma^{l}=0=\epsilon^{l}{}_{m}\gamma^{m}+\sigma\gamma^{l}-\gamma^{l}\sigma; \tag{3.27}$$

from which, by assuming a solution quadratic in the γ^{l},

$$\sigma=\tfrac{1}{4}\epsilon_{ij}\gamma^{i}\gamma^{j}. \tag{3.28}$$

Incidentally, here we have the same situation we had in the expression for the Γ_{l}. That is, there is a trace term omitted which we have set equal to zero. As it stands now, Eq. (3.28) contributes no traces to Γ_{l}, and hence the electromagnetic fields once set equal to zero remain zero. This also shows how the electromagnetic interaction terms may be incorporated into the spinor fields, and at the same time remain independent of the electron field.[12] If we put the expressions for the variations into Eq. (3.25), and remember the antisymmetry of the ϵ_{ij}, see (3.24), then the arbitrariness of the rotation coefficients allows us to write the two identities

$$\frac{\delta\mathfrak{M}}{\delta h^{a}{}_{m}}\{h^{ab}\delta_{m}{}^{a}-h^{aa}\delta_{m}{}^{b}\}+\frac{1}{4}\frac{\delta\mathfrak{M}}{\delta\psi}[\gamma^{a}\gamma^{b}-\gamma^{b}\gamma^{a}]\psi$$
$$+\frac{1}{4}\psi^{\dagger}[\gamma^{b}\gamma^{a}-\gamma^{a}\gamma^{b}]\frac{\delta\mathfrak{M}}{\delta\psi^{\dagger}}=0,$$
$$\frac{\partial\mathfrak{M}}{\partial h^{a}{}_{m,\lambda}}\{h^{ab}\delta_{m}{}^{a}-h^{aa}\delta_{m}{}^{b}\}+\frac{1}{4}\frac{\partial\mathfrak{M}}{\partial\psi_{,\lambda}}[\gamma^{a}\gamma^{b}-\gamma^{b}\gamma^{a}]\psi \tag{3.29}$$
$$+\frac{1}{4}\psi^{\dagger}[\gamma^{b}\gamma^{a}-\gamma^{a}\gamma^{b}]\frac{\partial\mathfrak{M}}{\partial\psi^{\dagger}{}_{,\lambda}}=0.$$

After multiplying the second of these identities by $h^{\mu}{}_{a}h^{\nu}{}_{b}$, and using Eq. (3.7), we see that

$$\frac{\partial\mathfrak{M}}{\partial h^{a}{}_{K,\lambda}}\{h^{\mu}{}_{K}g^{a\nu}-h^{\nu}{}_{K}g^{a\mu}\}+\frac{1}{4}\frac{\partial\mathfrak{M}}{\partial\psi_{,\lambda}}[\gamma^{\mu}\gamma^{\nu}-\gamma^{\nu}\gamma^{\mu}]\psi$$
$$+\frac{1}{4}\psi^{\dagger}[\gamma^{\nu}\gamma^{\mu}-\gamma^{\mu}\gamma^{\nu}]\frac{\partial\mathfrak{M}}{\partial\psi^{\dagger}{}_{,\lambda}}=0. \tag{3.30}$$

It is now possible with the help of Eq. (3.30) to eliminate $\partial\mathfrak{M}/\partial h_{,\lambda}$ in Eq. (3.22), and that equation now becomes

$$Z^{\lambda[\mu\nu]}=-\frac{1}{4}\frac{\partial\mathfrak{M}}{\partial\psi_{,\lambda}}[\gamma^{\mu}\gamma^{\nu}-\gamma^{\nu}\gamma^{\mu}]\psi$$
$$+\frac{1}{4}\psi^{\dagger}[\gamma^{\mu}\gamma^{\nu}-\gamma^{\nu}\gamma^{\mu}]\frac{\partial\mathfrak{M}}{\partial\psi^{\dagger}{}_{,\lambda}}. \tag{3.31}$$

Here $F_{(\psi)\nu}{}^{\mu}=0$ because the infinitesimal coordinate transformation does not change ψ; only a bein transformation affects the ψ field. The $U_{M}{}^{[\lambda\mu]\nu}$ thus assumes a particularly simple expression

$$U_{M}{}^{[\lambda\mu]\nu}=\tfrac{1}{2}\{Z^{\lambda[\mu\nu]}-Z^{\nu[\lambda\mu]}+Z^{\mu[\nu\lambda]}\}. \tag{3.32}$$

The expression $U_{M}{}^{[\lambda\mu]\nu}$ itself now contains no partial derivatives of $\mathfrak{M}$ with respect to the gravitational variables, and is quite easy to evaluate.

At this point, it remains only to carry out the operations indicated in the definition of $Z^{\lambda[\mu\nu]}$ with the electron Lagrangian. With reference to (3.5), after a short calculation, we have

$$Z^{\lambda[\mu\nu]}=-\tfrac{1}{8}ich(-g)^{\frac{1}{2}}\psi^{\dagger}\gamma^{\lambda}[\gamma^{\mu}\gamma^{\nu}-\gamma^{\nu}\gamma^{\mu}]\psi$$
$$-\tfrac{1}{8}ich(-g)^{\frac{1}{2}}\psi^{\dagger}[\gamma^{\mu}\gamma^{\nu}-\gamma^{\nu}\gamma^{\mu}]\gamma^{\lambda}\psi, \tag{3.33}$$

and

$$U_{M}{}^{[\lambda\mu]}{}_{\nu}=\tfrac{1}{8}ich(-g)^{\frac{1}{2}}\psi^{\dagger}\{2\gamma^{\dagger}\delta_{\nu}{}^{\mu}-2\gamma^{\mu}\delta_{\nu}{}^{\lambda}$$
$$-[\gamma^{\lambda}\gamma^{\mu}-\gamma^{\mu}\gamma^{\lambda}]\gamma_{\nu}\}\psi. \tag{3.34}$$

Because of the terms in $U_{M}{}^{[\lambda\mu]}{}_{\nu}$ in the expression for the matter energy-momentum tensor density, that quantity

[12] See for a fuller discussion of this point E. Schrödinger, Preuss. Akad. Wiss. Berlin, Ber. 11–12, 105 (1932).

has become somewhat complicated: it takes the form

$$\mathfrak{T}_\nu^\mu = \tfrac{1}{2}ich(-g)^{\frac{1}{2}}\{\psi^\dagger\gamma^\mu\psi_{;\nu} - \psi^\dagger_{;\nu}\gamma^\mu\psi\} - \tfrac{1}{8}ich(-g)^{\frac{1}{2}}\psi^\dagger_{;\lambda}\{[\gamma^\lambda\gamma^\mu - \gamma^\mu\gamma^\lambda]\gamma_\nu + 2\gamma^\mu\delta_\nu{}^\lambda - 2\gamma^\lambda\delta_\nu{}^\mu\}\psi$$
$$-\tfrac{1}{8}ich(-g)^{\frac{1}{2}}\psi^\dagger\{[\gamma^\lambda\gamma^\mu - \gamma^\mu\gamma^\lambda]\gamma_\nu + 2\gamma^\mu\delta_\nu{}^\lambda - 2\gamma^\lambda\delta_\nu{}^\mu\}\psi_{;\lambda}. \quad (3.35)$$

It should be emphasized that for our use the complete expression is necessary for the matter tensor. It will be remembered that in the special relativity theories the U part is added only to make the energy-momentum symmetric, and that if it is deleted entirely, the integrated energy and momentum is unchanged. In those theories the covariant divergence becomes an ordinary divergence and may be integrated out. In this generally covariant theory, however. Gauss' law may not be used in the same fashion for this term, and the entire expression, (3.35), must always be used.

We should like now to write down the expressions representing the angular momentum of the electron-gravitation field. In this connection we must bear in mind that the only unique aspect of the energy-momentum or the angular momentum is the total, or integrated, value taken over the whole three-dimensional space at some particular time t_0. This is because one may add to the four-dimensional density expression any divergence-less expression, and it would still be "conserved." In addition, it is easy to demonstrate that the integrated form of all such expressions gives identical values. But first we shall obtain the integrated expressions themselves. In order to obtain them, we integrate Eq. (2.20) over some four-dimensional region. We specialize the region to be a cylinder between two time surfaces, with the sides of the cylinder taken to spatial infinity, where the electron field is assumed zero and the metric flat. Designating the region by V_4, we have

$$\int \Omega^{\mu[\nu\lambda]}{}_{,\mu}d^4x = 0, \quad (3.36)$$

which because of Gauss' law, can be turned into

$$J^{\nu\lambda} = \int_{t_1} \Omega^{4[\nu\lambda]}d^3x = \int_{t_2} \Omega^{4[\nu\lambda]}d^3x. \quad (3.37)$$

$J^{\nu\lambda}$ is now the total angular momentum of the field, and is an invariant with respect to arbitrary coordinate transformations carried out within the region V_4, with the sole restriction that in any transformation, the new coordinates go over into the old ones on the boundary of V_4. Now it can be seen that if we add to $\Omega^{4[\nu\lambda]}$ some expression whose divergence vanishes $\chi^{4[\nu\lambda]}$, then it may be represented as the divergence of an antisymmetric quantity (a curl),

$$\chi^{4[\nu\lambda]} = V^{[4\sigma][\nu\lambda]}{}_{,\sigma}. \quad (3.38)$$

When $\chi^{4[\nu\lambda]}$ is integrated over the infinite three-space, then

$$\int V^{[4\sigma][\nu\lambda]}{}_{,\sigma}d^3x = \oint_{2\text{-surface}} V^{[4\sigma'][\nu\lambda]}dS_{\sigma'} + \int V^{[44][\nu\lambda]}{}_{,4}d^3x, \quad (3.39)$$
$$\sigma' = 1, 2, 3.$$

The second term on the right is zero by the symmetry assumed in the $V^{[\alpha\beta][\gamma\delta]}$ function. Hence, for all those functions $V^{[4\sigma'][\nu\lambda]}$ which fall off faster than $1/R^2$ (assumption of no radiation), the integrated value of the angular momentum is uniquely defined.

From Eq. (2.21), the matter contribution to $J^{\nu\lambda}$ may be written

$$J_M{}^{\nu\lambda} = \int \{\mathfrak{T}^{4\nu}x^\lambda - \mathfrak{T}^{4\lambda}x^\nu\}d^3x \quad (3.40)$$

or

$$J_M{}^{\nu\lambda} = \int \left\{\frac{\partial\mathfrak{M}}{\partial\psi_{,4}}\psi^{i\nu}x^\lambda + \psi^{\dagger i\nu}\frac{\partial\mathfrak{M}}{\partial\psi_{,4}}x^\lambda - \frac{\partial\mathfrak{M}}{\partial\psi_{,4}}\psi^{i\lambda}x^\nu \right.$$
$$\left. -\psi^{\dagger i\lambda}\frac{\partial\mathfrak{M}}{\partial\psi_{,4}}x^\nu + U_M{}^{[\sigma 4]\nu}{}_{;\sigma}x^\lambda - U^{[\sigma 4]\lambda}{}_{;\sigma}x^\nu\right\}d^3x. \quad (3.41)$$

Now $U_M{}^{[\sigma\mu]\nu}$ is a tensor density, so

$$U_M{}^{[\sigma 4]\nu}{}_{;\sigma} = \left\{\begin{matrix}\sigma\\ \sigma\beta\end{matrix}\right\}U_M{}^{[\beta 4]\nu} + \left\{\begin{matrix}\nu\\ \sigma\beta\end{matrix}\right\}U_M{}^{[\sigma 4]\beta}$$
$$+U^{[\sigma 4]\nu}{}_{,\sigma} - \left\{\begin{matrix}\sigma\\ \sigma\beta\end{matrix}\right\}U_M{}^{[\beta 4]\nu} \quad (3.42)$$

giving

$$J_M{}^{\nu\lambda} = \int \left\{\frac{\partial\mathfrak{M}}{\partial\psi_{,4}}\psi^{i\nu}x^\lambda - \frac{\partial\mathfrak{M}}{\partial\psi_{,4}}\psi^{i\lambda}x^\nu + \psi^{\dagger i\nu}\frac{\partial\mathfrak{M}}{\partial\psi^\dagger_{,4}}x^\lambda \right.$$
$$-\psi^{\dagger i\lambda}\frac{\partial\mathfrak{M}}{\partial\psi^\dagger_{,4}}x^\nu + \left\{\begin{matrix}\nu\\ \sigma\beta\end{matrix}\right\}U_M{}^{[\sigma 4]\beta}x^\lambda$$
$$-\left\{\begin{matrix}\lambda\\ \sigma\beta\end{matrix}\right\}U_M{}^{[\sigma 4]\beta}x^\nu - U_M{}^{[\lambda 4]\nu} + U_M{}^{[\nu 4]\lambda}$$
$$\left. -(U_M{}^{[\sigma 4]\nu}x^\lambda - U_M{}^{[\sigma 4]\lambda}x^\nu)_{,\sigma}\right\}d^3x. \quad (3.43)$$

The spatial divergence term in the integrand may be converted into a two-surface integral, but the original region V_4 was chosen so that the contribution is zero. (The $U_M{}^{[\sigma 4]\lambda}$ contains electron field functions, which

will be assumed to fall off faster than $1/R^2$.) The 4-component is zero again because of the antisymmetry of the U function. Thus we have, finally,

$$J_M{}^{\nu\lambda}=\int\Big\{\frac{\partial\mathfrak{M}}{\partial\psi_{,4}}\psi^{i;\nu}x^\lambda-\frac{\partial\mathfrak{M}}{\partial\psi_{,4}}\psi^{i;\lambda}x^\nu+\psi^{\dagger i;\nu}\frac{\partial\mathfrak{M}}{\partial\psi^\dagger_{,4}}x^\lambda-\psi^{\dagger i;\lambda}\frac{\partial\mathfrak{M}}{\partial\psi^\dagger_{,4}}x^\nu+U_m{}^{[\sigma 4]\beta}\left(\left\{\begin{matrix}\nu\\ \sigma\beta\end{matrix}\right\}x^\lambda-\left\{\begin{matrix}\lambda\\ \sigma\beta\end{matrix}\right\}x^\nu\right)+U_M{}^{[\lambda 4]\nu}-U_M{}^{[\nu 4]\lambda}\Big\}d^3x. \quad (3.44)$$

By using the expression (3.34) then the last equation becomes

$$J_M{}^{\nu\lambda}=\int\Big\{\frac{\partial\mathfrak{M}}{\partial\psi_{,4}}\psi^{i;\nu}x^\lambda-\frac{\partial\mathfrak{M}}{\partial\psi_{,4}}\psi^{i;\lambda}x^\nu+\psi^{\dagger i;\nu}\frac{\partial\mathfrak{M}}{\partial\psi^\dagger_{,4}}x^\lambda-\psi^{\dagger i;\lambda}\frac{\partial\mathfrak{M}}{\partial\psi^\dagger_{,4}}x^\nu+U_M{}^{[\sigma 4]\beta}\left(\left\{\begin{matrix}\nu\\ \sigma\beta\end{matrix}\right\}x^\lambda-\left\{\begin{matrix}\lambda\\ \sigma\beta\end{matrix}\right\}x^\nu\right)+\tfrac{1}{4}ich(-g)^{\frac{1}{2}}\psi^\dagger\gamma^4(\gamma^\nu\gamma^\lambda-\gamma^\lambda\gamma^\nu)\psi\Big\}d^3x. \quad (3.45)$$

To $J_M{}^{\nu\lambda}$ must be added the gravitational contribution:

$$J_G{}^{\nu\lambda}=\int\{\tau_G{}^{4\nu}x^\lambda-\tau_G{}^{4\lambda}x^\nu+U_G{}^{[\lambda 4]\nu}-U_G{}^{[\nu 4]\lambda}\}d^3x. \quad (3.46)$$

It is interesting to compare (3.45) with the quantity used in the special relativity theories. In the limiting case where the gravitational field is zero, and the space is flat, (3.45) degenerates precisely to the Lorentz-invariant angular momentum in general use.[8]

The expression of (3.45) in terms of the bein components has a particular significance.

$$J_M{}^{nl}=\int\Big\{\frac{\partial\mathfrak{M}}{\partial\psi_{,4}}\psi^{i;n}x^l-\frac{\partial\mathfrak{M}}{\partial\psi_{,4}}\psi^{i;l}x^n+\psi^{\dagger i;n}\frac{\partial\mathfrak{M}}{\partial\psi^\dagger_{,4}}x^l-\psi^{\dagger i;l}\frac{\partial\mathfrak{M}}{\partial\psi_{,4}}x^n+\left(\left\{\begin{matrix}\nu\\ \sigma\beta\end{matrix}\right\}x^\lambda-\left\{\begin{matrix}\lambda\\ \sigma\beta\end{matrix}\right\}x^\nu\right)h^l{}_\lambda h^n{}_\nu U_M{}^{[\sigma 4]\beta}+\tfrac{1}{4}ich(-g)^{\frac{1}{2}}\psi^\dagger\gamma^4[\gamma^n\gamma^l-\gamma^l\gamma^n]\psi\Big\}d^3x. \quad (3.47)$$

Equation (3.47) breaks into three parts. The first four terms are the usual orbital momentum terms, and the last term is the direct analog to the spin, provided we use the bein representation. This last term contributes the usual value of $\frac{1}{2}\hbar$ to the total angular momentum, since the γ^l matrices involved are simply the constant Dirac matrices. But the third term represents a correction to the usual expression of the *orbital* momentum (since it is seen to be proportional to the coordinates) which is due to the curvature of the space.

4. CONCLUSION

In conclusion, then, we have found a generally covariant representation for the angular momentum of a physical field which includes a matter field in addition to the gravitational field. A semiclassical discussion of the Dirac electron field shows that the intrinsic angular momentum of the electron has the expected value of $\frac{1}{2}\hbar$. The orbital momentum is a direct generalization of that of the usual theory, with some added terms that may be traced to the nonflatness of the space in the vicinity of the electron.

Further Results from the Study of Sea-Level Penetrating Showers

W. Y. Chang, G. Del Castillo,* and Leon Grodzins
Physics Department, Purdue University, Lafayette, Indiana

(Received August 21, 1952)

Thirty-five non-ionizing link showers (produced at a 17-g/cm² Pb plate) associated with sea-level penetrating showers are presented. These have their axes oriented toward the origins of the penetrating showers and are believed to be cascade electronic showers initiated by high energy photons, which are probably produced from the decay of π^0 mesons among the penetrating shower particles. The size distribution of these showers is given showing a spread from 2 to 20 particles per shower. The angular distribution of their axes with respect to the penetrating shower axes is also approximately determined.

Showers particles (of the penetrating showers) scattered by Be and Pb at angles greater than 10°, 15°, 20°, 30°, and 40° have been observed. The mean free path against scattering, and the corresponding scattering cross section per nucleon have been estimated in each case. The total scattering cross section per nucleon is of the order of magnitude of several millibarns. This figure may be compared with the total theoretical meson-nucleon scattering cross section calculated from pseudoscalar or scalar theory for meson energy equal to several times its rest energy. Perhaps, it is several times smaller than the total experimental nucleon-nucleon scattering cross section for, say, 300-Mev proton energy. Our experimental cross section probably represents the combined effect of meson-nucleon and nucleon-nucleon scattering.

1. INTRODUCTION

IN previous communications[1] we have presented our experimental results obtained at sea level for (1) the multiplicity distribution of the penetrating showers produced in Be, C, and Pb, (2) the angular distribution of the shower particles, and (3) the mean free path against total absorption in Be and Pb of the shower particles. In order to complete our preliminary study, we should like to report from further analysis, the following two more types of results: (*a*) the non-ionizing link showers associated with penetrating showers and (*b*) the scattering of the penetrating shower particles. These two types of events are very rare and, consequently, the statistics are bound to be poor. It is hoped, however, that they may help to throw some light into the nature of the penetrating-shower particles produced at sea level.

2. NON-IONIZING LINK SHOWERS ASSOCIATED WITH PENETRATING SHOWERS

Electronic components associated with penetrating showers have been observed by several workers.[2] These have been interpreted as due to the decay in flight, into two photons, of neutral pi-mesons which are assumed to be produced among the particles of the penetrating showers. However, in most of these cases the pictures are so complicated that it is not possible to decide whether the electrons arise from gamma-rays. The electrons very often appear to have come from the same place as the penetrating-shower particles. In the study of penetrating showers produced in Be, C, and Pb at sea level, we have found, in addition to the mixed showers of the above type, 35 missing-link showers at the bottom Pb plate (17 g/cm²) from about 350 penetrating showers.[1] Each of these showers has its approximate axis pointing toward the origin of the penetrating shower with no observable producing particle. A few pictures similar to these have also been reported recently by other workers.[2] The shower particles in all of the 35 cases have wide angular spread (most of the cases around 60°, some as large as 150°). In each shower all of the tracks show minimum ionization and some suffer from multiple scattering in the gas. Therefore, it is believed that these non-ionizing link showers are electronic showers.[3]

TABLE I. Size distribution of the non-ionizing link showers. N is the number of charged particles per shower.

Picture quality \ N	2	3	4	5	6	7	8	9	10	13	14	17	20
A showers	1	4	2	1	3		1	1	1			1	1
B showers	1	3	3	3	2	1		2	1	1	1		1
Total	2	7	5	4	5	1	1	3	2	1	1	1	2

Figures 1 and 2 are two examples of these events. Figure 1 shows a penetrating shower of three particles produced from the second Be plate. The two particles on the left-hand side pass through the Pb plate, while the one on the right suffers from backward scattering, moving upward to the front glass plate of the chamber. A missing-link shower of four particles is seen from the

* Supported in part by the Purdue Research Foundation and Institute Nacional de la Investigacion Cientifica, Mexico.

[1] Chang, Del Castillo, and Grodzins, Phys. Rev. **84**, 582, 584 (1951). In the 11-month study approximately 8000 pictures were taken. About 350 showed penetrating showers from the desired substances, of which 220 were suitable for analysis and have been published. More than 20 percent of the 350 showers are seen to contain electronic components, as determined by the multiplication at the Pb plate. Out of these, 35 are the missing link showers produced at the bottom Pb plate, 10 each associated with C and Pb showers and 15 with Be showers.

[2] For earlier references, see G. D. Rochester and W. G. V. Rosser, Repts. Progr. Phys. (London) **14**, 249 (1951). Also Gregory, Rossi, and Tinlot, Phys. Rev. **77**, 299 (1950); **81**, 675 (1951).

[3] As estimated roughly from the cascade-shower theory, the energy of the initiating photons varies from about 50 Mev to about 10 Bev. The best way would have been to count the number at maximum but, with only one thick Pb plate in the chamber, this could not be done.

TABLE II. Distribution of approximate projected angle in degree (at the origin of the penetrating shower) between the axes of the non-ionizing link and the penetrating showers.

Picture quality \ Degree	0–3	4–7	8–11	15	20
A showers	10	5		1	1
B showers	11	6	1		
Total	21	11	1	1	1

Pb plate, with its approximate axis pointing toward the origin of the penetrating shower. Figure 2 is a similar picture having a much larger electronic shower of at least 17 particles. The penetrating shower is produced again in the second Be plate, and all the three shower particles pass through the Pb plate. The large electronic shower with no observable initiating particle appears under the Pb plate on the left of the penetrating shower. The apex of this electronic shower is clearly separated from all of the particles of the penetrating shower, as can easily be seen in an enlarged print. It is to be noted that in both cases no heavily ionizing particles are seen among the particles of the missing-link showers, that the thin tracks have large angular spread, and that some show multiple scattering in the gas. It is, therefore, extremely unlikely that they are nuclear events.

FIG. 1. A penetrating shower of 3 particles produced in Be_2. One of the 3 particles is scattered upwards to the glass window, and the other two pass through the Pb plate (17 g/cm²). A non-ionizing link shower of 4 particles occurs at the Pb plate (on the right), which may be interpreted as due to decay of a neutral pi-meson into 2 photons. One of the two photons is converted into the cascade shower.

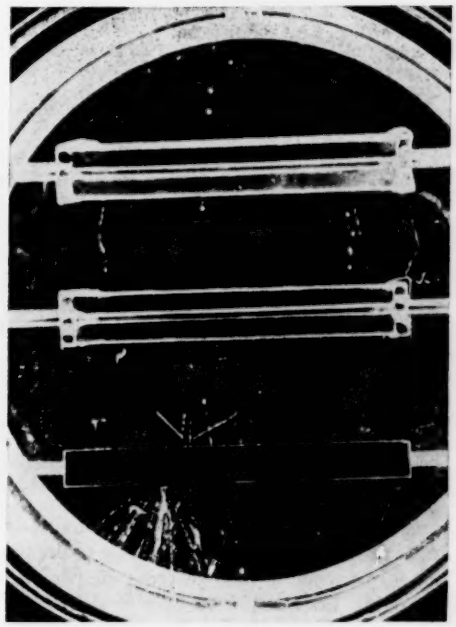

FIG. 2. An event similar to that shown in Fig. 1. All of the three penetrating-shower particles pass through the Pb plate. A missing link shower of at least 17 particles appears under the Pb plate (on the left) which may be similarly interpreted as in Fig. 1.

The size distribution of these showers is shown in Table I. The size of a shower may represent the energy[3] of the initiating photon, though for a given energy there is a large fluctuation in the number of the particles. It is seen that some showers have particles as many as 20. Table II shows the angular distribution of the missing-link shower axis from the penetrating-shower axis. The figures for the projected angles were only approximately determined because of the difficulty in defining the two shower axes. However, these two tables are good enough to indicate the angular (with respect to penetrating-shower axes) and energy spread of the initiating photons.

Because of the relatively small surface of the Pb plate in our arrangement, the chance to observe both photons from each decay is small.[4] This was particularly true when the penetrating showers and hence the neutral mesons were produced in the Pb or C which was placed above the chamber. So far, we have observed only one case where two missing-link showers are associated with a penetrating shower produced in Be with both their approximate axes pointing toward the origin of the penetrating shower. Unfortunately this picture is of poor quality. Several pictures have also been observed, where the non-ionizing link showers do

[4] For discussion on neutral mesons and related problems, see C. F. Powell, Repts. Progr. Phys. (London) **13**, 402 (1950), and B. Rossi, *High Energy Particles* (Prentice-Hall, Inc., New York, 1952).

TABLE III. Scattering cross section of penetrating-shower particles at different angles.[a] θ=projected angles of scattering in degrees larger than specified; N=No. of particles scattered at angles larger than specified; L=mean free path in g/cm²; σ=cross section per nucleon in millibarns.

Showers	Scatterer		>10°	>15°	>20°	>30°	>40°	No. of traversals
C−Pb		N	5	4	2	0	0	405
	Be	L	780	980	1950			
		σ	2.1	1.7	0.8			
		N	12	9	9	7	2	302
	Pb	L	430	570	570	740	2580	
		σ	3.9	2.9	2.9	2.3	0.7	
Be		N	9	8	3	0	0	142
	Pb	L	270	300	810			
		σ	6.2	5.6	2.1			

[a] The theoretical total cross section for meson-nucleon scattering at meson energy $\sim 5\mu c^2$ is as follows.
Pseudoscalar theory; $\sigma \sim 1$ millibarn, for $g^2/\hbar c \sim 1$.
Scalar theory: $\sigma \sim 3$ millibarn, for $g^2/\hbar c = 2.39\mu/M$ as determined from deuteron binding energy.

not have their axes oriented toward the origins of the penetrating showers. These could be due to decay at a distance (of very fast π^0 mesons) from the penetrating-shower origins. No attempt has been made to correlate these showers with the observed penetrating showers, because in each picture only one such non-ionizing link shower has been found.

From the solid angle of detection and probability of conversion of the photons, a crude estimate shows that the number of π^0 mesons is of the same order of magnitude as (though smaller than) that of the charged shower particles.

3. THE SCATTERING OF THE PENETRATING-SHOWER PARTICLES

Measurement has been carried out of the large angle scattering of the penetrating-shower particles previously reported,[1] in the hope that more knowledge may be obtained about the nature[5] of the shower particles produced particularly at sea level. The showers produced in C and in Pb have been grouped together to form the "C−Pb showers," because in these two elements they have been produced and propagating dowanwards under similar conditions. Some of the shower particles have been scattered by the two Be plates (9.6 g/cm² all together) and others by the Pb plate (17 g/cm²). The showers produced in the two Be plates have been put together as the "Be showers"; in this case, scattering greater than ten degrees has not been observed at the second Be plate but only at the Pb plate.

The particles scattered at angles larger than 10°, 15°, 20°, 30°, and 40° have been observed. The mean free path against scattering and the corresponding scattering cross section per nucleon have been estimated in each case from the number of particles so scattered and the number of traversals. The number of traversals in each element does not include those particles which are absorbed catastrophically. The results are presented in Table III. It is seen that all the cross sections lie between 10^{-26} and 10^{-27} cm²/nucleon. The figures for the mean free path and hence those for the cross section must not be taken too seriously because of low statistics. The angles for the two particles of C−Pb showers scattered by Pb at angles greater than 40° as listed are actually about 50° and 70°, respectively. We have also observed two events of backward scattering. One particle of a 3-particle Be shower has been scattered at about 130° and another of a 2-particle Pb shower at about 150°, both occurring at the Pb plate. These last two events have not been included in Table I.

It is very probable that the scattering events at the plates as described above are due to single nuclear scattering (by Coulomb or nuclear force) instead of multiple Coulomb scattering as may be judged from the fact that the scattering angles are fairly large yet the ionization of the scattered particles is only about minimum. Most of the particles of the penetrating showers must be nonelectronic, except those electrons found in the mixed showers as identified by the multiplications at the 17 g/cm² Pb plate. It may also be noticed that none of the particles of the C−Pb showers, which had been already scattered by Be, produces any multiplication at the Pb plate. Furthermore, nearly all the scattered particles, including those two backward scattered ones, do not show appreciable multiple scattering in the gas. Therefore, most of the charged shower particles as observed in the chamber must be either protons or π-mesons (or some other mesons) or both. For these particles, if the scattering process in the plates were multiple, the energies of the particles scattered at such angles must be low enough that their tracks should have ionization much greater than the minimum value. However, all the scattered particles (in fact, all the shower particles) appear to have minimum ionization. This seems to indicate, therefore, that most, if not all, of the scattering events are due to single nuclear scattering (more probably by nuclear force) instead of multiple Coulomb scattering, unless the charged shower particles were electrons which as mentioned above are improbable.

It may be interesting to see how the scattering cross sections obtained in our experiments are compared with some theoretical values for meson-nucleon scattering and with that of nucleon-nucleon scattering. Our results for scattering in Be at angles larger than 10° and 15°, respectively, are of the same order of magnitude as those obtained at high altitude by Green[6] for carbon at the corresponding angles. However, our results for scattering in Pb at angles larger than 15° are 10 to 20 times larger than that (at high altitude, too) of Fretter[7] for the same material and angular range. The results from our experiments at sea level seem to be in closer

[5] O. Piccioni, Phys. Rev. **77**, 1 (1950).

[6] F. R. Green, Phys. Rev. **80**, 832 (1950).

[7] W. B. Fretter, Phys. Rev. **76**, 511 (1949).

agreement than Fretter's with the theoretical meson-nucleon scattering cross sections calculated from certain meson theories for reasonably estimated meson energies. For example, our experimental cross sections are roughly comparable with the theoretical values of the pseudoscalar theory[8] for meson energies several times its rest energy, when the coupling constant (or the nucleon area for mesons) is properly chosen.[9] Moreover, they are also compatible with the values obtained from the scalar theory for similar meson energies, if in this latter case the coupling constant is determined from the binding energy of the deuteron. On the other hand, the total scattering cross sections obtained from experiment for nucleon-nucleon scattering at several hundred Mev proton energies would probably be several times larger than the values obtained from Table I. Closer comparison is not very meaningful at present because of the unknown momentum spectrum of the shower particles and because of the poor statistics. All one can say at present is: The sea-level penetrating-shower particles are very probably both mesons (of some kind) and protons.

Experiments with two large rectangular cloud chambers (16 in.×16 in.×14 in. each), one above the other, are being started at Purdue, in which efforts are being made to identify the shower particles, to reduce discriminations in the measurements of the multiplicity and angular distributions, and to observe multiplicity of penetrating showers produced from liquid hydrogen to be put above the top chamber.

In conclusion, we are grateful to Princeton University for the apparatus used in this work, which one of us (W. Y. C.) and his co-workers built at Princeton, and to our colleagues at Purdue, particularly R. M. Whaley, K. Lark-Horovitz, and R. Haxby, for their interest and support in these experiments.

[8] M. Peshkin, Phys. Rev. **81**, 425 (1951).
[9] H. A. Bethe and R. R. Wilson, Phys. Rev. **83**, 690 (1951).

PHYSICAL REVIEW VOLUME 89, NUMBER 2 JANUARY 15, 1953

Production of Negative Ions and Noise in Negative Ion Beams*†

WADE L. FITE‡
Lyman Laboratory of Physics, Harvard University, Cambridge, Massachusetts
(Received October 7, 1952)

In a search for high current sources of low energy (≈100 ev) negative atomic ions of hydrogen and oxygen, five types of sources were examined. The most promising practical source for both H^- and O^- was found to be the dc glow discharge from which beams of 10^{-7} ampere of either ion could be drawn. Hot cathode arc discharges yielded H^- currents of 7×10^{-8} ampere. Rf discharges, hollow cathode discharges, and sources involving the Arnot effect seem inferior as high current sources.

Two results were found which are of interest both for the mechanism of the discharge and for the production of negative ions. First, the most copious source of negative ions seems to be the anode side of well-formed striations such as are present in the two superior sources. Second, when either of these sources is used, the beam noise in the low audiofrequency range is much greater than shot noise and is related to fluctuations in the striations.

I. INTRODUCTION

IN the past twenty years, considerable attention has been given to certain negative ions. The theory of the opacity of the solar atmosphere, evolved primarily by Wildt and Chandrasekhar, has as its major thesis the absorption of light by negative atomic hydrogen ions (H^-). It is calculated that the absorption spectrum of these ions is a broad continuum in the visible and infrared light regions and that the presence of these ions in the sun's atmosphere would slightly alter the continuous spectrum of the sun from a blackbody spectrum to one such as is actually found.[1]

In the realm of upper atmosphere physics, attention has been directed to the negative atomic oxygen ion (O^-). The assumption of the presence of these ions in the ionosphere has been used in the past to account for the apparent coefficient of recombination between positive ions and electrons, the night-time persistence of the ionized layers, and the appearance of the green and red lines of the atomic oxygen spectrum in the air-glow or night sky spectrum.[2] For the most part, information about these ions has been acquired from theory. In the case of H^-, calculations appear to be trustworthy; for here the arbitrarily accurate Hylleraas wave function for the ion in the ground state can be used. In the case of O^-, exact calculations of quantities relevant to upper atmosphere physics are frequently replaced by little more than considered guesses.

It is clear that direct laboratory measurements on negative ions are desirable—in the case of H^-, to check

* The material in this paper is a portion of a thesis submitted to Harvard University in partial fulfillment of the requirements for the Ph.D. degree.
† This work was supported in part by the Office of Naval Research and by the Milton Fund of Harvard University.
‡ Present address: University of Pennsylvania, Philadelphia, Pennsylvania.
[1] S. Chandrasekhar, Revs. Modern Phys. **16**, 301 (1944); A. J. Deutsch, Revs. Modern Phys. **20**, 388 (1948); H. S. W. Massey, *Negative Ions* (Cambridge University Press, Cambridge, 1950), second edition, p. 122.
[2] H. S. W. Massey, reference 1, pp. 107–122; S. K. Mitra, *The Upper Atmosphere* (Royal Asiatic Society of Bengal, Calcutta, 1947), Chapters VI, X.

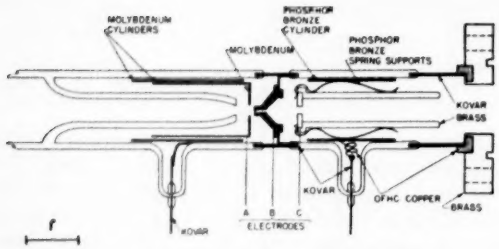

FIG. 1. The glow discharge negative ion source.

calculable quantities, and in the case of O^-, to obtain the various needed values directly. However, the experiments which can be performed on negative ions are few because of the great difficulties in obtaining sufficiently high ion concentrations. Nevertheless, some progress is being made in the directions indicated. For example, Lochte-Holtgreven recently reported observing the electron affinity emission spectrum of H^- in the laboratory.[3] Another experiment, suggested by E. M. Purcell in 1948, would give a direct measurement of the cross section of negative ions for the absorption of a photon (and consequent liberation of the extra bound electron). This latter experiment has been the concern of the author.

The experiment utilizes a beam of low energy negative ions of one variety and requires that the ion beam current be greater than 10^{-8} amp. A second criterion for the ion beam for the successful completion of this "photodetachment" experiment is that the fluctuations in beam current be little more than the shot noise which arises from the random arrival of the discrete charge carriers at the ion collector. Therefore, the experimental problem and the subject of the present paper is the production of such a beam.

II. APPARATUS

In order to meet the requirement that the ions investigated at any one time be of one variety, the apparatus chosen for the experiment on the photodetachment cross sections of negative ions was a small, low energy mass spectrometer. This instrument was also used in the evaluation of the suitability of the different ion source types. It should be remarked that many ions were undoubtedly lost at the slits of the mass spectrometer and that the ultimate currents obtainable from the various sources later discussed are believed to be somewhat higher than the values reported here.

III. NEGATIVE ION SOURCES

Five general types of sources for negative ions were examined: glow discharges, hot cathode arc discharges, radiofrequency discharges, hollow cathode discharges, and sources involving the Arnot effect (the appearance of a negative ion when a positive ion strikes a metal target).[4]

A. Glow Discharges

The first type of source to be examined was the glow discharge. The work of Bennett and Darby had demonstrated that large beams of high energy H^- ions were obtainable from such a discharge through water vapor.[5] Clearly, the beginning point was the further pursuit of their work, attempting to reduce the energy of the ions while increasing the beam current.

The simplest form of such a source of negatively charged ions is a dc glow discharge, in the anode of which is a small hole or canal. Modifications of this type of source introduced by Bennett and Darby to increase beam current include a glass funnel to concentrate the discharge onto a limited region on the anode. Another modification found in the course of the present experiments concentrates the discharge at the anode even further. A flat disk electrode having a $\frac{3}{16}$-in. diameter hole at the center is placed inside the discharge and close to the anode, with its plane perpendicular to the axis of the discharge tube. Then the anode is constructed with a snout-like probe which reaches up to the hole in the disk electrode. By making the disk electrode negative with respect to the anode, an electric field is established which tends to concentrate the discharge at the end of the probe. The canal was placed in the probe in a manner similar to that devised by Tüxen for his negative ion mass spectrograph.[6] The probe, with a $\frac{1}{16}$-in. diameter axial hole in it, was squared off and to this end a piece of 0.003-in. nickel foil was gold soldered. Then a 0.020-in. diameter hole was drilled through the foil. This type of canal minimized the chance of an ion striking a canal wall and either destroying itself or changing charge in the collision. The energy of the ions was controlled by the potential difference between the discharge tube's anode and the grounded body of the mass spectrometer.

It was found necessary to add one other electrode to accelerate the negative ions out of the canal and into the spectrometer. This electrode is maintained at a high positive potential with respect to the anode. In the diagram of the completed glow discharge source (Fig. 1), this third electrode is designated as "Electrode *C*." The flat disk electrode and the anode are called "Electrodes *A*" and "*B*", respectively.

Typical values of the various potentials on the electrode follow:

Mass Spectrometer Tube:	0 volts
Electrode *C*:	500 to 2000 volts
Electrode *B*:	−150 to −50 volts
Electrode *A*:	−500 to −200 volts

The potentials of electrodes *A* and *B* were more or less arbitrary but that of electrode *C* was not. This electrode had, in addition to its role as extractor of ions, an integral part in the ion optics of the mass spectrometer. In order to produce proper images under any given

[3] W. Lochte-Holtgreven, Naturwiss. **38**, 258 (1951).
[4] H. S. W. Massey, reference 1, pp. 79–81 (and papers referred to there).
[5] W. H. Bennett and P. F. Darby, Phys. Rev. **49**, 97 (1936).
[6] O. Tüxen, Z. Physik **103**, 463 (1936).

conditions, definite values of this potential were required.

The cathode end of the discharge tube terminated in the outer member of a ground joint made of Corning Code No. 7052 glass—the glass of which the entire tube was constructed. The cathode itself was mounted on a re-entrant seal to the inner member of the ground joint. The cathode most used was an open aluminum cylinder 2 in. long with an o.d. of $1\frac{1}{4}$ in.

O^- *Ions*

The first type of ion examined was negative atomic oxygen. Running a discharge through dried O_2 gas, currents of 90-ev O^- ions of up to 1.4×10^{-7} ampere were easily obtained. The current through the discharge was about 30 ma; the voltage drop between the anode and cathode was 600 volts; and the pressure in the discharge was about 0.1 mm Hg.

Pressure in the discharge was the first parameter to be varied in the attempt to increase ion yield. Bennett and Darby's observation that the pressure exerted a strong influence on H^- beam current only in so far as it affected the position of the striations in the discharge was confirmed for O^- ions. When the pressure was such that the probe on the anode just touched a striation, a peak beam current was observed, but when a slight pressure change caused the probed striation to shift a bit, the beam current immediately dropped. As the pressure was decreased, the striations moved toward the anode and as each striation touched the probe, a peak beam current was observed. These successive peak beam currents increased with decreasing pressure right up to the point when the discharge was starved and extinguished itself. Quite probably much of the loss of ion current at high discharge pressures was due to the increase of pressure in the mass spectrometer as gas leaked through the canal into the mass spectrometers at a higher rate than could be handled by the high speed diffusion vacuum pump.

Another variable of interest was the total current through the discharge. It was found that negative ion yield depended strongly on discharge currents when the latter were less than about 30 ma, and that this dependence was roughly linear. However, with high discharge currents (30 to 60 ma), the peak beam current for any given striation was independent of the discharge current.

It might be expected that the ions passing through the canal in the anode would possess some initial energy given them by the electric fields in the discharge (including the applied field between electrodes *A* and *B*) and also an energy spread attributable to the different ions being formed at different points in the discharge fields. The average initial energy was found to be about 25 ev from calculations involving the ion mass and charge, the radius of curvature and field strength in the magnet and the energy given the ions between the anode and the mass spectrometer. The energy spread was about 25 ev when observations of the beam current were made as either the magnetic field or the ion energy was swept.

A second and different type of check was made both both on the initial energy and the energy spread of the ions. The ion collector in the mass spectrometer was biased negative with respect to ground, and the measured current was considered as a function of collector bias. At each setting of the bias, the magnetic field was adjusted for maximum beam current. This check showed that the ion current did not drop at all until the collector became at least 10 volts negative with respect to the anode of the discharge. As the bias was increased, the collected current decreased to zero at a bias of about 35 volts below anode potential. These data are in agreement with the previous data.

H^- *Ions*

In general, the work on negative atomic hydrogen, extracted from a glow discharge, ran parallel to the work on O^-. The only difference was that the discharge was run through different gases. In picking up the work of Bennett and Darby, water vapor was the first gas examined. H^- beam currents of about 4×10^{-8} amp could be taken from this discharge. It was difficult to obtain beam currents of one-tenth this value when the gas used was pure hydrogen from which water vapor had been removed by a liquid air trap. The best gas turned out to be hydrogen gas with a trace of water vapor in it. With this mixture, it was possible to get currents of 1×10^{-7} amp of 140-ev H^- ions.

Other Negative Ions

Although no attempt was made to produce strong beams of ions other than H^- and O^-, several large current peaks were observed. In the discharge in oxygen, the only peak other than O^- was O_2^-. The beam current of the molecular ion was about $\frac{1}{3}$ that of the atomic ion. In the discharge in air, in addition to these two peaks, a strong peak of NO_2^- whose current was comparable to that of the O_2^- peak was found. In the moist hydrogen discharge a broad peak of about the same strength as H^- occurred at mass 16 to 18. Presumably this peak contained O^- and OH^-.

B. Hot Cathode Arc Discharges

The facts that hot cathode arcs have been among the most successful proton sources, and that Bennett and Darby had succeeded in getting currents of 8×10^{-8} amp of H^- from such a source,[5] led to an early investigation of hot cathode arcs. The first experimental arrangement used the tube already described and shown in Fig. 1. The only changes which needed to be made were the replacement of the cold cathode by a filament cathode which could be heated electrically and the lowering of the voltage across the tube to about 120 volts. Using this source, H^- beam currents of 2×10^{-8}

TABLE I. Maximum currents obtained.

Type of source	H^- current	O^- current
Glow discharge	1×10^{-7} amp	1.4×10^{-7} amp
Hot cathode arc	7×10^{-8} amp	
Hollow cathode discharge	None found	2×10^{-9} amp
Rf discharges	3×10^{-9} amp	
Arnot effect sources	5×10^{-11} amp	

amp of 140-ev ions could be obtained. Almost no dependence of beam current on discharge current was observed as the latter was varied from 0.05 to 1.5 amp. Except for being more intense, the positive column of the discharge was almost identical in appearance to that of the glow discharge. Striations were present and again negative ions seemed to be concentrated in the anode side of the striations.

A second discharge tube, modeled in part after a proton source built by Tuve, Dahl, and Hafstad,[7] was constructed out of brass. Using this tube, it was possible to obtain H^- beam currents of 7×10^{-8} amp. The tube's operating characteristics were very similar to those of the glass-bodied arc.[8]

C. Other Types of Sources

Other sources that were examined were radiofrequency electrodeless discharges, hollow cathode discharges, and sources in which the Arnot effect was operative. All these sources, in the embodiments used, were inferior to both the glow and the hot cathode arc discharges as producers of high current negative ion beams.[8]

D. Summary

Table I contains the maximum currents obtained from the various sources examined.

From the point of view of producing large beams, the most promising sources are the glow and hot cathode arc discharges, the two sources which possess striations. Of the two, the glow discharge is preferable because it can be used to produce both H^- and O^- whereas the arc is limited to H^- production and because the glow discharge is considerably less temperamental and demands much less attention than the arc.

IV. NOISE IN NEGATIVE ION BEAMS

The requirement that the ion beam be large for the proposed photodetachment experiment is met either by the glow or the hot cathode arc discharge. Each of these two sources had to be examined next to see if they met the second criterion for the beam—that the current fluctuations in the audiofrequency range be little more than shot noise.

In carrying this out, the current from the ion collector was sent through a 40-megohm resistor, and the resulting voltage signal was taken through a cathode follower into a narrow-band amplifier. The output signal was displayed on an oscilloscope.

The first measurements were made on the H^- beam from the glow discharge with the amplifier tuned to 20 cps (band width 1 cps). It was found that the mean square fluctuation for a 10^{-7} amp beam was about 10^{-20} amp^2 per cycle of band width, i.e., the rms noise current was about 1000 times that which would be expected if only shot noise were present.

To make certain that this noise did not originate in the amplifier, the noise in a temperature-limited diode was examined with the result that the noise here was close to that calculated for pure shot effect. In order to localize the origin of the noise further, all external sources of noise were checked: the power supply running the discharge, the voltage supplied for the various electrodes, the current to the magnet, and the current through the discharge were examined. Wherever 20 cps fluctuations were observed, they were removed. However, there was no substantial decrease in beam noise. Apparently the beam noise was of internal origin.

The investigation of internal sources of beam fluctuations began with an examination of striations. A brief investigation on what might be taking place in the striation was easily carried out by disconnecting the voltage supply between electrodes A and B and then using electrode A as a Langmuir probe. The probe assumed a floating voltage of about 35 volts below the anode. With a broad-band amplifier, it was found that the potential of the probe was very strongly modulated at 60 and 120 cps (due to incomplete filtering of the power supply for the discharge), and considerable high frequency fluctuations were present. When the 20-cps fluctuations only were measured, the rms value of the voltage (for the 1-cps band width) was about 1 millivolt.

In an attempt to see whether or not these striation *voltage* fluctuations were related to ion beam noise, the previous experiment was reversed. To electrode A was applied a potential which was the superposition of 200-dc volts below the anode and from 1 to 10 millivolts of 20-cps ac. With just 1 millivolt of the 20-cps signal applied, the ion beam was coherently modulated with about the same amplitude as the undesired current fluctuations. As the ac applied voltage was increased, the ac component in the ion beam increased proportionately. Thus, the fluctuations in the beam current and those of the potential at a fixed point in the discharge tube appear to be closely related.

Two different considerations suggest the hypothesis that the fluctuations in beam current can be attributed at least partly to the probe's extracting ions from different portions of the striation at different times. First, the mass spectrometer accepts only particles with a very narrow energy range about a definite energy. If the potentials in the discharge change a bit, those ions which are accepted by the mass spectrometer will have

[7] Tuve, Dahl and Hafstad, Phys. Rev. **48**, 241 (1935).

[8] For further details, see the author's thesis (Harvard University, 1951) (unpublished).

to come from a different region of the striation, the new region having the same potential as the region from which the ions were drawn prior to the potential change. And, since the density of ions in the striations varies from point to point, a change in beam current would be expected to accompany the small potential changes. The second consideration is the observation that the positions of the striations are shifted when the potential on electrode is changed. Conversely, the fluctuations observed on the Langmuir probe may indicate fluctuations in striation position (although these were too small to be discerned in the present experiments if they exist at all). However, if we suppose that striation position fluctuations do exist, then we would expect that the probe would be drawing ions from different portions of a striation at different times, for the probe is fixed with respect to the tube. Again, because the ion density varies from point in a striation, fluctuations in beam current would be expected.

In order to check this hypothesis, an examination of the noise as a function of position of creation of the ions was made. Slitting down the mass spectrometer and sweeping either the magnetic field or the energy given the ions gives a sweep of position of origin of the negative ions if the ions created at a given point have a well-defined characteristic energy as they reach the anode. That they do seems reasonable since there are large fields in the discharge near the anode. By observing the beam current and the 20-cps noise in the beam as the position of origin in a given striation was varied, it was found that the noise was far greater near the edges of the zone in which negative ions accumulated than in the middle of this zone (the middle being defined as the region from which the ions were being drawn when the beam current was maximum). This observation is not surprising because in the middle of the zone, where the total concentration of ions does not vary much from point to point, a change in the region being probed should not result in a great change in beam current. Similarly, shifting the probed region at the edge of the zone, where the gradient of the ion density is very large, should result in a great absolute change and a very great relative change in ion beam current.

It was also noted in passing that, when the power supply for the discharge was not filtered too well, the ions from the anode edge of a striation's negative ion zone gave a beam which was strongly modulated at 120 cps. The ions coming from the middle of this zone, where the 20-cps modulation was minimum gave a beam containing strong 60-cps modultaion. From the edge away from the anode came a negative ion beam strongly modulated at both 60 and 120 cps. The reason for this apparent localization of 60- and 120-cps modulation in different portions of the same striation is not known.

A last check on the noise in the negative ion beam was the examination of the noise spectrum in the low audio-frequency range (up to 3500 cps). By replacing the tuned components in the amplifier and measuring the band widths at the new frequencies, points could be taken on a plot of the ratio (R) of measured rms noise current to calculated rums shot noise current as a function of frequency (f). It was found that this ratio decreased with increasing frequency by a relationship approximating $R=1/f^n$, where n is a number whose value, as taken from several plots, ranged between 0.5 and about 1.5. No attempt to discover a better expression to describe the noise *vs* frequency relation was made.

The last experiment was a brief examination of the noise in the negative ion beam from the other high current source, the hot cathode arc discharge. That the beam noise characteristics of this source were every bit as bad as those of the glow discharge was immediately apparent. This is not surprising though, since in both sources the ions are taken from striations in the positive column. It is to be expected that the vices, as well as the virtues, of these two sources should be similar.

To lessen somewhat the impression given above that the noise in the ion beam is thoroughly bad, one useful application of the noise should be mentioned. This noise served as an excellent indicator of the beam's presence. Beams of 10^{-11} amp or less could not be detected by the galvanometers here used, but such beams were easily registered by the amplifier. Using this detector, a very weak beam of ions with a mass of about 12 was found after the glow discharge tube had been cleaned with CCl_4. Presumably this ion was negative atomic carbon.

V. SUMMARY

None of the various negative ions sources examined in the research described in this paper met both criteria for a source to carry out the proposed experiment on photodetachment of electrons from negative ions. The noise in the beams from the two sources which provided adequate dc currents was entirely too great to carry out the experiment as it had been originally planned—modifications in the experimental design were necessary before photodetachment cross sections could be measured.

The author wishes to express his appreciation for the guidance and direction of Professor O. Oldenberg during the progress of this research. Special thanks are also due Dr. L. M. Branscomb and Dr. G. D. Watkins for their interest and assistance and Professors E. M. Purcell, K. T. Bainbridge, and R. V. Pound for frequent consultations.

Absolute Light Emission Efficiency of Crystal Anthracene for Gamma-Ray Excitation*

MILTON FURST, HARTMUT KALLMANN, AND BERNARD KRAMER
Physics Department, New York University, Washington Square, New York, New York
(Received August 19, 1952)

The absolute light emission efficiency of crystal anthracene has been reported in the range from ¼ to 4 percent and in the vicinity of 10 percent. Further determinations involving integrated light intensity measurements are reported here, which give an efficiency of about 10 percent. The possibility of the discrepancies being due to the use of peak-height measurements in one set of experiments and integrated intensities in the others is discussed; preliminary experiments indicate that the difference in range of values is not due to this cause.

DISCREPANCIES of the order of ten for the absolute light output efficiency of anthracene or other organic crystals under gamma-ray excitation have been found reported in the literature.[1–5] (The relative light output is much more accurately known for the different organic materials.) The values given for the absolute efficiency may be divided into two groups, one ranging from between about ¼ percent to 4 percent and the other being in the vicinity of 10 percent. The measurements giving the lower range of values have been obtained using peak height determinations, whereas the larger values have been obtained with the integrated light output. The methods employed in some of the measurements were rather indirect; that reported by Harrison[2] used a "calibrated" photomultiplier.

On account of these differences, we have made a further determination of this efficiency. Only the integrated light output values were actually determined, but some information on the peak height efficiencies was also gained. Two methods were employed: 1. An indirect method—by comparing the light output of anthracene powder with that of ZnS powder and using the more or less accurate values known for ZnS. 2. A direct method—employing a photomultiplier and a calibrated thermopile and measuring the light output of both under the same geometrical conditions.

The first method was carried out by measuring the light output of powdered anthracene (~10 mg/cm²) on a glass plate under alpha-particle excitation. The light emission of ZnS (Type D—du Pont, 10 mg/cm²) was also obtained under identical conditions; their ratio was found to be about 50. Then, by using the known absolute α-particle efficiency of about 25 percent for ZnS, and the ratio[6,7] of ~15 between gamma-rays and alpha-particles for the light output of anthracene for the same absorbed energy, the amount of absorbed gamma-ray energy which is converted into light was computed to be 7 percent.

The second, more direct and probably more accurate, method measured the light from a 5-mm illuminated spot on a blue oscilloscope screen with suitable glass filters (Corning) which transmitted light only in the same spectral region as the anthracene crystal. A thermopile and a photomultiplier were placed at the same distance from the light source, and the emitted light was measured with both. A set of film neutral filters which were independently calibrated by two methods was used with the photomultiplier. Finally, a 5-mm anthracene flake at the same distance from the photomultiplier was excited by a 1-mC gamma-ray source (radium), and its light emission was measured. From the calculation of the amount of energy absorbed by the crystal in unit time by the measured mass of anthracene,[8] the efficiency was then determined by making use of the photomultiplier calibration. This measurement gave a value of 10 percent for the gamma-ray-to-light conversion efficiency of anthracene. These are close to the previously obtained value calculated by comparison with the light output of naphthalene.[5]

Although these experiments were carefully done, the values given above are only approximate, since sufficient repetitions were not made to give a more exact value. The major limiting factors are: (1) The differences in spectral distribution which exist between the calibration light from the oscilloscope screen and that of anthracene. This may not be very important, since the same spectral range was covered in both cases and the photomultiplier sensitivity does not vary very much in this blue region. (2) The amount of gamma-ray energy absorbed by the crystal was calculated rather than measured. (3) Another important source of error lies in slight differences in the geometry and in the solid angles of the incident calibrating light (oscilloscope screen spot) and the measured light (anthracene flake). This was minimized by using the same geometry and solid angle for both light sources. We feel that these limitations would not produce a large deviation, and, therefore, that the efficiency is actually close to 10 percent.

A possible explanation for these differences between

* This work was sponsored by the Signal Corps Engineering Laboratory, Fort Monmouth, New Jersey.
[1] J. I. Hopkins, Rev. Sci. Instr. **22**, 29 (1951).
[2] F. B. Harrison, Nucleonics **10**, 40 (1952).
[3] R. C. Sangster, Massachusetts Institute of Technology Technical Report No. 55, January, 1952.
[4] R. L. Paul, Ph.D. thesis, University of Oregon (unpublished).
[5] Broser, Kallmann, and Martius, Z. Naturforsch. **4a**, 204 (1949).
[6] Extrapolation from the data of Taylor *et al.* gives about 15.
[7] Taylor, Jentschke, Rembley, Eby and Kruger, Phys. Rev. **84**, 1034 (1951).
[8] One roentgen is equivalent to 83 ergs/g.

the integrated and peak-height measurements would be the existence of a tail in the decay curve of a light flash of the anthracene crystal. Such a tail could produce a considerable addition to the amount of light when integrated output is measured but would not show up in the peak height determinations Preliminary measurements on anthracene and CsBr carried out by Grace Marmor Spruch, however, tend to show that the emission of anthracene observed for the period of 10 milliseconds does not have a tail sufficient to account for the difference.

As a check, experiments with CsBr(Tl) were performed. With this crystal the integrated intensity is about 2 to 3 times as great as that of the same mass of anthracene for gamma-rays; the peak heights with a 1-megohm output resistance are, however, less than one-half of the anthracene value.[9] The light output of CsBr(Tl) takes place over a much more extended period than that of anthracene; certainly some light is still emitted after one millisecond, and this could account for the difference in peak heights. With longer circuit time constants, the peak heights of CsBr were considerably greater than those of anthracene. With anthracene, as remarked above, such an effect has not been detected; nevertheless, a very small, but long-time phosphorescence, sufficient to account for the above discussed differences, may exist. There are indications that some long-time phenomena do occur with anthracene, since a small but noticeable gamma-ray phosphorescence has been found, and also an energy storage which can later be released by light and does not instantaneously decay.

[9] Bittman, Furst, and Kallmann, Phys. Rev. **87**, 83 (1952).

PHYSICAL REVIEW VOLUME 89, NUMBER 2 JANUARY 15, 1953

Arbitrary Concentrations of Matter and the Schwarzschild Singularity

AMALKUMAR RAYCHAUDHURI*
Physics Laboratory, Asutosh College, Calcutta, India
(Received June 13, 1952)

A nonstatic solution of the Einstein gravitational equations representing a spherically symmetric cluster of radially moving particles in an otherwise empty space is obtained. While it has been presumed by Einstein that the Schwarzschild singularity is physically unattainable as matter cannot be concentrated arbitrarily, the present solution seems to show that there is no theoretical limit to the degree of concentration, and that the Schwarzschild singularity has no physical reality as it occurs only in some particular coordinate systems. Incidentally, it is shown that in case of spherical symmetry the condition of conservation of gravitational energy of an isolated system of fluid material is equivalent to the vanishing of pressure at the boundary.

1. INTRODUCTION

THE Schwarzschild field for a mass particle,

$$ds^2=-(1+m/2r)^4(dr^2+r^2d\theta^2+r^2\sin^2\theta d\varphi^2)+\frac{(1-m/2r)^2dt^2}{(1+m/2r)^2}, \quad (1)$$

has singularities at $r=0$ and $r=m/2$. While it is not unnatural to identify the singularity at the origin of the spatial coordinate system with the mass particle, the "Schwarzschild singularity" at $r=m/2$ (corresponding to the vanishing of g_{44}) has been the subject of considerable speculation. Considering the field inside matter, Schwarzschild showed that if one considers an incompressible perfect fluid ($T_k{}^i=-p\delta_k{}^i$, for $i, k=1, 2, 3$; $T_4{}^4=\rho=$const.), such a singularity corresponding to the vanishing of g_{44} can indeed be attained if the size of a sphere of given density be sufficiently large. However, as pointed out by Laue, the assumption of incompressibility is not consistent with the ideas of the theory of relativity. In order to avoid this difficulty, Einstein[1] has more recently examined the problem by considering a spherically symmetric assembly of particles moving in randomly oriented circles around a common center and in arbitrary phases. From the condition that the geodesics of the particles must be time-like, Einstein finds that there is a limit to the degree of concentration of matter, and it then follows that if matter be introduced in this particular form, the Schwarzschild singularity is physically unattainable. Further Einstein has expressed the view that it is not "subject to reasonable doubt that more general cases will have analogous results." However, the following considerations throw doubts on this presumption and have led to the present investigation.

2. FUNDAMENTAL IDEA OF THE PRESENT PAPER

If one considers the cosmologic solution corresponding to a spherically symmetric cluster of particles falling

* Present address: Theoretical Physics Department, Indian Association for the Cultivation of Science, Jadarpur, Calcutta, India.

[1] A. Einstein, Ann. Math. **40**, 922 (1939).

freely towards the center,[2] one finds that it is possible to reach any degree of concentration, there being no singularity except for infinite concentration. Now, suppose, we cut out a part R of such a contracting field and place it in an outside empty space. Outside we expect to have the Schwarzschild field,[3] while inside we expect the cosmologic solution. If the initial value of the radius of R be greater than that for Schwarzschild singularity (i.e., the concentration is less than the critical value required for this singularity), then there would be no singularity anywhere in the field. As the interior field goes on contracting, a singularity would appear in the exterior Schwarzschild solution as the radius crosses a certain critical value; however, so far as the interior field is concerned, no such singularity appears at any phase of its career. Such a situation is obviously inconsistent, so that either it is impossible to fit such a contracting field with the outside empty space for arbitrary concentrations or else the Schwarzschild singularity is only a property of some particular coordinate systems and would not appear in other properly chosen coordinate systems.

Einstein and Straus[4] have shown that in general it appears from the theory of differential equations that the cosmologic solution can be fitted to the Schwarzschild field; however, they have not considered whether the transformations which make the two solutions continuous are real and have also not considered the role of the Schwarzschild singularity in this problem of fit. In the present paper we shall show that it is possible to obtain a real solution of the gravitational equations for empty space which is continuous with the cosmologic solution at a time dependent boundary. No singularity corresponding to the Schwarzschild singularity appears at any phase in the exterior field for any arbitrary finite concentration in the cluster. The Schwarzschild singularity thus appears to be only a property of particular coordinate systems,[5] and there seems to be no theoretical limit to the degree of concentration.

[2] In the usual cosmologic solution for an expanding universe, the "particles" are running away from the center. However, the general theory of relativity is indifferent to the direction of time flux, and we are here considering the solution corresponding, so to say, to a contracting universe.

[3] Any spherically symmetric solution in empty space is known to be reducible to the Schwarzschild field. R. Birkhoff, *Relativity and Modern Physics* (Harvard University Press, Cambridge, 1923), p. 253.

[4] A. Einstein and E. G. Straus, Revs. Modern Phys. **17**, 120 (1945); **18**, 148 (1946).

[5] Some earlier workers also have given transformations which become singular at the Schwarzschild singularity, whereby the Schwarzschild singularity may be abolished. G. Lemaitre, Ann. soc. sci. de Bruxelles, Ser. I **53**, 51 (1933); J. L. Synge, Proc. Roy. Irish Acad. **A53**, 84–114 (1950).

3. FIELD EQUATIONS AND THEIR INTEGRATION

With the isotropic spherically symmetric line element,

$$ds^2=-e^{\mu}(dr^2+r^2d\theta^2+r^2\sin^2\theta d\varphi^2)+e^{\nu}dt^2, \qquad (2)$$
$$\mu=\mu(r,t), \quad \nu=\nu(r,t),$$

the Einstein gravitational equations give[6]

$$-8\pi T_1{}^1=e^{-\mu}[\mu'^2/4+\mu'\nu'/2+(\mu'+\nu')/r] -e^{-\nu}(\ddot{\mu}+\tfrac{3}{4}\dot{\mu}^2-\dot{\mu}\dot{\nu}/2), \qquad (3)$$

$$-8\pi T_2{}^2=-8\pi T_3{}^3=e^{-\mu}\left(\frac{\mu''+\nu''}{2}+\frac{\nu'^2}{4}+\frac{\mu'+\nu'}{2r}\right) -e^{-\nu}\left(\ddot{\mu}+\tfrac{3}{4}\dot{\mu}^2-\frac{\dot{\mu}\dot{\nu}}{2}\right), \qquad (4)$$

$$8\pi T_4{}^4=-e^{-\mu}(\mu''+\tfrac{1}{4}\mu'^2+2\mu'/r)+\tfrac{3}{4}e^{-\nu}\dot{\mu}^2, \qquad (5)$$

$$8\pi T_{14}=-(\dot{\mu}'-\tfrac{1}{2}\dot{\mu}\nu'), \qquad (6)$$

where dashes and dots denote differentiations with respect to r and t, respectively.

We now consider that in the region $0\leqslant r\leqslant r_1$, we have a spherically symmetric cluster of particles falling freely towards the origin. Such a situation is obviously obtained if we assume[7] that in this region we have the well-known solution

$$\left.\begin{aligned} e^{\mu}&=e^{q}\Big/\left(1+\frac{zr^2}{4R^2}\right)^2 \\ e^{\nu}&=1 \end{aligned}\right\} \quad \text{for} \quad r\leqslant r_1, \qquad (7)$$

where e^q is a decreasing function of t alone, $z=+1$, 0 or -1, and we take $r_1<2R$, so that so long as e^q is nonvanishing, there is no singularity in this region.

The coordinate system is co-moving, and the gravitational equations reduce to

$$0=-ze^{-q}/R^2-\ddot{q}-\tfrac{3}{4}\dot{q}^2, \qquad (8)$$

$$8\pi\rho=3ze^{-q}/R^2+\tfrac{3}{4}\dot{q}^2, \qquad (9)$$

where $\rho=T_4{}^4$ is the density $=nm$, n being the number density of the particles and m the mass of each particle. Equations (8) and (9) together give

$$\ddot{q}+\tfrac{1}{2}\dot{q}^2=-8\pi\rho/3, \qquad (10)$$

so that, ρ being essentially positive, $\ddot{q}$ is always negative. Thus q cannot have any minimum[8]; and the system once contracting ($\dot{q}$ negative) would go on contracting to infinite concentration.

[6] R. C. Tolman, *Relativity, Thermodynamics and Cosmology* (Oxford University Press, London, 1934), p. 252.

[7] With the form of solution assumed, ρ is a function of t alone. A spatially nonuniform distribution of particles (retaining spherical symmetry) would, however, lead to the same results so far as our investigation is concerned.

[8] A. Einstein, *The Meaning of Relativity* (Methuen and Company, Ltd., London, 1950), fourth edition, p. 113.

We next consider the field in the empty space $r \geqslant r_1$. The metric tensor must satisfy the field equations with $T_\nu^\mu = 0$ and along with the first derivatives must be continuous with (7) at $r = r_1$. Equation (6) gives on integration, $e^{-\nu}\dot{\mu}^2 = \varphi(t)$, where $\varphi(t)$ is a function of t alone. The condition of continuity now requires $\varphi(t) = \dot{q}^2$, so that we have

$$e^{-\nu}\dot{\mu}^2 = \dot{q}^2. \tag{11}$$

Using this result in Eq. (5), we get

$$0 = -e^{-\mu}(\mu'' + \tfrac{1}{4}\mu'^2 + 2\mu'/r) + \tfrac{3}{4}\dot{q}^2.$$

Now, with the substitution[9]

$$e^\mu r^2 = \xi^4, \quad x = \log r, \tag{12}$$

the above equation becomes

$$\partial^2\xi/\partial x^2 = \tfrac{1}{4}\xi + \tfrac{3}{16}\dot{q}^2\xi^5; \tag{13}$$

and, on integration, we get

$$(\partial\xi/\partial x)^2 = \tfrac{1}{4}\xi^2 + \tfrac{1}{16}\dot{q}^2\xi^6 + K, \tag{14}$$

where K is apparently a function of t alone.

The corresponding equation in the region $0 \leqslant r \leqslant r_1$ would be

$$(\partial\xi/\partial x)^2 = \tfrac{1}{4}\xi^2 + \tfrac{1}{16}\dot{q}^2\xi^6 - \tfrac{2}{3}\pi\rho\xi^6, \tag{15}$$

the function corresponding to K being here put equal to zero to avoid a singularity at the origin. Now the continuity of μ and μ' lead to the continuity of ξ^2 and $(\partial\xi/\partial x)^2$. Consequently, from (14) and (15),

$$K = -\left(\frac{2\pi\rho\xi^6}{3}\right)_{r=r_1} = -\frac{2\pi}{3}\rho\frac{e^{3q/2}}{(1+zr_1^2/4R^2)^3}r_1^3. \tag{16}$$

It is easy to see from (8) and (9) that $\rho e^{3q/2}$ is a constant independent of time as well, so that K also is a constant.

Equation (14) can be put into the Weierstrass form

$$(\partial y/\partial u)^2 = 4y^3 - q_2 y - q_3, \tag{17}$$

where

$$y = \frac{K^{\frac{1}{3}}}{\xi^2} + \frac{1}{12K^{\frac{1}{3}}}, \qquad q_2 = \frac{1}{12K^{4/3}}, \tag{18}$$

$$q_3 = -(1/6^3K^2 + \dot{q}^2/4), \quad u = K^{\frac{1}{3}}\log r.$$

The solution can now be expressed in terms of Weierstrass's elliptic function,

$$y = \wp(u - u_1 + c, q_2, q_3), \tag{19}$$

where

$$u_1 = K^{\frac{1}{3}}\log r_1 \quad \text{and} \quad c = \wp^{-1}(y_1),$$

y_1 being the value of y at $r = r_1$ determined from (7), (12), and (18).

Thus, in view of Eqs. (11) and (12), the field in the empty space $r \geqslant r_1$ is given by

$$e^\mu = \xi^4/r^2, \quad e^\nu = (4\dot{\xi}/\dot{q}\xi)^2, \tag{20}$$

with ξ given by (18) and (19). It is easy to see that (20) satisfies all the field Eqs. (3)–(6) and the necessary boundary conditions. For, if one substitutes from (20) and (14) in (3), one finds that the necessary and sufficient condition that T_1^1 should vanish is that K must be independent of t. This condition, as we have already noted, is satisfied. With (3), (5), and (6) now satisfied, (4) is satisfied in view of the divergence identity.

The choice of c in (19) and the fixing of K by (16) have already ensured the continuity of μ and μ'. If therefore the clocks on the two sides of the boundary be synchronized,[10] $\dot{\mu}$ and $\dot{\mu}'$ would also be continuous. Equations (11) and (6) then show that ν and ν' are also continuous.

4. TRANSFORMATION TO THE SCHWARZSCHILD FORM AND SINGULARITIES OF THE FIELD

If we make the transformation

$$(1 + m/2r_1)^4 r_1^2 = \xi^4,$$

$$dt_1 = \left(\frac{8r\xi\xi'}{|\dot{q}|(\xi^2 - 2m)}\right)dt + \frac{\xi^6|\dot{q}|}{2r(\xi^2 - 2m)}dr, \tag{21}$$

where $m = -2K$, the solution (20) goes over to the Schwarzschild form (1) in r_1 and t_1. (It is easy to verify that dt_1 is a perfect differential.)† It may be noted that the Schwarzschild singularity $r_1 = m/2$ corresponds to $\xi^2 = 2m$, and the transformation becomes singular there and is no longer real for $\xi^2 < 2m$.

We next investigate the singularities of our field; the region $0 \leqslant r \leqslant r_1$ is obviously free from singularities except when e^q vanishes (infinite concentration). In the exterior field, the continuity of μ and μ' insures that at $r = r_1$, the left-hand side of (14) is positive and that ξ is an increasing function[11] of x. It is not difficult now to see that ξ goes on increasing and becomes arbitrarily large at a finite value of r, giving rise to a singularity of e^μ. However, if one calculates the proper distance of the singularity from the origin defined by $\int_0^r e^{\mu/2}dr$ or the proper volume enclosed within the singular sphere, both these quantities are found to be infinite. Further, considering the transformation (21), this singularity ($\xi \to \infty$) corresponds to the infinite sphere in the Schwarzschild coordinate system. Thus, although occurring at a finite value of r, the singularity does not appear to be anywhere in the finite region.

[9] M. Wyman, Phys. Rev. **70**, 74 (1946).

[10] A time scale has already been chosen in the region $r \leqslant r_1$ by taking $e^\nu = 1$, because the general solution is $e^\nu = f(t)$. Hence, to make the time scales on either side of the boundary identical a suitable transformation of the time variable in the region $r \geqslant r_1$ may be necessary. This does not, however, affect Eq. (11).

† See H. P. Robertson, Trans. Am. Math. Soc. **29**, 481 (1927), especially p. 492. The author is indebted to the referee of the Physical Review for this reference.

[11] Actually the condition of continuity ensures the continuity of $(1/\xi)(\partial\xi/\partial r)$, this requires that ξ and $(\partial\xi/\partial r)$ are of the same sign, but their individual signs are undetermined. A negative value of ξ leads to the same results physically and so for simplicity we restrict our considerations to the positive sign of ξ.

In the next section we shall see that such a singularity occurs in the nonstatic form of even the Euclidean field.

The form (20) for e^{ν} shows that e^{ν} vanishes if ξ vanishes. We next investigate whether any singularity of this type is present. From (14), we get

$$\dot{\xi}_x=\frac{(\xi/2+3\dot{q}^2\xi^5/8)\dot{\xi}+\dot{q}\ddot{q}\xi^6/8}{2\xi_x}$$

and

$$\frac{\dot{\xi}}{\xi_x}=\frac{\dot{q}\ddot{q}}{16}\int_{\xi_1}^{\xi}\frac{\xi^6 d\xi}{\xi_x^3}+\dot{q}\left(\frac{\xi}{4\xi_x}\right)_1. \tag{22}$$

In the above equations, the subscript x indicates differentiation with respect to x, and the subscript 1 indicates the value of the quantity at the boundary $r=r_1$. Equation (22) gives at any particular time the behavior of $\dot{\xi}$ (or rather of $\dot{\xi}/\xi_x$) as we go away from r_1.

Let us consider the asymptotic value of $\dot{\xi}/\xi_x$ as $\xi\to\infty$. We have, from Eq. (22),

$$\left(\frac{\dot{\xi}}{\xi_x}\right)_{\xi\to\infty}=-\frac{\dot{q}\ddot{q}}{2\dot{q}^2}\int_{\xi_1}^{\infty}d\left(\frac{\xi}{\xi_x}\right)-\frac{\dot{q}\ddot{q}m}{4\dot{q}^2}\int_{\xi_1}^{\infty}\frac{d\xi}{\xi_x^3}+\dot{q}\left(\frac{\xi}{4\xi_x}\right)_1.$$

Since, from (14), (ξ/ξ_x) vanishes as $\xi\to\infty$, we get, after eliminating $\ddot{q}$ with the help of Eqs. (10) and (16),

$$\left(\frac{\dot{\xi}}{\xi_x}\right)_{\xi\to\infty}=\frac{m}{\dot{q}}\left\{-\frac{1}{\xi_1{}^5(\xi_x)_1}+\frac{1}{4}\left(\frac{\dot{q}^2}{2}+\frac{2m}{\xi_1{}^6}\right)\int_{\xi_1}^{\infty}\frac{d\xi}{\xi_x^3}\right\}. \tag{22'}$$

We note that

$$\left(\frac{\xi_x}{\xi}\right)_1=\frac{1}{2}\frac{(1-zr_1^2/4R^2)}{(1+zr_1^2/4R^2)}\equiv\alpha \quad \text{(say)}, \tag{23}$$

where α, as defined, is evidently a constant.

It is easy to see, from Eq. (9), that if we trace the history of the contracting cluster backwards in time, then for $z=-1$ or $z=0$, we can go to arbitrary large values of ξ_1. For $z=+1$, there is a maximum of ξ_1 determined by the zero of $\dot{q}$. We get for this maximum value of ξ_1, from Eqs. (9), (16), and (23),

$$(\xi_1^2)_{\max}=2m/(1-4\alpha^2)\geq 2m.$$

Hence, in all cases, the solution (7) allows a state at which $\xi_1^2=2m$. At this state we have

$$\int_{\xi_1}^{\alpha}\frac{d\xi}{\xi_x^3}<\int_{\xi_1}^{\alpha}\frac{64d\xi}{|\dot{q}|^3\xi^9}=\frac{8}{|\dot{q}|^3\xi_1{}^8} \tag{23a}$$

Also, from Eqs. (14) and (23), when $\xi_1^2=2m$,

$$(\xi_x)_1=|\dot{q}|\xi_1{}^3/4, \quad 2m/\xi_1{}^6=\dot{q}^2/16\alpha^2. \tag{23b}$$

Substituting from (a) and (b) we find that the quantity within the brackets in Eq. (22′) is definitely negative for $\alpha^2\geq 1/24$. Thus for $\alpha^2\geq 1/24$, and $\xi_1^2=2m$, $(\dot{\xi})_{\xi\to\infty}$ is of the opposite sign of $\dot{q}$, whereas for $\xi=\xi_1$, $\dot{\xi}$ is of the same sign as $\dot{q}$. Hence for $\alpha^2\geq 1/24$, and $\xi_1^2=2m$, $\dot{\xi}$ must have a zero for some value of $\xi>\xi_1$.

We can next generalize this result for arbitrary values of α and ξ_1. For we have, from Eqs. (22) and (23),

$$\frac{\ddot{q}}{16}\int_{\xi_1}^{\xi_s}\frac{\xi^6 d\xi}{\xi_x^3}=-\frac{1}{4\alpha},$$

where ξ_s is the value of ξ on the spherical surface at which $\dot{\xi}$ vanishes. From this we find that $d\xi_s/dt$ is always finite except for $e^{\nu}=0$ (when the field in the region $0\leq r\leq r_1$ becomes singular) and hence, since for $\alpha^2\geq 1/24$, and $\xi_1^2=2m$, we have a finite value of ξ_s, ξ_s will have a finite value at all stages provided $\alpha^2\geq 1/24$. Similarly, considering ξ_s as a function of the parameter α, we find that $\dot{\xi}$ will have a zero for all values of α as well.

It is thus clear that our solution, given by (20) has a singularity corresponding to the vanishing of q_{44}. However, it cannot be identified with the Schwarzschild singularity for it differs in two important respects. Firstly, this singularity does not in general occur at $\xi^2=2m$ and in fact, as a little consideration shows, it does not even occur at any fixed value of ξ. Secondly, while our singularity occurs for all concentrations, the Schwarzschild singularity appears only when the concentration exceeds a certain critical value. In the coordinate system which we have used, our singularity apparently is a surface separating a contracting space ($\dot{\xi}$ negative) in the neighborhood of the contracting cluster from an outside expanding space ($\dot{\xi}$ positive). However, when the solution is transformed to the static form, the singularity disappears. This suggests that the singularity has no physical reality.

Thus, in our solution there is no singularity at $\xi^2=2m$ (the Schwarzschild singularity). Further, our use of the co-moving coordinate system insures the vanishing of the coordinate velocity of the particles whose world lines are thus parallel to the time axis. Hence, no question of exceeding the velocity of light arises and, unlike the situation in Einstein's cluster, there appears to be no theoretical limit to the degree of concentration.

5. CASE OF ABSOLUTELY EMPTY SPACE

In case the space is absolutely empty, K in Eq. (14) is zero and Eq. (14) on integration gives, for ξ vanishing at the origin,

$$\xi^2=2ar/(a^2-\dot{q}^2r^2/4),$$

where a and $\dot{q}$ are two arbitrary functions of time. The solution now becomes

$$e^{\mu}=4a^2/(a^2-\dot{q}^2r^2/4)^2, \quad e^{\nu}=\dot{a}^2/\dot{q}^2.$$

If one makes the transformation,

$$r'=2ar/(a^2-\dot{q}^2r^2/4),$$

$$dt'=\frac{e^{\mu}}{2}|\dot{q}|rdr+e^{\mu/2}\frac{|\dot{a}|}{2|\dot{q}|a}(a^2+\dot{q}^2r^2/4)dt,$$

the line element goes over to the pseudo-Euclidean form

$$ds^2=-(dr'^2+r'^2d\theta^2+r'^2\sin^2\theta d\varphi^2)+dt'^2.$$

It is interesting to note that in this transformed form of even the pseudo-Euclidean field, one has a singularity at $r=2|a||\dot{q}|$ where e^μ becomes infinite. This confirms our conclusion of the preceding section that this singularity has no physical significance. It appears only because the infinite space is mapped out in a finite coordinate region.

Singularities, of the type $g_{44}=0$, may or may not be introduced into this solution as a and $\dot{q}$ are perfectly arbitrary functions of time.

6. CONSERVATION OF GRAVITATIONAL ENERGY OF AN ISOLATED SYSTEM

In this section, we are giving up the idea of a cluster of particles and consider instead a general spherically symmetric distribution of fluid material. We have seen that (20), with ξ defined by (14), is a solution of the field equations for empty space if K be a constant. Thus, any constant value of K gives rise to a solution. Further, from the transformation to the Schwarzschild form it is seen that the constancy of K means the constancy of the gravitational mass. Hence, for an isolated system in empty space, the gravitational energy must be conserved. It will now be shown that in the case of spherical symmetry this condition is equivalent to the requirement of the vanishing of the pressure at the boundary. For this purpose, it is more convenient to use the spherically symmetric line element in the form

$$ds^2=-e^\lambda dr^2-r^2(d\theta^2+\sin^2\theta d\varphi^2)+e^\nu dt^2. \tag{24}$$

The gravitational equations are[12]

$$8\pi T_1{}^1=e^{-\lambda}\left(\frac{\nu'}{r}+\frac{1}{r^2}\right)-\frac{1}{r^2}, \tag{25}$$

$$8\pi T_4{}^4=e^{-\lambda}\left(\frac{\lambda'}{r}-\frac{1}{r^2}\right)+\frac{1}{r^2}, \tag{26}$$

$$8\pi T_{14}=\dot{\lambda}/r, \tag{27}$$

$$-8\pi T_2{}^2=-8\pi T_3{}^3=e^{-\lambda}\left(\frac{\nu''}{2}-\frac{\lambda'\nu'}{4}+\frac{\nu'^2}{4}-\frac{\lambda'-\nu'}{2r}\right)-e^{-\nu}\left(\frac{\ddot{\lambda}}{2}-\frac{\lambda\dot{\nu}}{4}+\frac{\dot{\lambda}^2}{4}\right). \tag{28}$$

Equation (26), on integration gives

$$e^{-\lambda}=1-2m/r, \tag{29}$$

where

$$m=4\pi\int_0^r T_4{}^4r^2dr. \tag{30}$$

[12] Reference 6, p. 251.

Now, the condition to fit with the external space shows that $m(r_1)$ is the gravitational mass of the system, $r_1(t)$ being the coordinate of the boundary of the sphere. The rate of change of gravitational energy of the system is given by

$$\frac{dm}{dt}=m_{r_1}{}'\frac{dr_1}{dt}+\dot{m}_{r_1},$$

or, in view of (30), (29), and (27),

$$\frac{dm}{dt}=4\pi r_1{}^2\left(T_4{}^4\frac{dr_1}{dt}-T_4{}^1\right).$$

However, if p be the pressure and ρ the density of the fluid,[13]

$$T_4{}^4=\rho e^\nu(dt/ds)^2+pe^\nu(dt/ds)^2-p,$$
$$T_4{}^1=\rho e^\nu(dt/ds)(dr/ds)+p(dt/ds)(dr/ds)e^\nu,$$

so that the above equation gives

$$dm/dt=-4\pi r_1{}^2p_1dr_1/dt.$$

This is analogous to the classical relation that the rate of change of energy of an isolated system is equal to the rate of work done by the system. Thus, for a nonstatic field [$\dot{\lambda}\neq0$, $(dr/dt)\neq0$],‡ the condition of conservation of the gravitational mass is equivalent to the requirement of the vanishing of pressure at the boundary.

7. CONCLUDING REMARKS

It is interesting to note why our cluster can go on contracting indefinitely, while there exists an upper bound to the concentration in the case of Einstein's cluster. The null sphere [$r=m(2+\sqrt{3})/2$] lies beyond the Schwarzschild singularity ($r=m/2$), so that the Einstein particles, moving in circles, are constrained to lie beyond this singularity. In our case, however, for a radially moving particle, it is known[14] that it can cross the Schwarzschild singularity in finite proper time and without attaining the velocity of light.

As is clear, there is a singularity at a finite time, the whole region $0\leqq r\leqq r_1$ collapsing to zero volume. What happens after that, our equations cannot say.[15] It appears, indeed, that while we can trace the history of the birth of a particle, we cannot tell what happens when the particle is actually born. This perhaps can be attributed to the fact, as remarked by Einstein,[16] that the general theory of relativity would break down under such stringent conditions.

[13] P. G. Bergmann, *Introduction to The Theory of Relativity* (Prentice Hall, Inc., New York, 1947), p. 129.

‡ In case $\dot{\lambda}=0$ at the boundary, the conditions at the boundary are the same as in the static case and one gets the continuity of pressure in the usual manner.

[14] J. L. Synge, Proc. Roy. Irish Acad. **A53**, 84 (1950), especially p. 107.

[15] Reference 6, p. 438.

[16] Reference 8, p. 118, footnote.

Inelastic Events Induced by 32-Mev Protons on Helium

JACK BENVENISTE AND BRUCE CORK
Radiation Laboratory, University of California, Berkeley, California
(Received August 4, 1952)

A study of inelastic events induced by the bombardment of helium nuclei with 32-Mev protons has been made.

No low energy group of protons has been found which would indicate the existence of an excited, heavy-particle stable state of the helium nucleus. The absence of a bump on the continuum of protons from the reactions

$$p+\mathrm{He}^4\rightarrow\mathrm{He}^3+n+p',$$
$$p+\mathrm{He}^4\rightarrow\mathrm{H}^3+p''+p',$$

indicates a maximum cross section of 0.1 mb/sterad at 45° c.m. for the production of a single excited helium level as high as 23.3 Mev above the ground state. Further, the observed rather flat shape of the continuum requires the existence of at least two levels of about 1-Mev half-width, separated by about 1 Mev.

The angular variation of the differential cross section for the production of deuterons from the reaction

$$p+\mathrm{He}^4\rightarrow\mathrm{He}^3+d$$

has been measured. When the principle of detailed balancing is invoked, good agreement with the prediction of the theory of Butler is obtained for r_0 (range of nuclear forces plus radius of He^3 nucleus) $=4.2\times10^{-13}$ cm.

INTRODUCTION

EVIDENCE for the nature of nuclear forces comes from several sources. From binding energy measurements, especially of light nuclei, and from nucleon-nucleon scattering experiments, one may arrive at some conceptions of the character of the forces acting between elementary particles. Application of these ideas to the solution of more complex systems should then serve as a check on the accuracy of these concepts.

Thus, in 1936, it was shown theoretically[1] that, on the basis of what was then known about nuclear forces, the He^4 nucleus could be expected to have at least one excited level which was stable to particle disintegration. However, the analysis was based on sum rules valid only for neutron-proton potentials of the ordinary type. It was pointed out that if new sum rules are set up considering Majorana forces, the upper limit on the excitation energies which can be deduced from them are too high to be useful.

Bethe and Bacher[2] deduced the probable existence of two stable excited levels, a ^1P state at ≈16 Mev and a ^3P state at ≈10 Mev, and concluded that this was compatible with the experimental data available in 1936.

More recently, King and Goldstein,[3] pointed out that the observed $1/v$ behavior of the He^3 slow neutron absorption cross section indicated the absence of a bound excited state of the compound He^4 nucleus not too far below 20.5 Mev; furthermore, in view of the large (≈5000 barns) $He^3(n, p)H^3$ cross section[4] in the $1/v$ region, the existence of a broad unstable level in He^4 above 20.5 Mev is in the realm of possibility.

One of the more provocative recent experiments in this field is that of Argo *et al.*,[5] at Los Alamos. The yield of γ-rays from the reaction $T(p, \gamma)He^4$ was observed as a function of the incident proton energy. A cross section which increased more rapidly than could be explained by barrier penetration was interpreted as evidence for the existence of an excited level in the He^4 nucleus. Only the rising portion of the yield curve was observed in this work, since 2.5 Mev was the highest proton energy available. However, this curve was fitted with a Breit-Wigner single level resonance formula, and the constants evaluated. The presumed level was assigned an excitation energy of 21.6 Mev and a half-width ≈1 Mev.

Shortly after the first announcement[6] of these results, Professor W. K. H. Panofsky suggested that the 32-Mev proton linear accelerator was ideal equipment to resolve the question of the existence of an excited He^4 level by the method of inelastic scattering of protons from helium.

The inelastic scattering process may be described in the following way. As illustrated in Fig. 1, a proton incident on a target nucleus (A, Z) in its ground state E_0, may be considered to form a compound nucleus $(A+1, Z+1)$ in an excited state. One of the ways in which the excited compound nucleus might decay is by re-emitting a proton. If the proton (P) comes off with energy equal to that of the incident proton, the target nucleus is left in its ground state; however, if the target nucleus possesses an excited level E_n, the compound nucleus may decay to this level by emitting a proton (p') of less energy than that of the incident proton. This proton is said to be inelastically scattered. Thus, to search for excited levels of the target nucleus, one

[1] E. Feenberg, Phys. Rev. **49**, 328 (1936).
[2] H. A. Bethe and R. F. Bacher, Revs. Modern Phys. **8**, 147 (1936).
[3] L. D. P. King and L. Goldstein, Phys. Rev. **75**, 1366 (1949).
[4] J. H. Coon and R. A. Nobles, Phys. Rev. **75**, 1358 (1949).
[5] Argo, Gittings, Hemmendinger, Jarvis, and Taschek, Phys. Rev. **78**, 691 (1950).
[6] R. F. Taschek, Phys. Rev. **76**, 584 (1949).

requires detectors with which to analyze the energy spectrum of scattered particles.

EXPERIMENTAL DETAILS

Bombardment Geometry

A diagram of the bombardment geometry is shown in Fig. 2. The 32-Mev proton beam from the linear accelerator was first passed through a "stripping foil" to remove molecular ions and then through the pre-magnet collimator C_1, usually set at about $\frac{1}{8}$ in.$\times\frac{1}{8}$ in. After being deflected into the 20° port by the analyzer magnet M, the beam was further collimated to $\frac{1}{8}$ in. diameter at C_2 and C_3, before it entered the scattering chamber S. Then, the scattering chamber was carefully aligned, and the beam was collected in a Faraday cup and integrated.

Vacuum and Gas-Handling System

Before a bombardment, the chamber was evacuated, flushed thoroughly with the target gas, then pumped down to ≈10 microns. After isolating the chamber from the pumps, helium was slowly introduced through

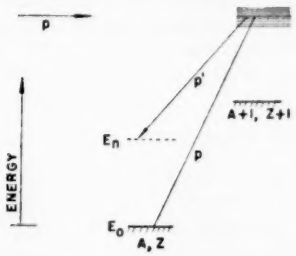

FIG. 1. Schematic description of elastic and inelastic scattering processes.

the charcoal-liquid air trap; the rate of flow was adjusted at the regulator. The combination of charcoal and the liquid air is capable of filtering out all gases but He, Ne and H_2. Since the producer specifies the bottled He to be 99.95 percent pure, with less than 0.03 percent H_2, target impurity was considered inconsequential. Actually, since the major impurity is hydrogen, a range spectrum of scattered particles would show the contributions from He and H_2 as separate.

The chamber was filled with the target gas to a pressure of about 1 atmosphere. This pressure was maintained at a constant differential with respect to atmospheric pressure by means of an oil-filled manometer through which the target gas bubbled continuously during the course of a run. The pressure differential was of the order of 10 in. of oil ("Litton" diffusion pump oil—0.9 g/cm³), i.e., about 2 percent of the total pressure. The atmospheric pressure was read before and after a run to 0.1 mm on a precision mercury barometer.

Beam Integrator

The beam was collected in a Faraday cup placed in a vacuum chamber. The charge was placed on a low

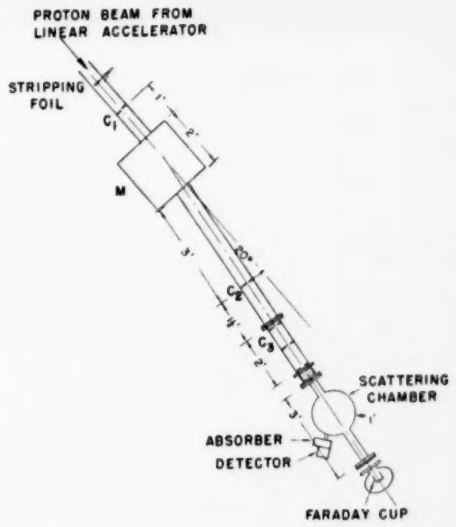

FIG. 2. Bombardment geometry.

leakage condenser connected to the grid of a 5803 electrometer tube used as a null indicator. The feedback voltage, or a fraction thereof, was applied to a Leeds and Northrup recording voltmeter which was self-calibrating against a standard cell.

The condenser used was compared on a General Radio Company impedance bridge with a G.R. standard condenser whose capacitance was known within 0.1 percent.

Electrons which might be coming down with the proton beam were kept from entering the Faraday cup by two permanent horseshoe magnets placed just beyond the scattering chamber. A second set of magnets provided a flux density of about 200 gauss just outside the Faraday cup to prevent secondary electrons from emerging.

Design and Characteristics of the Detector

Scattered particles were detected in a telescope of three gas proportional counters. Between the second and third counters was an aluminum foil 5.82 mg/cm² thick. By mixing pulses from the first two counters in coincidence and from the last counter in anticoincidence, the telescope counted all particles which stop in the foil. Hence, referring to the thickness of this foil as ΔR, if we place an absorber R in front of the telescope, it detects those particles having a range between R and $R+\Delta R$. Thus by changing R one obtains a differential range spectrum of the scattered particles.

The proportional counters were of the multiple-wire type—two-mil wolfram wires spaced $\frac{1}{4}$ inch apart over an area 2 inches in diameter, suspended with polystyrene spacers between thin aluminum ground planes $\frac{1}{2}$ in. apart. A trio of counters was designed as a unit; i.e., three counters were formed by alternating alumi-

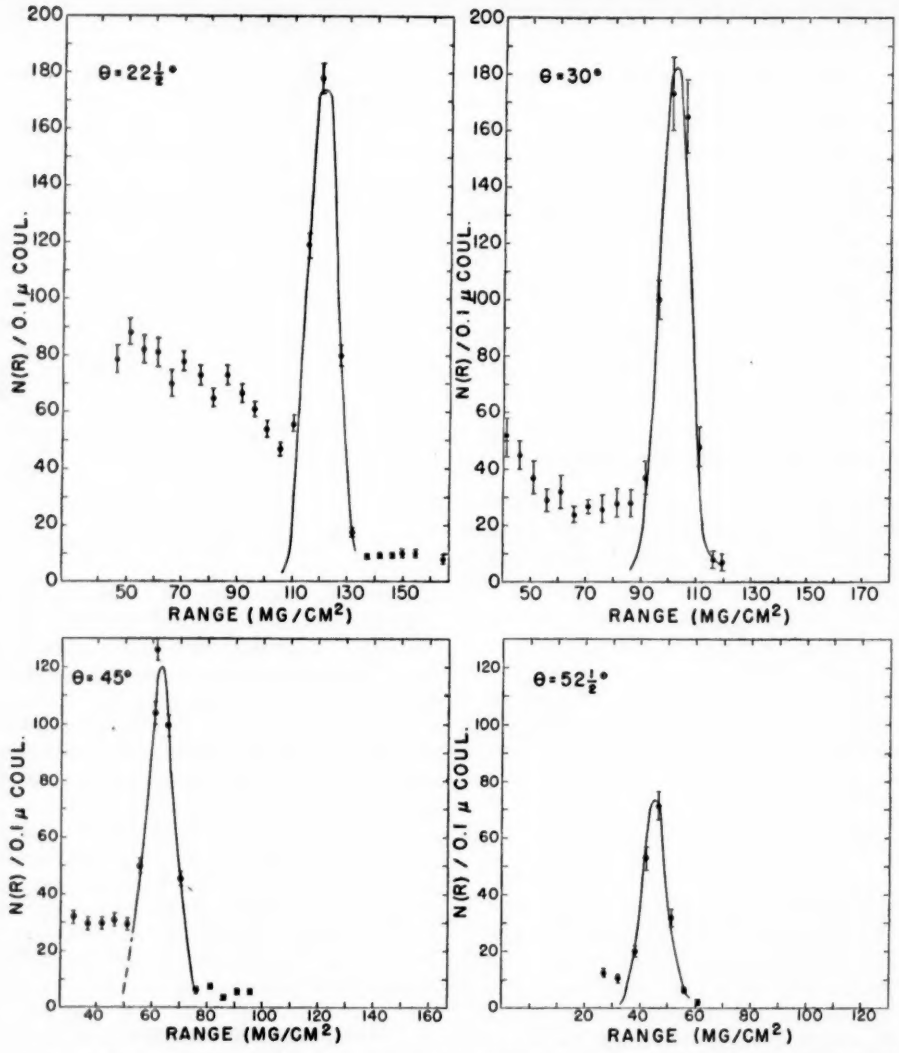

FIG. 3. Differential range spectra of charged particles inelastically scattered when He^4 is bombarded with 32-Mev protons. It is established in the text that the peak is made up of deuterons, and the continuum below the peak, of inelastically scattered protons.

num foils and multiple wire grids contained in a single chamber.

The counters were operated at about 950 volts, and the linear amplifier gains were adjusted so that the largest pulses were not quite overloading. Under these conditions, the coincidence counting rate (i.e., front two counters in coincidence and the last counter in anti-coincidence) as a function of discriminator voltage on the front two counters yielded plateaus which were quite adequate.

A proton transmitted through all three counters gives pulses having a maximum spread (jitter) of $\frac{1}{8}$ microsecond. The subsequent choice of 2-μsec gates for coincidence was made on the basis of the requirement of positive operation of the mixer-scaler.

Electronics

Pulses from proportional counters 1 and 2 generated 2-μsec gates which were fed into the coincidence channels of the mixer-scaler, while pulses from proportional counter 3 generated 3-μsec gates, straddling the 2-μsec gates of channels 1 and 2 in time, which were fed into the anti-coincidence channel of the mixer-scaler. Counting rates were low enough to make pile-up or dead-time corrections completely unnecessary. It was possible to monitor the accidental coincidences by splitting the

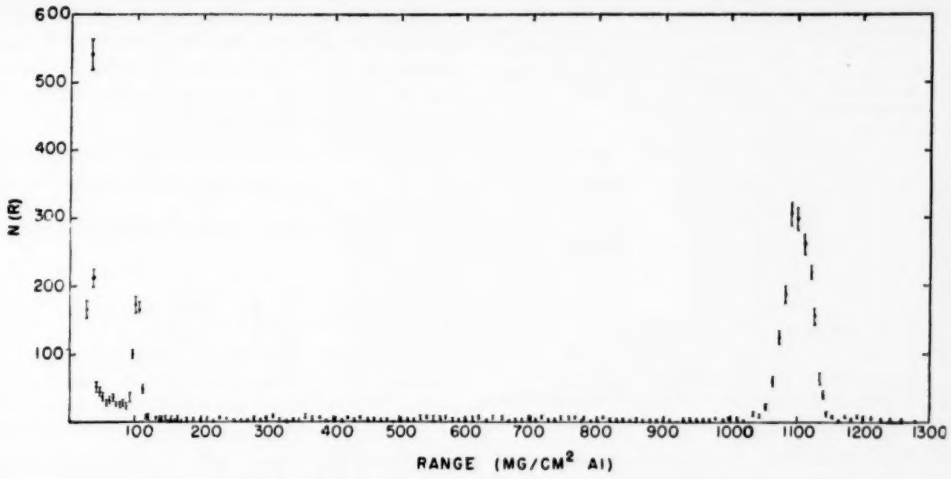

FIG. 4. Range spectrum of charged particles observed at 30°.

output of linear amplifier 2, introducing an arbitrary delay into another variable gate unit, and feeding this delayed gate into a separate mixer-scaler with the undelayed gates of the other channels. The mixer-scalers were effectively gated to count only during the beam by feeding a "beam gate" into the third coincidence channel.

Solid Angle Calculations

The solid angle calculations have been made.[7] The correction due to a finite beam width has been calculated and found negligible, and corrections due to the rapid variation of cross section with angle have been made.

Errors Affecting the Cross Section Measurement

The differential cross section for an observed process is proportional to

$$d\sigma/d\Omega \approx TN/[PCV(\Omega S)], \tag{1}$$

where T is the temperature in degrees absolute, P is the pressure of the target gas, C is the capacitance of the condenser which is charged by the collected beam to a voltage V, ΩS is the solid angle times scattering length determined by the slit geometry, and N is the number of particles detected.

In the course of a run one measured the number of particles which stopped in an aluminum foil of thickness ΔR, i.e., each point of the spectrum represents $(dN/dR)\Delta R$. Hence, to determine the number of particles scattered into the detector as a result of a given reaction, one measured the area under the peak and divided this by ΔR:

$$N=\frac{1}{\Delta R}\int\frac{dN}{dR}\Delta R dR. \tag{2}$$

[7] J. Benveniste, University of California Radiation Laboratory Report UCRL-1689, (thesis) (unpublished).

Area measurements were made by fitting theoretically derived line shapes to the experimental points as in Fig. 3. It is noted that Eq. (1) becomes

$$d\sigma/d\Omega_a \approx T/[PCV(\Omega S)\Delta R]. \tag{3}$$

Combining the several contributing errors quadratically, the estimated error in the measurement of the absolute differential cross section as a result of contributions from all sources except statistics was ±2.6 percent at 30°. Further, the estimated error of the relative cross section measurement as a result of contributions from all sources of error except statistics was ±1.5 percent at 30°.

RESULTS AND CONCLUSIONS

Search for Excited He^4 Level

A typical spectrum is shown in Fig. 4. The peak at 1100 mg/cm² represents elastically scattered protons; that at 30 mg/cm², elastically scattered alphas. The interesting group of particles is that at 100 mg/cm². As will be shown, they are deuterons from the reaction

$$p+He^4 \rightarrow He^3+d. \tag{4}$$

If they had proved to be protons, they would have indicated the existence of an excited level of the helium nucleus.

Identification of Low-Energy Peak

From the kinematics of the reaction (4) the energy of the deuterons is

$$E_d=\frac{2}{25}E\cos 2\phi+\tfrac{3}{5}(\tfrac{4}{5}E-18.3)+\frac{4}{25}E\left[6\left(1-\frac{22.9}{E}\right)\right]^{\frac{1}{2}} \times\cos\phi\left[1-\frac{\sin^2\phi}{6(1-22.9/E)}\right]^{\frac{1}{2}}, \tag{5}$$

TABLE I. Deuteron energies in the reaction $p+He^4 \rightarrow He^3+d$. The column headed E_d lists the deuteron energies expected from the kinematics of the reaction. The column headed E_d(obs) contains the energies of the particles having the observed ranges, assuming the particles to be deuterons. ϕ is the angle which the scattered deuteron makes with the beam direction.

ϕ_{lab}	E_d	E_d(obs)
15.0	12.41±0.15	12.40±0.05
22.5	11.47±0.15	11.25±0.05
30.0	10.54±0.15	10.35±0.05
37.5	9.29±0.1	9.32±0.07
45.0	7.94±0.1	7.85±0.07
52.5	6.56±0.1	6.27±0.1
60.0	5.25±0.1	5.40±0.1

where E is the energy in the laboratory system of the incident protons at the center of the scattering chamber, and ϕ is the angle which the scattered deuteron makes with the beam direction.

E may be quite accurately determined in the following way: The range of the elastically scattered protons includes, in addition to the aluminum absorber, a distance (equal to the radius of the scattering chamber) in the target gas, the entrance foil to the counter telescope, and the counter filling gas.

The nonaluminum portion of the range was equivalent to about 14 mg/cm² aluminum, and was the least precisely known contribution to the total range. However, the energy of the elastic protons was not sensitive to small uncertainties in the total range and was considered to be practically as precisely known as the range-energy data from which it is derived.[8] Then from the relation expressing the energy of protons elastically scattered from helium,

$$E_p=(E/25)[16+\cos 2\phi+8\cos\phi\{1-\tfrac{1}{16}\sin^2\}^{\frac{1}{2}}\phi], \quad (6)$$

one can find E. From range measurements of the elastic peak at seven different angles, $E=31.5\pm0.1$ Mev.

On the other hand, the precision with which the energy of the low-range particles was known depended strongly on how well known the nonaluminum portion of the range was known. It turned out that in addition to the calculations based on distances, gas pressures, and rates of energy loss, one had an excellent, independent, experimental check of this contribution. The energy of the elastically scattered alpha-particle is

$$E_{He^4}=(16/25)E\cos\phi, \quad (7)$$

and was as well known as E. The experimentally observed range of the alpha-particle must be that corresponding to E_{He^4} from the range-energy curves. Thus, the difference between this range and the aluminum absorbers plus counter foils was the nonaluminum contribution to the range.

In Table I, the column headed E_d lists the expected deuteron energies from reaction (4) as given by Eq. (5). The column headed E_d(obs) contains the energies of the particles having the observed ranges, assuming the particles to be deuterons. The agreement is seen to be quite good. However, it still remained to be seen whether the scattering data were explainable on the basis of inelastically scattered protons.

If there were an excited level of the helium nucleus,

$$p+He^4 \rightarrow Li^{5*} \rightarrow He^{4*}+p', \quad (8)$$

the inelastic proton energy would have the angular distribution

$$E_{p'}=\frac{E}{25}\cos 2\phi+\frac{16}{25}E\left(1-\frac{5}{4}\frac{\epsilon}{E}\right)+\frac{8}{25}E\left[1-\frac{5}{4}\frac{\epsilon}{E}\right]^{\frac{1}{2}}\cos\phi\left[1-\frac{\sin^2\phi}{16(1-5\epsilon/4E)}\right]^{\frac{1}{2}}, \quad (9)$$

where ϵ is the energy above the ground state of the presumed excited state. To determine a consistent value for ϵ, one measures the range of the low energy group of particles at some angle, say 45°. From the range-energy relations one can determine the energy of a proton having the range of the particles observed; then inserting this $E_{p'}$ and the previously determined E into Eq. (9), one finds that $\epsilon=21.2$ Mev. The column headed $E_{p'}$ in Table II lists the results of Eq. (9), using this value of ϵ. $E_{p'}$(obs) is the energy of a proton having the range experimentally measured. The discrepancy is seen to be quite significant.

Another identification of the low energy peak may be made by comparing the dE/dx of these particles with that of the elastic protons. It will be recalled from the description of the operation of the proportional counter telescope that all counted particles entering the counters have the same residual range. The dE/dx of deuterons and protons having the same residual range differs by about 30 percent; hence, one expects a difference of about 30 percent in the pulse height observed in the front counters. Inserting enough absorber before the counter telescope to see just the elastic protons and plotting counting rate *vs* discriminator voltage on the front two counters yields the curve of Fig. 5(a). Figure 5(b) is a similar curve obtained with the absorber required to see just the particles of the low energy peak.

TABLE II. Proton energies in the reaction $p+He^4 \rightarrow He^{4*}+p'$. The column headed $E_{p'}$ lists the expected energies of the scattered protons if there exists an excited state of the He^4 nucleus at 21.2 Mev. The column headed $E_{p'}$(obs) contains the energies of protons having the ranges experimentally measured.

ϕ	$E_{p'}$	$E_{p'}$(obs)
15	8.15±0.15	9.20±0.05
23.5	7.72±0.15	8.30±0.05
30	7.16±0.15	7.70±0.05
37.5	6.51±0.10	6.93±0.05
45	5.77±0.10	5.80±0.07
52.5	5.02±0.10	4.65±0.10
60	4.28±0.10	4.03±0.10

[8] J. H. Smith, Phys. Rev. **71**, 32 (1947).

The dE/dx of the particles of the low energy peak is seen to be about 25 percent larger than that of protons, and hence these particles are certainly deuterons.

Consideration of the Continuum

We now turn our attention to the continuum on the low range side of the deuteron peak.

The most likely sources for a continuum of protons of the observed range are the reactions

$$p+\mathrm{He}^4\rightarrow\mathrm{He}^3+n+p', \tag{10}$$

$$p+\mathrm{He}^4\rightarrow\mathrm{H}^3+p''+p', \tag{11}$$

where p' and p'' represent inelastically scattered protons. It is clear that observation of p' will yield information on the states of the $(n+\mathrm{He}^3)$ and $(p''+\mathrm{H}^3)$ systems which may also be referred to as the excited states of the He^4 nucleus (He^{4*}). For example, if the wave function describing the $(n+\mathrm{He}^3)$ system became unduly large for a given relative momentum, the probability that the proton (p') would come off with a related momentum (given by the conservation laws) would be correspondingly large. Reactions (10) and (11) may be rewritten

$$p+\mathrm{He}^4\rightarrow\mathrm{He}^{4*}+p', \tag{12}$$

$$\mathrm{He}^{4*}\rightarrow\mathrm{He}^3+n, \tag{13}$$

$$\mathrm{He}^{4*}\rightarrow\mathrm{H}^3+p'', \tag{14}$$

with somewhat less probability for the mode

$$\mathrm{He}^{4*}\rightarrow\mathrm{He}^4+\gamma. \tag{15}$$

The spectrum of p' should be a peak with an energy spread commensurate with the breadth of the excited He^4 level, while that of p'' would appear rather spread out due to the motion of its parent He^{4*}, and its area would be somewhat less than half that of the p' peak. If there were an excited level, therefore, one could expect to be able to detect a bump on the continuum. Actually, no bump (exhibiting the proper range-angle dependence) was discernible; therefore, all one can do is calculate a maximum cross section for the formation of an excited state by estimating the maximum area of a peak which might have been masked by the counting statistics. A calculation of this sort of the spectrum obtained at 22.5° (see Fig. 3) yields

$$\frac{(d\sigma)}{(d\Omega)_{\mathrm{lab}}}\leqslant 0.34 \text{ millibarn/steradian.}$$

Unfortunately, the intrusion of elastically scattered alpha-particles masks some of the low range portion of the small angle spectra where it would be desirable to hunt for a low energy group of protons. For example, at 22.5° it would not be possible to detect a small group of protons having a range less than 50 mg/cm² (5 Mev). Reference to the kinematical equation shows

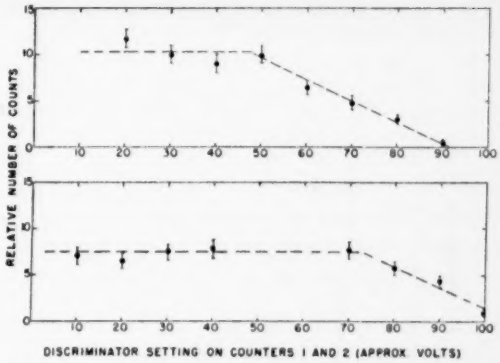

FIG. 5(a). dE/dx measurement of elastically scattered protons. The abscissa is the discriminator setting in volts. The pulse-height distribution in the front two counters of the proportional counter telescope yields a measurement of dE/dx which, with the known residual range, serves to identify the particle. (b) dE/dx measurement of the particles of the low energy peak.

that a group of protons of this energy would result if there were a level in He^4 at 23.3 Mev.

Finally, making the transformation to the c.m. system, we may conclude that the differential cross section for detecting an excited level in He^4 as high as 23.3 Mev above the ground state by means of inelastically scattered protons is less than 0.1 mb/sterad at 45° (c.m.).

If there exists a single excited level of the He^4 nucleus in the energy region and with the cross section indicated by Argo *et al.*,[8] a low energy proton group would have been seen. The absence of such a low energy proton group confirms and extends the findings of some other workers in this field.

The most natural extension to the work of the Los Alamos group was performed by Falk and Phillips,[9] who extended the excitation curve for the reaction $\mathrm{H}^3(p,\gamma)\mathrm{He}^4$ to incident proton energies of 3.4 Mev. No resonance is observed; rather, the γ-ray yield continues to increase in the way predicted by the calculations of Flowers and Mandl.[10] However, the existence of a weak (up to 30 percent), broad resonance superposed on the rising yield curve is not ruled out.

Allred,[11] in studying the reaction $\mathrm{He}^3(d,p)\mathrm{He}^4$, sought a group of low energy protons as evidence for the existence of an excited He^4 level. He reports an upper limit to the cross section for observing these protons at a c.m. angle of 102.7° of 0.2×10^{-27} cm², implying the absence of an excited He^4 level below 20.9 Mev.

Finally, the continued high level of the inelastically scattered protons, as far as we have been able to see, requires the existence of at least two levels, each having a half-width of about a million volts and a separation

[9] C. E. Falk and F. C. Phillips, Phys. Rev. **83**, 468 (1951).
[10] B. H. Flowers and F. Mandl, Proc. Roy. Soc. (London) **A206**, 131 (1951).
[11] J. C. Allred, Phys. Rev. **84**, 695 (1951).

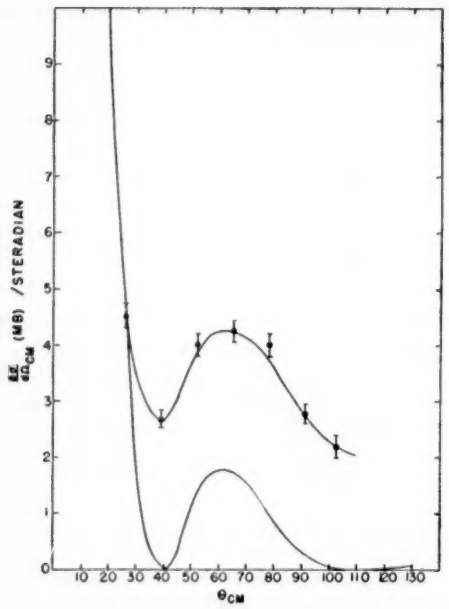

FIG. 6. Comparison of experimental yield of deuterons from the reaction $p+He^4 \rightarrow He^3+d$ with that predicted by the Butler theory. The curves have been normalized at the smallest angle observed, since the assumptions of the Butler theory are expected to be most valid for interactions involving small momentum transfers.

of about a million volts. However, whether there are just two levels or several closely spaced levels contributing to this region cannot be decided from this work.

Pick-Up Deuterons

It is interesting to compare the angular dependence of the differential cross section for the production of deuterons from the reaction $He^4(p, d)He^3$ with that predicted by the Butler theory.[12] Butler considers an incident deuteron to be stripped, with the neutron, say, deposited in the target nucleus. He finds that the angular distribution of the remaining proton depends in a distinctive way on the angular momenta and parities of the states of the initial and final nuclei. To date, the theory has been applied successfully to the assignment of angular momentum and parity to one nucleus when that of the other was known.[13–18]

Here, we are concerned with the inverse reaction, so we invoke the principle of detailed balancing which tells us that in the c.m. system, the differential cross section for the inverse reaction is directly proportional to that for the direct reaction; further, the proportionality factor includes only statistical weights, so that the angular dependences of the two differential cross sections are the same. Hence, applying the Butler theory to the reaction inverse to ours, $He^3(d, p)He^4$ will yield to us directly the angular dependence of the differential cross section for observation of our deuterons. Since the spins and parities of the initial and final nuclei are known, comparison of the theoretical and experimental data might be considered a check of the theory; or if the theory is considered to be a reasonable approximation to the truth, and if one believes the principle of detailed balancing, the theory may serve to fix the "size" of the He^3 nucleus.

If the captured neutron carries with it zero angular momentum, Butler gives

$$\sigma(\theta) \approx \left\{\frac{1}{K^2+a^2}-\frac{1}{K^2+(a+b)^2}\right\}^2 \times\left|\left[\left(\kappa_s+\frac{\partial}{\partial r}\right)\left\{\left(\frac{r}{2}\right)^{\frac{1}{2}}J_{\frac{1}{2}}(Zr)\right\}\right]_{r_0}\right|^2 \quad (17)$$

$$\approx\left\{\frac{1}{K^2+a^2}-\frac{1}{K^2+(a+b)^2}\right\}^2\left|\frac{\kappa_s}{Z}\sin Zr_0+\cos Zr_0\right|^2,$$

where

$$K^2=\tfrac{1}{4}K_d^2+k_{ps}^2-K_d k_{ps}\cos\theta,$$

$$Z^2=K_d^2+k_{ps}^2-2K_d k_{ps}\cos\theta,$$

$$K_d^2=(2M_d/\hbar^2)E_d, \quad k_{ps}^2=(2m_p/\hbar^2)E_p,$$

$$i\kappa_s=k_{ns}, \quad k_{ns}^2=(2m/\hbar^2)E_n,$$

$$E_n=E_d-\epsilon-E_p,$$

and ϵ is the deuteron binding energy; $a=0.23\times10^{13}$ cm^{-1} and $b=1.4\times10^{13}$ cm^{-1} are parameters of the internal wave function of the deuteron; r_0 is the interaction radius between the neutron and the target nucleus (He^3). Figure 6 is a comparison of the theoretical curve for $r_0=4.2\times10^{-13}$ cm, with a curve drawn through the experimental points. In spite of the somewhat meager experimental data, the fit, as determined by the coincidence of maxima and minima, is considered rather good. The increasing divergence of the two curves at large angles is not unexpected in view of the meaning of r_0. By definition, the proton does not penetrate the region of radius r_0 about the target nucleus; however, this assumption is expected to be violated in collisions involving high momentum transfers, i.e., large scattering angles.

Butler and Symonds[19] compared the theoretical angular distributions for the reactions $T(d, n)He^4$ and

[12] S. T. Butler, Proc. Roy. Soc. (London) **A208**, 559 (1951).
[13] L. Schecter, Phys. Rev. **83**, 695 (1951).
[14] Burrows, Powell, and Rotblatt, Proc. Roy. Soc. (London) **A209**, 461 (1951).
[15] Burrows, Powell, and Rotblatt, Proc. Roy. Soc. (London), **A209**, 478 (1951).
[16] Burrows, Gibson, and Rotblatt, Proc. Roy. Soc. (London), **A209**, 489 (1951).
[17] Burge, Burrows, Gibson, and Rotblatt, Proc. Roy. Soc. (London) **A210**, 534 (1952).
[18] W. M. Gibson and E. E. Thomas, Proc. Roy. Soc. (London) **A210**, 543 (1952).
[19] S. T. Butler and J. L. Symonds, Phys. Rev. **83**, 858 (1951).

$He^3(d, p)He^4$ for 10.5 deuterons with the experimental curves of Brolley *et al.*[20] and Allred[11] and found $r_0 = 4.3 \times 10^{-13}$ cm. The difference is not considered significant.

The authors are indebted to Professor W. K. H. Panofsky for his inspiration and guidance of this work from its inception, Professor L. W. Alvarez for his interest and encouragement, Dr. E. A. Martinelli, Dr. Val J. Ashby, and Dr. Robert W. Kenney for benefit derived from the discussion of mutual problems, Dr. Warren Heckrotte for several instructive discussions on the Butler theory, Dr. Joseph Lepore for illuminating discussions on the interpretation of the inelastic proton continuum, and Alex Stripeka, Harry Bowman, and Joel Harris of Mr. H. Farnsworth's Electronics Group, for their capable maintenance of the electronic equipment. Finally, the authors wish to express their gratitude to all members of the Linear Accelerator Crew, under the direction of Robert Watt and Wendell Olsen, for their enthusiastic cooperation in preparing for and performing the bombardments.

[20] Brolley, Fowler, and Stovall, Phys. Rev. **82**, 502 (1951).

PHYSICAL REVIEW VOLUME 89, NUMBER 2 JANUARY 15, 1953

States of Solid Methane as Inferred from Nuclear Magnetic Resonance*

KAZUHISA TOMITA
Department of Physics, Faculty of Science, University of Kyoto, Kyoto, Japan
(Received October 31, 1951, revised manuscript received June 30, 1952)

As there are different points of view concerning the molecular dynamical states in solid methane, especially concerning the λ-transition at 20.42°K, we have investigated the manner in which the new method of nuclear magnetic resonance throws light on the problem. Both the one-parameter theory and the method of perturbation were applied to the analysis of the proton resonance data given by Thomas, Alpert, and Torrey.

The characteristic time τ_c for molecular reorientation was estimated from the spin-lattice relaxation data, and it was found that above 20°K molecules may be considered to reorient against some fixed hindrances due to neighboring molecules. At about 65°K a marked alteration is present in the dominant mechanism of the above reorientation, which is considered to be either correlated or independent molecular rotation. However, below 20°K most of the molecules seem to be in the ground state of rotational oscillation and occasionally (about 10^7 times per second) tunnel or flip to neighboring equivalent orientations. It was proposed that we should discriminate between two pictures of the local magnetic field, possibly in relation to the frequency of resonance. This idea was confirmed by reproducing the line width data.

A perturbation calculation, assuming the $F\bar{4}3m$ arrangement of the molecules and taking account of the above situation, gave the entire shape of the absorption line, which was in close agreement with experimental data observed in the lowest temperature range.

I. INTRODUCTION

ABOUT ten years ago Clusius, Popp, and Frank[1–4] carried out a series of thermal measurements on solid methane and found a λ-change in the specific heat at 20.42°K. Although many authors have considered the mechanism of the λ-transition since that time, no decisive conclusions seem to have been obtained.

According to the results of x-ray analysis[5] the carbon atoms form a face-centered cubic lattice (see Fig. 1), and scarcely any difference was observed[6] between the lattice structures above and below the λ-point. The only remaining degrees of freedom being those of molecular reorientation, Clusius suggested that the transition should be a rotational one as suggested by Pauling.[7]

Because x-ray analysis could not fully locate the hydrogen atoms in the molecule, it seemed hopeless to verify the molecular rotation directly, and some indirect verifications have been attempted. These are connected with the thermal behavior of solid methane both above and below the λ-point.

Eucken examined[8] the rotational part of the specific heat and obtained a value of about 3 cal/mole deg between the λ-point and the fusion point, which seems to suggest that the molecules are rotating freely in the classical sense. Theoretical calculations showed,[9] however, that the free rotation of a single molecule may become classical only above 50°K.

At the lowest temperature the value of the zero-point entropy has been used as a starting point. Free rotation is excluded because it would require $S = S_0 + (2/16)R \ln 5$, which is definitely greater than the observed value $S_0 = R \ln 16$. Since $2^4 = 16$, Clusius proposed a random distribution of proton spin over the whole crystal, which implies that a spin is correlated equally with spins in the same molecule and with those in the other molecules. Were this the case, the resultant spin of a molecule could easily be changed, and sublimation from such a state should give a single species having

* Read on October 8, 1951, at the Sixth Annual Meeting of the Physical Society of Japan.

[1] Clusius, Popp, and Frank, Physica **4**, 1105 (1937).
[2] A. Frank and L. Popp, Z. physik Chem. **B36**, 291 (1937).
[3] Kruis, Popp, and Clusius, Z. Elektrochem. **43**, 664 (1937).
[4] K. Clusius and L. Popp, Z. physik. Chem. **B46**, 63 (1940).
[5] H. H. Mooy, Commun. Phys. Lab. Univ. Leiden **213** D(1931); **216** A(1931).
[6] A. Schallamach, Proc. Roy. Soc. (London) **A171**, 569 (1939).
[7] L. Pauling, Phys. Rev. **36**, 430 (1930).
[8] A. Eucken, Z. Elektrochem. **45**, 126 (1939).
[9] A. W. Maue, Ann. Physik **30**, 555 (1937).

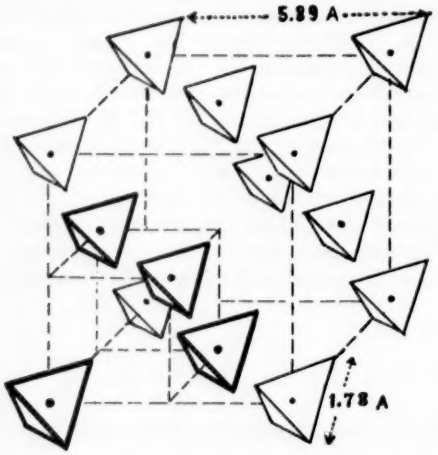

FIG. 1. The crystal structure of solid methane ($F\bar{4}3m$).

the lowest free energy, which seems improbable from our experience with hydrogen. However, recently Nagamiya[10] put forth another reasonable interpretation. He assumed that a molecule is in a state of rotational oscillation, which is quantized by a crystalline field having a definite symmetry due to the configuration of neighboring molecules, and looked for structures which give the proper value of the zero-point entropy. A crystalline field with tetrahedral symmetry was selected, in which molecules should be located parallel to each other, stretching their C−H bonds along the cubic body diagonals (see Fig. 1).

To verify the above viewpoint and to have a clear understanding of the nature of the transition, the recently developed method of nuclear magnetic resonance offers a powerful and promising tool. For this method is capable not only of giving the geometrical configuration[11,12] of protons but also of throwing light on their dynamical behavior.[13–17] The writer had already pointed out[18] that a methane molecule must be in a state of motion even in its lowest temperature modification, because the absorption line is definitely narrower than that expected for a rigid configuration.[19,20] Recently Thomas, Alpert, and Torrey[21] reported a proton magnetic resonance investigation on solid methane, giving not only the absorption line width but also the spin-lattice relaxation time (Figs. 2 and 4). They considered that the possibility of rotational transformation was eliminated, because there is no change in line width at the λ-point. Thus we have several conflicting opinions concerning the λ-transition.

The purpose of the present paper is to put in order the above diverse pictures by carefully analyzing the proton magnetic resonance data and to obtain a clear understanding of the mechanism of the λ-change.

II. DESCRIPTION BY THE ONE-PARAMETER THEORY

In a chemically saturated molecule like methane, protons are seldom influenced by their surroundings except through the magnetic interaction among themselves. The frequency associated with this interaction is only about 0.1 Mc/sec and that associated with molecular rotation is larger than 10^4 Mc/sec; therefore, spin-spin interaction can hardly affect the molecular rotation. Conversely, the rotation of the molecule cannot produce any significant magnetic field at the position of the nucleus, because the molecular charge distribution has no electric dipole moment owing to its high symmetry. Thus the coupling of the molecular motion with the nuclear spin system is involved only implicitly in the time change of the relative nuclear coordinates in the spin-spin interaction.

Magnetic resonance experiments are usually performed in the frequency range of 10 Mc/sec, where the Paschen-Back condition is well established; therefore the resonance line is well defined and perturbations due to spin-spin interaction affect only the attributes of the resonance line—i.e., its width and degree of saturation. Under these circumstances the following classification of the magnetic interaction is useful:

$$V=\sum_{i>j} V_{ij}, \tag{1}$$

$$V_{ij}=\gamma^2\hbar^2 r_{ij}^{-3}\{(\mathbf{I}_i\cdot\mathbf{I}_j)-3r_{ij}^{-2}(\mathbf{I}_i\cdot\mathbf{r}_{ij})(\mathbf{I}_j\cdot\mathbf{r}_{ij})\}$$
$$=\gamma^2\hbar^2 r_{ij}^{-3}(A+B+C+D+E+F), \tag{2}$$

$$\Delta m=0\begin{cases} A=-2(I_{iz}I_{jz})P_2^0(\cos\theta_{ij}), & (2.1)\\ B=\tfrac{1}{2}(I_i^+I_j^-+I_i^-I_j^+)P_2^0(\cos\theta_{ij}), & (2.2)\end{cases}$$

$$\Delta m=+1:\quad C=-\tfrac{1}{2}(I_i^+I_{jz}+I_{iz}I_j^+)P_2^1(\cos\theta_{ij})\times\exp[-i(\phi_{ij}-\gamma H_0 t)], \tag{2.3}$$

$$\Delta m=-1:\quad D=-\tfrac{1}{2}(I_i^-I_{jz}+I_{iz}I_j^-)P_2^1(\cos\theta_{ij})\times\exp[+i(\phi_{ij}-\gamma H_0 t)], \tag{2.4}$$

$$\Delta m=+2:\quad E=\tfrac{1}{4}(I_i^+I_j^+)P_2^2(\cos\theta_{ij})\times\exp[-2i(\phi_{ij}-\gamma H_0 t)], \tag{2.5}$$

$$\Delta m=-2:\quad F=\tfrac{1}{4}(I_i^-I_j^-)P_2^2(\cos\theta_{ij})\times\exp[+2i(\phi_{ij}-\gamma H_0 t)]. \tag{2.6}$$

Here $\mathbf{I}_i$ represents the spin operator of the nucleus i,

[10] T. Nagamiya, Progress Theor. Phys. **6**, 702 (1951).
[11] G. E. Pake, J. Chem. Phys. **16**, 327 (1948).
[12] Gutowsky, Kistiakowsky, Pake, and Purcell, J. Chem. Phys. **17**, 972 (1949).
[13] Bloembergen, Purcell, and Pound, Phys. Rev. **73**, 679 (1948).
[14] E. R. Andrew and R. Bersohn, J. Chem. Phys. **18**, 159 (1950).
[15] H. S. Gutowsky and G. E. Pake, J. Chem. Phys. **18**, 162 (1950).
[16] R. Newman, J. Chem. Phys. **18**, 669 (1950).
[17] E. M. Purcell, Physica **XVII**, 282 (1951).
[18] K. Tomita, Read on Nov. 4, 1950 at the fifth annual meeting of the Physical Society of Japan.
[19] N. L. Alpert, Phys. Rev. **75**, 389 (1949).
[20] Bitter, Alpert, Poss, Lehr, and Lin, Phys. Rev. **71**, 738 (1947); N. L. Alpert, Phys. Rev. **72**, 637 (1947).
[21] Thomas, Alpert, and Torrey, J. Chem. Phys. **18**, 1511 (1950).

and m is the z component (parallel to the constant field $\mathbf{H}_0$) of the resultant spin of the molecule. $\mathbf{r}_{ij}$ $(r_{ij}, \theta_{ij}, \phi_{ij})$ is the relative coordinate of spin i and j, and the P_i^μ $(\mu=1, 2, 3)$ are spherical harmonics of the second order. Semi-diagonal elements (A and B) represent adiabatic perturbations and are considered responsible for the spin-spin relaxation, while off-diagonal elements (C, D, E, and F) represent nonadiabatic perturbations which are considered responsible for the spin-lattice relaxation. However, we can observe only the stationary parts of the perturbation; therefore, an appropriate projection is necessary to select such stationary parts. The idea of Bloembergen *et al.* lies in approximating this process by adopting some specified harmonics in the Fourier spectrum of the intensity of perturbation. When we define $J_k(\nu)$ by the equation

$$\langle F_k^*(t)F_k(t)\rangle = \int_{-\infty}^{+\infty} J_k(\nu)d\nu$$

$$= \int_{-\infty}^{+\infty} d\nu \int_{-\infty}^{+\infty} \langle F_k^*(t)F_k(t-\tau)\rangle e^{2\pi i\nu\tau}d\tau, \quad (3)$$

where

$$F_0(t) = 2\sum_{i>j} P_2^0(\cos\theta_{ij}(t))/r_{ij}^3(t), \quad (3.1)$$

$$F_1(t) = \tfrac{1}{3}\sum_{i>j} P_2^1(\cos\theta_{ij}(t))e^{i\varphi_{ij}(t)}/r_{ij}^3(t), \quad (3.2)$$

$$F_2(t) = \tfrac{1}{3}\sum_{i>j} P_2^2(\cos\theta_{ij}(t))e^{2i\varphi_{ij}(t)}/r_{ij}^3(t), \quad (3.3)$$

the spin-lattice relaxation time T_1 (which is associated with the transition due to a nonadiabatic perturbation) is given by

$$(1/T_1) = \tfrac{3}{4}\gamma^4\hbar^2 I(I+1)[J_2(2\nu_0)+2J(\nu_0)], \quad (4)$$

where ν_0 is the Larmor frequency and is introduced as a result of the above projection. The spin-spin relaxation time T_2 (associated with the phase diffusion due to an adiabatic perturbation) is given by

$$(1/T_2)^2 = \mathrm{Spur}(\dot{I}_x^2)/\mathrm{Spur}(I_x^2)$$

$$= \frac{9}{4}\gamma^4\hbar^2\frac{I(I+1)}{3}\langle\{\textstyle\sum_j\{2P_2^0(\cos\theta_{ij})/r_{ij}^3\}^2\rangle$$

$$= \frac{9}{4}\gamma^4\hbar^2\frac{I(I+1)}{3}\int_{-\nu_m}^{+\nu_m} J_0(\nu)d\nu, \quad (5)$$

which is equivalent to the adiabatic second moment of the absorption line.[22] However, as a result of the above projection there appears the quantity ν_m, which is the maximum frequency of the spectrum that contributes to the stationary part of the local field.

In our case of solid methane, since the only remaining degree of freedom is that of molecular rotation, we may

[22] J. H. Van Vleck, Phys. Rev. **74**, 1168 (1948).

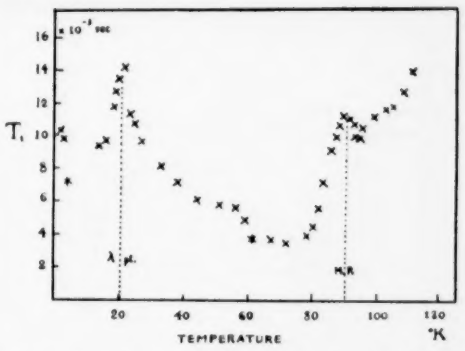

FIG. 2. Observed spin-lattice relaxation time T_1. (The data indicated by • seem unreliable as the result of our analysis (see Figs. 3 and 4).)

assume a single time constant τ_c (which represents the mean life of the relative orientation of nuclei) at least for the first approximation. This allows us to take a Brownian type correlation function,

$$\langle F_k^*(t)F_k(t-\tau)\rangle = \langle F_k^*(t)F_k(t)\rangle_{Av}\cdot\exp(-\tau/\tau_c), \quad (6)$$

from which we can obtain the Fourier intensity by the formula

$$J_k(\nu) = \int_{-\infty}^{+\infty}\langle F_k^*(t)F_k(t-\tau)\rangle\exp(2\pi i\nu\tau)d\tau$$

$$= 2\langle F_k^*(t)F_k(t)\rangle_{Av}\tau_c/[1+(2\pi\nu\tau_c)^2]. \quad (7)$$

Here $\langle F_k^*(t)F_k(t)\rangle_{Av}$ expresses the time average and should be calculated by using the orientational wave function $\phi_R(\theta, \varphi)$. However, as a methane molecule is highly symmetrical in shape, we may safely replace the time average by an average over a sphere. Admitting the above simplifying assumption, we have finally

$$(1/T_1) = K_1\left\{\frac{\tau_c}{1+(2\pi\nu_0\tau_c)^2}+\frac{2\tau_c}{1+(4\pi\nu_0\tau_c)^2}\right\}, \quad (8)$$

and

$$(1/T_2) = [(3K_1/\pi)\tan^{-1}(2\pi\nu_m\tau_c)]^{\frac{1}{2}}, \quad (9)$$

where

$$K_1 = (3/10)\gamma^4\hbar^2\sum_{j=2}^{4} r_{1j}^{-6}. \quad (10)$$

In this way, the two kinds of relaxation time are reduced to the single parameter τ_c.

1. Spin-Lattice Relaxation

In contrast to the monotonic variation of the line width with temperature, the spin-lattice relaxation time reveals a rather complex behavior below 90°K (the solidification point), and this suggests its greater sensitivity to the dynamical state of the protons. Accord-

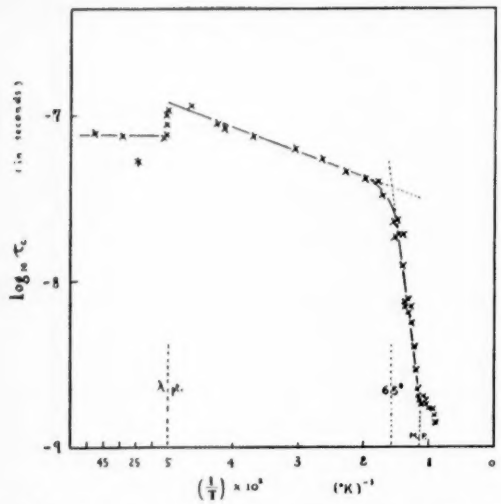

FIG. 3. Characteristic time τ_c determined from spin-lattice relaxation. ($\text{Log}_{10}\tau_c$ is plotted against reciprocal temperature.)

ingly, we have chosen the following procedure: By using the spin-lattice relaxation time we first determined τ_c as a function of temperature, and then, using this τ_c, we calculated the line width to be compared with observation. The first step is not a mere process of parameter fixing, but involves a crucial test of the basic model. For the minimum value of the lattice relaxation time is given by

$$(T_1)_{\min}=(3\sqrt{2}\pi/2)(\nu_0/K_1), \tag{11}$$

which is completely determined by the particular system of nuclei which reorient together as one rigid body, and by the applied frequency. If we take a single molecule as a unit whose reorientation is characterized by the time constant τ_c, the minimum relaxation time is calculated to be 3.5×10^{-3} sec, which is nearly equal to the observed value. This assures the validity of our picture, at least in the neighborhood of the minimum (at about 70°K).

By adopting the above picture over the entire temperature range and using (8), we have obtained the results shown in Fig. 3, where $\log_{10}\tau_c$ is plotted against reciprocal temperature. Figure 3 depends essentially on the nature of solid methane, although T_1 may also depend on the frequency used. It is observed that τ_c decreases with increasing temperature, and also that there exist rather sharp changes in the dominant mechanism for spin-lattice relaxation at about 20°K (λ-point), 65°K (this anomaly has not yet been detected by thermal measurements) and 90°K (melting point). The choice of scale enables us to obtain more information about the dynamical behavior of each molecule.

The linear character revealed in the plot above 20°K assures that τ_c may be expressed in the form

$$\tau_c^{-1}=\exp(-\theta/T)=\Omega\exp(-\epsilon/kT). \tag{12}$$

Equation (12) suggests that molecular reorientations appear only when the transitions (caused by the thermal agitation) occur between two distinct groups of levels, which are generally quantized by a more or less fixed crystalline field. The orientational flipping in the upper group is considered much more frequent than in the lower group, and ϵ is interpreted as the mean separation of the two groups. In the limit of weak quantization, the above process tends to a classical jumping over fixed potential peaks, the height of which is taken to be ϵ. The transition in τ_c at about 56°K is reproduced fairly well by adding two exponential formulas of the type (12), which seems to favor a classical terminology. The height ϵ of the peak and the frequency factor Ω in each range was estimated by (12) and are given in Table I. The relative magnitudes of ϵ and of Ω suggest that in the temperature range (*A*) (20∼65°K) the rate determining passage is rather narrow though it is not very high, whereas in the range (*B*) (65∼90°K) thermal agitation enables a molecule to jump over a broad front though its crest is considerably higher than in the former case. Above 90°K, it is obvious that our model becomes inadequate on account of the possible appearance of migration, but if we assume that only the molecular rotation is responsible for relaxation, ϵ and Ω are estimated to be between the values in (*A*) and (*B*).

Below the λ-point τ_c seems almost independent of temperature, which suggests that molecules are frozen into the lowest group of quantized levels, the width of which is much smaller than kT. It must be observed that the lowest temperature modification of methane does not give $\tau_c\to\infty$ (which is expected when molecules are immovably fixed), but it gives $\tau_c\sim10^{-7}$ sec, showing the existence of molecular reorientation at this very low temperature. This remarkable feature is, however, understood if we admit that the lowest group contains a number of levels. For then the transition inside this lowest group may be considered to correspond to the flipping reorientation. In fact, the value of the zero point entropy suggests that the lowest group contains a number of levels, even when quantized by the crystalline field.

2. Line Width

To confirm the considerations given above we calculated the line width of resonance absorption along the lines of the one-parameter theory, using values of τ_c determined from T_1. According to Bloembergen *et al.*, the effect of the nonadiabatic perturbation on line

TABLE I. Estimated values of ϵ and Ω.

Temperature range	Activation energy ϵ (or θ)	Frequency factor Ω
(A) 20∼65°K	68 cal/mole (34°K)	4.7×10^{7} sec^{-1}
(B) 65∼90°K	1380 cal/mole (695°K)	1.4×10^{12} sec^{-1}
Above 90°K	257 cal/mole (130°K)	2.0×10^{9} sec^{-1}

width becomes appreciable only when $2\pi\nu_0\tau_c<1$. In the present case this corresponds to the range $T>70°K$, where the observed line width is already very narrow (<0.5 gauss); therefore we may safely neglect the effect of the lattice relaxation on line width when $T<70°K$. It should be added that in the formula (9) ν_m is a rather ambiguous quantity, and this makes the estimate less accurate than in the case of spin-lattice relaxation. Bloembergen *et al.* took $\nu_m=(1/\pi T_2)$, but when applied to our case this formula does not give a good reproduction of line width even in the order of magnitude. In this situation we propose to discriminate between two pictures of local magnetic field, possibly in relation to the frequency which is used in the observation.

(1) In the range where τ_c is large, only the quasi-static or *kinematical* picture is observed. In this case the additional field due to magnetic interaction causes an adiabatic acceleration or decelerations of the main precession, which is expected to appear as a shift or width of the resonance line. However, the effect of the modes of molecular motion which are higher than the applied frequency is averaged out over one cycle of the radiofrequency and cannot be detected as a shift or a width. Therefore it is reasonable to adopt

$$\nu_m=d\cdot\nu_0, \quad (d\sim 1), \tag{13}$$

in this case. In fact, if we take $d=0.162$ in this formula, the line width in solid methane is reproduced fairly well, including its local characteristics in the range $T<50°K$ (in Fig. 4 the calculated values are represented by open circles and the broken line). Note that the single formula proves satisfactory both above and below the λ-point.

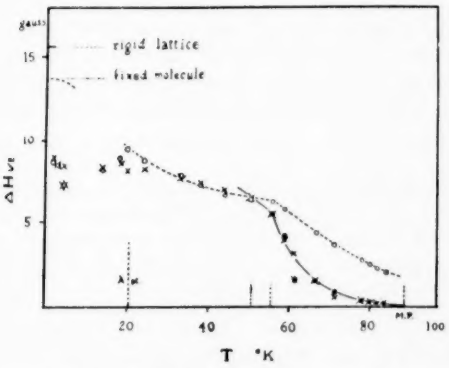

FIG. 4. Half-value width $\Delta H_{\frac{1}{2}}$ calculated from spin-lattice relaxation. (The open circles and the broken line represent the values calculated under the assumption of a quasi-static local field. The closed circles and the full line represent the values calculated under the assumption of a dynamic local field. The crosses represent observed values.)

(2) When τ_c becomes small, however, a marked discrepancy appears between the kinematical picture and the observations. (In methane this point is located at about 50°K, where there is no anomaly in τ_c.) An essentially *dynamical* treatment seems necessary in this case. However, we can also include this case in the scheme of the semi-phenomenological theory if we adopt a cooperative or correlated limit for ν_m, the procedure of Bloembergen *et al.* being one such example. However, in our case of methane their assumption proves to be inadequate, while a good reproduction of the line width is obtained if we assume

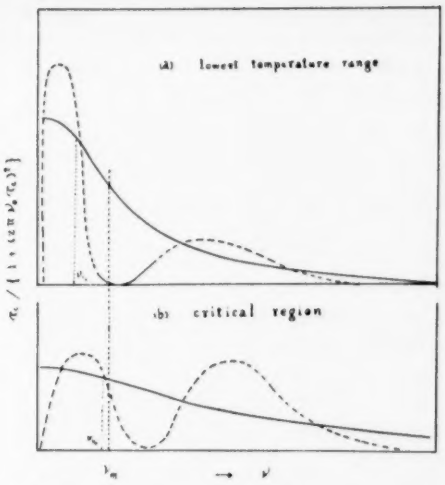

FIG. 5. The frequency spectrum of the intensity of perturbation (schematic). (a) corresponds to the lowest temperature range; (b) corresponds to the critical region.

$$\nu_m=e/(T_2)^n, \tag{14}$$

and take $e=0.184$ and $n=1.44$ above 50°K, as is shown in Fig. 4. (The calculated values are represented by solid circles and the full line.) It should be noted that this set of values is satisfactory over two regions which are different in the dominant mechanism for lattice relaxation.

In the transition region of the above two pictures, the line width becomes about one half that of a fixed molecule [the latter is estimated to be 13.6 gauss by taking $\nu_m\to\infty$ in (9)]. This seems to suggest that in this region the relative importance of the cut-off modes becomes comparable with the ones retained in (9). Conversely, if we tentatively set the critical region by the above condition, we have, according to (9),

$$\nu_m=\nu_{\frac{1}{8}}\equiv\tan(\tfrac{1}{8}\pi)/2\pi\tau_c, \tag{15}$$

which is also written as

$$(\tau_c^*\nu_0)=\tan(\tfrac{1}{8}\pi)/2\pi d=0.420. \tag{16}$$

The fact that $(\tau_c^*)^{-1}\sim\nu_0$ seems to suggest the significance of the critical condition. The observed value for $\tau_c^*\nu_0$ is 0.386, which is of the same order as (16) but somewhat smaller. This fact may be understood if

TABLE II. Reduced spin functions.

α_i and β_i represent spin functions for an individual nucleus i. I_t and M denote the resultant spin and its z-component respectively.

$A\ (I_t=2)$	ϕ_1	=	1									$\alpha_1\alpha_2\alpha_3\alpha_4$	$M=2$
$A\ (I_t=2)$	$2\,\phi_2$			1	1	1	1					$\beta_1\alpha_2\alpha_3\alpha_4$	$M=1$
$T\ (I_t=1)$	$2\sqrt{3}\,\phi_3$			1	1	1	−3					$\alpha_1\beta_2\alpha_3\alpha_4$	
	$\sqrt{6}\,\phi_4$			1	−1	−2	0					$\alpha_1\alpha_2\beta_3\alpha_4$	
	$\sqrt{2}\,\phi_5$			1	−1	0	0					$\alpha_1\alpha_2\alpha_3\beta_4$	
$A\ (I_t=2)$	$\sqrt{6}\,\phi_6$							1	1	1	1	1	1	$\beta_1\beta_2\alpha_3\alpha_4$	$M=0$
$E\ (I_t=0)$	$2\sqrt{3}\,\phi_7$							2	−1	−1	−1	−1	2	$\alpha_1\beta_2\beta_3\alpha_4$	
	$2\,\phi_8$							0	1	−1	1	−1	0	$\beta_1\alpha_2\beta_3\alpha_4$	
$T\ (I_t=1)$	$\sqrt{6}\,\phi_9$							1	1	1	−1	−1	−1	$\beta_1\alpha_2\alpha_3\beta_4$	
	$2\sqrt{3}\,\phi_{10}$							2	−1	−1	1	1	−2	$\alpha_1\beta_2\alpha_3\beta_4$	
	$2\,\phi_{11}$							0	1	−1	−1	1	0	$\alpha_1\alpha_2\beta_3\beta_4$	

we assume that the real spectrum is not simply the damped-oscillator type (the full line in Fig. 5), but that it is composed of two distinct humps (the dotted line in the figure). If ν_m should cut off a part of the lower frequency hump to satisfy the critical condition, the depression of $(\nu_m^*)_{\text{obs}}$ is to be expected. In the next section this idea is confirmed by an independent consideration.

As for the lowest temperature range, the protons in each molecule would also be affected by those in the neighboring molecules, if the molecules are immovably fixed. When we assume the $F\bar{4}3m$ arrangement (which is suggested by the x-ray analysis[5] and is supported by entropy considerations[10]; see Fig. 1), we expect a half-value width

$$\Delta H_{\frac{1}{2}}(\text{whole lattice}) = 15.5 \text{ gauss} \tag{17}$$

in this case.[23] Actually, however, only 8.7 gauss is observed as the half-value width, which apparently indicates the existence of a certain kind of molecular motion even below the λ-point. This situation is consistent with that which was inferred from spin-lattice relaxation.

III. THE SHAPE OF THE ABSORPTION LINE

Another independent test of our viewpoint is given by consideration of the detailed shape of the resonance. Accordingly, in this paragraph, we will treat the magnetic interaction by using the perturbation method, and the results will be compared with existing data observed in the lowest temperature range. If we consider a single molecule for the present, it is convenient to use a set of basic spin functions which are reduced with respect to the substitution group of four identical nuclei. This group is isomorphous to the real rotation group of the tetrahedron when we consider only reorientations which are equivalent to such rotations. In this case we may conveniently label their irreducible representations by using notations associated with the latter. Reducing the 16 spin functions, we have

$$5A+E+3T \tag{18}$$

as the irreducible members, to each of which there corresponds a definite value of resultant spin, as is shown in Table II. By using these basic functions, the matrix elements of the semidiagonal part of the spin-spin interactions are calculated. These are given in Table III, where

$$A_{ij} = -\gamma^2 h^2 r_{ij}^{-3} P_2^0(\cos\theta_{ij}). \tag{19}$$

As the constant field (which defines the z direction) is of uni-axial character and has in general no systematic relation to the figure axis, there are elements combining different irreducible representations.

Now the fact that below the λ-point a definitely narrower width is observed as compared with a rigid molecule suggests that we may not count all the elements in Table III as perfectly stationary. In order, then, to select the really stationary part of the perturbation, we must consider the spacial motion of a molecule. Since there is hardly any dynamical interaction between nuclear spin and space motion, the total wave function Φ of a molecule may be written as

$$\Phi = \phi_{\text{space}} \times \psi_{\text{spin}}. \tag{20}$$

However, ϕ_{space} and ψ_{spin} are not completely independent, because protons obey Fermi statistics. That is, Φ must belong to the totally symmetric representation, because we take only real rotations into account. In this case, physically real states are involved only in the combinations $\phi(A)\times\psi(A)$, $\phi(E)\times\psi(E)$, and $\phi(T)\times\psi(T)$, which correspond to what are called respectively *meta-*, *para-* and *ortho*-molecules. As the level

[23] The contribution of neighbors more distant than the tenth was replaced by an integration.

TABLE III. Matrix elements of the spin-spin interaction. (In view of the Paschen-Back situation we used only the adiabatic part of the perturbation.)

$A(\phi_1)$	a_2										$M=2$
$A(\phi_2)$		a_1	b_1	c_1	d						
$T\{(\phi_3)$		b_1	e	f	g						$M=1$
$T\{(\phi_4)$		c_1	f	h	k						
$T\{(\phi_5)$		d	g	k	l						
$A(\phi_6)$						a_0	b_0	c_0	0	0	0
$E\{(\phi_7)$						b_0	0	0	0	0	0
$E\{(\phi_8)$						c_0	0	0	0	0	0
$T\{(\phi_9)$						0	0	0	$-2e$	$-2f$	$2g$
$T\{(\phi_{10})$						0	0	0	$-2f$	$-2h$	$2k$
$T\{(\phi_{11})$						0	0	0	$2g$	$2k$	$2l$

$M=0$

separation in the rotational oscillation is more than 3×10^5 Mc/sec ($\sim$15°K), the population of the ground level may be considered to play a dominant role in our case ($T<14$°K). Thus a molecule resonates among the twelve equivalent lowest levels, which, under a crystalline field of tetrahedral symmetry, split into terms represented by

$$A+3T+E. \tag{21}$$

Transitions combining different terms offer the first possible cause of the molecular reorientation. Although the levels of $3T$ are degenerate as long as the crystalline field has the above symmetry, they may in practice be split or broadened, because the neighboring molecules are not really fixed. Transitions inside this $3T$ group may be considered the second cause of the molecular reorientation, although their frequency should be much lower than in the former case (see Fig. 6). Thus the molecular motions accompanied by a change in the resultant spin may have a relatively high frequency spectrum, and those accompanied by no change may have a low frequency one. These characteristics must be reflected in the local field intensity due to spin-spin interaction. In fact, the presence of such distinct groups in the local field spectrum is just what we expected in the previous section. In the lowest temperature range, however, ν_m is estimated as $1.76\nu_{1/4}$, which suggests that the greater part of the low frequency spectrum may contribute to the line width in contrast to the case in the critical region, while the frequency of the higher group may still be considered greater than ν_m (Fig. 5(a)). In this way, the process of cutting off higher frequency modes in the one-parameter theory corresponds to the elimination of the matrix elements combining different irreducible representations in our scheme. This elimination is the desired projection process required by the observations (see Fig. 3).

TABLE III.—*Continued*

$$\begin{pmatrix} -2a_2 \\ 4a_1 \\ 4b_1/\sqrt{3} \\ 8c_1/\sqrt{6} \\ 8d/\sqrt{2} \\ 12e \\ 24f/\sqrt{2} \\ 24g/\sqrt{6} \\ 6h \\ 6k/\sqrt{3} \\ 2l \\ 2a_0 \\ 4b_0/\sqrt{3} \\ 4c_0/\sqrt{6} \end{pmatrix} = \begin{pmatrix} 1 & 1 & 1 & 1 & 1 & 1 \\ 1 & 1 & 1 & 1 & 1 & 1 \\ 1 & 1 & 1 & -1 & -1 & -1 \\ 2 & -1 & -1 & 1 & 1 & -2 \\ 0 & -3 & 3 & 3 & -3 & 0 \\ -3 & -3 & -3 & 1 & 1 & 1 \\ 6 & -3 & -3 & -1 & -1 & 2 \\ 0 & -3 & 3 & -1 & 1 & 0 \\ 0 & 0 & 0 & -2 & -2 & 1 \\ 0 & 0 & 0 & 1 & -1 & 0 \\ 0 & 0 & 0 & 0 & 0 & -1 \\ 1 & 1 & 1 & 1 & 1 & 1 \\ -2 & 1 & 1 & 1 & 1 & -2 \\ 0 & -1 & 1 & -1 & 1 & 0 \end{pmatrix} \cdot \begin{pmatrix} A_{12} \\ A_{23} \\ A_{31} \\ A_{14} \\ A_{24} \\ A_{34} \end{pmatrix}$$

Changing to the coordinate system with a polar axis parallel to a cubic axis, and denoting the directions of constant field by (θ, φ), we may express the matrix elements as function of (θ, φ). As we retain only semi-diagonal elements of interaction with respect to both magnetic and crystalline fields, we may treat distinct molecular species separately, and the allowed transition between the roots of the secular equations appears as a shift from the Larmor frequency. The secular equations may be solved as follows.

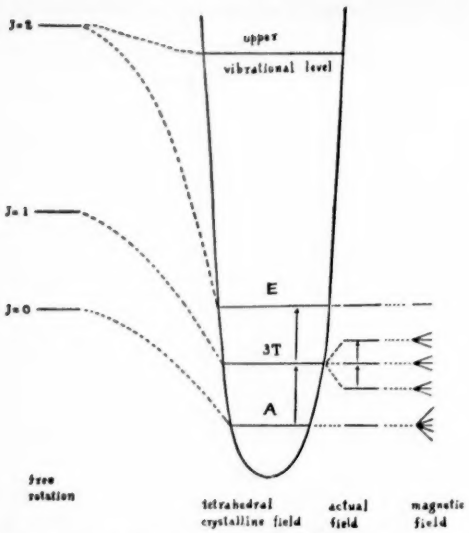

FIG. 6. Level scheme of a methane molecule under the crystalline field (schematic).

1. *Meta*-Methane (*A*)

Since the matrix elements themselves are a symmetric combination of A_{ij}, we have $a_2=a_1=a_0=0$ and no local field is present in this case. Therefore a resonance is expected exactly at the Larmor frequency. If we estimate the transition probability by the formula

$$J(M\to M')=|\langle M|\sum_{i=1}^{4} I_{ix}|M'\rangle|^2, \tag{22}$$

we find

$$J_{\text{meta}}(\pm 1\rightleftarrows 0)=\tfrac{3}{2}, \tag{23}$$

and

$$J_{\text{meta}}(\pm 2\rightleftarrows \pm 1)=1, \tag{24}$$

and finally we have

$$J_{\text{meta}}(\text{total})=5. \tag{25}$$

2. *Para*-Methane (*E*)

No resultant magnetic moment is present in this kind of molecule; therefore, it drops out of our magnetic observations.

3. *Ortho*-Methane (*T*)

Since the trace of the 3-dimensional matrix is zero, the secular equations may be written directly in standard forms. For the case $M=1$, we have explicitly

$$x^3-\tfrac{3}{16}x+\tfrac{1}{32}\cos\Psi(\theta,\varphi)=0, \tag{26}$$

where

$$\cos\Psi(\theta,\varphi)=1-(27/2)\sin^2 2\phi\cdot\cos^2\theta\cdot\sin^4\theta \tag{26.1}$$

represents the dependence on the constant field direction. Equation (26) has three real roots:

$$x_1=\tfrac{1}{2}\cos(\Psi/3), \tag{27.1}$$

$$x_2=-\tfrac{1}{2}\cos[(\pi-\Psi)/3], \tag{27.2}$$

$$x_3=-\tfrac{1}{2}\cos[(\pi+\Psi)/3]. \tag{27.2}$$

For the case $M=0$, the matrix elements are similar to the case $M=1$ except in sign and a factor 2; therefore we obtain three roots:

$$x_1'=-2x_1, \tag{28.1}$$

$$x_2'=-2x_2, \tag{28.2}$$

$$x_3'=-2x_3, \tag{28.3}$$

in the same way. Concerning the transition $M=\pm 1\rightleftarrows M=0$, only levels with the same suffix can be combined by the selection rule, and we have absorption lines at

$$\eta_i=3x_i \quad (i=1,2,3) \tag{29}$$

with respect to the Larmor frequency. Each of the three lines have the same intensity

$$J_{\text{ortho}}(\pm 1\rightleftarrows 0)=\tfrac{1}{2}. \tag{30}$$

and accordingly we have

$$J_{\text{ortho}}(\text{total})=3. \tag{31}$$

The dependence of the line position on the direction of the constant field in the case of a single crystal is shown in Fig. 7(a).

The solid samples used in the observations had been simply condensed from tank methane and cannot be considered as single crystals. Therefore a polycrystalline average was taken, assuming that every direction of a definite figure axis with respect to the constant field is equally probable. Then the probability with which an absorption line appears in the interval $\eta\sim\eta+d\eta$ is given by

$$W_\eta\Delta\eta=\frac{1}{4\pi}\int\int_{\eta\leqq\eta(\theta,\varphi)\leqq\eta+d\eta}\sin\theta d\theta d\varphi. \tag{32}$$

The results of the calculation, which is given in the Appendix, are shown in Fig. 7(b). Although generally we must take proper account of the mixing ratio of the three kinds of methane, this is proved by Maue[6] to be proportional to the spin weight only, on account of the statistical correlations. Therefore the correct relative weight is given by (25) and (31). After the polycrystalline average is taken, the area under the *ortho*-methane distribution should be normalized to be 3, when that of *meta*-methane (integrated value of δ-function) is normalized to be 5. In Fig. 7 the scale unit is

$$3\gamma^2\hbar^2/2\gamma^3=7.472 \text{ gauss}. \tag{33}$$

Hitherto we considered an aggregate of isolated molecules, but now we must take into account the interactions between molecules. The effect on a proton

of protons in the neighboring molecules is much smaller and less distinct than the effect of those in the same molecule, and we may take it into account as a broadening of each skeleton line, the resulting shape of which is expected to be proportional to

$$\frac{1}{(\langle \Delta H^2 \rangle_r)^{\frac{1}{2}}} \exp\left\{-\frac{(H-H_0)^2}{2\langle \Delta H^2 \rangle_r}\right\}. \tag{34}$$

Here $\langle \Delta H^2 \rangle_r$ is the second moment (in gauss^2) due to all protons except those in the same molecule. Assuming that the close neighbors (which play a dominant role) form a single crystal ($F\bar{4}3m$), this is calculated to be (7.34) gauss^2. Such Gaussian members, which are weighted by the polycrystalline average distribution, were summed to give the entire shape of the resonance. The presence of orthomethane broadens the foot of the Gaussian shape and the final result is shown in Fig. 8 (full line), which is in close agreement with the observed line contour at 1.29°K and 1.42°K.[24] This result is considered to be another independent support of our viewpoint, which was proposed in the previous section and interpreted in this section.

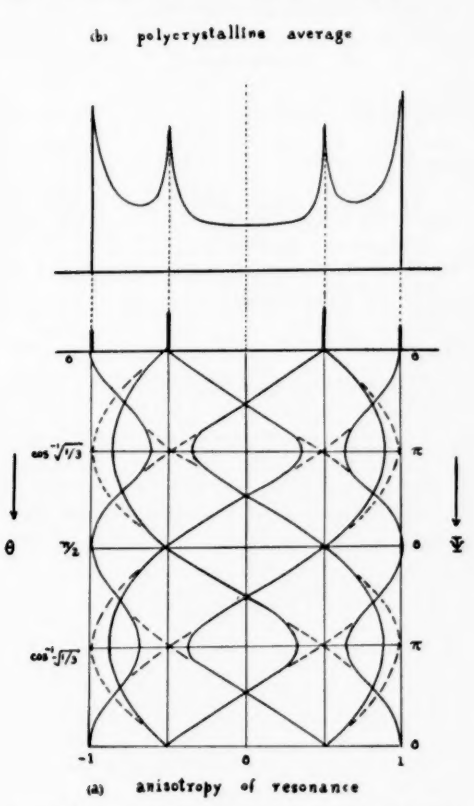

FIG. 7. Anisotropy of the resonance, (a), and the polycrystalline average (b). [Note that the same figure is obtained either when H_0 lies in one of the cubic planes ($\theta=\pi/2$, $\varphi=0$, or $\varphi=\pi/2$) or along one diagonal of the cubic body.]

[24] N. L. Alpert, private communication.

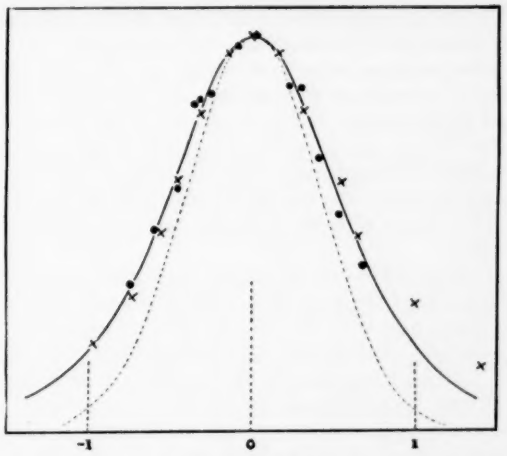

FIG. 8. The absorption line shape below the λ-point (the crosses represent the observed data at 1.29°K and the closed circles represent those observed at 1.42°K, both by Alpert, reference 24). The calculated results are shown by the full line, while the broken line represents the contour when there is only meta-methane. The scale unit equals 7.472 gauss.

IV. DISCUSSION AND CONCLUSION

As the result of the above analysis, we now have the following picture of the dynamical state of the molecules in solid methane.

1. Below the λ-Point (20°K)

(a) Molecules are located parallel to each other, stretching C—H bonds along the cubic body diagonals; or, more precisely, they are definitely confined to the ground state of the rotational oscillation.

(b) However, several states belong to the lowest level group on account of the figure symmetry, and a molecule resonates among them because of its small moment of inertia. This results in the occasional flipping of molecules to neighboring equivalent orientations (about 10^7 times per second on the average), and thus the spin-lattice relaxation time is rather short in this substance even at the lowest temperature.

(c) As the frequency of the flipping which is accompanied by a change in the resultant spin of a molecule is much larger than the Larmor frequency, the consequent local field cannot be detected as line width. Thus the observed width is only 57 percent of that which is expected for fixed molecules.

2. Between the λ-Point (20°K) and the Fusion Point (90°K)

(a) The λ-change in the specific heat at 20°K is associated with a rotational transformation, but the liberated motion is a hindered rotation rather than a free rotation.

(b) In the range between 20°K and 65°K, molecules are considered to rotate in gear with each other, slowly but less forcibly; while, in the range between 65°K and 90°K, molecules are considered to rotate more rapidly and independently, but occasionally collide with each other rather violently. The transition at about 65°K involves only the change in the dominant mechanism of relaxation and not a change in the degrees of freedom, for there is no anomaly in the thermal behavior in this region.

To examine the validity of the above pictures, and to make sure of the generality of the idea which leads us to them, it is most desirable to perform several more systematic experiments on methane. For example: (1) Careful measurements of line width using several different frequencies are necessary, because by such experiments discrimination will be obtained between phenomena depending on the frequency used and those inherent in the nature of the material. (2) Experiments on single crystals are desirable, for, by elaborating the fine structure of the resonance absorption, we may be able to test our model more conclusively. Also the direct determination of the proton lattice is desirable, if the method of neutron diffraction is available. (3) Similar measurements on deuterated methane, especially on CD_4, are needed. This will serve as another method to confirm the assumptions regarding the crystalline field. and will tell us about the electronic structure in the neighborhood of the deuteron.

The author wishes to express sincere gratitude to Professor M. Kotani, who encouraged him and gave valuable comments throughout the course of this investigation, and to Professor T. Nagamiya, Professor H. Takahashi and Mr. H. Narumi, who were interested in this work and gave advice on various points. Also he expresses thanks to Professor N. L. Alpert for his kind communications on the experimental data.

APPENDIX.

Solving for φ in terms of η in a form $\phi=\varphi(\theta,\eta)$, (32) becomes

$$W_\eta=\frac{1}{4\pi}\int_{\text{(allowed region)}}\frac{\partial\varphi(\theta,\eta)}{\partial\eta}d(\cos\theta), \tag{A.1}$$

which is convenient for calculation. Confining ourselves to the case of η_1 and putting

$$\gamma_1=\tfrac{2}{3}\eta_1=\cos(\Psi/3),\quad (\tfrac{1}{2}\leqq\gamma_1\leqq 1), \tag{A.2}$$

$$\Theta(\theta)=\cos^2\theta\sin^4\theta, \tag{A.3}$$

and

$$f_1(\gamma_1)=(2/27)(1+3\gamma_1-4\gamma_1^3)\geqslant 0, \tag{A.4}$$

we obtain

$$\frac{\partial\varphi}{\partial\gamma_1}=\frac{|\partial f_1/\partial\gamma_1|}{4[f_1(\Theta-f_1)]^{\frac{1}{2}}}, \tag{A.5}$$

from which it becomes clear that the integration in (A.1) should be taken over the regions where $\Theta\geq f_1\geq 0$. Changing the variable to

$$\xi=\cos^2\theta, \tag{A.6}$$

and making use of the roots α_1, α_2, α_3 $(\alpha_1\geq\alpha_2\geq\alpha_3)$ of the equation

$$\Theta=f_1, \tag{A.7}$$

(A.1) can be integrated to give

$$\begin{aligned}W_{\gamma_1}&=\frac{1}{4\pi}\frac{|f_1'|}{f_1^{\frac{1}{2}}}\int_{\alpha_3}^{\alpha_2}\frac{d\xi}{[(\alpha_1-\xi)(\alpha_2-\xi)(\xi-\alpha_3)\xi]^{\frac{1}{2}}}\\&=\frac{1}{4\pi}\frac{|f'|}{f_1^{\frac{1}{2}}}\frac{2}{[(\alpha_1-\alpha_4)\alpha_2]^{\frac{1}{2}}}K(k^2),\end{aligned} \tag{A.8}$$

where

$$k^2=[(\alpha_2-\alpha_3)\alpha_1]/[(\alpha_1-\alpha_3)\alpha_2], \tag{A.9}$$

and $K(k^2)$ is a complete elliptic integral. Although we have confined ourselves to the case of $\frac{1}{2}\leqq\gamma_1\leqq 1$, the same formula may be applied also to the entire range of γ. Taking into account the common probability of transition, we finally obtain the results shown in Fig. 7(b).

Superconducting Properties of Cobalt Disilicide

B. T. MATTHIAS AND J. K. HULM*
Bell Telephone Laboratories, Murray Hill, New Jersey
(Received October 3, 1952)

A solid rod of cobalt disilicide was found to have a superconducting transition temperature close to 1.4°K, a critical field gradient of 146 gauss per degree at the transition point, an ice-point resistivity of 16.5 micro-ohm cm and a residual resistivity of about 16 percent of the ice-point value.

INTRODUCTION

IN a recent paper[1] one of us reported the discovery of superconductivity in the Co–Si system, the transition being observed at about 1.39°K in a powdered cobalt-silicon specimen of approximate composition 1 Co+3 Si. Since from x-ray analysis this specimen appeared to consist of a mixture of the compound $CoSi_2$ and free silicon, it was deduced that $CoSi_2$ became superconducting. Against this, however, it was observed that a powder specimen composed solely of $CoSi_2$ remained normal down to 1.27°K, the lowest temperature then available. It was concluded, therefore, that the true transition temperature of $CoSi_2$ lay below 1.27°K, and that superconductivity appeared at 1.39°K in $CoSi_2$+Si owing to a rise in transition temperature caused by strain or some other effect of the free silicon. This hypothesis was later confirmed by measuring the pure $CoSi_2$ powder down to 1.1°K which revealed a superconducting transition at about 1.22°K.

The importance of this result, that a superconductor might be formed by combining a ferromagnetic metal with a nonmetal, made it imperative to check the above conclusions by measuring the various superconducting properties of a homogeneous, *solid* sample of the new material. In this paper we describe recent experiments in which detailed magnetic and electrical data were obtained down to 1.1°K for a solid rod of cobalt disilicide and which confirmed beyond doubt the superconducting behavior of this compound.

EXPERIMENTAL DETAILS

Several rods of about 8 cm in length and 6 mm in diameter were prepared by casting molten $CoSi_2$ in quartz tubes. A dark blue oxide film was removed from the surface of the rods using 280 carborundum paste, exposing a blue-grey surface in which crystal grains of about 0.1- to 1.0-mm edge could readily be observed. In both the magnetic and electrical measurements the specimens were placed in thin-walled Lucite capsules and lowered into a magnetic apparatus of the type described elsewhere,[2] with, however, the following modifications. To permit reliable critical field data to be obtained from the magnetic induction measurements, a detector coil consisting of a 2-cm length, single layer of enamelled 50-gauge wire containing 755 turns was wound directly upon a specimen rod at about a central position. For electrical resistance measurements, current and potential leads were attached to another specimen by forming each lead from eight

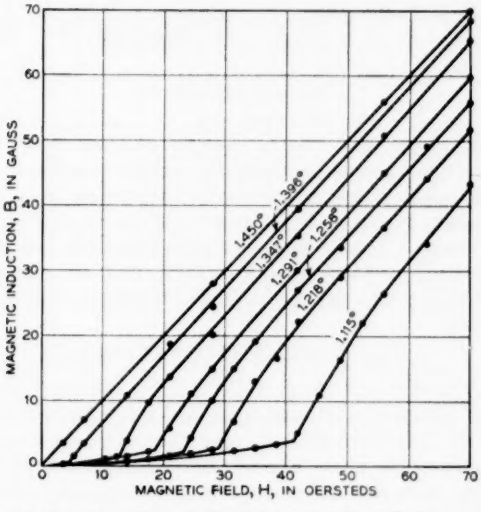

FIG. 1. Variation of magnetic induction with applied magnetic field at various temperatures for a cobalt disilicide rod.

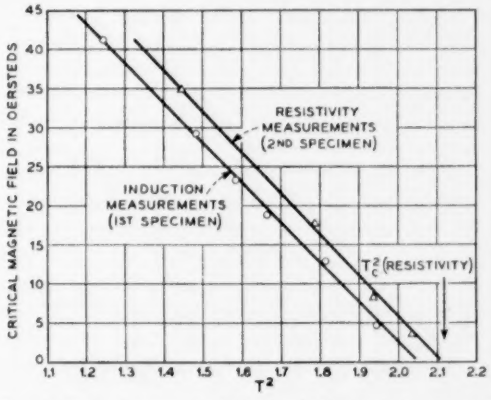

FIG. 2. Plot of magnetic field at which steep rise occurs in magnetic induction (circle points) and electrical resistance (cross points) for a cobalt disilicide rod *versus* T^2.

* On leave of absence from the University of Chicago, Chicago, Illinois.

[1] B. T. Matthias, Phys. Rev. **87**, 380 (1952).

[2] B. T. Matthias and J. K. Hulm, Phys. Rev. **87**, 799 (1952).

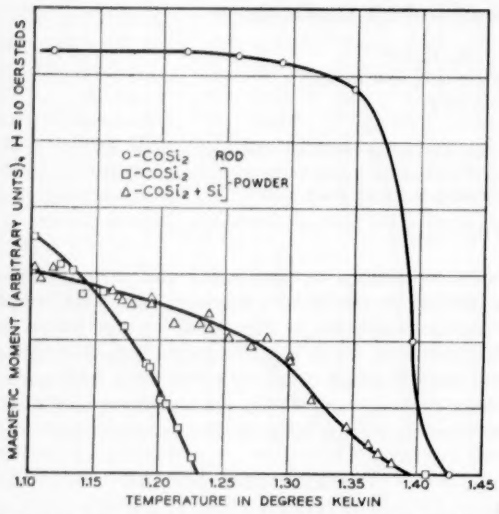

FIG. 3. Temperature variation of magnetic moment for rod and powder samples of $CoSi_2$ and powder sample of $CoSi_2$+Si, ($H = 10$ oersteds).

turns of bare 32-gauge copper wire wound tightly around the specimen and tacked with solder at one point. There was a negligible contact resistance between the specimen and these leads over the whole temperature range of measurement.

RESULTS AND DISCUSSION

(A) Magnetic Measurements

Magnetic induction—magnetic field curves obtained for a typical cobalt disilicide rod at various temperatures are shown in Fig. 1. Despite the slow approach to the complete normal state observed at higher fields, which probably indicates a rather poor Meissner effect, the beginning of the transition is quite well marked at each temperature, and it seems reasonable to identify the field at which a steep rise occurs with the thermodynamic critical field of the material. This is borne out by the fact that the field thus obtained is quite accurately proportional to T^2, as is shown by the circle points in Fig. 2. We therefore write the field equation for the particular sample in the form

$$H_c = 104.5[1-(T)^2/(1.43)^2] \text{ gauss},$$

which result suggests that $CoSi_2$ must be classified as a relatively soft superconductor from a magnetic point of view.

The temperature variation of the magnetic moment of the above rod sample in a field of 10 gauss is compared in Fig. 3 with the corresponding magnetic moment for the powder samples of $CoSi_2$ and $CoSi_2$+Si in which the superconducting studies were first carried out.[1] Since x-ray evidence and the residual resistivity data (next section) suggest that neighboring phases in the cobalt-silicon system are probably less than one percent soluble in $CoSi_2$, it seems that the differences of transition temperature between the $CoSi_2$ rod and the $CoSi_2$ powder of Fig. 3 are more likely to be due to differences of strain rather than differences in composition.[3]

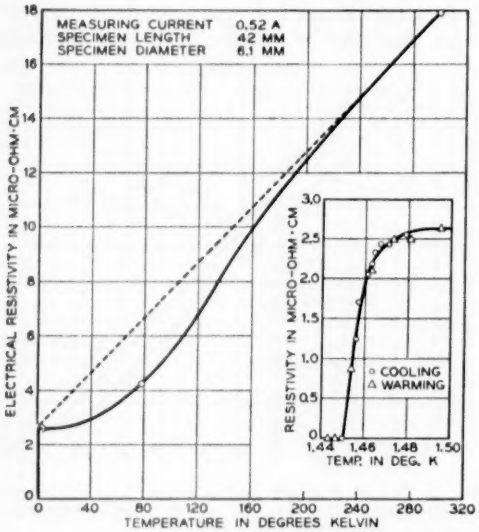

FIG. 4. Temperature variation of electrical resistivity of cobalt disilicide.

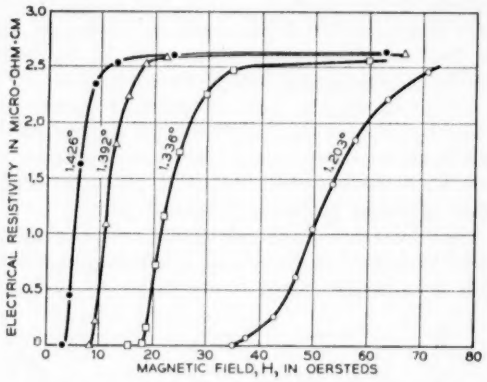

FIG. 5. Isothermal electrical resistance—magnetic field curves for cobalt disilicide.

(B) Electrical Measurements

The electrical resistivity of a $CoSi_2$ rod taken from the same batch of castings as the magnetic specimen of Sec. (A) was measured in zero magnetic field at room temperature, liquid nitrogen temperatures, and in the range from 4.2° down to 1.1°K, with the results shown in Fig. 4. As regards the high temperature resistivity, we may draw attention to the metallic behavior of the

[3] This assumption seems to be confirmed by Dr. S. Geller's observation that x-ray line broadening was observed to a greater extent in the solid rod than in the powdered sample.

sample despite the presence of 67 atomic percent of silicon, the ideal resistivity at the ice-point, about 13.9 micro-ohm cm, being comparable with that of pure metallic elements. The resistivity was constant between 4.2° and 1.5°K at about 16 percent of the ice-point value, which in comparison with corresponding data on solid solution alloys suggests that the deviation from stoichiometric composition was probably less than 1 percent.

The enlarged portion of Fig. 4 indicates that in zero field quite a sharp superconducting transition was observed at 1.455°K. The curves for restoration of resistance by a magnetic field at temperatures below the transition point were also studied and as shown in Fig. 5 were found to be of a rather gradual type. However, a plot of the field at which the first trace of resistance was restored against T^2 (cross points, Fig. 2) gave a straight line parallel to the critical field line obtained from induction measurements. Thus, allowing for the fact that the transition temperature of the electrical resistivity specimen (1.455°) is slightly higher than that of the magnetic specimen (1.432°K), the field at which resistance begins to be restored is probably quite close to the thermodynamic critical field in the present case.

CONCLUSION

Cobalt disilicide crystallizes in the calcium fluoride structure, in which, to our knowledge, no other superconducting compound has previously been found. Although this structure is usually regarded as typical for ionic compounds,[4] the present work indicates a clear exception in the case of $CoSi_2$. It remains to be seen whether similar exceptions are provided by other isomorphous intermetallic compounds such as $NiSi_2$ and $AuAl_2$, but it may be remarked for the present that neither of these compounds showed magnetic evidence of superconductivity down to 1.1°K.

We are grateful to E. Corenzwit for help in cryogenics, to D. H. Wenney and K. M. Olsen for casting the $CoSi_2$ rods, and to S. Geller for performing x-ray analyses.

[4] A. F. Wells, *Structural Inorganic Chemistry* (Clarendon Press, Oxford, 1945), p. 275.

PHYSICAL REVIEW VOLUME 89, NUMBER 2 JANUARY 15, 1953

Variational Principles for Three-Body Scattering Problems*

SIDNEY BOROWITZ, *Department of Physics, College of Engineering, New York University, University Heights, New York 53, New York*

AND

BERNARD FRIEDMAN, *Mathematics Research Group, Washington Square College, New York University, New York 3, New York*

Several stationary expressions for the direct and the exchange scattered amplitudes in three-body collisions are derived.

I. INTRODUCTION

THREE-BODY scattering problems have been solved approximately either by a Born approximation[1] or by variational methods involving a differential operator.[2] We shall discuss here several generalizations for three-body problems of the variational principle proposed by Schwinger[3] for two-body problems.

Important prototypes of three-body scattering problems are those involving the scattering of electrons by hydrogen atoms and the scattering of neutrons by deuterons. In both these cases the indistinguishability of the scattered particle and one of the scatterers creates some special difficulties due to the symmetry conditions imposed on the solution by the Pauli principle. In this paper we shall assume that two of the particles are identical and that exchange effects are consequently important.

In Sec. II of this paper we formulate the problem and indicate how a knowledge of the direct and exchange scattered amplitude enables us to satisfy the Pauli principle without explicitly working with symmetrical or antisymmetrical wave functions. In Sec. III we derive a stationary expression for the direct scattered amplitude, and in Sec. IV we derive a stationary expression for the exchange scattered amplitude.

Finally, we derive in Sec. V still another stationary expression for the scattered amplitudes which is more likely to converge to the correct solution when the trial field is the iterated unperturbed field.

* This work was performed at Washington Square College of Arts and Science, New York University, and was supported by contract with the U. S. Air Force through sponsorship of the Geophysics Research Division, Air Force Cambridge Research Center, Air Research and Development Command.

[1] For a resume of the literature see N. F. Mott and H. S. W. Massey, *Theory of Atomic Collisions* (Clarendon Press, Oxford, 1949), second edition.

[2] W. Kohn, Phys. Rev. **74**, 1793 (1948); S. S. Huang, Phys. Rev. **76**, 477 (1949); H. S. W. Massey and B. L. Moiseiwitsch, Proc. Roy. Soc. (London) **A205**, 483 (1951); M. Verde, Helv. Phys. Acta, **22**, 339 (1949); A. Troesch and M. Verde, Helv. Phys. Acta **24**, 39 (1951).

[3] J. Schwinger, hectographed notes on nuclear physics, Harvard University, unpublished.

II. GENERAL CONSIDERATIONS

In the problem which we treat, particle 1 is incident on a system consisting of particles 2 and 3 bound in their lowest state. The scattering cross section for this process can be found by considering the solution of the following Schrödinger equation with suitable boundary conditions:

$$\{\nabla_1^2+\nabla_2^2+2[E-v(r_1) -v(r_2)-V(r_{12})]\}\Psi_0(\mathbf{r}_1,\mathbf{r}_2)=0. \quad (1)$$

In setting down this equation we have chosen $m_1=m_2=\hbar=1$ and $m_3=\infty$. $\mathbf{r}_1$ and $\mathbf{r}_2$ are the position vectors of particles 1 and 2 with respect to the origin of coordinates, which is the position of particle 3. r_{12} is the distance between particles 1 and 2. E is the total energy of the system and the V's are the potentials between the particles. The results in all but the last section of this paper can be generalized in a useful way to m_3 finite by introducing the following change of variables in the Schrödinger equation,

$$\begin{aligned}\rho&=\mathbf{r}_2-\mathbf{r}_3,\\ R&=\mathbf{r}_1-[(m_2\mathbf{r}_2+m_3\mathbf{r}_3)/(m_2+m_3)],\\ P&=(m_1\mathbf{r}_1+m_2\mathbf{r}_2+m_3\mathbf{r}_3)/(m_1+m_2+m_3),\end{aligned} \quad (2)$$

and eliminating the coordinates of the center of mass.

We can now best specify the appropriate boundary conditions for the solution $\Psi_0(\mathbf{r}_1,\mathbf{r}_2)$ by separating off the incident wave. If we let $\phi_0(\mathbf{r}_2)$ describe the bound state of particles 2 and 3, then we may write

$$\Psi_0(\mathbf{r}_1,\mathbf{r}_2)=\exp(ik_0\mathbf{n}_0\cdot\mathbf{r}_1)\phi_0(\mathbf{r}_2)+\psi(\mathbf{r}_1,\mathbf{r}_2). \quad (3)$$

Here n_0 is the direction and $k_0=(E-\epsilon_0)^{\frac{1}{2}}$ the wave number of the incident particle; ϵ_0 is the binding energy of particles 2 and 3. $\psi(\mathbf{r}_1,\mathbf{r}_2)$, the scattered part of the solution, should be regular everywhere, and should behave either like an outgoing wave or a decreasing exponential as r_1 (or r_2) goes to infinity. A simple means for choosing the correct function $\psi(\mathbf{r}_1,\mathbf{r}_2)$ is to assume that the energy E has a small imaginary part and then to require that $\psi(\mathbf{r}_1,\mathbf{r}_2)$ vanish exponentially as either r_1 and/or r_2 goes to infinity.

The boundary conditions on Ψ_0 are, therefore, that

$$\operatorname*{Lim}_{r_1\to\infty}\Psi_0=\exp(ik_0\mathbf{n}_0\cdot\mathbf{r}_1)\phi_0(\mathbf{r}_2) +\left(\sum_n+\int\right)f_n(\theta,\phi)\frac{\exp(ik_nr_1)}{r_1}\phi_n(\mathbf{r}_2), \quad (4a)$$

$$\operatorname*{Lim}_{r_2\to\infty}\Psi_0=\left(\sum_n+\int\right)g_n(\theta,\phi)\frac{\exp(ik_nr_2)}{r_2}\phi_n(\mathbf{r}_1). \quad (4b)$$

In Eq. (4) $\phi_n(\mathbf{r})$ are the eigenstates, with energy ϵ_n, of the Hamiltonian

$$h=\nabla^2+2[\epsilon-v(r)]. \quad (5)$$

$k_n^2=E-\epsilon_n$, and the symbol $(\sum_n+\int)$ signifies a summation over discrete states and an integration over the continuum states. By analogy with the three-dimensional wave equation, and from physical considerations, it is presumed but has never been proven that Eq. (1) with the boundary conditions (4) specifies a unique solution Ψ_0. The coefficients f_n and g_n for those terms in (4) for which k_n is not imaginary, are called the scattered amplitudes for direct and exchange scattering.

A knowledge of f_n and g_n enables one to determine the effect of the Pauli principle on the cross section.[4] A solution Ψ_0' of (1) which satisfies this principle and the physical boundary conditions can be constructed from $\Psi_0(\mathbf{r}_1,\mathbf{r}_2)$ as follows:

$$\Psi_0'(\mathbf{r}_1,\mathbf{r}_2)=\Psi_0(\mathbf{r}_1,\mathbf{r}_2)\pm\Psi_0(\mathbf{r}_2,\mathbf{r}_1), \quad (6)$$

where the plus sign is taken for the antisymmetric spin state and the minus sign for the symmetric spin state. The scattering cross section for an unpolarized incident beam is given by

$$\sigma_n=\frac{k_n}{k_0}(w_a|f_n+g_n|^2+w_s|f_n-g_n|^2), \quad (7)$$

where w_a and w_s are statistical weight factors for the antisymmetric and symmetric spin states, respectively.

III. DIRECT SCATTERING

The first step in formulating a Schwinger variational principle is to replace Eq. (1) by an integral equation which includes the boundary conditions. For the case of direct scattering we consider

$$\zeta(\mathbf{r}_1,\mathbf{r}_2)=2[v(r_1)+V(r_{12})] \quad (8)$$

as a perturbation and introduce the Green's function for the operator

$$H_0=\nabla_1^2+\nabla_2^2+2[E-v(r_2)]; \quad (9)$$

this Green's function satisfies the equation

$$H_0G=-\delta(\mathbf{r}_1-\mathbf{r}_1')\delta(\mathbf{r}_2-\mathbf{r}_2'). \quad (10)$$

A convenient representation of G is

$$G(\mathbf{r}_1,\mathbf{r}_2;\mathbf{r}_1',\mathbf{r}_2') =\left(\sum_n+\int\right)\phi_n(\mathbf{r}_2)\phi_n^*(\mathbf{r}_2')\frac{\exp(ik_n|\mathbf{r}_1-\mathbf{r}_1'|)}{4\pi|\mathbf{r}_1-\mathbf{r}_1'|}. \quad (11)$$

In terms of G the solution ψ_0 of Eq. (1) can be written as

$$\Psi_0=\Phi_0(\mathbf{r}_1,\mathbf{r}_2)-\int G(\mathbf{r}_1,\mathbf{r}_2;\mathbf{r}_1',\mathbf{r}_2') \times\zeta(\mathbf{r}_1',\mathbf{r}_2')\Psi_0(\mathbf{r}_1',\mathbf{r}_2')d\mathbf{r}_1'd\mathbf{r}_2'. \quad (12)$$

In Eq. (12)

$$\Phi_0(\mathbf{r}_1,\mathbf{r}_2)=\exp(ik_0\mathbf{n}_0\cdot\mathbf{r}_1)\phi_0(\mathbf{r}_2). \quad (13)$$

The scattered amplitude f_n can be found by taking the limit of the right-hand side of (12) as $r_1\to\infty$; this gives

[4] Reference 1, Chap. VIII.

the following result:

$$f_n=-\frac{1}{4\pi}\int \exp(-ik_n\mathbf{n}\cdot\mathbf{r}_1)\phi_n^*(\mathbf{r}_2) \times\zeta(\mathbf{r}_1,\mathbf{r}_2)\Psi_0(\mathbf{r}_1,\mathbf{r}_2)d\mathbf{r}_1d\mathbf{r}_2. \quad (14)$$

The Born approximation consists of replacing Ψ_0 in (14) by the unperturbed wave Φ_0.

Starting with an integral equation it is a simple matter to write down a Schwinger variational principle. The usual algebraic complexities are simplified by first expressing this principle in operator form.

If K is a self-adjoint operator and if in the domain of K, x and y are vectors which satisfy the equations

$$Kx=a, \quad (15a)$$

$$Ky=b, \quad (15b)$$

where a and b are vectors, then the expression

$$(y, Kx)/(b, x)(y, a)=1/(b, x) \quad (16)$$

is stationary[5] with respect to arbitrary variations of x and y. The symbol (α, β) in Eq. (16) represents the inner products $\int\alpha^*\beta d\mathbf{r}$. The reciprocity condition is given by

$$(b, x)=(y, a), \quad (17)$$

and is a consequece of the fact that K is self-adjoint.

Our integral Eq. (12) corresponds to (15a), if we replace the abstract quantities in the latter according to the scheme

$$K\rightarrow\int d\mathbf{r}_1'd\mathbf{r}_2'[\delta(\mathbf{r}_1-\mathbf{r}_1')\delta(\mathbf{r}_2-\mathbf{r}_2')\zeta(\mathbf{r}_1',\mathbf{r}_2') +\zeta(\mathbf{r}_1,\mathbf{r}_2)G(\mathbf{r}_1\mathbf{r}_2;\mathbf{r}_1'\mathbf{r}_2')\zeta(\mathbf{r}_1',\mathbf{r}_2')],$$
$$x\rightarrow\Psi_0(\mathbf{r}_1',\mathbf{r}_2'), \quad (18)$$
$$a\rightarrow\zeta(\mathbf{r}_1,\mathbf{r}_2)\Psi_0(\mathbf{r}_1,\mathbf{r}_2).$$

For the equation corresponding to (15b) we choose

$$\Psi_n(\mathbf{r}_1,\mathbf{r}_2)=\Phi_n(\mathbf{r}_1\mathbf{r}_2)-\int G(\mathbf{r}_1,\mathbf{r}_2;\mathbf{r}_1',\mathbf{r}_2') \times\zeta(\mathbf{r}_1',\mathbf{r}_2')\Psi_n(\mathbf{r}_1',\mathbf{r}_2')d\mathbf{r}_1'd\mathbf{r}_2'), \quad (19)$$

with

$$\Phi_n=\exp(ik_n\mathbf{n}\cdot\mathbf{r}_1)\phi_n(\mathbf{r}_2). \quad (20)$$

Thus,

$$y\rightarrow\Psi_n(\mathbf{r}_1',\mathbf{r}_2'),$$
$$b\rightarrow\zeta(\mathbf{r}_1,\mathbf{r}_2)\Phi_n(\mathbf{r}_1,\mathbf{r}_2). \quad (21)$$

With the substitutions (18) and (21), Eq. (16) gives us a stationary expression for $-1/4\pi f_n$.

IV. EXCHANGE SCATTERING

In order to obtain the exchange scattered amplitude we consider

$$\eta(\mathbf{r}_1,\mathbf{r}_2)=2[v(r_2)+V(r_{12})] \quad (22)$$

as a perturbation and introduce the Green's function for the operator

$$H_0'=\nabla_1^2+\nabla_2^2+2[E-v(r_1)]; \quad (23)$$

this Green's function satisfies the equation

$$H_0'\mathcal{G}=-\delta(\mathbf{r}_1-\mathbf{r}_1')\delta(\mathbf{r}_2-\mathbf{r}_2'). \quad (24)$$

A convenient representation of $\mathcal{G}$ is

$$\mathcal{G}(\mathbf{r}_1,\mathbf{r}_2;\mathbf{r}_1',\mathbf{r}_2') =+\left(\sum_n+\int\right)\phi_n(\mathbf{r}_1)\phi_n^*(\mathbf{r}_1')\exp\frac{ik_n|\mathbf{r}_2-\mathbf{r}_2'|}{4\pi|\mathbf{r}_2-\mathbf{r}_2'|}. \quad (25)$$

The complication in this formulation is that the incident wave does not satisfy the equation

$$H_0'\Phi_0=0. \quad (26)$$

It is now most convenient to use the decomposition given by Eq. (3) to obtain the following integral equation for the scattered wave:

$$\psi(\mathbf{r}_1,\mathbf{r}_2) =-\int\mathcal{G}(\mathbf{r}_1\mathbf{r}_2;\mathbf{r}_1',\mathbf{r}_2')\eta(\mathbf{r}_1',\mathbf{r}_2')\psi(\mathbf{r}_1',\mathbf{r}_2')d\mathbf{r}_1'd\mathbf{r}_2' -\int\mathcal{G}(\mathbf{r}_1,\mathbf{r}_2;\mathbf{r}_1',\mathbf{r}_2')\zeta(\mathbf{r}_1',\mathbf{r}_2')\Phi_0(\mathbf{r}_1',\mathbf{r}_2')d\mathbf{r}_1'd\mathbf{r}_2'. \quad (27)$$

The exchange scattered amplitude is found by taking the limit of the right-hand side of (27) as $r_2\rightarrow\infty$; this gives the following result:

$$g_n=g_n'+b,$$

where

$$g_n'=-\frac{1}{4\pi}\int\exp(-ik_n\mathbf{n}\cdot\mathbf{r}_2')\phi_n(\mathbf{r}_1')\eta(\mathbf{r}_1',\mathbf{r}_2') \times\psi(\mathbf{r}_1',\mathbf{r}_2')d\mathbf{r}_1'd\mathbf{r}_2'=-\frac{1}{4\pi}\int\Phi_n(\mathbf{r}_2',\mathbf{r}_1') \times\eta(\mathbf{r}_1',\mathbf{r}_2')\psi(\mathbf{r}_1',\mathbf{r}_2')d\mathbf{r}_1'd\mathbf{r}_2',$$

$$b=-\frac{1}{4\pi}\int\exp(-ik_n\mathbf{n}\cdot\mathbf{r}_2')\phi_n(\mathbf{r}_1')\zeta(\mathbf{r}_1',\mathbf{r}_2') \times\exp(ik_0\mathbf{n}_0\cdot\mathbf{r}_1')\phi_0(\mathbf{r}_2')d\mathbf{r}_1'd\mathbf{r}_2')=-\frac{1}{4\pi}\int\Phi_n(\mathbf{r}_2',\mathbf{r}_1') \times(\mathbf{r}_1',\mathbf{r}_2')\Phi_0(\mathbf{r}_1',\mathbf{r}_2')d\mathbf{r}_1'd\mathbf{r}_2'.$$

The Born approximation involves setting $\psi\equiv0$ in (29) and thus gives $g_n=b$.

Our result for g_n in the Born approximation does not agree with that given by Mott and Massey,[6] namely,

$$-\frac{1}{4\pi}\int\Phi_n(\mathbf{r}_2',\mathbf{r}_1')\eta(\mathbf{r}_1',\mathbf{r}_2')\Phi_0(\mathbf{r}_1',\mathbf{r}_2')d\mathbf{r}_1'd\mathbf{r}_2'.$$

[5] N. Marcuvitz—Sec. III D, *Recent Developments in the Theory of Wave Propagation*, New York University, Institute for Mathematics and Mechanics (1949).

[6] Reference 1, Chap. VIII.

The two results are equivalent[7] when ϕ_n corresponds to a bound state, since their difference,

$$\int \Phi_n^*(\mathbf{r}_2', \mathbf{r}_1')[v(r_1')-v(r_2')]\Phi_0(\mathbf{r}_1', \mathbf{r}_2')d\mathbf{r}_1'd\mathbf{r}_2',$$

can be shown to be equal to zero as follows: Since $H_0'\Phi_n^*(\mathbf{r}_2, \mathbf{r}_1)=0$, replace $v(r_1')\Phi_n^*(\mathbf{r}_2', \mathbf{r}_1')$ by $\frac{1}{2}\{\nabla_1^2+\nabla_2^2+2E\}\Phi_n(\mathbf{r}_1', \mathbf{r}_2')$. Similarly replace $v(r_2')\Phi_0(\mathbf{r}_1', \mathbf{r}_2')$ by $\frac{1}{2}\{\nabla_1^2+\nabla_2^2+2E\}\Phi_0(\mathbf{r}_1', \mathbf{r}_2')$ Then integrate by parts.

However, when ϕ_n is in the continuum, the result of Mott and Massey in the Born approximation diverges, whereas Eq. (29) does not. The procedure that Mott and Massey use is open to question since they expand the entire solution including the incident wave in terms of the orthonormal set $\phi_n(\mathbf{r}_1)$. This procedure is not valid, as is shown in the Appendix.

We now proceed as in Sec. III to formulate a stationary expression for g_n'. Equation (27) corresponds to (15a) with

$$\begin{aligned} K\rightarrow & \int d\mathbf{r}'_1 d\mathbf{r}'_2[\delta(\mathbf{r}_1-\mathbf{r}_1')\delta(\mathbf{r}_2-\mathbf{r}_2')\eta(\mathbf{r}_1', \mathbf{r}_2') \\ & +\eta(\mathbf{r}_1, \mathbf{r}_2)\mathcal{G}(\mathbf{r}_1, \mathbf{r}_2; \mathbf{r}_1', \mathbf{r}_2')\eta(\mathbf{r}_1', \mathbf{r}_2')], \\ x\rightarrow & \psi, \\ a\rightarrow & -\eta(\mathbf{r}_1, \mathbf{r}_2) \\ & \times\int \mathcal{G}(\mathbf{r}_1, \mathbf{r}_2; \mathbf{r}_1', \mathbf{r}_2')\zeta(\mathbf{r}_1', \mathbf{r}_2')\Phi_0(\mathbf{r}_1', \mathbf{r}_2')d\mathbf{r}_1'd\mathbf{r}_2'. \end{aligned} \tag{30}$$

For the equation corresponding to (15b) we choose

$$\chi_n(\mathbf{r}_1, \mathbf{r}_2)=\Phi_n(\mathbf{r}_2, \mathbf{r}_1)-\int \mathcal{G}(\mathbf{r}_1, \mathbf{r}_2; \mathbf{r}_1', \mathbf{r}_2') \times\eta(\mathbf{r}_1', \mathbf{r}_2')\chi_n(\mathbf{r}_1', \mathbf{r}_2')d\mathbf{r}_1'd\mathbf{r}_2'. \tag{31}$$

Thus

$$\begin{aligned} y\rightarrow & \chi_n(\mathbf{r}_1', \mathbf{r}_2') \\ b\rightarrow & \Phi_n(\mathbf{r}_2, \mathbf{r}_1)\eta(\mathbf{r}_1, \mathbf{r}_2). \end{aligned} \tag{32}$$

With the substitutions (30) and (32), Eq. (16) gives us a stationary expression for $-1/4\pi g_n'$. A similar variational expression could be derived for $-1/4\pi f_n$.

V. OTHER FORMULATIONS

While the expressions corresponding to Eq. (16) with the replacements discussed in Secs. III and IV are stationary, their utility frequently depends to a large extent on whether or not one can use the unperturbed field as a trial function. There is some question as to whether the expressions derived in Secs. III and IV converge upon successive iterations of the unperturbed field. This applies especially to the case of exchange scattering.[8] In order to avoid this difficulty it might be useful to formulate additional stationary expressions for the scattered amplitude such that the use of the unperturbed field in their evaluation would be the first step in a converging process.

To do this we consider $2V(r_{12})$ of Eq. (1) as a perturbation. This step restricts the usefulness of the procedure to the situation in which one of the particles of the system has an infinite mass. Otherwise the unperturbed problem would be a true three-body problem and the Green's function for the unperturbed operator would in general be unobtainable.

Following the procedure of Sec. IV we introduce the Green's function corresponding to the operator

$$H_0''=\nabla_1^2+\nabla_2^2+2[E-v(\mathbf{r}_1)-v(\mathbf{r}_2)]; \tag{33}$$

this function is given by

$$\Gamma(\mathbf{r}_1, \mathbf{r}_2; \mathbf{r}_1', \mathbf{r}_2')$$

$$=\left(\sum_n+\int\right)\phi_n(\mathbf{r}_1)\phi_n^*(\mathbf{r}_1')\gamma_n(\mathbf{r}_2, \mathbf{r}_2') \tag{34a}$$

$$=\left(\sum_n+\int\right)\phi_n(\mathbf{r}_2)\phi_n^*(\mathbf{r}_2')\gamma_n(\mathbf{r}_1, \mathbf{r}_1'). \tag{34b}$$

In Eqs. (34a) and (34b) $\gamma_n(\mathbf{r}, \mathbf{r}')$ is the Green's function for the operator

$$h_n=\nabla^2+2[E-\epsilon_n-v(\mathbf{r})]. \tag{35}$$

We shall use Eq. (34a) to investigate the asymptotic behavior of the solution when $r_2\rightarrow\infty$: when $r_1\rightarrow\infty$ we shall use (34b).

The solution of Eq. (1) satisfying the boundary conditions is

$$\Psi_0=\phi_i(\mathbf{r}_1)\phi_0(\mathbf{r}_2)-2\int \Gamma(\mathbf{r}_1, \mathbf{r}_2; \mathbf{r}_1', \mathbf{r}_2')V(r_{12}') \times\Psi_0(\mathbf{r}_1', \mathbf{r}_2')d\mathbf{r}_1'd\mathbf{r}_2'. \tag{36}$$

In Eq. (36), $\phi_i(\mathbf{r}_1)$ is a solution of the equation $h_0\phi_i(\mathbf{r})=0$ which at infinity describes an incoming wave approaching the origin along the direction $\mathbf{n}_0$.

The scattered amplitudes can be found from the asymptotic forms of the Green's function[9]:

$$\operatorname*{Lim}_{r_2\rightarrow\infty}\Gamma(\mathbf{r}_1, \mathbf{r}_2; \mathbf{r}_1', \mathbf{r}_2')=-\left(\sum_n+\int\right)\phi_n(\mathbf{r}_1)\phi_n^*(\mathbf{r}_1') \times\frac{\exp(ik_nr_2)}{4\pi r_2}F_n(\mathbf{r}_2', \pi-\Theta) \tag{37a}$$

$$\operatorname*{Lim}_{r_1\rightarrow\infty}\Gamma(\mathbf{r}_1, \mathbf{r}_2; \mathbf{r}_1', \mathbf{r}_2')=-\left(\sum_n+\int\right)\phi_n(\mathbf{r}_2)\phi_n^*(\mathbf{r}_2') \times\frac{\exp(ik_nr_1)}{4\pi r_1}F_n(\mathbf{r}_1', \pi-\Phi). \tag{37b}$$

In Eqs. (37), F_n is a solution of the equation

$$h_nF_n=0, \tag{38}$$

[7] We are indebted to Major G. W. Griffing for this remark.
[8] W. Kohn, private communication.
[9] Reference 1, Chap. IV. It should be remarked that Eqs. (27) hold only for a $v(r)$ which goes to zero faster than $1/r$. For the Coulomb field one obtains a logarithmic phase factor in the exponential in the usual way.

which at infinity represents a wave approaching the origin at an angle of $\pi-\Theta$ (or $\pi-\Phi$) with the z axis; $\Theta(\Phi)$ is the angle between $\mathbf{r}_2$ and $\mathbf{r}_2'(\mathbf{r}_1$ and $\mathbf{r}_1')$.

From Eq. (37a) and (37b) one can immediately write down the amplitudes for direct and exchange scattering:

$$\alpha_n=-\frac{1}{2\pi}\int\phi_n^*(\mathbf{r}_2')F_n(\mathbf{r}_1',\pi-\Phi)V(r_{12}') \times\Phi_0(\mathbf{r}_1',\mathbf{r}_2')d\mathbf{r}_1'd\mathbf{r}_2', \quad (39)$$

and

$$\beta_n=-\frac{1}{2\pi}\int\phi_n^*(\mathbf{r}_1')F_n(\mathbf{r}_2',\pi-\Theta)V(r_{12}') \times\Phi_0(\mathbf{r}_1',\mathbf{r}_2')d\mathbf{r}_1'd\mathbf{r}_2'. \quad (40)$$

Equations (39) and (40) give correctly the inelastically scattered amplitudes as well as the elastically scattered exchange amplitude. To determine the direct elastically scattered amplitude f_0 it is necessary to add to α_0 the coefficient of the outgoing spherical wave contained in $\phi_i(\mathbf{r})$ as $r\to\infty$.

In formulating the stationary expression we shall again require, as in Secs. III and IV a solution of Eq. (1) satisfying different boundary conditions. The solution whose inhomogeneous term is $F_n^*(\mathbf{r}_1',\pi-\Phi)\phi_n(\mathbf{r}_2)$ will be designated by $\Psi_n(\mathbf{r}_1,\mathbf{r}_2)$, and the solution whose inhomogeneous term is $F_n^*(\mathbf{r}_2,\pi-\Theta)\phi_n(\mathbf{r}_1)$ will be designated by $\lambda_n(\mathbf{r}_1,\mathbf{r}_2)$.

A stationary expression for $-1/4\pi\alpha_n$ can be found using Eq. (16) with the following replacements:

$$K\to\int d\mathbf{r}_1'd\mathbf{r}_2'[\delta(\mathbf{r}_1-\mathbf{r}_1')\delta(\mathbf{r}_2-\mathbf{r}_2')2V(r_{12}) +4V(r_{12})\Gamma(\mathbf{r}_1,\mathbf{r}_2;\mathbf{r}_1',\mathbf{r}_2')V(r_{12}')], \quad x\to\Psi_0,\quad y\to\Psi_n, \quad (41)$$

$$a\to\phi_i(\mathbf{r}_1)\phi_0(\mathbf{r}_2),\quad b\to F_n^*(\mathbf{r}_1,\pi-\Phi)\phi_n(\mathbf{r}_2).$$

Similarly one can find the stationary expression for $-1/4\pi\beta_n$ as follows:

$$K\to\int d\mathbf{r}_1'd\mathbf{r}_2'[\delta(\mathbf{r}_1-\mathbf{r}_2')\delta(\mathbf{r}_2-\mathbf{r}_2')2V(r_{12}) +4V(r_{12})\Gamma(\mathbf{r}_1,\mathbf{r}_2;\mathbf{r}_1',\mathbf{r}_2')V(r_{12}')], \quad x\to\Psi_0,\quad y\to\lambda_n \quad (42)$$

$$a\to\phi_i(\mathbf{r}_1)\phi_0(\mathbf{r}_2),\quad b\to F_n^*(\mathbf{r}_2,\pi-\Phi)\phi_n(\mathbf{r}_1).$$

APPENDIX

We shall show that when a plane wave $\exp(ik_0r\cos\theta)$ is expanded in terms of a complete set of eigenfunctions of the Hamiltonian the expansion coefficients must contain singularities such as δ functions. If we assume that the Hamiltonian is spherically symmetric, it will be sufficient to consider the expansion of $\sin(k_0r)$ in terms of the eigenfunctions of the ordinary differential operator

$$-d^2/dr^2+V(r). \quad (A.1)$$

Let $u_n(r)$ be the discrete eigenfunctions and $\phi(r,k)$ be the continuum eigenfunctions of (A.1); that is

$$[d^2/dr^2+k^2-V(r)]\phi(r,k)=0.$$

We have the asymptotic formula $\phi(r,k)\sim\sin(kr+\eta)$, where η is the phase shift. Put

$$\phi(r,k)=\sin(kr+\eta)+w(r,k).$$

Then $w(r,k)$ will approach zero as r becomes infinite.

From the well-known relation,

$$\sum_n u_n(r)u_n(r')+\frac{2}{\pi}\int_0^\infty\phi(r,k)\phi(r',k)dk=\delta(r-r'),$$

we get the expansion

$$\sin k_0r=\sum_n u_n(r)\int_0^\infty\sin k_0r'u_n(r')dr' +\frac{2}{\pi}\int_0^\infty\phi(r,k)dk\int_0^\infty\phi(r',k)\sin k_0r'dr'.$$

Now the expansion coefficient in the continuum spectrum is

$$\frac{2}{\pi}\int_0^\infty\sin(k_0r')\phi(r',k)dr'=\frac{2}{\pi}\int_0^\infty\sin(k_0r')\sin(kr'+\eta)dr' +\frac{2}{\pi}\int_0^\infty\sin(k_0r')w(r',k)dr'.$$

The second term is a well-behaved function of k, but for the first term we have

$$\frac{2}{\pi}\int_0^\infty\sin(k_0r')\sin(kr'+\eta)dr' =k\cos\eta\frac{[\delta(k-k_0)+\delta(k+k_0)]}{k}-\frac{2}{\pi}\sin\eta\frac{k}{k^2-k_0^2} =\cos\eta\delta(E-E_0)-\frac{1}{\pi}\frac{\sin\eta}{E-E_0}, \quad (A.2)$$

if we put $k^2=E$, $k_0^2=E_0$. This coefficient is singular.

Conversion of an Amplified Dirac Equation to an Approximately Relativistic Form*

W. A. BARKER† AND Z. V. CHRAPLYVY
Physics Department, St. Louis University, St. Louis, Missouri
(Received September 3, 1952)

A fermion is described by a one-body relativistic wave equation of the Dirac type in which scalar, vector, tensor, pseudovector, and pseudoscalar interactions are included phenomenologically. This equation is converted to an approximately relativistic form by means of the Foldy-Wouthuysen transformation. The resulting relativistic correction terms associated with the five types of interaction are tabulated. The tables may be used to convert any one-body Dirac equation to its corresponding approximately relativistic form. The fine structure of the hydrogenic atom including the Lamb-Retherford shift is discussed as an illustration.

I. INTRODUCTION

A FERMION of mass m interacting with an external field may be described by a four-component wave function ψ satisfying the equation

$$\{\gamma_\mu(p_\mu+g_1\theta_\mu)-i(mc+g\theta) -(1/2!)g_{II}\gamma_\mu\gamma_\nu\theta_{\mu\nu}-(1/3!)g_{III}\gamma_\mu\gamma_\nu\gamma_\rho\theta_{\mu\nu\rho} -(i/4!)g^P\gamma_\mu\gamma_\nu\gamma_\rho\gamma_\sigma\theta_{\mu\nu\rho\sigma}\}\psi=0, \quad (1)$$

where $p_\mu=(-i\hbar\nabla, -i\hbar\partial/\partial x_4)$, $x_4=ict$, $\gamma_\mu=(-i\beta\boldsymbol{\alpha}, \beta)$; β and $\boldsymbol{\alpha}$ are the familiar Dirac matrices; c, $\hbar$ are the velocity of light and Planck's constant divided by 2π. The usual summation convention applies in expressions involving repeated Greek indices with the restriction that no two of the subscripts are equal in the same term. The external field is characterized by a scalar θ, a vector θ_μ, an antisymmetric tensor $\theta_{\mu\nu}$, a pseudovector $\theta_{\mu\nu\rho}$, and a pseudoscalar $\theta_{\mu\nu\rho\sigma}=\theta^P$, which have been added to the free particle Dirac equation in such a way as to satisfy the invariance requirements of special relativity under a Lorentz transformation. The strength of the interaction is determined by the coupling constants g, g_I, g_{II}, g_{III}, and g^P.

We do not identify the interaction terms with any particular type of external field nor the coupling constants with any specific coupling mechanism. For example, θ_μ may be identified with the electromagnetic potentials, the field strengths in scalar meson theory, or any other type of external field as long as it transforms like a four vector.

We propose to convert Eq. (1) into an approximately relativistic form, more amenable to physical interpretation and practical calculation, by a method recently developed by Foldy and Wouthuysen.[1] This technique has two advantages not shared by the method previously used to study this amplified Dirac equation[2]—the traditional method of eliminating the small components in terms of the large. First, the transformed Hamiltonian is Hermitian. Second, the transformed four-component wave function may be split into two sets of two-component wave functions which describe positive and negative energy states, respectively. The calculations are carried out to the second order in the expansion parameter, $(\hbar/mc)(\partial/\partial x_\mu)$.

By way of illustration, the results are applied to a study of the fine structure of the hydrogenic atom including the Lamb-Retherford shift.

II. REDUCTION OF THE AMPLIFIED DIRAC EQUATION TO AN APPROXIMATELY RELATIVISTIC FORM

In order to apply the Foldy-Wouthuysen method, it is necessary to write Eq. (1) in the form

$$H\psi=(\beta mc^2+\mathcal{O}+\mathcal{E})\psi=i\hbar\partial\psi/\partial t, \quad (2)$$

where the odd operators $\mathcal{O}$ and the even operators $\mathcal{E}$ are explicitly separated.[3] This may be readily done with the aid of the relations $\boldsymbol{\sigma}=(1/2i)(\boldsymbol{\alpha}\times\boldsymbol{\alpha})$, $\gamma_5=i\alpha_1\alpha_2\alpha_3$, and the following change of notation: $\theta_\mu\rightarrow(\boldsymbol{\theta}, \theta_4)$, $\theta_{\mu\nu}\rightarrow(\mathbf{M}, \mathbf{P})$, $\theta_{\mu\nu\rho}\rightarrow(\mathbf{S}, S_4)$. The result is

$$H\psi=\{\beta mc^2+cg\beta\theta+icg_1\theta_4+cg_{II}\beta\boldsymbol{\sigma}\cdot\mathbf{M}+cg_{III}\boldsymbol{\sigma}\cdot\mathbf{S} +c\boldsymbol{\alpha}\cdot(\mathbf{p}+g_1\boldsymbol{\theta})-cg_{II}\beta\boldsymbol{\alpha}\cdot\mathbf{P}-icg_{III}\gamma_5S_4 +cg^P\beta\gamma_5\theta^P\}\psi=i\hbar\partial\psi/\partial t. \quad (3)$$

The terms involving the matrices I, β, $\boldsymbol{\sigma}$, and $\beta\boldsymbol{\sigma}$ are even, those involving $\boldsymbol{\alpha}$, $\beta\boldsymbol{\alpha}$, γ_5, and $\beta\gamma_5$ are odd. The transformed wave equation generated by the Hermitian operator $S=-(i/2mc^2)\beta\mathcal{O}$ is of the form[4]

$$H'\psi'=\left\{\beta mc^2+\mathcal{E}+\frac{\beta}{2mc^2}\mathcal{O}^2 -\frac{1}{8m^2c^4}\left[\mathcal{O},[\mathcal{O},\mathcal{E}]_-+i\hbar\frac{\partial\mathcal{O}}{\partial t}\right]_-+\cdots\right\}\psi' =i\hbar\partial\psi'/\partial t. \quad (4)$$

Carrying this prescription out explicitly for Eq. (3) requires the evaluation of a large number of commutators and anticommutators. The calculations are facilitated by the use of the following identities of which the first two are well known and the last two

* This work was done under ONR auspices.
† Based on a thesis submitted to St. Louis University in partial fulfillment of the requirements for the degree of Doctor of Philosophy.
[1] L. L. Foldy and S. A. Wouthuysen, Phys. Rev. **78**, 29 (1950).
[2] G. Petiau, J. phys. et radium **10**, 264 (1949).
[3] An odd operator couples the upper and lower components of ψ; an even operator does not. See reference 1, p. 30, footnote 3.
[4] See reference 1, Eq. (32).

are easily verified.

$$[(\boldsymbol{\alpha}\cdot\mathbf{B}),(\boldsymbol{\alpha}\cdot\mathbf{C})]_{\mp}=\mathbf{B}\cdot\mathbf{C}+i\boldsymbol{\sigma}\cdot\mathbf{B}\times\mathbf{C}\mp\mathbf{C}\cdot\mathbf{B}\mp i\boldsymbol{\sigma}\cdot\mathbf{C}\times\mathbf{B}, \quad (5)$$

$$(\boldsymbol{\sigma}\cdot\mathbf{B})(\boldsymbol{\sigma}\cdot\mathbf{C})=\mathbf{B}\cdot\mathbf{C}+i\boldsymbol{\sigma}\cdot\mathbf{B}\times\mathbf{C}, \quad (6)$$

$$[(\boldsymbol{\alpha}\cdot\mathbf{B}),(\boldsymbol{\sigma}\cdot\mathbf{C})]_{\mp}=-\gamma_5\mathbf{B}\cdot\mathbf{C}+i\boldsymbol{\alpha}\cdot\mathbf{B}\times\mathbf{C}\pm\gamma_5\mathbf{C}\cdot\mathbf{B}\mp i\boldsymbol{\alpha}\cdot\mathbf{C}\times\mathbf{B}, \quad (7)$$

$$[(\boldsymbol{\alpha}\cdot\mathbf{B}),(\gamma_5 C)]_{\mp}=\mp(\boldsymbol{\sigma}\cdot\mathbf{B})C\pm C(\boldsymbol{\sigma}\cdot\mathbf{B}). \quad (8)$$

It is assumed that $\mathbf{B}$, $\mathbf{C}$, and C commute with the Dirac matrices but not necessarily with one another.

The five types of interaction generate relativistic correction terms of zero, first, and second order in the expansion parameter. These we have placed into six classifications, of which three involve $\boldsymbol{\sigma}$ and three do not.

A "Schrödinger term" is one which has the appearance of one or more of the terms in the ordinary Schrödinger equation, $(p^2/2m+V)\psi=E\psi$.

A "divergence term" is one which is similar to the term used by Foldy and Wouthuysen[1] to account for the "Darwin correction," to the S levels in a hydrogen atom, $-(e\hbar^2/8m^2c^4)\nabla\cdot\mathbf{E}$.

A "Darwin term" is one which is analogous to the term originally used by Darwin[5] to account for the "Darwin correction," $-(e\hbar^2/4m^2c^4)\mathbf{E}\cdot\nabla$.

A "spin-field term" is one which resembles the well-known term involving the normal magnetic moment of the electron, $(\beta e\hbar/2mc)\boldsymbol{\sigma}\cdot\mathbf{H}$.

A "spin-orbit term" is one which is similar to the well-known Thomas term,[6] $-(e\hbar/4m^2c^4)\boldsymbol{\sigma}\cdot(\mathbf{E}\times\mathbf{p})$.

Finally, a "spin-momentum term" is one which involves the dot product of $\boldsymbol{\sigma}$ and the linear momentum $\mathbf{p}$.

The results are presented in tabular form. In Table I are entered all those correction terms which do not involve mixed products between different types of interaction. In Table II are entered correction terms which do involve mixed products. It must always be considered along with Table I when a study is made of the correction terms arising from two or more types of interaction present in the original relativistic equation, say the vector and the tensor. The coupling constants have been suppressed in the tables, since how they should be reinserted is quite evident when a given term is to be used. Of course, the order of a term will be changed if the coupling constant includes any power of the Compton wavelength of the particle.

III. THE HYDROGENIC ATOM

In this section, we illustrate the use of the tables in demonstrating how one may obtain expressions for the major contributions to the Lamb-Retherford shift by applying the Foldy-Wouthuysen transformation to a relativistic one-body wave equation in which appropriate quantum-electrodynamic effects are included phenomenologically.

$$H\psi=\{\beta mc^2+e\phi+c\boldsymbol{\alpha}\cdot\mathbf{p}+(\mu_e-1)(e\hbar/2mc)i\beta\boldsymbol{\alpha}\cdot\mathbf{E}-e_1(\hbar/mc)^2\nabla\cdot\mathbf{E}\}\psi=i\hbar\partial\psi/\partial t. \quad (9)$$

The first three terms are the usual ones which occur in the wave equation for a Dirac particle of charge e coupled to the potential ϕ of an external electrostatic field. In addition, the anomalous magnetic moment of the electron (μ_e-1) Bohr magnetons is coupled to the external electric field $\mathbf{E}$, and e_1, a state-dependent quantity arising from a quantum-electrodynamic correction to the rest energy, is coupled to the d'Alembertian of the external field, which in the electrostatic case is simply $\nabla\cdot\mathbf{E}$. Two terms analogous to these have been used by Foldy[7] in a relativistic wave equation for the neutron to account for the magnetic and electrostatic contributions to the electron-neutron interaction.

Equation (9) is, of course, a specialization of Eq. (3) under the substitutions, $\theta_4=i\phi$, $g_{\mathrm{I}}=-e/c$; $\mathbf{P}=i\mathbf{E}$, $g_{\mathrm{II}}=-(\mu_e-1)(e\hbar/2mc^2)$; $\theta_4'=i\nabla\cdot\mathbf{E}$, $g_{\mathrm{I}}'=e_1\hbar^2/m^2c^3$; we assume all the remaining coupling constants to be zero. The corresponding approximately relativistic wave equation may be written by using the vector and tensor columns in Table I. Mixed product terms in Table II are neglected as they are of third or higher order. The result is

$$H'\chi'=\Big\{mc^2+\frac{p^2}{2m}+e\phi-\frac{e\hbar^2}{8m^2c^2}\nabla\cdot\mathbf{E}-\frac{e\hbar}{4m^2c^2}\boldsymbol{\sigma}\cdot\mathbf{E}\times\mathbf{p}-\frac{p^4}{8m^3c^2}-e_1\Big(\frac{\hbar}{mc}\Big)^2\nabla\cdot\mathbf{E}-\frac{(\mu_e-1)}{4m^2c^2}e\hbar^2\nabla\cdot\mathbf{E}-\frac{(\mu_e-1)}{2m^2c^2}e\hbar\boldsymbol{\sigma}\cdot\mathbf{E}\times\mathbf{p}\Big\}\chi'$$
$$=i\hbar\partial\chi'/\partial t, \quad (10)$$

where H' is the transformed Hamiltonian and χ' is a two-component wave function corresponding to positive energies. (The p^4 term in Eq. (10) does not come from the tables. It is obtained from $-\beta\mathcal{O}^4/8m^3c^6$ which is the next even term in the expansion (4).)

The last six terms in Eq. (10) may be considered as perturbations on the Balmer energy levels. Their individual contributions to the energy are given in Table III.

The kinetic energy, Darwin, and Thomas corrections are well known[8] and account for all the $Rch\alpha^2$ terms in the expansion of the Sommerfeld fine structure formula. R is the Rydberg, and α is the fine structure constant.

[5] C. G. Darwin, Proc. Roy. Soc. (London) **118**, 654 (1928).
[6] L. H. Thomas, Nature **117**, 514 (1926).

[7] L. L. Foldy, Phys. Rev. **83**, 688 (1951); Phys. Rev. **86**, 646 (1952).
[8] See, for example, E. U. Condon and G. Shortley, *The Theory of Atomic Spectra* (Cambridge University Press, New York, 1951), Chap. 5.

TABLE I. Relativistic correction terms associated with single-type interactions.

	Scalar	Vector	Tensor	Pseudovector	Pseudoscalar
Zero-Order Terms "Schrödinger" and "Spin-Field"	$\beta c\theta$	$ic\theta_4$	$\beta c\boldsymbol{\sigma}\cdot\mathbf{M}$	$c\boldsymbol{\sigma}\cdot\mathbf{S}$	
1st-Order Terms "Schrödinger" "Divergence"		$(\beta/2m)(\boldsymbol{\theta}\cdot\boldsymbol{\theta})$ $-(\beta i\hbar/2m)(\nabla\cdot\boldsymbol{\theta})$	$-(\beta/2m)(P^2)$ $-(i\hbar/2m)(\nabla\cdot\mathbf{P})$	$-(\beta/2m)(S_4^2)$	$-(\beta/2m)(\theta^P)^2$
"Darwin"		$(\beta/m)(\boldsymbol{\theta}\cdot\mathbf{p})$			
"Spin-Field"		$(\beta\hbar/2m)(\boldsymbol{\sigma}\cdot\nabla\times\boldsymbol{\theta})$	$(\hbar/2m)(\boldsymbol{\sigma}\cdot\nabla\times\mathbf{P})$	$(\beta\hbar/2m)(\boldsymbol{\sigma}\cdot\nabla S_4)$	$-(i\hbar/2m)(\boldsymbol{\sigma}\cdot\nabla\theta^P)$
"Spin-Orbit"			$-(i/m)(\boldsymbol{\sigma}\cdot\mathbf{P}\times\mathbf{p})$		
"Spin-Momentum"				$(i\beta/m)(S_4\boldsymbol{\sigma}\cdot\mathbf{p})$	
2nd-Order Terms "Schrödinger"	$-\dfrac{\beta}{2m^2c}(\theta p^2)$				
"Divergence"	$\dfrac{\beta\hbar^2}{8m^2c^2}(\nabla^2\theta)$	$-\dfrac{\hbar^2}{8m^2c}\left\{\nabla\cdot\left(-i\nabla\theta_4+\dfrac{1}{c}\dfrac{\partial\boldsymbol{\theta}}{\partial t}\right)\right\}$	$-\dfrac{\beta\hbar^2}{8m^2c^2}\left(\nabla\cdot\dfrac{\partial\mathbf{P}}{\partial t}\right)$	$\dfrac{\hbar}{4m^2c}(\nabla\cdot\mathbf{S}\times\mathbf{p})$	
"Darwin"	$\dfrac{\beta i\hbar}{2m^2c}(\nabla\theta\cdot\mathbf{p})$		$-\dfrac{\beta\hbar}{4m^2c}\left(\nabla\times\mathbf{M}+\dfrac{i}{c}\dfrac{\partial\mathbf{P}}{\partial t}\right)\cdot\mathbf{p}$		
"Spin-Field"		$-\dfrac{i\hbar^2}{8m^2c^2}\left(\boldsymbol{\sigma}\cdot\nabla\times\dfrac{\partial\boldsymbol{\theta}}{\partial t}\right)$ $-\dfrac{\hbar}{4m^2c}\left\{\boldsymbol{\sigma}\cdot\left(-i\nabla\theta_4+\dfrac{1}{c}\dfrac{\partial\boldsymbol{\theta}}{\partial t}\right)\times\boldsymbol{\theta}\right\}$	$\dfrac{\beta}{8m^2c}\Big\{-\hbar^2\boldsymbol{\sigma}\cdot\nabla\times\nabla\times\mathbf{M}+2i\hbar(\boldsymbol{\sigma}\cdot\nabla)(\mathbf{M}\cdot\mathbf{p})$ $+\hbar^2(\boldsymbol{\sigma}\cdot\nabla)(\nabla\cdot\mathbf{M})-i\hbar^2\boldsymbol{\sigma}\cdot\nabla\times\dfrac{\partial\mathbf{P}}{\partial t}-\dfrac{2\beta\hbar}{c}$ $\times\boldsymbol{\sigma}\cdot\mathbf{P}\times\dfrac{\partial\mathbf{P}}{\partial t}-2\beta i\hbar(\boldsymbol{\sigma}\cdot\nabla)(\mathbf{M}\cdot\mathbf{P})+2\beta i\hbar$ $\times(\mathbf{M}\cdot\nabla)(\boldsymbol{\sigma}\cdot\mathbf{P})+2\beta i\hbar\boldsymbol{\sigma}\cdot\mathbf{P}\times(\nabla\times\mathbf{M})$ $+4(\boldsymbol{\sigma}\cdot\mathbf{P})(\mathbf{M}\cdot\mathbf{p})\Big\}$	$(\lambda^2/8m^2c)\{(\boldsymbol{\sigma}\cdot\nabla)(\nabla\cdot\mathbf{S})-\boldsymbol{\sigma}\cdot\nabla\times(\nabla\times\mathbf{S})\}$ $-(i/c)(\boldsymbol{\sigma}\cdot\nabla\partial S_4/\partial t)\}-(i\hbar/4m^2c)(\boldsymbol{\sigma}\cdot\mathbf{S}\times\nabla S_4)$	$-\dfrac{\beta\hbar^2}{8m^2c^2}\left(\boldsymbol{\sigma}\cdot\nabla\dfrac{\partial\theta^P}{\partial t}\right)$
"Spin-Orbit"	$-\dfrac{\beta\hbar}{4m^2c}(\boldsymbol{\sigma}\cdot\nabla\theta\times\mathbf{p})$	$-\dfrac{\hbar}{4m^2c}\left\{\boldsymbol{\sigma}\cdot\left(-i\nabla\theta_4+\dfrac{1}{c}\dfrac{\partial\boldsymbol{\theta}}{\partial t}\right)\times\mathbf{p}\right\}$		$(1/2m^2c^2)\{\boldsymbol{\sigma}\cdot(\mathbf{S}\times\mathbf{p})\times\mathbf{p}\}$ $+(i\hbar/4m^2c)\{\boldsymbol{\sigma}\cdot(\nabla\times\mathbf{S})\times\mathbf{p}+\boldsymbol{\sigma}\cdot\nabla\times(\mathbf{S}\times\mathbf{p})\}$	
"Spin-Momentum"			$\dfrac{\beta}{4m^2c}(i\hbar\nabla\cdot\mathbf{M}-2\mathbf{M}\cdot\mathbf{p})(\boldsymbol{\sigma}\cdot\mathbf{p})$		$-\dfrac{\beta i\hbar}{4m^2c^2}\left(\dfrac{\partial\theta^P}{\partial t}\boldsymbol{\sigma}\cdot\mathbf{p}\right)$

TABLE II. Relativistic correction terms associated with mixed-type interactions.

	Scalar-Vector	Scalar-Tensor	Tensor-Pseudovector	Tensor-Pseudoscalar	Pseudovector-Pseudoscalar
1st-Order Terms "Spin-Field"				$-(\beta/m)(\theta^P\boldsymbol{\sigma}\cdot\mathbf{P})$	
2nd-Order Terms "Schrödinger"	$(\beta i\hbar/2m^2c)(\nabla\theta\cdot\dot{\boldsymbol{\theta}})$ $-(\beta/2m^2c)(\theta\dot{\boldsymbol{\theta}}\cdot\dot{\boldsymbol{\theta}})$	$(i\hbar/4m^2c)(\nabla\theta\cdot\mathbf{P})$ $+(\beta/2m^2c)(\theta P^2)$	$-(\beta\hbar/4m^2c)(2\mathbf{M}\cdot\nabla S_4$ $-\mathbf{P}\cdot\nabla\times\mathbf{S}+\mathbf{S}\cdot\nabla\times\mathbf{P})$	$(i\hbar/2m^2c)(\mathbf{M}\cdot\nabla\theta^P)$ $+(\beta/m^2c)(\theta^P\mathbf{M}\cdot\mathbf{P})$	$\dfrac{\beta\hbar}{4m^2c^2}\left(S_4\dfrac{\partial\theta^P}{\partial t}-\theta^P\dfrac{\partial S_4}{\partial t}\right)$
"Divergence"	$(\beta i\hbar/2m^2c)(\theta\nabla\cdot\dot{\boldsymbol{\theta}})$	$(i\hbar/2m^2c)(\theta\nabla\cdot\mathbf{P})$	$-(\beta\hbar/4m^2c)\{\nabla\cdot(\mathbf{P}\times\mathbf{S})+2S_4\nabla\cdot\mathbf{M}\}$	$(i\hbar/4m^2c)(\nabla\cdot\mathbf{M})\theta^P$	$-(\beta i\hbar/4m^2c)(\theta^P\nabla\cdot\mathbf{S})$
"Darwin"	$-(\beta/m^2c)(\theta\dot{\boldsymbol{\theta}}\cdot\mathbf{p})$		$-(i\beta/m^2c)\{(\mathbf{P}\times\mathbf{S})+S_4\mathbf{M}\}\cdot\mathbf{p}$		
"Spin-Field"	$-(\beta\hbar/4m^2c)$ $\times(\boldsymbol{\sigma}\cdot\nabla\theta\times\dot{\boldsymbol{\theta}}+2\dot{\theta}\boldsymbol{\sigma}\cdot\nabla\times\dot{\boldsymbol{\theta}})$	$-(\hbar/2m^2c)$ $\times(\boldsymbol{\sigma}\cdot\nabla\theta\times\mathbf{P}+\theta\boldsymbol{\sigma}\cdot\nabla\times\mathbf{P})$	$-\dfrac{\beta i\hbar}{4m^2c}\left\{\boldsymbol{\sigma}\cdot\nabla S_4\times\mathbf{M}+2S_4\boldsymbol{\sigma}\cdot\nabla\times\mathbf{M}+(\boldsymbol{\sigma}\cdot\mathbf{P})\right.$ $\times(\nabla\cdot\mathbf{S})+\boldsymbol{\sigma}\cdot\nabla\times(\mathbf{P}\times\mathbf{S})+\boldsymbol{\sigma}\cdot(\mathbf{S}\times\nabla)\times\mathbf{P}-\dfrac{i}{c}$ $\left.\times\dfrac{\partial}{\partial t}\boldsymbol{\sigma}\cdot(S_4\mathbf{P})\right\}+\dfrac{\beta}{2m^2c}\{S_4\boldsymbol{\sigma}\cdot\mathbf{P}\times\mathbf{S}+S_4^2\boldsymbol{\sigma}\cdot\mathbf{M}$ $-\beta\boldsymbol{\sigma}\cdot\mathbf{P}\times(\mathbf{P}\times\mathbf{S})\}$	$-(\hbar/4m^2c)(\theta^P\boldsymbol{\sigma}\cdot\nabla\times\mathbf{M}+\boldsymbol{\sigma}\cdot\nabla\theta^P\times\mathbf{M})$ $+(\beta/2m^2c)(\theta^{P2}\boldsymbol{\sigma}\cdot\mathbf{M})$	$-(\beta\hbar/4m^2c)$ $\times\{\boldsymbol{\sigma}\cdot(S\times\nabla\theta^P-\theta^P\nabla\times\mathbf{S})\}$
"Spin-Orbit"		$(i/m^2c)(\theta\boldsymbol{\sigma}\cdot\mathbf{P}\times\mathbf{p})$	$(\beta/2m^2c)(S_4\boldsymbol{\sigma}\cdot\mathbf{M}\times\mathbf{p})$		$-(i\beta/2m^2c)(\theta^P\boldsymbol{\sigma}\cdot\mathbf{S}\times\mathbf{p})$
	Scalar-Pseudovector	Scalar-Pseudoscalar	Vector-Tensor	Vector-Pseudovector	Vector-Tensor-Pseudovector
"Schrödinger"	$(\beta/2m^2c)(\theta S_4^2)$	$(\beta/2m^2c)(\theta^P)^2\theta$	$\dfrac{\beta i\hbar}{4m^2c}\left\{\mathbf{P}\cdot\left(-i\nabla\theta_4+\dfrac{1}{c}\dfrac{\partial\dot{\boldsymbol{\theta}}}{\partial t}\right)\right\}$ $-\dfrac{\beta\hbar}{4m^2c}\left\{\nabla\times\mathbf{M}+\dfrac{i}{c}\dfrac{\partial\mathbf{P}}{\partial t}\right\}\cdot\dot{\boldsymbol{\theta}}$		$-(i\beta/m^2c)$ $\times\{(\mathbf{P}\times\mathbf{S})+S_4\mathbf{M}\}\cdot\dot{\boldsymbol{\theta}}$
"Divergence"				$(\hbar/4m^2c)(\nabla\cdot\mathbf{S}\times\dot{\boldsymbol{\theta}})$	
"Spin-Field"	$-(\beta\hbar/2m^2c)$ $\times(\theta\boldsymbol{\sigma}\cdot\nabla S_4+S_4\boldsymbol{\sigma}\cdot\nabla\theta)$	$(i\hbar/4m^2c)$ $\times(\theta^P\boldsymbol{\sigma}\cdot\nabla\theta+2\theta\boldsymbol{\sigma}\cdot\nabla\theta^P)$	$-(i/m)(\boldsymbol{\sigma}\cdot\mathbf{P}\times\dot{\boldsymbol{\theta}})$[1st order] $\dfrac{\beta i\hbar}{4m^2c}\{(\nabla\cdot\mathbf{M})(\boldsymbol{\sigma}\cdot\dot{\boldsymbol{\theta}})+(\boldsymbol{\sigma}\cdot\nabla)(\mathbf{M}\cdot\dot{\boldsymbol{\theta}})+(\mathbf{M}\cdot\nabla)$ $\times(\boldsymbol{\sigma}\cdot\dot{\boldsymbol{\theta}})\}-\dfrac{\beta}{2m^2c}(\mathbf{M}\cdot\dot{\boldsymbol{\theta}})(\boldsymbol{\sigma}\cdot\dot{\boldsymbol{\theta}})$	$(i\beta/m)(S_4\boldsymbol{\sigma}\cdot\dot{\boldsymbol{\theta}})$[1st order] $\dfrac{1}{2m^2c}\{\boldsymbol{\sigma}\cdot(\mathbf{S}\times\dot{\boldsymbol{\theta}})\times\dot{\boldsymbol{\theta}}\}+(i\hbar/4m^2c)$ $\times\{\boldsymbol{\sigma}\cdot(\nabla\times\mathbf{S})\times\dot{\boldsymbol{\theta}}+\boldsymbol{\sigma}\cdot\nabla\times(\mathbf{S}\times\dot{\boldsymbol{\theta}})$ $-2\boldsymbol{\sigma}\cdot(\mathbf{S}\times\nabla)\times\dot{\boldsymbol{\theta}}\}$	$(\beta/2m^2c)(S_4\boldsymbol{\sigma}\cdot\mathbf{M}\times\dot{\boldsymbol{\theta}})$
"Spin-Orbit"				$\dfrac{1}{2m^2c}\{\boldsymbol{\sigma}\cdot(\mathbf{S}\times\dot{\boldsymbol{\theta}})\times\mathbf{p}-\boldsymbol{\sigma}\cdot\dot{\boldsymbol{\theta}}\times(\mathbf{S}\times\mathbf{p})\}$	
"Spin-Momentum"	$-(i\beta/m^2c)(\theta S_4\boldsymbol{\sigma}\cdot\mathbf{p})$		$-(\beta/2m^2c)(\mathbf{M}\cdot\dot{\boldsymbol{\theta}})(\boldsymbol{\sigma}\cdot\mathbf{p})$		
	Scalar-Tensor-Pseudoscalar	Scalar-Vector-Tensor	Scalar-Vector-Pseudovector	Vector Pseudoscalar	Vector-Pseudovector-Pseudoscalar
"Spin-Field"	$(\beta/m^2c)(\theta\dot{\theta}^P\boldsymbol{\sigma}\cdot\mathbf{P})$	$(i/m^2c)(\theta\boldsymbol{\sigma}\cdot\mathbf{P}\times\dot{\boldsymbol{\theta}})$	$-(i\beta/m^2c)(\theta S_4\boldsymbol{\sigma}\cdot\dot{\boldsymbol{\theta}})$	$\dfrac{\beta i\hbar}{4m^2c}\left\{\boldsymbol{\sigma}\cdot\left(-i\nabla\theta_4+\dfrac{1}{c}\dfrac{\partial\dot{\boldsymbol{\theta}}}{\partial t}\right)\theta^P\right.$ $\left.-\boldsymbol{\sigma}\cdot\dot{\boldsymbol{\theta}}\dfrac{1}{c}\dfrac{\partial\theta^P}{\partial t}\right\}$	$-(i\beta/2m^2c)(\theta^P\boldsymbol{\sigma}\cdot\mathbf{S}\times\dot{\boldsymbol{\theta}})$

TABLE III. Contributions of relativistic correction terms in Eq. (10) to hydrogenic energy levels.

Energy level correction	Term responsible
Kinetic energy correction	
$-\frac{Z^4Rch\alpha^2}{n^4}\left(\frac{n}{l+\frac{1}{2}}-\frac{3}{4}\right)$	$-\frac{p^4}{8m^3c^2}$
Darwin correction for S states	
$\frac{Z^4Rch\alpha^2}{n^3}$	$\frac{eh^2}{8m^2c^2}\nabla\cdot\mathbf{E}$
Thomas correction for states of $l\neq 0$	
$\left(\frac{Z^4Rch\alpha^2}{n^3}\right)\left(\frac{1}{(2l+1)(l+1)}\right)$ for $j=l+\frac{1}{2}$	$-\frac{eh}{4m^2c^2}\boldsymbol{\sigma}\cdot\mathbf{E}\times\mathbf{p}$
$-\left(\frac{Z^4Rch\alpha^2}{n^3}\right)\left(\frac{1}{l(2l+1)}\right)$ for $j=l-\frac{1}{2}$	
$(8e_1/e)\times$Darwin correction	
$8\frac{e_1}{e}\left(\frac{Z^4Rch\alpha^2}{n^3}\right)$	$-e_1\left(\frac{h}{mc}\right)^2\nabla\cdot\mathbf{E}$
$2(\mu_e-1)\times$Darwin correction	
$2(\mu_e-1)\left(\frac{Z^4Rch\alpha^2}{n^3}\right)$	$-(\mu_e-1)\frac{eh^2}{4m^2c^2}\nabla\cdot\mathbf{E}$
$2(\mu_e-1)\times$Thomas correction	
$2(\mu_e-1)\left(\frac{Z^4Rch\alpha^2}{n^3}\right)\left(\frac{1}{(2l+1)(l+1)}\right)$ for $j=l+\frac{1}{2}$	$-(\mu_e-1)\frac{eh}{2m^2c^2}\boldsymbol{\sigma}\cdot\mathbf{E}\times\mathbf{p}$
$-2(\mu_e-1)\left(\frac{Z^4Rch\alpha^2}{n^3}\right)\left(\frac{1}{l(2l+1)}\right)$ for $j=l-\frac{1}{2}$	

The quantum-electrodynamic factors are given by[9,10]

$$(\mu_e-1)=\alpha/2\pi, \tag{11}$$

$$e_1=e\frac{\alpha}{3\pi}\left\{\ln\frac{mc^2}{k_0(n,0)}-\ln 2-\frac{1}{5}+\frac{11}{24}+3\pi Z\alpha\left[1+\frac{11}{128}-\frac{1}{2}\ln 2+\frac{5}{192}\right]\right\}, \tag{12}$$

where $k_0(n,l)$ is the average atomic excitation energy for the level nl.

The contribution of the anomalous electron magnetic moment to the displacement of states of any l is easily calculated by using Table III and Eq. (11). The result is

$$E(n,l)=-\frac{2(\mu_e-1)Z^4Rch\alpha^2}{n^3}\left\{\frac{1+k}{(l+1)(2l+1)}\right\}, \tag{13}$$

where $k=-l-1$ for $j=l+\frac{1}{2}$ and $k=l$ for $j=l-\frac{1}{2}$. This expression agrees with that obtained by Breit[11] from an approximate evaluation. Upon inserting the 1951 constants of Bearden and Watts[12] into Eq. (13), the separation of the $2S$, $2P_{\frac{1}{2}}$ states of hydrogen due to the anomalous magnetic moment of the electron is 67.77 Mc/sec. Also the doublet separation of the $2P_{\frac{3}{2}}$, $2P_{\frac{1}{2}}$ states is increased by 25.41 Mc/sec from the value predicted by Dirac theory. These numerical values are in good agreement with the latest values quoted by Lamb.[13]

The contribution of e_1 to the displacement of the S states is also easily obtained by using Table III and Eq. (12):

$$E(n,0)=\frac{8Z^4Rch\alpha^2}{3\pi n^3}\left\{\ln\frac{mc^2}{k_0(n,0)}-\ln 2-\frac{1}{5}+\frac{11}{24}+3\pi Z\alpha\left[1+\frac{11}{128}-\frac{1}{2}\ln 2+\frac{5}{192}\right]\right\}. \tag{14}$$

[9] J. Schwinger, Phys. Rev. **73**, 416 (1948).
[10] Karplus, Klein, and Schwinger, Phys. Rev. **86**, 288 (1952); see also, Bethe, Brown, and Stehn, Phys. Rev. **77**, 370 (1950); J. B. French and V. E. Weisskopf, Phys. Rev. **75**, 1240 (1949).
[11] G. Breit, Phys. Rev. **72**, 984 (1947).
[12] J. A. Bearden and H. M. Watts, Phys. Rev. **81**, 73 (1951).
[13] W. E. Lamb, Jr., Phys. Rev. **85**, 259 (1952).

This agrees with the expression obtained by other authors.[10] Using the numerical value for $k_0(2, 0)$ as calculated by Bethe *et al.*,[10] the $2S$ state of hydrogen is shifted by 994.82 Mc/sec. Table III does not, however, predict the known additional displacement of the $2P_{\frac{1}{2}}$ state of hydrogen by 4.00 Mc/sec.

It is hoped that in future publications we may be able to demonstrate the utility of Tables I and II in beta-decay and meson theories.

We wish to express our appreciation to Professor G. Breit, Professor L. L. Foldy, and Professor H. Primakoff for valuable suggestions.

PHYSICAL REVIEW VOLUME 89, NUMBER 2 JANUARY 15, 1953

The Diffraction of Strong Shock Waves*

WAYLAND GRIFFITH AND DAVID E. BRICKL
Palmer Physical Laboratory, Princeton University, Princeton, New Jersey
(Received August 15, 1952)

The pseudostationary flow field resulting from diffraction of a strong shock in air over a convex corner has been investigated with the shock tube and interferometer. Only when the shock has turned nearly 180°, is it observed to become vanishingly weak. A potential flow theory for part of the field is inadequate to predict the extent of a Prandtl-Meyer expansion around the corner. Viscous forces produce a boundary layer which causes the flow to separate at the corner with significant changes in the density field as a result.

INTRODUCTION

THE diffraction of a plane shock wave by a convex corner is one example of the general problem of interacting shock and rarefaction waves. Since no unit of length is given for the flow, the pattern remains similar to itself in time, i.e., is pseudostationary, and may be described by the variables x/t and y/t. Like the complementary problem of Mach reflection, the nonlinear nature of the fluid mechanical equations present such formidable difficulties that no complete solution of the problem has been found. Jones, Martin, and Thornhill,[1] in a recent paper, have shown that a part of the flow field may be readily obtained when the incident shock is strong enough for the flow behind it to be supersonic. Previously, Lighthill[2] linearized the flow equations by retaining only terms of first order in the angle of the corner and calculated the pressure on the wall and the shape of the diffracted shock. This solution applies to shocks of any strength as long as the angle is sufficiently small. Previous experiments in this shock tube[3] established the validity of Lighthill's solution. Keller[4] has computed the density field for an acoustic wave rounding a 90° corner which is in good agreement with experimental data obtained for very weak shocks by White. The purpose of this paper will be to present the results of experiments with strong shocks (such that the flow behind them is supersonic) and any corner angle for comparison with the theory of reference 1 and as a guide to further theoretical work.

* This work was supported by the ONR.

[1] Jones, Martin, and Thornhill, Proc. Roy. Soc. (London) **A209**, 238 (1951).

[2] M. J. Lighthill, Proc. Roy. Soc. (London) **A198**, 454 (1949).

[3] Fletcher, Taub, and Bleakney, Revs. Modern Phys. **23**, 271 (1951).

[4] Mathematics Research Group Rept. EM-43, New York University, unpublished.

THEORETICAL CONSIDERATIONS

Consider a shock wave of velocity V advancing into still air in which the velocity of sound is a_1. According to one-dimensional shock theory, the flow velocity u_2 behind the shock is

$$u_2/a_1=2(M-1/M)/(\gamma+1), \tag{1}$$

where M is the shock Mach number V/a_1, and the local velocity of sound a_2 is

$$a_2/a_1=\{[2\gamma M^2-\gamma+1][2/M^2+\gamma-1]\}^{\frac{1}{2}}/(\gamma+1). \tag{2}$$

The flow behind the shock becomes supersonic when $u_2/a_2=1$ or for air with $\gamma=1.4$ when $M=2.068$.

When the incident shock passes the corner, a rarefaction wave advances back through the moving air with the velocity a_2, but the air itself is carried along with the velocity u_2. As a result, only the region below OAE in Fig. 1 will know of the existence of the corner. The strength of the diffracted shock EF varies in some unknown way so that the boundary conditions are difficult to establish.

A part of the flow can still be found, however. Jones, Martin, and Thornhill show that a Prandtl-Meyer expansion at the corner may be terminated in either one of two ways: (a) a uniform flow parallel to the wall, or (b) uniform flow parallel to a line on the other side of which some other flow maintains equal pressure, i.e., a slip stream. They predict that transition to the second case will occur when the Prandtl-Meyer flow expands to the ambient pressure p_1. The region below the slip stream would then be at rest at pressure p_1.

The radial extent of the Prandtl-Meyer flow may be found from the characteristics in the x/t, y/t system. One set consists of course of the radial lines through O. The other family must be found numerically. The

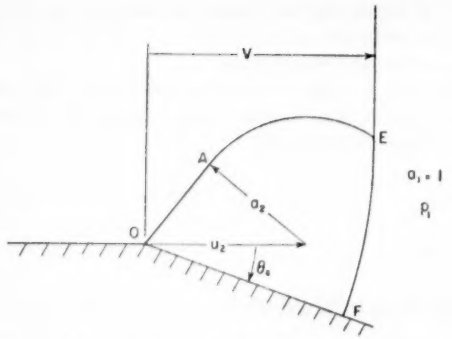

FIG. 1. Schematic drawing of shock diffraction pattern.

characteristic which passes through the point A was calculated for $M=3$ and is plotted in Fig. 2 as the dotted curve ABD. This provides an outer limit on the Prandtl-Meyer expansion. It will be seen that shocks appear which end the potential flow sooner.

EXPERIMENTAL RESULTS

Three models were made having corner angles $\theta_c=35°$, 90°, and 160°. In each case, the model completely spanned the four-inch width of the shock tube. The maximum distance past the corner which the shock could travel with the entire diffraction field still in view was about 2.5 in. Since the theory and operation of the tube have been described already,[5] no detailed explanation will be given here. Plane shock waves striking the model are photographed through a Mach-Zehnder interferometer with the aid of a 1-μsec spark triggered from an adjustable delay circuit. Thus any stage in the development of the flow could be recorded. This was especially significant in checking the assumption that the entire process was pseudostationary.

Figure 2 shows a typical density pattern obtained from an interferogram with a shock Mach number of 3.10. Numbers on the contours give the ratio of the density to the density ahead of the incident shock. The two discontinuities marked S may be either shocks or slip streams. Since we cannot decide which they are from these experiments alone, we shall arbitrarily refer to them as shocks. A small region of low density is observed below the slip stream (denoted by the dashed line) indicating that a vortex is shed from the corner. For comparison, the boundaries of the flow predicted theoretically for $M=3$ are shown by the dotted lines. OB is the final expansion wave which produces plane parallel flow at the ambient pressure in region OBD.

The influence of the corner angle on the flow pattern may be seen from Fig. 3 in which the shock and slip stream positions are drawn for three different corners with the same shock strength. For each case the pattern was found to grow similar to itself over a range of times varying by a factor of 5.

Only when the diffracted shock has turned nearly 180° does it become vanishingly weak. In the other cases the end moves forward to meet the wall normally. Except where the wall interferes directly, the subsidiary shocks S are nearly indistinguishable in the three experiments. An important result of this comparison is the observation that the slip stream angle and, therefore, the pressure to which the flow expands depend on the corner angle. This comes about through the action of viscosity in forming a boundary layer along the surface upstream from the corner. The vorticity so generated is shed from the corner in a sheet which then curls up to form the vortex already referred to in Fig. 2. Any such disturbance can make its presence felt in the entire region below the slip stream since there the air is nearly at rest.

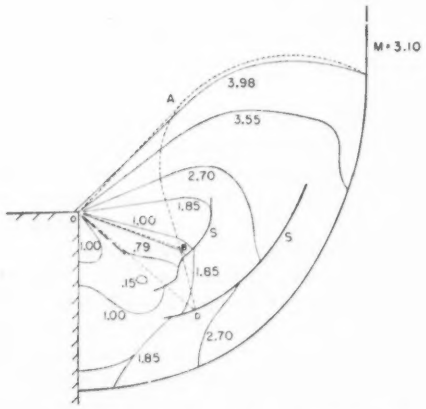

FIG. 2. Density field resulting from diffraction of a shock moving with a Mach number $M=3.10$ over a 90° corner. The dotted lines are the boundaries of the flow predicted theoretically for $M=3$.

Figure 4 shows the experimentally determined slip stream angle for each of the three corners as a function of M. The theoretical curve is obtained by computing the angle of turn necessary to expand the high pressure air behind the incident shock to ambient pressure. By coincidence, a corner angle of about 77° would give excellent agreement with the theory for all M between 2.06 and 3.2.

To study further the origin of viscous effects, the plate upstream from the corner was lengthened from 2 in. to 7 in. No changes could be detected. It appears, therefore, that the boundary layer thickness at the corner in these experiments was determined by the time since the flow was initiated by arrival of the shock rather than by the distance from the leading edge of the plate.

No theory is available for the growth of the boundary layer in the flow set up by a shock, but an order of

[5] Bleakney, Weimer, and Fletcher, Rev. Sci. Instr. **20**, 807 (1949).

magnitude for the thickness of such a layer may be obtained by applying the result for a plate suddenly set in motion.[6] The thickness is given by $2(\nu t)^{\frac{1}{2}}$, where ν is the kinematic viscosity and t is the elapsed time. For the earliest picture, where $t=10\ \mu$sec, this gives 0.007 inch. The surprising result is that such an exceedingly thin boundary layer causes the flow to

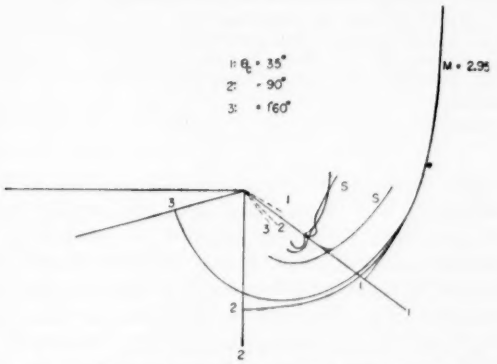

FIG. 3. Influence of corner angle on shock and slip stream position for $M=2.95$.

separate at the corner and depart significantly from the predictions of potential flow theory.

CONCLUSIONS

The strength of a plane strong shock diffracted at a convex corner decreases monotonically from the point

[6] W. F. Durand, *Aerodynamic Theory* (J. Springer, Berlin, 1934), Vol. 3, p. 65.

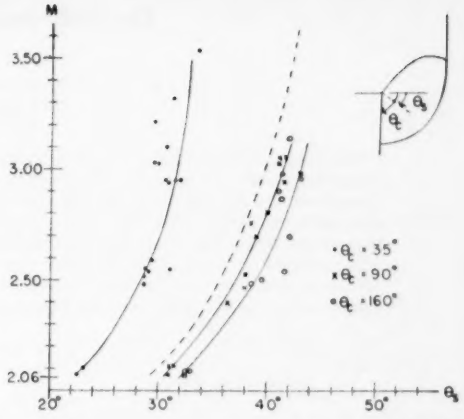

FIG. 4. Slip stream angle plotted as a function of M for each of the three corners. The dotted curve shows the theoretical dependence obtained by Thornhill.

of intersection with the leading edge of the rarefaction wave and reaches vanishing strength only in the neighborhood of a 180° turn. Predictions from potential theory concerning the flow field are only qualitatively correct in air. Viscous forces produce a boundary layer which causes the flow to separate at the corner with resulting modifications in pressure distribution. The location of the final wave in the Prandtl-Meyer expansion, therefore, becomes dependent upon the corner angle as well as the shock strength. Two subsidiary discontinuities occur whose positions are remarkably stable with respect to changes in corner angle and shock strength.

The Disintegration of Radium D

A. A. JAFFE AND S. G. COHEN
Department of Physics, Hebrew University, Jerusalem, Israel
(Received July 10, 1952)

The disintegration of radium D has been investigated using a gaseous source of lead tetramethyl in a proportional counter. The form of the low energy β-spectrum coincident with the 46.7-kev γ-ray has been determined. The end point has been found to be 15.2 ± 1 kev. The shape of the spectrum shows good agreement with the Fermi theory for an allowed transition, in which the effect of screening on the Coulomb factor is neglected. The results indicate that the number of β-particles below 3 kev is somewhat less than than predicted by theory, neglecting screening. It is also concluded that the change in binding energy of the atomic electrons (about 10 kev) released in the decay, is included in the energy of disintegration of the β-particles, and is shared between the β-particle and neutrino.

INTRODUCTION

THE disintegration of radium D has been investigated by many observers.[1] The exact measurement of the shape of the β-spectrum has, in particular, posed a difficult experimental problem, because of the extremely low energy of the β-particles. The form of a low energy spectrum for the high value of atomic number involved, i.e., $Z=82$, is also of considerable theoretical interest. Recently Insch, Balfour, and Curran[2] have examined the β-spectrum using proportional counters and a solid source, and have obtained the value of 18 ± 2.5 kev for the end point. In the work to be described, we have examined the disintegration using RaD, which is an isotope of lead, in the form of lead tetramethyl as a gaseous constituent in a proportional counter. (In one of the earliest investigations carried out on RaD, Richardson and Leigh-Smith[3] used radioactive lead tetramethyl in a cloud chamber.) This method clearly obviates the difficulties of self-absorption and backscattering and, as will also be seen, enables a very accurate energy calibration of the β-spectrum to be made and gives the form of the β-spectrum directly, in contrast with experiments using solid sources. The feasibility of the experiment was demonstrated by the preliminary verification of the following facts: (a) a counter filled with argon, methane, and including a few mm pressure of pure dry lead tetramethyl shows excellent proportionality; (b) the amount of sticking of the lead tetramethyl vapor to the counter walls, during the time of the experiment, was negligible; (c) the amount of RaE present in the counter during the experiment could be kept very small.

DESCRIPTION OF METHOD AND APPARATUS

Other work[4,5] has shown that a 46.7-kev γ-ray occurs in about 65 percent of disintegrations and is highly converted ($\sim$96 percent). If this γ-ray is emitted within a time short compared with the resolving time of the counter (a few microseconds) one would expect that 65 percent of the pulses obtained in a proportional counter containing RaD in the gas phase should correspond to the sum of the energies of the γ-ray and the β-particle, if all the secondary radiations are absorbed in the counter gas, giving rise to a peak in the region of 46.7 kev, and as the β-spectrum would be superposed on this gamma-line, one could get the shape of the β-spectrum from an analysis of the high energy side of the observed peak. An identical pulse distribution would also be produced by low energy β-particles coincident with cascade converted γ-rays, produced by indirect de-excitation of the 46.7-kev level, in some of the remaining 35 percent of the disintegrations. The counter was therefore designed to give the shape of this profile accurately. One might also expect, in relatively few cases, to get the pure low energy β-spectrum when all rays coincident with the decay are unconverted and escape from the counter, or if all the accompanying γ-rays are delayed due to metastability.

In order to minimize the wall effect and thus to diminish the distortion in the pulse distribution at low energies, the counter was made so that the range of the ionizing particles should be small compared with its dimensions. Most of the 46.7-kev γ-rays are converted in the L shell, resulting in conversion electrons of 30.5-kev energy and of maximum range (in the gas filling used, which was 60-cm argon+14 cm methane) about 1.2 cm. Only 12 percent of the γ-rays are converted in the MNO shells, giving rise to 44-kev conversion electrons of maximum range about 2.4 cm. The end effect, which causes distortion in the regions extending up to a distance of the order of a radius of the counter from each end, was kept small by making the counter long. The counter dimensions were thus chosen to be 9-cm in diameter and 72-cm long. The counter wall was made of brass and provided with a polythene window to permit energy calibrations using external sources of γ- and x-rays. The anode was a 4-mil diameter tungsten wire attached at each end to tungsten rods which were sealed into double metal-to-glass seals, the intermediate metal seals forming guard rings. The wire was shielded

[1] N. Feather, Nucleonics **5**, 22 (July, 1949).
[2] Insch, Balfour, and Curran, Phys. Rev. **85**, 805 (1952).
[3] H. O. W. Richardson and A. Leigh-Smith, Proc. Roy. Soc. (London) **A160**, 454 (1937).
[4] L. Cranberg, Phys. Rev. **77**, 155 (1950).
[5] D. K. Butt and W. D. Brodie, Proc. Phys. Soc. (London) **A64**, 791 (1951).

at each end of the counter by glass sleeves 5 mm in diameter. Electrostatic screening for the whole of the counter was provided by a large wire cage. The high voltage (working voltage was usually about 2400 volts) was obtained from a stabilized power supply, and the linear amplifier (E. K. Cole Ltd. Type 1008) was adjusted to work at a differentiation time of 10 microseconds and an integration time of 0.7 microsecond. The pulse distribution obtained from the counter could be recorded with an oscillograph equipped with a moving film camera, or by use of a single channel pulse analyzer. Good agreement was obtained using both methods, and the final results were obtained using the pulse analyzer.

The method of preparation of the radioactive lead tetramethyl is described in the appendix. Preliminary experiments in which nonradioactive lead tetramethyl was introduced in various amounts into a counter, together with argon and methane, showed that in order

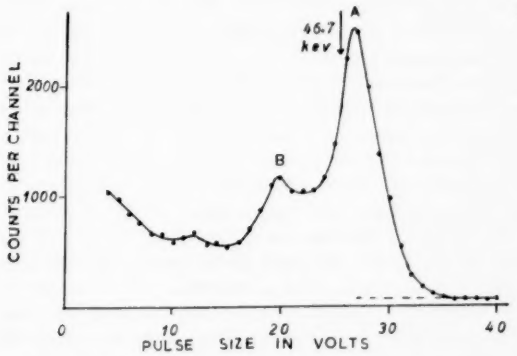

FIG. 1. Pulse-height distribution from proportional counter containing radioactive lead tetramethyl vapor, for the energy range 7 to 75 kev.

to obtain good proportionality (as checked by the line width obtained from external x-rays and γ-rays) the sample of lead tetramethyl must be thoroughly dried This was best achieved by desiccation with phosphorous pentoxide for periods of about 24 hours. It was at first thought that owing to the low energy of recoil of the Bi formed by the decay of RaD to RaE (0.08 ev for most of the disintegrations), there was some danger that volatile radioactive bismuth trimethyl might grow in the sample of liquid lead tetramethyl with a period of five days. Since, however, the age of the sample (from 1 to 3 days) produced no detectable difference in the pulse distribution obtained, it may be concluded that bismuth trimethyl is either not formed at all in the liquid lead tetramethyl or at the most in a very few percent of the disintegrations of the RaD. After introducing the lead tetramethyl vapor into the counter, however, measurements must be made within a few hours, because RaE, which has a half-life of 5 days, will grow inside the counter. Further preliminary experiments showed that when a few mm pressure of radioactive lead tetramethyl is introduced into the counter, only about 1 percent of it adheres to the walls, during times of the order of those used (not more than four hours).

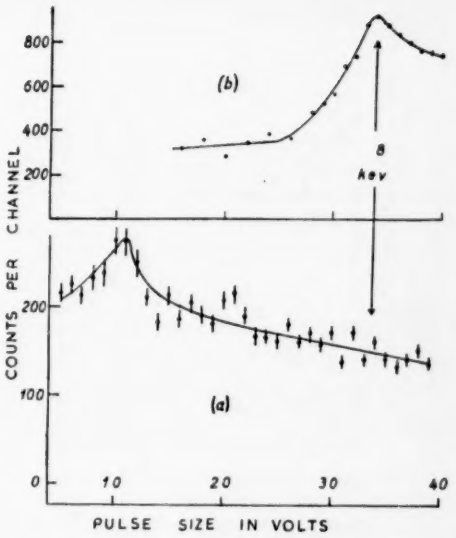

FIG. 2. (a) Pulse-height distribution from counter containing radioactive lead tetramethyl vapor, for the energy range from 1 to 9.5 kev. (b) Pulse distribution from a superimposed external source of RaD, taken with the same counter filling, to provide an energy calibration.

Energy calibrations were made by superimposing the L x-rays and γ-rays from an external source of RaD. The energies of the most intense of these radiations have already been investigated accurately, and we have also checked the values of these energies against the K x-rays of Fe^{55} which decays by K capture. As will be seen from the discussion of the results, the unconverted γ-ray at 46.7 kev provides a very useful calibration and defines the zero of the β-spectrum, since (as suggested above and, in fact, as confirmed) in the majority of the disintegrations the β-particles appear simultaneously with the quanta of 46.7 kev. At the same time the line widths obtained with the superimposed sources give a check of the proportionality of the gas mixture during the actual experiment.

EXPERIMENTAL RESULTS

The pulse distribution for the energy range of 7 to 75 kev is shown in Fig. 1. (This was obtained in an experiment in which 2 mm of lead tetramethyl vapor, together with 60-cm argon and 14-cm methane, gave a total counting rate of about 3000/sec.) The lower energies were examined at greater amplifications, and in Fig. 2(a) the range from 1 to 9.5 kev is shown. Figure 2(b) shows the distribution from the superimposed source of RaD (obtained by subtracting the pulse distribution without the external source from that ob-

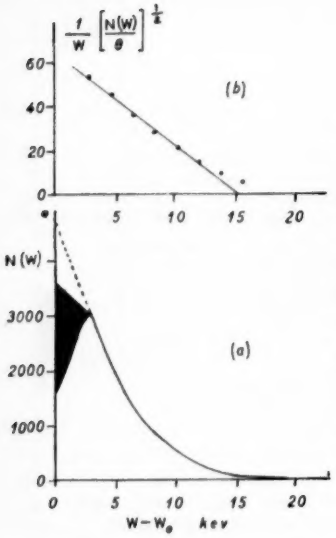

FIG. 3. (a) The solid curve shows the form of the β-spectrum found for RaD, the black area indicating the region of uncertainty below 3 kev. The dotted curve indicates the shape predicted by the Fermi theory, in the region where there is significant departure between the theoretical and experimental curves. (b) A Bleuler-Zünti plot of the experimentally found β-spectrum.

tained when the external source was superimposed) and displays the peak at about 8 kev, due to fluorescent x-rays of copper and zinc excited in the brass wall (see below).

Careful examination in the neighborhood of peak A, (Fig. 1), using the 46.7-kev γ-rays from an external source of RaD of approximate strength 0.5 millicuries, showed that the peak A was shifted towards higher energies by 2.7 ± 0.5 kev with respect to the peak of the superimposed 46.7-kev line. A strong external source must be used in this case owing to the low efficiency of the counter gas for the γ-rays and the necessity of obtaining a counting rate comparable with the internal counting rate; most of the softer L x-rays were removed by the use of a suitable filter.

THE SHAPE OF THE LOW ENERGY β-SPECTRUM

The width of the peak A (Fig. 1) is considerably greater than that obtained with an external source of 46.7-kev γ-rays (which has a semihalf-width of 1.7 kev as measured in the same counter with nonradioactive fillings). It is therefore to be interpreted as being due to the low energy β-spectrum coincident with quanta of total energy 46.7 kev as suggested above, and confirms that the lifetime of the 46.7-kev transition is less than the resolving time of the counter. Sometimes, however, the bismuth L x-rays produced after internal conversion in the L shell (mainly 10.8 and 13.0 kev) may escape from the counter. This gives rise to the peak B which occurs at 36.7 kev. The average escape probability has been very roughly estimated as 0.6–0.7, and using the value obtained by Kinsey[6] for the fluorescent yield of the L x-rays (0.47) it is possible to calculate the expected ratio of the areas of the two peaks; the experimental results are found to be in good agreement. The number of pulses corresponding to β-emission coincident with absorbed quanta of total energy 46.7 kev is found to be 73 percent of the number of disintegrations. The residual tail of low intensity on the high energy side of peak A can be accounted for by the random superposition of pulses due to the finite pulse duration and high counting rate, and probably also to the presence of a very small amount of RaE, perhaps in the form of bismuth trimethyl.

To determine the shape of the β-spectrum from the profile of peak A, after subtracting the extrapolated low intensity tail, it is necessary to take into account the statistical spread of pulse sizes, corresponding to a given energy, which is a characteristic of the proportional counter. Using the pulse distribution experimentally obtained from the 46.7-kev γ-rays from an external source, it is possible to estimate the amount of distortion of the β-spectrum associated with A. Since the semihalf-width at 46.7 kev is only 1.7 kev, it is found that the experimental curve must closely approximate to the shape of the β-spectrum down to about 3.5 kev (i.e., 50.2 kev in curve of Fig. 1). Below 3 kev, however, the shape cannot be uniquely determined from the results. Figure 3 shows the form of the β-spectrum obtained after correction for the statistical spread by successive approximations, and allowing for the small contribution from the peak B; the region of uncertainty below 3.5 kev is indicated by the shaded area. Further information on the β-spectrum below 3 kev is provided by the pulse distribution at low energies, shown in Fig. 2(a). As was explained above it may be expected that this distribution contains the pure low energy β-spectrum, though there may also be other causes contributing pulses to this region. It is interesting to see that the curve has a maximum at 2.4 kev. The existence of such a maximum in the β-spectrum would be consistent with the curve of Fig. 3(a).

COMPARISON OF THE β-SPECTRUM WITH THEORY

The Fermi theory for an allowed transition gives the form of the spectrum as

$$N(W)dW \propto p(W-W_0)^2F(Z,W)WdW.$$

The Coulomb factor $F(Z, W)$, neglecting the effects of screening, for which no adequate calculations are available (for high Z and such low energies), is given to a good approximation, for RaD, by $1/p$. Also W, the sum of the rest energy and the kinetic energy of the particle, is approximately constant over the range of the spectrum. Therefore, the form of the Fermi function approximates a parabola, $N(W) \propto (W-W_0)^2$. The effect of the Coulomb field is to increase the number of electrons in the low energy region and thus to remove the maximum normally obtained in allowed spectra of higher energies. Figure 3(b) shows a plot of $(1/W)\times[N(W)/\theta]^{\frac{1}{2}}$ against $W-W_0$ where θ is the funtcoin

[6] B. Kinsey, Can. J. Research **26**, 421 (1948).

defined and calculated by Bleuler and Zünti[7]), and it is seen that a good straight line is obtained from 3 to 13 kev; extrapolated, it gives an end point of 15.2 kev, which is also the mean value found from several sets of measurements. The accuracy of the above value is estimated as ±1 kev. In Fig. 3(a) the experimental curve closely coincides with the Fermi curve for $N(W)$ as a function of $W-W_0$, assuming an end point of 15.2 kev, down to 3 kev. The dotted curve below 3 kev shows the Fermi distribution in this region.

The results indicate that there are fewer electrons below 3 kev than predicted by the Fermi theory neglecting screening. It seems very likely that the departure can be explained by the effect of screening, since the latter reduces the effective Coulomb field and would thus tend to restore the maximum normally obtained.

As first pointed out by Schwartz and Edwards,[8] an experimental study of the β-spectrum of RaD should yield conclusive information on the effect of the change in binding energy of the atomic electrons on the shape of the β-spectrum. For RaD, calculations based on the Thomas-Fermi statistical model[9] lead to a value of about 10 kev for the change in atomic binding energy during the decay, and this is seen to be of the same order of magnitude as the maximum energy of the β-particles.

Since the above results show good agreement with the Fermi theory, at least down to 3 kev, it may be concluded that the relatively large change in atomic binding energy is included in the energy of the β-disintegration and is shared between the β-particle and the neutrino. This conclusion is in agreement with those recently obtained from theoretical considerations by Schwartz[10] and by Serber and Snyder.[11]

THE PULSE DISTRIBUTION IN THE LOW ENERGY REGION

In Fig. 1 the pulse distribution shows a rise towards low energies below 16 kev, and there is also an indication of a maximum at about 23 kev. A disturbing contribution to the low energy region is made by the wall and end effects which cause some of the high energy pulses to be thrown down into lower energies. The fraction of pulses thus distorted and their approximate distribution has been estimated theoretically (about 20 percent of the total number of pulses). Figure 4 shows the distribution obtained after subtracting this correction, the points below 7 kev being obtained from the results at higher amplifications [as shown in Fig. 2(a)] after normalizing the channel width. The correction hardly affects the pulse distribution at high energies, already discussed.

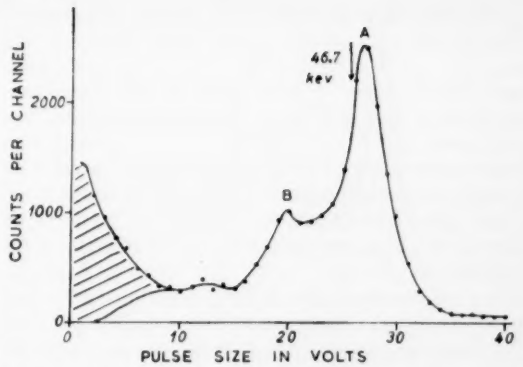

FIG. 4. The pulse-height distribution (obtained from results shown in Figs. 1 and 2) after correction for wall and end effects. The shaded area indicates the maximum possible contribution from the unaccompanied low energy β-spectrum.

The number of pulses below 15 kev in the corrected distribution amounts to about 13 percent of the total number of pulses. The low energy β-spectrum accompanied by unconverted 46.7-kev γ-rays (for which the counter efficiency is very low, and which therefore in most cases escape from the counter) should occur in only about 3.5 percent of the disintegrations.[1] This suggests that there is a contribution in this energy region from β-particles accompanied by metastable or unconverted γ-rays (the latter having a low efficiency for detection) other than the 46.7-kev γ-rays. The shaded area in Fig. 4 represents the largest contribution of the pure low energy β-spectrum which is compatible with the shape of the curve and also the form of the β-spectrum as previously found from the measurements at high energy described above. The exact significance of the remaining distribution (from 0–30 kev), obtained after deducting the shaded area, is not clear. It may include some low energy metastable γ-rays, in accordance with the hypothesis made above to account for the intensity of the pure low energy β-spectrum. In addition it is possible that a second more energetic β-spectrum exists of relatively low intensity; this would hardly affect the shape obtaining at high energies. This possibility has already been suggested by Cranberg[4] to explain his results using a magnetic β-ray spectrometer.

In a previous note[12] we have mentioned that there was evidence to believe that such a more energetic β-spectrum was in cascade with a γ-ray at 7.8 kev. A γ-ray of this energy has been reported by Curran, Angus, and Cockcroft[13] using proportional counters and was also apparently detected by the present authors.[14] Mr. D. West (of Harwell, England) has, however, kindly informed us in a private communication that he

[7] E. Bleuler and W. Zünti, Helv. Phys. Acta **19**, 375 (1946).
[8] H. M. Schwartz and R. R. Edwards, J. Chem. Phys. **19**, 385 (1951).
[9] Z. Hund, *Handbuch der Physik* (Julius Springer, Berlin), second edition, p. 621.
[10] H. M. Schwartz, Phys. Rev. **86**, 195 (1952).
[11] R. Serber and H. S. Snyder, Phys. Rev. **87**, 152 (1952).
[12] A. A. Jaffe and S. G. Cohen, Phys. Rev. **86**, 1041 (1952).
[13] Curran, Angus, and Cockroft, Phil. Mag. **40**, 36 (1949).
[14] S. G. Cohen and A. A. Jaffe, Phys. Rev. **86**, 800 (1952).

obtained no trace of a line at 7.8 kev using a proportional counter with *glass* walls and a thin mica window, and he suggests that the 7.8-kev line, found by the above-mentioned authors, has its origin in the fluorescent x-rays of copper (8.05 kev) excited in the wall of the counter by the L x-rays of RaD. We have since confirmed by absorption experiments, using the same *brass* walled counter with which we had previously observed the "7.8-kev line," that this line is in fact produced by fluorescent x-rays from the copper and zinc in the counter wall.

We wish to thank Dr. S. Israelshvili of the Department of Organic Chemistry, Hebrew University, for his advice on the synthesis of lead tetramethyl, and also Mr. S. Friedman, who built the pulse analyzer.

APPENDIX

Preparation of Radioactive Lead Tetramethyl

RaD (dissolved in nitric acid and in equilibrium with its products) was added to a carrier solution containing usually from about 5–10g of ordinary lead in the form of lead nitrate. By the addition of excess dilute HCl the RaD was precipitated with carrier as lead chloride, and this precipitate was washed several times with water and acetone and then thoroughly dried. It was found by preliminary experiment that the lead chloride so obtained contained less than 3 percent of the RaE and RaF originally in equilibrium with the RaD. This precipitate was refluxed with an ethereal solution of the freshly prepared Grignard reagent (methyl magnesium iodide) for about 3 hours. After destroying any excess Grignard by the addition of water, the resulting ethereal solution of lead tetramethyl was separated, dried with calcium chloride, and distilled, the lead tetramethyl (bp 110°C) being collected.

PHYSICAL REVIEW VOLUME 89, NUMBER 2 JANUARY 15, 1953

Proof That Probability Density Approaches $|\psi|^2$ in Causal Interpretation of the Quantum Theory

DAVID BOHM
Faculdade de Filosofia, Ciencias e Letras, Universidade de São Paulo, São Paulo, Brazil
(Received June 25, 1952)

In two previous papers a causal interpretation of the quantum theory was developed which involved the hypothesis that a quantum-mechanical system contains a precisely defined particle variable $\mathbf{x}$ but that, at present, we are restricted to calculating the probability density $P(\mathbf{x}, t)$ that the particle is at the position $\mathbf{x}$. It was shown that the assumption that $P(\mathbf{x}, t)=|\psi(\mathbf{x}, t)|^2$ is consistent, in the sense that if it holds initially, the equations of motion of the particles will cause this relation to be maintained for all time. In this paper, we extend the theory by showing that as a result of random collisions, an arbitrary probability density will ultimately decay into one with a density of $|\psi(\mathbf{x}, t)|^2$. Since all quantum-mechanical experiments to date have been concerned with statistical ensembles of systems that have been colliding with other systems for a very long time, it is therefore inevitable that as we draw samples from such ensembles, the probability density of systems with particles at the point $\mathbf{x}$ will be equal to $|\psi(\mathbf{x}, t)|^2$.

In the previous papers we also pointed out that, within the conceptual framework of the causal interpretation, it was possible to suggest mathematical theories more general than are permitted by the usual interpretation and that these more general theories might be needed in the domain of 10^{-13} cm, where present theories seem to fail. However, if these more general theories should apply at the level of 10^{-13} cm, then there would be a tendency to create discrepancies between P and $|\psi|^2$, a tendency whose cumulative effects should be felt even at the atomic level, where the more general theory ought to approach the usual theory. However, because those discrepancies have been shown to die out as a result of collisions, we can expect that under normal conditions the difference between P and $|\psi|^2$ would be negligible. Conditions are suggested, however, in which this difference might be appreciable, and experiments are indicated which might be able to test for the existence of such discrepancies.

I. INTRODUCTION

IN two recent papers,[1] (to be denoted hereafter by I and II, respectively) the author has proposed a causal reinterpretation of the quantum theory, based on the following hypotheses:

(a) A quantum-mechanical system, such as an electron, consists basically of a particle having a precisely defined position, which varies continuously as a function of the time.

(b) This particle is acted on not only by the classical potential $V(\mathbf{x}, t)$ but also by an additional quantum-potential $U(\mathbf{x}, t)$, which is important at the atomic level but negligible at the macroscopic level.

(c) If we write $\psi=Re^{iS/\hbar}$, where ψ is the wave function and R and S are real, then the quantum potential is given by

$$U(\mathbf{x}, t)=-(\hbar^2/2m)\nabla^2 R(\mathbf{x}, t)/R(\mathbf{x}, t). \quad (1)$$

The equation of motion of the particle then takes the form

$$m d^2\mathbf{x}/dt^2=-\nabla\{U(\mathbf{x}, t)+V(\mathbf{x}, t)\}. \quad (2)$$

To obtain the same predictions for all experimental results as are obtained from the usual interpretation of the quantum theory it is necessary, however, to make the following additional special assumptions (see paper I, p. 171):

(1) The ψ field satisfies Schrödinger's equation.

(2) The particle velocity is restricted to $\mathbf{v}=\nabla S(\mathbf{x})/m$.

[1] D. Bohm, Phys. Rev. **85**, 166 (1952) (paper I); **85**, 180 (1952) (paper II). See also, Phys. Rev. **87**, 389 (1952).

(3) We do not predict or control the precise location of a particle, but have a statistical ensemble of particles with a probability density, $P(\mathbf{x})=|\psi(\mathbf{x})|^2$.

It was suggested in paper I, Sec. 4, that if we gave up the special assumptions listed above, the causal interpretation of the quantum theory would permit the construction of new types of theories which might be needed in the treatment of certain domains, such as that involving distances of the order of 10^{-13} cm, where existing theories do not seem to be adequate. In support of this suggestion it was actually demonstrated in paper I, Sec. 9, that theories could be formulated, in which assumptions (1) and (2) ceased to be valid at the level of 10^{-13} cm but became approximately valid at the atomic level, where the usual theory is known to be applicable. No similar proof was given in papers I and II, however, with regard to assumption (3), although the conjecture was made in paper II, Sec. 7, that the effects of collisions and other random processes would be to cause any differences between $P(\mathbf{x})$ and $|\psi(\mathbf{x})|^2$ to decay with the passage of time, and thus to tend to establish the validity of assumption (3) at the atomic level, even under conditions in which it failed in the domain of 10^{-13} cm. The object of the present paper is to prove the above conjecture.

We begin our proof by noting that, in general, the probability density $P(\mathbf{x})$ may be an arbitrary function, restricted only by the requirement that it satisfies the conservation equation

$$(\partial P/\partial t)+\operatorname{div}(P\mathbf{v})=0. \tag{3}$$

But as shown in paper I, Sec. 4, provided that ψ is a solution of Schrödinger's equation and that $\mathbf{v}=\nabla S/m$, (i.e., provided assumptions (1) and (2) are valid), the function $|\psi(\mathbf{x}, t)|^2$ will satisfy a similar conservation equation

$$\begin{aligned}\partial|\psi|^2/\partial t+\operatorname{div}(|\psi|^2\nabla S/m)\\ =\partial|\psi|^2/\partial t+\operatorname{div}(|\psi|^2\mathbf{v})=0.\end{aligned} \tag{4}$$

Clearly, then if $P(\mathbf{x})$ is chosen initially equal to $|\psi(\mathbf{x})|^2$, the two will remain equal for all time; and thus, the consistency of assumption (3) is demonstrated. Any failure of assumptions (1) and (2) would, however, also result in the failure of (3), since $P(\mathbf{x})$ would be still conserved, while $|\psi(\mathbf{x})|^2$, in general, would not. Thus, if deviations from (1) and (2) really existed, for example, at the level of 10^{-13} cm, differences between P and $|\psi|^2$ would arise whose cumulative effects would in general be felt even at the atomic level, unless there exist opposing processes which tend continually to re-establish the equality of P and $|\psi|^2$. As we have already pointed out, we shall demonstrate in this paper that randomly distributed collisions furnish just such opposing processes, which in the absence of perturbations from the level of 10^{-13} cm would cause an arbitrary probability density $P(\mathbf{x}, t)$ to decay into $|\psi(\mathbf{x}, t)|^2$ with the passage of time. Clearly this result constitutes an important part of the causal interpretation of the quantum theory, since it shows that the causal interpretation could have an experimental content different from that of the usual interpretation at 10^{-13} cm and still lead to agreement with all experimental data that can now be understood in terms of the usual interpretation.

To show the importance of collisions in determining the probability density, we first note that all experiments in quantum mechanics to date have been concerned with statistics of systems (such as hydrogen atoms) drawn from large aggregates of matter, where they have been interacting with other systems for a very long time. When we do an experiment now, we have no choice but to drawn our samples from such an ensemble, whose members have undergone this lengthy process of collision with other atoms, electromagnetic waves, sound waves, and other disturbances which can alter the physical condition of the members of our ensemble. Now, each collision of, for example, a hydrogen atom with another atom can change the positions of the precisely defined particles located in each atom in a way that depends on the collision parameter and on the initial velocity of approach. Since there is a statistical ensemble of different kinds of collisions, we conclude that even if all the particles in our ensemble initially has the same positions, they would have some kind of distribution after collision.

To study how this probability distribution changes in a collision, we shall find it convenient to define a function $f(\mathbf{x}, t)$ through the equation

$$P(\mathbf{x}, t)=|\psi(\mathbf{x}, t)|^2 f(\mathbf{x}, t). \tag{5}$$

Since $P(\mathbf{x}, t)$ satisfies the conservation equation (3), while $|\psi(\mathbf{x}, t)|^2$ satisfies the similar Eq. (4), we readily find by subtracting (4) from (3) that

$$\partial f/\partial t+\mathbf{v}\cdot\nabla f=0. \tag{6}$$

But the above is just df/dt, the rate of change of f which results from following a particle orbit. We obtain, therefore, $df/dt=0$ and

$$f(\mathbf{x}, t)=f(\mathbf{x}', t'), \tag{7}$$

where $\mathbf{x}'$ is the position of a particle at the time t' which arrives at the position $\mathbf{x}$ at the time t.

Equation (7) is analogous to Liouville's theorem in classical statistical mechanics, with the important difference that in quantum theory, the ratio $f=P/|\psi|^2$ is what remains constant when we follow a moving particle, while in classical statistical mechanics it is the density $\rho(\mathbf{x}, \mathbf{p}, t)$ of points in phase space that remains constant. However, by methods that are very similar to those that can be used in classical statistical mechanics to show that $\rho(\mathbf{x}, \mathbf{p}, t)$ approaches a constant[2] along any

[2] Note that this result is not to be confused with the statement that $\rho(\mathbf{x}, \mathbf{p}, t)$ remains constant when $\mathbf{x}(t)$ and $\mathbf{p}(t)$ are solutions of the equations of motion. For in this case, even though ρ depends on $\mathbf{x}$, $\mathbf{p}$, and t, the dependence is such that there is no net change in ρ when we follow a trajectory of a particle in phase space. However, after many collisions, the functional form of ρ itself

surface of constant energy, we shall show in this paper that $f(\mathbf{x}, t)$ approaches a constant, so that P approaches $|\psi|^2$. Moreover, once P has become equal to $|\psi|^2$, no disturbance satisfying conditions (1) and (2) can possibly produce a difference between these two quantities, because the relation $P=|\psi|^2$ is then maintained for all time by the equations of motion of the particles.

The above results are deduced with the aid of assumptions (1) and (2), which certainly hold in the atomic domain. If, in this domain, perturbations arising at the level of 10^{-13} cm should create discrepancies between P and $|\psi|^2$, we should then expect that these discrepancies would die out in some mean time T, which is determined by the solutions of the equations of motion of the various particles involved and by the rates of collisions of these particles. In the steady state, the difference $P-|\psi|^2$ will be determined by the balance between the mean rate R, at which perturbations surge up from the level of 10^{-13} cm, and the mean rate $(P-|\psi|^2)/T$, at which a perturbation already in existence dies out. This yields

$$P-|\psi|^2=RT. \tag{8}$$

Now in the absence of any specific hypothesis as to what is happening at 10^{-13} cm, it is impossible for us to know anything about R, except that with the limitless number of conceivable hypotheses available any value at all is possible. Thus, if we assume the causal interpretation, we can always regard any experiments which show that P is equal to $|\psi|^2$ as *a posteriori* evidence that R is so small that discrepancies between P and $|\psi|^2$ have not yet been detected. This means that no experiment can possibly show that the usual interpretation must be chosen in preference to the causal interpretation. On the other hand, an experimentally observed discrepancy between P and $|\psi|^2$ would clearly indicate that the usual interpretation was untenable and that a causal interpretation was probably needed.[3]

An actual experimental test of the relation $P=|\psi|^2$ would be impracticably difficult at present, but as shown in paper II, the usual formulas for transition probabilities are, in the causal interpretation, consequencies of the assumption that $P=|\psi|^2$. Hence, if this assumption is not entirely true, we should expect to find discrepancies, probably rather small, between the observed mean rates of transitions and the rates predicted by present theories. We must study these discrepancies under conditions in which ψ is known to a high degree of accuracy. From this point of view, the best transition processes to study would probably be those involving radiation from atoms of hydrogen. However, to reduce the rate at which discrepancies between P and $|\psi|^2$ die out, we should avoid collisions by keeping the atoms under conditions of extreme isolation and avoid the effects of thermal radiation by keeping them at very low temperatures. To increase the rate R at which discrepancies between P and $|\psi|^2$ come up from the level of 10^{-13} cm, we should use atoms whose nuclei are very highly excited. Experimental evidence testing the accuracy of the predictions of the usual interpretation concerning rates of transition is at present rather rough and limited in quantity, and of course, no experiments have as yet been done with a view to finding conditions that are likely to lead to a maximum discrepancy between P and $|\psi|^2$.

II. PROOF THAT $P(x,t)$ APPROACHES $|\psi(x,t)|^2$

On the basis of the assumption that ψ satisfies Schrödinger's equation and that $\mathbf{v}=\nabla S/m$, we shall now show with the aid of a simple illustrative example that an arditrary probability density $P(\mathbf{x}, t)$ ultimately approaches $|\psi(\mathbf{x}, t)|^2$. This proof will be generalized in a more extensive paper to be published elsewhere.[4]

We choose for our example a hydrogen molecule excited to a doubly degenerate level of energy E_0, in which the component of the angular momentum in the direction of the axis of the molecule is, in the usual interpretation, said to be $\pm\hbar$. In terms of cylindrical polar coordinates, with the z axis along the axis of the molecule, the most general linear combination of these two degenerate eigenfunctions can be written as

$$\psi=\sqrt{2}g(\rho, z)(c_1\cos\phi+c_2\sin\phi)e^{-iE_0t/\hbar}, \tag{9}$$

where c_1 and c_2 are arbitrarily complex coefficients, satisfying the relation

$$|c_1|^2+|c_2|^2=1, \tag{10}$$

and where $g(\rho, z)$ is real and satisfies the normalization condition

$$\int_{-\infty}^{\infty}\int_{0}^{\infty}(g(\rho, z))^2\rho d\rho dz=1. \tag{11}$$

Equation (10) permits us to write

$$c_1=e^{i\alpha_1}\cos\omega; \quad c_2=e^{i\alpha_2}\sin\omega. \tag{12}$$

With these substitutions, we obtain (with $\psi=Re^{iS/\hbar}$,

$$\tan\frac{(S+E_0t)}{\hbar}=\frac{\cos\omega\sin\alpha_i\cos\phi+\sin\omega\sin\alpha_2\sin\phi}{\cos\omega\cos\alpha_1\cos\phi+\sin\omega\cos\alpha_2\sin\phi}. \tag{13}$$

We note that S is a function only of ϕ. This means that the velocity has a component only in the direction

changes and approaches a constant along any surface of constant energy. Similarly, from Eq. (7) we see that $f(\mathbf{x}, t)$ is a constant along any particle trajectory regardless of the form of f, but we now assert that after many collisions, the functional form of f changes in such a way that f approaches a constant.

[3] In fact, we can go further and say that after we reach the stage of postulating a particular example of a causal theory, experiments are conceivable (as shown in paper II, Sec. 6) which would permit us to infer the necessity of each element in the hypothesis underlying that particular theory; or in other words, to "observe" or detect that element.

[4] D. Bohm, *Anais da Academia Brasileira de Ciências* (to be published).

of ϕ, given by

$$V_\phi=\rho\frac{d\phi}{dt}=\frac{1}{\rho}\frac{\partial S}{\partial\phi}=\frac{1}{\rho}\frac{\cos\omega\sin\omega\sin(\alpha_2-\alpha_1)}{1+\sin\omega\cos\omega\cos(\alpha_2-\alpha_1)\sin 2\phi}. \quad (14)$$

Each electron moves in a circle, with a speed that depends on the angle ϕ, as well as on ρ. The solution of (13) is readily seen to be

$$-\tfrac{1}{2}\cos 2\phi\cos(\alpha_2-\alpha_1)\sin\omega\cos\omega+\phi-\phi_0 = (t/\rho^2)\cos\omega\sin\omega\sin(\alpha_2-\alpha_1), \quad (15)$$

where ϕ_0 is a constant of integration. Three types of orbits are possible. For $\omega=0, \pm\pi/2, \pm\pi$, we obtain ϕ constant, so that the particle does not move. For ω close to these values (and for ρ large), the particle oscillates on an arc of a circle. For large ratios of $\sin\omega\cos\omega/\rho$, the particle rotates in a complete circle with variable angular velocity.

Let us now consider, for any given ρ, a statistical ensemble of particles all having the same initial wave function, but having an arbitrary initial probability distribution $P_0(\phi)$. Although this distribution will, in general, change with time as a result of particle motions, it is clear that after the particles return to their initial positions, they will have the same separation as they had initially (since each follows a periodic orbit with the same period); so that as long as the molecule is isolated, we shall have only a periodically varying probability distribution. In practice, however, the molecule is not really isolated, since it is subjected to a continual series of collisions with other particles. To study the effects of these collision processes, we must, of course, first solve for the changes in the wave function resulting from the influence of the other particles and then use this solution to calculate the particle motions through the relation $\mathbf{v}=\nabla S/m$.

Now, in our simple illustrative example, it will be adequate to assume an incident particle whose mass M is so great that it can be treated classically (noting, however, that in our more complete article[4] it is shown that the same results will follow if this approximation is not made). In the causal interpretation, a classical approximation for the incident particle means that we can neglect the contribution

$$-(\hbar^2/2M)\nabla_{\mathbf{y}}^2|\Psi(\mathbf{x},\mathbf{y},t)|/|\Psi(\mathbf{x},\mathbf{y},t)|$$

of this particle (whose coordinates are denoted by $\mathbf{y}$) to the quantum potential and that we can approximate the wave equation as

$$i\hbar\frac{\partial\psi}{\partial t}=\frac{1}{2m}\left(\frac{\hbar}{i}\nabla_{\mathbf{x}}-\frac{e}{c}\mathbf{A}(\mathbf{x},\mathbf{y}(t))\right)^2\psi+V(\mathbf{x},\mathbf{y}(t))\psi,$$

where $\mathbf{y}(t)$ is regarded only as a parameter, whose time dependence is obtained by solving the equations of motion, and where $V(\mathbf{x},\mathbf{y})$ is the classical potential energy of interaction between $\mathbf{x}$ and $\mathbf{y}$, and $\mathbf{A}(\mathbf{x},\mathbf{y})$ the classical vector potential (due to magnetic interactions).

Let us further restrict ourselves to collisions so distant that perturbation theory may be applied. Now the major changes of the wave function will be due to transitions between degenerate levels, and as will soon be evident, no essential aspect of the problem will be altered if we made the further approximation of neglecting the comparatively unimportant transitions to levels of other energies. The changes in the wave function will then be determined by the three matrix elements

$$V_{11}(t)=2\int\cos\phi g(\rho,z)H_P(\mathbf{x},\nabla_{\mathbf{x}},t)g(\rho,z)\cos\phi d\mathbf{x}, \quad (14a)$$

$$V_{22}(t)=2\int\sin\phi g(\rho,z)H_P(\mathbf{x},\nabla_{\mathbf{x}},t)g(\rho,z)\sin\phi d\mathbf{x}, \quad (14b)$$

$$V_{12}(t)=V_{21}^*(t)=2\int\cos\phi g(\rho,z)H_P(\mathbf{x},\nabla_{\mathbf{x}},t) \times g(\rho,z)\sin\phi d\mathbf{x}, \quad (14c)$$

where $H_P(\mathbf{x},\nabla_{\mathbf{x}},t)$ is the part of the Hamiltonian operator corresponding to the perturbation. These matrix elements define the unitary transformation

$$c_1=\alpha_{11}(t)c_1'+\alpha_{12}(t)c_2', \quad c_2=\alpha_{21}(t)c_1'+\alpha_{22}(t)c_2',$$

where the α_{ij} satisfy the following condition for a unitary matrix

$$|\alpha_{11}|^2+|\alpha_{21}|^2=|\alpha_{12}|^2+|\alpha_{22}|^2=1, \quad \alpha_{11}\alpha_{12}+\alpha_{21}\alpha_{22}=0, \quad (16)$$

and where the c_j' represent the values of the coefficient of the wave function at time t' before collision, while the c_i represent those values at the time t after collision.

The transformation matrix $\alpha_{ij}(t)$ can in principle be obtained by carrying out a series of infinitesimal unitary transformations, with the transformation matrices $(1-iV_{ij}(t)dt/\hbar)$; but because the $V_{ij}(t)$ are all in general different functions of the time, the transformation coefficients $\alpha_{ij}(t)$ cannot in general be expressed in a closed form. Because the dependence of V_{ij} on the time will depend on the orbit of the incident particle, it is clear that the $\alpha_{ij}(t)$ will in general be different for different kinds of collisions. This means that the relation between c_i and c_j' will depend on the collision parameter $\mathbf{h}$ and on the initial velocity of approach $\mathbf{u}$, which quantities determine the orbit of the incident particle in a collision. Thus, we can write

$$c_j'=c_j'(c_i,\mathbf{h},\mathbf{u}).$$

Because the c_i and c_j' satisfy the identity $|c_1|^2+|c_2|^2=|c_1'|^2+|c_2'|^2=1$, which results from the unitary character of the transformation, it is better, however, to work in terms of the three independent parameters introduced in Eq. (12). We obtain

$$\omega'=\omega'(\omega,\alpha_1,\alpha_2,\mathbf{h},\mathbf{u});$$

$$\alpha_1'=\alpha_1'(\omega,\alpha_1,\alpha_2,\mathbf{h},\mathbf{u}); \quad \alpha_2=\alpha_2'(\omega,\alpha_1,\alpha_2,\mathbf{h},\mathbf{u}). \quad (17)$$

Now the various members of our ensemble of hydrogen molecules undergo collisions having a continuously and more or less randomly distributed set of values of $\mathbf{h}$ and $\mathbf{u}$; and as a result even if the c_j' were all initially the same before collisions, they would be distributed statistically after collisions.[b] We are therefore led to define the probability

$$Q(\omega, \alpha_i, \alpha_2, t)d\omega d\alpha_1 d\alpha_2 = Q(c_i, t)d\Omega,$$

where $d\Omega = d\omega d\alpha_1 d\alpha_2$ that the wave-function coefficients lie in the region $d\Omega$. Our problem is then to study how the function Q is changed during a collision. Now in any particular collision, carrying the coefficients from c_j' to c_i, the volume element $d\Omega'$ is carried into some other volume element $d\Omega$. It can then easily be shown that because of the unitary character of the collision,

$$d\Omega' = d\Omega. \tag{18}$$

This follows from the fact that a unitary transformation produces a rotation in the four-dimensional space, whose coordinates are the real and imaginary coefficients of the c_i. Thus, the volume element in the space is not changed, and from this fact we readily obtain Eq. (18). Since the number of systems does not change in a collision, we also have $Q(c_i, t)d\Omega = Q(c_j', t)d\Omega'$ and therefore obtain for the probability density of systems,

$$Q(c_i, t) = Q(c_i', t'). \tag{19}$$

Because the matrix elements $V_{ij}(t)$ vanish as $t \to \pm\infty$, the coefficients c_i will change only during the short time in which the potential is appreciable. Thus, if t represents any time after the n^{+n} collision and before the $(n+1)^{+n}$, while t' represents any time before the n^{+n} collision and after the $(n-1)^{+n}$, we do not need to consider the explicit time dependence of Q but can write instead

$$Q_{n+1}(c_i) = Q_n(c_j'), \tag{20}$$

where $Q_{n+1}(c_i)$ represents the value of $Q(c_i, t)$ after the n^{+n} collision.

We must now take into account the fact that there is a statistical ensemble of collisions of different types. To do this we define the probability $F(\mathbf{h}, \mathbf{u})d\mathbf{h}d\mathbf{u}$ that a collision occurs with collision parameter in the range $d\mathbf{h}$ and the velocity of approach in the range $d\mathbf{u}$. The next step is to eliminate the components of the collision parameter $\mathbf{h}$, in terms of the variables ω, α_1, α_2, with the aid of Eq. (17). This is permissible only if the Jacobian determinant $J(\partial\omega/\partial h_x, \partial\alpha_1/\partial h_y, \partial\alpha_2/\partial h_z)$, does not vanish identically. The identical vanishing of this determinant would imply that there was a functional relationship between ω, α_1, α_2. But as has already been shown, a three-parameter distribution of collisions (over the variable $\mathbf{h}$ for a given $\mathbf{u}$) will in general produce a three-parameter distribution of the c_i' for a given c_j', so that there can be no functional relationship between ω, α_1, α_2 and the determinant $J(\partial\omega/\partial h_x, \partial\alpha_1/\partial h_y, \partial\alpha_2/\partial h_z)$ cannot vanish identically. We can therefore define the probability,

$$G(c_j', c_i, \mathbf{u}, t, t')d\Omega' d\mathbf{u} = FJ(\partial h_x/\partial\omega, \partial h_y/\partial\alpha, \partial h_z/\partial\alpha_2)d\Omega' d\mathbf{u}, \tag{21a}$$

that the system makes a collision starting in the range $d\Omega' d\mathbf{u}$ and ending up with a given set of wave-function coefficients c_i. Clearly, by definition

$$\int G(c_j', c_i, \mathbf{u}, t')\, d\Omega' d\mathbf{u} = 1. \tag{21b}$$

The precise form of the function G is determined by the distribution function F and by the matrix elements $V_{ij}(t)$ in a very complicated way, but the only property of G that is of interest here is the fact that it is a continuous function of all its variables. This property of continuity follows from the continuity of F, the continuity of the relations (17), and the existence of the determinant $J(\partial h_x/\partial\omega, \partial h_y/\partial\alpha_1, \partial h_z/\partial\alpha_2)$. The continuity of F, however, follows from the assumption of a more or less random distribution of collision parameters and velocities of approach. It is here that we introduce the fundamental statistical element into our treatment.

To calculate the probability density $Q_{n+1}(c_i)$ of wave-function parameters existing after the nth collision, we need only average the contributions to Q_{n+1} coming from the various types of collisions. But each contribution satisfies Eq. (19). Thus, we obtain the following integral equation, which defines the way in which Q_n changes as a result of a collision:

$$Q_{n+1}(c_i) = \int G(c_i, c_j', \mathbf{u})Q_n(c_j')d\Omega' d\mathbf{u}. \tag{22}$$

We are now ready to show that $Q_n(c_j')$ approaches a constant as $n \to \infty$. First, we note that if $Q_n(c_j')$ is a constant, then by virtue of Eq. (21b), we obtain $Q_{n+1} = Q_n$. Thus, Q_n = constant is a possible equilibrium solution. If $Q_n(c_j')$ is not a constant, then let us denote by A_n its maximum value (as a function of all its variables). This maximum must exist, because by hypothesis, $Q_n(c_j')$ is a continuous function. Let us also denote by B_n the minimum value of $Q_n(c_j')$, and let us restrict ourselves for the time to the case in which there is only one point at which $Q_n(c_j')$ takes on the value A_n (and also only one point at which it takes the value B_n). Then since $Q_n(c_j') < A_n$ for all points except one we

[b] It is important to note here that the range of values of c_i, resulting from a given set of c_j', covers some three-dimensional region (or more precisely a set of finite measure) in the space of ω, α_1, α_2. This can be seen, from the fact that our group of infinitesimal transformations is isomorphic with the group of infinitesimal rotations on a two component spinor. As a result of the continuous distribution over $\mathbf{h}$, we shall have, in general, a continuous distribution of the $V_{ij}(t)$ for a given $\mathbf{u}$; and as a result of the continuous distribution over $\mathbf{u}$, a continuous distribution of the V_{ij} for a given $\mathbf{h}$. Thus, for each value of $\mathbf{h}$ (or of $\mathbf{u}$), we shall obtain a three-parameter distribution over ω, α_1, α_2, for a given ω', α_1', α_2' (or of ω', α_1', α_2' for a given ω, α_1, α_2).

obtain, with the aid of Eq. (21b),

$$Q_{n+1}(c_i) < \int G(c_i, c_j', \mathbf{u}) A_n d\Omega' d\mathbf{u} = A_n, \quad (22a)$$

and similarly, since $Q_n(c_j') > B_n$ except for one point, we have

$$Q_{n+1}(c_i) > \int G(c_i, c_j', u) B_n d\Omega' d\mathbf{u} = B_n. \quad (22b)$$

This means that $Q_{n+1}(c_i)$ can nowhere be as large as the maximum of $Q_n(c_j')$ nor as small as the minimum of $Q_n(c_j')$. Hence, the maximum of $Q_{n+1}(c_i)$ must be less than that of Q_n, and its minimum must be greater than that of Q_n. In other words,

$$A_{n+1} < A_n; \quad B_{n+1} > B_n. \quad (23)$$

On the basis of the above results, it seems clear on intuitive grounds that $Q_n(c_i)$ must approach a constant as $n \to \infty$. To prove that this happens, we shall show that the hypothesis that it does not approach a constant leads to a contradiction. We let $Q_\infty(c_i)$ represent the limiting form of $Q_n(c_i)$. We can then write $Q_n(c_i) = Q_\infty(c_i) + \epsilon_n(c_i)$, where $\epsilon_n(c_i)$ is a term that approaches zero uniformly as $n \to \infty$. Let us now evaluate $Q_n(c_i^m) - Q_{n+1}(c_i^m)$, where c_i^m is the point at which $Q_\infty(c_i)$ has its maximum value A_∞. We have

$$Q_n(c_i^m) - Q_{n+1}(c_i^m) = A_\infty - Q_{n+1}(c_i^m) + \epsilon_n(c_i^m),$$

and

$$A_\infty - Q_{n+1}(c_i^m) = \int G(c_i^m, c_j', \mathbf{u}) \times (A_\infty - Q_\infty(c_j') + \epsilon_n(c_j')) d\Omega' d\mathbf{u}.$$

But if $Q_\infty(c_j')$ is not a constant function of its arguments, then in the region in which G is appreciable, $A_\infty - Q_\infty(c_j')$ will be some finite number which does not approach zero as $n \to \infty$. We conclude then that $Q_n(c_i^m) - Q_{n+1}(c_i^m)$ also does not approach zero as $n \to \infty$. This contradicts the hypothesis that $Q_n(c_i)$ approaches $Q_\infty(c_i)$ as a limit, since such an approach requires that $Q_{n+1}(c_i) - Q_n(c_i)$ approach zero for all c_i. We conclude then that $Q_n(c_i)$ must approach a constant as $n \to \infty$.

We shall now remove the limitation that $Q_n(c_j')$ takes on its maximum (or minimum) value at only one point. First, we note that if $Q_n(c_j')$ takes on the value A_n (or B_n) on a set of isolated points, curves or surfaces, of dimensionality lower than that of the space of the ω, α_1, α_2 (or more generally, on a set of measure zero in this space), then it is obvious that the reasoning goes through precisely the same lines as before. If, however, $Q_n(c_j')$ should happen to take on the value A_n in a three-dimensional domain (or more generally in a region of finite measure in the space of ω, α_1, α_2) and if this region is bigger than the domain in which $G(c_i, c_j', \mathbf{u})$ is different from zero, the problem is a little more complicated, because one then obtains the result that $A_{n+1} = A_n$. However, if we evaluate $Q_{n+1}(c_i)$ near the edge of such a domain, we obtain contributions to the integral from regions in which $Q_n(c_j') < A_n$, so that at such points, $Q_{n+1}(c_i) < A_n$. Thus, in each collision, the special domain in which $Q_n(c_j') = A_n$ is narrowed until there is left only an isolated maximum point, and the problem is then reduced to the case originally considered.

The significance of our result is that after many collisions, the probability density for any set of wave-function coefficients, as defined by the ω, α_1, α_2, will be uniform. This means that each coefficient has a random phase and that there is a uniform probability for all values of ω (ω defines the absolute magnitude of the wave-function coefficients $\cos\omega$ and $\sin\omega$, of c_1 and c_2, respectively). But this is exactly what would be obtained from the usual quantum-statistical mechanics for the case of an ensemble of systems, each having two degenerate levels. This result is not surprising, since the causal interpretation treats the wave function in exactly the same way as does the usual interpretation.

It is important to note that the continuity of the function $G(c_i, c_j', \mathbf{u})$ played an essential role in the proof that $Q_n(c_i)$ approaches a constant as $n \to \infty$. Thus, if G had been a function that was zero everywhere except at certain isolated points, we could not have shown that $A_{n+1} < A_n$. For in this case, if the function $Q_n(c_j')$ had taken on its maximum value at precisely those points where G did not vanish, we should have obtained $A_{n+1} = A_n$. But the continuity of G guarantees that the integral expressing $Q_{n+1}(c_i)$ in terms of $Q_n(c_j')$ must obtain contributions from regions in which $Q_n(c_j')$ is less than its maximum, so that $A_{n+1} < A_n$. As we have seen, the continuity of G originates in the assumption of a more or less random distribution of types of collision. Thus, the approach of $Q_n(c_i)$ to its equilibrium value is based on the random character of the collision processes.

Let us now consider the particle motions. In general, these are rather difficult to solve for; but as in the case of the wave-function coefficients we are not interested in the details, but only in the fact that a statistical ensemble of collisions will lead to a corresponding statistical ensemble of changes in particle positions. By integrating the relation $\mathbf{V} = \nabla S/m$, we see that the initial position $\mathbf{x}'$ of a particle is a function of the final position $\mathbf{x}$, the final wave-function coefficients c_i, the collision parameter $\mathbf{h}$, and the initial velocity of approach $\mathbf{u}$. But as shown in Eq. (17), we can eliminate $\mathbf{h}$ in terms of c_i and c_j'. We then get

$$\mathbf{x}' = \mathbf{x}'(c_i, c_j', \mathbf{u}, \mathbf{x}, t, t'). \quad (24)$$

We must explicitly retain t and t' here, because the particles are in general moving both before and after the collision.[6] However, it will be convenient to define

[6] This can be seen from Eq. (14). Since the phase difference $\alpha_2 - \alpha_1$ appearing in this equation is not in general zero either before or after collision, and since $\cos\omega \sin\omega$ is also not in general zero, v_φ will in general differ from zero except in the very special cases mentioned above, which correspond to isolated possibilities of probability zero.

t' in such a way that it represents what may be called the "beginning" of the collision. This could be done, for example, by choosing it as the time when the distance of the incident particle is the smallest value d_0 for which the interactions can be neglected.

Now, because the relation between $\mathbf{x}'$ and $\mathbf{x}$ depends on $\mathbf{u}$, which is distributed statistically, we conclude that even if those particles having the same wave-function coefficients before and after collision had the same initial positions $\mathbf{x}'$, they would have a statistical distribution of positions $\mathbf{x}$ after collision.[7] This leads us to define the probability $P(c_i, \mathbf{x}, t)d\mathbf{x}$ that if a hydrogen molecule has wave-function coefficients c_i, its electron is located in the region $d\mathbf{x}$. In accordance with Eq. (5), we can write

$$P(c_i, \mathbf{x}, t) = |\psi(c_i, \mathbf{x}, t)|^2 f(c_i, \mathbf{x}, t), \tag{25}$$

where by definition,

$$\int P(c_i, \mathbf{x}, t)d\mathbf{x} = \int |\psi(c_i, \mathbf{x}, t)|^2 d\mathbf{x} = 1. \tag{26}$$

To obtain the probability density for the entire ensemble, we must multiply the above by the probability density $Q(c_i)$ that a molecule has the wave-function coefficients c_i. Using Eq. (7), we also have $f(c_i, \mathbf{x}, t) = f(c_j', \mathbf{x}', t')$; and using Eq. (19), we have $Q(c_i, t) = Q(c_j', t')$. Thus, we can write for the probability density in the space of $\mathbf{x}$, ω, α_1 and α_2,

$$Q(c_i, t)P(c_i, \mathbf{x}, t) = |\psi(c_i, \mathbf{x}, t)|^2 Q(c_j', t')f(c_j', \mathbf{x}', t'). \tag{27}$$

To calculate the probability density after the nth collision, we must average the contribution to $Q(c_i, t)P(c_i, \mathbf{x}, t)$ coming from the various types of collisions. Each contribution satisfies Eq. (27). But each contribution must be weighted with the proper weighting function. To obtain the weighting function, we begin with Eq. (21), which gives the probability of a collision with velocity of approach in the range $d\mathbf{u}$, that carries the wave-function coefficients from the region $d\Omega'$ to the definite values c_i. We must now eliminate $\mathbf{u}$ in terms of $\mathbf{x}$ with the aid of Eq. (24). However, we must note here that in our example of two degenerate levels, only ϕ will be changed in a collision,[8] and not ρ and z. Our simple example therefore serves only to illustrate the approach to equilibrium of the distribution in ϕ; but it is easily shown[4] that a more complex example would also demonstrate a similar approach to statistical equilibrium in ρ and z. In this example, we shall hereafter restrict ourselves to considering P and f as functions only of ϕ.

Now, even when c_i and c_j' are fixed, a continuous variation in any component of $\mathbf{u}$, say u_z, will in general produce a corresponding continuous variation[9] of ϕ'. In other words, if we solve for ϕ' with Eq. (24), we shall find that $\partial\phi'/\partial u_z$ is a continuous function, not identically zero. Thus, we can eliminate u_z in Eq. (21), expressing it in terms of ϕ', and obtain the probability,

$$K(c_i, c_j'; \phi, \phi'; u_x, u_y; t, t') = G(\partial u_z/\partial\phi')d\phi' d\Omega' du_x du_y,$$

that a collision occurs with approach velocity components in the range $du_x du_y$ and which carries the wave-function coefficients from $d\Omega'$ to c_i and the angle of the particle from $d\phi'$ to ϕ. Note that by definition

$$\int K d\Omega' d\phi' du_x du_y = 1. \tag{28}$$

The function $Kd\Omega' d\phi' du_x du_y$ is clearly the proper weighting function to use with Eq. (27). Denoting by f_{n+1} the value of f after the nth collision, we then obtain

$$Q_{n+1}(c_i)P_{n+1}(c_i, \phi, t) = |\psi(c_i, \phi, t)|^2 \int K(c_i, c_j'; \phi, \phi'; u_x, u_y, t, t') \times Q_n(c_j')f_n(c_j', \phi', t')d\Omega' du_x du_y d\phi'. \tag{29}$$

But the above must also be averaged over the times t' at which a collision begin, which are distributed at random. In doing this, it is convenient to average over a time T long compared to the time necessary to complete a collision but short compared with the time between collisions (such a case can always be obtained by making the pressure low enough). We then obtain [with the aid of (25)] an integral equation defining how $Q_n f_n$ is changed in these systems undergoing collision between t and $t-T$:

$$Q_{n+1}(c_i)f_{n+1}(c_i, \phi, t) = \int_{t-T}^{t} \frac{dt}{T} \int K Q_n(c_j') \times f_n(c_j'\phi', t')d\Omega' d\phi' du_x du_y. \tag{30}$$

From here on, the proof that $Q_n f_n$ approaches a constant as $n \to \infty$ is much the same as was the proof that Q_n approaches a constant. We let C_n be the maximum of $Q_n f_n$ and D_n its minimum. Then using (28), we readily show that

$$Q_{n+1}f_{n+1} < C_n; \quad Q_{n+1}f_{n+1} > D_n. \tag{31}$$

Note, however, that to obtain this result, we must, as

[7] This result is proved in detail in the more extensive paper mentioned in reference 4. However, it is very plausible, since different collision parameters will produce different changes of the wave-function coefficients throughout the collision, and therefore different velocities $\mathbf{v} = \nabla S/m$, so that different distances would be covered by the particles in the resulting motions.

[8] This can be seen from Eq. (14) and (14a, b, c). In the present approximation of neglecting transitions to nondegenerate levels, the phase S, and therefore the velocity $\mathbf{v} = \nabla S/m$, can depend only on ϕ; but if more terms were included in the expansion (9) of the wave function, S would clearly depend on ρ and z also. For a more detailed treatment of this point, see the paper mentioned in reference 4.

[9] As shown in paper II, Sec. 6, if the usual theory should fail in any domain, such as that associated with 10^{-13} cm, the positions of these particles could be observed with unlimited precision, so that it would be possible, at least in principle, to predict the precise time of decay of an individual nucleus.

in obtaining the similar result for Q_n, use the fact that K is a continuous function of all its variables. It is here that we bring in the basic hypothesis of a statistically distributed series of kinds of collisions.

Thus, we can deduce that $Q_n f_n$ approaches a constant. Since Q_n approaches a constant, we deduce that f_n also approaches a constant, which must be unity, since by (26) both P and $|\psi|^2$ are by definition normalized. This means that $P(c_i, \phi, t) = |\psi(c_i, \phi, t)|^2$, or that if we fix our attention on those cases in which the wave-function coefficients are c_i, the probability density is just $|\psi(c_i, \phi, t)|^2$.

Finally, let us note that no other solution of the conservation equation could have taken the place of $|\psi(c_i, \phi, t)|^2$ in our proof that after many collisions, $P(c_i, \phi, t) \rightarrow |\psi(c_i, \phi, t)|^2$. Although Eq. (7) would have followed from Eq. (5) if we had replaced $|\psi(\mathbf{x}, t)|^2$ by an arbitrary solution $H(\mathbf{x}, t)$ of the conservation equation, the step from Eq. (27) to Eq. (29) would not then have been possible. For in this step, we used the property that the value of $|\psi(c_i, \phi, t)|^2$ depends *only* on the final coefficients c_i of the wave function and not on the initial coefficients c_j'. This property makes it possible for us to take $|\psi(c_i, \phi, t)|^2$ out of the integral as a common factor, independent of the initial wave-functions coefficients c_j'. With any other solution of the conservation equation, the final value of the function would have depended on the initial coefficients c_j', as well as on the c_i, so that the function could not have been taken out of the integral and the proof would not have gone through.

III. SUMMARY AND CONCLUSIONS

We shall summarize the results of this paper in terms of the simple example of the α-decay of two uranium nuclei having the same wave function. Now one of these nuclei may disintegrate tomorrow and the other in two billion years. The usual interpretation of the quantum theory states, however, that *today* there can be no physically describable difference between these nuclei, since they both have the same wave function and since the wave function is said to determine all physically significant properties of a system. But the most elementary scientific procedure would suggest that if two objects are observed to act differently, this should be regarded as *a posteriori* evidence that there must in fact be some physical difference between them. Indeed, in the causal interpretation, the difference in the two uranium nuclei is explained very simply in terms of the assumption that each nucleus has in it a set of particles with precisely defined positions, which determine in principle exactly when that nucleus is going to decay (see paper I, Sec. 8). The difference in times of disintegration is then ascribed to the differences in positions of the various particles in the two nuclei. In fact, if we consider a statistical ensemble of such nuclei, all having the same wave function, then as has been shown in this paper, the particles in different nuclei will be in different positions as a result of collisions suffered by these nuclei over the past few billion years; and these collisions will have produced a probability density of $P = |\psi|^2$ that the particles in a particular nucleus take a given set of positions. Thus, we are able, as shown in paper I, Sec. 8, to explain the statistical ensemble in decay times of a large number of nuclei.

In the usual interpretation, however, the role of statistics is very different, for it is said that the precise future behavior of an individual system is completely arbitrary, in the sense that it cannot be related to any physically definable properties of that system or of anything else existing in the world today. Only the probability of decay in a statistical ensemble of systems is said to be determined by physical factors now in existence. Nevertheless, it is admitted that the behavior of an individual system such as a uranium nucleus can be physically significant, since, for example, if this nucleus disintegrates, the resulting particle can activate a Geiger counter, which can initiate a large scale process, such as the setting off of a bomb. In this situation, the question of when a particular nucleus decays clearly has physical significance, since it determines, for example, whether the bomb will explode tomorrow or in two billion years. In accordance with the postulate that only the behavior of a statistical ensemble of uranium nuclei can be determined by physical factors now in existence, however, the usual interpretation states that the time at which a particular bomb goes off is completely arbitrary, from a physical point of view.

The arbitrariness of the usual interpretation in the description of the behavior of an individual system is closely related to the assumption, already stated, that the wave function determines all physically significant properties of that system. Now, in the case of the uranium nucleus, the wave function takes the form of a packet initially entirely within the nucleus, which gradually "leaks" through the barrier and thereafter rapidly spreads without limit in all directions. Clearly, although this wave function is supposed to describe *all* physically significant properties of the system, it cannot explain the fact that each α-particle is actually detected in a comparatively small region of space and at a fairly well-defined instant of time. The usual interpretation states that this phenomenon must simply be accepted as an event that somehow manages to occur but in a way that is as a matter of principle forever beyond the possibility of a simultaneous and detailed "space-time and causal description." Indeed, even to ask for such a description is said to be a meaningless question within the framework of the usual interpretation of the quantum theory. In the causal interpretation, however, the postulated particles with precisely defined positions explain in a natural way why an α-particle can be detected at a fairly definite place and time, on the basis of the simple assumption that the particle existed all the time and just moved from its original location

to the place where it was finally found. Thus, even though we cannot yet[9] observe the precise locations of our postulated particles, they already perform a real function in the theory, namely, to explain certain properties of *individual* systems which are said in the usual interpretation to be just empirically given and forever unexplainable.

The postulation of particles with precisely defined (but not at present precisely measurable) positions not only makes possible a more connected description of the behavior of an individual system than is possible in the usual interpretation but also serves to increase the degree of unity in the treatment of the statistical aspects of the theory. Thus, in the usual interpretation, two completely different kinds of statistics are needed. First, there is the ordinary statistical mechanics, which treats of the distribution of systems among the quantum states, resulting from various chaotic factors such as collisions. The need for this type of statistics could in principle be avoided by means of more accurate measurements which would supply more detailed information about the quantum state, but in systems of appreciable complexity, such measurements would be impracticably difficult. Secondly, however, there is the fundamental and irreducible probability distribution, $P(\mathbf{x})=|\psi(\mathbf{x})|^2$, or more generally, $P_a=|C_a|^2$, where P_a is the probability that in the measurement of an arbitrary observable A we shall obtain the eigenvalue a, corresponding to the eigenfunction $\psi_0(\mathbf{x})$, and where $\psi=\sum_a C_a\psi_a(\mathbf{x})$. The need for this type of statistics cannot even in principle be avoided by means of better measurements, nor can it be explained in terms of the effects of random collision processes. The usual interpetation simply postulates the above probability distribution as a basic and not further analyzable property of matter, in addition to the more familiar type of probability that applies in the statistical distribution of systems among the quantum states. On the other hand, the causal interpretation requires only one kind of probability. For as we have seen, we can deduce the probability distribution $P(\mathbf{x})=|\psi(\mathbf{x})|^2$ as a consequence of the same random collision processes that give rise to the statistical distributions among the quantum states. Moreover, as shown in paper II, this result is sufficient to prove the more general result that the probability of obtaining the eigenvalue a in the measurement of an arbitrary observable A is $P_a=|C_a|^2$. In this way, the causal interpretation avoids the need for introducing *ad hoc* a completely new type of probability distribution, which does not represent incompleteness of information and which is not even in principle explainable in terms of random processes, such as collisions.

As the situation stands now, the causal interpretation and the usual interpretation each introduce one hypothesis that has not yet been proved experimentally, the causal interpretation assuming the existence of particles with precisely defined positions and the usual interpretation assuming that $P(\mathbf{x})=|\psi(\mathbf{x})|^2$ (or more generally, $P_a=|C_a|^2$).[10] The causal interpretation already has, however, the advantage of providing a more unified description of nature than is possible in the usual interpretation, one involving a smaller number of hypotheses that must simply be accepted as empirical facts without further explanation. For by making *one* postulate, that of the existence of particles with precisely defined positions, the causal interpretation explains two general properties of matter which must simply be postulated in the usual interpretation, i.e., the appearance of an individual particle in a fairly definite position and at a fairly well-defined instant of time after the wave function has spread over a wide region of space, and the probability distribution of these particles in a statistical ensemble of systems having the same wave function. For this reason, it would seem that the assumption of particles with precisely defined positions is likely to be on the right track, at least in its essential features, even if all of the details of the theory thus far suggested may perhaps not appear in a better theory of the phenomena associated with distances of the order of 10^{-13} cm.

The author wishes to thank Professor R. P. Feynman for several interesting and stimulating discussions.

[10] As shown in Sec. I of the present paper, the assumption that $P(\mathbf{x})=|\psi(\mathbf{x})|^2$ has not yet been verified experimentally, nor is it likely that experiments of the requisite precision will be possible in the near future.

Primitive Quantization in the Relativistic Two-Body Problem

J. L. SYNGE
Dublin Institute for Advanced Studies, Dublin, Ireland
(Received July 31, 1952)

A pair of events, one for each of two particles, is regarded as a point in 8-space (V_8). The technique of Hamilton's optical method is applied to V_8, giving rays and associated de Broglie waves. These waves are quantized by associating a phase-cycle with an increase of h in the characteristic function, and hence quantum rules appear as resonance conditions on the de Broglie waves, when the part of V_8 occupied by rays is multiply connected. A Hamiltonian equation is written down, the interaction between the particles being taken to be of Coulomb form, but with ordinary distance replaced by Minkowskian separation. This leads without approximation to a simple expression for quantized proper energies of the system, and from this expression follow the correct approximate energy levels for the hydrogenic atom (with $Z\alpha$), the mass-correction factor being included. There is no approximation based on smallness of relative velocity or ratio of masses, and mathematical complexities associated with retarded potentials are avoided by the use of the relativistic Coulomb interaction.

1. INTRODUCTION

THIS paper deals with the two-body problem (in particular, the problem of the hydrogenic atom) in a relativistic way, without any approximation based on the slowness of relative motion or smallness of the ratio of the masses. Complications due to the use of retarded potentials are avoided by employing two time coordinates, one for each particle, so that the manifold considered is a super-space-time of eight dimensions. For the hydrogenic atom, the interaction potential is assumed to have the Coulomb form, but with Euclidean distance replaced by Minkowskian separation.

From an assumed Hamiltonian equation connecting the coordinates and certain 4-vectors (slowness 4-vectors in the language of Hamilton, or equivalently momentum 4-vectors), Hamiltonian equations of motion follow, the solutions of these equations giving rays in super-space-time. These rays possess integrals, and we pick out those for which the integration constants have common values. Such rays form a manifold of six dimensions with two irreducible circuits, and the application of quantum rules to these circuits leads to quantized energy levels for the atom.

The Hamiltonian equation is taken in the form

$$\Omega=\frac{1}{2m}\sigma_r\sigma_r+\frac{1}{2m'}\sigma_r'\sigma_r'+\frac{ee'}{R}+\tfrac{1}{2}(m+m')c^2=0, \quad (1.1)$$

where m, m' are the proper masses of the particles, e, e' their charges, σ_r, σ_r' their slowness 4-vectors, and R their Minkowskian separation. The square of the quantized proper mass of the system comes out to be (without approximation)

$$\bar{m}^2=(m+m')^2-Z^2\alpha^2mm'/(n+j)^2, \quad (1.2)$$

$e'=-Ze$, $\alpha=e^2/ch$, $n=0, 1, 2, \cdots$; $j=1, 2, \cdots$, and so the proper energy of the atom is (approximately for small $Z\alpha$)

$$\bar{m}c^2=(m+m')c^2-\frac{1}{2}\frac{mm'}{m+m'}\frac{Z^2\alpha^2c^2}{(n+j)^2}. \quad (1.3)$$

This is the correct approximate formula with the mass-correction factor included. There is no fine structure, as is to be expected in a theory from which spin is omitted.

The theory is not, of course, to be regarded as physically satisfactory. It is a "classical" theory, with Bohr-Sommerfeld quantization imposed on it, and should be considered as a prototype (mathematically complete in itself) from which a correct wave-mechanical theory may be evolved inductively.

This treatment of the two-body problem is a particular application of a general method in the calculus of variations[1,2]; this method is described in Secs. 2 and 3 in a form suitable for application, with special reference to multiply connected domains. Primitive quantization is discussed in Sec. 4; this gives an intuitive validation of the quantum rules on the basis of the interference of de Broglie waves.

2. RAYS IN HAMILTONIAN SPACE

Let Greek suffixes have the range 1, 2, $\cdots N$, with the summation convention for repeated suffixes. Consider a space H_N with coordinates x_ρ. To make H_N a *Hamiltonian space* we write down an equation

$$\Omega(\sigma, x)=0, \quad (2.1)$$

connecting the coordinates x_ρ with a set of quantities σ_ρ, which (following Hamilton's nomenclature in geometrical optics) we call *slowness components*.

The *rays* in H_N are defined to be curves satisfying the variational condition,

$$\delta\int\sigma_\rho dx_\rho=0, \quad (2.2)$$

for fixed end points, the values of the σ's on the curves considered being arbitrary except for (2.1). We derive

[1] C. Carathéodory, *Variationsrechnung* (B. G. Teubner, Leipzig and Berlin, 1935).

[2] J. L. Synge, *Hamilton's Method in Geometrical Optics*, Institute for Fluid Dynamics and Applied Mathematics, University of Maryland, 1951.

at once the following differential equations for the rays:

$$dx_\rho/dw = \partial\Omega/\partial\sigma_\rho, \quad d\sigma_\rho/dw = -\partial\Omega/\partial x_\rho, \tag{2.3}$$

where w is a suitably chosen parameter.

If we assign initial values to x_ρ, σ_ρ for $w=0$, then Eqs. (2.3) give a unique ray. If, on the other hand, we assign initial values to x_ρ and give the direction of the ray (i.e., the ratios of dx_ρ), then the equations on the left of (2.3), together with (2.1), determine the initial values of σ_ρ and, hence, determine the ray. We note also that, from its variational definition, a ray is determined by two points on it.

From the totality of all possible rays we pick out a set filling a subspace R_M of $H_N (M<N)$, or possibly filling a portion of $H_N (M=N)$. In R_M σ_ρ are functions of position, since these quantities are determined by the direction of a ray at a point, and so the integral

$$I = -\int \sigma_\rho dx_\rho, \tag{2.4}$$

taken along any given curve in R_M, has a definite value. (The negative sign is inserted merely to make I positive in relativistic applications when the curve runs from the past into the future.) We call I the *action length* of the curve, and in the case of a closed curve or circuit C we call

$$I(C) = -\oint_C \sigma_\rho dx_\rho \tag{2.5}$$

the *action circulation* in C.

If R_M is multiply connected (and this is the case which interests us), it possesses independent irreducible circuits $C_1, C_2, \cdots C_p$. Then any circuit C in R_M may be deformed continuously into a linear combination of these irreducible circuits; this we express in the form

$$C \sim n_1 C_1 + n_2 C_2 + \cdots n_p C_p, \tag{2.6}$$

where the n's are integers. (The word *integer* will be used for the values $0, \pm 1, \pm 2, \cdots$.)

3. SYSTEMS OF RAYS. WAVES

We shall say that a set of rays R_M form a *system of rays* when the action circulation vanishes for every reducible circuit in R_M:

$$I(C) = 0 \tag{3.1}$$

(condition of Mayer in the calculus of variations). From now on we shall be concerned only with systems of rays.

The following theorem is fundamental: *The action circulations in two reconcilable circuits in R_M are equal.* This follows immediately from (3.1) if we join the circuits by a curve taken twice over in the two senses, thus producing a reducible circuit.

It follows then that the action circulation in any circuit C in R_M may be written

$$I(C) = -\oint \sigma_\rho dx_\rho = n_1 I_1 + \cdots + n_p I_p, \tag{3.2}$$

where the n's are the integers occurring in (2.6) and the I's are the fundamental action circulations

$$I_1 = I(C_1) = -\oint_{C_1} \sigma_\rho dx_\rho, \cdots I_p = I(C_p) = -\oint_{C_p} \sigma_\rho dx_\rho. \tag{3.3}$$

Let P_0, P be any two points of R_M and Γ a curve joining them. We define the *characteristic function* V of R_M by the formula

$$V_\Gamma(P_0, P) = -\int_\Gamma \sigma_\rho dx_\rho. \tag{3.4}$$

The value of this integral depends on the $2N$ coordinates of the points P_0, P, and also on the curve Γ. But it has the same value for all reconcilable curves. In general, if Γ' is a second curve joining P_0, P, then as in (2.6),

$$\Gamma' - \Gamma \sim n_1 C_1 + \cdots + n_p C_p, \tag{3.5}$$

and therefore

$$V_{\Gamma'}(P_0, P) - V_\Gamma(P_0, P) = n_1 I_1 + \cdots + n_p I_p. \tag{3.6}$$

If we use the symbol $V(P_0, P)$ to denote the set of all integrals (3.4) for fixed points P_0, P but for arbitrary choice of Γ, then this is a many-valued function of the $2N$ coordinates of the two points. Its multiplicity (in general infinite) is given by the formula

$$V(P_0, P) = V_\Gamma(P_0, P) + n_1 I_1 + \cdots + n_p I_p, \tag{3.7}$$

where the n's take all integer values.

We note that a change in P_0 alters $V(P_0, P)$, considered as a many-valued function of P, only by a constant.

If we give to P a displacement δx_ρ in R_M, then by (3.4)

$$\delta V = -\sigma_\rho \delta x_\rho. \tag{3.8}$$

If $M=N$, so that the rays fill a portion of H_N, the displacement of P is arbitrary, and it follows that

$$\partial V/\partial x_\rho = -\sigma_\rho; \tag{3.9}$$

and so, substituting in (2.1), we see that V satisfies the Hamilton-Jacobi equation

$$\Omega(-\partial V/\partial x, x) = 0. \tag{3.10}$$

But we are interested rather in the case $M<N$, so that δx_ρ in (3.8) are not independent, and consequently we do not get (3.9). The Hamilton-Jacobi equation does not play an important part in the theory; to bring it in we would have to regard the ray-space R_M as part of a larger ray-space filling a portion of H_N, and it is not always convenient to do this.

We now introduce waves in R_M. For fixed P_0, consider

the points P satisfying the equation

$$V(P_0, P)=K, \tag{3.11}$$

where K is some constant. If R_M is simply connected, the locus of P is a simple $(M-1)$-space. If R_M is multiply connected, then the locus of P is an $(M-1)$-space of many sheets (in general, infinitely many) on account of the fact that V is many-valued. In either case we shall call the $(M-1)$ space given by (3.11) an $(M-1)$ *wave*.

On giving all values to K in (3.11), we get a system of waves in R_M, uniquely determined by the system of rays. In the language of the calculus of variations, the rays are extremals and the waves transversals. Note that a change in the point P_0 does not alter the system of waves; it simply shifts the values of the constant K.

4. PRIMITIVE QUANTIZATION OF A SYSTEM OF WAVES

In a book not yet published,[3] I have shown that if H_N is space-time and if events of equal phase are given by measuring off action distances h along the rays, then the waves as defined in the preceding section have the properties usually associated with the histories of de Broglie waves. This suggests that we should consider a scalar disturbance in R_M, given by a formula

$$\psi=\psi_0 \cos(2\pi V/h+\text{const}), \tag{4.1}$$

where the amplitude ψ_0 is a function of position in R_M. But we pay no attention to this amplitude, concentrating rather on the phase angle. The imposition of phase according to (4.1) constitutes what may be called *primitive quantization*. On each ray it defines crests and troughs, the action length of the ray between consecutive crests being Planck's constant h.

But if R_M is multiply connected, then V is many-valued, and we are led to consider the disturbance as a superposition of waves as in (4.1), but with the various phases corresponding to the many values of V. Such waves will interfere destructively with one another, unless a condition of resonance obtains, and so we are brought to consider *resonant systems of waves* defined as follows: A system of waves associated with a system of rays R_M is a resonant system if the phase angles as shown in (4.1) differ by integral multiples of 2π when we take for V the various determinations according to (3.7).

Since the values of the n's in (3.7) are arbitrary, it is clear that the resonance conditions are

$$I_1=j_1h, \quad I_2=j_2h, \quad \cdots, \quad I_p=j_ph, \tag{4.2}$$

where the j's are integers.

It is hard to say to what extent the above derivation of these conditions represents a real advance on the method used by Sommerfeld[4] for quantizing the relativistic Kepler problem. They seem to come to very much the same thing in the applications. However, the present method avoids the apparently artificial device of separating the variables in the Hamilton-Jacobi equation and offers some intuitive justification for the conditions in terms of the interference of de Broglie waves.

5. THE TWO-BODY PROBLEM. SEPARATION INTO THE EXTRACULE AND THE INTRACULE

Consider Minkowskian space-time with rectangular Cartesian coordinates x_r ($x_4=\text{ict}$), Latin suffixes having the range 1, 2, 3, 4, with the summation convention. A point of the Hamiltonian space H_8 will correspond to a pair of events (x_r, x_r'), and we shall take for the Hamiltonian equation (2.1)

$$\Omega=(1/2m)\sigma_r\sigma_r+(1/2m')\sigma_r'\sigma_r'+f(\omega) +\tfrac{1}{2}(m+m')c^2=0. \tag{5.1}$$

Here m, m' are the proper masses of the two particles with which we are concerned and

$$\omega=(x_r-x_r')(x_r-x_r')>0, \tag{5.2}$$

this inequality making the vector x_r-x_r' space-like. The form of the function f remains for the present unspecified.

We define X_r, ξ_r, M_r, μ_r by the formulas

$$\begin{aligned} &X_r=(mx_r+m'x_r')/(m+m'), \quad M_r=\sigma_r+\sigma_r', \\ &\xi_r=x_r-x_r', \quad \mu_r=(m'\sigma_r-m\sigma_r')/(m+m'). \end{aligned} \tag{5.3}$$

We have then

$$\sigma_r dx_r+\sigma_r' dx_r'=M_r dX_r+\mu_r d\xi_r, \tag{5.4}$$

and

$$\begin{aligned} \Omega=\frac{1}{2(m+m')}M_rM_r+\frac{m+m'}{2mm'}\mu_r\mu_r \\ +f(\omega)+\tfrac{1}{2}(m+m')c^2=0, \\ \omega=\xi_r\xi_r>0. \end{aligned} \tag{5.5}$$

In the language of Eddington,[5] we may speak of (X_r, M_r) as connected with the extracule or exterior particle and (ξ_r, μ_r) with the intracule or interior particle.

In applying the general theory of the preceding sections, we take x_ρ to be (X_r, ξ_r) and σ_ρ to be (M_r, μ_r). Then by (2.3) the equations of the rays are

$$\begin{aligned} &\frac{dX_r}{dw}=\frac{\partial\Omega}{\partial M_r}=\frac{1}{m+m'}M_r, \quad \frac{dM_r}{dw}=-\frac{\partial\Omega}{\partial X_r}=0, \\ &\frac{d\xi_r}{dw}=\frac{\partial\Omega}{\partial\mu_r}=\frac{m+m'}{mm'}\mu_r, \quad \frac{d\mu_r}{dw}=-\frac{\partial\Omega}{\partial\xi_r}=-2f'(\omega)\xi_r. \end{aligned} \tag{5.6}$$

[3] J. L. Synge, *Geometrical mechanics and de Broglie waves* (Cambridge University Press).

[4] A. Sommerfeld, *Atomic Structure and Spectral Lines* (Methuen and Company, London, 1934), p. 608.

[5] A. S. Eddington, *Fundamental Theory* (Cambridge University Press, 1946), p. 51.

We see that a ray possesses ten integrals:

$$M_r = A_r = \text{const}, \quad \xi_r\mu_s - \xi_s\mu_r = B_{rs} = -B_{sr} = \text{const}. \tag{5.7}$$

6. THE SYSTEM OF RAYS WITH COMMON FIRST INTEGRALS

From the totality of all rays in H_8 we pick out those for which the integrals in (5.7) have common values. We shall show that these rays form a system [see Eq. (3.1)] and so have a system of waves associated with them. We shall explore the topology of the ray-space R_M and then apply the resonance conditions (4.2).

Of the constants B_{rs} only five are independent, not six as we might think. For, if we introduce the dual,

$$B_{rs}{}^* = \tfrac{1}{2}\epsilon_{rsmn}B_{mn}, \tag{6.1}$$

by means of the permutation symbol, we have by (5.7)

$$B_{rs}{}^*\xi_s = \epsilon_{rsmn}\xi_m\mu_n\xi_s = 0, \tag{6.2}$$

and so $\det B_{rs}{}^* = 0$. Therefore,

$$B_{23}{}^*B_{14}{}^* + B_{31}{}^*B_{24}{}^* + B_{12}{}^*B_{34}{}^* = B_{23}B_{14} + B_{31}B_{24} + B_{12}B_{34} = 0. \tag{6.3}$$

We shall use this relationship later.

In order to see whether the rays do form a system, we need to find (M_r, μ_r) in terms of (X_r, ξ_r), this being equivalent to finding σ_ρ in terms of x_ρ in the general theory preceding. We know M_r from (5.7). To find μ_r we have to solve the equations

$$\xi_r\mu_s - \xi_s\mu_r = B_{rs}, \tag{6.4}$$

$$\Omega = 0. \tag{6.5}$$

The general solution of (6.4) is

$$\mu_r = \omega^{-1}(\theta\xi_r - B_{rs}\xi_s), \tag{6.6}$$

where θ is arbitrary, this tensorial equation being easily verified by using the special coordinate system which we shall introduce below, making use of (6.3). The factor θ is then found by substituting (6.6) in (6.5) or (5.5). By (6.6) we have

$$\mu_r\mu_r = \omega^{-1}\theta^2 + \omega^{-2}B_{rm}\xi_m B_{rn}\xi_n, \tag{6.7}$$

and so we find for θ the two values

$$\theta = \epsilon\Theta \quad (\epsilon = \pm 1), \tag{6.8}$$

where Θ is the positive square root

$$\Theta = \left[-\frac{B_{rm}\xi_m B_{rn}\xi_n}{\omega} - \frac{2mm'\omega}{m+m'}\left\{ \frac{A_rA_r}{2(m+m')} + f(\omega) + \tfrac{1}{2}(m+m')c^2 \right\} \right]^{\frac{1}{2}}. \tag{6.9}$$

Substitution for θ in (6.6) gives μ_r, and so we have obtained (M_r, μ_r) in terms of (X_r, ξ_r) as required. On account of the factor ϵ there appear to be two rays through each point of the ray-space. Actually the ray-space is flattened, with two sides, and we may think of having one ray through each point if we associate the two values of ϵ with the two sides.

If the eight coordinates (X_r, ξ_r) were free, except for the inequality $\xi_r\xi_r > 0$ (signifying that ξ_r is space-like), the corresponding points would fill a portion of H_8. But they are not free on account of (6.2):

$$B_{rs}{}^*\xi_s = 0. \tag{6.10}$$

Of these four equations only two are independent on account of (6.3). *The ray-space is therefore of six dimensions* (R_6).

To explore R_6 we need a convenient coordinate system. Now

$$(B_{23}, B_{31}, B_{12}) \quad \text{and} \quad (B_{14}, B_{24}, B_{34})$$

are 3-vectors, orthogonal to one another by (6.3); and so by turning the space axes in the Galileian frame to which x_r, x_r' refer, we can make all the components of B_{rs} vanish except

$$B_{12} = -B_{21} = B, \text{ say}; \quad B_{24} = -B_{42} = iB^*, \text{ say}, \tag{6.11}$$

B and B^* being real constants. Then all the components of $B_{rs}{}^*$ vanish except

$$B_{31}{}^* = -B_{13}{}^* = iB^*, \quad B_{34}{}^* = -B_{43}{}^* = B. \tag{6.12}$$

From (6.10) it follows that

$$\xi_3 = 0, \quad \xi_1 = B\eta, \quad \xi_4 = -iB^*\eta, \tag{6.13}$$

η being a real parameter. We note that

$$\omega = \xi_r\xi_r = \xi_2{}^2 + (B^2 - B^{*2})\eta^2 > 0. \tag{6.14}$$

There is then a 1:1 correspondence between the points of R_6 and the real coordinate sextets $(X_1, X_2, X_3, X_4/i, \xi_2, \eta)$, these quantities taking all values subject to the inequality (6.14) and the condition that Θ as in (6.9) is real. As is easily verified,

$$B_{rm}\xi_m B_{rn}\xi_n = (B^2 - B^{*2})\omega, \tag{6.15}$$

and so we have

$$\Theta = \left[-(B^2 - B^{*2}) - \frac{2mm'\omega}{m+m'}\left\{ \frac{A_rA_r}{2(m+m')} + f(\omega) + \tfrac{1}{2}(m+m')c^2 \right\} \right]^{\frac{1}{2}}, \tag{6.16}$$

which is a function of ω only.

Before examining the topology of R_6, let us show that the rays form a system, the condition for which is that

$$\oint (M_r dX_r + \mu_r d\xi_r) = 0 \tag{6.17}$$

for every reducible circuit in R_6. Now

$$\oint M_r dX_r = \oint d(A_rX_r) = 0, \tag{6.18}$$

and by (6.6)

$$\oint \mu_r d\xi_r = \oint \omega^{-1}(\theta\xi_r - B_{rs}\xi_s)d\xi_r. \tag{6.19}$$

It is easily seen that

$$B_{rs}\xi_s d\xi_r = (B^2 - B^{*2})(\eta d\xi_2 - \xi_2 d\eta), \tag{6.20}$$

and so

$$\oint \mu_r d\xi_r = \tfrac{1}{2}\epsilon \oint \omega^{-1}\Theta(\omega)d\omega - (B^2 - B^{*2}) \oint \frac{\eta d\xi_2 - \xi_2 d\eta}{\xi_2^2 + (B^2 - B^{*2})\eta^2} = 0 \tag{6.21}$$

for a reducible circuit. Thus, (6.17) is true; the rays form a system.

As for the topology of R_6, it is easy to see that if

$$B^2 - B^{*2} < 0, \tag{6.22}$$

there is no irreducible circuit and hence no resonance conditions (4.2). If, on the other hand,

$$B^2 - B^{*2} > 0, \tag{6.23}$$

then there is an irreducible circuit C_1 in the (ξ_2, η) space (and hence in R_6) given by

$$\xi_2 = R\sin\phi, \quad (B^2 - B^{*2})^{\frac{1}{2}}\eta = R\cos\phi, \quad R = \text{const}, \quad 0 \leqslant \phi \leqslant 2\pi, \tag{6.24}$$

provided that Θ is real for $\omega = R^2$. If Θ has zeros R_1^2, R_2^2, with Θ real between them, we get another irreducible circuit C_2:

$$\xi_2 = R\sin\phi, \quad (B^2 - B^{*2})^{\frac{1}{2}}\eta = R\cos\phi, \quad \phi = \text{const}, \quad R_1 \leqslant R \leqslant R_2, \tag{6.25}$$

the circuit being obtained by taking R from R_1 to R_2 with one value of ϵ and returning with the other. This circuit goes round a flat sheet in ξ space.

If both these irreducible circuits exist, the resonance conditions (4.2) read

$$\oint_{C_1} \mu_r d\xi_r = jh, \quad \int_{C_2} \mu_r d\xi_r = nh, \tag{6.26}$$

where j and n are integers. Hence, using the expression in (6.21), valid for irreducible as well as reducible circuits, we get

$$2\pi(B^2 - B^{*2})^{\frac{1}{2}} = jh, \quad \int_{\omega_1}^{\omega_2} \omega^{-1}\Theta(\omega)d\omega = nh, \tag{6.27}$$

where ω_1 and ω_2 are zeros of Θ, with Θ real between them.

The condition (6.23) is stated for the special coordinate system; for arbitrary axes it reads

$$B_{rs}B_{rs} > 0. \tag{6.28}$$

7. THE HYDROGENIC ATOM

It remains only to apply (6.27) to the hydrogenic atom, and for that we choose, as a relativistic generalization of the Coulomb potential,

$$f(\omega) = ee'/R, \tag{7.1}$$

where $R^2 = \omega$, and e, e' the charges on the electron and nucleus, respectively.

The second condition in (6.27) reads

$$2\int_{R_1}^{R_2} R^{-1}\Theta dR = nh, \tag{7.2}$$

where

$$\Theta^2 = -(B^2 - B^{*2}) + \frac{2mm'ee'}{m+m'}R - \frac{2mm'}{m+m'}R^2 \times \left\{\frac{A_r A_r}{2(m+m')} + \tfrac{1}{2}(m+m')c^2\right\}, \tag{7.3}$$

and R_1, R_2 are the zeros of this quadratic expression. An easy calculation, which makes use of the integral

$$\int_{\rho_2}^{\rho_1} [(\rho_1 - \rho)(\rho - \rho_2)]^{\frac{1}{2}}\rho^{-2}d\rho = \pi[\tfrac{1}{2}(\rho_1 + \rho_2)(\rho_1\rho_2)^{-\frac{1}{2}} - 1], \tag{7.4}$$

leads from (7.2), combined with the first of (6.27), to the formula

$$A_r A_r + (m+m')^2c^2 = Z^2\alpha^2 mm'/(n+j)^2, \tag{7.5}$$

with Z, α as in (1.2). If we now define the proper mass $\bar{m}$ of the the atom by

$$\bar{m}^2c^2 = -M_r M_r = -A_r A_r, \tag{7.6}$$

then (7.5) gives us precisely (1.2), and this leads at once to the approximate formula (1.3).

The quantum numbers j, n occurring above are positive integers: this is due to an implicit choice of the senses of the fundamental circuits, made for the sake of simplicity. By (6.23) and (6.27), the value $j = 0$ is forbidden. But we can have $n = 0$. This degenerate case arises when $R_1 = R_2$ and corresponds to a circular orbit; the ray-space is then only of five dimensions.

We note that the resonance conditions are actually conditions on the two invariants $A_r A_r$ and $B_{rs}B_{rs}$, the former corresponding to the proper mass or proper energy of the system and the latter to its total angular momentum.

The Effect of Collisions upon the Doppler Width of Spectral Lines

R. H. DICKE
Palmer Physical Laboratory, Princeton University, Princeton, New Jersey
(Received September 17, 1952)

Quantum mechanically the Doppler effect results from the recoil momentum changing the translational energy of the radiating atom. The assumption that the recoil momentum is given to the radiating atom is shown to be incorrect if collisions are taking place. If the collisions do not cause broadening by affecting the internal state of the radiator, they result in a substantial narrowing of the Doppler broadened line.

QUANTUM mechanically, the Doppler effect results from the recoil momentum given to the radiating system by the emitted photon.[1] This recoil momentum implies a change in the kinetic energy of the radiating atom which is in turn mirrored by a corresponding change in the photon's energy. This change in the photon's energy is proportional to the component of the atom's velocity in the direction of emission of the photon and leads to the normal expression for the Doppler effect. Since for gas pressures commonly encountered the fraction of the time that an atom is in collision is negligibly small, it might seem reasonable to assume that the recoil momentum is absorbed by the single radiating atom or molecule rather than by an atomic aggregate. In this case the Doppler breadth would, within limits, be pressure-independent. Actually, under certain circumstances, this assumption is far from correct. Collisions which do not affect the internal state of the radiating system have a large effect upon the Doppler breadth.

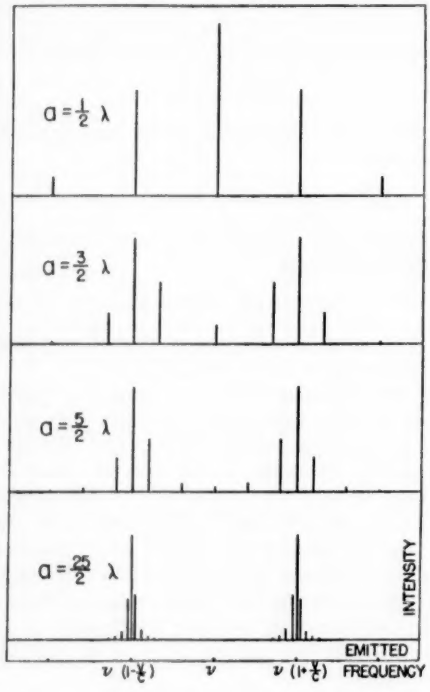

FIG. 1. Spectral distribution of radiation emitted by an atom confined to a one-dimensional box of width a.

The effect of collisions upon the Doppler effect is best illustrated with a simple example treated first classically and then quantum mechanically. Assume that the radiating atom, but not the radiation, is confined to a one-dimensional well of width a, and that it moves back and forth between the two walls with a speed v. The wave emitted by the atom is frequency modulated with the various harmonics of the oscillation frequency of the atom in the square well. For negligible collision and radiation damping, the spectral distribution of the emitted radiation is obtained from a Fourier series. A set of equally spaced sharp lines is obtained. They occur at the non-Doppler shifted frequency plus- or minus-integral multiples of the oscillation frequency of the atom in the square well. The intensity distribution of these lines is shown for several values of a/λ in Fig. 1.

In the quantum-mechanical description of this example, the radiating system possesses two types of energy, internal and external. The external energy is the quantized energy of the atomic center-of-mass moving in the one-dimensional square well. In a transition in which a photon is absorbed or emitted, both the internal and external quantum numbers may change. The frequency of the emitted photon is

$$\nu_{nm}=\nu+(h/8Ma^2)(n^2-m^2).$$

Here ν is the frequency of the non-Doppler shifted line, M is the mass of the radiator, and n, m are integers. A calculation of the transition probabilities gives results for the intensities which are for large n and m essentially the same as the classical results (Fig. 1).

The introduction of a Maxwellian distribution in v in the case of the classical calculation leads to a continuous distribution very similar to a normal Doppler distribution plus a sharp non-Doppler broadened line (see Fig. 2). The fraction of the energy radiated in the sharp line is

$$\frac{\sin^2(\pi a/\lambda)}{(\pi a/\lambda)^2}.$$

[1] E. Fermi, Revs. Modern Phys. 4, 105 (1932).

The sharp line has its origin in the fact that, for a non-integral value of $\pi a/\lambda$, the normal unshifted frequency is emitted by all atoms independent of their speed. Since for $a \geq \frac{1}{2}\lambda$ the dominant noncentral lines in Fig. 1 are always close to the normal Doppler shifted frequencies, the broad distribution has a line contour nearly identical with the normal Doppler line. For $a < \frac{1}{2}\lambda$, the distribution increases in breadth but becomes much weaker.

For the quantum-mechanical treatment, a Maxwell-Boltzmann distribution among the various energy levels leads to a fine complex of lines having frequencies ν_{nm}. If the zero-point energy of oscillation of the atom in the well is very small compared with kT, the degenerate frequency $\nu = \nu_{nn}$ is usually the most intense single frequency emitted. For a small amount of collision or natural broadening, the complex of lines becomes a continuous distribution (Fig. 2) essentially identical with that given by the classical calculation. Note that although the atom is in contact with the walls of the cavity only an infinitesimal part of the time, the probability of the photon's momentum being given to the walls rather than to the atom is finite, being

$$\frac{\sin^2(\pi a/\lambda)}{(\pi a/\lambda)^2}.$$

For a gas confined to a large volume but with a mean free path small compared with a wavelength, the shape of a Doppler broadened line has been calculated treating the radiation classically and using a statistical procedure. In this treatment the phase of the radiation emitted as a function of the time is given by the position of the radiator as a function of the time. The probability distribution of position given by diffusion theory is used to calculate the mean intensity as a function of frequency. Substantially the same result is obtained also quantum mechanically, using a method similar to Foley's.[2] This quantum-mechanical calculation is valid only if the recoil energy of the radiator is small compared with kT. Assuming that the Doppler

[2] H. M. Foley, Phys. Rev. **69**, 616 (1946).

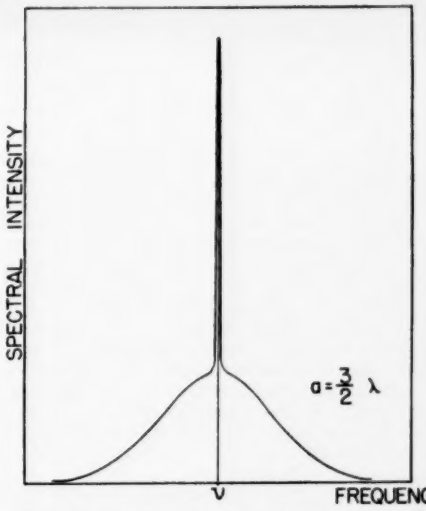

FIG. 2. Doppler broadened line of a gas in a one-dimensional box.

effect is the only appreciable source of the line breadth, it is found that the line has a Lorentz rather than Gaussian shape. The line contour is given by

$$I(\alpha) = I_0 \frac{2\pi D/\lambda^2}{(\alpha-\nu)^2 + (2\pi D/\lambda^2)^2}.$$

The width of the line at half-intensity is, in cycles per second, $4\pi D/\lambda^2$. Here D is the self-diffusion constant of the gas. This line width is roughly $2.8L/\lambda$ times that of a normal Doppler broadened line (L is the mean free path). Therefore, under those conditions for which the calculation is valid, the line breadth which is wholly Doppler is greatly reduced.

Because of the requirement that the gas collisions should not influence the internal state of the radiator, the above results are ordinarily valid only for certain magnetic dipole transitions. Nuclear magnetic resonance absorption, paramagnetic resonance absorption, and S-state hyperfine transitions are examples of transitions which are but weakly affected by collisions.

Lifetimes of Nuclear Isomers*

STEVEN A. MOSZKOWSKI†
University of Chicago, Chicago, Illinois
(Received August 29, 1952)

Lifetimes of nuclear isomers for gamma-transitions are calculated theoretically on the basis of various independent particle models; e.g., single proton, single neutron, and states of several particles (Sec. II). The calculations of this paper are essentially restricted to the most common type of transition *viz.*, multipole order equal to spin change. The lifetime is expressed in terms of a matrix element, M, whose theoretical value depends on the particular model of the nucleus. Radial integrals are calculated numerically, assuming that the nuclear wave functions are given by single particle wave functions for a spherical square well.

Empirical values of M^2 can be deduced from measured isomeric lifetimes, corrected for internal conversion. An analysis of empirical M^2 for some gamma transitions points to a number of regularities which, in general, speak in favor of an independent particle model (Sec. III).

The regularities are the following:

Empirical values of M^2 for $M4$ transitions are of order unity and show little scattering and no distinction between odd proton and odd neutron nuclei. The lack of scattering within each group of transitions is consistent with predictions of a single particle model. However, according to this model, one would expect odd proton nuclei to have lifetimes about half as large as odd neutron nuclei for the same transition energy, and also would expect lifetimes about 1/10 as large as found empirically. Empirical values of M^2 for $M4$ transitions appear to be larger for transitions in nuclei with nearly closed shells.

According to an independent particle model, M^2 for $E3$ transitions of energy 100 kev should be of order 10^{-6} for single neutron transitions, and vanish for many particle transitions, such as those between $p_{\frac{1}{2}}$ and 7/2+states. The fact that empirical M^2 for $E3$ transitions are small can be interpreted as resulting from small deviations from an independent particle model. In fact, empirical M^2 for transitions between $p_{\frac{1}{2}}$ and 7/2+states in odd-neutron nuclei appear to be smaller the more nearly the nucleus can be represented as a closed shell nucleus.

The empirical value of M^2 for an $M1$ isomeric transition in Li^7 is slightly larger than expected according to an independent particle model.

A graph of energy levels for a spherical square well potential is presented (Appendix, Fig. 2).

I. INTRODUCTION

IT was first suggested by v. Weizsacker,[1] and has become generally accepted, that nuclear isomeric states decay into each other by gamma-emission, but that the lifetime is large if the spin of the two states differs by several units of $\hbar$.

The emitted quantum may carry off angular momentum $L(\geq 1)$, giving rise to electric or magnetic 2^L pole radiation (denoted in this paper by EL or ML), according to whether the quantum has parity $(-1)^L$ or $(-1)^{L-1}$. It follows that the selection rules for EL and ML radiation, i.e., radiation of various multipolarities, are

$$|I_i - I_f| \leq L \leq I_i + I_f, \tag{1}$$

parity change $(-1)^L$ for EL, $(-1)^{L-1}$ for ML. Here I_i and I_f denote the spins of the initial and final states, respectively.

Electromagnetic radiation is not the only mode of decay for a nuclear excited state. Instead, an internal conversion electron may be emitted; i.e., an orbital electron may be ejected and carry off the energy of excitation. The number of electrons emitted from a given shell per quantum is called the conversion coefficient for that shell. Values of conversion coefficients depend on the multipolarity of the transition and on the electronic configuration. However, they do not depend on the detailed structure of the nucleus, and can therefore be calculated, in principle, to the same accuracy as spectroscopic problems.

K-conversion coefficients have been calculated by Rose *et al.*[2] neglecting the effect of screening, for energies above 150 kev, and by Reitz[3] for selected cases, including the effect of screening. Calculations of K, L_{I}, L_{II} and L_{III} conversion coefficients over a wide range of energies and including screening effects are now in progress.[4]

Conversion data are extremely useful for obtaining multipolarity of a transition, but not for obtaining information regarding detailed nuclear structure (apart from the spin and parity change). Goldhaber and Sunyar[5] have made multipolarity assignments for many transitions by comparing observed K-coefficients with Rose's theoretical values, and also from a semi-empirical analysis of K/L ratios, which indicates that K/L ratios are a function of Z^2/E and multipolarity alone (except for $M1$ transitions).[6] The work of Mihelich and Church[7] indicates that ratios of L-subshell conversion coefficients can be of use for assigning multipolarities and for analyzing transitions which involve a mixture of multipolarities.

The lifetime of an excited state for gamma-emission depends not only on the multipolarity and energy of the transition, but also on the detailed structure of the nucleus. It is, thus, not possible to identify the multi-

* This work was carried out in partial fulfillment of the requirements for a Ph.D. degree at the University of Chicago. It was supported by an AEC Predoctoral Fellowship.
† Now at Columbia University, New York, New York.
[1] C. F. v. Weizsacker, Naturwiss. **24**, 813 (1936).
[2] Rose, Goertzel, Spinrad, Harr, and Strong, Phys. Rev. **83**, 79 (1951).
[3] J. R. Reitz, Phys. Rev. **77**, 10 (1950).
[4] M. E. Rose and G. Goertzel (to be published).
[5] M. Goldhaber and A. W. Sunyar, Phys. Rev. **83**, 906 (1951).
[6] M. Goldhaber (private communication).
[7] J. W. Mihelich and E. L. Church, Phys. Rev. **85**, 733 (1952); J. W. Mihelich, Phys. Rev. **87**, 646 (1952).

polarity of a transition from a lifetime measurement alone, without specific assumptions as to nuclear structure.

However, information regarding nuclear structure can be obtained by comparing the measured lifetime of a transition with the lifetime calculated using a specific nuclear model, e.g., the independent particle model,[8] provided the multipolarity of the transition has already been identified, say, from conversion data.

II. THEORETICAL CALCULATIONS OF LIFETIMES FOR GAMMA-DECAY

a. Single Proton for Spin Change Equal to Multiple Order-Central Potential

The transition probability per unit time for a system to undergo an electromagnetic transition from an initial state i to a final state f is given by the well-known equation[9]

$$W=\frac{2\pi}{\hbar}|\mathcal{H}_{fi}'|^2N(E). \tag{2}$$

Here $\mathcal{H}_{fi}'$ is the matrix element of the electromagnetic interaction between particles and field, $N(E)$ is the number of final states available per unit energy interval. The total nonrelativistic Hamiltonian of proton and electromagnetic field can be written[10]

$$\mathcal{H}=\frac{(\mathbf{p}-e\mathbf{A}/c)^2}{2M}+V(r)-\mu_P\frac{e\hbar}{2Mc}(\boldsymbol{\sigma}\cdot\mathbf{H})+\textstyle\sum_k n_k\hbar\omega_k. \tag{3}$$

Here M denotes mass of proton, μ_P is the proton magnetic moment in nuclear magnetrons. The vector potential, normalized to one quantum per unit volume is given by

$$\mathbf{A}=\boldsymbol{\varepsilon}(2\pi\hbar c^2/\omega)^{\frac{1}{2}}e^{i\mathbf{k}\cdot\mathbf{r}}. \tag{4}$$

The radiation interaction is contained in (3) and is given by

$$\mathcal{H}'=-\frac{e}{Mc}\mathbf{p}\cdot\mathbf{A}-\mu_P\frac{e\hbar}{2Mc}(\boldsymbol{\sigma}\cdot\mathbf{H}). \tag{5}$$

[The term $(e^2/2Mc^2)\mathbf{A}^2$ is neglected here, as are second order perturbation terms, both of which give rise to double quantum emission, with a transition probability which is usually several orders of magnitude less than the transition probability for single quantum emission.][11,12] The first term in (5) is the interaction energy of a point charge with an electromagnetic field, while the second term is the interaction energy of an intrinsic magnetic moment with the field. The transition probability between states is calculated using (2), summing over polarizations, and integrating over all directions of emission:

$$W=\frac{2\omega}{\hbar c}\int_\pi\frac{d\Omega_n}{4\pi}\sum_\varepsilon|J_{fi}|^2. \tag{6}$$

Here $d\Omega_n$ is the solid angle for direction of emission,

$$J_{fi}=\left|\left(\frac{e}{Mc}(\mathbf{p}\cdot\boldsymbol{\varepsilon})+\frac{i\omega}{c}\mu_P\frac{e\hbar}{2Mc}(\boldsymbol{\sigma}\cdot\boldsymbol{\varepsilon}')\right)e^{i\mathbf{k}\cdot\mathbf{r}}\right|_{fi}. \tag{7}$$

$\boldsymbol{\varepsilon}'=\mathbf{n}\times\boldsymbol{\varepsilon}$, and $\mathbf{n}=\mathbf{k}c/\omega$, the unit vector in direction of emission. The exponential in (7) can be expanded in ascending powers of $\mathbf{k}\cdot\mathbf{r}$, which is assumed to be $\ll1$.

Using elementary relations of quantum mechanics, one can write J_{fi} as follows:

$$\begin{aligned}J_{fi}=&\sum_{L=1}^{\infty}\frac{e}{L!}\left(\frac{i\omega}{c}\right)^L\left[(\mathbf{r}\cdot\boldsymbol{\varepsilon})(\mathbf{r}\cdot\mathbf{n})^{L-1}\right]_{fi}\\&+\sum_{L=1}^{\infty}\frac{e\hbar}{Mc}\frac{1}{(L-1)!}\left(\frac{i\omega}{c}\right)^L\left[\left(\frac{\mathbf{l}\cdot\boldsymbol{\varepsilon}'}{L+1}+\frac{\mu_P\boldsymbol{\sigma}\cdot\boldsymbol{\varepsilon}'}{2}\right)\right.\\&\left.\times\frac{(\mathbf{r}\cdot\mathbf{n})^{L-1}}{2}+\frac{(\mathbf{r}\cdot\mathbf{n})^{L-1}}{2}\left(\frac{\mathbf{l}\cdot\boldsymbol{\varepsilon}'}{L+1}+\frac{\mu_P\boldsymbol{\sigma}\cdot\boldsymbol{\varepsilon}'}{2}\right)\right].\end{aligned} \tag{8}$$

Here $\mathbf{l}$ is the orbital angular momentum operator in units of $\hbar$.

A transition between two given states can usually proceed by radiation of several multipolarities, consistent with the selection rules (1). In this paper, only those transitions are considered for which the radius of the nucleus, a, is much smaller than the wavelength of the radiation, $\omega a/c\ll1$; e.g., most nuclear isomeric transitions. For such cases, the calculations presented here, and also independent calculations of Weisskopf[13] and of Stech,[14] indicate, in accord with experimental evidence, that the transition will go primarily by the lowest multipole order permitted by the selection rules, *viz.*, EL for $\Delta I=L$, parity change $(-1)^L$. The only exceptions to this found experimentally to date are a few $M1+E2$ mixtures.[5,7]

Interaction terms which give rise to pure 2^L pole radiation transform under space rotation of the nucleus as the components of the irreducible tensor of order L,[15] denoted by $\mathfrak{D}^{(L)}$. For transitions involving $\Delta I=L$, but only for these, terms which result from an expansion of the interaction into powers of $\mathbf{k}\cdot\mathbf{r}$ transform as $\mathfrak{D}^{(L)}$. In particular, the Lth term of the first and second series of (8) corresponds to an EL and ML transition, respectively.

To evaluate (8) and the transition probability (6), one uses the fact that for a central potential, the wave

[8] M. G. Mayer, Phys. Rev. **78**, 16, 22 (1950).
[9] L. I. Schiff, *Quantum Mechanics* (McGraw-Hill Book Company, Inc., New York, 1949), first edition, p. 193.
[10] W. Heitler, *The Quantum Theory of Radiation* (Oxford University Press, London, 1947), second edition, p. 91.
[11] M. Goeppert-Mayer, Ann. Physik **9**, 273 (1931).
[12] R. G. Sachs, Phys. Rev. **57**, 194 (1940).
[13] V. F. Weisskopf, Phys. Rev. **83**, 1073 (1951).
[14] B. Stech, Z. Naturforsch. **7a**, 401 (1952).
[15] E. Wigner, *Gruppentheorie und iher Anwendung auf die Quantenmechanik der Atom Spektren* (Edwards Brothers, Ann Arbor, Michigan, 1944), p. 164.

function of initial and final state of the proton can be written as product of a radial function R and of an angular function $\theta_{l\,I}{}^{m}$ (for intrinsic spin $\frac{1}{2}$). Integrations over the angular functions can be performed exactly, since they involve only the symmetry properties of the nucleus. However, values of integrals over radial functions depend on the particular nuclear potential chosen.

Since the transition probability and thus the gamma-decay lifetime $\tau_\gamma=1/W$ is independent of the direction quantum number of the initial state m_i,[16] one can calculate the gamma-ray lifetime for a transition for which $I_i=I_f+L$ and take $m_i=I_i$; then the summation over final m-substates reduces to a single term, with $m_f=I_f$. Thus the gamma-ray lifetime is given by the following equations[17]:

$$\tau_{\gamma EL}{}^{\Delta l=L}_{\Delta l=L}=\left[\frac{2(L+1)}{L}\,\frac{1}{(2L+1!!)^2}\,\frac{e^2}{\hbar c}\omega\left(\frac{\omega a}{c}\right)^{2L}SM_{EL}{}^2\right]^{-1}, \quad (9a)$$

$$\tau_{\gamma ML}{}^{\Delta l=L}_{\Delta l=L-1}=\left[\frac{2(L+1)}{L}\,\frac{1}{(2L+1!!)^2}\,\frac{e^2}{\hbar c}\omega\left(\frac{\omega a}{c}\right)^{2L}\times\left(\frac{\hbar}{Mca}\right)^{2}SM_{ML}{}^2\right]^{-1}, \quad (9b)$$

where

$$M_{EL}{}^2=|(r/a)^L|_{fi}{}^2, \quad (10a)$$

$$M_{ML}{}^2=\left(\mu_P L-\frac{L}{L+1}\right)^2\left|\left(\frac{r}{a}\right)^{L-1}\right|_{fi}^2, \quad (10b)$$

$$2L+1!!=1\times3\times5\times\cdots\times(2L+1), \quad (11)$$

$$|(r/a)^L|_{fi}=\int_0^\infty R_f(r/a)^L R_i r^2 dr, \quad (12)$$

the radial integral in units of a^L, S is a statistical factor, whose value depends only on the spins involved in the transition and is defined as

$$S(I_i, L, I_f)=4\pi\sum_{m_f}\sum_{m}\left|\int_{4\pi}\theta_{l_f,\,I_f}{}^{m_f*}Y_L{}^{m_e}\theta_{l_i,\,I_i}{}^{m_i}d\Omega\right|^2. \quad (13)$$

$Y_L{}^m$ are spherical harmonics.

This gives

$$S(I_i, L, I_f)=\frac{(I_i-\frac{1}{2})!\times(2L+1)!!\times(2I_f)!!}{(2I_i)!!\times L!\times(I_f-\frac{1}{2})!} \quad (14a)$$

for $I_i=I_f+L$, namely, when the spin of the initial state is larger than the spin of the final state. For transitions with $I_f=I_i+L$ the statistical factor is given as follows, in accordance with a simple statistical weight argument:

$$S(I_i, L, I_f)=S(I_i+L, L, I_i)\times\frac{2I_i+2L+1}{2I_i+1}. \quad (14b)$$

Note that S equals 1 for any transition for which $I_f=\frac{1}{2}$ and $I_i=L+\frac{1}{2}$. M is the only term in the equation which depends on the detailed nuclear structure. It is called here the "matrix element." According to Eqs. (10), M is expected to be of order unity, if the radial integral is (see Sec. IIg). To bring Eqs. (9) into correspondence with Weisskopf's equations,[13] one writes them as follows:

$$\tau_{\gamma EL}=\frac{L(2L+1!!)^2}{4.4(L+1)}\left(\frac{197\text{ Mev}}{\hbar\omega}\right)^{2L+1}\times(a\text{ in }10^{-13}\text{ cm})^{-2L}10^{-21}S^{-1}M_{EL}{}^{-2}\text{ sec}, \quad (15a)$$

$$\tau_{\gamma ML}=\frac{L(2L+1)!!}{0.19(L+1)}\left(\frac{197\text{ Mev}}{\hbar\omega}\right)^{2L+1}\times(a\text{ in }10^{-13}\text{ cm})^{-(2L-2)}\cdot10^{-21}S^{-1}M_{ML}{}^{-2}\text{ sec}. \quad (15b)$$

TABLE I. Values of S for $E1$ and $E2$ transitions.

I_f	S_{E1}	S_{E2}
I_i+2	...	$\frac{15}{32}\frac{(2I_i+3)(2I_i+5)}{(I_i+1)(I_i+2)}$
I_i+1	$\frac{3}{4}\frac{(2I_i+3)}{(I_i+1)}$	$\frac{15}{16}\frac{(2I_i+3)}{I_i(I_i+1)(I_i+2)}$
I_i	$\frac{1}{4I_i(I_i+1)}$	$\frac{5}{16}\frac{(2I_i-1)(2I_i+3)}{(I_i-1)(I_i)}$
I_i-1	$\frac{3}{4}\frac{(2I_i-1)}{I_i}$	$\frac{15}{16}\frac{(2I_i-1)}{(I_i-1)(I_i)(I+1)}$
I_i-2	...	$\frac{15}{32}\frac{(2I_i-3)(2I_i-1)}{(I_i-1)(I_i)}$

b. Electric Transitions for Spin Change Less than Multipole Order

The EL transition probability now has to be derived by expanding the radiation interaction explicitly into terms which transform as $\mathfrak{D}^{(L)}$ under space rotation of the nucleus. It can be shown, and is stated here without proof, that Eqs. (9a), (10a), (13) still hold in the limit $\omega a/c\ll1$. For a given I_i, L, I_f, of the four possible kinds of transitions ($l_i=I_i\pm\frac{1}{2}$, $l_f=I_f\pm\frac{1}{2}$), two have the parity change $(-1)^L$ required for an EL transition, *viz.*, those transitions for which l_i-l_f-L is an even integer. S is the same for these two transitions, as can be seen by inserting the relation

$$\frac{\boldsymbol{\sigma}\cdot\mathbf{r}}{r}\theta_{I\pm\frac{1}{2},\,I}{}^{m}=\theta_{I\mp\frac{1}{2},\,I}{}^{m} \quad (16)$$

into (13), and taking into account the fact that $Y_L{}^m$ commutes with $\boldsymbol{\sigma}$. Thus S for electric transition is a

[16] S. R. de Groot and H. A. Tolhoek, Physica **15**, 833 (1949).
[17] S. A. Moszkowski, Phys. Rev. **83**, 1071 (1951).

function of I_i, L and L_f alone. Table I shows values of S for $E1$ and $E2$ transitions.

c. Transitions of a Single Neutron

The calculation of transition probabilities for a single neutron is similar to the calculation for a single proton. The interaction Hamiltonian is given, as before, by (5). However, the first term vanishes due to the absence of electric charge of the neutron. More rigorously, if one considers the nucleus as a two-body system of neutron and core moving about a common center of gravity, one obtains an electric moment term due to the motion of the core.

For this model of the nucleus

$$\mathcal{H}'(\mathbf{r})=-\frac{Ze}{Mc}\left[\mathbf{p}\cdot\mathbf{A}\left(\frac{-\mathbf{r}}{A}\right)\right]-\mu_N\frac{e\hbar}{2Mc}\left[\boldsymbol{\sigma}\cdot\mathbf{H}(\mathbf{r})\right], \quad (17)$$

where μ_N is the neutron magnetic moment in nuclear magnetons.

Thus, transitions between single neutron states involving $\Delta I=L$ and parity change $(-1)^{L-1}$ will proceed by magnetic 2^L pole radiation as in the single proton case. With respect to Eqs. (9b), obtained for the single proton case, the only change is that the term $[\mu_P L-(L/L+1)]^2$ is replaced by $(\mu_N L)^2$. However, electric 2^L pole transitions between states involving $\Delta I=L$ and parity change $(-1)^L$ now have probabilities only $(Z/A^L)^2$ as large as for the single proton case. One can also get a contribution to the transition probability from the second term in (17), because of interaction of intrinsic magnetic moment with the electromagnetic field.[13] It is easy to convince oneself that the EL and $M(L+1)$ transition probabilities resulting from intrinsic magnetic moment are smaller than the corresponding EL probabilities for a single proton (9a) (resulting from the EL moment) by a factor of order $(\hbar\omega/Mc^2)^2$. It is thus seen that the EL matrix elements for gamma-ray transitions involving $L\geq 2$, for odd neutron nuclei, assuming an independent particle model, are expected to be much smaller than 1.

d. Effect of a Spin-Orbit Interaction on $M1$ Transitions

Sachs and Austern[18] have shown that the introduction of a velocity-dependent interaction will leave electric transition probabilities the same as calculated above, but that it will result in different magnetic transition probabilities. In particular, Jensen and Mayer[19] have shown that the introduction of a spin-orbit coupling for a single proton leads to finite $M1$ transition probabilities, both for $\Delta l=0$, and for $\Delta l=2$. In contrast, for a pure central potential, in the absence of spin-orbit coupling, no $M1$ transitions can occur, because either the $M1$ matrix element between initial and final state vanishes, or the two states are degenerate.

[18] R. G. Sachs and N. Austern, Phys. Rev. **81**, 705, 710 (1951).
[19] J. H. D. Jensen and M. G. Mayer, Phys. Rev. **85**, 1040 (1952).

With reasonable assumptions regarding the strength of spin-orbit coupling in nuclei ($\Delta E=2$ Mev for $A=100$, $l=4$),[20] Jensen and Mayer obtain $M^2=0.26$ for an $M1$ transition in an odd proton nucleus involving $\Delta l=2$.

e. Transitions between States of Several Particles

Strictly speaking, all nuclear states, except those of a single nucleon, are states of several particles. In most cases involving an odd number of particles, the spins of all but one particle couple to spin zero, and the state has the I of the odd particle.[8] These particular states will be referred to as "states of normal coupling." Such states behave in many ways like the corresponding states of a single particle, e.g., have the same spin and magnetic moment. It shall be assumed that the particles can be treated as independent; i.e., that the wave function of a state of several particles can be written as a sum of products of single particle wave functions.

States in which an odd number of identical particles couple to a spin different from the spin of the odd particle; e.g., $(g_{9/2})_{7/2+}$ [3,5 or 7] are also known to occur.[6,17] Such states are called here "states of abnormal coupling." Calculations of Kurath[21] and of Talmi[22] of energy levels for the different configurations of three identical particles in a $d_{5/2}$ or $f_{7/2}$ orbit indicate that the state of normal coupling is expected to be the ground state, provided the forces between particles are of short range, compared to the nuclear radius. However, for a range of forces comparable to the nuclear radius, Kurath and also Talmi find that the state $(j)_{j-1}{}^3$ can be the ground state. In view of these results, the existence of states of abnormal coupling should not be surprising.

The wave functions of individual nucleons in various quantum states shall be labeled $\psi_{j_k}{}^{m_k}$ and one writes symbolically for the properly antisymmetrized linear combination of single particle wave functions of n nucleons; i.e., for the Slater determinant,

$$\Psi=\psi_{j_1}{}^{m_1}\psi_{j_2}{}^{m_2}\cdots\psi_{j_n}{}^{m_n}. \quad (18)$$

The wave function for $2s$ identical particles, each of spin j, and differing only in m, which couple to a total spin 0, denoted by $\Psi(j^{2s})_0{}^0$ can be written as

$$\Psi(j^{2s})_0{}^0=\left(\sum_{m=\frac{1}{2}}^{j}(-1)^{j-m}\psi_j{}^m\psi_j{}^{-m}\right)^s\Big/\left[\frac{(j+\frac{1}{2})!s!}{(j+\frac{1}{2}-s)!}\right]^{\frac{1}{2}}. \quad (19)$$

It is easily seen that $\Psi(j^{2s})_0{}^0$ is an eigenfunction of I^2 and of I_z with the proper eigenvalues $I(I+1)=0$, $M=0$.

Any term containing the same value of m twice automatically vanishes. Since there are $(j+\frac{1}{2}!)/(s!j+\frac{1}{2}-s!)$ different nonvanishing terms, and each one occurs $s!$ times, the normalization of (19) is warranted.

[20] M. G. Mayer, Phys. Rev. **74**, 235 (1948).
[21] D. Kurath, Phys. Rev. **80**, 98 (1950).
[22] I. Talmi, Phys. Rev. **82**, 101 (1951).

A wave function of $2s+1$ particles, each of spin j, which couple to $I=j$, $M=j$ is given by

$$\Psi(j^{2s+1})_j{}^j = \psi_j{}^j\left(\sum_{m=\frac{1}{2}}^{j}(-1)^{j-m}\psi_j{}^m\psi_j{}^{-m}\right)^s \Big/ \left[\frac{(j-\frac{1}{2})!s!}{(j-\frac{1}{2}-s)!}\right]^{\frac{1}{2}}. \quad (20)$$

For $j\leq 7/2$, these wave functions are the only ones which can be constructed.

The total wave function of a number of identical particles can thus be written, apart from normalization factors, as products of wave functions of pairs of identical particles coupling to a spin 0, and that of the wave function of the odd particle, if any. The total normalization factor is not equal to the product of the separate normalization factors, because many terms in the product can vanish.

The total wave function of n_a particles in an orbit a and n_b particles in a different orbit b is just the product of $\Psi(j_a{}^{n_a})$ and of $\Psi(j_b{}^{n_b})$, including the value of the normalization factor.

Using the wave functions (19) and (20), and assuming an interaction operator which can be written as a sum of terms, each of which acts on one particle at a time, and which is symmetric in all the particles (called a symmetric single-particle interaction operator),

$$O=\sum_{\text{particles } k} O_k, \quad (21)$$

one can evaluate the probability for transitions between states of normal coupling involving configurations of only protons (or neutrons).[23]

This transition probability is equal to the transition probability between the corresponding single particle states, multiplied by a factor denoted here by ρ, which depends on the number of particles in the two orbits involved in the transition and also on the spins of these orbits. We must consider two cases, according to whether the particle undergoing the transition is an odd one or an even one.

Let the initial state of spin j_a contain $2s_a+1$ particles in orbit a and $2s_b$ particles in orbit b, and the final state of spin j_b have $2s_a$ and $2s_b+1$ particles in orbits a and b, respectively.

Then (odd particle jumping), ρ is given by

$$\rho=\frac{j_a+\frac{1}{2}-s_a}{j_a+\frac{1}{2}}\times\frac{j_b+\frac{1}{2}-s_b}{j_b+\frac{1}{2}}. \quad (22a)$$

Alternatively, let the initial state of spin j_a be composed of $2s_a-1$ particles and $2s_b$ particles in orbits a and b, and the final state of spin j_b contain $2s_a$ and $2s_b-1$ particles in these orbits.

Then (even particle jumping), ρ is given by

$$\rho=\frac{s_a}{j_a+\frac{1}{2}}\times\frac{s_b}{j_b+\frac{1}{2}}. \quad (22b)$$

According to Eqs. (22), the transition probability between states of partially filled orbits is less than that between the corresponding single particle states. Physically, this reduction comes about from the fact that a fraction of the substates, which would be available to the particle in the corresponding transition between single particle states, are not available in this case to the jumping particle, because they are already occupied.

It can also be shown that certain kinds of transitions cannot occur, according to an independent particle picture, assuming a symmetric single-particle interaction operator. These follow:

1. Transitions which require change of orbit for several particles.

This is an immediate consequence of the form of the interaction operator.

2. Transitions between a state of normal coupling and a state of abnormal coupling of only protons (or neutrons), involving a change of orbit for one particle.

Such a transition would require that several particles change their state, since not only is one particle changing its orbit, but at least two other particles must change from being lined up antiparallel to being lined up in a different way.

3. M1 transitions between two states of the same configuration, consisting exclusively of protons (or neutrons), and differing only in coupling and no change of orbit.

The transition matrix element is

$$\int\Psi_f(\textstyle\sum_k O_k)\Psi_i d\tau = c\int\Psi_f(\sum_k j_k)\Psi_i d\tau \quad (23)$$

which follows from the relation[24]

$$\int\psi_j{}^{m'}O\psi_j{}^m d\tau = c\int\psi_j{}^{m'}j\psi_j{}^m d\tau \quad (24)$$

[23] For many nuclear states, e.g. ground and low-lying isomeric states of heavy nuclei with $N\geq 50$ and also of some light nuclei, all orbits partially or completely filled by protons are also completely filled by neutrons. The isotopic spin of such a state is uniquely given as $(N-Z)/2$. A transition between two such states involving a particle jump between orbits a and b can be characterized as a proton (or neutron) transition if the orbits a and b are partially filled by protons (or neutrons).

According to the independent particle model, the transition probability between these two states is equal to the transition probability between two corresponding states of a hypothetical nucleus for which there are protons (or neutrons) only in orbits a and b. Thus, although in this section states consisting exclusively of protons (or neutrons) are considered, the results are applicable to heavy nuclei, in so far as the independent particle model is valid.

[24] E. U. Condon and G. H. Shortley, *The Theory of Atomic Spectra* (University Press, Cambridge, England, 1951), first edition, p. 61.

where c is independent of the values of m and m'. Since the operator $I=\sum_k j_k$ does not mix wave functions of different states, the integral (23) must vanish.

f. Numerical Calculations of Radial Integrals

The radial integrals in Eqs. (10) depend on the form of the nuclear potential. It is questionable whether the single particle wave functions calculated for a central potential are good approximations to the real nuclear wave functions. However, the success of the independent particle model in explaining many observed phenomena[8] makes the attempt to use single particle wave functions at least plausible.

The radial integrals Eq. (12) have been evaluated for several cases:

1. *Wave Function Constant Inside Nucleus—Vanishing Outside*[13]

For EL radiation $$|(r/a)^L|_{fi}=3/(L+3). \quad (25a)$$

For ML radiation $$|(r/c)^{L-1}|_{fi}=3/(L+2). \quad (25b)$$

2. *Spherical Square Well Potential—No Spin-Orbit Coupling*

The wave functions are obtained by solving the eigenvalue problem for a square well (of radius a and depth V_0), i.e., by obtaining the solutions of the Schroedinger equation for $r\leq a$ and for $r\geq a$ and fitting the values of the wave functions and their derivatives at $r=a$.

Calculations of the radial integrals were made for several cases which represent typical isomeric transitions in nuclei. All states are assumed to be bound by 8 Mev. (V_0 is slightly different for initial and final state. The radius a has been taken as $1.5\times10^{-13}\,A^{\frac{1}{3}}$ cm.)

The results of these calculations are shown in Table II.

The radial integrals (in units of proper power of nuclear radius), are nearly independent of the size of the nucleus. This is a consequence of the fact that for the cases treated here, the binding energy is much smaller than the depth of the potential well.

The results of Table II suggest, in agreement with expectations, that values of radial integrals depend less on the particular nuclear model for large multipole orders of the radiation than for small multipole order, and that they do not depend strongly on the particular states nor on nuclear size for a given multipole order.

3. *Spherical Square Well Potential with Spin-Orbit Coupling*

The radial integral was evaluated for a square well potential with an additional spin-orbit interaction given by

$$-K-\frac{1}{r}\frac{dV}{dr}(\mathbf{l}\cdot\boldsymbol{\sigma}) \quad (26)$$

TABLE II. Calculated values of radial integral.

Transition[a]	Cases of interest	Radial integral $\lvert(r/a)^{L \text{ or } L-1}\rvert_{fi}$ for EL or ML: Square well $A=100$	Square well $A=140$	Constant wave function
$1h-3s$	$E5\ h_{11/2}\rightarrow s_{1/2}$	0.43	0.40	0.38
$1g-2p$	$M4\ g_{9/2}\rightarrow p_{1/2}$	0.45	0.43	0.50
$1h-2d$	$M4\ h_{11/2}\rightarrow d_{3/2}$ $E3\ h_{11/2}\rightarrow d_{3/2}$	0.43	0.42	0.50
$2d-3s$	$E2\ d_{3/2}\rightarrow s_{1/2}$	0.52	0.50	0.60

[a] For each state, the number denotes radial quantum number n (number of radial nodes $+1$), letter corresponds to orbital quantum number l.

(which is infinite at $r=a$ and vanishes everywhere else), for the special case of an $M4$ transition between a $1g_{9/2}$ and $2p_{1/2}$ state in In^{113}.

The value of K and of well depth V_0 were so chosen that both initial and final state are bound by 8 Mev. The radial wave functions are assumed to be of the same kind as those of a square well, but the boundary conditions require a finite discontinuity in the derivative at $r=a$. The value of the radial integral for this case is 0.53 compared to 0.44 for the same transition in a square well potential without a spin-orbit interaction.

g. Summary of Theoretical Results

The lifetime for a nuclear isomeric state for gamma-decay can be written as follows (Sec. IIa):

$$\tau_{\substack{\gamma EL\\ \Delta I=L\\ \Delta I=L}}=\left[\frac{2(L+1)}{L}\frac{1}{(2L+1!!)^2}\omega\frac{e^2}{\hbar c}\left(\frac{\omega a}{c}\right)^{2L}SM_{EL}{}^2\right]^{-1}; \quad (9a)$$

$$\tau_{\substack{\gamma ML\\ \Delta I=L\\ \Delta I=L-1}}=\left[\frac{2(L+1)}{L}\frac{1}{(2L+1!!)^2}\omega\times\frac{e^2}{\hbar c}\left(\frac{\omega a}{c}\right)^{2L}\left(\frac{\hbar}{Mca}\right)^{2}SM_{ML}{}^2\right]^{-1}. \quad (9b)$$

For transitions for which $I_i=I_f+L$,

$$S(I_i, L, I_f)=\frac{(I_i-\frac{1}{2})!}{(2I_i)!!}\frac{2L+1!!}{L!}\frac{(2I_f)!!}{(I_f-\frac{1}{2})!}, \quad (14a)$$

and a simple statistical weight argument gives S for transitions for which $I_i=I_f-L$.

In the later discussion of $M4$ transitions (Sec. IIIa), the following values of S will be of particular interest:

$$S(9/2, 4, \tfrac{1}{2})=1; \quad (27a)$$

$$S(\tfrac{1}{2}, 4, 9/2)=5; \quad (27b)$$

$$S(11/2, 4, \tfrac{3}{2})=15/11; \quad (27c)$$

$$S(13/2, 4, 5/2)=225/143. \quad (27d)$$

The value of M^2 depends on the particular model of the

nucleus. For a single proton (Sec. IIa),

$$M_{EL}^2 = |(r/a)^L|_{fi}^2; \tag{10a}$$

$$M_{ML}^2 = \left(\mu_P L - \frac{L}{L+1}\right)^2 \left|\left(\frac{r}{a}\right)^{L-1}\right|_{fi}^2. \tag{10b}$$

For a single neutron (Sec. IIc),

$$M_{EL}^2 = \left(\frac{Z}{A^L}\right)^2 \left|\left(\frac{r}{a}\right)^L\right|_{fi}^2, \tag{28a}$$

or of order $(\hbar\omega/Mc^2)^2$, whichever is larger.

For $E3$ transitions of energy 100 kev, $M^2 \sim 10^{-8}$.

$$M_{ML}^2 = (\mu_N L)^2 |(r/a)^{L-1}|_{fi}^2. \tag{28b}$$

Theoretical values of M^2 for $M4$ transitions square-well potential, $A=100$ (Secs. IIf, IIIa), follow:

	Transition	Group	M_{M4}^2	
proton	$1g_{9/2} \leftrightarrow 2p_{1/2}$	$(4P)$	22	(29a)
neutron	$1g_{9/2} \leftrightarrow 2p_{1/2}$	$(4N)$	11.8	(29b)
neutron	$h_{11/2} \leftrightarrow 2d_{3/2}$	$(5N)$	10.8	(29c)

For transitions between states of normal coupling, involving configurations of only protons (or neutrons), calculations based on an independent particle model (Sec. IIe), give as result that M^2 is equal to M^2 for the corresponding transition between pure single particle states, times a factor ρ.

For $[(j_a)^{2s_a+1}(j_b)^{2s_b}]_{j_a} \rightarrow [(j_a)^{2s_a}(j_b)^{2s_b+1}]_{j_b}$,

$$\rho = \frac{j_a + \frac{1}{2} - s_a}{j_a + \frac{1}{2}} \times \frac{j_b + \frac{1}{2} - s_b}{j_b + \frac{1}{2}}. \tag{22a}$$

For $[(j_a)^{2s_a-1}(j_b)^{2s_b}]_{J_a} \rightarrow [(j_a)^{2s_a}(j_b)^{2s_b-1}]_{J_b}$,

$$\rho = \frac{s_a}{j_a + \frac{1}{2}} \times \frac{s_b}{j_b + 1}. \tag{22b}$$

TABLE III. Distribution of $\log M^2$ values for $M4$ transitions in odd-A nuclei; subscript denotes group of transition.

				Xe_{5N}^{135}
				Te_{5N}^{125}
				Te_{5N}^{123}
				Te_{5N}^{121}
				Sn_{5N}^{117}
		Ba_{5N}^{137}		Tc_{4P}^{99}
		Ba_{5N}^{135}	Pb_{6N}^{207}	Tc_{4P}^{97}
	Hg_{6N}^{199}	Xe_{5N}^{131}	Xe_{5N}^{133}	Tc_{4P}^{95}
	Hg_{6N}^{197}	Te_{5N}^{129}	Te_{5N}^{127}	Nb_{4P}^{95}
Pt_{6N}^{195}	Pt_{6N}^{197}	In_{4P}^{115}	Y_{4P}^{87}	Zr_{4N}^{89}
Ba_{5N}^{133}	Xe_{5N}^{129}	In_{4P}^{113}	Sr_{4N}^{87}	Kr_{4N}^{85}
Nb_{4P}^{97}	Zn_{4N}^{69}	Y_{4P}^{91}	Sr_{4N}^{85}	
$\bar{9}.7$[a]	$\bar{9}.8$	$\bar{9}.9$	0.0	0.1
	Sn_{5N}^{119}	Y_{4P}^{89}	Te_{5N}^{131}	Nb_{4P}^{91}
	0.2	0.3	0.4	0.9

$\log_{10} M^2$

[a] $\bar{9}.7$ denotes $9.7-10$.

Example: The transition $[p_{\frac{1}{2}}(g_{9/2})^2]_{\frac{1}{2}-} \rightarrow [(g_{9/2})^3]_{9/2+}$ has a transition probability 4/5 as large as $p_{\frac{1}{2}} \rightarrow g_{9/2}$ transition. A $[p_{\frac{1}{2}}(g_{9/2})^2]_{\frac{1}{2}-} \rightarrow [(p_{\frac{1}{2}})^2(g_{9/2})]_{9/2+}$ transition has a transition probability only 1/5 as large as the transition between single particle states. Thus the three transitions are all between $\frac{1}{2}-$ and $9/2+$ states yet the transition probabilities are different.

Transitions requiring change of orbit for several particles cannot occur according to an independent particle model (Sec. IIe); neither can transitions between a state of normal coupling and one of abnormal coupling of only protons (or neutrons), involving a change of orbit for one particle, e.g., $[p_{\frac{1}{2}}(g_{9/2})^2]_{\frac{1}{2}-} \rightarrow [(g_{9/2})^3]_{7/2+}$.

$M1$ transitions between two states of the same configuration of only protons (or neutrons), and differing only in coupling, and involving no change of orbit, e.g., $[(g_{9/2})^3]_{9/2+} \rightarrow [(g_{9/2})^3]_{7/2+}$, cannot occur either.

III. SOME INTERPRETATIONS—VALUES OF M^2

Values of empirical squares of matrix elements M^2, obtained by comparing the experimental lifetime, corrected for internal conversion, with the theoretical lifetime of Eqs. (9) or (15), show some interesting regularities, which may have significance in connection with nuclear shell structure.[8]

A comprehensive summary of the classification of isomeric transitions as well as a discussion of values of empirical matrix elements has been given by Goldhaber and Sunyar.[5] Some of their conclusions were derived independently by the author.[17] It is found that most magnetic transitions have empirical M^2 values of order 1, while most electric transitions (except some $E2$), have smaller M^2 values, generally of order 10^{-3}, resulting in comparable lifetimes for EL and ML transitions of the same energy.

However, some additional results of an analysis of M^2 values, which were not discussed in the above papers, can be mentioned at this point; *viz.*, $M4$ transitions in odd-A nuclei, $E3$ transitions in odd-A nuclei, and the $M1$ transition in Li^7.

a. $M4$ Transitions in Odd-A Nuclei

$M4$ transitions are found precisely where they are expected according to the j-j coupling shell model.[8] These transitions may be divided into four groups, according to the number of the shell in which they occur (near the end), and according to whether N or Z is odd. The shells containing up to 50, 82, and 126 particles are denoted by 4, 5, and 6 (corresponding transitions: $g_{9/2} \leftrightarrow p_{1/2}$, $h_{11/2} \rightarrow d_{3/2}$, and $i_{13/2} \rightarrow f_{5/2}$), respectively, in accordance with the order of filling of shells in the j-j coupling model.

Empirical values of M^2 for $M4$ transitions (calculated with the aid of Eqs. (10b) and (27), are in good agreement with the estimates of Weisskopf,[13] $M^2=1$, and show surprising lack of scattering, as can be seen from Table III. The average and scatter of $\log M^2$ values for

TABLE IV. Average and scatter of $\log M^2$ values for various groups of $M4$ transitions in odd-A nuclei.

Group	Number of cases	Average	Scatter[a]
$4P$ $g_{9/2}-p_{1/2}$	11	$\underline{0}.08$	0.32
$4N$ $g_{9/2}-p_{1/2}$	5	$\overline{9}.99$	0.09
$5N$ $h_{11/2}-d_{3/2}$	15	$\underline{0}.03$	0.16
$6N$ $i_{13/2}-f_{5/2}$	5	$\overline{9}.83$	0.10
Total odd$-Z$	11	$\underline{0}.08$	0.32
Total odd$-N$	25	$\overline{9}.98$	0.16
Total	36	0.01	0.23

[a] As measured by root mean square deviation.

$M4$ transitions of the various groups ($4P$, $4N$, $5N$, and $6N$) are shown in Table IV. It is seen that the average value of $\log M^2$ is nearly identical for the $4P$, $4N$, and $5N$ groups, and slightly smaller for the small $6N$ group. Goldhaber and Sunyar[5,25] have calculated M^2 by putting $S=1/(2I_i+1)$, rather than values given by Eq. (27), their idea probably being that lifetimes should be proportional to the number of initial m-substates. Owing to this difference, they find a considerably larger average value for M^2 in the $5N$ group than in the $4N$ group. As the statistical factors used here, Eqs. (14, 27) are uniquely given by integration of the angular parts of the nuclear wave functions, their adoption seems more realistic than the use of the factors proposed by Goldhaber and Sunyar.[5]

Theoretical values of M^2 for $M4$ transitions (assuming a single proton or neutron in a spherical square well, nucleus of $A=100$, $a=1.5\times10^{-13}\,A^{\frac{1}{3}}$ cm), are given by Eqs. (29) for $4P$, $4N$, and $5N$ transitions.

On the basis of a single particle model, one would thus expect M^2 values for odd proton nuclei as well as odd neutron nuclei to show very little scattering, and also very little difference between the $4N$ and $5N$ groups.

One would, however, expect a considerable difference in M^2 values between odd proton and odd neutron nuclei, with the former expected to be about twice as large as the latter. No such difference between M^2 values is found experimentally, as far as can be ascertained from the data available to date. According to Eqs. (29), M^2 values predicted by the single particle model are of order 10, while empirical M^2 values are of order 1. One might attempt to reduce this apparent discrepancy by modifying the theoretical predictions; e.g., by substituting for μ_P and μ_N not the magnetic moment of a free particle, but the effective intrinsic magnetic moment for an odd particle, which can be inferred from a magnetic moment measurement of the ground state, on the assumption that the spin and magnetic moment of the nucleus is determined by that of the odd particle.[26] This would give values of theoretical M^2 lower than the values of Eqs. (29). However, a large amount of scattering of theoretical M^2 values would now result, due to scattering of values of μ_P and μ_N for ground states.

Furthermore, the difference between theoretical M^2 values for odd-proton and odd-neutron transitions would still exist. In any case, it is questionable whether any relation exists between matrix elements for $M4$ transitions and static $M1$ momenta of ground states, since the "intrinsic magnetic moments," which are assumed to influence the magnitude of these quantities, may be quite different from each other.

Empirical values of $\log M^2$ as function of neutron number (Fig. 1) show some interesting regularities. For $4P$ isomers, $\log M^2$ as function of N has a maximum at $N=50$, while for $5N$ isomers, it tends to increase as function of $N(N<82)$ and decreases as function of $Z(Z>50)$. In general, M^2 values appear to be larger, the more closely the nucleus can be represented by closed shells. The apparent tendency of empirical M^2 to be larger for nearly closed shell nuclei than for others receives some support from theoretical values of M^2 calculated for transitions between states containing several particles on the basis of an independent particle model [Sec. IIe, Eqs. (22)].

The M^2 values for transitions between states of normal coupling are, in general, found to be smaller than those for the corresponding true single particle states.

b. $E3$ Transitions in Odd-A Nuclei

Most known $E3$ transitions in odd-A nuclei are either in odd neutron nuclei or between $p_{1/2}$ and $7/2+$ states (the latter for odd particle number 43, 45, or 47). For a single neutron transition, the value of M^2, according to an independent particle model, should be of order $(Z/A^{\frac{1}{3}})^2$ because of the recoil of the core, or of order $(\hbar\omega/Mc^2)^2$ because of the intrinsic magnetic moment of the $(\hbar\omega/Mc^2)^2$ neutron, whichever is the larger (Sec. IIc); i.e., be of order 10^{-8} for $L=3$, $A=100$, $E=100$ kev. The empirical value of M^2 for the $E3$ transition in $Cd^{111}(h_{11/2}\rightarrow d_{5/2}$, energy 149 kev) is 4.5×10^{-6}.

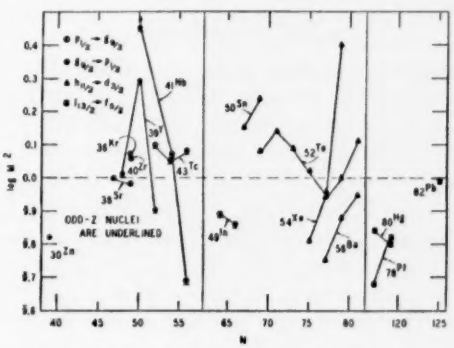

FIG. 1. Values of $\log M^2$ for $M4$ transitions *versus* neutron number (odd-A nuclei).

[25] The term "$|M|^2$" used by Goldhaber and Sunyar is the same as SM^2 used in this paper, while their "$|M'|^2$" is equivalent to M^2 used here, the latter normalized to an average value of 1.

[26] F. Bloch, Phys. Rev. **83**, 839 (1951).

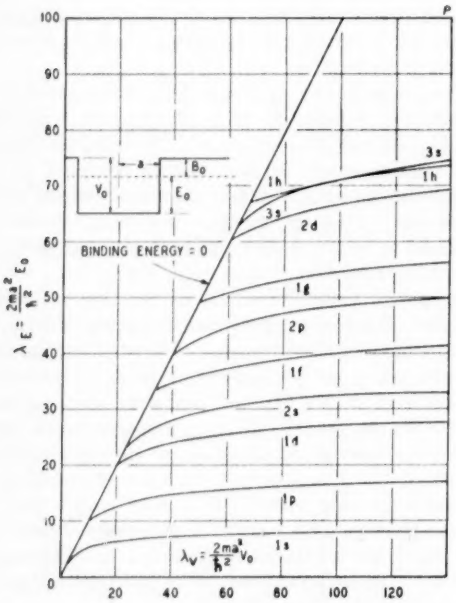

FIG. 2. Energy levels for a spherical square well.

For a transition between $p_{1/2}$ and 7/2+ states, M^2 vanishes according to the independent particle model (Sec. IIe). It is thus not surprising that the empirical values of M^2 for $E3$ transitions are small and show considerable scattering, as shown in Table V.

The size of the M^2 can be taken as a measure of the deviations from a pure independent particle model. As it is likely that the size of these deviations will probably be different nuclei, the variation of $\log M^2$ values shown in Table V can be understood in this picture. In fact, it can be seen that $\log M^2$ decreases as function of N for N between 43 and 47; i.e., as the neutron number approaches 50. This is not surprising, since one would expect greater validity of the independent particle model for a given nucleus, the more nearly it is a closed shell nucleus.

c. $M1$ Transition in Li^7

The $\frac{1}{2}\rightarrow\frac{3}{2}$-transition in Li^7 (energy 479 kev), is the only one of the $M1$ group known for which the independent particle model (including the effect of spin-orbit coupling) predicts matrix elements of order 1.

The theoretical M^2 value according to this model is $(\mu_P-\frac{1}{2})^2=5.25$ for a free proton undergoing a $p_{\frac{1}{2}}\rightarrow p_{\frac{3}{2}}$ transition. According to calculations similar to the ones described in section IIe, M^2 is 2.7 for a $[(p_{\frac{3}{2}})^3]_{\frac{1}{2}-}\rightarrow [(p_{\frac{3}{2}})^3]_{\frac{3}{2}-}$ transition, and 1.0 for a $[(p_{\frac{3}{2}})^2(p_{\frac{1}{2}})]_{\frac{1}{2}-}\rightarrow [(p_{\frac{3}{2}})^3]_{\frac{3}{2}-}$ transition, for a system of two neutrons and one proton with isotopic spin $\frac{1}{2}$ in both initial and final state.

The empirical value of M^2 is 7.6. The fact that the empirical value of M^2 is larger than the theoretical M^2 for any of the configurations mentioned, is somewhat surprising, but is probably not significant, due to the questionable validity of the assumptions made in the calculations.

The author wishes to express his deep gratitude to Professor Maria G. Mayer, who has been a constant source of inspiration throughout his graduate studies, and who gave him so much valuable advice during the course of this work. He also wishes to thank Dr. Valentine L. Telegdi for many stimulating discussions and criticisms.

The author held an Atomic Energy Commission Predoctoral Fellowship during most of the academic year 1951–1952 and gratefully acknowledges the financial aid received.

TABLE V. Empirical $\log M^2$ values for some $E3$ transitions between $p_{1/2}$ and 7/2+ states in odd-N nuclei.

	Z	34	36
N 43		$\bar{7}.4$[a]	$\bar{6}.6$
45		$\bar{6}.6$	$\bar{6}.5$
47		$\bar{5}.8$	$\bar{6}.2$

[a] $\bar{7}.4$ denotes 7.4 − 10.

APPENDIX. ENERGY LEVELS FOR A SPHERICAL SQUARE-WELL POTENTIAL

To evaluate the radial wave functions (Sec. IIf), it was first necessary to obtain energy levels. A graph of energy levels is given here in the hope that it may be useful for related problems of energy levels in a spherical square-well potential. Assume,

$$\lambda_E \quad \text{(30a)}$$

$$\lambda_B=\frac{2Ma^2}{\hbar^2}\begin{Bmatrix}E_0\\B_0\\V_0\end{Bmatrix}, \quad \text{(30b)}$$

$$\lambda_V \quad \text{(30c)}$$

where a=radius of well, V_0=depth of potential, E_0 =kinetic energy of particle in nucleus, and B_0=binding energy ($E_0+B_0=V_0$). Specifically, assuming $a=1.5\times10^{-13}\times A^{\frac{1}{3}}$ cm and taking energies in Mev, we obtain

$$2Ma^2/\hbar^2=0.1084A^{\frac{1}{3}}\ \text{Mev}^{-1}. \quad (31)$$

The energy value solutions of the Schroedinger equation for states with radial quantum numbers n (number of radial nodes +1), and orbital angular momentum numbers l are plotted as function of λ_V in Fig. 2. Using Fig. 2 it is possible to obtain the position of energy levels for square wells for a wide range of radii and well depths.

Magnetic Analysis of the Deuteron-Beryllium Reactions*

R. W. GELINAS AND S. S. HANNA
Department of Physics, Johns Hopkins University, Baltimore, Maryland
(Received September 23, 1952)

The charged particle spectra from the deuteron bombardment of Be^9 have been analyzed magnetically with a spectrograph employing a second-order focus. Previously established transitions to states in Be^{10} and Li^7 were observed, and a careful search of the proton and alpha-spectra failed to disclose additional states in these nuclei, throughout the region explored. The excitation energy of the second excited state of Li^7 was determined as 4.62 ± 0.02 Mev. The transition to the broad first excited state of Be^8, as well as to the ground state, was revealed in the triton spectrum. Alpha- and triton continue resulting from the three-particle disintegrations, $Be^9(d,\alpha)Li^{7**}(\alpha)t$ and $Be^9(d,t)Be^{8*}(\alpha)\alpha$, were also observed and examined in some detail. Other three-particle disintegrations appear improbable but cannot be definitely excluded, at the bombarding energies employed from 0.5 to 1.0 Mev.

I. INTRODUCTION

THE charged particles emitted during the deuteron bombardment of beryllium have previously been investigated by both range and magnetic analysis. With the former method two groups of alpha-particles,[1] two groups of protons,[2] and a single group of tritons[3] have been observed. With magnetic analysis several investigators[4] have examined these groups and have carefully measured the Q values. In addition, the spectrum of the alpha-particles has been observed up to an excitation energy in Li^7 of about 3.6 Mev by Buechner and Strait[4] and by Inglis,[5] at different bombarding energies. Above an excitation energy in Li^7 of 2.5 Mev, Inglis observed the rise of a broad peak or plateau of alpha-particles. Using range analysis, Gove and Harvey[6] examined the alpha-particle spectrum, at a bombarding energy of 14 Mev. In a careful series of measurements with this reaction and with the inelastic scattering of protons, deuterons, and alphas by the Li^7 nucleus itself, they found a new level in Li^7 at about 4.7 Mev. Other investigators have subsequently observed transitions to this state under a variety of conditions.[7,8] In a study of the angular distributions of the Be^9+d reactions, the emission of tritons of less energy than the ground-state group was observed by Resnick and Hanna.[9]

In the present experiment we have investigated, by means of magnetic analysis, the alpha-spectrum from the deuteron bombardment of beryllium up to an excitation energy in Li^7 of 5.3 Mev, the proton spectrum up to 4.0 Mev in Be^{10}, and the triton spectrum up to 4.8 Mev in Be^8. Bombarding energies ranging from 0.47 to 1.02 Mev were used in various phases of the work. The presence of the short-range alpha-group observed by Gove and Harvey[6] was confirmed, as previously reported.[7] In addition to the well-defined triton group forming the ground state of Be^8, broad structure was observed in a region corresponding to the known state in Be^8 at about 3 Mev. In addition to these features the alpha- and triton continua, previously observed,[5,9] have been studied in some detail. Recently, Cuer and Jung[10] have reported a similar investigation of the triton spectrum using range analysis aided by magnetic deflection.

II. EXPERIMENTAL PROCEDURE

The magnetic spectrograph used in the investigation has been described by Inglis,[5] and the theory has been given by Hafner, Donoghue, and Snyder.[11] The apparatus is now equipped with a more compact magnet and is mounted so that it can be rotated for observations at all angles from about 20° to 160° to the beam. Figure 1 shows a perspective view of the instrument in operation in the present investigation. The angular aperture in the vertical plane was approximately 5°, considerably smaller than was necessary. Because of the relatively high yield of the deuteron-beryllium reactions, the small solid angle was not inconvenient. It did, however, facilitate the identification by range in emulsion of the numerous kinds of particles observed, inasmuch as all the particles entered the emulsion with small angular divergence (at an angle of about 35° to the emulsion). The manner in which the energy coverage of the instrument varies with the magnetic field is illustrated by Fig. 2. At a field of approximately 14 kilogauss, for example, the range covered is from

* Assisted by a contract with the AEC.
[1] E. R. Graves, Phys. Rev. **57**, 855 (1940).
[2] Oliphant, Kempton, and Rutherford, Proc. Roy. Soc. (London) **A150**, 241 (1935); Lattes, Fowler, and Cuer, Proc. Phys. Soc. (London) **59**, 883 (1947).
[3] Williams, Haxby, and Shepherd, Phys. Rev. **52**, 1031 (1937).
[4] W. W. Buechner and E. N. Strait, Phys. Rev. **76**, 1547 (1949); Buechner, Strait, Stergiopoulos, and Sperduto, Phys. Rev. **74**, 1569 (1948); Strait, Van Patter, Buechner, and Sperduto, Phys. Rev. **81**, 747 (1951); W. Whaling and C. W. Li, Phys. Rev. **81**, 150 (1951); Williamson, Browne, Craig, and Donahue, Phys. Rev. **84**, 731 (1951); E. D. Klema and G. C. Phillips, Phys. Rev. **86**, 951 (1952).
[5] D. R. Inglis, Phys. Rev. **78**, 104 (1950).
[6] H. E. Gove and J. A. Harvey, Phys. Rev. **82**, 299, 658 (1951).
[7] Gelinas, Class, and Hanna, Phys. Rev. **83**, 1260 (1951).
[8] A. Ashmore and J. F. Raffle, Proc. Phys. Soc. (London) **A65**, 296 (1951); W. Franzen and J. G. Likely, Phys. Rev. **87**, 667 (1952).
[9] I. Resnick and S. S. Hanna, Phys. Rev. **82**, 463 (1951).
[10] P. Cuer and J. J. Jung, Compt. rend. **234**, 204 (1952).
[11] Hafner, Donoghue, and Snyder, privately circulated report.

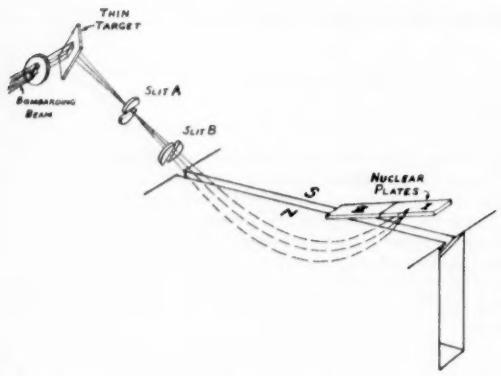

FIG. 1. Perspective view of the spectrograph in this experiment.

4.1 to 2.9 Mev on the first photographic plate, and from 2.9 to 1.95 Mev on the second plate (on a proton or alpha-energy scale, the two scales being nearly the same). At each field setting the ratio of maximum to minimum energy is about 2.1, when two 3-inch plates are used. The upper energy limit for protons (alphas) is about 6 Mev at present, the limiting factor being the heating of the field coils. Since the plate holder, which is three-sided, accommodates three pairs of plates, it is possible to cover the range from $E_p=0.8$ to 6.0 Mev, for example, in three exposures without breaking the vacuum in the spectrograph.

The energy scale for each exposure was established by using the known bombarding energy and accurate Q values to establish the energies of prominent particle groups. The energy of a group is related to its position on the plate by the expression $E=A(s-x)^2$, where E is the energy, A depends only on the magnetic field and hence is a constant for a given exposure, s is a geometrical constant of the instrument, and x is the displacement from the high energy end of the plate. By using two groups of particles of known energy (preferably protons) both A and s could be determined. The above expression is theoretically correct for a spectrograph with a uniform field in the gap and no fringing field outside. In practice, these conditions are not completely satisfied, but the procedure was satisfactory in that it predicted the location of other known peaks within the accuracy of the measurements. In establishing the energy scale, corrections were applied to account for energy losses in the target.

The chief contribution to the widths of the observed peaks came from the thickness of the targets employed. At the low bombarding energies used in this series of observations, the energy spread produced in the incident deuterons by the target thickness is relatively large, on the order of 30–40 kev, for most of the targets used. The maximum broadening of the peaks from other sources, such as fluctuations in the energy of the deuteron beam or in the magnetic field of the spectrograph, is estimated at 10–20 kev. For many of the runs an unbacked beryllium foil of approximately 0.07 mg/cm² was placed at an angle of 45° with respect to the beam. To reduce broadening of the observed peaks, the setting was made so that the beam impinged on the front and the reaction products emerged from the back of the foil, as illustrated in Fig. 1. The observations on the $Be^9(d,t)Be^8$ reaction were made on a beryllium layer of about the same thickness deposited on a solid backing, and the setting was made so that the reaction products emerged from the front surface. The investigation of the structure in the vicinity of the Li^{+++} recoils was obtained with a considerably thinner deposit of beryllium (~0.02 mg/cm²) on thick backing. The best value obtained in the investigation for the ratio of the energy of a group to the width of its peak at half-maximum was about 100. The sharpest group observed had a width of 25 kev at an energy of 1.6 Mev.

In all some 15 exposures were made at 10 different field settings to obtain the spectra presented. (A cut-off valve with a wide aperture, installed between the target chamber and the spectrograph, makes it possible to change photographic plates while the target remains in vacuum.) All the observations were made at 90° to the beam. The nuclear plates (25-micron emulsions) were counted in a microscope at a magnification of 450. Swaths about 200 microns wide were counted at 1-mm intervals along the plate for a preliminary survey. When better statistics or greater resolution were needed, each adjacent swath was counted. Identification of particles was by means of their deflection in the magnetic field and range in the emulsion. Because the

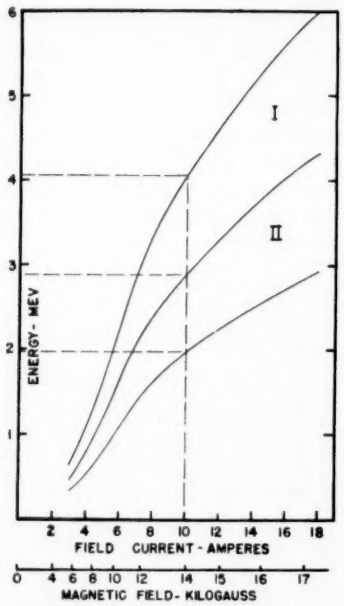

FIG. 2. Energy coverage of the spectrograph. Regions I and II correspond to the nuclear plates labeled in Fig. 1.

directions of particles striking the plate vary through the acceptance angle of the spectrograph, the projected range which was the observed quantity is not a sensitive criterion. In the present observations the method does not distinguish among H^{3+}, He^{4++}, and Li^{7+++} particles. All other particles were readily identified. In order to be acceptable, tracks had to satisfy a length criterion and enter the emulsion in the proper direction.

For convenience the spectra are plotted on an energy scale. Each type of particle therefore has a different scale, the relationship between any two scales being given by the factor $(m_1/m_2)(q_2/q_1)^2$. For alphas and protons the scales are the same to within 0.8 percent. The tracks observed in a swath of fixed width in the microscope are the count in a fixed momentum interval. This was converted to the number in a fixed energy interval by means of the factor $dx/dE=(s-x)/2E$, the symbols having been defined above. In the ideal case when the target spot is restricted so that particles passing through slit B (in Fig. 1) do not encounter the pole faces of the magnet, the solid angle of the spectrograph is independent of the radius of curvature. This ideal geometry is not readily achieved, and it limits the aperture of the instrument in any practical arrangement. In the present investigation, slit B was not employed. Although the instrumental scattering was not serious, the solid angle was no longer independent of the radius of curvature. In the vertical dimension (Fig. 1) the angular aperture is determined only by the height of the target spot and the distance of slit A from the target. In the horizontal dimension, however, the particle trajectories are limited by the pole faces of the magnet at the point where the rays emerge from the gap. Hence, the solid angle decreases linearly with increasing radius of curvature, the ratio of maximum to minimum solid angle being 1.24. This correction has been applied to the observations.

III. RESULTS

Figure 3 shows the spectrum of charged particles below $E_p=6$ Mev resulting from the bombardment of beryllium by 0.68-Mev deuterons. Starting at the high energy end of Fig. 3 there is a low background of tritons which declines towards lower energy. The strong alpha-peaks at about 4.8 and 4.5 Mev are from $Be^9(d,\alpha)Li^7, Li^{7*}$. The triton background continues to fall slowly, but at about 3.2 Mev a rise in the background is evident. This rise and subsequent plateau[5,7,10] are attributed to alphas from the following three-particle disintegrations: $Be^9(d,\alpha)Li^{7**}(\alpha)H^3$, and $Be^9(d,t)Be^{8*}(\alpha)He^4$. A third source of alphas might be the simultaneous three-body breakup of the compound nucleus B^{11}. The triton spectrum bears on the interpretation of this continuum, and the question is discussed below. Below 3 Mev and the alpha-yield reaches a maximum and then falls gradually until an energy of about 2.0 Mev is reached. Here a prominent peak occurs which is

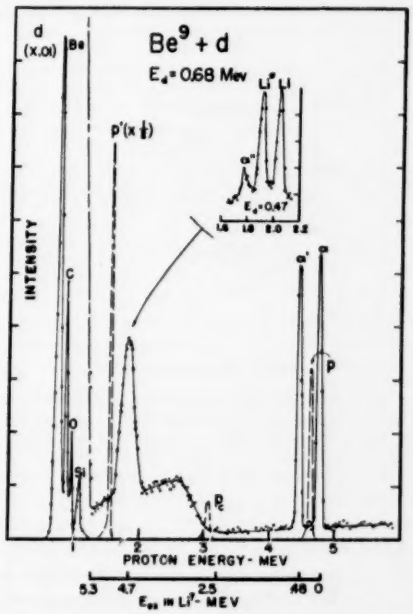

FIG. 3. The charged-particle spectrum at 90° resulting from the deuteron bombardment of Be^9. Above 1.3 Mev the solid curve represents alphas, tritons, or Li^{+++} particles; below 1.3 Mev the curve represents elastically scattered deuterons to a reduced scale. The dashed curve represents protons; the group labeled p_c is from carbon.

due to the triply charged Li^7 nuclei formed in the reactions, $Be^9(d,Li^7)He^4$ and $Be^9(d,Li^{7*})He^4$, but the two groups are unresolved. This region of the spectrum was also examined at a bombarding energy of 1.02 Mev, but no significant change in the structure was observed. Also contributing to the peak at 2 Mev is the alpha-group resulting from the $Be^9(d,\alpha)Li^{7**}$ reaction. At the time that these data were obtained, this new state in Li^7 had not yet been discovered. After Harvey and Gove had announced evidence for the state,[6] we were also able to detect it using the more favorable bombarding energy of 0.47 Mev (see Fig. 4) and a thinner target. This observation is shown in an insert in Fig. 3.

The measured separation of this short-range alpha-group from the Li^7 group is 264 ± 10 kev (alpha-energy scale), and from the Li^{7*} group it is 128 ± 10 kev, at the bombarding energy of 0.47 Mev. The corresponding excitation energy in Li^7 may be calculated from the expression:

$$E_x=(\tfrac{8}{6})Q+(\tfrac{8}{6}+4M_1/9M_2-M_1/M_3)E_1 +(M_2+M_3)S/M_3.$$

Q is the energy release for a lithium group, S is the separation of the alpha-group from this lithium group, and E_1 is the bombarding energy. The subscripts 1, 2, and 3 refer, respectively, to the deuteron, alpha-, and lithium particle. When values for the Li^{7*} group are used, the formula gives the excitation energy above the

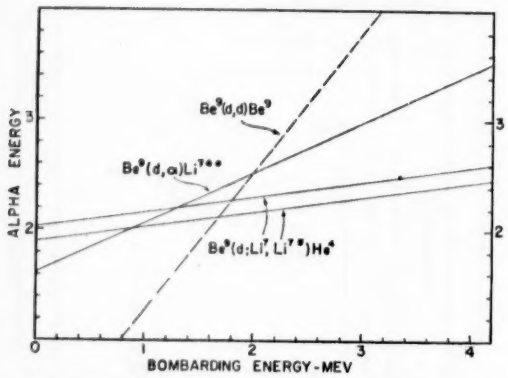

FIG. 4. The variation with bombarding energy of the energy of the alpha-group from the $Be^9(d,\alpha)Li^{7**}$ ($E_{ex}=4.62$ Mev) reaction, showing the relationship to other groups observed with magnetic deflection. The ordinate, labeled "alpha energy," must be multiplied by the factor $(m_\alpha/m)(q/q_\alpha)^2$ to give the energies of the other groups shown.

0.478-Mev state in Li^7. Using $Q=7.153\pm0.006$ Mev and the masses given by Li *et al.*,[12] we obtain an excitation energy of 4.62 ± 0.02 for the second excited state.

Below 1.6 Mev the alpha-background continues to fall and is completely obscured below 1.25 Mev by elastically scattered deuterons. Four well-resolved groups of deuterons are observed, corresponding to scattering from beryllium, carbon, oxygen, and silicon (the latter arising from the use of pump oil containing silicon). Each surface contamination, undoubtedly present on both sides of the unbacked beryllium foil, gives rise to a single peak only, because of the compensation obtained with the setting of the target. A deuteron scattered from the front surface must subsequently pass through the target to reach the spectrograph, while one from the back surface will have already traversed the foil. In either case one traversal of the target is required. The proton peaks at about 4.7 and 1.6 Mev are the well-known groups from beryllium,

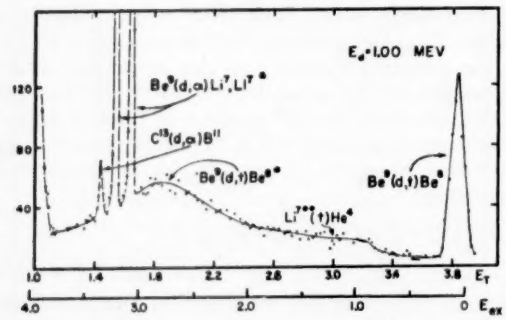

FIG. 5. The charged-particle spectrum at 90° resulting from the deuteron bombardment of Be^9. The solid curve represents tritons, the dashed curve alphas. Proton groups were not included. E_{ex} signifies the excitation energy in Be^8.

[12] Li, Whaling, Fowler, and Lauritsen, Phys. Rev. **83**, 512 (1951).

and the one at 3.1 Mev is from carbon. No trace of other structure which could be attributed to beryllium was observed in the proton spectrum.

With magnetic deflection a triton having the same radius of curvature as an alpha has only one-third the energy. Thus the maximum energy of tritons which can be focused in the spectrograph is about 2 Mev, and absorbing aluminum foils were used at slit *A* (Fig. 1) to obtain the spectrum of higher energy tritons. Five runs were made at $E_d=1.0$ Mev, with a different foil thickness for each run, in order to cover the triton spectrum above 1.8 Mev. Another run without foil covered the range from 1.2 to 1.8 Mev. In the latter

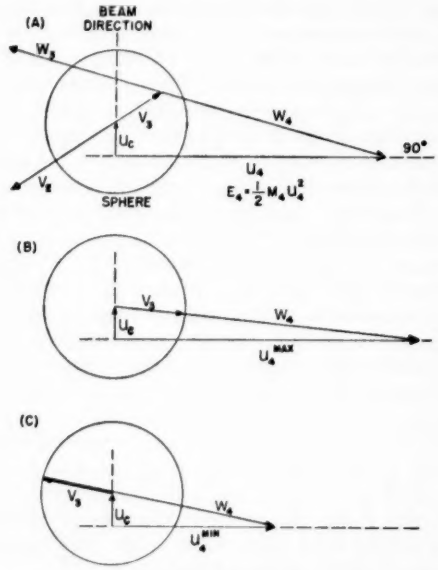

FIG. 6. Velocity diagrams for three-particle disintegrations of the type $P_0(P_1,P_2)P_3(P_4)P_5$. U_c represents the velocity in the laboratory frame of the center of mass of all the particles. V_2 and V_3 are velocities of P_2 and P_3 in the c.m. system of the particles. W_4 and W_5 represent velocities of P_4 and P_5 in the c.m. system of P_3. U_4 is the velocity of P_4 in the laboratory. (A) represents a general case in which P_4 is observed at $\theta=90°$ in the laboratory. (B) and (C) denote, respectively, orientations of the vectors for which U_4 attains its maximum and minimum, at $\theta_L=90°$.

exposure the alpha-group arising from the $C^{13}(d,\alpha)B^{11}$ reaction was detected on the trailing edge of the strong alpha-group from Be^9 (30 times more intense).

The triton spectrum covering triton energies from 1.0 to 3.9 Mev appears in Fig. 5. Again the ordinate of the energy spectrum represents the yield in a fixed energy interval and includes the solid angle correction. An additional correction was necessary because of the use of absorbing foils, which distort the energy scale. When these corrections were made, the results from the five runs joined smoothly together. The energy scale for the triton spectrum was calculated with the aid of the range energy curves for aluminum given by

Gross.[13] The nominal foil thickness as given by the manufacturer could be checked and if necessary adjusted by means of the shift in energy observed in the proton groups from carbon and oxygen impurities on the target. The ground-state triton group also provided a determination of the foil thickness used in obtaining the high energy end of the spectrum. The uncertainty in the energy scale in Fig. 5 is estimated to be ± 50 kev.

At the highest triton energy there appears the discrete triton group from the ground state $Be^9(d,t)Be^8$ reaction. The background from 3.7 to 3.3 Mev is very low, but just below 3.3 Mev it shows a definite rise. The yield remains constant to about 2.6 Mev, where it again begins to rise, reaching a broad peak at 1.8 Mev. Below 1.8 Mev the yield falls, and is about the same at 1.1 Mev as at 2.6 Mev. By referring to the scale of energy of excitation in Be^8, it will be seen that the broad peak is at the correct energy and of the proper width to be identified with the broad state at 2.9 Mev in Be^8. The rise in the background just below 3.3 Mev and subsequent plateau may be attributed to the triton

TABLE I. Maximum and minimum energies of particles produced in the various possible three-particle disintegrations. $E_d = 1.0$ Mev and $\theta = 90°$.

	Tritons		Alphas	
	E_{max}	E_{min}	E_{max}	E_{min}
$Be^9(d,\alpha)Li^{7*}\cdots(t)\alpha$				
$E_{ex}=4.62$ Mev	3.27 Mev	0.09 Mev	3.13 Mev	0.00 Mev
6.56	3.90	1.06	3.38	0.54
7.46	3.80	1.91	3.10	1.21
$Be^9(d,t)Be^{8*}(\alpha)\alpha$				
$E_{ex}=2.0$			2.84	0.05
2.9			3.20	0.34
3.8			3.40	0.79
$Be^9(d,t)2\alpha$	3.96	0.00	3.43	0.00

continuum which would result from the breakup into an alpha and a triton of recoiling Li^7 nuclei formed in the second excited state at 4.62 Mev. The calculated maximum energy of tritons from this reaction is 3.27 Mev at the bombarding energy of 1.0 Mev (see Fig. 6 and Table I). Considering the straggling produced by the absorbing foils, and the uncertainty in the energy scale, the agreement between the experimental rise in the background and the calculated maximum energy is quite satisfactory. The appearance of the triton spectrum in this region, and its interpretation, agree with the observations and conclusions of Cuer and Jung.[10] It is interesting on the basis of this interpretation to estimate the intensity of the triton continuum produced by the disintegration of Li^{7**} nuclei, and hence the intensity of the transition to the 4.62-Mev state. Since the shape of the continuum is not established throughout, only a rough estimate can be given. It would appear that at the bombarding energy of 1.0 Mev

[13] E. P. Gross, *Range, Energy Ionization Curves* (Princeton University Press, Princeton, 1947).

TABLE II. Relative intensities of transitions from Be^9+d. Values in most cases are only approximate, and were measured at 90° in the laboratory system. The value for $Be^9(d,\alpha)Li^{7**}$ at $E_d = 1.0$ Mev was estimated from the triton continuum from the disintegration of Li^{7**}. The yields at each energy have been normalized to make the ground-state alpha-yield = 10.

	$E_d = 0.47$ Mev	0.68 Mev	1.0 Mev
$Be^9(d,\alpha)Li^7$	10	10	10
$Be^9(d,\alpha)Li^{7*}$	10	9.5	7.0
$Be^9(d,\alpha)Li^{7**}$	2		10
$Be^9(d,t)Be^8$			3.5
$Be^9(d,t)Be^{8*}$		10	15
$Be^9(d,p)Be^{10}$		5	4.5
$Be^9(d,p)Be^{10*}$		8	

the transition to the 4.62-Mev state is about as probable as the transition to the ground state (Table II). This is in contrast to the situation at $E_d = 0.47$ Mev, where the intensity is at most one-quarter the intensity of the ground-state transition. This relative increase is not necessarily surprising, but it may be simply a result of overestimating the number of tritons from the Li^{7**} disintegration possibly because of the presence of tritons produced by some other mechanism. Table I lists the maximum and minimum energy of the continuous distributions for the various possible three-particle processes. It is seen that the disintegration of lithium nuclei in the next two known excited states, at $E_{ex} = 6.56$ and 7.47 Mev, will produce tritons throughout this region, as will also the simultaneous three-particle disintegration. All three of these processes have high energy limits beyond the limit of the distribution corresponding to the 4.62-Mev state. One or more of these processes may therefore account for the low background observed between 3.3 and 3.8 Mev in the triton spectrum, although at least some of this background may be attributed to instrumental scattering.

The high energy end of the alpha-continuum is shown in greater detail in Fig. 7, at the higher bombarding energy of 1.02 Mev. The yield first begins to rise

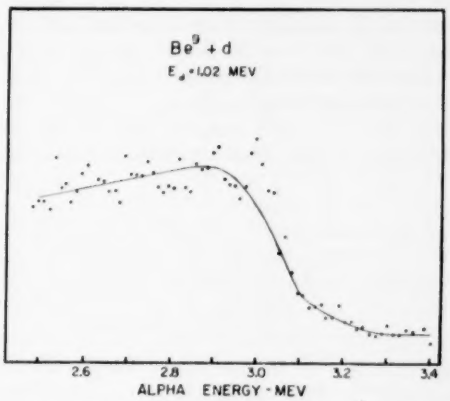

FIG. 7. Detailed view of the spectrum near the high energy limit of the alpha-continuum. The structure at 3.0 Mev is probably due to the $O^{16}(d,\alpha)N^{14}$ reaction.

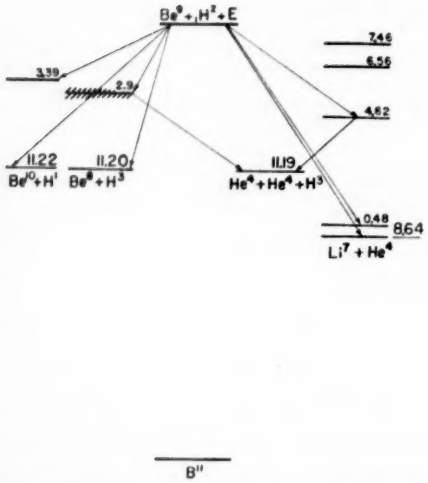

FIG. 8. Energy-level diagram showing the transitions observed in this investigation. With the exception of the value 4.62 Mev, the energies are taken from the literature.

slightly, at about an alpha-energy of 3.3 Mev. The rise becomes more pronounced at 3.1 Mev and reaches a maximum in the vicinity of 2.9 Mev, and then declines slowly. At about 3.0 Mev there appears to be a peak in the spectrum, somewhat in excess of a likely statistical fluctuation. The alpha-group from $O^{16}(d,\alpha)N^{14}$ should fall at 3.10 Mev. If this identification is correct, it establishes that there is an average loss of approximately 100 kev for alpha-particles coming from the target which was oriented as shown in Fig. 1. Taking this loss into account, it is seen from Table I that the maximum energy for alphas from the $Be^9(d,\alpha)Li^{7**}(t)\alpha$ ($E_{ex}=4.62$ Mev) process is about 3.0 Mev. For the $Be^9(d,t)Be^{8*}(\alpha)\alpha$ reaction, which is also established by the triton spectrum, a discrete upper limit cannot be given because of the great breadth of the state in Be^8. Above about 3.1 Mev, however, the yield should decline and practically vanish in the neighborhood of 3.3 Mev. Qualitatively the observed fall in the spectrum is in agreement with these high energy limits. Unfortunately, the distributions corresponding to the next two excited states in Li^7, $E_{ex}=6.56$ and 7.47 Mev, would not be detected unless they had appreciable intensities. In agreement with the triton spectrum, these reactions, as well as the simultaneous process, are apparently much less likely than the other two processes at these bombarding energies.

A summary of all the transitions observed in this investigation is given in Fig. 8. The observations extended up to 5.3 Mev in Li^7, 4.0 Mev in Be^{10}, and 4.8 Mev in Be^8. Because of the alpha-continuum from the three-particle processes, the region above 3.8 Mev in Be^8 and 2.6 Mev in Li^7 could not be examined in as great detail as elsewhere. The ratios of the alpha-yields

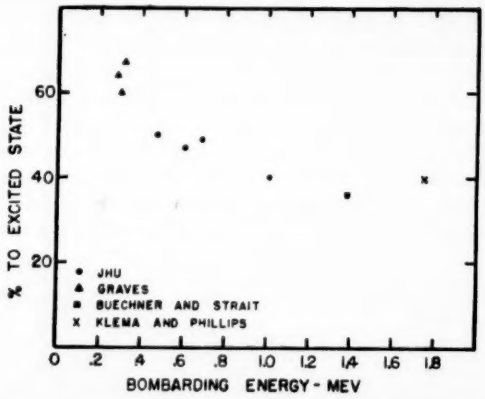

FIG. 9. Fraction of the alphas from $Be^9(d,\alpha)Li^7$, Li^{7*} which go to the 480-kev state. At about 0.3 Mev the results given by Graves (reference 1) indicate about 63 percent to the first excited state. The present work, including the measurement of Inglis (reference 5), indicates a decrease to about 40 percent at 1.0 Mev. The values at 1.4 and 1.75 Mev are estimated from the spectra presented, respectively, by Buechner and Strait and by Klema and Phillips (reference 4); they indicate a fairly constant percentage of transitions to the first excited state, above 1.0 Mev.

to the doublet ground state of Li^7 where rather accurately determined and are summarized in Fig. 9, together with results of other investigators.

It is a pleasure to acknowledge the original impetus given this investigation by D. R. Inglis, who also designed and put into operation the spectrograph used in the investigation. P. Milich was responsible for a major part of the construction and assembly of the new mounting and magnet which were installed before the present investigation. We are also indebted to R. T. Frost for several helpful discussions.

Magnetic Analysis of the $Sr^{88}(d,p)Sr^{89}$ Reaction*

CHARLES E. MCFARLAND AND FRANKLIN B. SHULL
Physics Department, Washington University, St. Louis, Missouri
(Received October 8, 1952)

A magnetic analyzer was used to study proton groups produced when a $SrCO_3$ target was bombarded with 10.43-Mev deuterons. Three excited states of Sr^{89} were found in addition to the ground state. The corresponding Q values are 4.33, 3.26, 2.26, and 1.79 Mev.

THE $Sr^{88}(d,p)Sr^{89}$ reaction has previously been examined by Harvey,[1] who found a reaction energy of $Q=4.32\pm0.2$ Mev when Sr^{89} is formed in its ground state. He also states that "the first excited level to occur (*viz.*, in Sr^{89}) will be separated from the ground state by about 1 Mev." No information about energy levels in Sr^{89} can be obtained from beta- and gamma-decay studies, since its radioactive parent, Rb^{89}, has a rather short half-life.

In the present investigation, a target was prepared from natural $SrCO_3$. The abundance of Sr^{88} in natural strontium is about 82 percent, and we have assumed that any prominent groups of protons can be attributed to reactions involving this isotope. The carbonate was ground to a fine powder in water and then allowed to fall out of this semisuspension onto a 0.2-mil polyethylene foil. The average thickness of carbonate on the target was 1.35 mg/cm². The presence of carbon and oxygen in the substrate and the target compound proves to be helpful in evaluating data. We have employed the $C^{12}(d,d')C^{12}$, $C^{12}(d,p)C^{13}$, and $O^{16}(d,p)O^{17}$ reactions as convenient standards for comparison. In particular, we used these reactions to determine the energy of the incident deuteron beam.

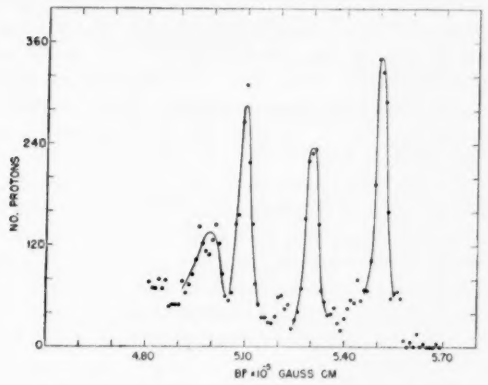

FIG. 1. Proton spectrum from the $Sr^{88}(d,p)Sr^{89}$ reaction.

The reaction products were analyzed with a uniform-field magnetic spectrometer, whose mean radius of curvature is 42.25 cm. The angle between the collimated deuteron beam and the direction of the measured protons was 90°. Photographic plates were used to detect and record charged particles from the reaction. A series of 12 exposures at gradually increasing values of the magnetic field was sufficient to cover the desired momentum range with thoroughness. Each exposed plate encompassed an effective momentum spread of about 0.3×10^5 gauss-centimeters. The total spread covered by the 12 plates was about 1.2×10^5 gauss-centimeters. It is obvious that there was a considerable degree of overlap by adjacent plates. In fact, each of the proton groups plotted in Fig. 1 was observed on at least four different plates. The incident deuteron beam was generated by the Washington University cyclotron; its mean energy, as determined from reaction studies, was 10.43 Mev. To make this determination, the same set of 12 photographic plates was used.

The proton spectrum from the $Sr^{88}(d,p)Sr^{89}$ reaction is pictured in Fig. 1, which shows relative numbers of protons in equal intervals of momentum as a function of momentum measured in gauss-centimeters. The three peaks of greatest momentum seem to be fairly well defined and represent about the maximum resolving power of which the equipment is capable in practice. The fourth peak is less intense and less definite; conceivably, it could result from the superposition of two weak and unresolved groups, but we have chosen to ignore this possibility when computing reaction energies. Should this peak eventually prove to be double, the reaction energy which we have computed from it would correspond to the more energetic member of the pair.

The reaction energies computed from the four proton groups are 4.33, 3.26, 2.26, and 1.79 Mev. The accuracy is estimated to be ±0.1 Mev for the first three and ±0.2 Mev for the fourth. The ground-state Q value compares favorably with the one reported by Harvey. The corresponding excitation energies for nuclear states of Sr^{89} are 0, 1.07, 2.07, and 2.54 Mev. Thus, the first excited state also occupies approximately the position which Harvey claims for it.

* Sponsored by the joint program of the ONR and AEC.
[1] J. A. Harvey, Phys. Rev. 81, 353 (1951).

PHYSICAL REVIEW VOLUME 89, NUMBER 2 JANUARY 15, 1953

Multiple Scattering and Radiation Damping. II*

H. EKSTEIN
Armour Research Foundation, Illinois Institute of Technology, Chicago, Illinois
(Received September 22, 1952)

The analysis of multiple elastic scattering by a system of fixed scatterers in terms of two-body collision matrices is extended to large bodies. The dynamical theory of particle wave propagation in crystals is formulated and discussed from this viewpoint, as an extension of Ewald's theory to scatterers of finite size. A theory of wave propagation in a random medium, including disordered crystals, is obtained as the limiting case for a crystal with infinite unit cell. Contrary to the usual approach, this analysis considers a definite "frozen" configuration of the medium; statistical averaging over configurations may be used on the intensities obtained.

In crystals and dense liquids, radiation damping is compensated by the reaction of surrounding scatterers. Therefore, it is found convenient to restate the basic equations of multiple scattering in terms of a matrix β which is essentially the Green's function for the single scattering event, with "standing wave" rather than "outgoing wave" boundary conditions. This has the advantage of eliminating the spurious radiation damping terms at the outset; one obtains nonattenuated waves in nondissipative crystals or dense liquids by a simple expansion method.

Application is made to the following problems: the equivalent of the Lorentz-Lorenz formula for matter waves; index of refraction for an interaction of the form of a one-level Breit-Wigner formula; attenuation of long waves in a disordered crystal containing protons with random spins; double refraction effect in a liquid or crystal containing protons with partially oriented spin.

I. INTRODUCTION

IN Part I of this paper, the elastic scattering by a system of fixed centers of force was treated by replacing the interaction potential by a matrix α which describes rigorously the single scattering event. This reformulation has three advantages over the usual perturbation method: first, the iteration solution converges for short-range forces, where Born's approximation diverges; second, the first approximation to the present equations tends toward the correct solution for a system of widely separated scatterers, whereas the perturbation method gives only a first approximation; third, the results are applicable where the interaction potential is not known, but the single scattering amplitudes are.

The matrix α is essentially the Green's function of the single scattering problem, with the usual boundary condition describing outgoing (or retarded) waves. In this Part II, an alternative formulation is developed in which α is replaced by a matrix β which is essentially the Green's function for boundary conditions describing half-retarded, half-advanced (standing) waves. The new formulation which is rigorously equivalent to the previous one is advantageous for the following reasons: In crystals and in sufficiently dense liquids, the radiation damping effect on the single scatterer is compensated by the reaction of surrounding scatterers. Hence, it is logical that for the purpose of successive approximation, one should start with a description of the single scattering event from which radiation damping has been eliminated. In Sec. III, the theory of an infinite crystal is developed on this basis, and applied to the following problems: the equivalent of the Lorentz-Lorenz formula for scalar waves; the refractive index for long waves of a crystal consisting of absorbing scatterers; in particular, the case of a one-level Breit-Wigner dispersion formula for the single scatterer.

In Sec. IV, a dynamical theory of liquid scattering is formulated as a generalization of the crystal theory, starting from the remark that the most general configuration may be considered as the limit of a crystal with infinite unit cell. Boundary conditions for the semi-infinite medium are discussed, and an approximate solution is found.

Section V discusses the extension of the theory to the case where the scatterers are not simple centers of force, but many-body systems such as nuclei. In this case, the preceding results are approximately correct if the elastic submatrix of a more general matrix α or β is inserted. This approximation amounts to disregarding inelastically scattered particles. The properties of β for this general case are discussed.

II. INTRODUCTION OF HALF-ADVANCED, HALF-RETARDED SOLUTIONS

Let us examine more closely the convergence of the imaginary part of the expansion (I, 66).[1] The imaginary part of the forward scattered amplitude in the first approximation is $N\,\mathrm{Im}f(k_0)$, i.e., that corresponding to N non-interfering point scatterers. Since $\mathrm{Im}F(k_0)$ is proportional to the total scattering cross section, this approximation is good when the scatterers are located at random (total cross section $=N\times$single cross section), but poor when interference is predominant. In the latter case, the first approximation is incorrect even in the event of vanishing single cross section, so that higher terms of the expansion in α must outweigh the first approximation. This situation is illustrated by the example of a spherical crystal discussed in (I). For a small phase δ_0,

$$\mathrm{Im}\alpha\approx\delta^2/2\pi^2k_0,\quad \alpha^2\approx\delta^2/(2\pi^2k_0)^2,$$

so that the first imaginary term, $iN\delta^2/2\pi^2k_0$ is compensated by the second term of the second approximation (I, 95), i.e., $-i\alpha^2 2\pi^2k_0N$; the first term of Eq. (I, 95) represents the correct first approximation to the

* Work supported in part by the U. S. Office of Naval Research.

[1] H. Ekstein, Phys. Rev. **83**, 721 (1951). Further referred to as I.

imaginary part of the forward scattering amplitude. In general, several terms of the expansion in terms of α will be needed to extricate the correct first approximation, because the diverse powers of δ are awkwardly distributed among the terms of the power series in α.

This awkwardness is due to the unusual circumstance that the parameter of expansion is complex, an undesirable feature for many purposes. For instance, the elegant method of calculating the nth order of the iteration from the previous orders[2] can be used only when the expansion parameter is real.

Physically, the complex nature of α is due to radiation damping, where the single scattering event is purely elastic. In a more extended body, most of the scatterers are symmetrically surrounded by other scatterers so that radiation damping is largely compensated by the reaction of the surrounding scatterers. This situation suggests that a more suitable approximation method could be obtained if the single scattering event were described by the sum of the retarded and advanced solutions of the Schrödinger equation, rather than by the retarded solution describing outgoing waves only.[3]

If the Green's function $\cos(k_0 r)/r$ is chosen for the unperturbed Schrödinger equation, the solution of the single scattering problem will appear as half-advanced, half-retarded spherical wave. The steps analogous to Eqs. (I, 24 to 29) lead to Eq. (I, 30) which defines the matrix β.

To relate the multiple scattering problem to β, we rewrite Eq. (I, 43) by using the definition (I, 7),

$$F_n(\mathbf{k})-P\int\frac{d\mathbf{k}'}{k'^2-k_0^2}\exp[-i\mathbf{r}_n\cdot(\mathbf{k}-\mathbf{k}')]u(\mathbf{k}-\mathbf{k}')F_n(\mathbf{k}')$$
$$=u(\mathbf{k}-\mathbf{k}_0)\exp[-i\mathbf{r}_n\cdot(\mathbf{k}-\mathbf{k}_0)]+\frac{i\pi k_0}{2}\int_S u(\mathbf{k}-\mathbf{k}')$$
$$\times\exp[-i\mathbf{r}_n\cdot(\mathbf{k}-\mathbf{k}')]F_n(\mathbf{k}')d\Omega$$
$$+\sum_{m\neq n}\int_h\frac{d\mathbf{k}'}{k'^2-k_0^2}\exp[-i\mathbf{r}_n\cdot(\mathbf{k}-\mathbf{k}')]$$
$$\times u(\mathbf{k}-\mathbf{k}')F_m(\mathbf{k}'). \quad (1)$$

If now Eq. (I, 30) is used for comparison, the procedure used in Eq. (I, 44 to 52) gives

$$F_n(\mathbf{k})=\beta(\mathbf{k},\mathbf{k}_0)\exp[-i\mathbf{r}_n\cdot(\mathbf{k}-\mathbf{k}_0)]$$
$$+\sum_{m\neq n}\int_h\frac{d\boldsymbol{\kappa}}{\kappa^2-k_0^2}\exp[-i\mathbf{r}_n(\mathbf{k}-\boldsymbol{\kappa})]\beta(\mathbf{k},\boldsymbol{\kappa})F_m(\boldsymbol{\kappa})$$
$$+\frac{i\pi k_0}{2}\int_S\exp[-i\mathbf{r}_n\cdot(\mathbf{k}-\boldsymbol{\kappa})]\beta(\mathbf{k},\boldsymbol{\kappa})F_n(\boldsymbol{\kappa})d\Omega, \quad (2)$$

so that now only the principal value of the nth term is missing from the sum over m, rather than the total hook integral as in Eq. (I, 52).

Equation (2) is merely a restatement of the original problem; the boundary conditions still describe outgoing waves, since $F(\mathbf{k})$ is connected with $\psi(\mathbf{r})$ by Eq. (I, 8). The identity of the two formulations can easily be seen for point scatterers. Equation (I, 52) can then be written, with the definition (I, 44),

$$G_n(\mathbf{k})=\alpha_0\exp(i\mathbf{r}_n\cdot\mathbf{k}_0)$$
$$+2\pi^2\alpha_0\sum_{m\neq n}\frac{\exp[ik_0|\mathbf{r}_n-\mathbf{r}_m|]}{|\mathbf{r}_n-\mathbf{r}_m|}G_m(\mathbf{k}). \quad (3)$$

Since, in this case $\alpha_0=f_0(k_0)$, $\beta_0=g_0(k_0)$, Eq. (I, 19) can be used:

$$G_n=\beta_0\Big[\exp(i\mathbf{r}_n\cdot\mathbf{k}_0)$$
$$+2\pi^2\sum_{m\neq n}\frac{\exp(ik_0|\mathbf{r}_n-\mathbf{r}_m|)}{|\mathbf{r}_n-\mathbf{r}_m|}G_m+2i\pi^2k_0G_n\Big], \quad (4)$$

and this is the form which Eq. (2) takes for this particular case.

The reformulation of the scattering problem given in Eq. (2) has the advantages of Born's approximation with respect to the relation between imaginary and real parts. For instance, the well-known theorem connecting the imaginary part of the forward scattering amplitude to the total cross section is satisfied also by first and second iteration approximations, i.e., the cross section to the first nonvanishing order can be calculated either by integrating the first approximation or by determining the imaginary part of the second approximation. To see this, we compare the cross section

$$\sigma=\int|\psi_{sc}|^2r^2d\Omega=(2\pi^2)^2\int|F(\mathbf{k})|^2d\Omega, \quad (5)$$

or, using the first approximation to Eq. (2),

$$\sigma^{(1)}=(2\pi^2)^2\int|\beta(\mathbf{k},\mathbf{k}_0)|^2|\sum\exp[-i\mathbf{r}_n\cdot(\mathbf{k}-\mathbf{k}_0)]|^2d\Omega, \quad (6)$$

with the imaginary part of the forward scattering amplitude,

$$\mathrm{Im}\psi_{sc}=2\pi^2\,\mathrm{Im}F(\mathbf{k}_0,\mathbf{k}_0). \quad (7)$$

If the second iteration of Eq. (2) is used,

$$F^{(2)}(\mathbf{k}_0)=\int_h\frac{d\boldsymbol{\kappa}}{\kappa^2-k_0^2}\beta(\mathbf{k}_0,\boldsymbol{\kappa})\sum\exp[-i\mathbf{r}_n\cdot(\mathbf{k}_0-\boldsymbol{\kappa})]$$
$$\times\beta(\boldsymbol{\kappa},\mathbf{k}_0)\textstyle\sum_n\exp[-i\mathbf{r}_n(\boldsymbol{\kappa}-\mathbf{k}_0)]$$
$$-PN\int\frac{d\boldsymbol{\kappa}}{K^2-k_0^2}\beta(\mathbf{k}_0,\boldsymbol{\kappa})\beta(\boldsymbol{\kappa},\mathbf{k}_0). \quad (8)$$

[2] Jost, Luttinger, and Slotnick, Phys. Rev. **80**, 189 (1950).

[3] That a many-body problem can be described by using half-retarded, half-advanced solutions for the single scatterer to obtain a retarded total effect, is shown by J. A. Wheeler and R. P. Feynman, Revs. Modern Phys. **17**, 157 (1945).

It is shown in Sec. V that the matrix β is Hermitean when the scattering is purely elastic. Hence,

$$\mathrm{Im}F^{(2)}(\mathbf{k}_0)=\frac{\pi k_0}{2}\int|\beta(\mathbf{k},\mathbf{k}_0)|^2 \times|\sum\exp[-i\mathbf{r}_n(\mathbf{k}-\mathbf{k}_0)]|^2 d\Omega, \quad (9)$$

and therefore

$$\sigma^{(1)}=(4\pi/k_0)\,\mathrm{Im}\psi_{sf}{}^{(2)}, \quad (10)$$

in agreement with the exact theorem, whereas the expansion in terms of α does not show this relation. We may conclude, in general, that for dense media the formulation of the scattering problem in terms of half-advanced, half-retarded single scattering solutions is more convenient for the purpose of approximations.

III. THE INFINITE CRYSTAL

The theory of wave propagation in an infinite periodic medium was developed by v. Laue[4] for x-rays and adapted to the case of electrons by Bethe and others.[5] For scalar particles, the solution has the form

$$\psi=\exp(i\mathbf{K}_0\cdot\mathbf{r})\sum c_n\exp(2\pi i\mathbf{A}_n\cdot\mathbf{r}), \quad (11)$$

where the $\mathbf{A}_n$ are the reciprocal lattice vectors. If the potential v is expanded into a Fourier series,

$$v=\sum V_n\exp(2\pi i\mathbf{A}_n\cdot\mathbf{r}), \quad (12)$$

the introduction of Eqs. (11) and (12) into the Schrödinger equation leads to

$$[(\mathbf{K}_0+2\pi\mathbf{A}_n)^2-\mathbf{k}_0^2]c_n+(2m/h^2)\sum V_{n-m}c_m=0, \quad (13)$$

where $k_0^2=2mE/h^2$. Laue's method for solving Eq. (13) is to disregard all but a small number of c_n's [for which $(\mathbf{K}_0+2\pi\mathbf{A}_n)^2\approx k_0^2$] and to solve the remaining equations. To determine the range of validity of this approximation, let us consider the case where only c_0 is retained in first approximation. We have

$$K_0^2-k_0^2+(2m/h^2)V_0=0, \quad (14)$$

$$-c_n=\frac{2m}{h^2}\frac{V_nc_0}{(\mathbf{K}_0+2\pi\mathbf{A}_n)^2-k_0^2}(n\neq0). \quad (15)$$

Hence, in second approximation,

$$K_0^2-k_0^2+\frac{2m}{h^2}\left(V_0-\frac{2m}{h^2}\sum{}'\frac{|V_m|^2}{(\mathbf{K}_0+2\pi\mathbf{A}_m)^2-k_0^2}\right)=0. \quad (16)$$

If (14) is to be a good approximation, it is necessary that

$$\frac{2m}{h^2}\sum{}'\frac{|V_m|^2}{(\mathbf{K}_0+2\pi\mathbf{A}_m)^2-k_0^2}\ll|V_0|. \quad (17)$$

Assuming that the geometrical orientation of $\mathbf{K}_0$ is such that the lower terms do not contribute much to the sum, the validity of Eq. (16) depends on the rapidity with which the Fourier coefficients V_m decrease, and on their numerical magnitude. For high values of m, the sum can be approximated by the integral

$$\int^{\infty}\frac{|V(k)|^2}{k^2}d\mathbf{k}.$$

If the potential v represents point-scatterers, the Fourier transform of the delta-function will become asymptotically constant and the sum diverges. More generally, for small scatterers, Laue's approximation method must fail. For the extreme case of point-scatterers, an alternative method is given by Ewald's method which has been applied to the case of scalar particles by Goldberger and Seitz.[6]

In addition to its mathematical convenience in these cases, Ewald's method has the more general advantage that it correlates the properties of the crystal with the scattering properties (polarizability) of the single ion, rather than with the potential or electronic density which is not directly measurable. However, the theory has been established only for point scatterers, so that a generalization of Ewald's method for finite scatterers seems desirable. An attempt to fill this gap has been made recently by Lax,[7] but it has not been quite successful. Following Schwinger and Lippmann, Lax describes the single scattering process by the equation

$$\psi_a=\phi_a+\frac{1}{E-H}T\phi_a,$$

where ψ_a is the total wave function, ϕ_a an eigenfunction of the unperturbed Hamiltonian H belonging to the energy E, and T is the matrix which is denoted by f in the present paper. Lax concludes that in a multiple scattering problem, the foregoing equation can be interpreted by

$$(\text{scattered wave})=(E-H)^{-1}T\ (\text{incident wave}).$$

However, since ϕ_a is an eigenfunction of H belonging to the energy E, this generalization implies that the field incident on one scatterer can be represented as a superposition of plane waves of definite energy E. In general, this assumption is unwarranted; for instance, the incident field

$$e^{ik(r-r_0)}/r-r_0$$

has all energies in its Fourier spectrum.

To represent the scattering under the influence of a general incident field, an operator more general than T is required, *viz.*, either α of which T is a submatrix or β, according to the boundary conditions chosen for the

[4] M. von Laue, *Roentgenstrahlinterferenzen* (Akademische Verlagsgesellschaft, Leipzig, 1941).
[5] A. Sommerfeld and H. Bethe, *Handbuch der Physik* (J. Springer, Berlin, 1933), XXIV, 2.
[6] M. L. Goldberger and F. Seitz, Phys. Rev. **71**, 294 (1947).
[7] M. Lax, Phys. Rev. **85**, 621 (1952).

single scattering event.[8] In the following, the generalization for finite scatterers will be formulated rigorously.

The usual theory which starts from single scattering amplitudes meets a certain difficulty in eliminating the effect of radiation damping for long waves. From elementary dispersion theory[9] one expects n^2-1 (n refractive index) to be proportional to the single scattering amplitude, which, because of radiation damping, is necessarily complex. It was pointed out already by Lorentz on intuitive grounds that in a nonabsorbing crystal the radiation damping of a single scatterer must be exactly compensated by the influence of the other scatterers, so that the absurdity of a single attenuated wave in a nonabsorbing crystal can be avoided. However, a rigorous proof of this compensation has been given only for the case of a simple lattice of electromagnetic point-dipoles by Ewald.[10] Any approximate treatment which starts from the retarded solution for a single scatterer, has difficulties to avoid the appearance of the spurious imaginary terms.[11]

It seems more natural, in view of the intuitive knowledge of the cancellation of radiation damping, to start from the half-retarded, half-advanced solutions in constructing the total field. In this manner, spurious imaginary parts are avoided at the outset, regardless of the degree of approximation.

We first generalize Eq. (2) for the case where there are N different scattering centers described by matrices β_m. In an obvious way, one finds

$$F_n(\mathbf{k})=\beta_n(\mathbf{k},\mathbf{k}_0)\exp[-i\mathbf{r}_n\cdot(\mathbf{k}-\mathbf{k}_0)]+\sum_{m\neq n}\int_h\frac{d\boldsymbol{\kappa}}{\kappa^2-k_0^2}\exp[-i\mathbf{r}_n\cdot(\mathbf{k}-\boldsymbol{\kappa})]\beta_n(\mathbf{k},\boldsymbol{\kappa})F_m(\boldsymbol{\kappa})+\frac{i\pi k_0}{2}\int_S\beta_n(\mathbf{k},\boldsymbol{\kappa})\exp[-i\mathbf{r}_n\cdot(\mathbf{k}-\boldsymbol{\kappa})]F_n(\boldsymbol{\kappa})d\Omega. \quad (18)$$

We consider an infinite crystal with translation vectors $\mathbf{a}_n$ and scatterers of type j located with their centers at $\mathbf{a}_n+\mathbf{r}_j$, where $\mathbf{r}_j$ is located in the first unit cell. We label the scatterers by the numbers n, j, specifying the unit cell and type. Further, we omit now the first term in Eq. (18) which describes the incident wave, since we are now interested in self-sustained waves in the infinite crystal. Equation (18) becomes

$$F_{nj}=\sum_{ml}{}'\int_h\frac{d\boldsymbol{\kappa}}{\kappa^2-k_0^2}\exp[-i(\mathbf{a}_n+\mathbf{r}_l)\cdot(\mathbf{k}-\boldsymbol{\kappa})]\times\beta_j(\mathbf{k},\boldsymbol{\kappa})F_{ml}(\boldsymbol{\kappa})+\frac{i\pi k_0}{2}\int_S\beta_j(\mathbf{k},\boldsymbol{\kappa})\times\exp[-i(\mathbf{r}_n+\mathbf{a}_j)\cdot(\mathbf{k}-\boldsymbol{\kappa})]F_{nj}(\boldsymbol{\kappa})d\Omega, \quad (19)$$

where the prime sign means now omission of the term $m=n$, $l=j$. This infinite set of integral equations can be reduced to a finite set by assuming the solutions to have the form of lattice waves, i.e.,

$$F_{nj}=G_j\exp[-i(\mathbf{a}_n+\mathbf{r}_j)\cdot(\mathbf{k}+\mathbf{K}_0)], \quad (20)$$

where the propagation vector $\mathbf{K}_0$ is to be determined. By inserting Eq. (20) into Eq. (19) and making the transformation $\mathbf{a}_n\rightarrow\mathbf{a}_{n+1}$, one can verify that Eq. (20) is a solution provided that it satisfies the equation

$$G_j(\mathbf{k})=\sum_{ml}{}'\exp[i\mathbf{K}_0\cdot(\mathbf{a}_m+\mathbf{r}_l-\mathbf{r}_j)]\int_h\frac{d\boldsymbol{\kappa}}{\kappa^2-k_0^2}\times\exp[i\boldsymbol{\kappa}\cdot(\mathbf{r}_j-\mathbf{a}_m-\mathbf{r}_l)]\beta_j(\mathbf{k},\boldsymbol{\kappa})G_l(\boldsymbol{\kappa})+\frac{i\pi k_0}{2}\int_S\beta_j(\mathbf{k},\boldsymbol{\kappa})G_j(\boldsymbol{\kappa})d\Omega, \quad (21)$$

where the prime means omission of $m=0$, $l=j$. To carry out the summation we use the well-known formula,

$$\sum_n\exp(i\mathbf{a}_n\cdot\mathbf{k})=[(2\pi)^3/\tau]\sum_h\delta(\mathbf{k}-2\pi\mathbf{A}_h), \quad (22)$$

where $\mathbf{A}_h$ are the reciprocal lattice vectors and τ is the volume of the unit cell. Hence,

$$G_j(\mathbf{k})=\frac{(2\pi)^3}{\tau}\sum_{hl}\frac{\exp[-i2\pi\mathbf{A}_h\cdot(\mathbf{r}_l-\mathbf{r}_j)]\times\beta_j(\mathbf{k},\mathbf{K}_0+2\pi\mathbf{A}_h)G_l(\mathbf{K}_0+2\pi\mathbf{A}_h)}{(\mathbf{K}_0+2\pi\mathbf{A}_h)^2-k_0^2}-P\int\frac{d\boldsymbol{\kappa}\beta_j(\mathbf{k},\boldsymbol{\kappa})}{\kappa^2-k_0^2}G_j(\boldsymbol{\kappa})d\boldsymbol{\kappa}. \quad (23)$$

It is clear that $\mathbf{K}_0$ must be such that $(\mathbf{K}_0+2\pi\mathbf{A}_h)^2$ is different from k_0^2, for every h. This remark permits a simplification of Eq. (21). If the two contributions to the hook-integral are separated, the surface integrals will be

$$\frac{i\pi k_0}{2}\sum_{\text{all }m,l}\exp[i\mathbf{K}_0(\mathbf{a}_m+\mathbf{r}_l-\mathbf{r}_j)]\times\int_S\exp[i\boldsymbol{\kappa}\cdot(\mathbf{r}_j-\mathbf{a}_m-\mathbf{r}_l)]\beta_j(\mathbf{k},\boldsymbol{\kappa})G_l(\boldsymbol{\kappa})d\Omega,$$

and if Eq. (22) is used, all terms must vanish, since the requirement $\kappa^2=k_0^2$ implicit in the symbol S conflicts with $\boldsymbol{\kappa}=\mathbf{K}_0+2\pi\mathbf{A}_h$. Therefore, the surface integrals do

[8] For point scatterers, the distinction between T and α becomes irrelevant. Hence, Lax's calculations are approximations valid within the same range as Ewald's, i.e., for scatterers very small as compared to the interatomic distance and to the wavelength, or, more generally, whenever $\alpha\approx f$.

[9] E. Fermi, *Nuclear Physics* (University of Chicago Press, Chicago, 1950).

[10] P. P. Ewald, Ann. Inst. Henri Poincaré **VIII**, 79 (1932).

[11] An ingenious attempt to avoid the paradox in the general case has been made by M. Lax, Phys. Rev. **85**, 621 (1952).

not contribute to Eq. (21), and it can be written

$$G_j(\mathbf{k})=\sum_{m,l}{}' \exp[i\mathbf{K}_0\cdot(\mathbf{a}_m+\mathbf{r}_l-\mathbf{r}_j)]P\int \frac{d\boldsymbol{\kappa}}{\kappa^2-k_0^2} \times\exp[i\boldsymbol{\kappa}\cdot(\mathbf{r}_j-\mathbf{a}_m-\mathbf{r}_l)]\beta_j(\mathbf{k},\boldsymbol{\kappa})G_l(\boldsymbol{\kappa}). \quad (24)$$

To illustrate the meaning of this equation, consider the case of point scatterers in a Bravais lattice:

$$G=\frac{\tan\delta_0}{k_0}\sum{}' \frac{\cos|a_n|k_0}{|a_n|}\exp[i\mathbf{a}_n\cdot\mathbf{K}_0]G, \quad (25)$$

which is obtained from Eq. (24) by letting all β_l's except $\beta_1=\beta$ vanish, and letting β and hence G tend toward constants. The value of β is then determined by Eq. (I, 22). This is to be compared with

$$G=\frac{\exp(2i\delta_0)-1}{2ik_0}\sum{}' \frac{\exp(i|\mathbf{a}_n|k_0)}{|\mathbf{a}_n|}\exp(i\mathbf{a}_n\cdot\mathbf{K}_0)G, \quad (26)$$

which is obtained from Eq. (3). The two equations, although mathematically identical, differ in that all radiation damping effects are eliminated from Eq. (25).

Rigorous solutions can be obtained only for point-scatterers, by evaluating the right-hand side of Eq. (23) through a limiting process which lets the β and G tend toward constants. Following Ewald,[10] we may choose

$$G_j=\lim_{E\to\infty}\left\{\frac{(2\pi)^3}{\tau}\sum_{hl}\frac{\exp[-2\pi i\mathbf{A}_h\cdot(\mathbf{r}_l-\mathbf{r}_j)-(1/4E^2) \times\{(\mathbf{K}_0+2\pi\mathbf{A}_h)^2-k_0^2\}]G_l\beta_j}{(\mathbf{K}_0+2\pi\mathbf{A}_h)^2-k_0^2} -P\int\frac{d\boldsymbol{\kappa}\exp[-(1/4E^2)(\kappa^2-k_0^2)]G_j\beta_j}{\kappa^2-k_0^2}\right\}. \quad (27)$$

We consider the limiting case of large wavelengths, i.e., k_0, $K_0\to 0$ in a Bravais lattice. Then

$$1=\frac{(2\pi)^3\beta}{\tau(K_0^2-k_0^2)}+\beta\lim_{E\to\infty}\left\{\frac{(2\pi)^3}{\tau}\sum{}'\frac{\exp[-\pi^2A_h^2/E^2]}{4\pi^2A_h^2} -P\int\frac{d\boldsymbol{\kappa}\exp(-\kappa^2/4E^2)}{\kappa^2}\right\}. \quad (28)$$

For evaluation of the sum, it is desirable to have E as small as possible. To obtain the error due to using a finite value of E, we consider the curly bracket as a function of $1/E$ and write

$$f\left(\frac{1}{E}\right)=f(0)+\int_0^{1/E}\frac{df}{d\eta}d\eta, \quad (28)$$

$$\frac{df}{d\eta}=-\frac{2\pi}{\tau}2\pi^2\eta\sum{}'\exp(-\pi^2\eta^2A_h^2)+\frac{4\pi^3}{\eta^2}, \quad (29)$$

or by theta-transformation of the sum

$$\frac{df}{d\eta}=-\frac{4\pi^3}{\eta^2}\sum_n\exp(-a_n^2/\eta^2)+\frac{4\pi^3}{\tau}\eta+\frac{4\pi^3}{\eta^2}. \quad (30)$$

If η is large as compared to the lattice distance, only the term $n=0$ contributes to this sum, and we have

$$f\left(\frac{1}{E}\right)\approx f(0)+\int_0^{1/E}\frac{4\pi^3}{\tau}\eta d\eta=f(0)+\frac{2\pi^3}{\tau}\frac{1}{E^2}. \quad (31)$$

In the simplest case, i.e., a cubic Bravais lattice, one finds that $aE=10$ is sufficient to make the corrective term one percent. One finds

$$\{\ \}=-(2\pi/a)9.4. \quad (32)$$

With $n^2=K_0^2/k_0^2$, Eq. (28) gives

$$n^2-1=\frac{4\pi\cdot 2\pi^2\beta/a(k_0a)^2}{1+(2\pi^2\beta/a)\cdot 3}, \quad (33)$$

the equivalent of the Lorentz-Lorenz formula for matter waves. Since, for small cross section, $2\pi^2\beta$ is the scattering length, it is clear that the corrective term in the denominator is noticeable only when the scattering length is of the order of the distance between scatterers. This does not happen for any slow-neutron scattering process, so that the Lorentz correction is unimportant for this case.

The experience obtained with the electromagnetic Lorentz correction leads to the belief that Eq. (33) remains substantially correct for a more general dense assembly of scatterers, even when they are not rigorously point scatterers. Hence, it is plausible that in a phenomenological theory of meson scattering by heavy nuclei, if the nucleus is considered as a refracting sphere, Eq. (33) should be used in estimating the refracting index, using for β the observed scattering amplitude of the single nucleon. The main effect of the correction will be to smooth out the maxima of β in the heavy nucleus as compared to the single nucleon.

Returning to the general case, we seek to solve Eq. (23) by approximation. In general, a few terms of the sum will have small denominators, *viz.*, those for which the Laue-Bragg condition,

$$(\mathbf{K}_0+2\pi\mathbf{A}_n)^2\approx k_0^2,$$

is approximately realized. If N large terms are retained, the remaining equation can be written

$$[k^2-k_0^2]c_j(\mathbf{k})=\frac{(2\pi)^3}{\tau}\sum_{h,l}^{h=N}\exp[i(\mathbf{K}_h-\mathbf{k})\cdot\mathbf{r}_j] \times\beta_j(\mathbf{k},\mathbf{K}_h)G_l(\mathbf{K}_h), \quad (34)$$

where

$$\mathbf{K}_h=\mathbf{K}_0+2\pi\mathbf{A}_h, \quad (35)$$

and

$$G_j(\mathbf{k})=c_j(\mathbf{k})[k^2-k_0^2]\exp[i(\mathbf{k}-K_0)\cdot\mathbf{R}_j] \quad (36)$$

In this approximation, a further simplification is possible, by summing over the index j:

$$[k^2-k_0^2]C(\mathbf{k})=\frac{(2\pi)^3}{\tau}\sum_h^N\beta(\mathbf{k},\mathbf{K}_h)C(\mathbf{K}_h), \quad (37)$$

where

$$C(\mathbf{k})=\sum_j c_j(\mathbf{k}) \tag{38}$$

and

$$\beta(\mathbf{k},\boldsymbol{\kappa})=\sum_j \exp[i(\boldsymbol{\kappa}-\mathbf{k})\cdot\mathbf{r}_j]\beta_j(\mathbf{k},\boldsymbol{\kappa}). \tag{39}$$

To solve Eq. (34), only the values at $\mathbf{k}=\mathbf{K}_h$ are required. Hence, with the notation

$$C(\mathbf{K}_h)=C_h, \tag{40}$$

we have

$$[K_h^2-k_0^2]C_h=\frac{(2\pi)^3}{\tau}\sum_m^N \beta(\mathbf{K}_h,\mathbf{K}_m)C_m. \tag{41}$$

Equation (41) is similar to Laue's equations, if all but N terms are omitted in the sum. β takes the place of the structure factor V_{n-h} and β_j the place of the atomic form factor. However, Eq. (41) is more general in two respects: (1) the value of β depends on the unknown K_0, (2) β is not merely a function of the difference of its two arguments: this would be true only if β was identified with the two-body interaction potential, which is an inadequate approximation for nuclear interactions.[12]

Comparison with Eq. (13) suggests the following simple interpretation: in Laue's equations, substitute $\beta(\mathbf{K}_h,\mathbf{K}_m)$ as "pseudopotential," and proceed by Laue's approximation method. This rule has a particularly simple form when the scatterers are very small: β becomes a constant and can be considered as having been derived from an effective potential $\delta(\mathbf{r}-\mathbf{a}_n)$ in coordinate representation with an appropriate constant coefficient.

However, this simple rule does not hold for higher approximations. In particular, when β and, hence, G are constants, the second approximation would diverge if one used only the reinterpreted Laue equation. However, Eq. (23) shows that the contributions for $|K|\gg k_0$ are small: indeed, when the denominator has become a smooth function, sum and integral are equal.

Thus, we can formulate a heuristic rule similar to that found in (I), but not deducible from it: for small scatterers, substitute β as pseudopotential in Laue's equation, and proceed by Laue's approximation method, cutting off all integrals and sums at some point $|\mathbf{A}_m|\gg k_0$.

This situation provides an explanation for a curious coincidence found by Goldberger and Seitz.[6] Besides a correct calculation of neutron refraction and diffraction, based on Ewald's method, they present another derivation which uses delta-functions as effective potentials to describe the nuclei. They point out the inadequacy of this method, but find that it gives the same result as the correct method.

This coincidence is now explained by the mutual cancellation of two omissions: they first disregard, in effect, the integral in Eq. (23), calculate the first approximation by Eq. (41) and omit the second approximation which, with their formalism, would have been infinite. It can be seen now that the integral in Eq. (23) serves precisely to make this second approximation finite, and in their case, very small.

Returning to the general case of finite scatterers, we consider the simplest case, where only the contribution of the first term is large:[13] we have as a first approximation

$$K_0^2-k_0^2-[(2\pi)^3/\tau]\beta(\mathbf{K}_0,\mathbf{K}_0)=0. \tag{42}$$

It is shown in Sec. V that β is Hermitean where no inelastic scattering is present: hence, n^2 is real. If, as it happens often, the third term is small, we can solve this transcendental equation by successive approximations:

$$K_0^2-k_0^2=[(2\pi)^3/\tau]\beta(\mathbf{k}_0,\mathbf{k}_0), \tag{43}$$

where

$$\mathbf{k}_0=(\mathbf{K}_0/|\mathbf{K}_0|)k_0, \tag{44}$$

and so forth. Equation (43) is a sufficient approximation for all known cases of slow neutron scattering.

For point scatterers

$$n^2-1=(4\pi/k_0^3\tau)\tan\delta_0. \tag{45}$$

If we had used the retarded solution α instead of β we would have obtained

$$n^2-1=[(2\pi)^3/\tau k_0^2]\alpha(\mathbf{k}_0,\mathbf{k}_0), \tag{46}$$

and for point scatterers

$$n^2-1=\frac{4\pi}{k_0^3\tau}\frac{\exp(2i\delta_0)-1}{2i}. \tag{47}$$

Equation (47) is a slight generalization of the elementary theory[9] which predicts wave attenuation in a case where it obviously cannot exist. The use of the half-retarded, half-advanced solution has avoided this difficulty.

As an illustration of the effect of radiation damping, we consider again the case of small scatterers, *viz.*, nuclei whose scattering is described by a one-level Breit-Wigner formula. In this case[14] with the usual notation

$$e^{2i\delta_0}-1=4\pi^2ik_0f=e^{2i\eta}-1-\frac{i\Gamma_1e^{2i\eta}}{E-E_c+\frac{1}{2}i\Gamma}. \tag{48}$$

From Eq. (I, 19) we have[15]

$$n^2-1=\frac{(2\pi)^3}{\tau k_0^2}\frac{1}{2\pi^2ik_0}\frac{e^{i\eta}[E-E_c+\frac{1}{2}i(\Gamma_2-\Gamma_1)]-e^{-i\eta}[E-E_c+\frac{1}{2}i(\Gamma_2+\Gamma_1)]}{e^{i\eta}[E-E_c+\frac{1}{2}i(\Gamma_2-\Gamma_1)]+e^{-i\eta}[E-E_c+\frac{1}{2}i(\Gamma_2+\Gamma_1)]}. \tag{49}$$

[12] The question as to whether the generalization of Ewald's method to finite scatterers leads precisely to the form of Laue's equations has been discussed, but not entirely clarified by Ewald (Z. Krist. **97**, 1 (1937)).

[13] This approximation does not mean that the wave function is essentially a plane wave, as in Eq. (14). On the contrary, for point scatterers the wave function has singularities of the type $1/r$. The higher terms $G(\mathbf{K}_h)$ are omitted not because they are small, but because they are compensated by the integral on the right hand side of Eq. (23).

[14] N. E. Mott and H. S. W. Massey, *The Theory of Atomic Collisions* (The Clarendon Press, Oxford, 1949).

[15] The use of Eq. (I, 19), which has been derived for pure potential scattering only, will be justified in Sec. V.

In particular, if Γ_2 is very small, we can neglect η near resonance,

$$n^2-1=\frac{-2\pi}{\tau k_0^3}\frac{\Gamma_1}{E-E_c+\frac{1}{2}i\Gamma_2}, \tag{50}$$

whereas, by using the retarded solution, we would have obtained

$$n^2-1=-\frac{2\pi}{k_0^3\tau}\frac{\Gamma_1}{E-E_c+\frac{1}{2}i(\Gamma_1+\Gamma_2)}. \tag{51}$$

The correction for radiation damping has the effect of removing the natural line width from the terms composing the total line width. If no competing processes are present, i.e., $\Gamma_2=0$, the correct formula (50) shows that the index of refraction is either real or imaginary whereas the uncorrected Eq. (51) predicts attenuated waves. Hence, a good mirror for slow neutrons should have nuclei with large scattering, but small absorption cross section.

It is shown in Sec. V that for finite scatterers, and including absorption

$$\mathrm{Im}\beta(\mathbf{k}_0,\mathbf{k}_0)=[k_0/(2\pi)^3]\sigma_{\mathrm{in}}, \tag{52}$$

where σ_{in} is the cross section for inelastic and absorption processes of the single, fixed scatterer. Hence, we have, for long waves or, more generally, far from Laue-Bragg reflections

$$\mathrm{Im}(n^2-1)=\sigma_{\mathrm{in}}/k_0\tau. \tag{53}$$

Equation (53) is just what one would expect intuitively; since in the present approximation all inelastically scattered particles are considered lost, the attenuation is clearly proportional to the inelastic cross-section under conditions where no attenuation by radiation damping occurs.

Equation (53) is important in interpreting slow neutron transmission measurements. The attenuation coefficient varies from σ_{in} (long waves) to σ_{total} (e.g., in case of exact Bragg reflection from a crystal).

We discuss the second approximation to Eq. (42). We have, from Eq. (34), as a first approximation

$$(k^2-k_0^2)c_j(\mathbf{k})=[(2\pi)^3/\tau]\beta_j(\mathbf{k},\mathbf{K}_0)\times\exp[i\mathbf{r}_j\cdot(\mathbf{K}_0-\mathbf{k})]C_0, \tag{54}$$

and, by introducing this into the small terms of Eq. (23),

$$K_0^2-k_0^2=\frac{(2\pi)^3}{\tau}\beta(\mathbf{k}_0,\mathbf{k}_0)+\frac{(2\pi)^6}{\tau^2}\sum_{h\neq 0}\frac{\beta(\mathbf{k}_0,\mathbf{K}_h)\beta(\mathbf{K}_h,\mathbf{k}_0)}{K_h^2-k_0^2}$$
$$-\frac{(2\pi)^3}{\tau}P\int d\boldsymbol{\kappa}\sum_j\frac{\beta_j(\mathbf{k}_0,\boldsymbol{\kappa})\beta_j(\boldsymbol{\kappa},\mathbf{k}_0)}{\kappa^2-k_0^2}, \tag{55}$$

It is apparent that the second approximation does not diverge, even for point scatterers. Just as in the case of finite scattering systems, the integral compensates the nonoscillatory terms of the sum, because the self-action of each scatterer has been eliminated at the outset, whereas in Laue's approximation method the self-action causes divergence.

IV. THE RANDOM MEDIUM

In this section, the random medium will be studied from the viewpoint of a dynamical theory, i.e., we seek the properties of solutions in the infinite medium rather than considering the scatterer as a cause of perturbation of an incident beam.

There are, at present, two approaches to wave propagation in random media: (1) the perturbation (or geometric) theory which calculates the scattered wave for a definite configuration, and averages intensities by weighting all possible configurations with their probability. (2) a dynamical theory originated by Foldy[16] and extended by Lax[7,11] which determines the properties of a mean wave obtained by statistical averaging of some scatterer positions. Now, the outstanding fact about a random medium such as glass is that measurable properties do not vary from sample to sample: one can say that the sample is so large that its various parts constitute already a statistical ensemble. Hence, it seems that the purpose of a deductive theory is to show that observable properties don't depend on the precise configuration, but only on certain autocorrelation functions, in other words, to show that scattering is not "structure sensitive."

The present analysis considers a definite "frozen" configuration of the random medium, and does not make use of any statistical averaging. It is found that the only assumption necessary is the mathematical existence of a correlation function. To avoid a misunderstanding, it may be remembered that the autocorrelation function has by itself nothing to do with statistics; it is a definite functional of a given function.

We consider first a definite time-independent potential $v(\mathbf{r})$. The "random medium" is defined by the existence of the correlation function

$$\lim_{\tau\to\infty}\frac{1}{\tau}\int v(\mathbf{r}'+\mathbf{r})v(\mathbf{r})d\mathbf{r}=w(\mathbf{r}), \tag{56}$$

where τ is the volume of integration. To define the problem completely, we must select a class of solutions by some means. We do not wish to this by the introduction of boundary conditions at infinity, because it is clear from analogy with the crystal that the solutions needed to satisfy boundary conditions in a problem involving a finite scatterer are of very different types, increasing exponentially in various space directions.[17] In the case of the crystal, the selection of solutions is made by Floquet's theorem, which is expressed by Eq. (11). What we need for the random medium is evidently an analog of Floquet's theorem.

[16] L. L. Foldy, Phys. Rev. **67**, 107 (1945).

[17] In the simplest case of a homogeneous medium, the solutions needed to solve the problem of total reflection are exponentially increasing normal to the boundary.

Our choice is based on the simple remark that the crystal can be considered as the most general medium provided that the unit cell is extended to infinity. Hence, we shall follow the formalism of Sec. III, going to the limit $\tau\to\infty$ at the appropriate point. This selection is not equivalent to the periodic boundary conditions frequently used in physics, mainly because complex values of the wave numbers must be admitted

We consider now the second-order solution to the crystal problem. By inversion of Eq. (12) we have

$$V_n=\frac{1}{\tau}\int_\tau \exp(-2\pi i A_n\cdot\mathbf{r})v(\mathbf{r})d\mathbf{r}. \tag{57}$$

In the limit the reciprocal lattice vectors will form a dense set $\mathbf{R}$ and V_n will tend toward $V(\mathbf{R})$. But

$$\lim_{\tau\to\infty}\frac{1}{\tau}\left|\int \exp(-2\pi i\mathbf{R}\cdot\mathbf{r})v(\mathbf{r})d\mathbf{r}\right|^2=\lim\tau|V(\mathbf{R})|^2 \tag{58}$$

will exist in the limit, if the correlation function $w(\mathbf{r})$ exists, and will be given by the Wiener-Khinchin formula

$$\lim\tau|V(\mathbf{R})|^2=\int d\mathbf{r}\exp(-2\pi i\mathbf{r}\cdot\mathbf{R})w(\mathbf{r})=G(\mathbf{R}). \tag{59}$$

The Fourier coefficients V_n tend to zero as $1/\sqrt{\tau}$, except V_0, the mean value, which remains finite. Therefore, V_0 and the coefficient a_0 must be singled out. Instead of Eqs. (14) and (15), we have

$$[K_0^2+(2m/\hbar^2)V_0-k_0^2]c_0+\sum{}' v_m c_m=0, \tag{60}$$

$$(n\neq 0)[(\mathbf{K}_0+2\pi\mathbf{A}_n)^2+(2m/\hbar^2)V_0-k_0^2]c_n+V_n c_0+\sum{}' V_{n-m}c_m=0. \tag{61}$$

Assuming again c_0 to be large, we obtain

$$c_n=-\frac{2m}{\hbar^2}\frac{V_n c_0}{(\mathbf{K}_0+2\pi\mathbf{A}_n)^2+(2m/\hbar^2)V_0-k_0^2}, \tag{62}$$

and

$$K_0^2-k_0^2+\frac{2m}{\hbar^2}V_0-\left(\frac{2m}{\hbar^2}\right)^2\sum{}'\times\frac{|V_m|^2}{(\mathbf{K}_0+2\pi\mathbf{A}_n)^2+(2m/\hbar^2)V_0-k_0^2}=0. \tag{63}$$

For finite cell dimensions, $\mathbf{K}_0$ is obviously such that none of the denominators in Eqs. (62, 63) vanishes. As the vectors $\mathbf{A}_n$ become a dense set, it is no longer possible to avoid the vanishing of the denominators, and a suitable limiting process must be defined. By analogy with usual scattering theory, we define the limiting process so that k_0^2 has a small positive imaginary part, which is made to vanish after the sum has been converted into an integral.

In converting the sum in Eq. (63) into an integral, we note that the number of reciprocal lattice points in the unit volume of Fourier space is τ. Hence, we obtain

$$K_0^2-k_0^2+\frac{2m}{\hbar^2}V_0-\left(\frac{2m}{\hbar^2}\right)^2\int_h \times\frac{G(\mathbf{R})d\mathbf{R}}{(\mathbf{K}_0+2\pi\mathbf{R})^2-k_0^2+(2m/\hbar^2)V_0}=0, \tag{64}$$

to the second order.

We now turn to the boundary value problem of a semi-infinite medium, with an incident plane wave. Rigorously, the solution of the boundary value problem would require an infinite number of solutions for the infinite medium, and not only the one approximated by Eqs. (62, 64), but we follow the usual procedure[18] in omitting all but the strongest. The tangential components of $\mathbf{K}_0$ are then determined by the requirements of continuity: they must be equal to those of the incident wave, and the only unknown is the component of $\mathbf{K}_0$ normal to the boundary which is determined by Eq. (64). The reflected and transmitted strong waves are determined as in homogeneous refraction, with a refractive index

$$n^2-1=-\frac{2m}{k_0^2\hbar^2}V_0+\frac{(2m)^2}{k_0^2\hbar^4}\int_h \times\frac{G(\mathbf{R})d\mathbf{R}}{(\mathbf{k}_0+2\pi\mathbf{R})^2-k_0^2+(2m/\hbar^2)V_0}, \tag{65}$$

where we have substituted $\mathbf{k}_0$, the wave vector of the incident wave, for $\mathbf{K}_0$ in the denominator of the integral. By the definition of the integral, the imaginary part of n^2 is given by

$$\mathrm{Im}n^2=\frac{m^2}{(2\pi)^2k_0\hbar^4}\int_S G\left(\frac{\mathbf{R}-\mathbf{k}_0}{2\pi}\right)d\Omega. \tag{66}$$

which is the equivalent of the formulas for turbidity in the optics of liquids.[19]

In contrast to the crystal case, the weak reflected or scattered vacuum waves cannot be disregarded, because the resonance denominator vanishes for some of the internal weak waves.

The calculation of the weak reflected waves is somewhat facilitated by remarking that those internal waves for which the tangential component of $\mathbf{K}_h$ is larger than k_0, can be only continued into the vacuum by waves decaying exponentially from the surface as in total reflection of homogeneous bodies. Hence, most of the weak waves will give rise only to surface waves which are hardly observable. Furthermore, it is clear that waves with propagation vectors greatly different

[18] M. von Laue, *Materiewellen und ihre Interferenzen* (Akademische Verlagsgesellschaft, Leipzig, 1948).

[19] S. Bhagavantam, *Scattering of Light and the Raman Effect* (Chemical Publishing Company, Brooklyn, 1942).

from k_0 suffer strong, if not total, reflection in penetrating through the boundary. It is, hence, plausible to assume that the only important contribution to the weak external field is given by internal waves with propagation vectors $|\mathbf{K}_h| \approx |\mathbf{K}_0| \approx k_0$. But these waves suffer little refraction, so that we may simply continue them into the vacuum without change.

By Eqs. (11) and (62), the wave function in the vacuum is

$$\psi \approx -\exp(i\mathbf{K}_0\cdot\mathbf{r})\sum_h \frac{2m}{\hbar^2}\frac{V_n c_0}{K_h^2-k_0^2}\exp(2\pi i\mathbf{A}_h\cdot\mathbf{r}), \quad (67)$$

the summation being extended over a small range $|\mathbf{K}_h| \approx k_0$. Passing to the continuum, we have for $c_0=1$

$$\psi = -\frac{2m}{\hbar^2}\tau\int_h \frac{\exp[i(\mathbf{K}_0+2\pi\mathbf{R})\cdot\mathbf{r}]V(\mathbf{R})}{(\mathbf{K}_0+2\pi\mathbf{R})^2-k_0^2}d\mathbf{R}. \quad (68)$$

For large values of r, one obtains the asymptotic value

$$\psi \sim -\frac{2m}{\hbar^2}\frac{\tau}{4\pi}V\left(\frac{\mathbf{k}-\mathbf{K}_0}{2\pi}\right)\frac{\exp(ik_0 r)}{r},$$

where $\mathbf{k}$ is a vector of length k_0 and parallel to $\mathbf{r}$. Hence, by Eq. (59)

$$|\psi|^2 \sim \left(\frac{2\pi m}{\hbar^2}\right)^2\frac{\tau}{r^2}G\left(\frac{\mathbf{k}-\mathbf{K}_0}{2\pi}\right). \quad (69)$$

Equation (69) is almost identical with Born's approximation for the scattered waves, but it contains instead of the propagation vector of the incident wave $\mathbf{k}_0$, the vector $\mathbf{K}_0$ which has a complex normal component, so that only a surface layer of the medium contributes to scattering.

This approach to the dynamical theory of the random medium may become inadequate either because the potential has strong singularities (point scatterers) so that the second term in Eq. (64) becomes very large even diverges; or because the interaction cannot be described by a potential. In either case, we can use the alternative formulation in terms of two-body matrices β.

Conversion of the sums into integrals, in the manner previously described, gives by Eq. (55)

$$K_0^2-k_0^2 = \frac{(2\pi)^3}{\tau}\beta(\mathbf{K}_0,\mathbf{K}_0) + \frac{(2\pi)^3}{\tau}P\int\frac{\beta(\mathbf{K}_0,\boldsymbol{\kappa})\beta(\boldsymbol{\kappa},\mathbf{K}_0)-\sum\beta_j(\mathbf{K}_0,\boldsymbol{\kappa})\beta_j(\boldsymbol{\kappa},\mathbf{K}_0)}{\kappa^2-k_0^2}d\boldsymbol{\kappa} + \frac{(2\pi)^3}{\tau}\frac{i\pi k_0}{2}\int\beta(\mathbf{K}_0,\boldsymbol{\kappa})\beta(\boldsymbol{\kappa},\mathbf{K}_0)d\Omega. \quad (70)$$

This expression is meaningful if the limits

$$\lim_{\tau\to\infty}\frac{\beta(\mathbf{K}_0,\mathbf{K}_0)}{\tau} \quad \text{and} \quad \lim_{\tau\to\infty}\frac{\beta(\mathbf{K}_0,\boldsymbol{\kappa})\beta(\boldsymbol{\kappa},\mathbf{K}_0)}{\tau}(\boldsymbol{\kappa}\neq\mathbf{K}_0) \quad (71)$$

exist. The first limit is clearly the mean value of $\beta_i(\mathbf{K}_0,\mathbf{K}_0)$ and exists by assumption. To investigate the second limit, we may disregard the matrices β_i and consider

$$\lim_{\tau}\frac{1}{\tau}|\sum\exp(i\mathbf{k}\cdot\mathbf{r}_i)|^2.$$

The existence of this limit is implied in the existence of $G(\mathbf{R})$ as defined in Eq. (59), for, if the potential is due to individual scatterers, with potentials $v_i(\mathbf{r})$, V has the form

$$V=(1/\tau)\sum_i\exp(i\mathbf{R}\cdot\mathbf{r}_i)V_i(\mathbf{R}), \quad (72)$$

with

$$V_i=\int_\infty v_i(\mathbf{r})\exp(i\mathbf{R}\cdot\mathbf{r})d\mathbf{r}. \quad (73)$$

Hence, the refractive index is

$$n^2-1=(2\pi)^3\left[\frac{\langle\beta_i(\mathbf{K}_0,\mathbf{K}_0)\rangle}{k_0^2}+P\frac{1}{k_0^2}\int\frac{G''(\mathbf{K}_0,\boldsymbol{\kappa})}{\kappa^2-k_0^2}d\boldsymbol{\kappa} + \frac{i\pi}{2k_0}\int_S G'(\mathbf{K}_0,\boldsymbol{\kappa})d\Omega\right], \quad (74)$$

where

$$G'(\mathbf{K}_0,\boldsymbol{\kappa})=\lim(1/\tau)\beta(\mathbf{K}_0,\boldsymbol{\kappa})\beta(\boldsymbol{\kappa},\mathbf{K}_0), \quad (75)$$

$$G''(\mathbf{K}_0,\boldsymbol{\kappa})=\lim(1/\tau)[\beta(\mathbf{K}_0,\boldsymbol{\kappa})\beta(\boldsymbol{\kappa},\mathbf{K}_0) - \sum\beta_j(\mathbf{K}_0,\boldsymbol{\kappa})\beta_j(\boldsymbol{\kappa},\mathbf{K}_0)], \quad (76)$$

and

$$\langle\beta_i(\mathbf{K}_0,\mathbf{K}_0)\rangle=\lim(1/\tau)\sum\beta_i(\mathbf{K}_0,\mathbf{K}_0). \quad (77)$$

If one or several scatterers are point scatterers (β_i constant), the principal value still exists in this formulation because the constant part of the first term of G'' is canceled by the second term.

The first term in Eq. (74) has the same form as in the crystal case, and needs no further discussion. The third term has a simple meaning only when the single scattering event is purely elastic. In this case, the integral is essentially the cross section, in first approximation, of a unit volume of liquid, by comparison with Eqs. (9) and (10). This is in agreement with well-known results on turbidity.[19] The second term is purely real for nonabsorbing liquids, and is evidently the equivalent of the Lorentz correction. From the comparison with the Lorentz correction for crystals we may infer that its order of magnitude, relative to the first term is β/a, where a is a mean distance between scatterers. This term constitutes the main contribution to the first nonvanishing correction for the refractive index of a liquid as used in the experiments of Burgy, Ringo, and Hughes.[20]

Since the third term vanishes when the density of scatterers is so large that destructive interference prevails, we find that the refractive index is real for very dense, nonabsorbing liquids. This result is in agreement

[20] Burgy, Ringo and Hughes, Phys. Rev. **84**, 1160 (1951).

with theoretical results usually reported.[19] These, however, are obtained by arbitrarily disregarding radiation damping contrary to the present derivation.

As an example, we consider the imaginary part of n^2 for the case of a crystal with protons having random spins. The disordered crystal is a special case of a random medium, and can be treated dynamically by the present method. However, the particular approximation method used to derive Eq. (70) assumes that no Bragg reflection has importance, so that the following result is only valid for a wavelength large enough to avoid Bragg reflection in a polycrystal, or for a nonreflecting position of a single crystal.

The elements of the matrix β for the n-p scattering are derived in Sec. V.

The contribution of the first term in the bracket [Eq. (74)] is

$$(a_1-a_3)^2\nu_p/16\pi^2k_0,$$

where ν_p is the number of protons per unit volume. This contribution is in agreement with Eq. (53), since the inelastic (usually called incoherent) cross section of the unpolarized proton is $(4\pi/8)(a_1-a_3)^2$. The second term in the bracket is real to the second order in the scattering length, and does not contribute. The integrand of the third term can be easily evaluated on the assumption of random spins.[21] It is

$$\nu_p(\langle\beta^2\rangle-\langle\beta\rangle^2)=\frac{\nu_p}{16\cdot 4\pi^4}(a_1-a_3)^2.$$

Hence,

$$\mathrm{Im}n^2=\frac{4\pi\nu_0}{k_0}\frac{3}{2}\cdot\frac{1}{8}(a_1-a_3)^2. \tag{77}$$

In other words, the apparent cross section of the protons, as measured by a transmission experiment, is $\frac{3}{2}$ times the "incoherent" n-p cross section. This result could also have been obtained from the elementary theory, i.e., by determining in first approximation, the number of incident neutrons scattered by a thin sheet.

Specifically dynamical phenomena, not described by a kinematic theory, are to be expected when the scatterers have their spins partially aligned by an external field. In this case, the spinor character of the neutrons cannot be disregarded, and the coefficients C_n in Eq. (41) must be considered as spinors. For a liquid, all coefficients but C_0 may be disregarded in first approximation, so that two refractive indices must be considered, for neutron spin parallel and antiparallel to the field direction, as in the theory of neutron propagation in a ferromagnet.[22] We have

$$n^2-1=-\frac{4\pi}{k_0^2}\left[\frac{\nu_0}{4}(3a_3+a_1)\pm\frac{\epsilon}{2}\nu_p(a_3-a_1)+\nu_M a_M\right], \tag{78}$$

where ν_p and ν_M are the numbers per unit volume, of protons and other spinless nuclei, respectively, a_M the scattering length of these, and ϵ the relative excess of protons aligned:

$$\epsilon=(\nu_+-\nu_-)/\nu-\tfrac{1}{2}. \tag{79}$$

A measurement of the angle of total reflection provides a means for determining the difference of triplet and singlet amplitude.

V. PROPERTIES OF THE MATRICES α AND β

The basic assumption of this paper is that equations derived for the simplest case of potential scattering remain approximately valid if the matrices α and β describing the elastic scattering of a more general single scatterer are substituted. We shall now express these quantities in terms of the general theory of scattering and derive some of their properties.

It would be desirable to relate the multiple scattering to a general time-independent theory of single scattering. Neither of the three presentations known to us[23–25] is quite sufficient to describe absorption, creation and rearrangement processes which occur in the nuclear phenomena under study. We have to make the further assumption that the general properties of the scattering matrices are preserved in a more general theory, and we shall use Pauli's formalism.

The scattering of an incident plane wave is described by the matrix

$$(k|f|0)=U(k|\phi|0), \tag{80}$$

where U is the interaction Hamiltonian, and $(k|\phi|0)$ the wave function in momentum representation. If U is a scalar potential in coordinate space,

$$(\mathbf{k}|f|0)=\frac{1}{(2\pi)^3}\int u(\mathbf{r})\psi(\mathbf{r})\exp(-i\mathbf{k}\cdot\mathbf{r})d\mathbf{r}, \tag{81}$$

where ψ is that wave function which has the asymptotic form $\exp(i\mathbf{k}_0\cdot\mathbf{r})$. Hence, it is seen by comparison with Eq. (I, 4) that

$$f(\mathbf{k})=-(2m/\hbar^2)(\mathbf{k}|f|0) \tag{82}$$

in the simplest case.[26] The generalization consists in substituting for f that submatrix which describes elastic scattering, i.e.,

$$f(\mathbf{k})=-(2m/\hbar^2)(\mathbf{k}|f|0)\delta_{nn_0}, \tag{83}$$

where n and n_0 characterize two unperturbed states of the scatterer. In the following, it will be useful to

[21] Reference 4, p. 177.
[22] H. Ekstein, Phys. Rev. **76**, 1328 (1949).
[23] C. Møller, Kgl. Danske Videnskab. Selskab Mat.-fys. Medd. **23**, No. 1 (1945); **22**, No. 19 (1946).
[24] W. Pauli, *Meson Theory of Nuclear Forces* (Interscience Publishers, Inc., New York, 1948).
[25] B. Lippmann and J. Schwinger, Phys. Rev. **79**, 469 (1950).
[26] Pauli's equation giving the connection between the asymptotic value of the wave function in coordinate space and the matrix $(k|f|0)$ differs from our Eq. (I, 8) by a factor $(-(2\pi)^{-1})$. The minus sign is presumably omitted by mistake; the constant factor is due to our use of unnormalized plane waves $\exp(i\mathbf{k}\cdot\mathbf{r})$ as usual in the theory of scalar scattering, instead of normalized plane waves $(2\pi)^{-\frac{1}{2}}\exp(i\mathbf{k}\cdot\mathbf{r})$.

distinguish between variables characterizing the scatterer (n) and the incident particle (k). Thus, we can write

$$f(\mathbf{k}) = -(2m/h^2)(k, n_0|\, f\,|k_0, n_0). \quad (84)$$

Generalizing Eq. (I, 28) we can define a matrix $(k|\,\alpha\,|\kappa)$ for the general scattering problem by the integral equation

$$(k|\,\alpha\,|\kappa) - \sum_l \frac{(k|\,U\,|l)}{E_0 - E_l}(l|\,\alpha\,|\kappa) + i\pi \int_A (k|\,U\,|A)(A|\,\alpha\,|\kappa) = (k|\,U\,|\kappa), \quad (85)$$

which reduces to Pauli's equation (5) for $(k|\,f\,|0)$ in the special case where $E(\kappa) = E_0$. In Pauli's notation, the symbol A stands for all variables except the energy, and the integral is extended over the "energy shell" $E = E_0$. The matrix $\alpha(\mathbf{k}, \boldsymbol{\kappa})$ used in the theory of multiple scattering is proportional to that submatrix of $(k|\,\alpha\,|\kappa)$, which describes elastic processes only:

$$\alpha(\mathbf{k}, \boldsymbol{\kappa}) = -(2m/h^2)(nk|\,\alpha\,|n_0\kappa)\delta_{nn_0}. \quad (86)$$

The matrix $(k|\,\alpha\,|\kappa)$ has no direct physical meaning, but it can be connected with the scattering of a beam of particles issued from a point source at a finite distance, in the manner described by Eqs. (I, 23, 29).

For the theory of multiple scattering in extended bodies, we need the generalization of the matrix $\beta(\mathbf{k}, \boldsymbol{\kappa})$ introduced in Eq. (I, 30).

This matrix differs from α by the elimination of radiation damping in elastic, but only in elastic scattering. Hence, the appropriate generalization is given by the equation

$$(n, k|\,\beta\,|n_0, \kappa) - \sum_{l, m} \frac{(n, k|\,U\,|m, l)(m, l|\,\beta\,|n_0, \kappa)}{E_0 - E_{ml}} + i\pi \sum_{m \neq n_0} \int_A (n, k|\,U\,|m, A)(m, A|\,\beta\,|n_0, \kappa) = (n, k|\,U\,|n_0, \kappa), \quad (87)$$

in which the term describing radiation damping by loss of the elastically scattered particles has been omitted. The matrix $\beta(\mathbf{k}, \boldsymbol{\kappa})$ is again proportional to the elastic submatrix of $(n, k|\,\beta\,|n_0, \kappa)$:

$$\beta(\mathbf{k}, \boldsymbol{\kappa}) = -(2m/h^2)(n, k|\,\beta\,|n_0, \kappa)\delta_{nn_0}. \quad (88)$$

If the Hamiltonian of the single scattering process is not known, the matrix α can, at least in principle, be measured by a set of double-scattering experiments, using Eq. (I, 52), but β is not directly related to an experiment using a small number of scatterers. Therefore, it is useful to show how β can be calculated if α is known.

We write the equation defining α (Eq. (85)) under the form

$$(n, k|\,\alpha\,|n_0, \kappa) - \sum_{l, m} \frac{(n, k|\,U\,|m, l)(m, l|\,\alpha\,|n_0, \kappa)}{E_0 - E_m} + i\pi \sum_{m \neq n_0} (n, k|\,U\,|m, A)(m, A|\,\alpha\,|n_0, \kappa) = (n, k|\,U\,|n_0, \kappa) - i\pi \int_A (n, k|\,U\,|n_0, A) \times (n_0, A|\,\alpha\,|n_0, \kappa). \quad (89)$$

Comparison with Eq. (87) shows that

$$(n, k|\,\alpha\,|n_0, \kappa) = (n, k|\,\beta\,|n_0, \kappa) - i\pi \int_A (n, k|\,\beta\,|n_0, A)(n_0, A|\,\alpha\,|n_0, \kappa). \quad (90)$$

This equation allows us to calculate β if α is known. It is similar to Heitler's integral equation, except for the circumstance that in general $E_0 \neq E_{n_0\kappa}$. The solution can be obtained in two steps: since only values of β on the energy shell occur under the integral, we can write, for the particular set of values $\kappa = k_0$ such that $E_0 = E_{n_0\kappa}$:

$$(n, k|\,f\,|n_0, k_0) = (n, k|\,g\,|n_0 k_0) - i\pi \int_A (n, k|\,g\,|n_0, A)(n_0, A|\,f\,|n_0, k_0). \quad (91)$$

If g is determined by solving this equation, β is given by

$$(n, k|\,\beta\,|n_0, \kappa) = (n, k|\,\alpha\,|n_0, \kappa) + i\pi \int_A (n, k|\,g\,|n_0, A)(n_0, A|\,\alpha\,|n_0, \kappa). \quad (92)$$

In first approximation, when β differs only slightly from α, we have

$$(n, k|\,\beta\,|n_0, \kappa) = (n, k|\,\alpha\,|n_0, \kappa) + i\pi \int_A (n, k|\,\alpha\,|n_0, A)(n_0, A|\,\alpha\,|n_0, \kappa). \quad (93)$$

This equation can be used to estimate the importance of the correction for radiation damping. For point scatterers, Eq. (90) becomes

$$(n|\,\alpha\,|n_0) = (n|\,\beta\,|n_0) - i(4\pi^2 k_0 m/h^2)(n|\,\beta\,|n_0)(n_0|\,\alpha\,|n_0), \quad (94)$$

or, if we write, in accordance with Eqs. (86, 88),

$$\alpha_n = -(2m/h^2)(n|\,\alpha\,|n), \quad \beta_n = -(2m/h^2)(n|\,\beta\,|n), \quad (95)$$

$$\beta_n = \alpha_n/(1 + 2i\pi^2 k_0 \alpha_n). \quad (96)$$

Hence, if α_n is written under the form $1/4\pi^2 i k_0$

$\times[\exp(2i\delta_n)-1]$ where δ is now complex, we have

$$\beta_n=(1/2\pi^2k_0)\tan\delta_n, \tag{97}$$

which justifies the generalized use of Eq. (I, 22) made in Sec. III.

As an example, we calculate β for n-p scattering. The only nonvanishing matrix elements of α are, with obvious notation:[27]

$$\downarrow\downarrow \rightarrow \downarrow\downarrow \text{ or } \uparrow\uparrow \rightarrow \uparrow\uparrow : {}^3\alpha,$$
$$\downarrow\uparrow \rightarrow \downarrow\uparrow \text{ or } \uparrow\downarrow \rightarrow \uparrow\downarrow : \tfrac{1}{2}({}^3\alpha+{}^1\alpha),$$
$$\downarrow\uparrow \rightarrow \uparrow\downarrow \text{ or } \uparrow\downarrow \rightarrow \downarrow\uparrow : \tfrac{1}{2}({}^3\alpha-{}^1\alpha),$$

where ${}^3\alpha$ and ${}^1\alpha$ are the corresponding quantities for triplet and singlet scattering. The diagonal elements of β are, by Eq. (97)

$${}^3\alpha/(1+2i\pi^2k_0\,{}^3\alpha) \quad \text{(parallel spins)},$$

$$\tfrac{1}{2}({}^3\alpha+{}^1\alpha)/[1+i\pi^2k_0({}^3\alpha+{}^1\alpha)] \quad \text{(antiparallel spins)}.$$

By Eq. (I, 21) we have, for each of the elements ${}^3\alpha$ and ${}^1\alpha$,

$$2\pi^2\alpha=\delta_0/k_0+i\delta_0^2/k_0 \tag{98}$$

to the second order of the small phase angle. In terms of the scattering length,

$$a=-\delta_0/k_0, \tag{99}$$

we have then

$$2\pi^2\beta=-a_3 \quad \text{(parallel spins)}, \tag{100}$$

and

$$2\pi^2\beta=-\tfrac{1}{2}(a_3+a_1)+\tfrac{1}{4}ik_0(a_3-a_1)^2 \quad \text{(antiparallel spins)}. \tag{101}$$

The scattering lengths a_1 and a_3 are here those of the bound proton, i.e., twice the scattering length for the free collision.

Equation (87) can be written

$$\beta=U(1-T), \tag{102}$$

where

$$(nk|T|n'k')=\frac{(nk|\beta|n'k')}{E(nk)-E_0}$$
$$+i\pi(nk|\beta|n'k')\delta\{E(nk)-E_0\}(1-\delta_{nn'}). \tag{103}$$

[27] L. Rosenfeld, *Nuclear Forces* (North-Holland Publishing Company, New York, 1948).

Because of the Hermitean character of U, we have also

$$\beta^*=(1-T^*)U. \tag{104}$$

Multiplication of Eq. (102) by $(1-T^*)$ from the left and of Eq. (104) by $(1-T)$ from the right, gives

$$(1-T^*)\beta-\beta^*(1-T)=0. \tag{105}$$

In particular, when only elastic scattering exists, i.e., all matrix elements of U except $(n_0k|U|n_0k')$ vanish,

$$\beta-\beta^*=0, \tag{106}$$

which proves the statement made in Sec. II. In general we obtain from Eq. (105) for the matrix element n, $k=n'$, $k'=n_0$, k_0:

$$2\,\mathrm{Im}(n_0, k_0|\beta|n_0, k_0)$$
$$=-2\pi\sum_{m\neq n_0}\int_A|(m, A|\beta|n_0, k_0)|^2. \tag{107}$$

By Eq. (93) β differs from α only by second-order terms. Hence, we can substitute α for β in the right-hand side, with an error of third order in β. We can use this approximation consistently to evaluate $\beta(\mathbf{k}_0, \mathbf{k}_0)$ in Eq. (43). The elements of α appearing under the integral belong to the submatrix f of α, since $E_0=E(n_0, k_0)$. The relation between the asymptotic form of the scattered wave and f is[24]

$$\psi_m(\mathbf{r})\sim-(2\pi)^{\frac{1}{2}}\frac{\exp(ik_m)}{r}k_m\left(\frac{dk}{dE}\right)_{k=k_m}(m, A|f|n_0k_0). \tag{108}$$

Hence, the partial differential cross section $d\sigma_m$ for the process $n_0\rightarrow m$ is[28]

$$d\sigma_m=(2\pi)^4\frac{k_m}{k_0}\frac{m^2}{h^4}|(m, A|f|n_0, k_0)|^2d\Omega. \tag{109}$$

Therefore,

$$\mathrm{Im}\beta(\mathbf{k}_0, \mathbf{k}_0)=[k_0/(2\pi)^3]\sigma_{in}, \tag{110}$$

where

$$\sigma_{in}=\sum_{m\neq n_0}\int d\sigma_m. \tag{111}$$

This result was anticipated in Sec. III.

The author is indebted to Miss Irene Corvin for numerical calculations leading to Eq. (33).

[28] The factor $(2\pi)^3$ is due to different normalization, as pointed out in footnote 26.

Radiations of 6.7-Day U^{237}

F. WAGNER, JR., M. S. FREEDMAN, D. W. ENGELKEMEIR, AND J. R. HUIZENGA
Chemistry Division, Argonne National Laboratory, Chicago, Illinois

(Received September 19, 1952)

The radiations of U^{237} have been studied using a magnetic lens beta-ray spectrometer and scintillation spectrometers for betas and gammas singly and in coincidence. A beta with an end-point energy of 245±5 kev was found along with evidence for the existence of a lower energy component. Gammas of energy 27, 43, 59, 165, 207, 269, 334, 370, and 430 kev were found, and probably a gamma of 102 kev. The decay scheme constructed gives a total decay energy for this isotope of 551±5 kev.

INTRODUCTION

SINCE U^{237} was first observed by Nishina *et al.*[1] and independently by McMillan,[2] several studies[2-5] of the radiations from this isotope have been made, but none have led to a definite assignment of the total decay energy, and there has been a lack of agreement among the several investigators as to the character of these radiations.

McMillan's[2] absorption data indicated the presence of a simple beta-ray ($E_{max}=0.25$ Mev) and two soft gamma-rays. Later work by Brady and Rubinson,[3] counting with the use of aluminum and lead absorbers, led them to assign the activity to three beta-particles ($E_{max}=1.5$, 1.2, and 0.25 Mev) and to gammas of energies 0.53, 0.23, and 0.14 Mev.

A more extensive study of this isotope by Engelkemeir and Turkevich[4] using coincidence methods as well as straight absorption counting enabled them to give a more detailed picture of these radiations. They reported gammas of 0.050, 0.220, and 0.450 Mev, conversion electrons at *ca* 0.1 and *ca* 0.3 Mev, and a beta-continuum with $E_{max}=0.3$ Mev. They also detected the presence of neptunium x-rays (14 and 95 kev).

More recently Melander and Slätis[5] studied the beta-ray and conversion line spectrum of samples of U^{237} with a magnetic lens spectrometer. They reported the presence of a beta-continuum ($E_{max}=0.23$ Mev), possibly a lower energy beta, and eight conversion lines corresponding to gammas of energy 0.057, 0.204, and 0.260 Mev. Gamma-absorption measurements were in agreement with these results.

The experiments reported here were undertaken in order to furnish data as to the total decay energy of the U^{237} nucleus for use in formulating the energy cycles among the heavy elements.[6]

EXPERIMENTAL

The U^{237} used in these experiments was formed by neutron irradiation of enriched uranium (*ca* 50 percent U^{236}) in the Argonne heavy water pile.

After irradiation uranium was chemically separated from fission products and other activities by the following chemical procedure.

1. Uranyl nitrate was dissolved in HNO_3 after irradiation.
2. $(NH_4)_2U_2O_7$ was precipitated; the precipitate was then washed.
3. $(NH_4)_2U_2O_7$ was dissolved in concentrated HNO_3. Urea and Fe^{++} were added (to reduce neptunium to Np^{+4}), the solution was diluted to $0.4M$ H^+ and saturated with NH_4NO_3.
4. Uranium was diethyl ether extracted from aqueous solution, washed with saturated NH_4NO_3, and then re-extracted back into water (activities such as iodine remain in ether).
5. The water solution was re-extracted with ether several times to remove traces of halogens.
6. $NaUO_2(Ac)_3$ was precipitated from the water solution.
7. Steps 2 to 6 were repeated five times, omitting step 6 in the last cycle.

The final extraction resulted in a solution of uranyl nitrate in water.

Evidence for the decontamination achieved with this procedure is the fact that no change was observed in the spectrum taken on a sample after several additional extraction cycles were performed. A sample showed a linear decay over a period of thirteen half-lives in agreement with the 6.75±0.01 days half-life measured by Huizenga and Flynn.[7]

BETA-RAY SPECTROMETER STUDIES

The samples for the beta-ray spectrometer were prepared by evaporating a solution of uranium on thin (10 $\mu g/cm^2$) LC-600 films, which were made conducting by a coat of Aquadag on the back side.

The instrument used was a double lens magnetic spectrometer having a transmission of *ca* 2 percent and a resolution for the Ba^{137} conversion line of *ca* 2 percent.

The detector was an atmospheric pressure flow-type methane proportional counter. For energies below 135

[1] Nishina, Yaseki, Ezoe, Kimura, and Ikawa, Phys. Rev. **57**, 1182 (1940).
[2] E. McMillan, Phys. Rev. **58**, 178 (1940).
[3] E. L. Brady and W. Rubinson, *Radiochemical Studies: The Fission Products* (McGraw-Hill Book Company, Inc., New York, 1951), Paper No. 3.21, National Nuclear Energy Series, Plutonium Project Record, Vol. 9, Div. IV.
[4] D. W. Engelkemeir and A. Turkevich, *Radiochemical Studies: The Fission Products* (McGraw-Hill Book Company, Inc., New York, 1951), Paper No. 3.22, National Nuclear Energy Series, Plutonium Project Record, Vol. 9, Div. IV.
[5] L. Melander and H. Slätis, Arkiv Mat. Astron. Fysik **A36**, No. 15 (1948-1949).
[6] Huizenga, Magnusson, Freedman, and Wagner, Phys. Rev. **84**, 1264 (1951).
[7] J. R. Huizenga and K. F. Flynn (unpublished results).

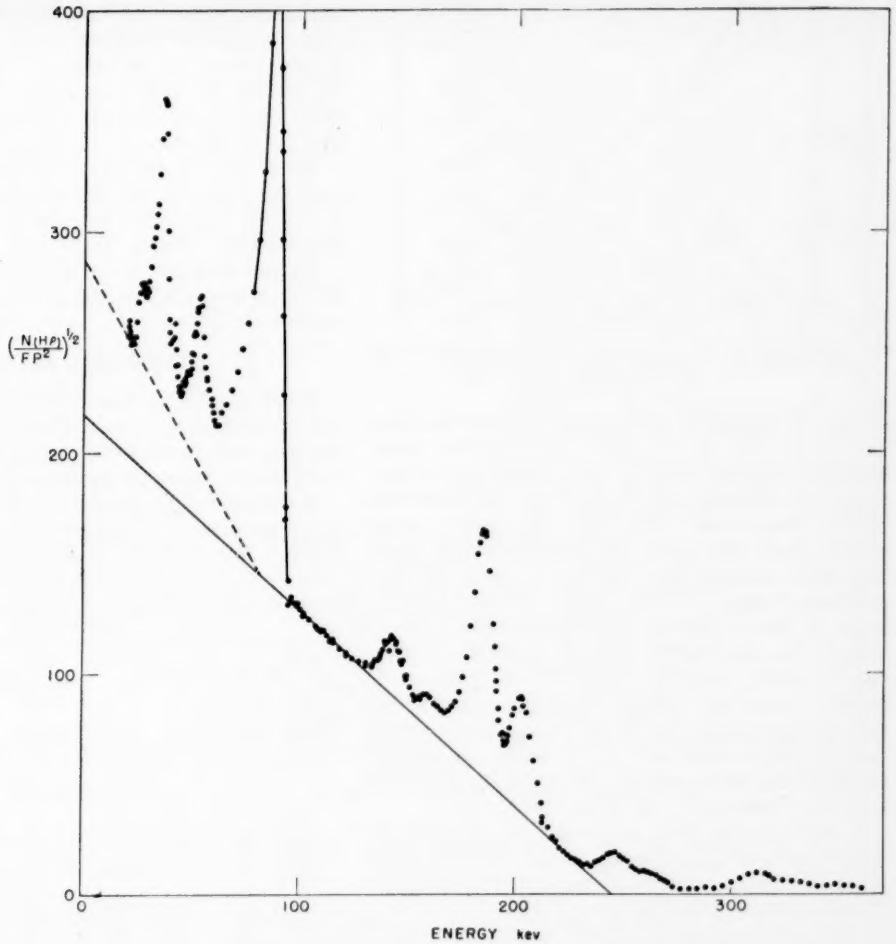

FIG. 1. Kurie plot of electron spectrum of U^{237}.

kev a thin window (*ca* 60 $\mu g/cm^2$) supported by a 50 percent transmission grid was used; above 95 kev a 1.3 mg/cm^2 mica window was used without the supporting grid.

The window transmission characteristics were determined with the use of a sample of Pm^{147} of average thickness <5 $\mu g/cm^2$. This sample was vacuum volatilized onto a 10-$\mu g/cm^2$ LC-600 film as a chelation compound of prometheum with trifluoro-acetylacetone $[Pm(F_3C_5H_4O_2)_3]$. It has been shown[8] that the Kurie plot of such thin samples of Pm^{147} is straight to less than 8 kev. The Kurie plots of our samples then indicated that the 60-$\mu g/cm^2$ window did not affect the shape above 20 kev, and the 1.3 mg/cm^2 above 80 kev. The two sets of data were normalized over the range (95 to 135 kev) where the slope of the momentum plot is low. The normalizing factor was determined at ten separate points in the overlap region. No single value of this factor varied by more than 1.5 percent from the average value.

The data from the beta-ray spectrometer show the presence of at least one beta-continuum with superimposed conversion lines. The Kurie plot (Fig. 1) of the beta-continuum, although masked for a considerable section owing to intense conversion lines, appears to be straight from an end point of 245 ± 5 kev back to approximately 95 kev. Beta-gamma coincidence measurements on a scintillation sepectrometer (see below), which avoid the obscuring effects of the conversion lines, show a beta-component of 255 ± 10 kev, of allowed shape. In this coincidence spectrum, the upturn in the Kurie plot (Fig. 2) observed below 100 kev corresponds to that normally seen in scintillation spectrometry of beta-rays, and so cannot be taken as evidence for the presence of a low energy beta-component.

Below *ca* 95 kev the continuum found in the lens spectrometer is masked by a number of conversion electrons as well as by distortion from source thickness

[8] Langer, Mott, and Price, Phys. Rev. **77**, 798 (1950).

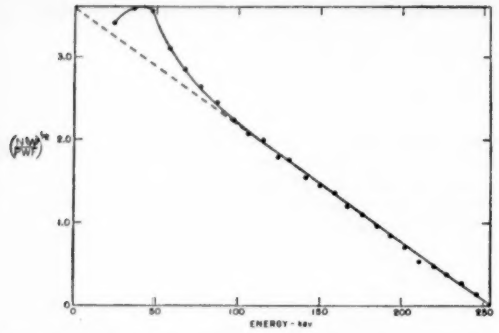

FIG. 2. Kurie plot of electron spectrum of U^{237} in coincidence with 208-kev gamma.

effects. The magnitude and sharpness of the rise below this energy (Fig. 1), in consideration of the source thickness, suggests strongly the presence of a beta-component of energy, say 80 to 95 kev (consistent with Slätis's observations). The only self-consistent decay scheme compatible with the gamma-energies found (see below) requires the existence of a beta of 81-kev maximum energy. If the sharp upturn in the Kurie plot below 95 kev is treated as adequate evidence for an 81-kev beta, analysis of the Kurie curve in the usual manner leads to beta branching ratios of $\gtrsim 80$ percent for the 245-kev, and $\lesssim 20$ percent for an assumed 81-kev beta (see dotted line, Fig. 1). However, it may be noted (see discussion) that calculations based on gamma-intensities furnish a minimum value for the branching ratio (*ca* 5 percent) for the 81-kev beta.

A higher energy beta-component was searched for without avail using a source of approximately three times the activity of the source used for the main study. The data indicated that the upper limit for the intensity of a beta of 511-kev energy (ground-to-ground transition for the suggested decay scheme, Fig. 6) was 0.1 percent of the intensity of the 245-kev beta.

The conversion lines (Table I) are assigned to levels in Np^{237} corresponding to gammas of 59, 165, 207, 334, 43, 269, 370, and 430 kev. The first four have been found in the gamma scintillation spectrometer. Careful search failed to reveal any line in the neighborhood of 118 kev, or of K_α Auger lines, contrary to the results of Slätis.[8] Values for the energies of the shell edges were obtained from unpublished tables of Hill *et al.*[9]

The K conversion line of the 334-kev gamma at 215 kev would not be observable due to the high intensity of the M conversion line of the 207-kev gamma at 201 kev. Similarly the K conversion line of the 269-kev gamma is masked by the L conversion line of the 165-kev gamma.

The K conversion line of the 165-kev gamma falls on the tail of line $M_I(59)$; in each experiment a discernible fluctuation was observed at 47.3 kev (750 $H\rho$), which is therefore assigned as the $K(165)$ line. Its maximum intensity, estimated by unfolding the tail of line $M_I(59)$, using as a guide the tailing edge of line $K(207)$ is 0.2 of the intensity of $L_I(165)$, which indicates that the multipolarity of the transition is at least 2^3.[10]

The K line of the 370-kev gamma is not resolved from the L line of the 269-kev gamma, but it is evidenced by a slight but reproducible decrease in slope at point $K(370)$ in Fig. 3.

A momentum plot of the spectrum is given in Fig. 3. The data from the lens spectrometer studies are summarized in Table I.

GAMMA-RAY STUDIES

To supplement the lens spectrometer data and aid in the formulation of a decay scheme a scintillation spectrometer and an argon-CO_2 proportional spectrometer were used to study the gamma ray spectrum.

A sodium iodide (thalliated) crystal in the scintillation spectrometer which had been calibrated with the 282-kev line of Hg^{203} [11] (resolution 17 percent), was

TABLE I. Summary of data of electron conversion lines and of gammas.

Lens spectrometer data				Scintillation spectrometer data		Transition data	
Conversion electron energy; kev	Shell converted in	γ energy kev	Relative[a] intensity	γ energy kev	Relative[b] intensity	Best value of energy; kev	Relative[c] intensity
...	...	...	...	27	...	27	
20.5	L_I	42.9	...	...	...	43	
26.7	L_{III}	44.3	...				
36.9	M_I	42.6	...				
41.7	N_I	43.2	0.013				
36.9	L_I	59.3	0.15	60	0.37	59	0.58
53.5	M_I	59.2	0.05				
57.6	N_I	59.1	...				
...	...	...	...	102[d]	0.53	102	0.53
47.3	K	165.5	...	163	...	165	
143.1	L_I	165.5	0.025				
159.1	M_I	164.8	0.003				
88.5	K	206.7	0.53	210	0.21	207	0.88
185.1	L_I	207.5	0.11				
202.5	M_I	208.2	0.03				
246.7	L_I	269.1	0.0022	...	...	269	
263.6	M_I	269.3	0.0007				
312.0	L_I	334.4	0.0007	340	0.025	334	
327.9	M_I	336.6	0.0002				
~251	K	~369.2		...	...	370	
348.0	L_I	370.4	0.00011				
312	K	430.2	...	...	...	430	

[a] Relative intensity = conversion electrons per 245-kev β.
[b] Relative intensity = gammas per 245-kev β.
[c] Relative intensity = conversion electrons plus gammas per 245-kev β.
[d] K x-rays. (Assumed.)

[8] Hill, Church, and Mihelich, Rev. Sci. Instr. **23**, 523 (1952). We wish to thank the authors for a pre-publication copy of these tables.

[10] M. Goldhaber and A. W. Sunyar, Phys. Rev. **83**, 906 (1951).
[11] H. Slätis and K. Siegbahn, Phys. Rev. **75**, 318 (1949).

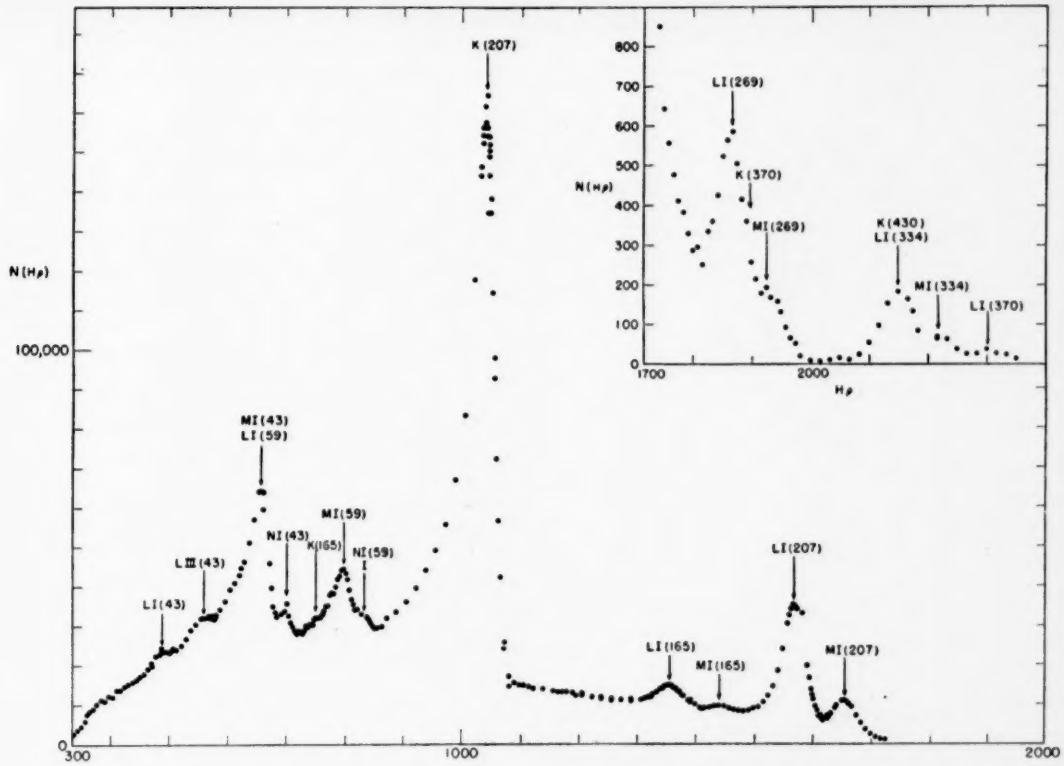

FIG. 3. Momentum plot of electron spectrum of U^{237}. (Note change of scale on inset.)

used. Gammas of approximately 60, 210, and 340 kev were found (Fig. 4). A search for gammas of higher energy than 340 kev was carried out using very intense source with lead absorbers (*ca* 1.9 g/cm²) to keep the *ca* 210-kev gamma from flooding the counter. No gammas were found at these higher energies although the presence of these gammas in intensity 10 percent that of the *ca* 340-kev gamma would have been observable.

The argon-CO_2 counter was used to examine the quantum spectrum below 60 kev. The *K* x-rays of silver (22.1 kev) were used to calibrate this instrument which gave a resolution width of 14 percent at this energy. The results showed a large amount of *L* x-ray present in the U^{237} spectrum but no evidence for the existence of the 43-kev gamma found from the conversion line spectrum. However, Prohaska[12] has reported the presence of an approximately 100 percent converted 42-kev gamma in the α-decay of Am^{241} (see discussion). The 27-kev gamma did not show up directly but could have been lost in the tailing out of the x-ray lines whose counting rates were significantly above background at this setting. The results of these studies (including estimates of relative gamma-ray intensities) are listed in Table I.

COINCIDENCE STUDIES

Two sodium iodide (thalliated) scintillation spectrometers were used in coincidence to study the energy level structure of the Np^{237} product nucleus.

With one set to count the 210-kev gamma, a survey of the energy spectrum with the other showed coincidence with gammas of energies 27, 60, and 165 kev (Fig. 5). The 165-kev gamma was hidden under the intense 210-kev line in the singles measurement.

A search for gammas in coincidence with the 340-kev gave negative results.

Substituting an anthracene crystal beta-counter for one of the gamma counters showed the 210-kev gamma to be in coincidence with a beta of an end-point energy of 255±10 kev (Fig. 2).

An attempt to find coincidence between the 340-kev gamma- and beta-rays was not successful owing to the limitations on the total singles counting rates of the instruments available.

[12] C. A. Prohaska, University of California Radiation Laboratory Report UCRL-1395 (1951) (unpublished); Asaro, Reynolds, and Perlman, Phys. Rev. **87**, 277 (1952); F. Asaro *et al.* from their α-spectrum data in the decay of Am^{241} construct a decay scheme which leads to a ground state in Np^{237} 11 kev lower than that reported here. Consequently in referring to energy levels in Np^{237}, their designation of any particular level differs from ours by 11 kev. The 11-kev transition has not been observed.

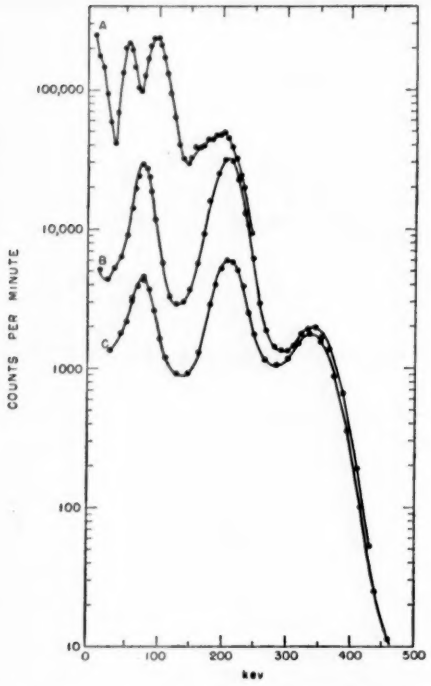

FIG. 4. Gamma-spectra of U^{237} in sodium iodide scintillation spectrometer. [The vertical position of the curves with respect to each other has no significance. The peak on curves *B* and *C* at *ca* 75 kev is lead x-ray.] A. 0.00-g/cm² lead absorber; B. 1.10-g/cm² lead absorber; C. 4.00-g/cm² lead absorber.

SUMMARY AND CONCLUSIONS

A decay scheme (Fig. 6) has been assembled from the data of the several experiments performed on this isotope. Many of the features of this scheme are only tentative; however, it is felt that the main features are well established and that the total decay energy of U^{237} is correctly defined. This energy is given by the 245-kev beta in cascade with the 207- and 59-kev gammas; this is the only plausible scheme in view of the intensity and coincidence measurements.

The position of the 165-kev gamma is fixed by the fact of its coincidence with the 207-kev gamma, and by its low intensity which indicates that the intense 268-kev level[12] cannot feed it.

The fitting together of other features of the decay scheme is somewhat tenuous.

Studies of the fine structure[12] in the alpha-decay of Am^{241} have given some information about the energy level structure of Np^{237}. The results of these studies indicate a level at 59 kev[12] and one at approximately 100 kev,[12] the 59- and 100-kev gammas having been observed. This data has been incorporated into our decay scheme.

The scintillation spectrometer showed a line at 102 kev which could well be a mixture of *K* x-rays and *ca* 100-kev gammas. The *L* conversion line from a 100-kev gamma would fall on the side of the *K* line from the 210-kev gamma and was not seen (see text). The results of the coincidence experiments indicate that the 334-kev gamma is not all in cascade with the 59-kev gamma, since a crude calculation shows that, had this been the case, the coincidences would have been numerous enough to have been observed. This indicates that the 100-kev gamma must be comparable in intensity to the 334-kev gamma (*ca* 3 percent of the 245-kev β).

The intensity values given in Table I are based on the assumption that all of the 102-kev quanta found in the scintillation spectrometer are *K* x-rays arising from the conversion of the 207-kev gamma, and that there is one *K* x-ray per *K* electron; that is, small corrections for *K* fluorescent yield are neglected.[13]

These assumptions are based on the following facts: (1) The energy measured is in reasonable agreement with predicted K-α x-ray energies (97 to 101 kev); (2) From the beta-spectrum data it is known that the 207 gamma is *ca* 50 percent *K* converted; (3) No gamma of 102 kev was found in coincidence with the 207-kev gamma, thus eliminating such a gamma from the main cascade of the U^{237} nucleus and consequently eliminating it as a component of any important intensity (see Fig. 6). Although the relative intensity of the 59-kev transi-

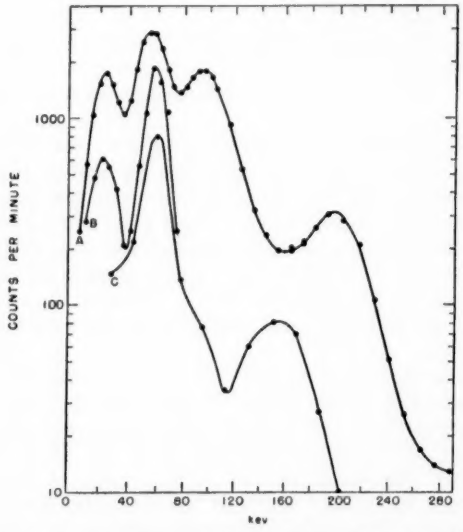

FIG. 5. Gamma-gamma coincidence spectra of U^{237} in sodium iodide scintillation spectrometers. [The vertical position of the curves with each other has no significance.] Abscissas denote energy setting of spectrometer I; coincidences observed with: A. Gammas above 20 kev in spectrometer II; B. 200-kev gammas in spectrometer II, 1.0 g/cm² of copper absorber over counter II; C. 200-kev gammas in spectrometer II, 1.4 g/cm² of copper absorber over each counter.

[13] Extrapolation of the data given by A. H. Compton and S. K. Allison [*X-Rays in Theory and Experiment* (D. Van Nostrand Company, Inc., New York), second edition, p. 488] leads to estimates for the *K*-fluorescence yields in heavy isotopes of within a few percent of unity.

tion (Table I) is lower than that of the 207-kev, it is evident that it must be in sequence with the 207-kev transitions, and from the data on the Am^{241} alpha-decay[17,14] it is located below the latter.

The energy level scheme proposed by Asaro *et al.*[12] based on alpha- and gamma-decay studies on Am^{241} includes 26.43- and 33.36-kev transitions in sequence, in parallel with the 59-kev transition (shown dotted in Fig. 6), and with intensities of the unconverted gamma one-third that of the 59-kev gamma. As noted above the 27-kev was found in coincidence with the 207-kev gamma, although the 33-kev gamma was not seen. We have also observed the 27-kev gamma in Am^{241} [14] but not the 33-kev gamma, on a scintillation and on a proportional counter spectrometer, in agreement with the results of Beling *et al.*[15] (Fig. 7). We did not survey the electron spectrum to low enough energies (<20 kev) to find the L lines of 26.4- or 33.3-kev gammas. On the assumption that the results of Asaro *et al.*[12] on the existence and intensity of the 33-kev gamma are correct,

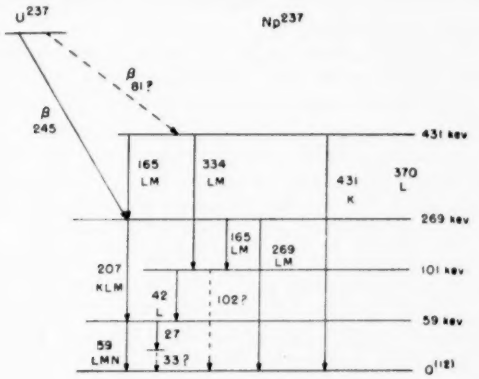

FIG. 6. Decay scheme of U^{237}.

quite reasonable values of the conversion coefficients of the 27- and 33-kev transitions lead to a matching of the intensities of the 207-kev transitions with the intensities of the transitions (59, 27, and 33 kev), which deplete the 59-kev level), and thus affirm the validity of the proposed decay scheme.

The K conversion coefficient of the 207-kev transition and the K/L conversion ratio have been calculated from the lens spectrometer data. An attempt to correlate these values with the character and multipolarity of the 207-kev gamma predicted by the K/L conversion ratio and by the K conversion coefficient was unsuccessful. According to the tables of Rose *et al.*[16] the K conversion coefficient ($\alpha=1.6$) corresponds to an $E4$ transition ($E4=1.1$, $E5=2.3$, $M1=4$, $M2=10$) whereas according

[14] Freedman, Wagner, and Engelkemeir, Phys. Rev. **88**, 1155 (1952).
[15] Beling, Newton, and Rose, Phys. Rev. **86**, 797 (1952).
[16] Rose, Goertzel, and Perry, Oak Ridge National Laboratory Report ORNL-1023 (1951) (unpublished).

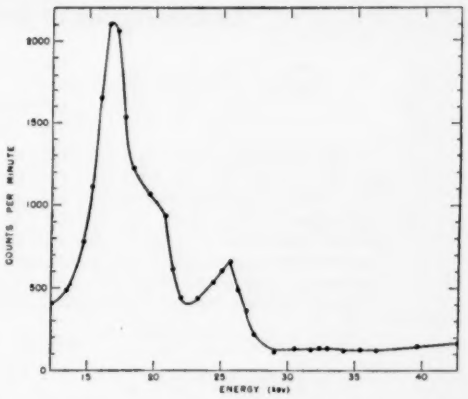

FIG. 7. Gamma-spectrum of Am^{241} taken with argon$-CO_2$ proportional counter. 440 mg/cm² Al over sample.

to the work of Goldhaber and Sunyar[10] the K/L conversion ratio (5) corresponds to an $M2$ transition (Goldhaber and Sunyar values: $M1=7.8$, $M2=5$, $M3=2$, $E1=3$, $E2-E4<1$).

The branching ratio between the 245-kev beta and 81-kev beta can be estimated from the Kurie plot and from the intensities of the gammas in the decay of the 431-kev level of the Np^{237} nucleus (Fig. 6). The maximum amount of 81-kev beta possible on the basis of the Kurie plot is approximately 20 percent of the total betas. The minimum amount necessary to account for the intensity observed for the 165-kev gamma (+conversion lines) is of the order of 5 percent.

On the basis of a 20 percent branching to an 81-kev beta and 80 percent to a 245-kev beta, the logft values for these two betas are 5.9 and 6.6, respectively; for a 5 percent and 95 percent division the logft values become 6.5 and 6.5.

A value of 511 kev for the decay energy of the U^{237} leaves a residual unbalance of *ca* 160 kev in the following decay cycle if one assumes the alpha-decay energy for U^{227} to be 4.28 (larger than the 4.25-Mev alpha-decay energy of U^{238}).

$$\begin{array}{ccc} & \overset{\alpha}{\longleftarrow} & \\ Pa^{233} & & Np^{237} \\ \beta^- \uparrow & \alpha & \uparrow \beta^- \\ Th^{233} & \longleftarrow & U^{237} \end{array}$$

However, work is being carried out at this laboratory[17] searching for gammas in cascade with the Np^{237} alphas, and preliminary experimental results indicate that there is gamma-energy of the required order of magnitude to account for the unbalance in sequence with the alpha-decay.

Therefore, although many features of the presented decay scheme are uncertain, these experiments serve to determine the decay energy of U^{237}.

[17] L. B. Magnusson and D. W. Engelkemeir (private communication).

Disintegration of Helium by 90-Mev Neutrons

PETER E. TANNENWALD*
Radiation Laboratory, Department of Physics, University of California, Berkeley, California
(Received August 11, 1952)

A detailed study of the fragments produced from helium when bombarded by 90-Mev neutrons was made in a 22-inch cloud chamber filled with helium gas and operated in a pulsed magnetic field of 22 000 gauss. The particles were identified by curvature and relative ionization, or by change of curvature with range when they stopped in the chamber. The energy of the incident neutron could be calculated from measured quantities for most modes of disintegration. The total number of events, for incident neutrons above 40 Mev, was normalized to the interpolated n-He^4 total cross section of 1.9×10^{-25} cm²; thus absolute cross sections were established for the various disintegration processes. Energy dependences were compared and energy and angular distributions have been determined.

I. INTRODUCTION

NUCLEON–NUCLEON scattering provides one of the most direct ways of gaining information about the forces between nucleons. Yet the scattering and disintegration of nuclei by nucleons has been a most fruitful approach in establishing various models of the nucleus and in revealing the behavior of large numbers of nucleons in close proximity. The disintegration of helium presents a unique case in that there are so few particles that a theoretical analysis of the interactions between individual nucleons can be hoped for; and on the other hand, due to the tightly bound structure of helium, it will show some of the properties of heavier nuclei. If it is true, as is sometimes believed, that the alpha-particle exists as a sub-structure in heavier nuclei, then the disintegration of helium will be of value in interpreting the disintegrations of heavier nuclei.

The charged particles ejected from nuclei when bombarded by 90-Mev neutrons have been studied in a number of experiments,[1] and the results indicate that the nature of the collision process for high energies is determined predominantly by the interaction of the bombarding particle with an individual nucleon rather than with the struck nucleus as a whole.

Neutron-induced stars are especially suited for study in a cloud chamber. In the first star experiment using 90-Mev neutrons, Tracy and Powell[2] filled their chamber with a mixture of oxygen and helium gas. In the present investigation a more complete analysis was possible due to the use of helium gas alone in the chamber, a more powerful magnetic field,[3] and experience with neutron-deuteron scattering.[4]

II. EXPERIMENTAL PROCEDURE

The 90-Mev neutrons produced in the stripping process by bombarding a 2-inch thick beryllium target with 190-Mev deuterons were collimated outside the concrete shielding of the 184-inch Berkeley cyclotron by means of a rectangular copper collimator four feet long passing a beam $2\frac{3}{4}$ in. wide and $\frac{3}{4}$ in. high (see Fig. 1). The neutrons were then allowed to enter a 22-inch Wilson cloud chamber[3] through a 3×1 inch aluminum foil 1 mil thick, and to pass out through a similar window in order to reduce backscattering from the rear wall of the chamber.

The cloud chamber was operated in a pulsed magnetic field of 22 000 gauss. The cycle of operations, which was repeated once a minute, was as follows: the current through the magnet is turned on in advance so that its maximum coincides with the expansion of the chamber. The cyclotron beam is pulsed through the chamber at the instant the moving diaphragm of the chamber hits the bottom, and the lights are flashed 0.03 sec later.

The chamber was filled with 99 percent pure helium gas to a total pressure of 81.5 cm Hg; in the expanded equilibrium position 1.8 cm of this pressure was due to the partial water vapor pressure from the moist gelatine covering the diaphragm. Immediately after expansion the ration of helium to oxygen nuclei was 51.8. The expansion ratio during the experiment was approximately 17 percent.

The pictures were taken by a twin-lens camera and reprojected to natural size through the same lenses in a stereo-projector.[5] (See Fig. 2.)

III. METHOD OF ANALYSIS OF EVENTS

On the average, three two-prong stars and about an equal number of heavily-ionizing single tracks appear in each picture. The possible reactions when a neutron strikes a helium nucleus are as follows:

Inelastic	$n+He^4\rightarrow d+t$	(dt)
	$\rightarrow p+t+n$	(pt)
	$\rightarrow d+d+n$	(dd)
	$\rightarrow p+d+2n$	(pd)
	$\rightarrow p+p+3n$	(pp)
	$\rightarrow He^3+2n$	(He^3)
Elastic	$\rightarrow He^4+n$	(He^4)

* Present address: Project Lincoln, Massachusetts Institute of Technology, Cambridge, Massachusetts.

[1] K. Brueckner and W. Powell, Phys. Rev. **75**, 1274 (1949); and J. Hadley and H. F. York, Phys. Rev. **80**, 345 (1950).

[2] J. Tracy and W. Powell, Phys. Rev. **77**, 594 (1950).

[3] W. Powell, Rev. Sci. Instr. **20**, 402 (1949).

[4] W. Powell (to be published). See also University of California Radiation Laboratory Report UCRL-1191.

[5] Brueckner, Hartsough, Hayward, and Powell, Phys. Rev. **75**, 555 (1949).

Analysis of an event involving the helium nucleus requires identification of protons, deuterons, tritons, He^3 nuclei, and He^4 nuclei. Stars with three or more prongs are observed occasionally; they are due to oxygen nuclei in the water vapor. The identification of the particles involved in the two-prong stars rests mainly on measurement of their radii of curvature and an estimate of their relative ionizations. If one knows the strength of the magnetic field at the position of the tracks, two out of the following three quantities determine the third: curvature, ionization, particle identity.

Two-Prong Stars

A two-prong star from helium can only include singly charged particles, and over the range of energies observed in this experiment, a simple rule holds. For a given radius of curvature the ionization of a deuteron is approximately three times that produced by a proton and of a triton is six times that for a proton. A table was constructed which gives $H\rho$ *vs* ionization for p, d, t, He^3, and He^4, and it is used in the following way.

In each picture a more or less parallel beam of lightly ionizing particles can be seen to come through the entrance window with radii around 35 cm. The fact that the ionization of these tracks is the lightest observed for these curvatures plus the fact that occasionally tracks are observed to come in with these curvatures which appear denser but never lighter, establishes these background tracks as protons. This verifies the expectation that protons are knocked out of the walls of the collimator and window by the incident neutrons. Since their identities and curvatures are established, their ionizations can be obtained from the table, and thus a starting point has been made in finding reference ionizations. Furthermore if the ionization of a track from helium falls in the proper range, it can be bracketed between two background proton tracks.

Various other aids can be employed in identifying particles. If, for example, one prong of a star is a deuteron and the two prongs are not coplanar with the neutron beam direction, then it is very unlikely that the other prong is a triton. Or, one prong may end in the chamber giving rise to a characteristic ending. A unique

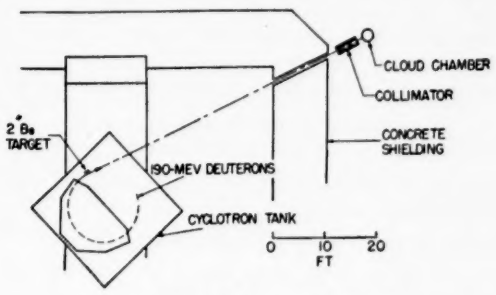

FIG. 1. Sketch of cyclotron, cloud chamber, and collimation arrangement.

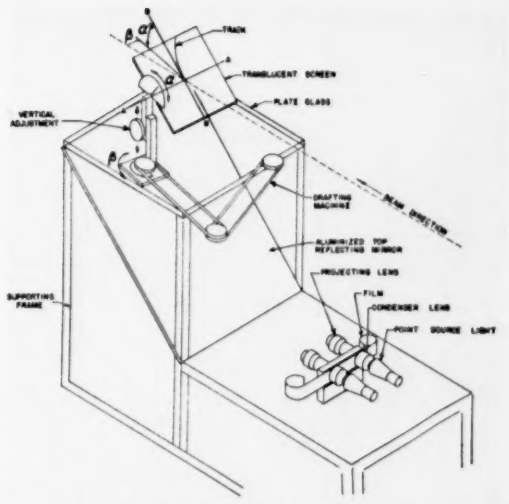

FIG. 2. Stereo-projector used to reproject events to natural size. Dip angle α and beam angle β are indicated.

theoretical relation exists for each particle which relates $H\rho$ *vs* residual range, and the ending of the track in question can be compared with the theoretically computed track shape or with an experimental characteristic ending in the same gas mixture which has previously been well established from other evidence.

By such reference and bracketing procedures it has been possible to identify the fragments from two-prong stars in most cases. Out of 179 two-prong stars whose tracks lay within angles of $\pm 30°$ to the horizontal plane, eight could not be analyzed with certainty. Of these eight, four had one or both prongs too short, and four were either pd's or pt's. The latter uncertainty stems from the fact that when a track has an ionization with respect to minimum starting at about 70 times minimum, it is very difficult to decide whether the ionization is 70 times or twice as great.

Single-Prong Stars

The single tracks from helium are He^3's and He^4 recoils. These tracks turn out to be most frequently of low energy and they will then be extremely heavy and often also short. Ionizations fall in the range above 100 where estimates of density are not sufficiently accurate to distinguish between He^3 and He^4. However, if the track stops in the chamber, it can be compared with a characteristic ending; if it does not stop in the chamber, the change in curvature along the track is insufficient to determine whether it is He^3 or He^4.

Figures 3 and 4 show some representative stars and characteristic endings.

Measurements

The technique used in reprojecting the events and the whole question of accuracy of measurements have been discussed by Powell and associates.[4]

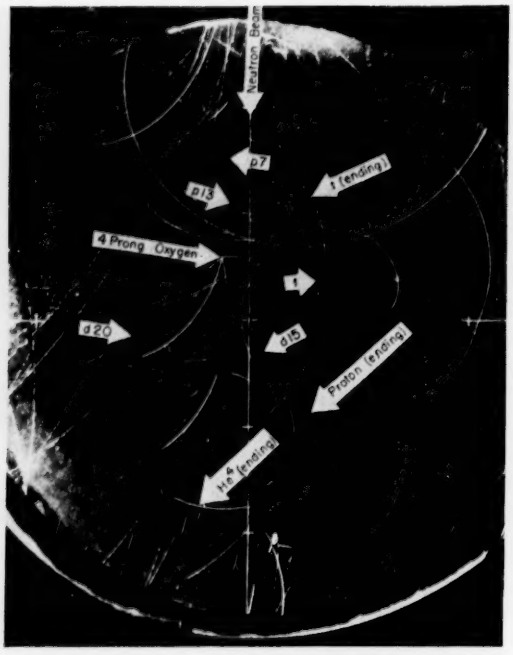

FIG. 3. Photograph showing examples of events that were analyzed. The letters are abbreviations for the particles and the numbers stand for the dE/dx values with respect to minimum ionization.

All angular measurements rest on the assumption that the incident neutrons entered the chamber in a parallel beam. This assumption is verified by the fact that the number of stars produced outside the volume swept out by the neutron beam is negligible.

In the present experiment complete analysis of stars was limited to those events which had all their prongs lying within dip angles of less than $\pm 30°$. (Dip angle is the angle between the initial track direction and its projection on the horizontal plane containing the neutron beam.) This restriction is necessary because when the prong under consideration is too slanted, accurate measurement of curvature and dip angle is impossible in a large number of cases. A very slanted track is usually short because it passes quickly out of the lighted region, and the extreme stereoscopic effect required of the lenses makes the superposition of the two images insensitive to variations of the slant plane. Imposition of this restriction necessitated an extended correction procedure, which is discussed below.

Calculations

The energy of the incident neutron causing a particular event can be calculated for most cases. Since the disintegration of helium by a neutron into a deuteron and triton is a two-body problem, the incident neutron energy can be calculated in two ways—momentum balance and energy conservation. In the case of *pt* and *dd* disintegrations, in which one secondary neutron comes off, it is still possible to calculate the energy of the incident neutron. But for *pd* events, in which two neutrons come off in addition to the proton and deuteron, only a minimum incident neutron energy can be computed if the two ejected neutrons are lumped together and treated as one particle with two neutron mass units with the requisite momentum to balance the problem.

In the elastic scattering cases, the measured energy of a He^4 recoil leads directly to the energy of the incident neutron, and the corresponding scatter angle of the neutron is independent of the particular He^4 recoil energy.

IV. CORRECTIONS

Single-Prong Stars

Only those events have been measured whose tracks lay within an angle of $\pm 30°$ to the horizontal plane. In order to find the number of events which would have been observed without this restriction on the dip angle, a weighting factor has to be assigned to each event. This factor is the reciprocal of the fraction of total solid angle available to the track if one uses the assumption of isotropic azimuthal distribution about the neutron beam direction. The appropriate correction factor was applied to each track individually. (See Appendix I for details.)

Two-Prong Stars

In the case of events with two prongs the correction procedure is complicated by the fact that the rejection of an event may be due to one or both prongs lying outside the $\pm 30°$ limit; and, furthermore, the fraction of total solid angle available to the event depends on the difference in azimuthal angles of the two tracks. The appropriate correction factor was applied to each event individually. (See Appendix I for details.)

As a check on this computed correction procedure, the events for which one or both prongs lay outside the $\pm 30°$ limit have been counted, and whenever possible, identified. The total number of these partially analyzed stars plus the total number of completely analyzed stars should be equal, within statistical errors, to the number of completely analyzed stars corrected by the computed solid angle correction. Such a check would also assure one that nothing significant was overlooked by confining α to less than $\pm 30°$. Certain few two-

TABLE I. Results of inelastic events.

	pt	*dt*	*pd*	*dd*	*pp*	He^3	Total
1. Measured	88.0	33.0	31.0	17.0	2.0		171.0
2. Not identified	5.1	0.8	1.7	0.4			8.0
3. Sum	93.1	33.8	32.7	17.4	2.0		179.0
4. Corrected total	212.6	75.5	76.3	37.0	3.8		
5. Total with He^3 assumption	212.6	75.5	76.3	37.0	3.8	83.5	488.7
6. Total for neutrons >40 Mev	209.1	66.5	76.3	35.2	3.8	80.8	471.7
7. Probable error	7.3%	12.3%	12.1%	16.8%	48.0%		5.2%

prong stars are conceivable where both prongs would never fall inside the 30° limits regardless of how the configuration was rotated about the beam axis. This situation would amount to an infinite computed solid angle correction factor, but it will be shown from the data that no significant contributions could have come from this type of star.

The He^3 Assumption

As has been mentioned before, it was impossible to determine whether a single track was He^3 or He^4 when it did not end in the chamber. In order to estimate what fraction of all the single tracks was He^3's, some assumption must be made regarding the He^3 formation mechanism.

The pt and He^3 events can be considered as similar processes—in one case the incoming neutron interacts with and strips a proton off the helium nucleus, while in the second case it strips off a neutron. As a simple approximation, it seems reasonable to expect the ratio of He^3 to pt events to be the same as the ratio of the free $n-n$ to the $n-p$ cross section at 90 Mev. To the extent of present knowledge, the numerical value of σ_{pp} must be employed for σ_{nn}; then the ratio becomes about $\frac{1}{3}$.[6]

Furthermore, those cases of the dt events in which a pick-up deuteron comes off in the forward direction must be included as a type of pt event because the deuteron is actually not formed until some time after the disintegration.[7] The number of He^3's is thus estimated to be

$$\tfrac{1}{3}\,[\text{No. of } pt \text{ events} + \text{pick-up } dt \text{ events}].$$

V. RESULTS AND DISCUSSION

1. Inelastic Events

The first row in Table I shows the inelastic events which had dip angles less than ±30° and were thus subject to a detailed analysis. In addition there were four stars which could not be identified and four stars where the interpretation could have been either pd's or pt's. These eight unidentified events were arbitrarily divided into groups with the same relative distribution as the identified events in the first row. The numbers in the second row show the grouping of these eight events.

Line 3 is the sum of line 1 and line 2. The fourth row gives the total number of events of each type which would have been observed if α had not been restricted to less than ±30°.

The fifth row shows the total number of inelastic events of each type including 83.5 events for He^3 obtained by using the assumption made in the section on

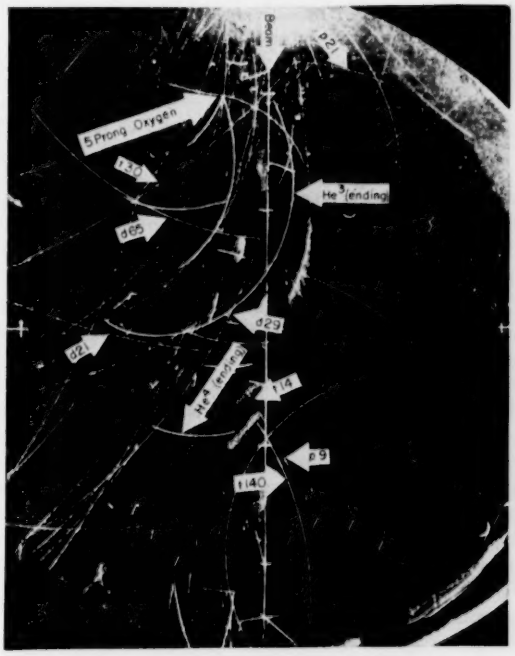

FIG. 4. Another sample picture. The lightest tracks which were dealt with are about 4–5 times with respect to minimum ionization and are only barely visible in the reproduction; the heaviest tracks encountered are as high as 400 times.

Corrections. Row 6 is the same as row 5 except it includes only events from neutrons above 40 Mev.

Line 7 gives the statistical probable error based on events actually analyzed from neutrons above 40 Mev.

Results of Solid Angle Corrections

The following summarizes the evidence that no significant information was missed due to the fact that some stars might have had "unusual" configurations so as to have both prongs always outside the 30° limits:[8]

1. The number of events as computed from application of solid angle corrections to the analyzed stars in the 30° group is equal, within statistical error, to the number of counted (and partially analyzed) events outside the 30° limits. This proves that the number of "unusual" stars must be small.

2. The stars analyzed in the 30° group yield a certain distribution as to type of event. Those stars that were successfully analyzed in the group having one or both prongs outside have the same distribution of events.

3. The remaining stars in the group having one or both prongs outside, with one or both prongs not identified, can be arranged so as to give this same distribution.

Hence one can conclude that it is highly unlikely that there is any considerable number of stars of an "unusual" character among the events of item (3) whose presence would change the distribution in item (2) by a significant amount.

[6] Estimated from Hadley, Kelley, Leith, Segrè, Wiegand, and York, Phys. Rev. **75**, 351 (1949); and Chamberlain, Segrè, and Wiegand, Phys. Rev. **83**, 923 (1951).

[7] G. Chew and M. Goldberger, Phys. Rev. **77**, 470 (1950).

[8] For details see P. E. Tannenwald, University of California Radiation Laboratory Report UCRL-1767.

TABLE II. Results of elastic events.

He^4's ending in the chamber	139
Single tracks not ending	125
He^3's ending	2
Tracks less than 2 cm long	105
Tracks counted, with $\alpha > \pm 30°$ (ending and not ending)	349
Computed solid angle correction to He^3's ending	218
Computed solid angle correction to tracks not ending	127
Weighted single prong events due to neutrons >40 Mev	441

2. Elastic Events

Table II shows the results of measurements of the single prong stars. One has to determine now the number of single tracks which would have been observed if all solid angles had been looked at and if no tracks had been missed because they were too short. In order to correct for the solid angle limitation, a proper weighting factor has been applied to each individual event—as explained in detail previously. The angular distribution of the scattered neutrons shows a lack of neutrons in the forward direction, which is due to the short range of the recoils. It is proposed to extrapolate the experimental spectrum to zero scatter angle according to a reasonable theoretical assumption as to the shape of the spectrum, and it will be shown that 124 He^4 events from neutrons above 40 Mev are contributed by this extrapolation.

If the total number of neutron-helium collisions is to be normalized to the total n-He^4 cross section as determined indirectly by carbon disk detectors, those helium collisions must be excluded which were due to neutrons not present in the total cross-section experiment beam. The carbon activation reaction has a threshold at 20 Mev, and the number of neutrons detected between 20 and 40 Mev is small because of the sharp drop of the activation curve near the threshold and the small number of neutrons in that part of the spectrum.[9] Hence no serious error is introduced if only helium events from neutrons above 40 Mev are included in the normalization. There are very few inelastic events from neutrons between 20 and 40 Mev (see Table I)—the thresholds range from 17.5 Mev to 25.9 Mev—and also it will be shown that it is not feasible to correct for missed short elastic recoils from neutrons below 40 Mev.

In order to examine the question of why only two He^3's were observed ending in the chamber, one can again consider the analogy between the He^3 and pt processes. It is found that while 23 percent of the tritons from pt events stop in the chamber, only 5 percent of the He^3's stop (the total number of He^3's being based on the He^3 assumption). The following reasons could account for this:

1. The number of He^3's was grossly over-estimated in the He^3 assumption.

2. The He^3 energy distribution might differ from the triton energy distribution such that no low energy He^3's are emitted. (They would have to have less than a few Mev in order to end in the chamber.)

3. The He^3 energy distribution might differ from the triton energy distribution such that most He^3's received very little energy. In this case the short tracks could be confused with He^4. It should also be noted that for a given energy the range of a He^3 is only about one-third that of a triton.

3. Cross Sections

In order to obtain absolute cross sections the total number of events (472 inelastic+484 elastic), for incident neutrons above 40 Mev, is normalized to the interpolated n-He^4 total cross section from the work of Cook *et al.*[9] When σ is plotted *vs* $A^{\frac{2}{3}}$ for H, D, Li, and Be, σ for He turns out to be 1.9×10^{-25} cm^2 when the points are connected by a smooth curve. A probable error of 10 percent is arbitrarily assigned to this value.

On the basis of the inelastic and elastic events listed, the results are: $\sigma_{\text{elastic}}=96\pm17$ mb; $\sigma_{pt}=42\pm6$ mb; $\sigma_{dt}=13\pm2.5$ mb; $\sigma_{pd}=15\pm2.5$ mb; $\sigma_{dd}=7\pm1.5$ mb; $\sigma_{pp}=0.8\pm0.4$ mb; $\sigma_{He^3}=16$ mb (assumed). The ratio $\sigma_{\text{inelastic}}/\sigma_{\text{total}}$ is 0.49 ± 0.07.

4. Errors

The errors quoted in Table I are the statistical probable errors based on the number of events actually analyzed. For each quantity making up the 484 elastic events a statistical probable error can be associated based on the number of events actually measured. But it is more realistic to consider the magnitude of the extrapolation that had to be made for missed tracks and the uncertainty in the 80.8 assumed He^3 events, and consequently a probable error of ±60 was assigned to the 484 recoils.

5. Comparison with Theory

In 1950 Heidmann published an analysis of the 90-Mev neutron-helium scattering problem;[10] it is interesting to compare his predictions for the relative cross sections with the present experimental findings (Table III[10,11]).

If Heidmann's revised theoretical results were diminished by the ratio 190 mb/244 mb so as to make his

TABLE III. Comparison of experiment with Heidmann's theory.

Process	Theory[a]	Theory revised[b]	Experiment
elastic He^4	180 mb	160 mb	96±17 mb
pt	63	60±10	42±6
dt	16	16	13±2.5
pd	~0	~2	15±2.5
dd	~0	~0	7±1.5
pp	~0	~0	0.8±0.4
He^3	6	~6	16 (assumed)

[a] See reference 10.
[b] See reference 11.

[9] Cook, McMillan, Peterson, and Sewell, Phys. Rev. **75**, 7 (1949).

[10] J. Heidmann, Phil. Mag. **41**, 444 (1950).
[11] J. Heidmann (private communication).

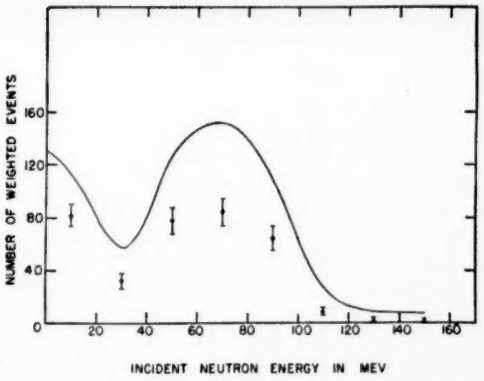

FIG. 5. Incident neutron spectrum weighted by the n-He elastic scattering cross section, as measured from He^4's ending in the chamber (single points), and as measured from all single prong events on the assumption that they are all He^4's (solid curve).

total cross section equal to the interpolated experimental value, the agreement would be excellent for the He^4, pt, and dt modes of disintegration. In any case the agreement is remarkable because, as the author himself points out, the calculations should be criticized for use of Gaussian functions for the potential and for the use of deuteron wave functions, which were employed to simplify the integrations. Heidmann apparently underestimates the occurrence of the pd and dd processes, but agrees that complete disintegration of helium by a neutron (pp) is rare.

In arriving at the number of He^3 disintegrations, Heidmann was the first to consider the pt and He^3 events as similar processes. However, he estimated that the ratio of He^3 to pt events would be given by

$$\frac{\frac{1}{4}}{\frac{1}{4}+\frac{3}{4}}\left(\frac{V\ \text{singlet}}{V\ \text{triplet}}\right)^2,$$

or about one-tenth. As discussed in the section on Corrections, in the present investigation the ratio of He^3 to pt events is assumed to be

$$\sigma_{nn}/\sigma_{np}=\sigma_{pp}/\sigma_{np}=\tfrac{1}{3},$$

which leads to about three times the He^3 cross section. Only the He^3 and He^4 cross sections and the ratio $\sigma_{\text{inelastic}}/\sigma_{\text{total}}$ are affected if one uses one or the other assumption. One piece of evidence which speaks in favor of the $\frac{1}{3}$ ratio comes from $n-d$ scattering at 90 Mev. Powell[4] found that the cross section for the production of protons with less than 10 Mev is 14.6 mb and that for protons with more than 10 Mev is 51.1 mb. The low energy protons are roughly isotropic and are left behind when the incident neutron hits the neutron in the deuteron, while the higher energy protons come off predominantly forward and result from the incident neutron striking the proton in the deuteron. The ratio between these two processes, which can be considered as n-n and n-p interactions in a light nucleus, is $\frac{1}{3}$.

6. Energy Dependence

The experimental information available is the incident neutron spectrum weighted by the n-He scattering cross section. In Fig. 5, the single points give this function as measured from He^4 recoils ending in the chamber. If all the single tracks which do not end in the chamber are included, the upper curve results. It is seen to have a quite similar shape, which is to be expected since the He^3's have been estimated to constitute only about 10 percent of the total spectrum. (Of course below 20.5 Mev the events must all be due to He^4 since this is the threshold for the $He^4(n, 2n)He^3$ reaction.) The peak occurs at about 70 ± 5 Mev. The distribution has the general features resulting experimentally from the deuteron stripping process, namely a peak near half the deuteron energy and an apparent peak of low energy neutrons. Since both the energy dependence of elastic n-He scattering and the exact shape of the low energy end of the neutron spectrum are unknown, one cannot draw any conclusions as to the reality of the low energy neutron peak. The broadness of the spectrum and the shift of the main peak down to 70 Mev is due to the fact that the stripping target used in this part of the experiment was 2-inch Be rather than the more desirable $\frac{1}{2}$-inch Be.

For the various inelastic processes, the number of events *vs* incident neutron energy is plotted in Fig. 6; the peaks occur at about

pt: 75 ± 5 Mev
dt: 65 ± 5 Mev
pd: 67 ± 5 Mev.

(The neutron energy in the pd cases is a minimum.)

Since the incident neutron spectrum was the same in each case, the qualitative nature of the curves can be compared. The small shift of the pd curve to lower energies with respect to the pt curve may simply reflect the fact that the calculated value of the neutron energy gives a minimum only. The dt curve shows a decided energy dependence, and this agrees with the sharp falling off with energy of the pick-up process, which is

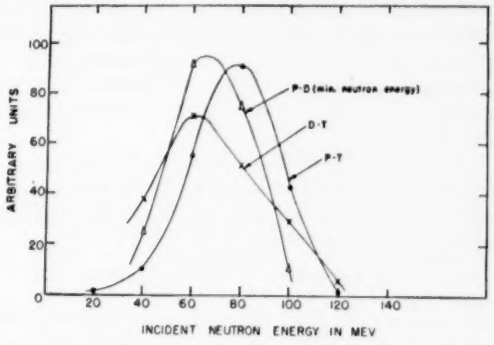

FIG. 6. Incident neutron spectrum weighted by n-He cross sections as measured from various inelastic events. Curves have been normalized to have the same area.

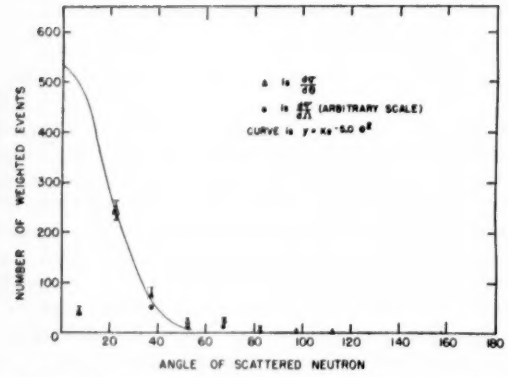

FIG. 7. Relative number of elastically scattered neutrons per unit scatter angle and per unit solid angle from incident neutrons above 40 Mev. Solid curve comes from theory.

theoretically expected. Preliminary experimental results on *n-d* pick-up deuterons verify this sharp energy dependence.[12]

7. Energy and Angular Distributions

Elastically Scattered Neutrons

The elastic events were divided into two groups—those due to incident neutrons below 40 Mev and those due to incident neutrons above 40 Mev. The reasons for this division are first that there exists evidence that low energy neutrons scatter from helium in a different manner than high energy neutrons;[13] second to be able to make a comparison with theory, in particular that due to Heidmann;[10] and third for a reason which will become evident in the next paragraphs.

The points denoted by triangles in Fig. 7 show the angular distribution of elastically scattered neutrons ($d\sigma/d\theta$) from incident neutrons with energies greater than 40 Mev; the points denoted by circles were obtained by dividing the $d\sigma/d\theta$ points by the average value of the sine over the 15° intervals and represent thus $d\sigma/d\Omega$. All single prongs not ending in the chamber have been included in this plot, but little error was made since only about 15 percent of the events above 40 Mev are estimated to be contributed by He^3's. Evidently there is a hole in the experimental distribution near the forward direction; it is due to the corresponding recoils being too short to be measured with certainty.

According to Heidmann's theory the angular distribution of 90 Mev elastically scattered neutrons is a Gaussian curve centered on the forward direction. His predicted curve has the equation

$$d\sigma/d\Omega = 4.50 \exp(-7.86\theta^2) \times 10^{-25} \text{ cm}^2$$

in the c.m. system. Since the present experimental data are consistent with a Gaussian, it was decided to draw a Gaussian curve through the experimental points; its form is

$$d\sigma/d\Omega = K \exp(-5.0\theta^2).$$

It is shown by the solid line in Fig. 7 and was extrapolated to zero degrees scatter angle.

Advantage has been taken previously of the opportunity to associate the events under the extrapolated part of the curve with the events missed because the tracks were too short. The reason why the angular distribution was plotted in 15° groups is that when a 40-Mev neutron is scattered at 15°, the corresponding recoil will just be 2 cm long. (This was the criterion selected below which recoils were merely counted instead of measured.) Consequently one begins to lose measurable tracks for neutron scatter angles of 15° and less. The critical alpha recoil angle corresponding to the neutron scatter angle of 15° is 80.5°. Recoils have been observed at angles as high as 84°; they are due to neutrons of energies higher than 40 Mev.

Figure 8 shows the angular distribution of elastically scattered neutrons from incident neutrons with energies less than 40 Mev. Here again a substantial number of neutrons are known to be missing near the forward direction. But since they can be missing up to fairly large neutron scatter angles (when a 5-Mev neutron is scattered at 45°, its alpha-recoil will just be 2 cm long), it is not possible to estimate the distribution of the missing tracks. However, the distribution confirms the general trend found by Swartz[13] that elastic scattering is peaked less in the forward direction at lower energies. The picture is qualitatively that the forward peak of diffraction scattering on the basis of the opaque nucleus model is spread out at lower energies, and that more nearly isotropic scattering is approached.

The $He^4(n, d)t$ *Reaction*

The angular distribution of deuterons from *dt* events is plotted in Fig. 9 and shows the expected peak of pick-up deuterons in the forward direction. The distribution is plotted both in terms of $d\sigma/d\theta$ and $d\sigma/d\Omega$.

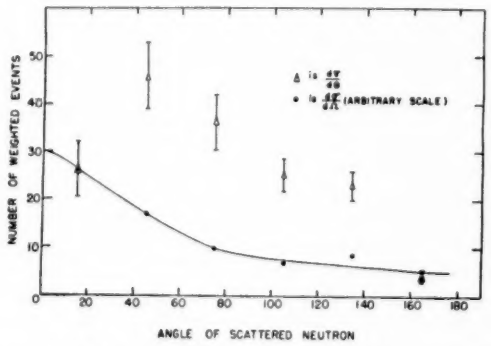

FIG. 8. Relative number of elastically scattered neutrons per unit scatter angle and per unit solid angle from incident neutrons below 40 Mev.

[12] A. Bratenahl (private communication).
[13] C. Swartz, Phys. Rev. **85**, 73 (1952).

The solid line representing the differential cross section $d\sigma/d\Omega$ is subject to some error due to the inaccuracy introduced by averaging $\sin\theta$ over a 30° interval; but it is included to show the approximate half-width of the forward peak, which is estimated to be 25°. On the other hand, the $d\sigma/d\theta$ points are useful in comparing the relative forward to backward scattering; they show that the events under the peak constitute about one-half of the total dt cross section. Heidmann has pointed out[11] that the critical tests between theory and experiment are, in order of increasing sensitivity to large momentum changes (and thus small interaction distances): the total dt cross section, the angular half-width of fast forward deuterons, and the ratio of forward to backward deuterons. The following is a comparison between theory and experiment on these points:

	Theory	Experiment
Total σ_{dt}	16 mb	13±2.2 mb
Half-width	8.4°	~25°
Ratio forward/backward[14]	1000/1	1/1

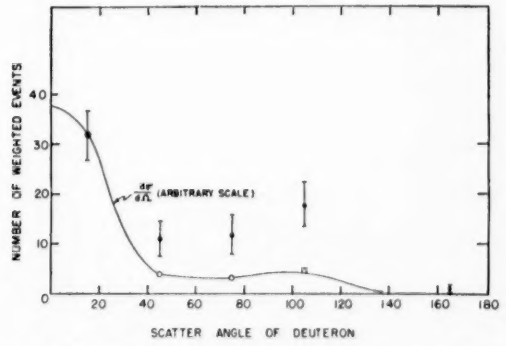

FIG. 9. Relative number of deuterons per unit scatter angle and per unit solid angle from dt events. The solid line connects points obtained from division by the average number of steradians in 30° scatter angle intervals.

The discrepancies increase exactly in the order listed above, with only the total σ_{dt} being in satisfactory agreement.

The one event plotted in the 165° group is a low energy deuteron with an associated triton going forward with 75 Mev. The process responsible for this is undoubtedly triton pick-up.

In Fig. 10 the energy distribution of the deuterons from dt events is plotted. The peak corresponding to pick-up deuterons falls at 50 Mev. Although the dt process is a two-body problem, there is no one-to-one correspondence between a point on the angular distribution plot and a point on the energy distribution plot because of the variety of energies of the incident neutrons. This fact, incidentally, must be kept in mind in making all comparisons with Heidmann's theory,

[14] Strictly, the experimental ratio observed is pick-up deuterons to non-pick-up deuterons.

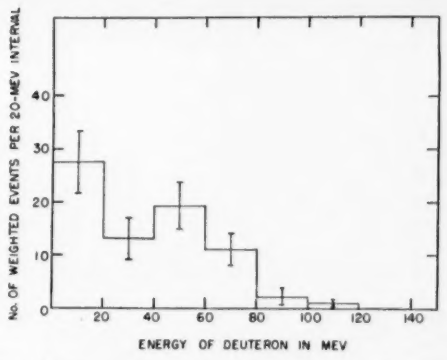

FIG. 10. Energy distribution of deuterons from dt events.

since he analyzed the problem for monochromatic 90-Mev incident neutrons.

The $He^4(n, pn)t$ *Reaction*

According to Heidmann's prediction the tritons from the pt reaction are of low energy (2 Mev on the average) and are distributed almost isotropically. Figure 11 shows the energy distribution of the tritons, and agreement is seen to be excellent. However, Fig. 12 shows that the angular distribution of the tritons is not isotropic but concentrated in the forward direction. The proton energy distribution is shown in Fig. 13.

The proton angular distribution from pt events is plotted in Fig. 14 together with the proton angular distribution from pd events. For both distributions it can be said that the free nucleon n-p scattering is reflected to some extent. This would be expected on the basis of a model first proposed by Serber,[15] developed in greater detail by Goldberger,[16] and whose general features were verified by Hadley and York.[1] According to this picture, the bombarding particle interacts with an individual nucleon rather than with the struck nucleus as a whole, and probably leading to the ejection of a fast particle in the forward direction.

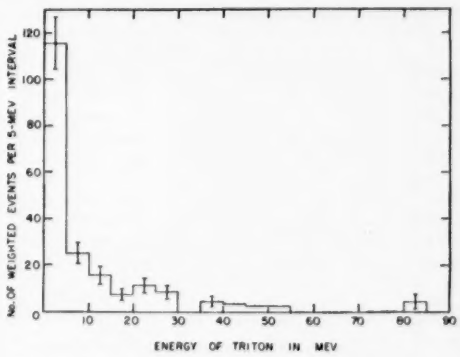

FIG. 11. Energy distribution of tritions from pt events.

[15] R. Serber, Phys. Rev. **72**, 1114 (1947).
[16] M. Goldberger, Phys. Rev. **74**, 1269 (1948).

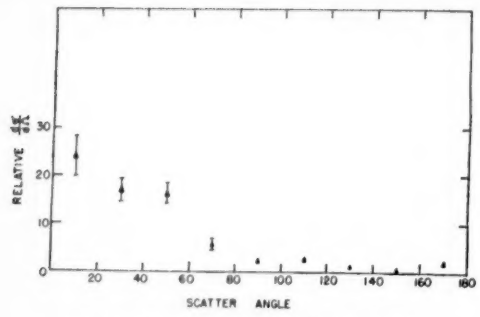

FIG. 12. Relative number of tritons per unit solid angle from *pt* events.

Figure 15 gives the energy distribution of protons from *pd* events. The statistics are not good because of the low frequency of occurrence of this type of event. Nor does any theory exist at present with which comparison can be made.

8. Experimental Checks

Stopping Power of Gas Mixture

A check was made of the range-energy relations expected from the calculated stopping power of the gas mixture in the chamber. The energies of a few long proton tracks ending in the chamber were determined from $H\rho$ measurements. The measured ranges agreed well within experimental error with the calculated ranges based on a stopping power of 0.185.

Oxygen Stars

From the partial pressures existing in the chamber immediately after expansion, the ratio of helium to oxygen nuclei was computed to be 51.8. If one assumes roughly that the ratio of inelastic events to total events (σ_i/σ_t) is the same for oxygen and helium, then the number of two-prong helium stars can be compared with the number of oxygen stars which show two or more prongs. The observed ratio is 12.2, and the ratio expected on the basis of the cross sections from reference 8 is 12.9.

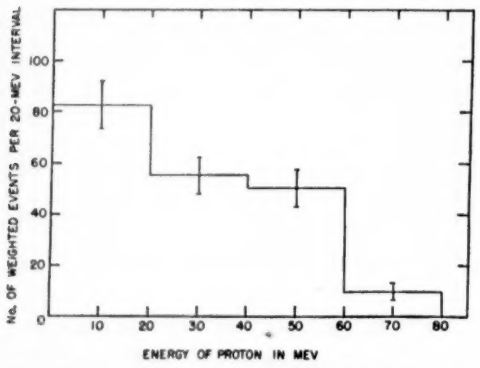

FIG. 13. Energy distribution of protons from *pt* events.

Azimuthal Symmetry

One of the implied assumptions of this experiment is that all processes occur with azimuthal symmetry. This is borne out, within statistical errors, when He^4 recoils, and tritons from *pt* events, are compared in four azimuthal angle groups.

VI. CONCLUSIONS

When helium is bombarded by 90-Mev neutrons, the dominant process is elastic scattering, which exhibits the characteristic forward diffraction peak for incident neutron energies above 40 Mev. For neutron energies below 40 Mev, elastic scattering tends to become more isotropic. The most frequent inelastic process is the disintegration in which the incident neutron strips off a proton from the helium nucleus leaving a low energy triton behind. A special case of this process occurs when the outgoing neutron and proton proceed together as a high energy forward deuteron—the so-called pick-up process. Pick-up accounts for about one-half of the events in which a deuteron and a triton are emitted; in the other half the deuteron comes off in a random direction with low energy. Although Heidmann's theory may be criticized in a number of ways, as pointed out by the author, it is in good agreement with the cross sections for elastic scattering and *pt* and *dt* disintegrations. The most serious discrepancies arise when the theoretical ratio of forward pick-up deuterons to backward deuterons of 1000/1 is compared with the experimental ratio of 1/1; also the theory predicts a much smaller number of *pd* and *dd* disintegrations than is observed. As far as the energy dependences are concerned, no sharp dependence is evident for elastic scattering (above 40 Mev) and for *pt* and *pd* disintegrations, while the *dt* disintegrations fall off with increasing energy, as is expected at least for the pick-up part of the process.

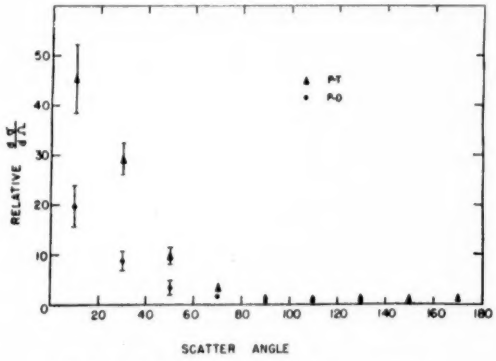

FIG. 14. Relative number of protons per unit solid angle from *pt* and *pd* events.

Noteworthy in the angular distributions is the fact that the proton angular distributions from *pt* and *pd* disintegrations reflect to some extent the free *n-p* interaction. Since He^{3}'s could not be distinguished from He^{4}'s in this investigation, the mechanism leading to He^{3} production has been assumed to be similar to that leading to triton production. The possible errors arising from this assumption would seriously affect only the $He^{4}(n, 2n)He^{3}$ cross section.

Since at higher incident neutron energies, say 270 Mev, the theoretical approximation that the bombarding particle interacts only with one nucleon in the target nucleus becomes much better, the calculations become simplified, and hence neutron-helium scattering at this energy should prove to be of decisive interest. Further, the parallel experiment to the present one, namely proton-helium scattering at high energies would, together with the results of the present investigation, provide further comparison between the *n-n* and *n-p* and *p-p* forces.

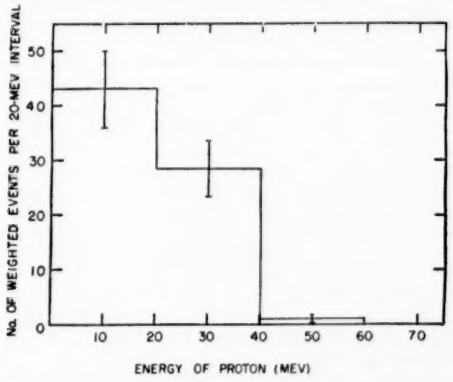

FIG. 15. Energy distribution of protons from *pd* events.

The author wishes to express his sincere gratitude to Professor Wilson Powell for suggesting this problem and for his helpful advice and constant encouragement throughout the investigation. The cooperation of many members of the cloud-chamber group is also acknowledged with pleasure, and special thanks are due to Dorothy Gardner for carrying out a large share of the calculations and to Beverly Lee who did the computation in the earlier stages.

APPENDIX I

In order to find the solid angle correction for a single prong event, one computes what fraction of the azimuthal angle ϕ (the angle between the projection of the initial track direction on a plane perpendicular to the neutron beam and the horizontal plane) meets the requirement at the given scatter angle θ that the dip angle α be less than $\pm 30°$.

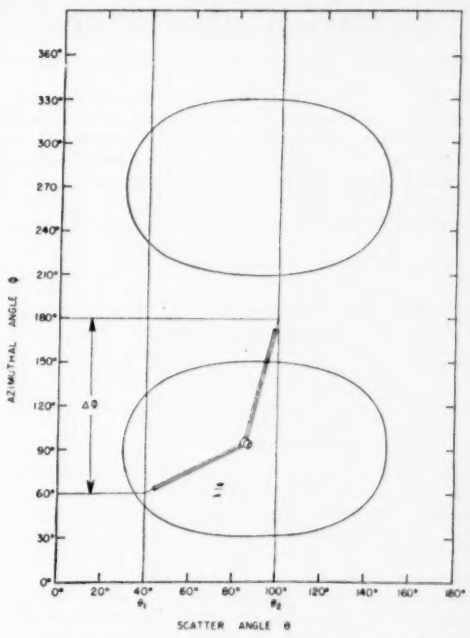

FIG. 16. Graph used for solid angle correction. Regions inside the ovals are excluded when dip angle α is restricted to the range from $+30°$ to $-30°$.

In Fig. 16 the direction in space of any track is given by a point in the $\phi-\theta$ plane; the oval regions are defined by the equation

$$\sin\phi = \sin\alpha/\sin\theta,$$

with $\sin\alpha = \pm\frac{1}{2}$. The interpretation of the plot is as follows: A track with a given scatter angle θ would be measured for those azimuthal angles ϕ which fall outside the oval regions. Consequently the probability of having observed a track when it has a given scatter angle θ is simply the ratio of the number of ϕ degrees outside the ovals to 360 degrees.

A two-prong event is geometrically defined by the three parameters θ_1 (prong 1), θ_2 (prong 2), and $\Delta\phi$ on the assumption of azimuthal symmetry. The correction factor is obtained graphically from Fig. 16 as follows: One leg of a pair of dividers is always kept on θ_1 while the other leg is always kept on θ_2. The angle between the legs is fixed by the parameter $\Delta\phi$. The dividers are then moved vertically up the plot so that θ_1 moves from $\phi=0°$ to $\phi=360°$. Everytime one or the other leg crosses into or out of the restricted regions the fact is recorded. From this information one can calculate two correction factors—one factor gives the number of events to be expected in the azimuthal region where one prong is too slanted; the other gives the number where both prongs are too slanted. The sum of the measured event and the two correction factors is the number of events which would have been observed if there had been no restriction on the dip angle α.

Letters to the Editor

PUBLICATION of brief reports of important discoveries in physics may be secured by addressing them to this department. The closing date for this department is five weeks prior to the date of issue. No proof will be sent to the authors. The Board of Editors does not hold itself responsible for the opinions expressed by the correspondents. Communications should not exceed 600 words in length and should be submitted in duplicate.

Microwave Resonance Absorption in Gadolinium Metal*

A. F. KIP, C. KITTEL, AND A. M. PORTIS,† *Department of Physics, University of California, Berkeley, California*
AND
R. BARTON, AND F. H. SPEDDING, *Institute for Atomic Research, Iowa State College, Ames, Iowa*
(Received November 24, 1952)

MICROWAVE resonance absorption in gadolinium metal has been measured near 9000 and 24 000 Mc/sec in the ferromagnetic and paramagnetic regions. Gadolinium is known to exhibit a saturation magnetization[1] corresponding closely (±2 percent) to the value expected for an ^8S state, where the magnetic moment of each atom is due to the seven electrons in the $4f$ shell. It is therefore likely, as Van Vleck[2] has emphasized, that Gd is a good realization of the atomic model of a ferromagnet, in contrast to the ferromagnetic metals of the iron group, all of which show saturation magnetizations which cannot be explained on such a simple basis. From this point of view, we wished to determine how closely the g value corresponds to the value for free electron spin, as expected for a half-filled shell. Our results suggest that there may be spin-orbit coupling effects, perhaps between the spin of $4f^7$ shell and the orbit of the $5d$ electron, which partly spoil the purity of the assumed ^8S ionic state.

An annealed circular disk of polycrystalline Gd, 2.3 cm in diameter and 0.04 cm thick, was used in these experiments. The sample contained no more than 0.1 percent of other rare earth elements. Absorption measurements were made by clamping the sample behind a hole of area 0.049 cm² drilled into the end wall of a resonant cavity, so that the sample effectively forms a small part of this wall. Figure 1 shows a typical resonance curve.

Results in the 9000 Mc/sec range were consistent with the 24 000 Mc/sec results, but because of the greater accuracy of the measurements at the higher frequency, only the latter will be given. Measurements were made in the temperature range between −196°C and +105.5°C. The Curie temperature is 16°C, according to Trombe. Figure 2 summarizes the results at 24.30×10^9 Mc/sec for the positions of maximum absorption *vs* temperature. The principal cause of the shift of the peak position in going from the paramagnetic to the ferromagnetic region is the increase in magnetization of the sample. The individual absorption curves in the paramagnetic range exhibit the typical shape of resonance curves in metals, as found by Yager[3] and Bloembergen[4] in the case of supermalloy and nickel. The width of the absorption curves in the paramagnetic region is approximately 1000 oersteds at the half-power points. Below 20°C the width increases rapidly, and below 0°C the width is so great that no estimate can be made of the width, using external fields from 0 to 10 000 oersteds. The cause of the extreme width in the ferromagnetic region is not understood, but may be associated with a high crystalline anisotropy energy and polycrystalline broadening. The value of the magnetization in the ferromagnetic range was obtained from unpublished data of Elliott, Legvold, and Spedding.

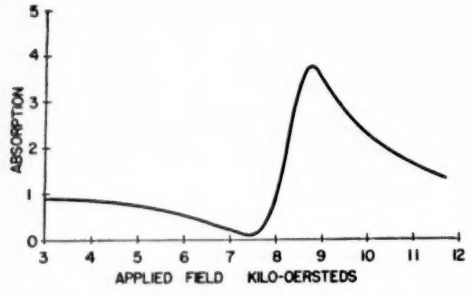

FIG. 1. Gadolinium metal resonance absorption at 24.3×10^9 Mc/sec, $T=105.5$°C.

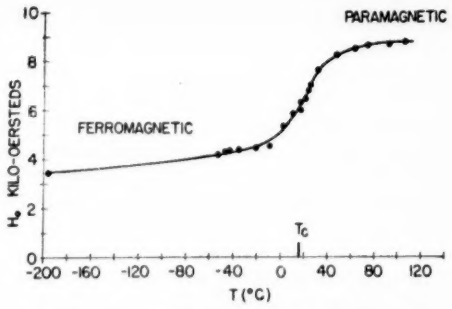

FIG. 2. Gadolinium metal peak position *vs* temperature, at 24.3×10^9 Mc/sec.

The g factor obtained in the paramagnetic region is 1.95±0.03, taking into account shifts in the peak position due to demagnetizing factors and relaxation effects, as well as the effect of varying eddy current losses. In the ferromagnetic region the extreme breadth of the absorption curve prevents accurate determination of the g value. However, we have made calculations of the ferromagnetic g value, ignoring possible shifts in peak positions arising from relaxation effects. These calculations lead to a ferromagnetic g value of 1.94. A limit of uncertainty cannot be assigned to this value because of the extreme breadth of the absorption curves, but the g value is not inconsistent with that in the paramagnetic range.

Our results are to be compared with recent unpublished results of Elliott, Legvold, and Spedding on the saturation magnetization extrapolated to 0°K and infinite applied field. The g value obtained from this value of saturation magnetization is 1.96.

* U. S. Atomic Energy Commission Fellow
† This research was assisted in part by the U. S. Office of Naval Research and the U. S. Atomic Energy Commission.
[1] F. Trombe, Ann. phys. **7**, 385 (1937).
[2] J. H. Van Vleck, Physica **15**, 197 (1949).
[3] W. A. Yager, Phys. Rev. **75**, 316 (1949).
[4] N. Bloembergen, Phys. Rev. **78**, 572 (1950).

Electronic Structure of the Germanium Crystal

FRANK HERMAN AND JOSEPH CALLAWAY*
David Sarnoff Research Center, RCA Laboratories Division, Princeton, New Jersey
(Received November 25, 1952)

THE method of orthogonalized plane waves,[1] recently applied to the diamond crystal,[2] has been used to study the energy band structure of the germanium crystal. The calculation is based on the usual one-electron approximation. A crystal model constructed from isolated atoms [$Ge(4s)^1(4p)^3$] arranged as a germanium lattice was used to determine the Coulomb potential. The constituent atomic wave functions were taken from the self-consistent field calculations for Ge.[3] The effect of exchange was not considered due to the complexity of available approximate treatments.

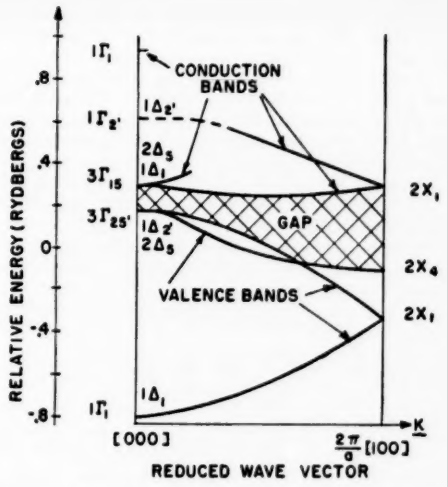

FIG. 1. Energy band structure of the germanium crystal. The present study was restricted to the points $\mathbf{k}=000$ and $k=2\pi(100)/a$. The curves joining the calculated eigenvalues indicate the estimated trends, based on the slopes and curvatures at the end points. The symbols denote degeneracy and symmetry classification. The notation is fully described in references 4 and 5.

The energy band structure predicted for germanium is shown in Fig. 1. The notation used is fully described by Bouckaert *et al.*[4] and Herring.[5] The nondegenerate conduction bands represented by Γ_1 and Γ_2' at $\mathbf{k}=000$ have spherical energy surfaces at this point. The energy surfaces associated with the three lower-lying conduction bands do not have spherical symmetry in E *vs* $\mathbf{k}$. A similar band structure was found for diamond.[2] Although the theory of electron mobility commonly employs spherical energy surfaces for the lowest conduction band for reasons of mathematical simplicity,[6] recent measurements[7,8] have led to interpretations to the contrary.[9,10] These inferences are borne out by the present calculation.

While the numerical results are highly dependent upon the assumed crystal potential and core wave functions, the Γ_2' and Γ_{15} eigenvalues are found to lie far enough apart to suggest that the present study reliably predicts their relative position.

The $\mathbf{k}$ value at which the minimum vertical separation between valence and conduction bands occurs cannot now be predicted with certainty. One of the three conduction bands, degenerate at $\mathbf{k}=000$ (at Γ_{15}), has a downward curvature at this point in certain crystallographic directions; the largest downward curvature occurs along the screw axis (100). The other two bands have upward curvature at $\mathbf{k}=000$ in all directions. The lowest conduction band has a smaller downward curvature at $\mathbf{k}=000$ than any of the three valence bands degenerate at this point (at Γ_{25}'). An exploratory calculation at $\mathbf{k}=2\pi(100)/a$ on the reduced zone face indicates that the separation between valence and conduction bands is considerably greater at this point than at the reduced zone center ($\mathbf{k}=000$). In view of these results, it appears likely that the minimum vertical (optical) separation occurs at $\mathbf{k}=000$.

That the lowest energy value reached by the lowest conduction band does not lie much below its value at $\mathbf{k}=000$ is suggested by the approximate equality of the energy gaps determined by optical and thermal measurements. The calculated energy gap at $\mathbf{k}=000$, 1.45 ev, is in reasonable agreement with the experimental value, 0.75 ev.[6] The valence bands are found to span an energy range of 13.3 ev; experimental data bearing on this prediction are lacking.

In the limit of an empty diamond-type lattice ($V=0$), the states Γ_{15} and Γ_{25}' coalesce. The crystal potential removes this degeneracy. In the case of diamond,[2] Γ_{15} and Γ_{25}' are automatically orthogonal to the core bands formed from the ($1s$) atomic states. The crystal potential, representing Coulomb and exchange interactions, separates these states by about 5.7 ev. In germanium, these states must be orthogonalized to the core bands arising from the ($2p$), ($3p$), and ($3d$) atomic states. The existence of a smaller energy gap in germanium may be attributed to the partial cancellation of the attractive crystal potential by a repulsive potential introduced by the orthogonalization. The convergence properties of the germanium eigensolutions are improved, relative to the diamond eigensolutions, by the additional orthogonality terms.

A more detailed account of the present investigation will be submitted for publication shortly.

The authors wish to express their appreciation to Dr. D. O. North of the RCA Laboratories for valuable guidance, to Dr. C. Herring of the Bell Telephone Laboratories for informative discussions, and to Dr. W. J. Eckert of the Watson Scientific Computing Laboratory at Columbia University for permission to use IBM calculating facilities. The authors are grateful to Dr. I. Wolff, Mr. E. W. Herold, and Dr. L. P. Smith of the RCA Laboratories for their continued interest and support.

* Present address: Palmer Physical Laboratory, Princeton University, Princeton, New Jersey.

[1] C. Herring, Phys. Rev. **57**, 1169 (1940).
[2] F. Herman, Phys. Rev. **88**, 1210 (1952).
[3] W. Hartree and D. R. Hartree, Phys. Rev. **59**, 306 (1941).
[4] Bouckaert, Smoluchowski, and Wigner, Phys. Rev. **50**, 58 (1936).
[5] C. Herring, J. Franklin Inst. **233**, 525 (1942).
[6] W. Shockley, *Electrons and Holes in Semiconductors* (D. Van Nostrand Company, Inc., New York, 1950).
[7] G. L. Pearson, Phys. Rev. **78**, 646 (1950).
[8] H. Suhl, Phys. Rev. **78**, 646 (1950).
[9] W. Shockley, Phys. Rev. **78**, 173 (1950).
[10] Pearson, Haynes, and Shockley, Phys. Rev. **78**, 295 (1950).

Proton-Proton Scattering at Intermediate Energies

ANDRÉ MARTIN AND LOUP VERLET
Laboratoire de Physique, Ecole Normale Supérieure, Paris, France
(Received November 28, 1952)

RECENTLY the nucleon-nucleon interaction yielded by the pseudoscalar meson theory (with pseudoscalar coupling) has been analyzed by Lévy.[1] At low energies, this interaction reduces to a potential which has the following form:

$$V(r)=\infty \quad \text{for} \quad r<r_c,$$
$$V(r)=V_c(r)+S_{12}V_t(r) \quad \text{for} \quad r>r_c,$$

where

$$V_c(r)=\frac{G^2}{4\pi}\left(\frac{\mu}{2M}\right)^2\frac{(\boldsymbol{\tau}_1\cdot\boldsymbol{\tau}_2)(\boldsymbol{\sigma}_1\cdot\boldsymbol{\sigma}_2)}{3}\frac{e^{-\mu r}}{r}-3\left(\frac{G^2}{4\pi}\right)^3\left(\frac{\mu}{2M}\right)^2\frac{1}{\mu r^2}$$
$$\times\left\{\frac{2}{\pi}K_1(2\mu r)+\frac{\mu}{2M}\left[\frac{2}{\pi}K_1(\mu r)\right]^2\right\}, \quad (1)$$

$$V_t(r)=\frac{G^2}{4\pi}\left(\frac{\mu}{2M}\right)^2\frac{(\boldsymbol{\tau}_1\cdot\boldsymbol{\tau}_2)}{3}\left[1+\frac{3}{\mu r}+\frac{3}{\mu r^2}\right]\frac{e^{-\mu r}}{r},$$

its validity being limited to energies not greater than about 50 Mev. With this potential, Lévy has studied the low and intermediate energy experimental data for the neutron-proton system. The two constants $G^2/4\pi$ and r_c were determined to fit the binding energy of the deuteron and the neutron-proton zero energy singlet scattering length, with the following results:

$$G^2/4\pi=9.7\pm1.3,$$
$$r_c=(0.38\pm0.03)(\hbar/\mu c). \quad (2)$$

It seemed interesting to investigate proton-proton scattering at intermediate energies (18.3 and 32 Mev), where the accuracy of the measurements and the sensitivity of the differential cross sections to the characteristics of the potential presumably provide a more severe test for the theory.

The calculations were carried out as follows: direct numerical integration of the Schrödinger equation for $L=0$, to obtain the S phase shift K_0; Born approximation with Coulomb wave function

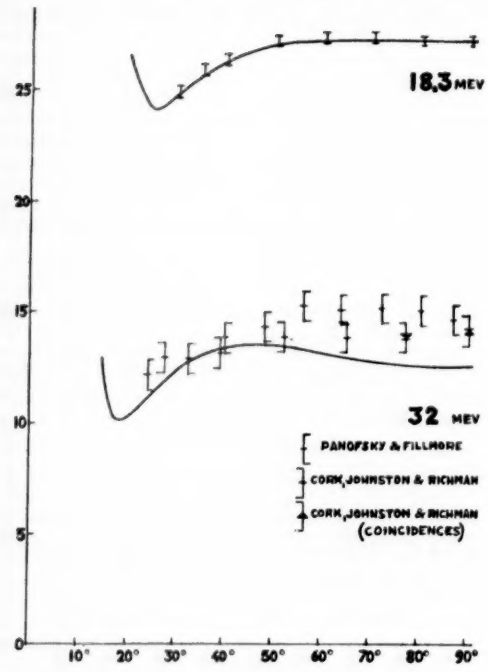

FIG. 1. The angular distribution of the differential cross section (in millibarns per steradian), at 18.3 and 32.0 Mev. In the latter case appropriate errors have been assumed so that the two series of experimental data (see reference 6) are consistent with each other.

for the determination of the D phase shift K_2 and the three P phase shifts $K_1^{(0)}$; $K_1^{(1)}$, $K_1^{(2)}$ corresponding to tensor scattering with $J=L-1$, $J=L$, $J=L+1$, respectively. (In computing K_1, the coupling with F state has been neglected.) For a potential including a repulsive core the Born approximation gives

$$\tan K_L^{(J)} = -\frac{M}{\mu}\int_{r_c}^{\infty}[F_L(kr)-\rho_L(kr_c)G_L(kr)]^2 V_L^{(J)}(r)dr \\ -(-1)^L\rho_L(kr_c), \quad (3)$$

where F_L and G_L are, respectively, the regular and irregular Coulomb wave functions, and $\rho_l(kr_c)=F_L(kr_c)/G_L(kr_c)$. The contribution of the core to the D phase shifts was found negligible for the range of energy investigated. To obtain the Coulomb wave function, the Schrödinger equation, corresponding to the Coulomb field alone, was solved numerically since the existing tables[3] do not cover the required range of (kr) values at high energy. The solution which vanishes for $r=r_c$ was normalized by comparison with the tables for sufficiently large values of (kr).

(1) 18.3 Mev.—For this energy, there exists excellent measurements.[3] Keeping a core radius of $0.38(\hbar/\mu c)$, we observed that the cross section at 90° is very sensitive to the variation of the coupling constant within the interval defined by Eq. (2). When $G^2/4\pi$ varies from 9.7 to 11, K_0 increases from 34.77° to 75.13°. The accuracy of the 18.3-Mev experiments provides, therefore, a severe restriction on the possible values of the coupling constant: we found[4] $G^2/4\pi = 10.36\pm0.02$ for $r_c=0.38(\hbar/\mu c)$. With these constants we obtained the following values of the phase shifts: $K_0=52.8°$, $K_1^{(0)}=6.82°$, $K_1^{(1)}=-1.45°$, $K_1^{(2)}=1.85°$, $K_2=0.35°$.

The corresponding differential cross section[5] is plotted in Fig. 1. It is seen that the agreement with experiment is excellent.

(2) 32.0 Mev.—For this energy the experimental results[6] are not so good as for 18.3 Mev. The following phase shifts have been obtained: $K_0=44.85°$, $K_1^{(0)}=11.79°$, $K_1^{(1)}=-1.62°$, $K_1^{(2)}=3.79°$, $K_2=0.97°$.

The corresponding differential cross section is plotted in Fig. 1. One can notice a discrepancy of about 10 percent with the experimental data. This discrepancy can be compared with the similar one observed by Lévy for $n-p$ scattering at 40 Mev. It is consequently probably not fortuitous and might be due to several causes: the energy dependence of the potential presumably starts to be felt at these energies (see, for instance, reference 1, end of Sec. III); the detailed structure of the interaction at short distances might also become more significant. These problems will be investigated in more detail for the analysis of high energy nucleon-nucleon scattering.

The authors wish to acknowledge the kind hospitality they have received at the Laboratoire de Physique of the Ecole Normale Supérieure. They are also deeply indebted to Dr. Maurice Lévy for suggesting this problem and for continued guidance in the calculations.

[1] M. Lévy, Phys. Rev. **86**, 806 (1952); **88**, 725 (1952).
[2] Bloch, Hull, Broyles, Bouricius, Freeman, and Breit, Phys. Rev. **23**, 147 (1951).
[3] J. L. Yntema and M. G. White, Technical Report NYO 3478, Princeton University, 1952 (unpublished).
[4] These figures would, of course, be modified if r_c were varied within the allowed interval of Eq. (2). The new value of $G^2/4\pi$ presumably improves the agreement with the low energy data.
[5] Breit, Kittel, and Thaxton, Phys. Rev. **57**, 255 (1940).
[6] W. K. H. Panofsky and F. Fillmore, Phys. Rev. **79**, 57 (1950); Cork, Johnston, and Richman, Phys. Rev. **79**, 71 (1950).

New Long-Lived Magnesium-28 Isotope*

R. K. SHELINE AND N. R. JOHNSON
Department of Chemistry, Florida State University, Tallahassee, Florida
(Received December 1, 1952)

MAGNESIUM-28, a 21-hr β^- emitter, has been produced in both a betatron irradiation and a cyclotron bombardment. The nuclear reactions are

$$Si^{30}(\gamma,2p)Mg^{28}, \quad (1)$$

$$Mg^{26}(\alpha,2p)Mg^{28}. \quad (2)$$

The half-lives observed are 21.7 ± 1.0 hr in the case of nuclear reaction (1) and 21.3 ± 0.2 hr in the case of nuclear reaction (2).

In nuclear reaction (1) elemental silicon was irradiated for eight hours in the gamma-spectrum of the 100-Mev University of Chicago betatron. The silicon was dissolved in hot conc sodium hydroxide and carrier magnesium ion added. The solution was neutralized with hydrochloric acid precipitating silicon dioxide and filtered. Magnesium ammonium phosphate was precipitated from the filtrate which was buffered with ammonium chloride by the addition of primary ammonium phosphate. The magnesium ammonium phosphate precipitation was repeated twice more to insure purity.

In nuclear reaction (2) a disk of magnesium metal of ordinary isotopic composition was bombarded in an external beam of 39-Mev alpha-particles for ten hours in the University of California 60-inch cyclotron. The magnesium disk was coated with Krylon plastic spray except for the area in which the beam was concentrated. The magnesium could then be dissolved in dil hydrochloric acid in such a way as to produce the highest possible specific activity. The magnesium ammonium phosphate was then precipitated from the appropriately buffered solution, to which sodium chloride was added as a hold-back carrier. This precipitation was repeated four additional times.

The evidence for the assignment of this activity as Mg^{28} is very strong. Perhaps the strongest piece of evidence is the observation in milking experiments of Al^{28}, the daughter of Mg^{28}, with which it is in secular equilibrium. Al^{28}, which is a well-studied activity,[1] has a 2.3-min half-life and decays via a 3.01-Mev β^- and a 1.80-Mev gamma to Si^{28}. The half-life observed in the milking experiments agrees very closely with the reported 2.3-min half-life for Al^{28}. In addition, aluminum absorption curves on the activity, after it has been allowed to attain radioactive equilibrium, show the

existence of the 3-Mev β^- of Al^{28}. When one adds to this the evidence from cross bombardment and nuclear systematics from this part of the isotope chart, the assignment as Mg^{28} seems unequivocal.

Mg^{28} has a half-life slightly more than 130 times that of the longest-lived magnesium activity previously known, Mg^{27} ($t_{\frac{1}{2}}=9.6$ min).[1] For this reason Mg^{28} should find considerable use as a tracer, particularly in the study of photosynthesis. Its use in plant physiology, soil science, and certain parts of biochemistry is immediately evident. Preliminary experiments using Mg^{28} as a tracer in plants have been encouraging.

It is probable that Mg^{28} could be produced by high energy cyclotron spallation reactions on elemental silicon or calcium chloride. Such methods of production of this activity might have the advantage of producing a large amount of high specific activity particularly advantageous in tracer experiments.

Because of the very considerable application which this isotope may find in other fields, this work is reported without a decay scheme for Mg^{28}. Work is continuing on the project and a complete report on this activity will be published in this journal in the near future. Thanks are due the staffs and crews of the University of Chicago betatron and the University of California 60-inch cyclotron.

* This work was assisted by the U. S. Atomic Energy Commission.

[1] K. Way *et al.*, *Nuclear Data*, National Bureau of Standards Circular No. 499 (1950), pp. 24, 22.

Thermal Rayleigh Disk Measurements in He^3-He^4 Mixtures

BERNARD WEINSTOCK, *Argonne National Laboratory, Lemont, Illinois*
AND
JOHN R. PELLAM, *National Bureau of Standards, Washington, D. C.*
(Received November 17, 1952)

PRELIMINARY investigations of the propagation of second sound in a 4 percent mixture of He^3 and He^4 have been carried out during a joint Argonne-NBS program conducted at the NBS Cryogenics Laboratory. For these experiments a thermal Rayleigh disk[1] apparatus was employed. The volume of the disk chamber was limited to $\frac{3}{4}$ cc by the amount of mixture available, and the diameter of the mirrored disk was accordingly reduced to 2.8 mm. A satisfactory fiber for suspending the disk and with small restoring constant was prepared from Duco cement. Second sound was generated by passing an alternating electrical current through a carbon strip resistance, and the frequency corresponding to maximum deflection of the disk from its equilibrium orientation gave a direct measurement of the wave velocity. The actual torque on the disk was computed from the observed deflection and the measured value of the restoring constant of the suspension, so that the kinetic energy density of the thermal wave was determined. Evaluation of the thermal resonance properties of the system permitted the kinetic energy density for unit heat current density to be computed and allowed a comparison with pure He^4. The apparatus was checked by measurements with pure He^4 directly, and reasonable agreement was obtained with the previously observed values. In the work with the mixture the power input to the system was severely limited by phenomena associated with the heat flush effect, and it was therefore necessary to amplify the resulting small disk deflection. This was achieved by turning the power on and off with a frequency corresponding to that of the freely swinging disk suspension. In this way a detection sensitivity of 10^{-8} dyne-centimeter was obtained in a system where the maximum torque was of the order of 1 microdyne centimeter.

We have found that the velocity of second sound in the 4 percent mixture increases continuously with decreasing temperature to a value of 38 meters per second at about 0.9°K. Table I gives representative values of the observed velocities for various temperatures. These results are in qualitative agreement with the earlier observations of Lynton and Fairbank,[2] who measured a 0.8 percent mixture down to 1.2°K. From this it appears likely that

TABLE I. Wave velocity of second sound in 4 percent He^3-He^4 mixture *versus* temperature.

Temperature (°K)	Wave velocity (m/sec)
0.9	38
1.0	36
1.25	31
1.5	28
1.75	24
1.95	16
2.0	0

the quantitative aspects of Pomeranchuk's[3] theory for the second sound velocity of He^3-He^4 mixtures are incorrect. In his theory the second sound velocity of mixtures at first increases above that of pure He^4 but then decreases and extrapolates to a small value at absolute zero. For this to occur, he would have predicted the appearance of a maximum in the velocity of second sound for the 4 percent mixture at a temperature of about 1°K. Dingle,[4] on the other hand, suggests that, owing to strong interaction between the particles, the velocity of second sound in mixtures will behave at very low temperatures similarly to that of pure He^4 and in fact near absolute zero will approach the same value of first sound velocity divided by $\sqrt{3}$. So far our results are consistent with this latter prediction; choice, however, between Dingle and Pomeranchuk's views must await measurement at much lower temperatures.

Regarding the torque measurement, Koide and Usui[5] have suggested that thermal Rayleigh disk measurements with He^3-He^4 mixtures would be a sensitive test of a hypothesis that the He^3 component remains stationary in the center-of-mass system in the presence of second sound, rather than participate in the normal fluid excursion. They treated theoretically cases of He^3 concentration up to 0.8 percent for temperatures above 1.5°K, and predicted a marked decrease in torque resulting from the dilution. We have checked this effect in our investigations under even more extreme conditions and have found that at 0.9°K in the 4 percent mixture the torque has fallen to a few tenths percent of that for pure He^4. While our measurements agree with their prediction, it might be possible to explain our results without assuming that the He^3 does not participate in the normal fluid particle motion. In this connection, specific heat values for the mixture obtainable from our torque measurements agree well with calculated values deduced from the de Boer-Gorter[6] theory.

[1] J. Pellam and P. Morse, Phys. Rev. **78**, 474 (1950); J. Pellam and W. Hanson, Phys. Rev. **85**, 216 (1952).
[2] E. Lynton and H. Fairbank, Phys. Rev. **80**, 1043 (1950).
[3] L. Pomeranchuk, J. Exptl. Theoret. Phys. (U.S.S.R.) **19**, 42 (1949).
[4] R. Dingle, Phil. Mag. **42**, 1080 (1951).
[5] S. Koide and T. Usui, Prog. Theoret. Phys. **6**, 506 (1951).
[6] J. de Boer and C. J. Gorter, Physica **16**, 225 (1950).

The Structure of Deformation Bands

EDWARD W. HART
General Electric Research Laboratory, Schenectady, New York
(Received December 4, 1952)

IT is well known[1] that two parallel dislocations with opposite Burger's vectors, as shown in Fig. 1, and gliding on distinct planes can block each other's motion because of their mutual stress interaction. The angle, ϕ, between the line joining the two dis-

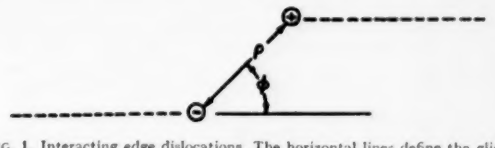

FIG. 1. Interacting edge dislocations. The horizontal lines define the glide planes containing Burger's vectors.

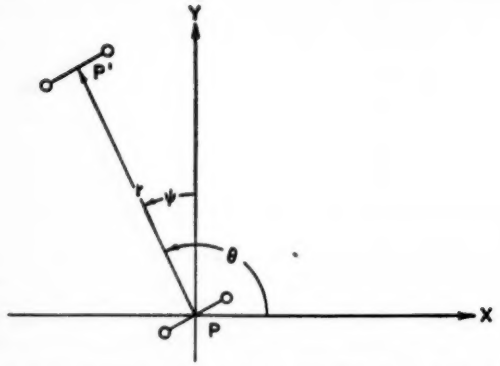

FIG. 2. Interacting pairs of dislocations. The glide planes are parallel to the x axis.

locations of the pair and the slip plane is determined ideally by the applied stress in the neighborhood. If there were a group of such pairs in any local region of a crystal they would then all have the same orientation angle, ϕ. It is the purpose of this note to show that, if the components of the pairs were edge type dislocations, such a group could form a stable array and that this array would have a property which has been observed for deformation bands in metal crystals deformed in tension.

Consider the interaction of two similarly oriented pairs, P and P', such that the spacing, r, between them is large compared to the spacing, ρ, of the component dislocations of either pair. The configuration is shown in Fig. 2 where the x direction is chosen to be the slip direction, P is taken to be at the origin, and θ is the angle between the positive x direction and the line connecting P and P'. The force per unit length, F, exerted on P' by P is readily found to be given by

$$F=Gbb'(\rho\rho'/r^3)\{\alpha^2[\cos3\theta-3\cos5\theta]+3\beta^2[\cos3\theta+\cos5\theta]-2\alpha\beta[\sin3\theta+3\sin5\theta]\},$$

where $\alpha=\cos\phi$, $\beta=\sin\phi$, and b and b' are the component dislocation strengths of P and P', respectively. The equilibrium orientation of the array is given by the value of θ for which $F=0$. It is seen immediately that the equilibrium value of θ is dependent only on the magnitude of ϕ, and so the orientation of a group of more than two pairs is the same as for two.

The variation of the equilibrium orientation angle, ψ (equal to $\theta-90°$), against ξ (equal to $\cot\phi$) is shown in Fig. 3. If an array of this sort is taken as a model of a deformation band, the angle ψ is the angle between the deformation band and the normal to the slip plane. Cahn[2] reported measurements of this angle (it is the angle designated θ in Cahn's paper) for ten specimens. His results, tabulated in Tables I and II of reference 2, comprise a range from 11° to 21°. The range of values of ξ which would correspond to these angles is reasonable. When r is equal to or smaller than ρ, the result above does not hold, and the angle ψ becomes much smaller.

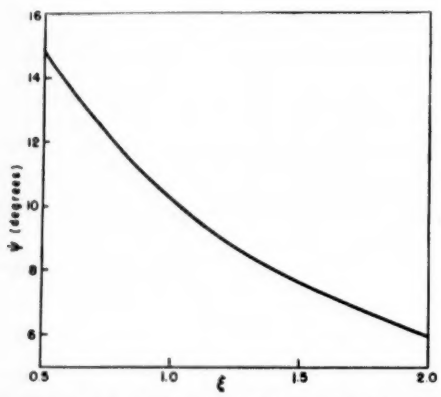

FIG. 3. Static equilibrium configurations for interacting dislocation pairs.

It seems reasonable then to infer that deformation bands as observed in aluminum could be composed of widely spread pair elements of the sort treated here. This would be in agreement with the explanation of asterism proposed by Burgers,[3] based on only one pair. Although the components of the pairs have been represented here as single dislocations, they can equally well be groups of dislocations piled up at the end of slip regions so long as the total dislocation strength of each component in a pair is the same as that of the component with which it is paired.

[1] See, for example, A. H. Cottrell, *Progress in Metal Physics* (Interscience Publishers, Inc., New York, 1949), p. 103.
[2] R. W. Cahn, J. Inst. Metals **79**, 129 (1951).
[3] J. M. Burgers, Proc. Phys. Soc. (London) **52**, 23 (1940).

Unified Field Theory and Born-Infeld Electrodynamics

G. RICKAYZEN, *Christ's College, Cambridge, England*
AND
B. KURŞUNOĞLU,* *Fitzwilliam House, Cambridge, England*
(Received November 24, 1952)

IN a recent paper by one of us,[1] a new version of Einstein's generalized theory of gravitation was proposed. In this note, we show that in the limit of a point charge distribution of an "electron," this theory reduces to that of Born-Infeld electrodynamics.[2]

The Lagrangian of the proposed theory was given as

$$2p^2\mathfrak{L}=\mathfrak{g}^{\alpha\beta}(R_{\alpha\beta}-ip^2B_{\alpha\beta})+2p^2\{\sqrt{(-g)}-\sqrt{(-b)}\}, \tag{1}$$

where

$$B_{\alpha\beta}=\partial_\alpha B_\beta-\partial_\beta B_\alpha \tag{2}$$

is an auxiliary field variable that can be eliminated from the field equations, and the metric of the unified space-time is given by

$$ds^2=b_{\alpha\beta}dx^\alpha dx^\beta, \tag{3}$$

$$b^{\alpha\beta}=\mathfrak{g}^{\alpha\beta}/[\sqrt{(-\mathrm{Det}\mathfrak{g}^{\alpha\beta})}], \tag{4}$$

$$b_{\alpha\beta}b^{\beta\gamma}=\delta_\alpha{}^\gamma. \tag{5}$$

If we let $p\to\infty$, the Lagrangian (1) reduces to

$$\mathfrak{L}'=-\tfrac{1}{2}i\mathfrak{g}^{\alpha\beta}B_{\alpha\beta}+\{\sqrt{(-g)}-\sqrt{(-b)}\}. \tag{6}$$

The variations of the action, with $\mathfrak{L}'$ as the action-density, with respect to the field variables $\mathfrak{g}^{\alpha\beta}$ and B_α of the unified field theory lead to the field equations,

$$a_{\alpha\beta}=b_{\alpha\beta}, \tag{7}$$

$$\phi_{\alpha\beta}=B_{\alpha\beta}, \tag{8}$$

$$\mathfrak{g}^{\alpha\beta}{}_{,\beta}=0. \tag{9}$$

Now Eqs. (7), (8), and (9) are the field equations of unified field theory in the limit $p\to\infty$, in which case the field $\phi_{\alpha\beta}$ degenerates into the curl of a four-vector B_α. By using (7) and (8) in (6), we obtain a different action-density,

$$L=\tfrac{1}{2}\mathfrak{g}^{\alpha\beta}\phi_{\alpha\beta}+\{\sqrt{(-g)}-\sqrt{(-b)}\} \tag{10}$$

$$=\sqrt{(-a)}(\Omega+2\Lambda^2)(1-\Omega-\Lambda^2)^{-\frac{1}{2}}+\{\sqrt{(-g)}-\sqrt{(-a)}\} \tag{11}$$

$$=-\sqrt{(-g)}+\sqrt{(-a)}(1+\Lambda^2)(1-\Omega-\Lambda^2)^{-\frac{1}{2}}+\{\sqrt{(-g)}-\sqrt{(-a)}\}$$

$$=\sqrt{(-a)}\left\{\frac{1+\Lambda^2}{\sqrt{(1-\Omega-\Lambda)^2}}-1\right\}. \tag{12}$$

We define the tensor

$$q_{\alpha\beta}=a_{\alpha\beta}+iF_{\alpha\beta}, \qquad (13)$$
$$F_{\alpha\beta}=-\tfrac{1}{2}\epsilon_{\alpha\beta\mu\nu}g^{\mu\rho}g^{\nu\sigma}.$$

Then, from (9), it follows that F can be written

$$F_{\alpha\beta}=\partial_\alpha A_\beta-\partial_\beta A_\alpha. \qquad (14)$$

The determinant of (13) is

$$q=a\{1-Q-\Lambda^2\}=a(1+\Lambda^2)^2/(1-\Omega-\Lambda^2), \qquad (15)$$
$$Q=\tfrac{1}{2}F_{\mu\nu}F^{\mu\nu}.$$

From (15), it follows that

$$L=\sqrt{(-a)}\{\sqrt{(1-Q-\Lambda^2)}-1\}, \qquad (16)$$

which is the Lagrangian of the Born-Infeld theory.

It was shown in reference 1 that $\sqrt{2}p=\kappa$ is the reciprocal of the range of charge distribution in the linear approximation. Hence, we infer that in the limit $p\to\infty$ the charge distribution tends to a point. This comparison suggests that $F_{\alpha\beta}$ is the electromagnetic field tensor, while B_α is the antipotential defined by Born and Infeld.

As in the Maxwell-Lorentz electrodynamics, the Born-Infeld theory does not prescribe the law of distribution of the charges, but introduces this law as an extra postulate. On the contrary, unified field theory implies this law in the field equations, and this must be regarded as an important consequence of the unification of physical fields.

* Now at the Laboratory of Nuclear Studies, Cornell University, Ithaca, New York.

[1] B. Kurşunoğlu, Phys. Rev. **88**, 1369 (1952).
[2] M. Born and L. Infeld, Proc. Roy. Soc. (London) **A144**, 425 (1934).

Second-Sound Velocity below 1°K as a Function of Pressure*

VICTOR MAYPER, JR., AND MELVIN A. HERLIN
Research Laboratory of Electronics, Massachusetts Institute of Technology, Cambridge, Massachusetts
(Received November 24, 1952)

THE publication of Gorter's recent letter[1] has prompted us to submit the following, which is essentially the text of a paper delivered at the ONR–GE Cryogenics Conference at Schenectady on October 6, 1952.

Measurements of the velocity of second sound have contributed significantly to an understanding of the nature of the excitations of liquid helium II. The results of Atkins and Osborne[2] along the vapor pressure line seem to confirm approximately the prediction of Landau[3] that c_2 should approach the constant $c_1/\sqrt{3}$, which results from the proposal that the liquid should approach an ideal phonon gas at low temperatures. Further evidence that the excitations of the liquid are due solely to phonons at low temperatures is given by the specific-heat measurements of Kramers,[4] showing a T^3 dependence for C_v below approximately 0.6°K. There is some discrepancy between the second-sound measurements and the specific-heat measurements quoted above, in that the second-sound velocities depart radically from the phonon-gas model above approximately 0.35°K instead of the 0.6°K of the specific-heat measurements.

Measurements now in progress by the authors, both at vapor pressure and at higher pressure, are being made by the pulse method of Pellam,[5] later used by Maurer and Herlin.[6] A second-sound chamber 3.035 cm long and 3.2 mm in diameter employs carbon-composition films on Bakelite disks for both transmitter and receiver. The transmitted pulse for the measurements reported here was 20 μsec long, of intensity 3.5 mw/cm², and repeated 30 times per second. (The results did not seem to depend appreciably on these parameters.) The received pulse is displayed on a Dumont type 256-D A/R scope; the internal time marker of the scope is used to measure the delay time. Temperatures are measured with an ac mutual inductance bridge, calibrated against the vapor pressure of helium from 1° to 4°. Warm-up times of three to four minutes are typical.

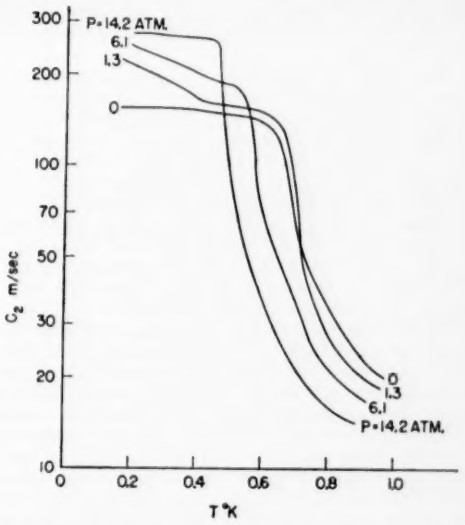

FIG. 1. Second-sound velocity *vs* temperature at various pressures. Experimental points have been omitted for clarity, but the various regions of the curves are unmistakable. Each curve represents twenty to thirty points, obtained from several demagnetizations.

Our results at vapor pressure are in reasonably good agreement with Kramers' specific heat data and with the results of DeKlerk, Hudson, and Pellam,[7] just announced, at least above approximately 0.3°K. At vapor pressure, we find no trace of the rise in velocity that they report at lower temperatures, but this may be due to our more rapid warm-up time. Our extrapolated value for $c_2(0)$ is 155 m/sec, in agreement with Atkins and Osborne, and in reasonably good agreement with the value reported by DeKlerk, Hudson, and Pellam for a temperature just below that of the sharp drop in c_2. Our results at higher pressure, as may be seen in Fig. 1, tend to bear out the supposition that this low temperature rise in velocity is a real phenomenon, becoming more apparent at higher pressure. It will be noted that our values for c_2 at a temperature just below that of the sharp drop in c_2 are, at each pressure, just about 10 percent higher than $c_1/\sqrt{3}$ for that pressure. (In the case of 14.2 atmospheres, the low temperature rise apparently has begun before the sharp rise at intermediate temperature is complete.) At the very lowest temperatures, velocities have risen to near c_1.

A possible explanation of this behavior is as follows:[8] If we consider liquid helium at temperatures below the sharp drop in c_2 to be phonon gas, then, as in the usual picture, heating at some point in the helium will cause a concentration gradient in this gas. This gradient may revert toward equilibrium in one of three ways. First, if the mean free path for inelastic phonon-phonon collisions (such as Umklapp collisions) is short, the phonons will diffuse away and ordinary heat conduction will result. In liquid helium II in the pure phonon-gas region, the temperature is lower, and the inelastic mean free path is long, while the mean free path for elastic collision is still short, so that a compression wave of phonons is propagated, resulting in second sound. At still lower temperatures, the phonons are becoming more rarefied and their total mean free path may become larger than the dimensions of the measuring apparatus, in which case we get a flow of phonons analogous to Knudsen flow of a gas. Some will travel straight from the transmitter to the receiver at their velocity c_1, and others will be reflected from the walls of the tube and eventually reach the receiver, thus building up a received pulse which looks as though it were caused by diffusive heat flow. The foot of this pulse will indicate a velocity which be-

comes nearer to c_1 as the temperature is decreased (i.e., as the mean free path becomes longer) and as the sensitivity of the receiver is increased.

In this picture, the sharp rise in velocity at intermediate temperatures is caused by the disappearance of the high temperature excitations (bosons or rotons). As soon as these have disappeared, the velocity of heat pulses should become $c_1/\sqrt{3}$, and remain there until the mean free path for phonon-phonon collision becomes long, at which temperature it should rise to near c_1. The pressure dependence should be in the direction found experimentally, since (as mentioned by Maurer and Herlin) the number of phonons at a given temperature decreases with pressure, and hence any long mean-free-path effect should increase with pressure.

The shape of the received pulse at low temperatures and at all pressures observed shows the behavior reported by Pellam and Scott[9] and by Atkins and Osborne. At the lowest temperatures, where the velocity is high and does not vary rapidly with temperature, the pulse shape is essentially that reproduced in the letter of Atkins and Osborne. The rise is fairly sharp, with a well-defined foot, but the tail is extremely long. At the intermediate temperatures, coincident with the rapid drop in velocity with temperature, the tail becomes shorter, the rise longer, and the foot less well defined, so that the pulse becomes symmetrical and assumes a roughly Gaussian shape. At the higher temperatures the entire pulse becomes well defined. The extremely large dispersion in the intermediate-temperature region may possibly be due to the interaction of the phonons and the higher temperature excitations, since in this region they are competing for dominance.

* This work was supported in part by the Signal Corps, the Air Materiel Command, and the U. S. Office of Naval Research.

[1] C. J. Gorter, Phys. Rev. **88**, 681 (1952).
[2] K. R. Atkins and D. G. Osborne, Phil. Mag. **41**, 1078 (1950).
[3] L. Landau, J. Phys. (U.S.S.R.) **5**, 71 (1941).
[4] H. A. Kramers, Proc. Int. Conf. on Low Temp. Phys., Oxford, 1951, p. 93 (unpublished).
[5] J. R. Pellam, Phys. Rev. **74**, 841 (1948).
[6] R. D. Maurer and M. A. Herlin, Phys. Rev. **76**, 948 (1949) and **81**, 444 (1951).
[7] DeKlerk, Hudson, and Pellam, read at ONR-GE Cryogenics Conference, Schenectady, October 6, 1952 (unpublished).
[8] See J. C. Ward and J. Wilks, Phil. Mag. **42**, 314 (1951) and **43**, 48 (1952).
[9] J. R. Pellam and R. B. Scott, Phys. Rev. **76**, 869 (1949).

Activities in Light Nuclei from Nitrogen Ion Bombardment

L. D. WYLY AND A. ZUCKER
Oak Ridge National Laboratory, Oak Ridge, Tennessee
(Received October 14, 1952)

RECENTLY Breit, Hull, and Gluckstern[1] have pointed out the possibility of obtaining information regarding nuclear structure by bombarding nuclei with heavy nuclei. A cyclotron has been constructed at Oak Ridge National Laboratory to accelerate triply ionized nitrogen ions to an energy of approximately 25 Mev. The machine is designated the Oak Ridge National Laboratory 63-inch cyclotron, since its pole pieces are 63 inches in diameter. Beam currents of approximately 1 μa have been measured at maximum radius. During the time devoted primarily to the "tune-up" and adjustment of the accelerator, several light elements were exposed to the internal beam, to investigate induced radioactivities. The targets bombarded and the activities observed are shown in Table I. Several activities may be interpreted as resulting from the fusion of a substantial portion of the nuclear matter in the two nuclei.

TABLE I. Observed activities.

Isotope bombarded	Half-lives observed	Reaction products Observed	Remaining
Deuterium	124 sec	O^{15}	n
Beryllium	110 min	F^{18}	He^4
Carbon	15 hr	Na^{24}	$2H^1$
	110 min	F^{18}	Be^8
	long	Na^{22}	He^4
Nitrogen	10 min	N^{13}	N^{15}
	2 min	O^{15}	C^{13}
Oxygen	113 min	F^{19}	C^{12}
	2.4 min	Al^{28}	$2H^1$

TABLE II. Observable activities.[a]

	Q (Mev)	M_3	M_4	$T_{\frac{1}{2}}(M_3)$
$N^{14}+Be^9 \rightarrow M_3+M_4$	+ 1.8	F^{18}	He^5	112 min
$E_{Av}=9.78$ Mev	− 3.8	N^{18}	Be^{10}	10.1 min
$E_B=6.4$ Mev	− 5.3	F^{17}	He^6	72 sec
	− 9.6	O^{15}	Li^8	118 sec
	−10.0	C^{11}	B^{12}	20.5 min
$N^{14}+C^{12} \rightarrow M_3+M_4$	− 3.0	F^{18}	Be^8	112 min
$E_{Av}=11.5$ Mev	− 3.1	Na^{24}	$2H^1$	15 hr
$E_B=9.2$ Mev	− 5.7	N^{13}	C^{13}	10.1 min
	− 7.9	C^{11}	N^{15}	20.5 min
	− 8.6	O^{15}	B^{11}	118 sec
$N^{14}+N^{14} \rightarrow M_3+M_4$	+ 0.2	N^{13}	N^{15}	10.1 min
$E_{Av}=12.5$ Mev	− 0.3	O^{15}	C^{13}	118 sec
$E_B=10.5$ Mev	− 4.1	C^{11}	O^{17}	20.5 min
	− 4.9	F^{17}	B^{11}	72 sec
	− 5.4	O^{14}	C^{14}	76 sec
	− 6.5	Na^{25}	$3H^1$	60 sec
	− 7.2	F^{18}	B^{10}	112 min
$N^{14}+O^{16} \rightarrow M_3+M_4$	+18	P^{30}	γ	2.5 min
$E_{Av}=13.3$ Mev	+ 0.73	Al^{28}	$2H^1$	2.3 min
$E_B=11.7$ Mev	− 2.9	F^{18}	C^{12}	112 min
	− 4.8	O^{15}	N^{15}	118 sec
	− 6.4	N^{13}	O^{17}	10.1 min
	− 7.0	F^{17}	C^{13}	72 sec
	− 8.8	Mg^{27}	$3H^1$	9.6 min
	−11	C^{15}	F^{19}	20 min
	−23	Na^{24}	$2He^3$	15 hr

[a] E_{Av} is the energy available in the center-of-mass system, assuming a 25-Mev beam. E_B is the Coulomb barrier: $z_1z_2e^2/(r_1+r_2)$, where $r=1.4\times10^{-13}A^{\frac{1}{3}}$ cm.

The beam energy, corresponding to the $H\rho$ at the target radius of 24.25 in., is 25 Mev for N^{+++} ions. The range of these ions in Ilford C-2 emulsions has been measured. The maximum range of the ions is approximately 16 microns with the peak of the beam energy distribution at 10.5 microns. The half-width at half-maximum is 4 microns. From the calculation of Knipp and Teller[2] we find the maximum energy of the nitrogen ions to be approximately 26 Mev, with the peak of the distribution at 21 Mev. Since the range-energy relations for heavy ions in solids are not well known, these energy determinations may not be final.

The target is mounted on a water-cooled brass probe which is inserted into the upper dee. Bombardments are from 2 to 30 minutes. Upon termination the probe is immediately removed through a vacuum lock, and the target is inserted in a lead-shielded Geiger counter; the transfer usually requires only two or three minutes. This method does not detect all reactions produced, but only those which lead to radioactive products with half-lives between one minute and a few days.

The deuterium target was prepared by evaporating a zirconium film on a platinum backing and heating it in an atmosphere of deuterium. The activity observed is that expected from the $N^{14}(d,n)O^{15}$ reaction. We may conclude that the cyclotron beam does indeed contain N^{+++} ions, since N^+ ions, accelerated by the third harmonic of the rf, would have insufficient energy to produce reactions with deuterium. Owing to the energy carried by the center of mass, 25-Mev nitrogen ions correspond to 3.6-Mev deuterons on a stationary nitrogen target.

The beryllium target was a 5-mil foil, obtained commercially, and the carbon targets were graphite plates $\frac{1}{32}$ in. thick. Oxygen was bombarded in two forms, as oxidized copper and as TiO_2 powder pressed into a zirconium backing; identical activities of 113 minutes and 2.4 minutes were found in both targets. Since no 15-hour activity was found in oxygen targets, we may conclude that there is no carbon contamination and, conversely, since there was no short half-life in the carbon we may assume it to be oxygen free. The assignment of the 2.4-minute activity to Al^{28} is not

unquestionable; as a possible alternative, P^{30} would be a radiative capture of nitrogen on oxygen, a reaction which is not as probable as one involving emission of two protons.

Nitrogen was bombarded in the form of tantalum nitride, prepared by passing nitrogen over clean tantalum at 1000°C. Upon bombardment, the target showed 2-minute, 10-minute, and 112-minute activities. It is possible that the TaN target contains oxygen contamination. The 2-minute activity may be a mixture of O^{15} produced from the nitrogen in the target and of Al^{28} produced in the oxygen contaminant. The 10-minute half-life can be assigned to N^{13} and arises from a nitrogen-nitrogen reaction. The 110-minute half-life is assigned to F^{18}, which may be due entirely to oxygen contamination in the target.

The observable activities are listed in Table II, in the order of decreasing Q values. The Q values were computed from the mass values of Mattauch and Flammersfeld.[3] It is to be noted that in general the reactions observed are the most exoergic ones. For this reason the F^{18} found in the nitrogen is attributed to oxygen contamination. We did not find a 10.1-minute, 20.5-minute, or 118-second activity in any of the carbon targets, even though the formation of the respective isotopes is energetically possible, and easily observable.

We wish to thank Mr. J. B. Dial for the preparation of the deuterium target. It is a pleasure to acknowledge the many fruitful discussions with Dr. J. L. Fowler. We are indebted to Dr. H. L. Reynolds for the beam energy determination in nuclear emulsions.

[1] Breit, Hull, and Gluckstern, Phys. Rev. **87**, 74 (1952).
[2] J. Knipp and E. Teller, Phys. Rev. **59**, 659 (1941).
[3] J. Mattauch and A. Flammersfeld, *Isotopic Report* (Verlag der Zeitschrift für Naturforschung, Tübingen, 1949).

Paramagnetic Resonance in Copper Acetate at 47 000 Mc/sec

TOSIHIKO OKAMURA, YOSIHARU TORIZUKA, AND MUNEYUKI DATE
Research Institute for Scientific Measurements, Sendai, Japan
(Received November 10, 1952)

ANOMALOUS paramagnetic resonance absorption in copper acetate was first reported by Lancaster and Gordy.[1] Resonance experiments on single crystals of this substance were made by Bleaney[2] and Kumagai *et al.*,[3] and the experimental results were analyzed by Kambe.[4]

The present experiments were made on single crystals at a wavelength of 6.38 mm. The results were compared with the theory and were found in sufficient agreement with it. Figures 1 and 2 are, respectively, the changes in resonance field and g value with crystal orientation, when the direction of the applied field was varied by 180° in the $(11\bar{1})$ plane of the crystal from the [110] direction, which was perpendicular to the external field.

According to the theory by Kambe and Bleaney, four Cu^{++} ions in a unit cell comprise two pairs of ions and strong exchange forces are postulated between two ions in a pair; the resonance field for a

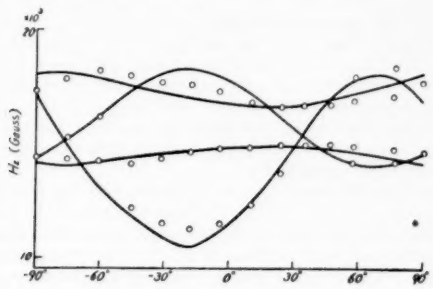

FIG. 1. Resonance field *vs* crystal orientation; the full lines denote the theoretical curves.

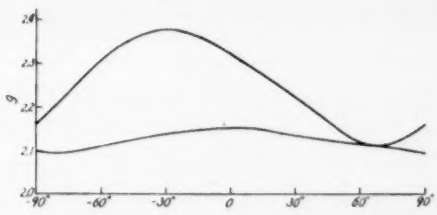

FIG. 2. Angular dependence of g value for each pair of Cu^{++} ions.

pair of Cu^{++} ions is expressed as

$$H=(h\nu/g\beta)\pm P(3\cos^2\theta-1), \tag{1}$$

where P denotes a constant having the dimensions of magnetic field and θ is the angle between the applied field and an axis passing through two Cu^{++} ions in a pair.

Substituting the observed values, $g_\perp=2.10$, $g_{\parallel}=2.37$ in Eq. (1), where the value of P is taken to be 2000 gauss, the curves in Fig. 1 were obtained by projection on the $(11\bar{1})$ plane; for a pair of curves that had the larger amplitude, the angle between an axis passing through two Cu^{++} ions in a pair and the $(11\bar{1})$ plane was calculated to be 4°, and for another pair of curves that had smaller amplitude the angle was calculated to be 59°.

The authors wish to express their thanks for valuable discussions with Dr. H. Kumagai and Mr. E. Abe at the Institute of Science and Technology, Tokyo University.

[1] F. W. Lancaster and W. Gordy, J. Chem. Phys. **19**, 1181 (1951).
[2] B. Bleaney *et al.* Phil. Mag. **43**, 373 (1952).
[3] Kumagai, Abe, and Shimada, Phys. Rev. **87**, 385 (1952).
[4] K. Kambe (unpublished).

The Half-Life of W^{187}†

G. G. EICHHOLZ
Radioactivity Division, Department of Mines and Technical Surveys, Ottawa, Canada
(Received November 18, 1952)

THE half-life of W^{187} has been determined by a number of workers since it was first discovered in 1935.[1,2] Most of these measurements resulted in a half-life value of 24.0±0.1 hours.[3–6] More recently, however, Cork, Keller, and Stoddard[7] have published a value of 25.0 hours, well above previous readings. As a knowledge of the half-life of this isotope was considered important for some experiments carried out in this laboratory, a careful redetermination of the half-life has been carried out.

The measurements were performed by means of an argon-filled pressure ionization chamber, a vibrating reed electrometer, and a pen recorder. The stability of this apparatus has been described before[8] and is more than adequate for the purpose. Two samples were used, a chemically pure calcium tungstate powder and a piece of pure tungsten metal. Each sample was irradiated for one day with slow neutrons from a radium-veryllium source with paraffin moderator. The decay of each sample was plotted over a period of four half-lives, two different runs being carried out on both samples. Both samples were analyzed spectrographically for impurities. The calcium tungstate contained less than 0.1 percent Mg and trace amounts of Fe, Sn, Cu, and K. The tungsten metal contained trace amounts of Mo, Fe, Si, and Cu, all less than 0.05 percent.

The weighted mean obtained from the four determinations by least squares analysis of each decay curve was 23.85±0.08 hours.

Weighting was carried out by taking into account the probable error of the individual runs. The error includes contributions from the other wolfram isotopes which are very small, W^{181} has a half-life of 140 days and its production rate is very low; W^{185} has a half-life of 5.5 sec. W^{185} emits only very soft gamma-rays and in its normal isotopic abundance contributes not more than 0.08 percent of the total initial activity. Over three days its contribution to the

measured decay rate, if detected, would not exceed 0.0004 percent. The contribution to the detected radiation from all the calcium isotopes is also quite negligible.

† Published by permission of the Director-General of Scientific Services, Department of Mines and Technical Surveys, Ottawa, Canada.

[1] McLennan, Grimmett, and Read, Nature **135**, 147 (1935).
[2] Amaldi, d'Agostino, Fermi, Pontecorvo, Rasetti, and Segrè, Proc. Roy. Soc. (London) **A149**, 522 (1935).
[3] R. Jaeckel, Z. Physik **104**, 762 (1937).
[4] O. Minakawa, Phys. Rev. **57**, 1189 (1940).
[5] W. Fajans and W. H. Sullivan, Phys. Rev. **58**, 276 (1940).
[6] Seren, Friedlander, and Turkel, Phys. Rev. **72**, 888 (1947).
[7] Cork, Keller, and Stoddard, Phys. Rev. **76**, 575 (1949).
[8] G. G. Eichholz and L. A. Ficko, Phys. Rev. **86**, 794 (1952).

Cross Terms in β-Decay

O. Kofoed-Hansen and Aage Winther
Institute for Theoretical Physics, University of Copenhagen, Copenhagen, Denmark
(Received December 2, 1952)

THE cross terms between S and V and between T and A interaction in β-decay, the so-called Fierz terms, are in general assumed to vanish. This assumption is based on the apparent straightness of Kurie plots for allowed transitions, where the general expression for the β-spectra is given by[1]

$$P_{\mp}=C\cdot pE(E_{\max}-E)^2F(Z,E)(1\pm b/E),$$

$$b_{\mp}=\pm\frac{2[1-(Z/137)^2]^{\frac{1}{2}}\{g_Sg_V|\int 1|^2+g_Tg_A|\int\boldsymbol{\sigma}|^2\}}{[g_S^2+g_V^2]|\int 1|^2+[g_T^2+g_A^2]|\int\boldsymbol{\sigma}|^2}.$$

For low and medium maximum energies, the most important effect of the cross term b/E is a change of the slope of the Kurie plot. This change is, however, not detected since it is equivalent to a change of C. What remains is a curvature which appears as a small deviation from a straight line, the slope of which is adjusted to the experimental points.

If a β-spectrum can be measured accurately from 100 kev up to 100 kev below the maximum energy, and a straight line is drawn in the Kurie plot through these points, the maximum deviation from this line will be a function of $E_{\max}$ and b. This function in percent of the ordinate is illustrated in Fig. 1.

It is seen that even large values of $b(-1\leq b\leq 1)$ give only small deviations and that, consequently, it is difficult to obtain very narrow limits for b. In fact, an analysis of the published β-spectra indicates that in no case can b values as large as 0.4 be excluded. In such experimental comparisons, one should of course remember that b has opposite sign for positron and negatron emission. Furthermore, it should be remembered that b, besides being a function of the coupling constants, also depends on the nuclear matrix elements. The dependence of b on the coupling constants is

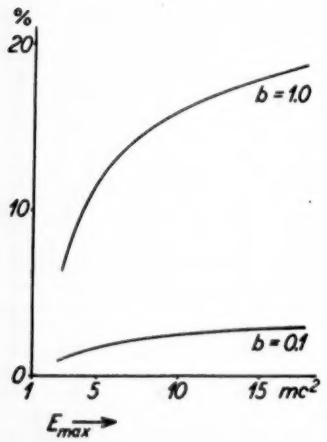

FIG. 1. Maximum deviation of the curved Kurie plot from a straight line drawn through points 100 kev above zero energy and 100 kev below maximum energy for different values of the cross term coefficient b and as a function of $E_{\max}$.

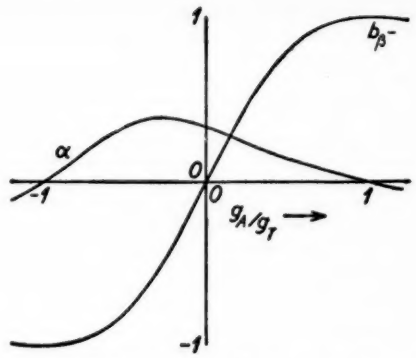

FIG. 2. The experimental angular correlation parameter α and the cross term parameter $b\beta^-$ for allowed G-T transitions.

especially simple in the case where either $|\int 1|^2$ or $|\int\boldsymbol{\sigma}|^2$ vanish. In Fig. 2, we have plotted b as a function of g_A/g_T in the $|\int 1|^2=0$ case.

The possible existence of cross terms will also influence the interpretation of recoil experiments, where the electron-neutrino angular correlation is investigated. If cross terms exist, this correlation is given by[1]

$$W(\theta_{\beta\nu})=1+a(p/E)\cos\theta_{\beta\nu}+b/E,$$

and the measured angular correlation coefficient will be given by

$$\alpha=a/(1+b/E),$$

where E is a certain mean energy of those electrons for which the angular correlation is measured. In Fig. 2, we have plotted α as a function of g_A/g_T in the case $|\int 1|^2=0$ for $E=2$.

It is seen that a determination of α does not permit a unique determination of g_A/g_T, and therefore, it seems valuable to combine β-spectroscopic measurements with the recoil experiments.

Precision measurements of the shape of allowed β-spectra with high maximum energy are therefore very desirable, and especially for transitions where the ratio $|\int 1|^2/|\int\boldsymbol{\sigma}|^2$ can be estimated so that one can interpret the results in terms of the coupling constants.

A more detailed account of these considerations will be given in *Kongelige Danske Videnskabernes Selskab, Matematisk-fysiske Meddelelser*.

[1] See, e.g., S. R. de Groot and H. A. Tolhoek, Physica **16**, 456 (1950).

Heat Pulses in Liquid Helium II below 1°K

K. R. Atkins
University of Toronto, Toronto, Canada
(Received November 21, 1952)

GORTER[1] has suggested that the propagation of heat pulses in liquid helium II well below 1°K can be explained if we assume that the phenomena are not due to second sound but to normal thermal conduction. The purpose of this letter is to agree partially with this suggestion, while pointing out that it is not, as Gorter suggests, inconsistent with the views of Landau,[2] but receives a satisfactory explanation in terms of the development of these views by Khalatnikov.[3,4]

According to Khalatnikov, the mean free path of a phonon at 0.2°K is of the order of 10^3 cm and this is incompatible with the propagation of second sound with a wavelength less than this. The events resulting in the propagation of a heat pulse may therefore be visualized as follows. Phonons are generated at the transmitter and subsequently describe paths during which they suffer no collisions with other phonons. A few phonons travel directly to the

receiver, and the received signal starts after a finite time determined by the velocity of first sound u_1. In this respect the situation cannot be adequately described by the classical equations of thermal conduction, which always give a received signal starting at time zero. Most phonons travel to the wall of the propagation tube where they are diffusely scattered once or many times before reaching the receiver. The signal therefore builds up gradually and the apparent arrival time may depend on the noise level or amplification of the receiver giving an apparent velocity somewhat less than u_1.

The thermal conductivity of the material of the propagation tube is usually so low that heat generated inside the tube leaks out with a long relaxation time of the order of several milliseconds. The excess phonons therefore distribute themselves uniformly throughout the enclosure, producing inside it a uniform excess temperature which then dies away with this long relaxation time, thus producing the long tail observed on the received pulse. It is worth noticing that the maximum amplitude depends only on the heat supplied per pulse and the thermal capacity of the enclosed liquid, suggesting a possible method for measuring the specific heat of the liquid at very low temperatures.

These considerations apply only to the lowest temperatures where the mean free path is large. Khalatnikov's theory would restrict their validity to the temperature range below about 0.6°K. The rise in the velocity of second sound just below 1°K is not so readily explained in terms of dispersion effects. Applying, for example, Dingle's[5] theory of viscous attenuation, the 20 percent rise[6] in velocity at 0.85°K would require a viscosity of the order of 0.1 poise, which appears rather large. A complete set of velocity and attenuation measurements in this region must be available before it can be concluded that the rise in velocity can be explained in any other way than that suggested by Landau.

I should like to thank Professor W. H. Watson for many stimulating discussions.

[1] C. J. Gorter, Phys. Rev. **88**, 681 (1952).
[2] L. D. Landau, J. Phys. (U.S.S.R.) **5**, 495 (1941).
[3] L. D. Landau and I. M. Khalatnikov, J. Exptl. Theoret. Phys. (U.S.S.R.) **19**, 637, 709 (1949).
[4] I. M. Khalatnikov, J. Exptl. Theoret. Phys. (U.S.S.R.) **20**, 243 (1950).
[5] R. B. Dingle, Physica **18**, 789 (1952).
[6] R. D. Maurer and M. A. Herlin, Phys. Rev. **76**, 948 (1949).

Pseudo-Quadrupole Effect for Nuclei in Molecules*

NORMAN F. RAMSEY
Harvard University, Cambridge, Massachusetts
(Received December 4, 1952)

SEVERAL years ago, Foley,[1] following a suggestion of Van Vleck,[2] calculated the pseudo-quadrupole effect for nuclei in diatomic molecules. This effect was a perturbation of the energy levels similar to that by a nuclear electrical quadrupole moment but due instead to the second-order paramagnetic interaction between the nuclear magnetic moment and the electron orbital moments.

It is the purpose of this note to point out that in addition to the effect considered by Foley there are two other magnetic terms which give rise to apparent nuclear quadrupole moments which are of similar magnitude to the term considered by Foley. One of these corresponds to the direct or low frequency term in the diamagnetic susceptibility of molecules.[3] The terms considered by Foley correspond to high frequency[3] (or second-order paramagnetism) terms of the diamagnetic susceptibility. The other new contribution is that due to the electron spins of the molecule. As recently pointed out by Ramsey and Purcell,[4] the effects of the electron spins cannot be neglected even in $^1\Sigma$ molecules when the perturbations entering in a second-order perturbation calculation correspond to magnetic fields that are not uniform throughout the molecule. In such cases the second-order contributions from the triplet state must be included. Since the magnetic field of the nuclear magnetic moment is far from uniform in the molecule, the contribution from the interaction between the nuclear magnetic moment and electron spin magnetic moment must therefore be included.

These terms can best be discussed quantitatively with the aid of the Hamiltonian used by Ramsey and Purcell:[4]

$$\mathcal{H}=\mathcal{H}_1+\mathcal{H}_2+\mathcal{H}_3,$$

where

$$\mathcal{H}_1=\Sigma_k[1/2m_k][(\hbar/i)\nabla_k+(e\hbar/c)\Sigma_i\gamma_i\mathbf{I}_i\times\mathbf{r}_{ki}/r_{ki}^3]^2+V+\mathcal{H}_{LS}+\mathcal{H}_{SS}+\mathcal{H}_{II},$$

$$\mathcal{H}_2=2\beta\hbar\,\Sigma_{kl}\gamma_l\{3(\mathbf{S}_k\cdot\mathbf{r}_{kl})(\mathbf{I}_l\cdot\mathbf{r}_{kl})r_{kl}^{-5}-\mathbf{I}_l\cdot\mathbf{S}_k r_{kl}^{-3}\},$$

$$\mathcal{H}_3=(16\pi\beta\hbar/3)\Sigma_{kl}\gamma_l\delta(\mathbf{r}_k-\mathbf{r}_l)\mathbf{S}_k\cdot\mathbf{I}_l.$$

The only terms that were considered by Foley were the cross products of the two terms inside the bracket of $\mathcal{H}_1$. The additional term corresponding to simple diamagnetism is the square of the second term in the bracket of $\mathcal{H}_1$. Since Foley's term enters only in second order, these two contributions are of comparable magnitude. The other, and, in general, larger effect from the electron spin is that which results from $\mathcal{H}_2$, $\mathcal{H}_3$, and their cross terms. Although the term $\mathcal{H}_3$ gives rise to the largest matrix elements for a molecule such as D_2, it alone, even in a second-order perturbation calculation, gives rise to no pseudo-quadrupole effect since it is independent of the molecular orientation. However, the cross terms between $\mathcal{H}_2$ and $\mathcal{H}_3$ in the second-order perturbation and the terms dependent on $\mathcal{H}_2$ alone both give rise to pseudo-quadrupole effects with the contribution of the former considerably exceeding the latter in the case of D_2. If Q' is the apparent electric quadrupole moment of the nucleus produced by these magnetic interactions, the apparent quadrupole interaction $eQ'(\partial^2V^{ext}/\partial z^2)$ produced by Foley's term for D_2 is approximately -1 cycle per second when estimated by the procedure in his paper. The contribution of the simple diamagnetic term is approximately $+0.4$ cycle per second when estimated with Heitler-London wave functions. The contribution of the electron spins when estimated with Heitler-London wave functions is -2.4 cycles per second. Although all of these pseudo-quadrupole interactions are smaller than those of any nuclear quadrupole moment so far measured, they are comparable to the effects which can be measured in present precision experiments.

* This work was assisted by the joint program of the U. S. Office of Naval Research and the U. S. Atomic Energy Commission.
[1] H. M. Foley, Phys. Rev. **72**, 504 (1947).
[2] J. H. Van Vleck (private communication to I. I. Rabi).
[3] J. H. Van Vleck, *Electric and Magnetic Susceptibilities* (Oxford University Press, London, 1932), pp. 275–276.
[4] N. F. Ramsey and E. M. Purcell, Phys. Rev. **85**, 143 (1952).

A New Approach to the Problem of Higher Order Corrections in the Meson Theory of Nuclear Forces

J. WERLE
Institute for Theoretical Physics, Warsaw, Poland
(Received November 28, 1952)

THE method of successive approximations,[1] outlined for classical meson field equations in a previous note,[2] is here applied to consistent quantum-mechanical calculations. For the sake of generality we present here a formalism, which contains both classical and quantum mesodynamics. Adopting the usual notations, all the equations for the meson fields can be written in the general form

$$(\Box-\mu^2)\varphi=-4\pi\Omega\delta(\mathbf{x}-\mathbf{x}_{(1)}), \tag{1}$$

where $\delta(\mathbf{x})$ is the three-dimensional Dirac function, $\mathbf{x}$ is the vector of position in ordinary space, and Ω is a linear operator characterizing the sources of the meson field component φ. In all cases considered we assume that Ω commutes with the Laplacian operator Δ.

If we suppose now that the solution of Eq. (1) has the form of an expansion $\varphi=\sum_l \varphi^{(l)}$ according to the orders of the time derivatives,[2] we are led to the following form for it:

$$\varphi=\sum_{l=0}^{l_\infty}(-1)^l\frac{1}{2\pi^2}\frac{d^{2l}}{dt^{2l}}\Omega\int\frac{e^{i(\mathbf{k}\cdot\mathbf{r}_{(1)})}}{(k^2+\mu^2)^{l+1}}d_3k$$
$$=\sum_{l=0}^{\infty}(-1)^l\frac{d^{2l}}{dt^{2l}}\left\{\Omega\frac{\sqrt{2}r_{(1)}^{l-\frac{1}{2}}}{r^{\frac{1}{2}}2^l l!\mu^{l-\frac{1}{2}}}K_{l-\frac{1}{2}}(\mu r_{(1)})\right\}, \quad (2)$$

where K denotes modified Hankel functions; $\mathbf{r}_{(1)}=\mathbf{x}-\mathbf{x}_{(1)}$.

As an application of the above general expansion formula to quantum theory, we present the case of the pseudoscalar meson field with pseudoscalar coupling to the nucleons. We have to solve the following set of equations for the meson field φ and the wave function of the nucleon ψ:

$$(\Box-\mu^2)\varphi(\mathbf{x},t)=-4\pi g\psi^*(\mathbf{x},t)\rho_2^{(1)}\psi(\mathbf{x},t)$$
$$=-4\pi g\int\psi^*(\mathbf{x}_{(1)},t)\rho_2^{(1)}\delta(\mathbf{r}_{(1)})\psi(\mathbf{x}_{(1)},t)\cdot d_3\mathbf{x}_{(1)}, \quad (3)$$

$$i\partial\psi(\mathbf{x}_{(1)}t)/\partial t=H^{(1)}\psi(\mathbf{x}_{(1)},t). \quad (4)$$

We have written the sources of the meson field in this integral form corresponding to that postulated by Eq. (1). In order to have more freedom in applying our formalism we do not specify the form of $H^{(1)}$ now. Using expansion (2) we obtain for the field generated by the nucleon denoted by (1):

$$\varphi(\mathbf{x},t)=g\sum_l\frac{(-1)^l\sqrt{2}}{r^{\frac{1}{2}}2^l l!\mu^{l-\frac{1}{2}}}\frac{d^{2l}}{dt^{2l}}$$
$$\times\int\psi^*(\mathbf{x}_{(1)},t)\rho_2^{(1)}r_{(1)}^{l-\frac{1}{2}}K_{l-\frac{1}{2}}(\mu r_{(1)})\psi(\mathbf{x}_{(1)},t)d_3x_{(1)}$$
$$=g\int\psi^*(\mathbf{x}_{(1)},t)\left\{\rho_2^{(1)}\frac{e^{-\mu r_{(1)}}}{r_{(1)}}\right.$$
$$\left.+\frac{1}{2\mu}[H^{(1)},[H^{(1)},\rho_2^{(1)}e^{-\mu r_{(1)}}]]+\cdots\right\}\psi(\mathbf{x}_{(1)},t)d_3x_{(1)}. \quad (5)$$

In transforming the expression for φ to this last form we have utilized the equations of "motion" (4), substituting $H^{(1)}\psi$ for $i\partial\psi/\partial t$ and replacing all the time derivatives by commutators in the known manner.

Now the interaction energy of two given sources can be obtained in a way analogous to that given for electrodynamics by Møller:[3] The source density of the second particle (divided by 4π) is to be multiplied by the field created by the first particle and the result integrated over the whole space. Thus we get

$$-g\int\psi^*(\mathbf{x}_{(2)},t)\rho_2^{(2)}\psi(\mathbf{x}_{(2)},t)\varphi(\mathbf{x}_{(2)}t)d_3x_{(2)}$$
$$=\int\psi^*(1)\psi^*(2)\{\mathcal{U}(2\leftarrow1)\}\psi(1)\psi(2)d_3x_{(1)}d_3x_{(2)}. \quad (6)$$

The quantity

$$\mathcal{U}(2\leftarrow1)=-g^2\left\{\rho_2^{(2)}\rho_2^{(1)}\frac{e^{-\mu r_{12}}}{r_{12}}\right.$$
$$\left.+\frac{1}{2\mu}\rho_2^{(2)}[H^{(1)},[H^{(1)},\rho_2^{(1)}e^{-\mu r_{12}}]]+\cdots\right\}, \quad (7)$$

defined by Eq. (6), can be considered as representing the action of the first particle upon the second one.

It can easily be proved that in the simplest case, when we treat the motion of the sources as given, and especially when we take the simplest possible form for $H^{(1)}$—the free particle Hamiltonian —we get the same results as those obtained by other quantum methods in this approximation (e.g., the second quantization of φ gives the same result in the second-order perturbation treatment). For the sake of comparison of our result with those of other authors let us compute the matrix element of our $\mathcal{U}(2\leftarrow1)$ corresponding to the following transition:

particle (1) from a state of definite momentum and energy $(\mathbf{p}_1, E_1)$ to another such state $(\mathbf{p}_1', E_1')$;
particle (2) from $(\mathbf{p}_2, E_2)$ to $(\mathbf{p}_2', E_2')$.

We obtain

$$-\frac{g^2}{2\pi^2}n'^*(1)n'^*(2)\rho_2^{(1)}\rho_2^{(2)}n(1)n(2)\left\{\frac{1}{(\mathbf{p}_1'-\mathbf{p}_1)^2+\mu^2}\right.$$
$$\left.+\frac{(E_1'-E_1)^2}{\{(\mathbf{p}_1'-\mathbf{p}_1)^2+\mu^2\}^2}+\cdots\right\}\delta(\mathbf{p}_1'+\mathbf{p}_2'-\mathbf{p}_1-\mathbf{p}_2). \quad (8)$$

[$n(1)$ denotes a constant spinor satisfying $(\boldsymbol{\alpha}_{(1)}\mathbf{p}_1+\rho_3^{(1)}M_1)n(1)=E_1n(1).$] The expansion (8) is convergent for all $\mathbf{p}_1$ and $\mathbf{p}_1'$, if we assume Dirac's hole theory and a constant number of nucleons, and therefore exclude the transitions between states of different energy sign (creations and annihilations of nucleon pairs). Then we can sum the expansion (8) and obtain the known result

$$-\frac{g^2}{2\pi^2}\frac{n'^*(1)n'^*(2)\rho_2^{(1)}\rho_2^{(2)}n(1)n(2)}{(\mathbf{p}_1'-\mathbf{p}_1)^2+\mu^2-(E_1'-E_1)^2}\delta(\mathbf{p}_1+\mathbf{p}_2-\mathbf{p}_1'-\mathbf{p}_2'). \quad (9)$$

Because of the good convergence (for all $\mathbf{p}_1$ and $\mathbf{p}_1'$) of (8) in the momentum representation, we are entitled to neglect in (7) all higher order terms, retaining, e.g., only terms to the second order.

However, the formalism presented is not restricted to the above unnecessarily simplified case. It can easily be seen that this method can be used for an iterative solution of the two-body problem (generally, for an iterative solution of simultaneous equations of field and motion). For instance, if we take $H^{(1)}$ in (4) with static Yukawa potential, as a first approximation of the interaction potential between two particles, and insert it in the first two terms in (7), we get a second, better approximation. This second approximation will also contain terms of higher order in g^2. It is interesting that these terms of higher order in g appear in our method always together with higher order (at least second) relativistic corrections, and cannot be separated from them. Therefore, this suggests that the above approximation method presents a new method of expanding the solutions of the quantum equations, which allows us to account for processes of higher order in g. A consistent application of our method to the two-body problem, forces us to use the many-time formalism analogous to that of Dirac, Fock, and Podolski.

Finally we give a simple equivalence proof for pseudovector and pseudoscalar couplings in the case of a pseudoscalar meson field, based on the above convenient form of writing the sources of the meson field. If we consider the case in which these couplings appear together, we obtain for the meson field the same equation as (3) but with an additional term,

$$\frac{f}{\mu}\frac{\partial}{\partial x^\nu}(\psi^*\sigma_\nu^{(1)}\psi)=\frac{f}{\mu}\frac{\partial}{\partial x^\nu}\int\psi^*(\mathbf{x}_{(1)},t)\sigma_\nu^{(1)}\delta(\mathbf{r}_{(1)})\psi(\mathbf{x}_{(1)},t)d_3x_{(1)}. \quad (10)$$

The equation of "motion" has now the form

$$i\frac{\partial\psi(\mathbf{x}_{(1)},t)}{\partial t}=H^{(1)}\psi=\left\{-i\alpha_{(1)}{}^k\frac{\partial}{\partial x_{(1)}{}^k}+\rho_3^{(1)}M\right.$$
$$\left.+g\rho_2\varphi+\frac{f}{\mu}\sigma_\nu\varphi_{,\nu}\right\}\psi(\mathbf{x}_{(1)},t). \quad (11)$$

Using Eq. (11) we can transform expression (10) in a way similar to (5), and after carrying out the calculations we obtain

$$\frac{f}{\mu}\frac{\partial}{\partial x^\nu}(\psi^*\sigma_\nu^{(1)}\psi)=\frac{f}{\mu}\int\psi^*(\mathbf{x}_{(1)},t)\left\{\sigma_k^{(1)}\frac{\partial\delta(\mathbf{r}_{(1)})}{\partial x^k}\right.$$
$$\left.+i[H^{(1)},\rho_1^{(1)}\delta(\mathbf{r}_{(1)})]\right\}\psi(\mathbf{x}_{(1)},t)d_3x_{(1)}$$
$$=-\frac{2f}{\mu}\int\psi^*(\mathbf{x}_{(1)},t)\{M\rho_2^{(1)}-g\rho_3^{(1)}\varphi\}$$
$$\times\delta(\mathbf{r}_{(1)})\psi(\mathbf{x}_{(1)},t)d_3x_{(1)}. \quad (12)$$

Thus we see that the pseudovector coupling is equivalent to pseudoscalar coupling plus a term containing the meson function φ in the sources. (This term vanishes if we take $g=0$.) Therefore we propose to use the following density of the interaction Lagrangian:

$$g'\psi^*\rho_2\psi\varphi+(f'/\mu)\psi^*\rho_3\psi\varphi^2. \quad (13)$$

As regards the equations for meson fields, this form is strictly equivalent to the usual form, $g\psi^*\rho_2\psi\varphi+(f/\mu)\psi^*\sigma_\nu\psi\varphi_{,\nu}$. It is

interesting that recently Sachs[4] suggested the necessity of the existence of such a coupling term to account for the data.

A full text of this work will be published elsewhere.

The author wishes to thank Prof. L. Infeld for many valuable suggestions and helpful criticism.

[1] Einstein, Infeld, and Hoffman, Ann. Math. **39**, 65 (1938); L. Infeld, Phys. Rev. **53**, 836 (1938).
[2] J. Werle, Phys. Rev. **87**, 159 (1952).
[3] C. Møller, Z. Physik **70**, 786 (1931).
[4] R. G. Sachs, Phys. Rev. **87**, 1100 (1952).

Theory of the Microwave Permeability Tensor and Faraday Effect in Nonsaturated Ferromagnetic Materials

GEORGE T. RADO
Naval Research Laboratory, Washington, D. C.
(Received November 26, 1952)

THE microwave Faraday rotation in a ferromagnetic material is calculated below without invoking the restriction, implicit in Roberts'[1] and Hogan's[2] adaptation of Polder's[3] theory, that the material be magnetized to saturation. Under certain conditions the rotation θ is shown to be proportional to the static magnetization M throughout the magnetization curve or hysteresis loop of the material.

If the magnetic inhomogeneities are larger than the domain wall thickness, the exchange torque may be neglected at points not contained within walls, so that at such points the time-dependent saturation magnetization and effective field vectors are related by

$$\partial \mathbf{M}_s(t)/\partial t = \gamma \mathbf{M}_s(t) \times \mathbf{H}(t), \tag{1}$$

where the damping torque is omitted for simplicity, and $ge/2mc$ is denoted by γ. Letting $\mathbf{H}(t)=\mathbf{H}_0+\mathbf{h}(t)$, $\mathbf{M}_s(t)=\mathbf{M}_s+\mathbf{m}(t)$, and $\mathbf{m}(t)\times h(t)\approx 0$, one obtains with $\exp(i\omega t)$ type time-dependence

$$\mathbf{m}=(\gamma/i\omega)(H_0\mathbf{m}-M_s\mathbf{h})\times\mathbf{u}, \tag{2}$$

where $\mathbf{u}$ is a time-independent unit vector defined by $\mathbf{M}_s=M_s\mathbf{u}$. The vector $\mathbf{H}_0=H_0\mathbf{u}$ is an effective, local, static field and represents the resultant of the applied, anisotropy, and magnetic interaction fields at the equilibrium orientation defined by $\mathbf{M}_s(t)=\mathbf{M}_s$. (Although H_0 is not calculable, it may be characterized by the energy increase $M_sH_0\varphi^2/2$ caused by a small deflection φ of $\mathbf{M}_s(t)$ relative to $\mathbf{M}_s$.) The vectors $\mathbf{m}$, $\mathbf{h}$, $\mathbf{u}$, and the scalar H_0 are functions of position.

Assume that $H_a\gamma \ll \omega$, where H_a is some applied field capable of saturating the material and corrected, if necessary, for demagnetization due to the shape of the specimen. Since $H_0 \lesssim H_a$, it follows that $H_0\gamma \ll \omega$. Assume, in addition, that $4\pi M_s\gamma \ll \omega$. Equation (2) then leads to

$$\mathbf{b}\equiv\mathbf{h}+4\pi\mathbf{m}\approx\mathbf{h}+i(4\pi M_s\gamma/\omega)\mathbf{h}\times\mathbf{u}, \tag{3}$$

where H_0 does not occur explicitly.

Consider a polycrystalline material containing randomly oriented crystallites and let it be statically magnetized to some definite state. The internal dynamic demagnetizing field, which contributes to $\mathbf{h}$, may be sufficiently random so that the probability of $\mathbf{h}$ having any specified value at a given point is independent of the direction of $\mathbf{u}$ at that point. This lack of correlation justifies the equation

$$\langle \mathbf{h}\times\mathbf{u}\rangle_{Av}=\langle\mathbf{h}\rangle_{Av}\times\langle\mathbf{u}\rangle_{Av}. \tag{4}$$

The symbol $\langle\ \rangle_{Av}$ is introduced to indicate an average[4] taken over a volume whose linear dimensions are large compared to domain sizes but small compared to a distance L in which $\langle\mathbf{h}\rangle_{Av}$ changes appreciably; clearly $L \lesssim \lambda/4$, where λ is the wavelength in the material. Letting $\mathbf{u}=\mathbf{i}\alpha_1+\mathbf{j}\alpha_2+\mathbf{k}\alpha_3$, where $\mathbf{i}$, $\mathbf{j}$, $\mathbf{k}$ are unit vectors along the x, y, z coordinate axes, respectively, and noting that in a polycrystal magnetized parallel to $\mathbf{k}$ the relations $\langle\alpha_1\rangle_{Av}=\langle\alpha_2\rangle_{Av}=0$ and $\langle\alpha_3\rangle_{Av}=M/M_s$ are valid, one obtains from Eqs. (3) and (4)

$$\langle b_x\rangle_{Av}=\langle h_x\rangle_{Av}+i(4\pi M\gamma/\omega)\langle h_y\rangle_{Av}, \tag{5a}$$

$$\langle b_y\rangle_{Av}=-i(4\pi M\gamma/\omega)\langle h_x\rangle_{Av}+\langle h_y\rangle_{Av}, \tag{5b}$$

$$\langle b_z\rangle_{Av}=\langle h_z\rangle_{Av}. \tag{5c}$$

In general, domain wall displacements may also contribute to the (diagonal) components of the tensor relating $\langle\mathbf{b}\rangle_{Av}$ and $\langle\mathbf{h}\rangle_{Av}$, but if such contributions are neglected, and the other assumptions of Eqs. (5) apply, then these equations (or their obvious generalizations for finite damping)[5] should be used instead of Polder's[3] tensor for the Faraday effect and other applications.

If $\langle\mathbf{b}\rangle_{Av}$, $\langle\mathbf{h}\rangle_{Av}$, and $\langle\mathbf{E}\rangle_{Av}$ are proportional to $\exp(i\omega t-pz)$, Maxwell's curl equations in an unbounded, nonconducting, medium lead to

$$\langle\mathbf{b}\rangle_{Av}=(p^2c^2/\omega^2\epsilon)(\langle h_x\rangle_{Av}\mathbf{k}-\langle\mathbf{h}\rangle_{Av}), \tag{6}$$

where $\epsilon=\epsilon_1-i\epsilon_2$ is the dielectric constant. Combining Eqs. (5) and (6) one obtains two circularly polarized waves described by $p_\pm^2=-(\omega^2\epsilon/c^2)(1\mp 4\pi M\gamma/\omega)$. With the abbreviation $\epsilon_{eff}=(|\epsilon|+\epsilon_1)/2$, it follows that

$$\theta=(z/2)[\mathrm{Im}(p_-)-\mathrm{Im}(p_+)]\approx(2\pi\gamma\epsilon_{eff}^{\frac{1}{2}}/c)zM, \tag{7}$$

a result derived by others[1,2] for $M=M_s$ and not, as they believed, for an arbitrary M.

The published data[1,2] suggest that the predicted proportionality of θ and M may apply even under wave guide conditions provided M is uniform throughout the sample. In the case of a thin disk possessing a large demagnetizing factor in the z direction, of course, no remanence (or hysteresis) of θ or M is to be expected.

[1] F. F. Roberts, J. phys. et radium **12**, 305 (1951).
[2] C. L. Hogan, Bell System Tech. J. **31**, 1 (1952).
[3] D. Polder, Phil. Mag. **40**, 99 (1949).
[4] It was pointed out previously [See G. T. Rado, Revs. Modern Phys. (to be published)] that the validity of such an average is a prerequisite for the interpretation of the measured complex initial permeability of polycrystalline ferrites.
[5] If the damping term $-\eta\{[\mathbf{H}(t)\cdot\mathbf{M}_s(t)]\mathbf{M}_s(t)/M_s^2-\mathbf{H}(t)\}$ is included in the right-hand side of Eq. (1), and it is assumed that $\eta'=4\pi\eta/\omega \ll 1$, then the nondiagonal components of the tensor in Eqs. (5) remain unchanged; the diagonal components become $\mu_{11}=\mu_{22}=1-i\eta'$ and $\mu_{33}=1-i\eta'[1-(M/M_s)^2]$. The Faraday rotation, Eq. (7), remains unchanged.

The Half-Life of Ca^{45}

C. F. G. DELANEY AND J. H. J. POOLE
Physical Laboratory, Trinity College, Dublin, Ireland
(Received December 1, 1952)

THE half-life of Ca^{45} has been estimated by Walke, Thompson, and Holt[1] to be 180±10 days, and by Matthews and Pool[2] to be 152 days. The discrepancy between these values seemed to warrant the redetermination described below.

The decay of 2.3 g of calcium carbonate which had been irradiated for about a day in the Harwell pile, was followed with a G.E.C. end-window G-M counter, type EHM2. Day to day variations in the response of this counter (which, however, never exceeded 2 percent) were corrected for by counting a standard uraninite source. The active material was contained in a brass source holder sealed off with thin cellophane to prevent any change or losses. The activity fell from 3934 counts/min to 1668 counts/min in 202 days. A least squares semilogarithmic plot of the decay gave a value of 163.5 days for the half-life, with a calculated maximum error of ±4 days.

Since an interval of over 100 days was allowed to elapse between the irradiation of the material and the first measurement, any short-lived radioisotopes produced during the activation will have almost completely disappeared. As regards long-lived contaminants, a consideration of the analysis of the calcium carbonate shows that the greatest contribution will be made by S^{35}. Even this, however, will be less than 0.1 percent of the calcium activity. The

Harwell impurity specification and the linearity of the decay curve confirm the absence of appreciable amounts of such contaminants.

A more detailed account of this work will be published elsewhere.

[1] Walke, Thompson, and Holt, Phys. Rev. **57**, 177 (1940).
[2] D. E. Matthews and M. L. Pool, Phys. Rev. **72**, 163 (1947).

The Mass Difference $Si^{27}-Al^{27}$†

J. D. KINGTON, J. K. BAIR, R. R. CARLSON, AND H. B. WILLARD
Oak Ridge National Laboratory, Oak Ridge, Tennessee
(Received October 21, 1952)

THE $Al^{27}(p,n)Si^{27}$ threshold has been found to be 5.819±0.010 Mev using the 5.5-Mev electrostatic generator at Oak Ridge. From this the calculated value of the mass difference $Si^{27}-Al^{27}$ is 0.00519 amu and the Si^{27} disintegration energy is 3.81±0.01 Mev.

In each magnet cycle the calibration of the magnet was effected by locating in order the $F^{19}(p,\alpha\gamma)O^{16}$ levels at 1.355 Mev and 1.381 Mev[1] with mass two beam, the $Al^{27}(p,n)Si^{27}$ threshold, and the $F^{19}(p,\alpha\gamma)O^{16}$ level at 0.669 Mev[1] with mass three beam. The gamma-rays were detected with a NaI crystal counter and the neutrons with a "Bonner-Butler" type[2] counter.

Previously reported values for the $Al(p,n)$ threshold were 6.1±0.1 Mev,[3] and 5.93 Mev.[4] These measurements were done with cyclotrons using essentially a stacked-foil technique. The maximum positron energy from Si^{27} disintegration has been reported as 3.54±0.01 Mev,[5] 3.74,[6] 3.48±0.10 Mev,[7] and 3.6 Mev.[4]

† This document is based on work performed for the U. S. Atomic Energy Commission at Oak Ridge National Laboratory.
[1] Chao, Tollestrup, Fowler, and Lauritsen, Phys. Rev. **79**, 108 (1950).
[2] T. W. Bonner and J. W. Butler, Phys. Rev. **83**, 1091 (1951).
[3] G. Kuerti and S. N. Van Voorhis, Phys. Rev. **56**, 614 (1939).
[4] Blaser, Boehm, Marmier, and Scherrer, Helv. Phys. Acta **24**, 465 (1951).
[5] Barkas, Creutz, Delsasso, Sutton, and White, Phys. Rev. **58**, 383 (1940).
[6] McCreary, Kuerti, and Van Voorhis, Phys. Rev. **57**, 351 (1940).
[7] F. I. Boley and D. J. Zaffarano, Phys. Rev. **84**, 1059 (1951).

The Ground State Hyperfine Structure and Nuclear Magnetic Moment of Praseodymium

HIN LEW
Division of Physics, National Research Council, Ottawa, Canada
(Received November 10, 1952)

THE hyperfine structure of the ground state of praseodymium has been studied by the atomic beam magnetic resonance method. Transitions between magnetic levels belonging to the same total quantum number F and between magnetic levels belonging to different F have been observed. From the former transitions and the previously known nuclear spin value of 5/2, the total electronic angular momentum of the atom in the ground state has been found to be 9/2 and the g_J value of this state to be 0.727±0.005. Since this value of the Landé g factor is exactly that of a $^4I_{9/2}$ state in Russell-Saunders coupling, it seems most likely that the atomic ground state of Pr is a $^4I_{9/2}$. This state is also, according to Hund's rules, the most probable ground state of the $4f^3 6s^2$ configuration which has been predicted for this element.[1]

Of the five hyperfine intervals which exist for the ground state of Pr with $I=5/2$ and $J=9/2$, only two have been observed, *viz.*, the intervals $F=4\rightarrow F=3$ and $F=3\rightarrow F=2$. Their values are 3708.10±0.05 Mc/sec and 2782.20±0.05 Mc/sec, respectively. Attempts to obtain other intervals were unsuccessful, probably because of insufficient microwave power in the transition region. If it is assumed that the hyperfine levels of the $^4I_{9/2}$ state are unperturbed by neighboring states, the observed intervals may be expressed in terms of two constants A and B which measure, respectively, the interaction between the nuclear magnetic moment and the electrons, the interaction between the nuclear electric quadrupole moment and the electrons.[2] We find

$$A=+926.11\pm0.09 \text{ Mc/sec},$$
$$B=-12.9\pm1.0 \text{ Mc/sec},$$
$$B/A=-0.014.$$

The sign of A has been found to be positive by an analysis of the trajectory of the atoms in the apparatus, following the method of Davis, Feld, Zabel, and Zacharias.[2]

A deviation from the interval rule in hyperfine structure may arise from perturbations by neighboring states as well as from a nuclear electric quadrupole moment. In the case of Pr, however, an estimate of the perturbing effect of the $^4I_{11/2}$ state lying about 1450 cm^{-1} above the ground state[3] indicates that the perturbation is not sufficient to account for the observed deviation.

From the magnetic dipole interaction constant A, the contribution a_{4f} due to a single f electron has been calculated by the method of Goudsmit.[4] We obtain

$$a_{4f}=0.7626A(f^3, {}^4I_{9/2})=706.25 \text{ Mc/sec}.$$

From a_{4f} the nuclear gyromagnetic ratio is calculated from the relation

$$a_{4f}=\frac{g_I}{1836}\frac{R\alpha^2(Z-\sigma)^3}{n^3 l(l+\frac{1}{2})(l+1)},$$

using $n=4$ and $\sigma=35.5$. This value of the screening constant σ is calculated from the fine structure multiplet of the ground state of neodymium.[5] A value nearly the same as this is also obtainable from the fine structure of Pr I as deduced from Pr II.[3] We find $g_I=1.53$ and hence

$$\mu=+3.8 \text{ nm}.$$

As a check, this crude method of evaluating the magnetic moment has been applied to the configurations $3d4s^2$, $3d^24s^2$, $3d^34s^2$ of Sc I, Cu I, V I, respectively, for which the magnetic moments are accurately known, and the errors in the calculated moments have been found to be from 10 to 15 percent. Therefore the accuracy of the above value of μ is probably no better than 10 percent. It is interesting to note the close agreement between this value and that calculated by Brix[6] from Pr II. This value also lends support to the view in the independent particle picture of nuclei that the nuclear moments of Pr arise mainly from a $d_{5/2}$ proton.

A detailed report of the experiment and calculations, together with an estimate of the nuclear quadrupole moment, will be given in a later paper.

[1] P. Schuurmans, Physica **12**, 589 (1946).
[2] The exact definitions of A and B are that given by Davis, Feld, Zabel, and Zacharias [Phys. Rev. **76**, 1076 (1949)] except that we have used capital letters instead of small ones. Capital letters are used here because the interaction constants belong to the term $4f^36s^2\,{}^4I_{9/2}$ rather than to a single electron. The contributions to A and B due to a single $4f$ electron will be denoted by small letters.
[3] An estimate of the fine structure splitting of the $f^25s^2\,{}^4I$ multiplet of Pr I may be obtained from the known levels of the f^25s, ${}^3,{}^5I$ multiplet of Pr II in the manner illustrated for Nd in reference 5.
[4] S. Goudsmit, Phys. Rev. **37**, 663 (1931).
[5] P. Schuurmans, Physica **11**, 419 (1946).
[6] P. Brix, Phys. Rev. (to be published).

THE AMERICAN INSTITUTE OF PHYSICS

INCORPORATED

57 East 55 Street New York 22, N.Y.

MEMBER SOCIETIES:

American Physical Society
KARL K. DARROW, *Secretary*, Columbia University, New York 27, New York.

Optical Society of America
ARTHUR C. HARDY, *Secretary*, Massachusetts Institute of Technology, Cambridge 39, Massachusetts.

Acoustical Society of America
WALLACE WATERFALL, *Secretary*, 57 East 55th Street, New York 22, New York.

Society of Rheology
G. J. DIENES, *Secretary*, Brookhaven National Laboratory, Upton, Long Island, New York.

American Association of Physics Teachers
R. F. PAUSH, *Secretary*, University of Illinois, Urbana, Illinois.

AFFILIATED SOCIETIES:

American Crystallographic Association
American Society for Metals
Electron Microscope Society of America
Physical Society of Pittsburgh
Physics Club of Chicago
Physics Club of Philadelphia
Cleveland Physics Society
Physics Club of the Lehigh Valley
Sigma Pi Sigma

ASSOCIATES:

Over seventy-five leading industrial enterprises and other institutions which contribute to the support of the Institute.

JOURNALS:

The Physical Review
S. A. GOUDSMIT, *Editor*, Brookhaven National Laboratory, Upton, Long Island, New York.

Reviews of Modern Physics
J. W. BUCKTA, *Editor*, University of Minnesota, Minneapolis, Minnesota.

Journal of the Optical Society of America
WALLACE R. BRODE, *Editor*, National Bureau of Standards, Washington 25, D. C.

The Journal of the Acoustical Society of America
FLOYD A. FIRESTONE, *Editor*, 57 East 55th Street, New York 22, New York.

American Journal of Physics
THOMAS H. OSGOOD, *Editor*, Michigan State College, East Lansing, Michigan.

The Review of Scientific Instruments
GAYLORD P. HARNWELL, *Editor*, Randal Morgan Laboratory of Physics, University of Pennsylvania, Philadelphia, Pennsylvania.

The Journal of Chemical Physics
CLYDE A. HUTCHISON, JR., *Editor*, Institute for Nuclear Studies, University of Chicago, Chicago 37, Illinois.

Journal of Applied Physics
ELMER HUTCHISSON, *Editor*, Case Institute of Technology, Cleveland 6, Ohio.

Physics Today
GAYLORD P. HARNWELL, *Editorial Director*; ROBERT E. DAVIS, *Managing Editor*, American Institute of Physics, 57 East 55 Street, New York 22, New York.

OFFICERS
GEORGE R. HARRISON, *Chairman*
Massachusetts Institute of Technology
GEORGE B. PEGRAM, *Treasurer*
Columbia University

GOVERNING BOARD
KARL K. DARROW
G. J. DIENES
S. A. GOUDSMIT
G. P. HARNWELL
GEORGE R. HARRISON
F. V. HUNT
RUDOLPH KINGSLAKE
HUGH S. KNOWLES
C. C. LAURITSEN
F. W. LOOMIS
WILLIAM F. MEGGERS
GEORGE B. PEGRAM
I. I. RABI
DUANE ROLLER
FREDERICK SEITZ
FRANCIS G. SLACK
JOHN C. STEINBERG
RICHARD M. SUTTON
MARK W. ZEMANSKY

Consultant on Printing
MELVIN LOOS

ADMINISTRATIVE STAFF
HENRY A. BARTON, *Director*
WALLACE WATERFALL, *Executive Secretary*
THEODORE VORBURGER, *Advertising Manager*
RUTH F. BEYANS, *Publication Manager*
BETTY H. GOODWEILER, *Assistant Secretary*
EILEEN B. NEUBERGER, *Circulation Manager*
KATHRYN SEITZ, *Assistant Treasurer*

THE American Institute of Physics was founded in 1931 as a federation of leading societies in the field of Physics. It combines into one operating agency those functions on behalf of physics which can best be done by the Societies jointly. Its purpose is the advancement and diffusion of physics and its applications to human welfare. To this end it publishes for itself or the Societies the nine journals listed on this page; promotes unity and effectiveness of effort among all who are interested in physics; renders numerous direct services to physicists and to the public; and cooperates with government agencies, national associations, educational institutions, technical industries, and others in such manner as to realize the opportunities and fulfill the responsibilities of physics as an important and constructive human activity.

CONTENTS

THE PHYSICAL REVIEW SECOND SERIES, VOLUME 90, No. 2 JANUARY 15, 1953

Distribution in Energy of the Neutrons from the Interaction of 14-Mev Neutrons with Some Elements . . . . . ELIZABETH R. GRAVES AND LOUIS ROSEN 343

Elastic Scattering of 6.8-Mev Protons from Copper . . . . . L. M. GOLDMAN 349

Transition Probability for Photoelectric Emission from Semiconductors . . . . H. B. HUNTINGTON AND L. APKER 352

Extension of Mahlman's Theory of Photoelectric Emission to a Periodic Potential . . . . . H. B. HUNTINGTON 357

Electron Capture by Protons Passing through Hydrogen . . . . . J. DAVID JACKSON AND RAMEY SCHIFF 359

$C^{12}(p,p)C^{12}$ Differential Cross Section . . . H. L. JACKSON, A. L. GOLDSMITH, F. J. ROPLEKE, R. W. HILL, R. COLEBROOK, AND J. R. CAMERON 365

Excited States of the F^{19} Nucleus . . . . . HERBERT L. JACKSON AND AARON I. GOLDSMITH 370

Neutron Capture Gamma-Rays from Titanium, Chromium, Iron, Nickel, and Zinc . . . . . R. B. KINSEY AND G. A. BARTHOLOMEW 375

Neutron Capture Gamma-Rays from Scandium, Vanadium, Manganese, Cobalt, and Copper . . . . . G. A. BARTHOLOMEW AND R. B. KINSEY 385

Angular Distributions of Protons from the Reaction $T^{(d,p)}T^{2}$ . . . . . D. A. BROMLEY, J. A. KUEHNER, AND E. W. PUTHEBOOT 395

Thermal Treatment of Silicon Rectifiers . . . . . LEO ESAKI 395

Spin and Angular Momentum in General Relativity . . . . . PETER G. BERGMANN AND ROBB THOMSON 400

Further Results from the Study of Sea-Level Penetrating Showers . . . . . W. Y. CHANG, G. DEL CASTILLO, AND LEON GROSSIC 408

Production of Negative Ions and Holes in Negative Ion Beams . . . . . WARD L. FITE 411

Absolute Light Emission Efficiency of Crystal Anthracene for Gamma-Ray Excitation . . . . . MILTON FURST, HARTMUT KALLMANN, AND BERNARD KRAMER 416

Arbitrary Constructions of Matter and the Schwarzschild Singularity . . . . . ANNALENDRAM RATCHAUDHURI 417

Inelastic Events Induced by 33-Mev Protons on Helium . . . . . JACK BENEVIDES AND BRUCE COLE 422

Source of Solid Methane as Inferred from Nuclear Magnetic Resonance . . . . . KAZUMIRA TOMITA 429

Superconducting Properties of Cobalt Disilicide . . . . . B. T. MATTHIAS AND J. K. HULM 439

Variational Principles for Three-Body Scattering Problems . . . . . SIDNEY BOROWITZ AND BERNARD FRIEDMAN 441

Conversion of an Amplified Dirac Equation to an Approximately Relativistic Form . . . . . W. A. BARKER AND Z. V. CHRAPLYVY 446

Diffraction of Strong Shock Waves . . . . . WATLAND GRIFFITHS AND DAVID R. BRIGGS 451

Disintegration of Radium D . . . . . A. A. JAFFE AND S. G. COHEN 454

Proof That Probability Density Appreciation $|\psi|^2$ in Causal Interpretation of the Quantum Theory . . DAVID BOHM 462

Primitive Quantization in the Relativistic Two-Body Problem . . . . . J. L. SYNGE 467

Effect of Collisions upon the Doppler Width of Spectral Lines . . . . . R. H. DICKE 472

Lifetimes of Nuclear Isomers . . . . . STEVEN A. MOSZKOWSKI 474

Magnetic Analysis of the Deuteron-Beryllium Reactions . . . . . R. W. GELLIAS AND S. S. HANNA 483

Magnetic Analysis of the $Sr^{86}(d,p)Sr^{90}$ Reaction . . . . . CHARLES E. MCFARLAND AND FRANKLIN S. SHULL 489

Multiple Scattering and Radiation Damping. II . . . . . H. EISTEIN 490

Radiations of 6.7-Day U^{237} . . . . F. WAGNER, JR., M. S. FREEDMAN, D. W. ENGELKEMEIR, AND J. R. HUIZENGA 502

Disintegration of Helium by 90-Mev Neutrons . . . . . PETER R. TAUSSENWALD 505

Letters to the Editor:

Microwave Resonance Absorption in Gadolinium Metal . . . . . A. F. KIP, C. KITTEL, A. M. PORTIS, R. BARTON, AND F. H. SPEDDING 515

Electronic Structure of the Germanium Crystal . . . . . FRANK HERMAN AND JOSEPH CALLAWAY 518

Proton-Proton Scattering at Intermediate Energies . . . . . ANDRÉ MARTIN AND LOUP VERLET 519

New Long-Lived Magnesium-26 Isotope . . . . . R. K. SHEELINE AND N. R. JOHNSON 520

Thermal Rayleigh Disk Measurements in He^3—He^4 Mixtures . . . . . BERNARD WEINSTOCK AND JOHN R. PELLAM 521

Structure of Deformation Bands . . . . . EDWARD W. HART 521

Unified Field Theory and Born-Infeld Electrodynamics . . . . G. RICKAYZEN AND B. KURŞUNOĞLU 522

Second-Sound Velocity below 1°K as a Function of Pressure . . . . . VICTOR MAYER, JR., AND MELVIN A. HERLIN 523

Activities in Light Nuclei from Nitrogen Ion Bombardment . . . . . L. D. WYLY AND A. ROGERS 524

Paramagnetic Resonance in Copper Acetate at 47 000 Mc/sec . . . . . TOSHIMIO OKAZAWA, YOSHIHARU TOMIZUKA, AND MUNETOSHI DATE 525

Half-Life of W^{187} . . . . . G. G. EICHHOLZ 525

Cross Terms in β-Decay . . . . . O. KOFOED-HANSEN AND AAGE WINTHER 526

Heat Pulses in Liquid Helium II below 1°K . . . . . K. R. ATKINS 526

Pseudo-Quadrupole Effect for Nuclei in Molecules . . . . . NORMAN F. RAMSEY 527

New Approach to the Problem of Higher Order Corrections in the Meson Theory of Nuclear Forces . . . . . J. WEELE 527

Theory of the Microwave Permeability Tensor and Faraday Effect in Nonsaturated Ferromagnetic Materials . . . . . GEORGE T. RADO 529

Half-Life of Ca^{45} . . . . . C. F. G. DELANEY AND J. H. J. POOLE 529

Mass Difference Si^{29}—Al^{29} . . . J. D. KNOTOR, J. K. BAIR, R. R. CARLSON, AND H. B. WILLARD 530

Ground-State Hyperfine Structure and Nuclear Magnetic Moment of Praseodymium . . . KIN LAU 530

LANCASTER PRESS, INC., LANCASTER, PA.